

NASA/CP-2000-210325



National Educators' Workshop: Update 99

Standard Experiments in Engineering, Materials Science, and Technology

Compiled by

*Ginger L. F. Arrington and James E. Gardner
Langley Research Center, Hampton, Virginia*

James A. Jacobs

Norfolk State University, Norfolk, Virginia

John E. Fillion

DaimlerChrysler Corporation, Auburn Hills, Michigan

P. K. Mallick

University of Michigan, Dearborn, Michigan

October 2000

U.S. AIR FORCE
VAFB TECHNICAL LIBRARY

The NASA STI Program Office . . . in Profile

Since its founding, NASA has been dedicated to the advancement of aeronautics and space science. The NASA Scientific and Technical Information (STI) Program Office plays a key part in helping NASA maintain this important role.

The NASA STI Program Office is operated by Langley Research Center, the lead center for NASA's scientific and technical information. The NASA STI Program Office provides access to the NASA STI Database, the largest collection of aeronautical and space science STI in the world. The Program Office is also NASA's institutional mechanism for disseminating the results of its research and development activities. These results are published by NASA in the NASA STI Report Series, which includes the following report types:

- **TECHNICAL PUBLICATION.** Reports of completed research or a major significant phase of research that present the results of NASA programs and include extensive data or theoretical analysis. Includes compilations of significant scientific and technical data and information deemed to be of continuing reference value. NASA counterpart of peer-reviewed formal professional papers, but having less stringent limitations on manuscript length and extent of graphic presentations.
- **TECHNICAL MEMORANDUM.** Scientific and technical findings that are preliminary or of specialized interest, e.g., quick release reports, working papers, and bibliographies that contain minimal annotation. Does not contain extensive analysis.
- **CONTRACTOR REPORT.** Scientific and technical findings by NASA-sponsored contractors and grantees.

- **CONFERENCE PUBLICATION.** Collected papers from scientific and technical conferences, symposia, seminars, or other meetings sponsored or co-sponsored by NASA.
- **SPECIAL PUBLICATION.** Scientific, technical, or historical information from NASA programs, projects, and missions, often concerned with subjects having substantial public interest.
- **TECHNICAL TRANSLATION.** English-language translations of foreign scientific and technical material pertinent to NASA's mission.

Specialized services that complement the STI Program Office's diverse offerings include creating custom thesauri, building customized databases, organizing and publishing research results . . . even providing videos.

For more information about the NASA STI Program Office, see the following:

- Access the NASA STI Program Home Page at <http://www.sti.nasa.gov>
- Email your question via the Internet to help@sti.nasa.gov
- Fax your question to the NASA STI Help Desk at (301) 621-0134
- Telephone the NASA STI Help Desk at (301) 621-0390
- Write to:
NASA STI Help Desk
NASA Center for AeroSpace Information
7121 Standard Drive
Hanover, MD 21076-1320

NASA/CP-2000-210325



National Educators' Workshop: Update 99

Standard Experiments in Engineering, Materials Science, and Technology

*Compiled by
Ginger L. F. Arrington and James E. Gardner
Langley Research Center, Hampton, Virginia*

*James A. Jacobs
Norfolk State University, Norfolk, Virginia*

*John E. Fillion
DaimlerChrysler Corporation, Auburn Hills, Michigan*

*P. K. Mallick
University of Michigan, Dearborn, Michigan*

Proceedings of a workshop sponsored jointly by the National Aeronautics and Space Administration, Washington, DC; Norfolk State University, Norfolk, Virginia; the Department of Defense, Washington, DC; the National Institute of Standards and Technology, Gaithersburg, Maryland; DaimlerChrysler Corporation, Auburn Hills, Michigan; and the University of Michigan, Dearborn, Michigan
and held in
Dearborn and Auburn Hills, Michigan
October 31–November 3, 1999

National Aeronautics and
Space Administration

Langley Research Center
Hampton, Virginia 23681-2199

October 2000

The use of trademarks or names of manufacturers in this report is for accurate reporting and does not constitute an official endorsement, either expressed or implied, of such products or manufacturers by the National Aeronautics and Space Administration.

Available from:

NASA Center for AeroSpace Information (CASI)
7121 Standard Drive
Hanover, MD 21076-1320
(301) 621-0390

National Technical Information Service (NTIS)
5285 Port Royal Road
Springfield, VA 22161-2171
(703) 605-6000

PREFACE

NEW:Update 99, hosted by the University of Michigan-Dearborn and the DaimlerChrysler Corporation, was held October 31 - November 3, 1999.

The 14th Annual NEW:Update was built on themes, activities and presentations based on extensive evaluations from participants of previous workshops as we continued efforts to strengthening materials education. About 100 participants witnessed demonstrations of experiments, discussed issues of materials science and engineering (MS&E) with people from education, industry, government, and technical societies, heard about new MS&E developments, and chose from nine, three-hour mini workshops in state-of-the-art laboratories. Faculty in attendance represented high schools, community colleges, smaller colleges, and major universities. Undergraduate and graduate students also attended and presented.

As in past years, we were fortunate to have excellent support from our hosts. DaimlerChrysler and the University of Michigan Dearborn helped to coordinate the many scientist, engineers, professors and other staff, by providing funding, opening their facilities, developing presentations and activities.

NEW:Update 99 participants saw the demonstration of about fifty experiments and aided in evaluating them. We also heard updating information relating to materials science, engineering and technology presented at mini plenary sessions.

The experiments in this publication can serve as a valuable guide to faculty who are interested in useful activities for their students. The material was the result of years of research aimed at better methods of teaching materials science, engineering and technology. The experiments developed by faculty, scientists, and engineers throughout the United States and abroad add to the collection from past workshops. There is a blend of experiments on new materials and traditional materials.

Experiments underwent an extensive peer review process. After submission of abstracts, selected authors were notified of their acceptance and given the format for submission of experiments. Experiments were reviewed by a panel of specialists through the cooperation of the International Council for Materials Education (ICME). Comments from workshop participants provided additional feedback which authors used to make final revisions, which were then submitted to the NASA editorial group for this publication.

The ICME encourages authors of experiments to make submissions for use in the Journal of Materials Education (JME). The JME offers valuable teaching and curriculum aids including instructional modules on emerging materials technology, experiments, book reviews, and editorials to materials educators.

As with previous NEW:Updates, critiques were made of the workshop to provide continuing improvement of this activity. The evaluations and recommendations made by participants provide valuable feedback for the planning of subsequent NEW:Updates.

NEW:Update 99 and the series of workshops that go back to 1986 are, to our knowledge, the only national workshops or gatherings for materials educators that have a focus on the full range of issues on strategies for better teaching about the full complement of materials. NEW:Update 98, with its diversity of faculty, industry, and government MSE participants, served as a forum for both formal and informal issues facing MSE education that ranged from the challenges of keeping faculty and students abreast of new technology to ideas to ensure that materials scientists, engineers, and technicians maintain the proper respect for the environment in the pursuit of their objectives.

We demonstrated the second edition of Experiments in Materials Science, Engineering & Technology, (EMSET2) CD-ROM with over 300 experiments from NEW:Updates. This CD-ROM is another example of cooperative efforts to support materials education. The primary contributions came from the many authors of the demonstrations and experiments for NEW:Updates. Funding for the CD came from both private industry and federal agencies. Please see the attached information for obtaining the CD.

We express our appreciation to all those who helped to keep this series of workshops viable. Special thanks goes to those on our national organizing committee, management team, hosts, sponsors, and especially those of you who developed and shared your ideas for experiments, demonstrations, and novel approaches to teaching.

We hope that the experiments presented in this publication will assist you in teaching about materials science, engineering and technology. We would like to have your comments on their value and means of improving them. Please send comments to Jim Jacobs, School of Science and Technology, Norfolk State University, Norfolk, Virginia 23504.

The use of trademarks or manufacturers' names in this publication does not constitute endorsement, either expressed or implied, by the National Aeronautics and Space Administration.

MANAGEMENT TEAM

James A. Jacobs
Workshop Co-chairperson
Norfolk State University

John E. Fillion
Workshop Co-chairperson
DaimlerChrysler

P. K. Mallick
Workshop Co-chairperson
University of Michigan

Diana P. LaClaire
Assistant Director
Norfolk State University

Robert Berrettini
International Council for Materials Education

James M. Boileau
Ford Motor Company

Paul Brown
International Council for Materials Education

L. Roy Bunnell
Southridge High School

S. Raj Chaudhury
Norfolk State University

James Clum
University of Detroit-Mercy

Martin A. Crimp
Michigan State University

Leonard W. Fine
Columbia University

Morton Friedman
Gateway Engineering Coalition

Kenneth L. Jewett
National Institute of Standards &
Technology

Thomas F. Kilduff, Emeritus
Thomas Nelson Community College

James V. Masi
Northeast Center for Telecommunication
Technologies

Alfred E. McKenney
IBM Corporation, Retired

Thomas C. Pederson
General Motors Company

Edwin Prior
National Aeronautics and Space
Administration

Heidi Ries
Air Force Institute of Technology

Philip S. Sklad
Oak Ridge National Laboratory

Laura L. Sullivan
American Society for Engineering
Education

Charles V. White
Kettering University

Steven M. Yalisove
University of Michigan-Dearborn

Acknowledgements

We greatly appreciate the support provided by these organizations:

**American Society for Engineering
Columbia University
Kettering University
Michigan State University
University of Detroit-Mercy
ASM International
Delphi Automotive Chassis Systems
International Council for Materials Education
Northeast Center for Telecommunication Technologies
University of Michigan-Ann Arbor**

CONTENTS

PREFACE	iii
MANAGEMENT TEAM	v
REVIEWERS OF EXPERIMENTS	xi
LISTING OF EXPERIMENTS FROM NEW:UPDATES	xiii
PARTICIPANTS	xxxi
UNIVERSITY OF MICHIGAN DEARBORN	xliv
CONTINUOUS LEARNING NETWORK (CLN)	1
Robert Kleinhans, Marina Arizpe, - LightSpeed Technologies, Inc.	
STUDY OF MOLECULAR DEGRADATION OF POLYMERS BY INTRINSIC VISCOSITY	27
Ping Liu - Eastern Illinois University, Danuta Ciesielska - Poznan University of Technology, Poland	
MICROWAVE DIELECTRIC RESPONSE OF WATER AS A FUNCTION OF FREQUENCY	37
J. N. Dahiya - Southeast Missouri State University	
CHALLENGES AND OPPORTUNITIES FOR MATERIALS RESEARCH IN THE AUTOMOTIVE INDUSTRY	51
Christine S. Sloane - General Motors R&D Center and Advanced Technology Vehicles	
SHAPE MEMORY ALLOYS	69
John A. Marshall - University of Southern Maine	
ACCELERATED AGING STUDY OF ABS COPOLYMER	75
Wayne L. Elban, Scott N. Hornung, Matthew C. Reinhardt - Loyola College	
FRICITION AND LUBRICATION OF HIGHLY DEFORMABLE POROUS BEARINGS: LEARNING FROM ARTICULAR CARTILAGE OF HUMAN JOINTS	101
Michael A. Soltz, Gerard A. Ateshian - Columbia University	
EXPERIMENTS IN MAGNETICS FOR TELECOMMUNICATIONS: ORGANIC AND SOL-GEL	109
James V. Masi - Northeast Center for Telecommunications Technologies	
EFFECT OF TEMPERATURE ON THE IMPACT BEHAVIOR AND DIMENSIONAL STABILITY OF THERMOPLASTIC POLYMERS	121
Wayne L. Elban - Loyola College, Matthew J. Elban - Carroll Christian High School	

BIOSPHERE 2 CENTER - PAST, PRESENT AND FUTURE	145
William C. Harris, Leonard W. Fine, Morton B. Friedman - Columbia University	
IONIC BONDING, AN INTRODUCTION TO MATERIALS AND TO SPREADSHEETS	151
Mike L. Meier - University of California, Davis	
TABLETOP EXPERIMENTS FOR MATERIAL PROPERTIES DETERMINATION	167
R. E. Smelser, E. M. Odom, S. W. Beyerlein - University of Idaho	
ACCELERATED FATIGUE TEST	187
Yulian Kin, Dennis Holler - Purdue University Calumet	
FOUR WINDOWS PROGRAMS FOR THE MATERIALS SCIENCE LABORATORY	197
Mike L. Meier - University of California, Davis	
EGG BUNGEE CORD DROP	205
Robert A. McCoy - Youngstown State University	
DESIGN PRACTICES FOR AUTOMOTIVE AND LIGHT TRUCK ALUMINUM BODIES	213
M. J. Wheeler on behalf of Alcan Global Automotive Products and the Aluminum Association	
ALUMINUM MATERIALS FOR ENVIRONMENTALLY FRIENDLY VEHICLES	225
M. J. Wheeler - Alcan International Limited	
THE DRIVE FOR LIGHT WEIGHT VEHICLES IN NORTH AMERICA	235
M. J. Wheeler - Alcan International Limited	
STRUCTURAL DESIGN OF ALUMINUM COMPONENTS WITH ADS SOFTWARE	249
J. Randolph Kissell - The TGB Partnership	
OPPORTUNITIES FOR RECYCLING OF ALUMINUM FROM END-OF-LIFE VEHICLES	255
M. P. Thomas, C. L. Wood, Jr. - The Aluminum Association Inc.	
THERMOSET COMPOSITES (SMC & RRIM) FOR AUTOMOTIVE COMPONENTS	267
Ken C. Rusch, Bruce Budde and Carolyn Hamilton, LARSS Students - The Budd Company Plastics Division representing The Automotive Composites Alliance	
SIMPLE AND INEXPENSIVE METHOD FOR TESTING SHEAR STRENGTH OF ADHESIVE BONDS	297
L. Roy Bunnell - Southridge High School	

MICROWAVE DRIVEN ACTUATORS POWER ALLOCATION AND DISTRIBUTION	303
Timothy Forbes, Kyo D. Song - Norfolk State University	
STRETCHY "ELASTIC" BANDS III CONTAMINANT EFFECTS	313
Alan K. Karplus - Western New England College	
GALVANOSTATIC POLARIZATION CURVES FOR TEACHING PURPOSES, PART II.....	329
Carlos E. Umana - University of Costa Rica	
DIGITAL SHEAROGRAPHY AND APPLICATIONS.....	341
Y. Y. Hung - Oakland University	
LARC™ RP46 POLYIMIDE LOW COST HIGH TEMPERATURE TECHNOLOGY.....	387
Ruth H. Pater - NASA Langley Research Center	
MECHANICAL PROPERTIES OF SHEET STEELS USED IN STAMPING AND DRAWING.....	391
Harvey Abramowitz - Purdue University - Calumet	
EVERY-DAY OBJECTS AND CLASS DEMONSTRATION IN MATERIAL SCIENCE CLASS, DESIGNED TO HELP STUDENTS LEARN	423
Neda S. Fabris - California State University, Los Angeles	
ENGINEERING PLAN BEHIND THE ULTRA LIGHT STEEL AUTO BODY AND AISI/CARS '98 OVERVIEW.....	431
Darryl Martin, Samuel K. Errera - American Iron and Steel Institute	
MST-ONLINE: THE DESIGN OF AN INTERNET GATEWAY FOR EDUCATIONAL RESOURCES IN MATERIALS SCIENCE AND TECHNOLOGY.....	461
S. Raj Chaudhury, Matthew Sanders, Curtiss Wall, James A. Jacobs - Norfolk State University	
VISIO-PLASTIC MODELING OF METAL FORGING AND EXTRUSION.....	475
Ghassan T. Kridli - University of Michigan - Dearborn	
CORPORATE PARTNERSHIPS: WIN-WIN-WIN.....	481
David H. Devier - Owens Community College	
A SIMPLE EXPERIMENT FOR DETERMINING ELASTIC PROPERTIES OF POLYMERS	489
P. K. Mallick, Subrata Sengupta - University of Michigan - Dearborn	
THE MATERIALS EDUCATION LIBRARY: SHARING EDUCATIONAL RESOURCES VIA THE WORLD WIDE WEB	499
Darcy J. M. Clark - University of Michigan	

TEACHING THE PRINCIPLES OF MATERIALS SCIENCE USING OUR NATURAL SURROUNDINGS: SPIDER SILK	513
Robert J. Scheer - Winona State University	
SIMPLE CLASSROOM DEMONSTRATIONS IN CHEMISTRY AND MATERIALS SCIENCE	519
John B. Hudson - Rensselaer Polytechnic Institute	
ARTIFACTS IN X-RAY DIFFRACTION EXPERIMENTS	529
Bruce J. Pletka, Ruth I. Schultz Kramer, Edward A. Laitila - Michigan Technological University	
THE ADVANCED MATERIALS AND PROCESSING EDUCATION CENTER	543
R. S. Goldman, D. Clark, A. Ghosh, L. P. Kendig, J. F. Mansfield, K. McIntyre, X. Pan, K. Worth - University of Michigan	
PREVIEW OF NEW:UPDATE 2000.....	547
Richard Lee - National Composite Center	
USCAR LIFE CYCLE INVENTORY STUDY.....	573
J. L. Sullivan - Ford, R. Williams - GM, S. Yester - Chrysler, S. Hentges - APC, S. Pomper - AA, S. Chubbs - AISI	
USE OF A WEBSEM (REMOTE SCANNING ELECTRON MICROSCOPE)TO CHARACTERIZE AUTOMOTIVE WEAR DEBRIS	597
Stephen K. Kennedy - RJ Lee Group, Inc., Michael Gaston - West Greene High School	
TEENAGED MATERIALS SCIENCE.....	605
Joanna Mirecki Millunchick - University of Michigan	
INTRODUCTION TO EMSET2	617
James A. Jacobs, Alfred E. McKenney, Matthew Sanders, - Norfolk State University	
A METHOD FOR THE MEASUREMENT OF MAGNETOSTRICTION IN FERROMAGNETIC ALLOYS	633
O. Garcia-Hernandez, R. Galindo, K. L. Garcia, R. Valenzuela - National University of Mexico	
CORKING AN OPEN-ENDED TANK.....	647
Edward L. Widener - Purdue University	
MEASUREMENT OF VISCOSITY: CLASSROOM DEMONSTRATION.....	655
Richard B. Griffin, Lance Terrill - Texas A&M University	
THE ROLE OF PLASTICS IN THE AUTOMOBILE	665
Bruce Cundiff - American Plastics Council	

REVIEWERS FOR NEW:Update 99

Else Breval
Senior Research Associate
Materials Research Laboratory
The Pennsylvania State University

Paul W. Brown
Professor Ceramics Science and Engineering
Materials Research Laboratory
The Pennsylvania State University

Witold Brostow
Professor of Materials Science
Center for Materials Characterization
University of North Texas

L. Roy Bunnell
Southridge High School

William Callister
Adjunct Professor of Metallurgy
University of Utah

James Clum
Director Manufacturing Engineering
College of Engineering and Science
University of Detroit Mercy

Michael Grutzcek
Associate Professor
Materials Research Laboratory
The Pennsylvania State University

Technical notebooks were provided by
NASA LANGLEY RESEARCH CENTER

Announcements of the workshop were provided by
Northeast Center for Telecommunication Technologies

Page intentionally left blank

LISTING OF EXPERIMENTS FROM NEW:UPDATES

EXPERIMENTS & DEMONSTRATIONS IN STRUCTURES, TESTING, AND EVALUATION

NEW:Update 88

NASA Conference Publication 3060

Sastri, Sankar. "Fluorescent Penetrant Inspection"

Sastri, Sankar. "Magnetic Particle Inspection"

Sastri, Sankar. "Radiographic Inspection"

NEW:Update 89

NASA Conference Publication 3074

Chowdhury, Mostafiz R. and Chowdhury, Farida. "Experimental Determination of Material Damping Using Vibration Analyzer"

Chung, Wenchiang R. "The Assessment of Metal Fiber Reinforced Polymeric Composites"

Stibolt, Kenneth A. "Tensile and Shear Strength of Adhesives"

NEW:Update 90

NIST Special Publication 822

Azzara, Drew C. "ASTM: The Development and Application of Standards"

Bates, Seth P. "Charpy V-Notch Impact Testing of Hot Rolled 1020 Steel to Explore Temperature Impact Strength Relationships"

Chowdhury, Mostafiz R. "A Nondestructive Testing Method to Detect Defects in Structural Members"

Cornwell, L. R., Griffin, R. B., and Massarweh, W. A. "Effect of Strain Rate on Tensile Properties of Plastics"

Gray, Stephanie L., Kern, Kristen T., Harries, Wynford L., and Long, Sheila Ann T.

"Improved Technique for Measuring Coefficients of Thermal Extension for Polymer Films"

Halperin, Kopl. "Design Project for the Materials Course: To Pick the Best Material for a Cooking Pot"

Kundu, Nikhil. "Environmental Stress Cracking of Recycled Thermoplastics"

Panchula, Larry and Patterson, John W. "Demonstration of a Simple Screening Strategy for Multifactor Experiments in Engineering"

Taylor, Jenifer A. T. "How Does Change in Temperature Affect Resistance?"

Wickman, Jerry L. and Corbin, Scott M. "Determining the Impact of Adjusting Temperature Profiles on Photodegradability of LDPE/Starch Blown Film"

Widener, Edward L. "It's Hard to Test Hardness"

Widener, Edward L. "Unconventional Impact-Toughness Experiments"

NEW:Update 91

NASA Conference Publication 3151

Bunnell, L. Roy. "Tempered Glass and Thermal Shock of Ceramic Materials"

Lundeen, Calvin D. "Impact Testing of Welded Samples"

Gorman, Thomas M. "Designing, Engineering, and Testing Wood Structures"

Strehlow, Richard R. "ASTM - Terminology for Experiments and Testing"

Karplus, Alan K. "Determining Significant Material Properties, A Discovery Approach"

Spiegel, F. Xavier and Weigman, Bernard J. "An Automated System for Creep Testing"

Denton, Nancy L. and Hillsman, Vernon S. "Isotropic Thin-Walled Pressure Vessel Experiment"

Allen, David J. "Stress-Strain Characteristics of Rubber-Like Materials: Experiment and Analysis"

Dahl, Charles C. "Computer Integrated Lab Testing"

Cornwell, L. R. "Mechanical Properties of Brittle Material"

NEW:Update 92**NASA Conference Publication 3201**

- Bunnell, L. Roy. "Temperature-Dependent Electrical Conductivity of Soda-Lime Glass and Construction and Testing of Simple Airfoils to Demonstrate Structural Design, Materials Choice, and Composite Concepts"
- Marpert, Mark I. "Walkway Friction: Experiment and Analysis"
- Martin, Donald H. "Application of Hardness Testing in Foundry Processing Operations: A University and Industry Partnership"
- Masi, James V. "Experiments in Corrosion for Younger Students By and For Older Students"
- Needham, David. "Micropipet Manipulation of Lipid Membranes: Direct Measurement of the Material Properties of a Cohesive Structure That is Only Two Molecules Thick"
- Perkins, Steven W. "Direct Tension Experiments on Compacted Granular Materials"
- Shih, Hui-Ru. "Development of an Experimental Method to Determine the Axial Rigidity of a Strut-Node Joint"
- Speigel, F. Xavier. "An Automated Data Collection System For a Charpy Impact Tester"
- Tipton, Steven M. "A Miniature Fatigue Test Machine"
- Widener, Edward L. "Tool Grinding and Spark Testing"

NEW:Update 93**NASA Conference Publication 3259**

- Borst, Mark A. "Design and Construction of a Tensile Tester for the Testing of Simple Composites"
- Clum, James A. "Developing Modules on Experimental Design and Process Characterization for Manufacturing/Materials Processes Laboratories"
- Diller, T. E. and A. L. Wicks, "Measurement of Surface Heat Flux and Temperature"
- Denton, Nancy and Vernon S. Hillsman, "An Introduction to Strength of Materials for Middle School and Beyond"
- Fisher, Jonathan H. "Bridgman Solidification and Experiment to Assess Boundaries and Interface Shape"
- Gray, Jennifer "Symmetry and Structure Through Optical Diffraction"
- Karplus, Alan K. "Knotty Knots"
- Kohne, Glenn S. "An Automated Digital Data Collection and Analysis System for the Charpy Impact Tester"
- Olesak, Patricia J. "Scleroscope Hardness Testing"
- Speigel, F. Xavier, "Inexpensive Materials Science Demonstrations"
- Wickman, J. L. "Plastic Part Design Analysis Using Polarized Filters and Birefringence"
- Widener, Edward L. "Testing Rigidity by Torque Wrench"

NEW:Update 94**NASA Conference Publication 3304**

- Bruzan, Raymond and Baker, Douglas, "Density by Titration"
Dahiya, Jai N., "Precision Measurements of the Microwave Dielectric Constants of Polyvinyl Stearate and Polyvinylidene Fluoride as a Function of Frequency and Temperature"
Daufenbach, JoDee and Griffin, Alair, "Impact of Flaws"
Fine, Leonard W., "Concrete Repair Applications and Polymerization of Butadiene by an "Alfin" Catalyst"
Hillsman, Vernon S., "Stress Concentration: Computer Finite Element Analysis vs. Photoelasticity"
Hutchinson, Ben, Giglio, Kim, Bowling, John, and Green, David, "Photocatalytic Destruction of an Organic Dye Using TiO₂"
Jenkins, Thomas J., Comtois, John H., and Bright, Victor M., "Micromachining of Suspended Structures in Silicon and Bulk Etching of Silicon for Micromachining"
Jacobs, James A. and Jenkins, Thomas J., "Mathematics for Engineering Materials Technology Experiments and Problem Solving"
Karplus, Alan K., "Paper Clip Fatigue Bend Test"
Kohne, Glenn S., "Fluids With Magnetic Personalities"
Liu, Ping and Waskom, Tommy L., "Ultrasonic Welding of Recycled High Density Polyethylene (HDPE)"
Martin, Donald H., Schwan, Hermann, Diehm, Michael, "Testing Sand Quality in the Foundry (A Basic University-Industry Partnership)"
Shull, Robert D., "Nanostructured Materials"
Werstler, David E., "Introduction to Nondestructive Testing"
White, Charles V., "Glass Fracture Experiment for Failure Analysis"
Wickman, Jerry L. and Kundu, Nikhil K., "Failure Analysis of Injection Molded Plastic Engineered Parts"
Widener, Edward L., "Dimensionless Fun With Foam"

NEW:Update 95**NASA Conference Publication 3330**

- Brown, Scott, "Crystalline Hors d'oeuvres"
Karplus, Alan K., "Craft Stick Beams"
Kern, Kristen, "ION Beam Analysis of Materials"
Kozma, Michael, "A Revisit to the Helicopter Factorial Design Experiment"
Pond, Robert B., Sr., "Recrystallization Art Sketching"
Roy, Rustum, "CVD Diamond Synthesis and Characterization: A Video Walk-Through"
Saha, Hrishikesh, "Virtual Reality Lab Assistant"
Spiegel, F. Xavier, "A Novel Approach to Hardness Testing"
Spiegel, F. Xavier, "There are Good Vibrations and Not So Good Vibrations"
Tognarelli, David, "Computerized Materials Testing"
Wickman, Jerry L., "Cost Effective Prototyping"

NEW:Update 96**NASA Conference Publication 3354**

- Chao, Julie, Currotto, Selene, Anderson, Cameron, Selvaduray, Guna, "The Effect of Surface Finish on Tensile Strength"
Fabris, Neda S., "From Rugs to Demonstrations in Engineering Materials Class"
Ferguson, Luke, Stoebe, Thomas, "Hysteresis Loops and Barkhausen Effects in Magnetic Materials"
Karplus, Alan K., "Holy Holes or Holes Can Make Tensile Struts Stronger"
Koon, Daniel W., "Relaxation and Resistance Measurements"
Liu, Ping, Waskom, Tommy L., "Composite of Glass Fiber with Epoxy Matrix"
Song, Kyo D., Ries, Heidi R., Scotti, Stephen J., Choi, Sang H., "Transpiration Cooling Experiment"
South, Joe, Keilson, Suzanne, Keefer, Don, "In-Vivo Testing of Biomaterials"
Thorogood, Michael G., "Tensile Test Experiments With Plastics"
Widener, Edward L., "Brinelling the Malay Snail"

NEW:Update 97**NASA Conference Publication 208726**

- Banerjee, Gautam, Miller, Albert E. "Understanding Galvanic Corrosion Tricks to Prevent Some Expensive Failures"
- Cadwell, John and Eric, Piippo, Steven. "Strength Testing of Composite Materials"
- Diez, C. Ray. "Case Hardening: An Activity to Demonstrate Brinnell Hardness"
- Draayer, B. F., Dahiya, J. N. "A Computerized Microwave Spectrometer for Dielectric Relaxation Studies"
- Erickson, Glen C., Chung, W. Richard. "Effectiveness of Ultrasonic Testing Method in Detecting Delamination Effects in Thick Composites"
- Fabris, Neda S. "Learning More From Tensile Test Experiment"
- Ferguson, Luke, Stoebe, Thomas. "Properties of Magnetic Ferrites With a Simple Fabrication Method"
- Fine, Leonard W. "Demonstrating the Critical Properties of Carbon Dioxide"
- Goranson, Ulf. "Jet Transport Structures Performance Monitoring"
- Gorman, Thomas M. "Relationship Between Moisture Changes and Dimensional Change in Wood"
- Griffin, R. B., Cornwell, L. R. "Measurement of the Modulus of Elasticity Using a Three-Point Bend Test"
- Homidany, Mtrook Al, Weick, Brian L. "A Device for Measuring the Elastic Modules of Spherical Materials"
- Hudson, John B., Svanes, Torkel, Bryson, Daniel, Sawyer, W. Gregory, "An Interactive Molecular Dynamics Simulation of Atomic Behavior"
- Karplus, Alan K. "Stretchy "Elastic" Bands"
- Liu, Paul Cheng-Hsin, Moore, Kenneth, Ogu, Chris. "Rapid Prototyping Processes and Procedures"
- Loutts, George B. "Crystal Growth of Mixed Optical Materials With the Automatic Czochralski Puller"
- Lund, David W. "High Speed Civil Transport - Design Challenges"
- Masi, James V. "Experiments in Diffusion: Gases, Liquids, and Solids For Under Five Dollars"
- McCoy, Robert A. "How a Heat Pack Works"
- Nydam, Andrew. "Low Dollar Tensile (Torsion) Tester"
- Song, Kyo D. "Design of Hypervelocity Flow Generator and Its Flow Visualizations"
- Spiegel, F. Xavier. "Medicine, Magic, Materials, and Mankind"
- Umana, Carlos E. "The Combined Effect of Thermal Conductivity and Thermal Expansion in a PMMA Plastic Heated by Thermal Radiation"
- Vanasupa, Linda, Braun, David. "The Human Half-Adder: Understanding the Big Picture of Digital Logic"
- Warren, Matthew E., Loutts, George. "Optical Experiments With Manganese Doped Yttrium Orthoaluminate, A Potential Material For Holographic Recording and Data Storage"
- Werstler, David. "Case Studies in Metal Failure and Selection"
- Whang, Kyumin and Hsu, Matthew. "Evaluating the Strength and Biodegradation of a Gelatine-Based Material"
- Williams, John R. "Corrosion Demonstration Utilizing Low Cost Materials"

NEW:Update 98**NASA Conference Publication 209549**

- Griffin, Richard B., Cornwell, L. Roy, Yapura, Carlos, Krishnan, Sivasubramaniam, Hallford, John. "Use of a Four-Point Bend Apparatus to Determine the Modulus of Elasticity"
- Karplus, Alan K. "Stretchy "Elastic" Bands II"
- McWhan, Denis. "Materials Science With Photons and Neutrons"
- Meier, Mike L., Ewald, Karl. "The Underlying Structure of Engineering Materials"
- Meier, Mike L., "Artificial Microstructures"
- Rudes, Merrill. "Crystal Growth"
- Song, Kyo D., Budde, Bruce, Hamilton, Carolyn. "System Upgrade of Atomic Oxygen Generator for Space Materials Research"
- Stang, Robert G. "Room Temperature Creep of Solder"
- Umana, Carlos E. "Galvanostatic Polarization Curves for Teaching Purposes"

Fabris, Neda S. "Every-Day Objects and Class Demonstration in Material Science Class, Designed to Help Students Learn"

Griffin, Richard, Terrill, Lance. "Measurement of Viscosity: Classroom Demonstration"

Hudson, John B. "Simple Classroom Demonstrations in Chemistry and Materials Science"

Karplus, Alan K. "Stretchy "Elastic" Bands III Contaminant Effects"

Kennedy, Stephen K. "Use of a WEBSEM (Remote Scanning Electron Microscope) to Characterize Automotive Wear Debris"

Kin, Yulian, Holler, Dennis. "Accelerated Fatigue Test"

Meier, Mike L. "Ionic Bonding, an Introduction to Materials and to Spreadsheets"

Meier, Mike L. "Four Windows Programs for the Materials Science Laboratory"

McCoy, Robert A. "Egg Bungee Cord Drop"

Pletka, Bruce J., Schultz Kramer, Ruth I., Laitila, Edward A. "Artifacts in X-Ray Diffraction Experiments"

Scheer, Robert J. "Teaching the Principles of Materials Science Using Our Natural Surroundings: Spider Silk"

Smelser, R. E., Odom, E. M., Beyerlein, S. W. "Tabletop Experiments for Material Properties Determination"

EXPERIMENTS & DEMONSTRATIONS IN METALS

NEW:Update 88

NASA Conference Publication 3060

- Nagy, James P. "Sensitization of Stainless Steel"
Neville, J. P. "Crystal Growing"
Pond, Robert B. "A Demonstration of Chill Block Melt Spinning of Metal"
Shull, Robert D. "Low Carbon Steel: Metallurgical Structure vs. Mechanical Properties"

NEW:Update 89

NASA Conference Publication 3074

- Balsamel, Richard. "The Magnetization Process - Hysteresis"
Beardmore, Peter. "Future Automotive Materials - Evolution or Revolution"
Bunnell, L. Roy. "Hands-On Thermal Conductivity and Work-Hardening and Annealing in Metals"
Kazem, Sayyed M. "Thermal Conductivity of Metals"
Nagy, James P. "Austempering"

NEW:Update 90

NIST Special Publication 822

- Bates, Seth P. "Charpy V-Notch Impact Testing of Hot Rolled 1020 Steel to Explore Temperature Impact Strength Relationships"
Chung, Wenchiang R. and Morse, Margery L. "Effect of Heat Treatment on a Metal Alloy"
Rastani, Mansur. "Post Heat Treatment in Liquid Phase Sintered Tungsten-Nickel-Iron Alloys"
Spiegel, F. Xavier. "Crystal Models for the Beginning Student"
Yang, Y. Y. and Stang, R. G. "Measurement of Strain Rate Sensitivity in Metals"

NEW:Update 91

NASA Conference Publication 3151

- Cowan, Richard L. "Be-Cu Precipitation Hardening Experiment"
Kazem, Sayyed M. "Elementary Metallography"
Krepiski, Richard P. "Experiments with the Low Melting Indium-Bismuth Alloy System"
Lundeen, Calvin D. "Impact Testing of Welded Samples"
McCoy, Robert A. "Cu-Zn Binary Phase Diagram and Diffusion Couples"
Patterson, John W. "Demonstration of Magnetic Domain Boundary Movement Using an Easily Assembled Videocam-Microscope System"
Widener, Edward L. "Heat-Treating of Materials"

NEW:Update 92

NASA Conference Publication 3201

- Dahiya, Jai N. "Phase Transition Studies in Barium and Strontium Titanates at Microwave Frequencies"
Rastani, Mansur. "Improved Measurement of Thermal Effects on Microstructure"
Walsh, Daniel W. "Visualizing Weld Metal Solidification Using Organic Analogs"

NEW:Update 93

NASA Conference Publication 3259

- Guichelaar, Philip J. "The Anisotropy of Toughness in Hot-Rolled Mild Steel"
Martin, Donald H. "From Sand Casting TO Finished Product (A Basic University-Industry Partnership)"
Petit, Jocelyn I. "New Developments in Aluminum for Aircraft and Automobiles"
Smith, R. Carlisle "Crater Cracking in Aluminum Welds"

NEW:Update 94

NASA Conference Publication 3304

- Gabrykewicz, Ted, "Water Drop Test for Silver Migration"
Kavikondala, Kishen and Gambrell, Jr., S. C., "Studying Macroscopic Yielding in Welded Aluminum Joints Using Photostress"
Krepiski, Richard P., "Exploring the Crystal Structure of Metals"
McClelland, H. Thomas, "Effect of Risers on Cast Aluminum Plates"
Weigman, Bernard J. and Courpas, Stamos, "Measuring Energy Loss Between Colliding Metal Objects"

NEW:Update 95**NASA Conference Publication 3330**

Callister, William, "Unknown Determination of a Steel Specimen"

Elban, Wayne L., "Metallographic Preparation and Examination of Polymer-Matrix Composites"

Shih, Hui-Ru, "Some Experimental Results in the Rolling of Ni₃Al Alloy"**NEW:Update 96****NASA Conference Publication 3354**

Callister, Jr., William D., "Identification of an Unknown Steel Specimen"

Elban, Wayne L., "Metallurgical Evaluation of Historic Wrought Iron to Provide Insights into Metal-Forming Operations and Resultant Microstructure"

Griffin, R. B., Cornwell, L. R., Ridings, Holly E., "The Application of Computers to the Determination of Corrosion Rates for Metals in Aqueous Solutions"

Hilden, J., Lewis, K., Meararipous, Selvaduray, Guna, "Measurement of Springback Angle in Sheet Bending"

Moss, T. S., Dye, R. C., "Experimental Investigation of Hydrogen Transport Through Metals"

Olesak, Patricia J., "2nd Steel Heat Treatment Lab: Austempering"

Spiegel, F. Xavier, "A Magnetic Dilemma: A Case Study"

Werstler, David E., "Lost Foam Casting"

NEW:Update 97**NASA Conference Publication 208726**

Dalton, William K., Olesak, Patricia J. "Making a Phase Diagram"

Hartwig, K. T., Haouaoui, M., Cornwell, L. R. "Alloy Composition Determinations"

Kin, Yulian, Abramowitz, Harvey, Hentea, Toma, Xu, Ying. "Life Estimate Based on Fatigue Crack Propagation"

NEW:Update 98**NASA Conference Publication 209549**

Biancaniello, Frank S., Jiggetts, Rodney D., Ridder, Stephen D. "Characterization of High Nitrogen Stainless Steel (HNSS) Produced via Inert Gas Atomization and Hip Consolidation"

Cooke, Archie M. "Cast Iron, Wrought Iron & Steel (Historical Perspective of Properties of Ferrous Material"

Kin, Yulian, Abramowitz, Harvey, Hentea, Toma, Higley, Jim, Richards, Jason. "Laboratory Measurement of J-Integral"

NEW:Update 99**NASA Conference Publication**

Kridli, Ghassan T. "Visio-Plastic Modeling of Metal Forging and Extrusion"

Marshall, John A. "Shape Memory Alloys"

Umaña, Carlos E. "Galvanostatic Polarization Curves for Teaching Purposes Part II"

EXPERIMENTS & DEMONSTRATIONS IN POLYMERS

NEW:Update 89

NASA Conference Publication 3074

- Chung, Wenchiang R. "The Assessment of Metal Fiber Reinforced Polymeric Composites"
Greet, Richard and Cobaugh, Robert. "Rubberlike Elasticity Experiment"
Kern, Kristen T., Harries, Wynford L., and Long, Sheila Ann T. "Dynamic Mechanical Analysis of Polymeric Materials"
Kundu, Nikhil K. and Kundu, Malay. "Piezoelectric and Pyroelectric Effects of a Crystalline Polymer"
Kundu, Nikhil K. "The Effect of Thermal Damage on the Mechanical Properties of Polymer Regrinds"
Stibolt, Kenneth A. "Tensile and Shear Strength of Adhesives"
Widener, Edward L. "Industrial Plastics Waste: Identification and Segregation"
Widener, Edward L. "Recycling Waste-Paper"

NEW:Update 90

NIST Special Publication 822

- Brostow, Witold and Kozak, Michael R. "Instruction in Processing as a Part of a Course in Polymer Science and Engineering"
Cornwell, L. R., Griffin, R. B., and Massarweh, W. A. "Effect of Strain Rate on Tensile Properties of Plastics"
Gray, Stephanie L., Kern, Kristen T., Harries, Wynford L., and Long, Sheila Ann T. "Improved Technique for Measuring Coefficients of Thermal Extension for Polymer Films"
Humble, Jeffrey S. "Biodegradable Plastics: An Informative Laboratory Approach"
Kundu, Nikhil. "Environmental Stress Cracking of Recycled Thermoplastics"
Wickman, Jerry L. and Corbin, Scott M. "Determining the Impact of Adjusting Temperature Profiles on Photodegradability of LDPE/Starch Blown Film"

NEW:Update 91

NASA Conference Publication 3151

- Allen, David J. "Stress-Strain Characteristics of Rubber-Like Materials: Experiment and Analysis"
Chowdhury, Mostafiz R. "An Experiment on the Use of Disposable Plastics as a Reinforcement in Concrete Beams"
Gorman, Thomas M. "Designing, Engineering, and Testing Wood Structures"
Lloyd, Isabel K., Kolos, Kimberly R., Menegaux, Edmond C., Luo, Huy, McCuen, Richard H., and Regan, Thomas M. "Structure, Processing and Properties of Potatoes"
McClelland, H. T. "Laboratory Experiments from the Toy Store"
Sorensen, Carl D. "Measuring the Surface Tension of Soap Bubbles"
Wickman, Jerry L. and Plocinski, David. "A Senior Manufacturing Laboratory for Determining Injection Molding Process Capability"

NEW:Update 92

NASA Conference Publication 3201

- Kundu, Nikhil K. "Performance of Thermal Adhesives in Forced Convection"
Liu, Ping. "Solving Product Safety Problem on Recycled High Density Polyethylene Container"
Wickman, Jerry L. "Thermoforming From a Systems Viewpoint"

NEW:Update 93

NASA Conference Publication 3259

- Csernica, Jeffrey "Mechanical Properties of Crosslinked Polymer Coatings"
Edblom, Elizabeth "Testing Adhesive Strength" & "Adhesives The State of the Industry"
Elban, Wayne L. "Three-Point Bend Testing of Poly (Methyl Methacrylate) and Balsa Wood"
Labana, S. S. "Recycling of Automobiles an Overview"
Liu, Ping and Tommy L. Waskom, "Application of Materials Database (MAT.DB) to Materials Education and Laminated Thermoplastic Composite Material"
Marshall, John A. "Liquids That Take Only Milliseconds to Turn into Solids"
Quaal, Karen S. "Incorporating Polymeric Materials Topics into the Undergraduate Chemistry Curriculum: NSF-Polyed Scholars Project: Microscale Synthesis and Characterization of Polystyrene"

NEW:Update 94**NASA Conference Publication 3304**

Fine, Leonard W., "Concrete Repair Applications and Polymerization of Butadiene by an "Alfin" Catalyst"
Halperin, Kopl, Eccles, Charles, and Latimer, Brett, "Inexpensive Experiments in Creep and Relaxation of Polymers"

Kern, Kristen and Ries, Heidi R., "Dielectric Analysis of Polymer Processing

Kundu, Mukul and Kundu, Nikhil K., "Optimizing Wing Design by Using a Piezoelectric Polymer"

Kundu, Nikhil K. and Wickman, Jerry L., "An Affordable Materials Testing Device"

Stienstra, David, "In-Class Experiments: Piano Wire & Polymers"

NEW:Update 95**NASA Conference Publication 3330**

Fine, Leonard W., "Polybutadiene (Jumping Rubber)"

Liu, Ping, and Waskom, Tommy L., "Plastic Recycling Experiments in Materials Education"

Liu, Ping, and Waskom, Tommy L., "Compression Molding of Composite of Recycled HDPE and Recycled Tire Chips"

Masi, James V., "Experiments in Natural and Synthetic Dental Materials: A Mouthful of Experiments"

NEW:Update 96**NASA Conference Publication 3354**

Brindos, Richard, Selvaduray, Guna, "Effect of Temperature on Wetting Angle"

Liu, Ping, Waskom, Tommy L., "Making Products Using Post Consumer Recycled High Density Polyethylene: A Series of Recycling Experiments"

Spiegel, F. Xavier, "Elasticity, Plasticity and Anelasticity: Demonstrations"

NEW:Update 97**NASA Conference Publication 208726**

Liu, Ping, Waskom, Tom L. "Study of Rheological Behavior of Polymers"

Sullivan, Laura L. "Correlation of Birefringent Patterns to Retained Orientation in Injection Molded Polystyrene Tensile Bars"

NEW:Update 98**NASA Conference Publication 209549**

Tomalia, Donald A. Dendritic Polymer Properties and Macromolecular Architecture"

NEW:Update 99**NASA Conference Publication**

Bunnell, L. Roy. "Simple and Inexpensive Method for Testing Shear Strength of Adhesive Bonds"

Elban, Wayne L., Elban, Matthew J. "Effect of Temperature on the Impact Behavior and Dimensional Stability of Thermoplastic Polymers"

Elban, Wayne L., Hornung, Scott N., Reinhardt, Matthew C. "Accelerated Aging Study of ABS Copolymer"

Forbes, Tomothy, Song, Kyo D. "Microwave Driven Actuators Power Allocation and Distribution"

Liu, Ping. "Study of Molecular Degradation of Polymers by Intrinsic Viscosity"

Mallick, P. K. "A Simple Experiment for Determining Elastic Properties of Polymers"

EXPERIMENTS & DEMONSTRATIONS IN CERAMICS

NEW:Update 88

NASA Conference Publication 3060

- Nelson, James A. "Glasses and Ceramics: Making and Testing Superconductors"
Schull, Robert D. "High T_c Superconductors: Are They Magnetic?"

NEW:Update 89

NASA Conference Publication 3074

- Beardmore, Peter. "Future Automotive Materials - Evolution or Revolution"
Bunnell, L. Roy. "Hands-On Thermal Conductivity and Work-Hardening and Annealing in Metals"
Link, Bruce. "Ceramic Fibers"
Nagy, James P. "Austempering"
Ries, Heidi R. "Dielectric Determination of the Glass Transition Temperature"

NEW:Update 90

NIST Special Publication 822

- Dahiya, J. N. "Dielectric Behavior of Superconductors at Microwave Frequencies"
Jordan, Gail W. "Adapting Archimedes' Method for Determining Densities and Porosities of Small Ceramic Samples"
Snail, Keith A., Hanssen, Leonard M., Oakes, David B., and Butler, James E. "Diamond Synthesis with a Commercial Oxygen-Acetylene Torch"

NEW:Update 91

NASA Conference Publication 3151

- Bunnell, L. Roy. "Tempered Glass and Thermal Shock of Ceramic Materials"
Craig, Douglas F. "Structural Ceramics"
Dahiya, J. N. "Dielectric Behavior of Semiconductors at Microwave Frequencies"
Weiser, Martin W., Lauben, David N., and Madrid, Philip. "Ceramic Processing: Experimental Design and Optimization"

NEW:Update 92

NASA Conference Publication 3201

- Bunnell, L. Roy. "Temperature-Dependent Electrical Conductivity of Soda-Lime Glass"
Henshaw, John M. "Fracture of Glass"
Stephan, Patrick M. "High Thermal Conductivity of Diamond"
Vanasupa, Linda S. "A \$.69 Look at Thermoplastic Softening"

NEW:Update 93

NASA Conference Publication 3259

- Bunnell, L. Roy and Stephen Piippo, "Property Changes During Firing of a Typical Porcelain Ceramic"
Burchell, Timothy D. "Developments in Carbon Materials"
Dahiya, J.N., "Dielectric Measurements of Selected Ceramics at Microwave Frequencies"
Ketrn, L.A. "Preparation of Simple Plaster Mold for Slip Casting and Slip Casting"
Masi, James V. "Experiments in Diamond Film Fabrication in Table Top Plasma Apparatus"
Werstler, David E. "Microwave Sintering of Machining Inserts"

NEW:Update 94

NASA Conference Publication 3304

- Bunnell, L. Roy and Piippo, Steven, "The Development of Mechanical Strength in a Ceramic Material During Firing"
Long, William G., "Introduction to Continuous Fiber Ceramic Composites"
Reifsnider, Kenneth L., "Designing with Continuous Fiber Ceramic Composites"
West, Harvey A. & Spiegel, F. Xavier, "Crystal Models for the Beginning Student: An Extension to Diamond Cubic"

NEW:Update 95

NASA Conference Publication 3330

- Louden, Richard A., "Testing and Characterizing of Continuous Fiber Ceramic Composites"

NEW:Update 96

NASA Conference Publication 3354

Bunnell, L. Roy, Piippo, Steven W., "Evaluation of Chemically Tempered Soda-Lime-Silica Glass by Bend Testing"

Dahiya, J. N., "Microwave Measurements of the Dielectric Relaxation in Different Grain Size Crystals of BaTiO₃"

Masi, James V., "Experiments in Sol-Gel: Hydroxyapatite and YBCO"

Stang, Robert G., "The Effect of Surface Treatment on the Strength of Glass"

Thomas, Shad, Hasenkamp, Erin, Selvaduray, Guna, "Determination of Oxygen Diffusion in Ionic Solids"

NEW:Update 98

NASA Conference Publication 209549

Ferguson, Luke, Stoebe, Thomas. An Inexpensive 1600°C (2912°F) Miniature Electric Furnace for Teaching Materials Science.

Welch, David. "Superconducting Magnets and Applications"

EXPERIMENTS & DEMONSTRATIONS IN COMPOSITES

NEW:Update 88

NASA Conference Publication 3060

Nelson, James A. "Composites: Fiberglass Hand Laminating Process"

NEW:Update 89

NASA Conference Publication 3074

Beardmore, Peter. "Future Automotive Materials - Evolution or Revolution"

Chung, Wenchiang R. "The Assessment of Metal Fiber Reinforced Polymeric Composites"

Coleman, J. Mario. "Using Template/Hotwire Cutting to Demonstrate Moldless Composite Fabrication"

NEW:Update 90

NIST Special Publication 822

Bunnell, L. R. "Simple Stressed-Skin Composites Using Paper Reinforcement"

Schmenk, Myron J. "Fabrication and Evaluation of a Simple Composite Structural Beam"

West, Harvey A. and Sprecher, A. F. "Fiber Reinforced Composite Materials"

NEW:Update 91

NASA Conference Publication 3151

Greet, Richard J. "Composite Column of Common Materials"

NEW:Update 92

NASA Conference Publication 3201

Thornton, H. Richard. "Mechanical Properties of Composite Materials"

NEW:Update 93

NASA Conference Publication 3259

Masters, John "ASTM Methods for Composite Characterization and Evaluation"

Webber, M. D. and Harvey A. West. "Continuous Unidirectional Fiber Reinforced Composites: Fabrication and Testing"

NEW:Update 95

NASA Conference Publication 3330

Craig, Douglas F., "Role of Processing in Total Materials"

Wilkerson, Amy Laurie, "Computerized Testing of Woven Composite Materials"

NEW:Update 97

NASA Conference Publication 208726

Gardea, Luis, Weick, Brian L. "A Method for Measuring the Shear Strength of Polymers and Composites"

NEW:Update 99

NASA Conference Publication

Lee, Richard. "National Composite Center"

Marshall, John A. "Shape Memory Alloys"

Rusch, Ken. "Thermoset Composites (SMC & RRIM) for Automotive Components"

EXPERIMENTS & DEMONSTRATIONS IN ELECTRONIC AND OPTICAL MATERIALS

NEW:UPDATE 88

NASA Conference Publication 3060

Sastri, Sankar. "Magnetic Particle Inspection"

NEW:Update 89

NASA Conference Publication 3074

Kundu, Nikhil K. and Kundu, Malay. "Piezoelectric and Pyroelectric Effects of a Crystalline Polymer"

Molton, Peter M. and Clarke, Clayton. "Anode Materials for Electrochemical Waste Destruction"

Ries, Heidi R. "Dielectric Determination of the Glass Transition Temperature"

NEW:Update 90

NIST Special Publication 822

Dahiya, J. N. "Dielectric Behavior of Superconductors at Microwave Frequencies"

NEW:Update 91

NASA Conference Publication 3151

Dahiya, J. N. "Dielectric Behavior of Semiconductors at Microwave Frequencies"

Patterson, John W. "Demonstration of Magnetic Domain Boundary Movement Using an Easily Assembled Videocam-Microscope System"

NEW:Update 92

NASA Conference Publication 3201

Bunnell, L. Roy. "Temperature-Dependent Electrical Conductivity of Soda-Lime Glass"

Dahiya, Jai N. "Phase Transition Studies in Barium and Strontium Titanates at Microwave Frequencies"

NEW:Update 94

NASA Conference Publication 3304

Elban, Wayne L., "Stereographic Projection Analysis of Fracture Plane Traces in Polished Silicon Wafers for Integrated Circuits"

Parmar, Devendra S. and Singh, J. J., "Measurement of the Electro-Optic Switching Response in Ferroelectric Liquid Crystals"

NEW:Update 95

NASA Conference Publication 3330

Dahiya, Jai N., "Temperature Dependence of the Microwave Dielectric Behavior of Selected Materials"

Marshall, John, "Application Advancements Using Electrorheological Fluids"

Ono, Kanji, "Piezoelectric Sensing and Acoustic Emission"

Ries, Heidi R., "An Integrated Approach to Laser Crystal Development"

NEW:Update 96

NASA Conference Publication 3354

Jain, H., "Learning About Electric Dipoles From a Kitchen Microwave Oven"

NEW:Update 97

NASA Conference Publication 208726

Marshall, John A. "Magneto-Rheological Fluid Technology"

Umana, Carlos E. "How to Compute the Atomic Magnetic Dipole Moment of An Element: An Engineering Approach"

NEW:Update 98

NASA Conference Publication 209549

Abramowitz, Harvey. "Use of Piezoelectric Crystals for Voice Recognition"

Dahiya, J. N. "Liquid Crystal p-Azoxyanisole in Microwave Field"

Draayer, Bret. "Simulating Optical Correlation on a PC"

Kasdan, Matthew, Kennedy, Stephen K. "Microchemistry and the New Scanning Electron Microscopes"

Loutts, George B., Noginov, Mikhail A., Wynne, Rosalind, Ross, Kai T., Grandy, Talia. "Investigation of thermal Bleaching in Manganese Doped Orthoaluminum Single Crystals"

Marshall, John A. "Magneto-Rheological Fluid Technology"

Noginov, M. A., Warren, M., Loutts, G. B. "X-ray Excited Emission of Mn^{2+} ions in Mn: $YAlO_3$

Valenquela, R., Amano, E. "Determination of the Curie Temperature in Ferro and Ferrimagnets"

NEW:Update 99

NASA Conference Publication

Dahiya, J. N. "Microwave Dielectric Response of Water as a Function of Frequency"

Masi, James V. "Experiments in Magnetics for Telecommunications: Organic and Sol-Gel"

Widener, Edward L. "Corking an Open-Ended Tank"

EXPERIMENTS & DEMONSTRATIONS IN MATERIALS SYSTEMS

NEW:Update 96

NASA Conference Publication 3354

Aceves, Salvador M., Smith, J. Ray, Johnson, Norman L., "Computer Modeling in the Design and Evaluation of Electric and Hybrid Vehicles"

Benjamin, Robert F., "Experiments Showing Dynamics of Materials Interfaces"

Daugherty, Mark A., "Electrolytic Production of Hydrogen Utilizing Photovoltaic Cells"

Fine, Leonard W., "The Incandescent Light Bulb"

MacKenzie, James J., "Hydrogen -- The Energy Carrier of the Future"

NEW:Update 97

NASA Conference Publication 208726

Bunnell, L. Roy. "Weakening of Latex Rubber by Environmental Effects"

Chadwick, Margaret. "Automotive Materials For the Next Millennium"

NEW:Update 98

NASA Conference Publication 209549

Fabris, Neda S. "Teaching Statistical Quality Control and Process Analysis in Materials Laboratory"

Widener, Edward L. "The Colorful Character of Materials"

EXPERIMENTS & TOPICS IN MATERIALS CURRICULUM

NEW:Update 93

NASA Conference Publication 3259

Bright, Victor M. "Simulation of Materials Processing: Fantasy or Reality?"

Diwan, Ravinder M. "Manufacturing Processes Laboratory Projects in Mechanical Engineering Curriculum"

Kundu, Nikhil K. "Graphing Techniques for Materials Laboratory Using Excel"

McClelland, H. T. "Process Capability Determination of New and Existing Equipment and Introduction to Usable Statistical Methods"

Passek, Thomas "University Outreach Focused Discussion: What Do Educators Want From ASM International"

NEW:Update 94

NASA Conference Publication 3304

Brimacombe, J. K., "Transferring Knowledge to the Shop Floor"

Burte, Harris M., "Emerging Materials Technology"

Constant, Kristen P. and Vedula, Krishna, "Development of Course Modules for Materials Experiments"

Coyne, Jr., Paul J., Kohne, Glenn S., Elban, and Wayne L., "PC Laser Printer-Generated Cubic Stereographic Projections with Accompanying Student Exercise"

Masi, James V., "Bubble Rafts, Crystal Structures, and Computer Animation"

McKenney, Alfred E., Evelyn D., and Berrettini, Robert, "CD-ROM Technology to Strengthen Materials Education"

Olesak, Patricia J., "Understanding Phase Diagrams"

Scheer, Robert J., "Incorporating "Intelligent" Materials into Science Education"

Schwartz, Lyle H., "Technology Transfer of NIST Research"

Spiegel, F. Xavier, "Demonstrations in Materials Science From the Candy Shop"

Uhl, Robert, "ASM Educational Tools Now and Into the Future"

NEW:Update 95

NASA Conference Publication 3330

Belanger, Brian C., "NIST Advanced Technology Programs"

Berrettini, Robert, "The VTLA System of Course Delivery and Faculty in Materials Education"

Kohne, Glenn S., "An Autograding (Student) Problem Management System for the Compeuwtir Ilittur8"

Russ, John, "Self-Paced Interactive CD-ROMS"

NEW:Update 96

NASA Conference Publication 3354

Chaudhury, S. Raj, Escalada, Larry, Zollman, Dean, "Visual Quantum Mechanics - A Materials Approach"

Gulden, Terry D., Winter, Patricia, "Explorations in Materials Science"

McKelvy, Michael J., Birk, James P., Ramakrishna, B. L., "Bringing Advanced Experimental Technology Into Education"

McMahon, Jr., Charles J., "Labs on Videotape for Materials Science and Engineering"

Parkin, Don M., "Los Alamos - The Challenging World of Nuclear Materials Science"

Pendleton, Stuart E., "Next Generation Multimedia Distributed Data Base Systems"

Russ, John C., "Impact of Multimedia and Network Services on an Introductory Level Course"

Spiegel, F. Xavier, "NEW:Update, The Experience of One College"

Wilkerson, Amy, Self, Donna, Rodriquez, Waldo J., Ries, Heidi R., "A "Problem Based Learning" Approach to Reflection and Refraction"

Winter, Patricia S., "Business Involvement in Science Education"

NEW:Update 97**NASA Conference Publication 208726**

- Chaudhury, S. Raj. "The National Educators' Workshop WEB"
- Hudson, John B., Shadler, Linda S., Palmer, Mark A., Moore, James A. "Integration of Laboratory Experiences Into An Interactive Chemistry/Materials Course"
- Jacobs, James A., McKenney, Alfred E. "213 Experiments on CD-ROM From 10 Years of NEW:Updates"
- Kayser, Jack R. "Structural Laboratory Manual"
- Russ, John C. "Impact of Multimedia and Network Services on an Introductory Level Course"
- Sawyer, W. Gregory, Bryson, Daniel, Svanes, Torkel, and Hudson, John B. "Effective Learning Through Interactive Computer Simulation and Experimentation."
- Shackelford, James F., Meier, Michael. "Computer Applications For The Materials Laboratory/Classroom: Illustrating Structure and Diffraction"
- Swyler, Karl J., Fine, Leonard W. "Preview of NEW:Update 98"
- Winter, John M. Jr., Lipetzky, Kirsten G. "X-Ray Radiographic Exercises for an Undergraduate Materials Lab"

NEW:UPDATE 98**NASA CONFERENCE PUBLICATION 209549**

- Berndt, C. C. "Internet Research and the Undergraduate Learning Experience"
- Chaudhury, S. Raj, Golembiewski, Gae. "Educational and Public Outreach for the Mars Sample Return Project"
- Halada, Gary. "Earthquake Resistant Engineering Design"
- Halada, Gary. "Teaching Through Engineering Disaster"
- Higley, James B. "Concurrent Engineering"
- McKenney, Alfred E. "Producing PDF Files Using Adobe Acrobat Capture V2.01"
- McMahon, Charles J., Jr. "Tutorials for Introduction to Materials Engineering"
- Petrakis, Leon. "Rendering Asbestos Harmless"
- Swyler, Karl. "Educational Programs at BNL and Other DOE Labs"

NEW:Update 99**NASA Conference Publication**

- Chaudhury, S. Raj, Sanders, Matthew, Wall, Curtiss, Jacobs, James A. "MST-Online: The Design of an Internet Gateway for Educational Resources in Materials Science and Technology"
- Clark, Darcy J. M. "The Materials Education Library: Sharing Educational Resources Via the World Wide Web"
- Devier, David H. "Corporate Partnerships: WIN-WIN-WIN"
- Gardia-Hernandez, O., Galindo, R., Garcia, K. L., Valenzuela, R. "A Method for the Measurement of Magnetostriction in Ferromagnetic Alloys"
- Millunchick, Joanna Mirecki "Teenaged Materials Science"

EMSET CD ROM
EXPERIMENTS IN MATERIALS SCIENCE, ENGINEERING & TECHNOLOGY
 ISBN: 0-13-648486-7
James A. Jacobs

A Multimedia Tool of Laboratory Experiments and Classroom Demonstrations

FEATURES:

- Over 200 laboratory experiments and classroom demonstrations which you can modify to suit your teaching objectives, environment, and students' needs.
- Access to instructional aids developed by hundreds of materials educators and industry specialists in the field of materials science, engineering and technology.
- Provides students with "hands-on" activities that cover the full range of materials science and technology: topics such as woods, metals, and emerging technologies including processing and structures of advanced composites and sol-gel ceramics.
- Flexibility: emphasis is placed on low-cost, multi-concept exercises in recognition of the many settings in which materials education occurs.
- The CD-ROM allows you to read, navigate, search for other experiments/documents, print, and edit.

CATEGORIES OF EXPERIMENTS:

TESTING & EVALUATION, POLYMERS, METALS, CERAMICS, COMPOSITES, ELECTRONIC MATERIALS & MATERIALS CURRICULUM

A BONUS CD OF VIDEO CLIPS:

A bonus CD provides video segments on selected concepts.
STM & AFM MICROSCOPY, POLYMERS, CERAMICS, AND COMPOSITES

PLATFORMS SUPPORTED:

This CD-ROM can be used on Windows and Macintosh platforms. Acrobat Reader and QuickTime software is included on the disk for Windows 3x, Windows 95 and Macintosh. The disk may be used on other platforms provided the appropriate software is installed.

TO ORDER A COPY	
Call: 1 (800) 947-7700 OR Visit our web site: www.prenhall.com	
OR simply fill out and mail this to:	
Prentice Hall, Order Processing Dept. 200 Old Tappan Road, Old Tappan, NJ 07675	
Date _____	Tax Exempt Cert. No. _____
P.O. Number _____	
BILL TO:	SHIP TO:
Account No. _____	Cust. Key No. _____
Name _____	Name _____
Dept. _____	Dept. _____
School/Org. _____	School/Org. _____
Address _____	Address _____
City _____	City _____
State, Zip _____	State, Zip _____
<i>CD-ROM Price: \$150.00</i>	

Page intentionally left blank



**National Educators' Workshop
1999 Participants**

- Row 1. W. Elban, R. Valenzuela, R Pater, L. Smith, S. Bhonsle, E. Widener, D. LaClaire
Row 2. M. Arizpe, M. Fu, P. K. Mallick, B. Callister, B. Patbl, P. Liu, M. Hung, J. Jacobs, D. Finlow, J. Fillion, B. Snedeker, L. Santos
Row 3. R. Goldman, L. Bao, R. Smelser, A. Nye, B. McCoy, R. Singh, A. Karplus, J. Masi, L. Huang, G. Arrington, D. Wells
Row 4. R. Raffo, S. Yalisove, M. Meier, S. R. Chaudhury, S. Kennedy, Z. Wang, S. Gerritsma, M. Churma
Row 5. C. Alderman, T. Kilduff, C. Gallinat, C. Reichel, D. Gerbus, C. R. Diez, P. Alesso, J. Hudson, R. Griffin, P. Sklad, M. Hjelmstad, C. Smith, C. Chrovian, H. Tang
Row 6. R. Yang, D. Clark, J. Clum, C. White, H. Card, R. Bunnell, B. Berrettini, J. Gardner, J. Stuef
Row 7. M. Sanders, S. Errera, D. Schiavello, R. Kissell, G. Johnson, M. Friedman, B. Pletka, M. Crimp, T. Pederson, J. Morrison, H. Abramowitz, Y. Kin, C. Umana, N. Fabris, S. Helba, M. Rudes

Page intentionally left blank

NATIONAL EDUCATORS' WORKSHOP
1999 PARTICIPANTS

Harvey Abramowitz
Department of Engineering
Purdue University - Calumet
2200 169th Street
Hammond, IN 46323
219-989-2473
harveya@calumet.purdue.edu

Cheryl Alderman
North Carolina State University at UNCA
CPO 2360
One University Heights
Asheville, NC 28804-8511
828-251-6943
alderman@eos.ncsu.edu

Lori Aldridge
Northwestern High School
2503 W. Main Street
Rockhill, SC 29732
803-547-0969
ll1516@aol.com

Philip Alesso
SUNY College of Technology at Alfred
Alfred, NY 14802
607-587-8576
allessopf@alfredtech.edu

Marina Arizpe
Lightspeed Technologies, Inc.
7005 Double Eagle Court
St. Louis, MO 63129
314-846-0082

Ginger Arrington
NASA Langley Research Center
Mail Stop 211
Hampton, VA 23681-2199
757-864-9696
g.l.freeman@larc.nasa.gov

Lingyun Bao
University of Michigan-Dearborn

Robert Berrettini
209 Kenmar Drive
Monroeville, PA 15146-1717
412-373-7975
berrettini@juno.com

Steve R. Bhonsle
Valparaiso University
ME Department
Valparaiso, IN 46383
219-464-5119
suryaji.bhonsle@valpo.edu

L. Roy Bunnell
6119 W. Willamette
Kennewick, WA 99336
509-734-3800
Bunnro@ksd.org

William D. Callister
University of Utah
2419 East 3510 South
Salt Lake City, UT 84109
801-278-8611
bill.callister@m.cc.utah.edu

Hershey Card
Farmington High School
32000 Shiawassee
Farmington, MI 48336
248-489-3456
card.hershey@farmington.k12.mi.us

Joseph Carpenter
Department of Energy
202-586-1022

Cindy Carter
Prentice Hall
445 Hutchinson Avenue
Columbus, OH 43235

C. Raj Chaudhury
Norfolk State University
2401 Corprew Avenue
Norfolk, VA 23504
757-823-2241
srchaudhury@nsu.edu

Michelle Churma
Prentice-Hall, Inc.
445 Hutchinson Avenue 4th floor
Columbus, OH 43235
614-841-3636
michele_churma@prenhall.com

Darcy J. M. Clark
MSE Department
University of Michigan-Ann Arbor
H. H. Dow Building
2300 Hayward Street
Ann Arbor, MI 48109-2136
734-764-3377
darcyc@engin.umich.edu

James Clum
Director Manufacturing Engineering
College of Engineering & Science
University of Detroit Mercy
4001 W. McNichols Road
P. O. Box 19900
Detroit, MI 48219-0900
313-992-1510
clumja@udmercy.edu

Martin Crimp
Department of Materials Science & Mechanics
Michigan State University
East Lansing, MI 48824-1226
517-355-0294
Crimp@EGR.MSU.EDU

Bruce Cundiff
Director of Automotive
American Plastics Council
1800 Crooks Road, Suite A
Troy, MI 48084
bcundiff@ameriplas.org

Jai N. Dahiya
Physics Department
Southeast Missouri State University
One University Plaza
MS 6600
Cape Girardeau, MO 63701
573-651-2390
dahiya@physics.semo.edu

Steve Dairy
Harper Creek High School

David H. Devier
Owens Community College
Oregon Road
P. O. Box 10,000
Toledo, OH 43669-1947
ddevier@owens.cc.oh.us

C. Ray Diez
Industrial Technology
University of North Dakota
Box 7118
Grand Forks, ND 58202-7118
701-777-2198

Wayne L. Elban
Loyola College
Department of Electrical Engineering
and Engineering Science
4501 N. Charles Street
Baltimore, MD 21210
410-617-2853
welban@loyola.edu

Samuel K. Errera
American Iron and Steel Institute
2000 Town Centre
Suite 320
Southfield, MI 48075-1199
248-945-4770
erreras@autosteel.org

Neda S. Fabris
Mechanical Engineering
California State University, Los Angeles
5151 State University
Los Angeles, CA 90032
323-343-5218
nfabris@calstatela.edu

Ron Fasca
Owens Community College
P. O. Box 10,000
Toledo, OH 43612
419-661-7469
rfasca@owens.cc.oh

John E. Fillion
Manager of Body Materials Engineering
CIMS: 482-00-11
DaimlerChrysler Corporation
800 Chrysler Drive
Auburn Hills, MI 48326-2757
248-576-7472
jef2@chrysler.com

Leonard W. Fine
Department of Chemistry
Columbia University in the
City of New York
Havemeyer Hall
New York, NY 10027
212-854-2017
fine@chem.columbia.edu

David E. Finlow
Shawnee State University
940 Second Street
Portsmouth, OH 45662
740-355-2686
dfinlow@shawnee.edu

Timothy Forbes
Norfolk State University
700 Park Avenue
Norfolk, VA 23504

Morton Friedman
Columbia University
500 West 120th Street
Room 510 Mudd
New York, NY 10027
212-854-2986
friedman@columbia.edu

Maofeng Fu
University of Michigan-Detroit

James E. Gardner
Technical Staff Assistant
NASA Langley Research Center
Building 1219, Room 217
MS 118
Hampton, VA 23681-0001
757-864-6003
j.e.gardner@larc.nasa.gov

Dan Gerbus
University of Idaho
Mechanical Engineering Dept.
Moscow, ID 83844-0902

Steve Gerritsma
University of Michigan-Dearborn

Rachael S. Goldman
Dow Corning
Dept. of Materials Science & Engineering
2300 Hayward Street
Ann Arbor, MI 48109-2136
734-647-6821
rsgold@engin.umich.edu

Richard B. Griffin
Department of Mechanical Engineering
Texas A&M
College Station, TX 77843
409-845-9779
rgriffin@mengr.tamu.edu

Jeremiah Habets
Columbia University
510 SW Mudd
500 W. 120th Street
New York, NY 10027
212-854-4729
joh18@columbia.edu

W. C. Harris
Columbia University Biosphere 2 Center
P. O. Box 689
Oracle, AZ 85623
520-896-6453
wharris@bio2.edu

Steve Helba
Prentice Hall
445 Hutchinson Avenue
Columbus, OH 43235
800-228-7854

Donald Heckelman
Engineering Science Program
Hudson Valley Community College
80 Vandenberg Avenue
Troy, NY 12180
heckedon@hvcc.edu

Luke Hamming Huang
University of North Dakota
152 Starcher Hall
Grand Forks, ND 58203
701-777-2202
Luke_huang@und.nodak.edu

John B. Hudson
Rensselaer Polytechnic Institute
Materials Science & Engineering Dept.
Troy, NY 12180
518-276-6447
hudsonj@rpi.edu

Michael Y. Y. Hung
John F. Dodge Chair Professor
Mechanical Engineering Dept.
Oakland University
Rochester Hills, MI 48309
248-370-2238
hung@oakland.edu

James A. Jacobs
Norfolk State University
700 Park Avenue
Norfolk, VA 23504
757-823-8109
jajacobs@nsu.edu

Glenn E. Johnson
Andrews University
Mail Stop 0370
Berrien Springs, MI 49104616-471-3191
johnsong@andrews.edu

Alan K. Karplus
Department of Mechanical Engineering
Western New England College
Springfield, MA 01119-2684
413-782-1220
akarplus@wnec.edu

Stephen K. Kennedy
RJ Lee Group, Inc. 350 Hochberg Road
Monroeville, PA 15146
724-325-1776
skennedy@rjlg.com

Thomas F. Kilduff
504 Brafferton Circle
Hampton, VA 23663
757-857-0272
tkilduff@whro.net

Yulian Kin
Purdue University Calumet
2200 169th Street
Hammond, IN 46323
219-989-2684
kin@calumet.purdue.edu

Gary Kinzel
The Ohio State University
Department of Mechanical Engineering
1063 West 18th Avenue
Columbus, OH 43210-1107
614-292-6884
kinzel.1@osu.edu

Randy Kissell
The TGB Partnership
1325 Farmview Road
Hillsborough, NC 27278
919-644-8250
tgb@mindspring.com

Robert Kleinhans
Lightspeed Technologies
5987 Royal Country
St. Louis, MO 63129
636-394-0012
rk@lightspeed-tech.com

Steve Kosmos
Grosse Point High School

Ghassan T. Kridli
University of Michigan-Dearborn
4901 Evergreen Road
Dearborn, MI 48128
313-593-5467
gkridli@umich.edu

Diana P. LaClaire
Norfolk State University
2401 Corprew Avenue
Norfolk, VA 23504
757-823-9072
dplaclaire@nsu.edu

Richard E. Lee
National Composites Center
2000 Composites Drive
Kettering, OH 45420
937-297-9453
teamelks@ix.netcom.com

Ping Liu
Eastern Illinois University
101 Klehm Hall
Charleston, IL 61920
217-581-6267
cfpl@eiu.edu

P. K. Mallick
Department of Mechanical Engineering
University of Michigan-Dearborn
Dearborn, MI 48128
313-593-5119
pkm@umich.edu

John Marshall
University of Southern Maine
John Mitchell Center
Gorham, ME 04038
207-780-5447
jmarshal@usm.maine.edu

Darryl Martin, Sr. Director
American Iron and Steel Institute
2000 Town Center
Suite 320
Southfield, MI 48075-1199
248-945-4760
martin@autosteel.org

James V. Masi, Director
Northeast Center for Telecommunications
Technologies
One Federal Street
Springfield, MA 01105
413-731-3155
masi@stcc.mass.edu

Robert A. McCoy
Mechanical Engineering Department
Youngstown State University
Youngstown, OH 44555
330-742-1736
ramccoy@cc.yzu.edu

Mike Meier
University of California Davis
Department Chemical Engineering & Materials
Science
Davis, CA 95616
530-752-5166
mlmeier@ucdavis.edu

Kay Milewski
Ford Research Laboratory
P. O. Box 2053
20000 Rotunda Drive
Dearborn, MI 48121-2053
313-248-8196

Joanna Mirecki Millunchick
Dept. of Materials Science and Engineering
University of Michigan
2300 Hayward Street
Ann Arbor, MI 48109-2136

Jim Morrison
Lightspeed Technologies
5987 Royal Country
St. Louis, MO 63129
jm@lightspeed-tech.com

Wayne A. Noll
Delphi Auto
937-455-6757
wayne.a.oll@delphiauto.com

Alan Nye
Rochester Institute of Technology
76 Lomb Drive
Rochester, NY 14623
716-475-6121
ahneme@rit.edu

Debby Parker
Department of Mechanical Engineering
University of Michigan-Dearborn
Dearborn, MI 48128
313-593-5882
dparker@umich.edu

Ruth Pater
Mail Stop 226
Materials Div. Research & Technology Group
NASA Langley Research Center
Hampton, VA 23681-2199
757-864-4277
r.h.pater@larc.nasa.gov

Thomas C. Pederson
Senior Staff Research Scientist
Research & Development Center
General Motors Corporation
Mail Code 480-103-001
30500 Mound Road 103
Box 9055
Warren, MI 48090-9055
810-986-1650
thomas_c._pederson@gmr.com

Bruce J. Pletka
Michigan Technological University
1400 Townsend Drive
Houghton, MI 49931-1295
906-487-2639
bjpletka@mtu.edu

Federico Raffo
University of Michigan-Dearborn

Carl Reichel
Augusta Technical Institute
3116 Deans Bridge Road
Augusta, GA 30906
706-771-4092
creichel@mindspring.com

Anthony Renshaw
Columbia University in the City
of New York
School of Engineering & Applied Science
New York, NY 10027

Bill Ross
Muskegon Community College
221 S. Quarterline Road
Muskegon, MI 49442
616-777-0367
rossb@muskegon.cc.mi.us

Merrill Rudes
Energy Concepts, Inc.
595 Bond Street
Lincolnshire, IL 60069
847-821-1900 ext. 312
ecieng1@aol.com

Kenneth Rusch
Budd Plastic Division
1850 Research Drive
Troy, MI 48083-2167
248-619-2235
rushkr@troyrd.buddcompany.com

Constance L. Rutherford
DaimlerChrysler Corporation
800 Chrysler Drive
Auburn Hills, MI 48326-2757
248-576-7501
CR15@daimlerchrysler.com

Lori Rysdorp
American Iron and Steel Institute
2000 Town Center
Southfield, MI 48075-1199
248-945-4768
rysdorpl@autosteel..org

Matthew Sanders
Norfolk State University
700 Park Avenue
Norfolk, VA 23504
717-683-8109

Leslie Santos
3310 West Big Beaver Road
Suite 144
Troy, MI 48084
248-649-4888
lsantos@wwnet.net

Jessica Schroeder
Materials & Processes Laboratory
GM R&DE Center
Warren, MI
810-986-1176

Subrata Sengupta
College of Engineering and Computer Science
University of Michigan-Dearborn
Dearborn, MI 48128

Daniel V. Schiavello
Desktop Engineering International
1200 MacArthur Blvd.
Mahwah, NJ 07430
201-818-9700
schiavello@deiusa.com

Ram N. Singh
St. Louis Community College at Florissant Valley
3400 Pershall Road
St. Louis, MO 63135-1408
314-595-1822
rsingh@fd.stlcc.cc.mo.us

Philip S. Sklad
Oak Ridge National laboratory
Bldg. 4515, MS-6065
P. O. Box 2008
Oak Ridge, TN 37831-6065
423-574-5069
pxi@ornl.gov

Christine S. Sloane
General Motors R & D Center and
Advanced Technology Vehicles
MC: 483-619-409
1996 Technology Drive
Troy, MI 48007-7083
248-680-5754
christine.s.sloane@gm.com

Ron Smelser
University of Idaho
Mechanical Engineering Department
Moscow, ID 83844-0902
208-885-4049
rsmelser@uidaho.edu

Ann Smith
Automotive Composites Alliance
3310 W. Big Beaver
Suite 144
Troy, MI 48098
248-649-4888

L. Brent Smith
Shawnee State University
940 Second Street
Portsmouth, OH 45662
740-355-2686
bsmith@shawnee.edu

Becky Snedeker
The Aluminum Association
900 19th Street, N.W.
Washington, DC 20006

Michael E. Soltz
Columbia University in the
City of New York
New York, NY 11027

Jim Stuef
ECI
32900 W. 13 Mile Road
Farmington Public Schools
Farmington Hill, MI 48334

Michael P. Thomas
Alcan Global Automotive Products
37676 Enterprise Court
Farmington Hills, MI 48331
248-487-5633
Mike.Thomas@Alcan.com

Brian Thompson
Michigan State University
Mechanical Engineering
517-355-2179

Yinghao Tian
University of Michigan-Dearborn

Gary Tibbetts
Materials & Processes Laboratory
GM R&D Center
Warren, MI
810-986-0655

Carlos E. Umana
School of Mecanical Engineering
University of Costa Rica
San Pedro, Costa Rica
506-207-4548
caruma@terraba.fing.ucr.ac.cr

Alejandro Vadillo
University of Michigan-Dearborn

Raul Valenzuela
Institute for Materials Research
National University of Mexico
P. O. Box 70-360
Mexico 04510 Mexico
525-622-46 53
monjaras@servidor.unam.mx

Marcel vanSchaik
AISI-Southfield
vanschaikm@autosteel.org

Dave Vebecky
Farmington High School
Farmington Public Schools
Farmington Hills, MI 48336

Anthony S. Warren
Alcan Aluminum
37676 Enterprise court
Farmington Hills, MI 48331
248-489-5631
tony.warren@alcan.com

David L. Wells
Focus: Hope
Wayne State University
1400 Oakman Boulevard
Detroit, MI 48128
313-494-4293
wellsd@focushope.edu

Michael Wheeler
Alcan Global Automotive Products
136 Bagot Street
Kingston, Ontario K7L 3E5
Canada
Mike.Wheeler2@sympatico.ca

Barbara White
810-659-2269

Charles V. White
Professor of Manufacturing Engineering
Kettering University
1700 West Third Avenue
Flint, MI 48504-4898
810-762-7884
cvwhite@kettering.edu

Edward L. Widener
Purdue University
Knob Hall 119
West Lafayette, IN 47907-1317
765-494-7521
elwidener@tech.purdue.edu

Steven Yalisove
Director, Center for Nanomaterials Science
Department of Materials Science and Engineering
University of Michigan
2300 Hayward Street
Ann Arbor, MI 48109-2136
734-764-4346
smy@umich.edu

Robert L. Yang
NASA Langley Research Center
MS 211
Hampton, VA 23681-0001
757-864-8020
r.l.yang@larc.nasa.gov

Susan G. Yester
DaimlerChrysler Corporation
800 Chrysler Drive
Auburn Hills, MI 48326

Page intentionally left blank

NATIONAL EDUCATORS' WORKSHOP

Update 99: Standard Experiments
in Engineering Materials, Science,
and Technology

October 31 - November 3, 1999 - Dearborn and Auburn Hills, Michigan

Sponsored by



Department of Energy
Office of Energy Efficiency and
Renewable Energy



National Aeronautics & Space
Administration
Langley Research Center



Norfolk State University
School of Science and
Technology

MSEL

Materials Science &
Engineering Laboratories-
NIST

DAIMLERCHRYSLER

DaimlerChrysler Corporation



Scientific Research Laboratory
Ford Motor Company



General Motors Corporation



Energy Efficiency & Renewable
Energy Program
Oak Ridge National Laboratory

USAMP

United States Automotive
Materials Partnership



Center for Lightweight Materials
and Processing
University of Michigan-Dearborn



Gateway Engineering Coalition



American Iron & Steel Institute



Aluminum Association



American Plastics Council



Automotive Composites Alliance

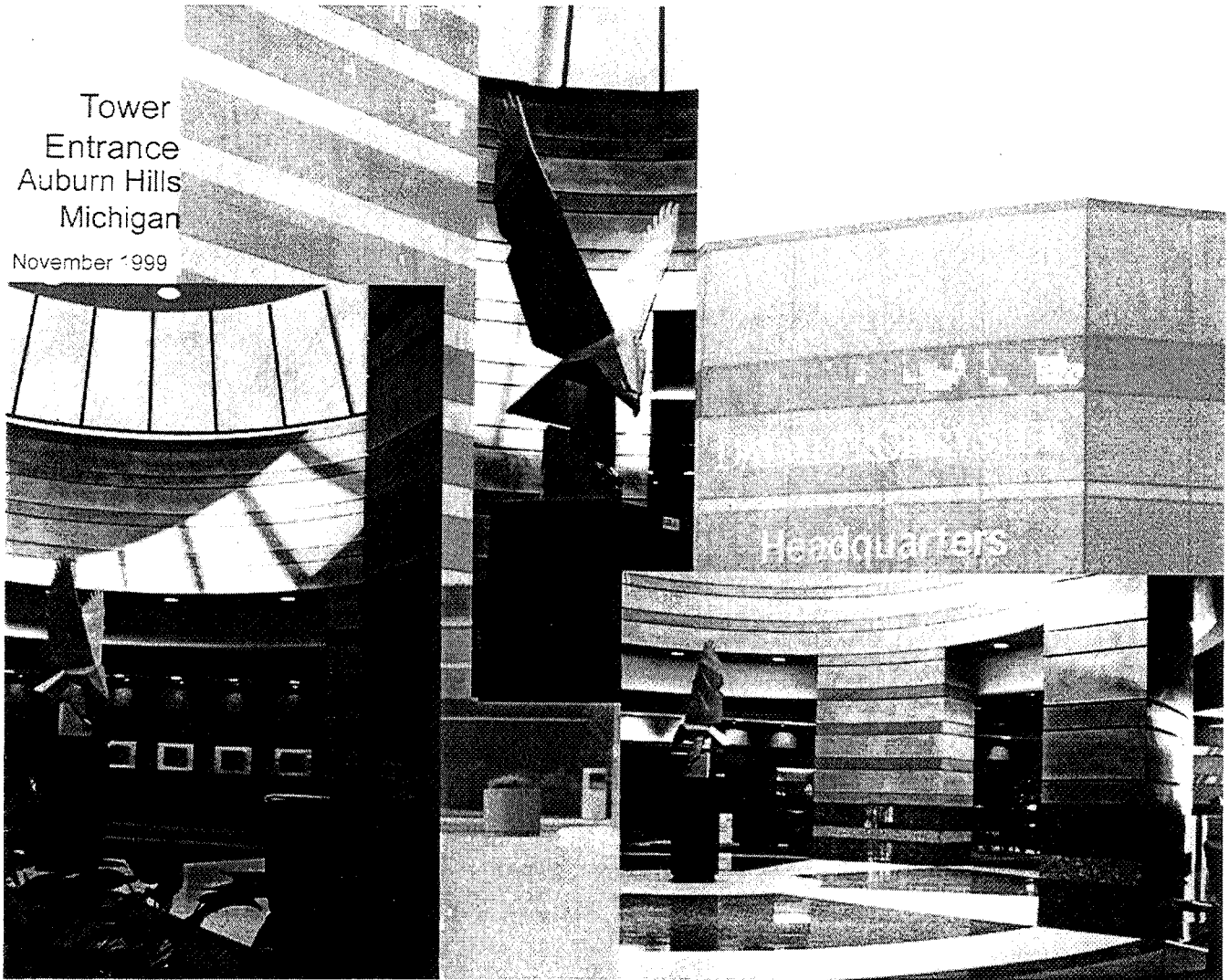
with the support of

American Society for Engineering
Columbia University
Kettering University
Michigan State University
University of Detroit-Mercy

ASM International
Delphi Automotive Chassis Systems
International Council for Materials Education
Northeast Center for Telecommunication Technologies
University of Michigan-Ann Arbor

Tower
Entrance
Auburn Hills
Michigan

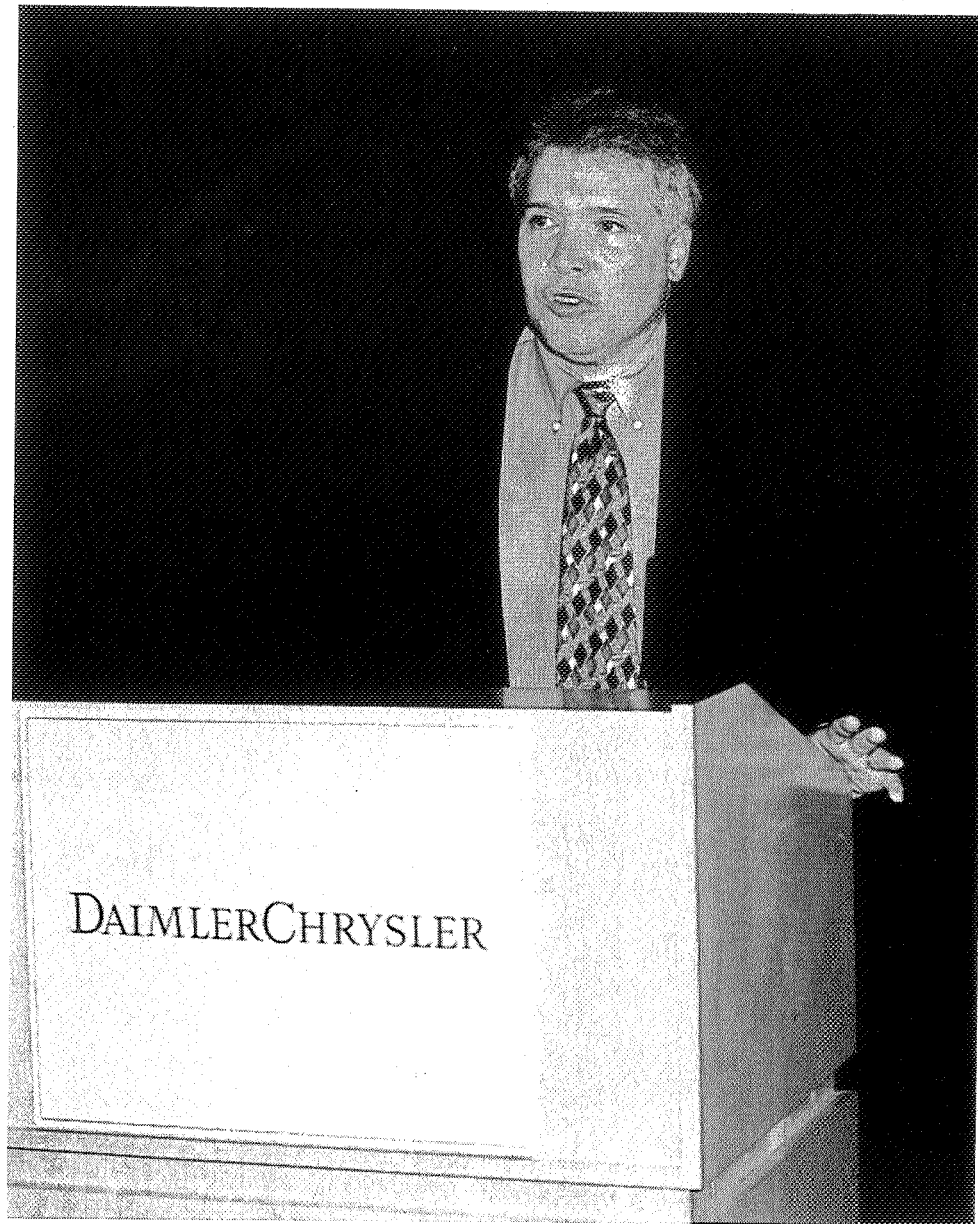
November 1999



WELCOME



James Jacobs



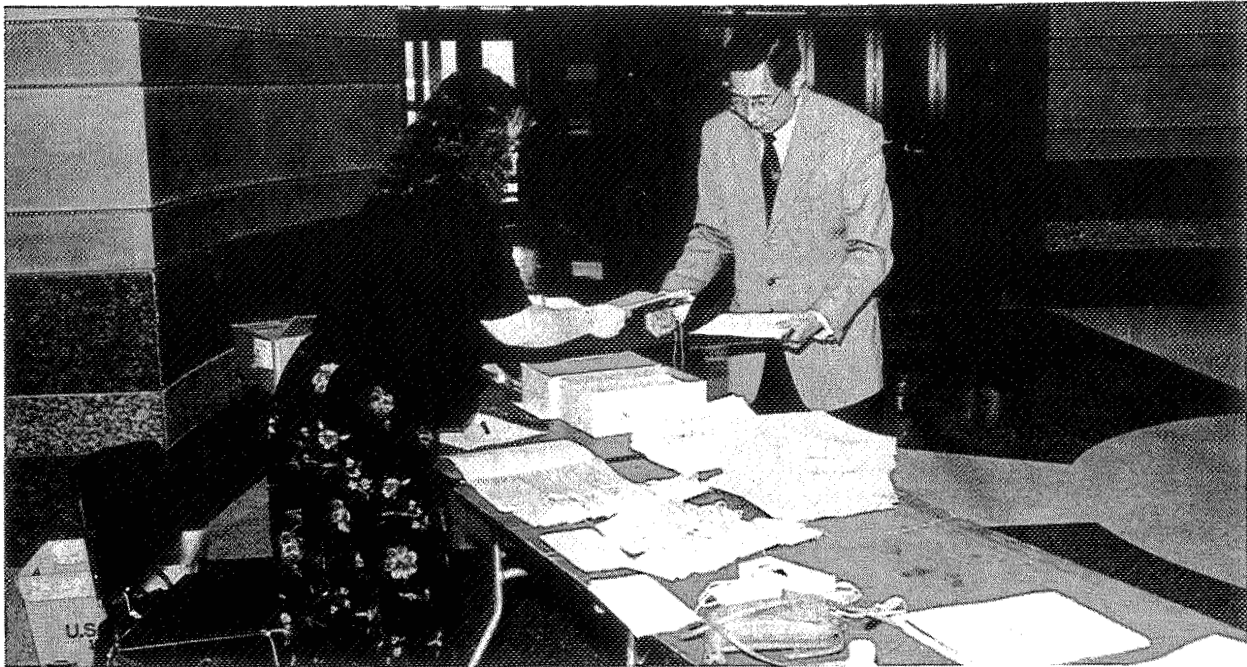
John Fillion

CONTRIBUTIONS



James Clum and James Gardner

REGISTRATION

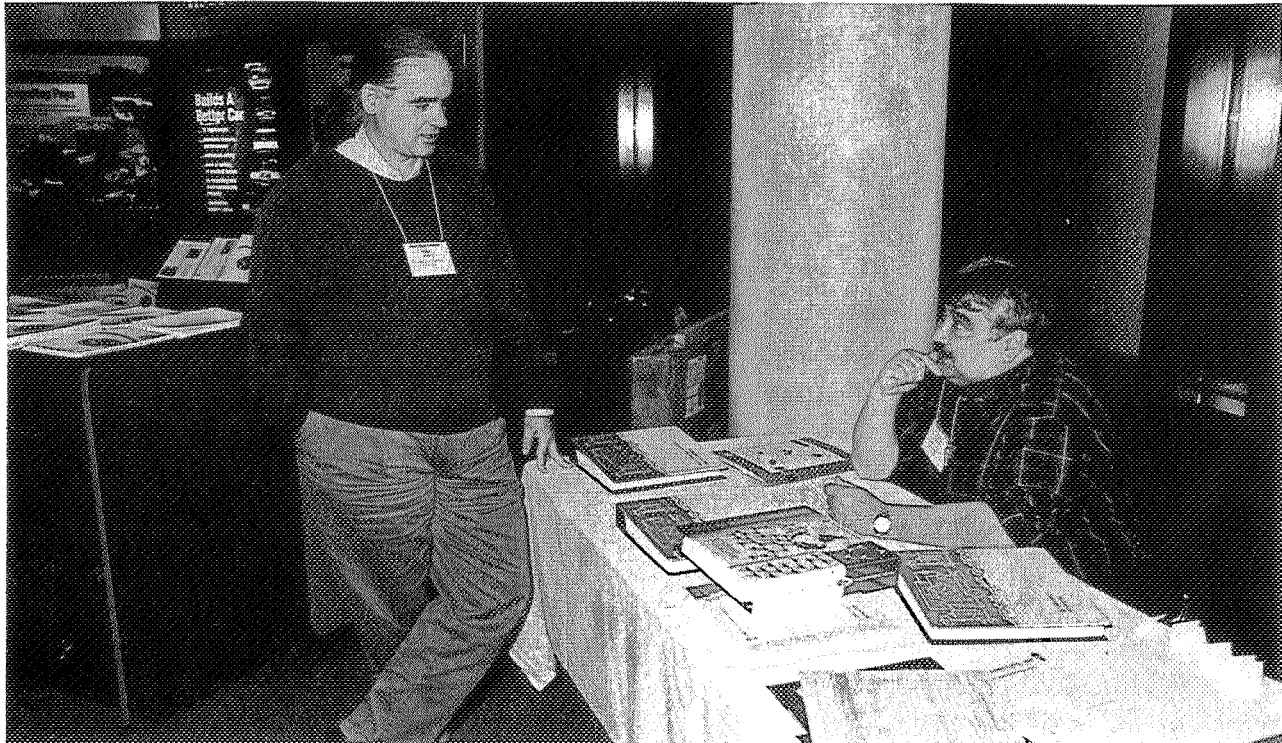
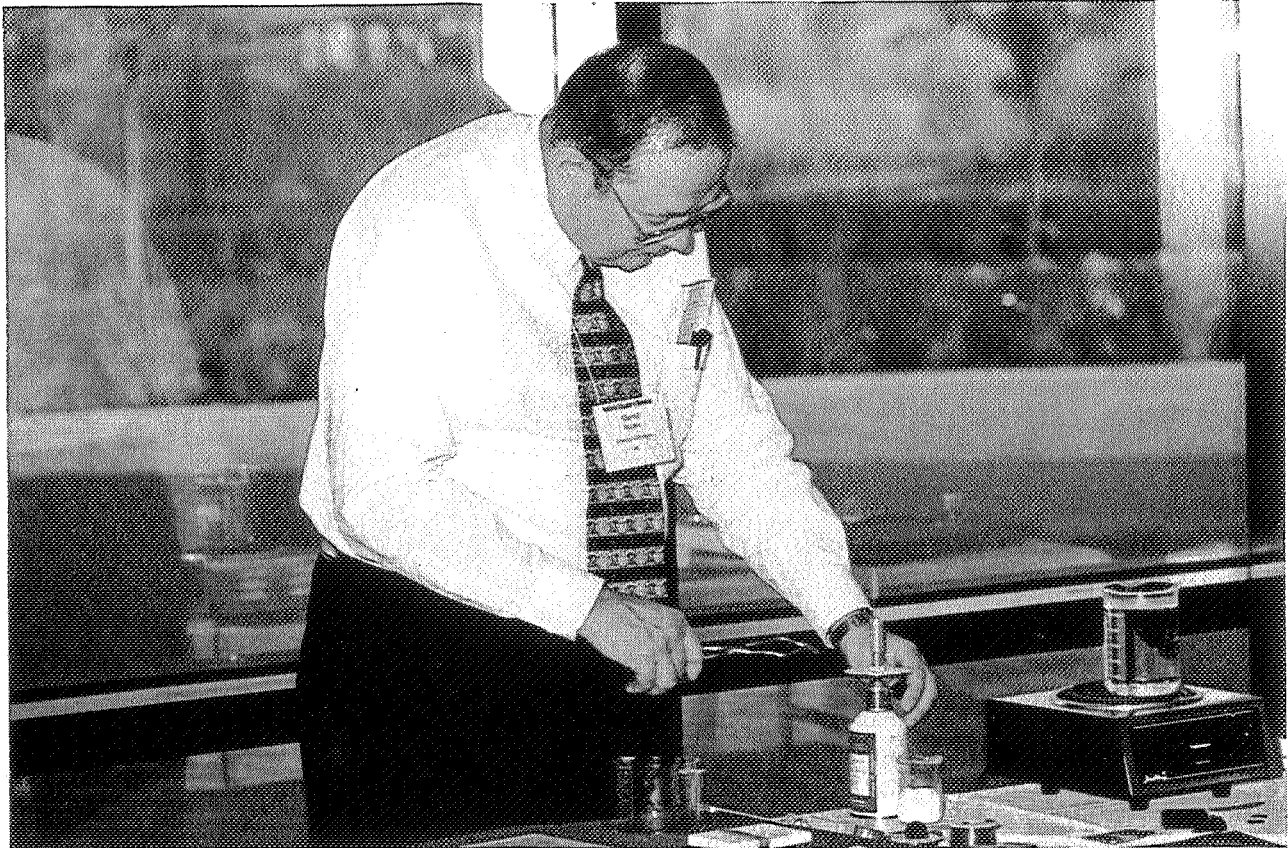


Ginger Arrington

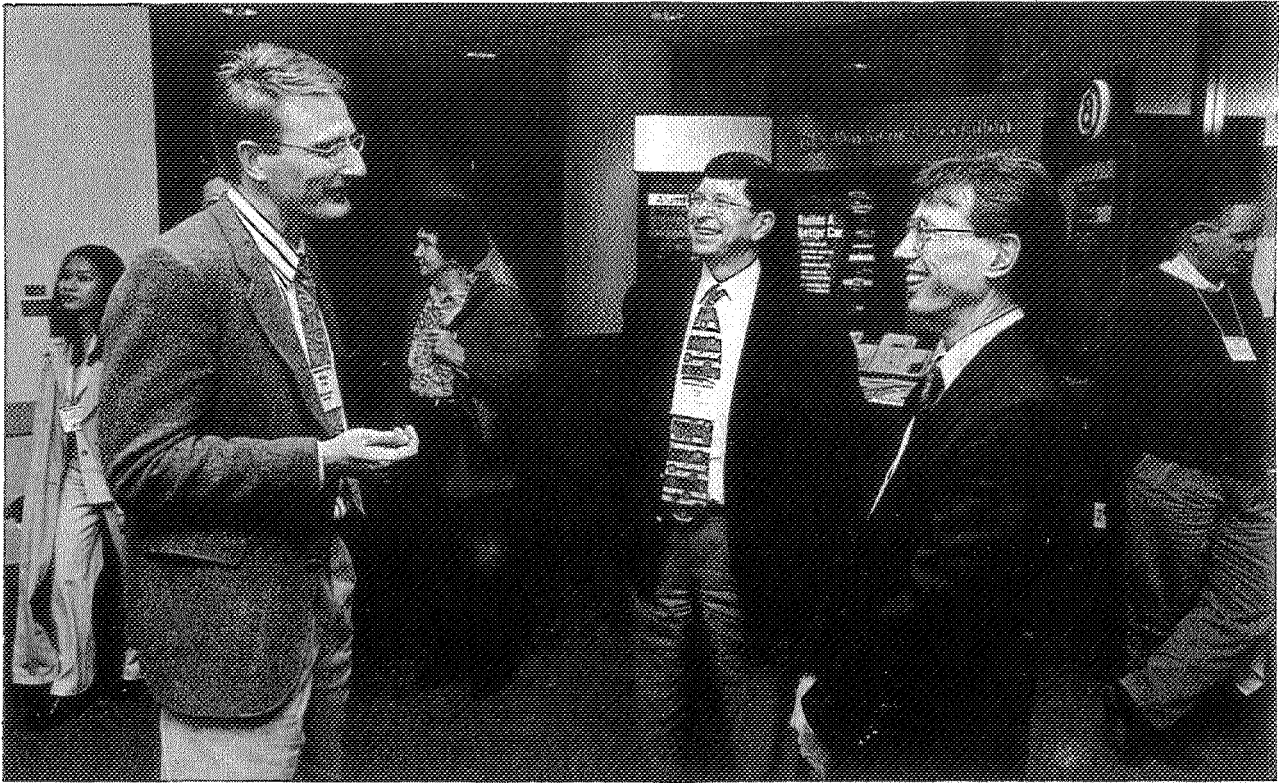


Diana LaClaire and Constance Rutherford

POSTER SESSIONS



POSTER SESSIONS AND DISPLAYS



**University of Michigan
Dearborn**

Tour of Henry Ford Estate and National Historic Landmark

Graduate Curriculum on Lightweight Automotive Materials

Demonstration on Lightweight Automotive Materials Database

Seminar

Concurrent Engineering and Rapid Prototyping

Gary Kinzel

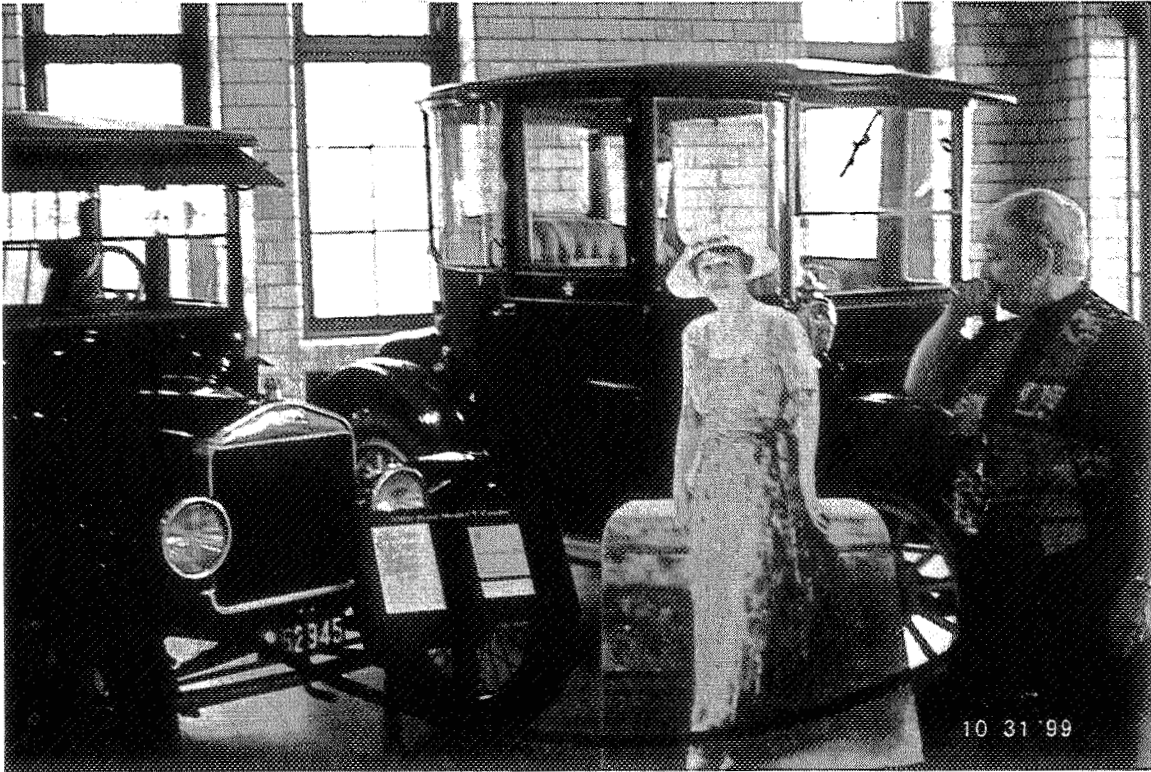
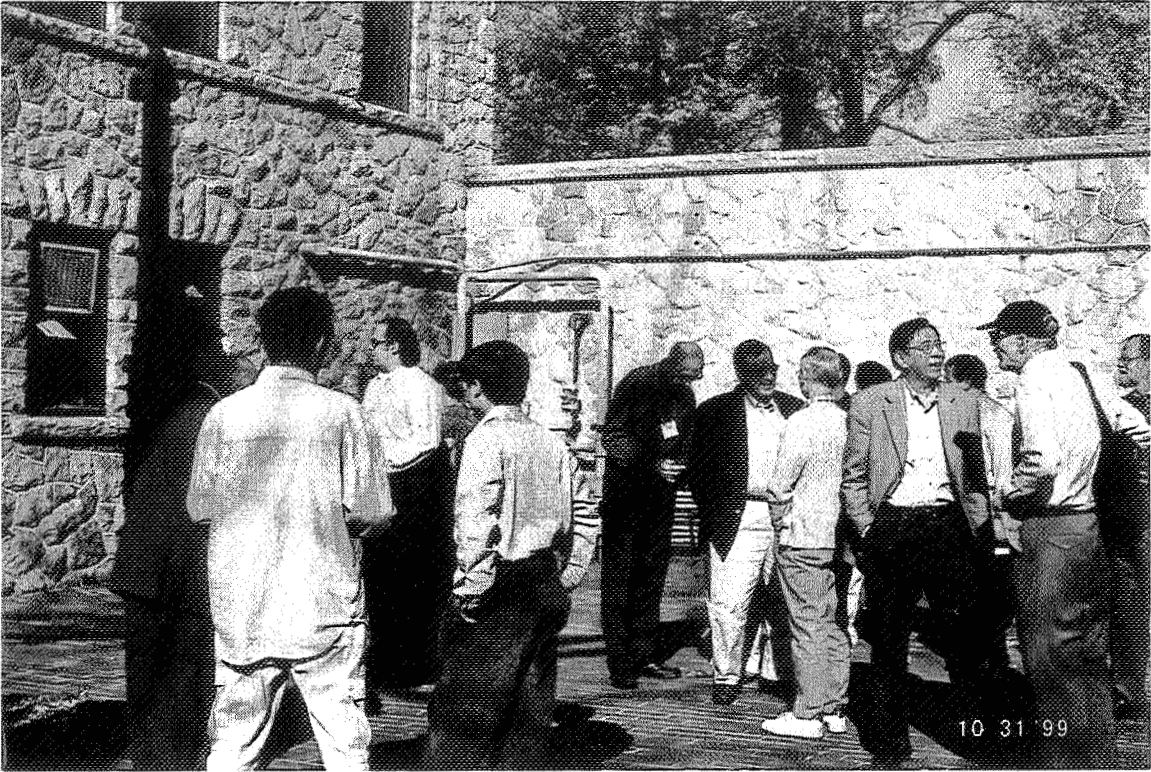
The Ohio State University

Research on Lightweight Automotive Materials and Processes

University of Michigan – Dearborn Faculty and Students

Lab Tour

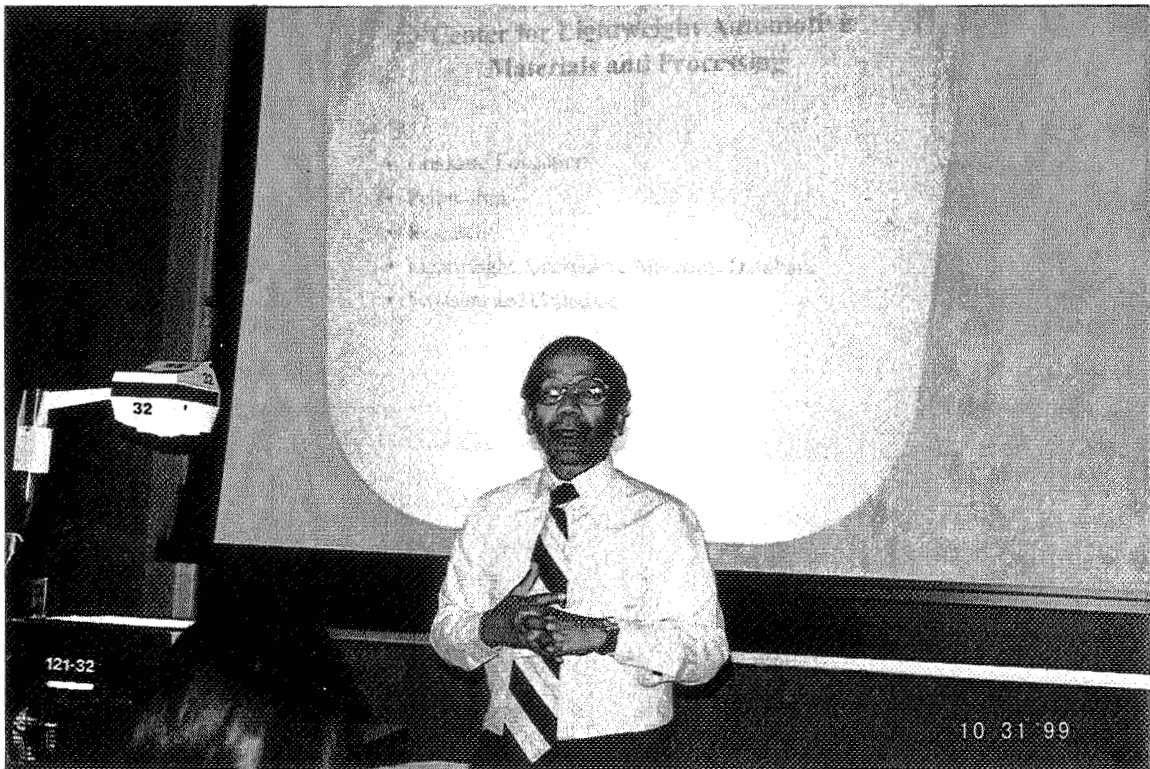
Tour of Henry Ford Estate and National Historic Landmark



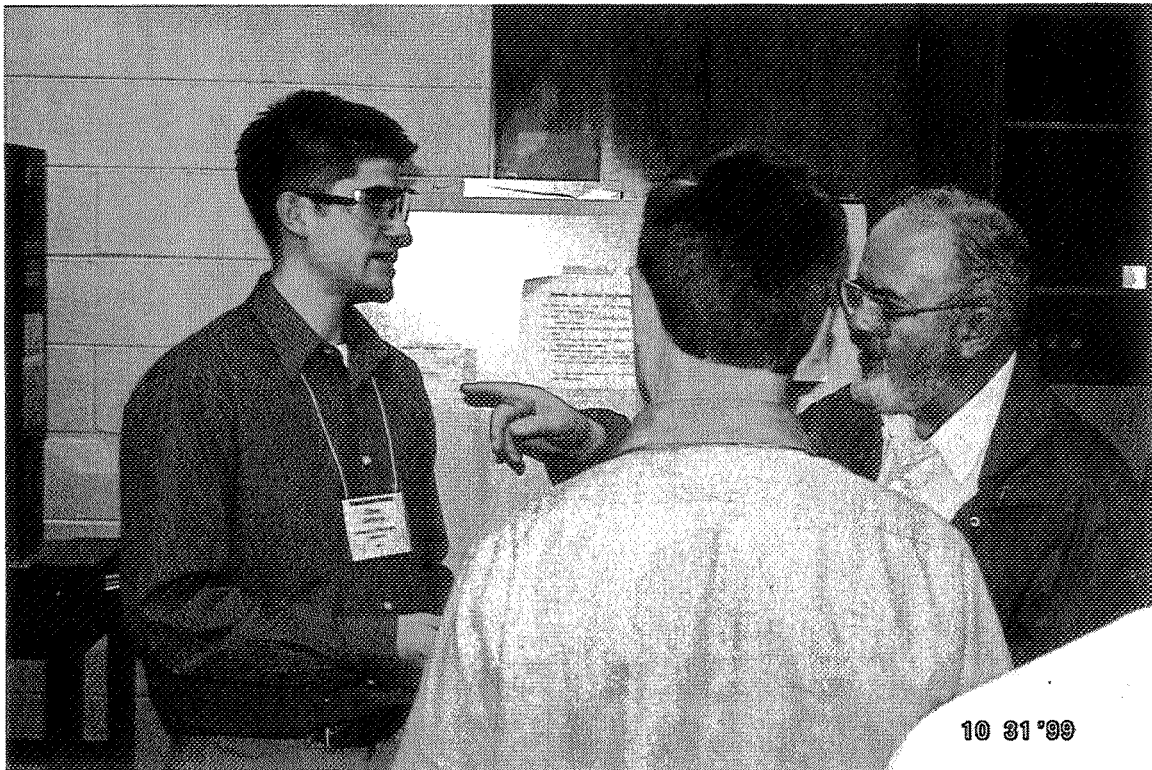
Seminar— Concurrent Engineering and Rapid Prototyping
Gary Kinzel, The Ohio State University



Research on Lightweight Automotive Materials and Processes
University of Michigan – Dearborn Faculty and Students



LAB TOUR UNIVERSITY OF MICHIGAN – DEARBORN



MINI WORKSHOPS

LIGHTSPEED TECHNOLOGIES

Web-Based Training System:
Hands-on activities with materials design,
tooling, finishing and
injection molding

GENERAL MOTORS

Demonstration of carbon fibers from Natural Gas:
formation and application and nondestructive
testing of bonded composites using Shearography
(optical technique for evaluating polymer matrix composite)

ALUMINUM ASSOCIATION

Design Practices for Automotive and Light Truck
Aluminum Bodies Computer Aided Design,
Welding and Recycling

AUTOMOTIVE COMPOSITE ALLIANCE

Interactive tours of plastics and composites
production facilities at Budd Plastics
and
Cambridge Industries

DAIMLERCHRYSLER

Tour of DaimlerChrysler production development
facilities for Prowler and Viper

AMERICAN IRON & STEEL INSTITUTE

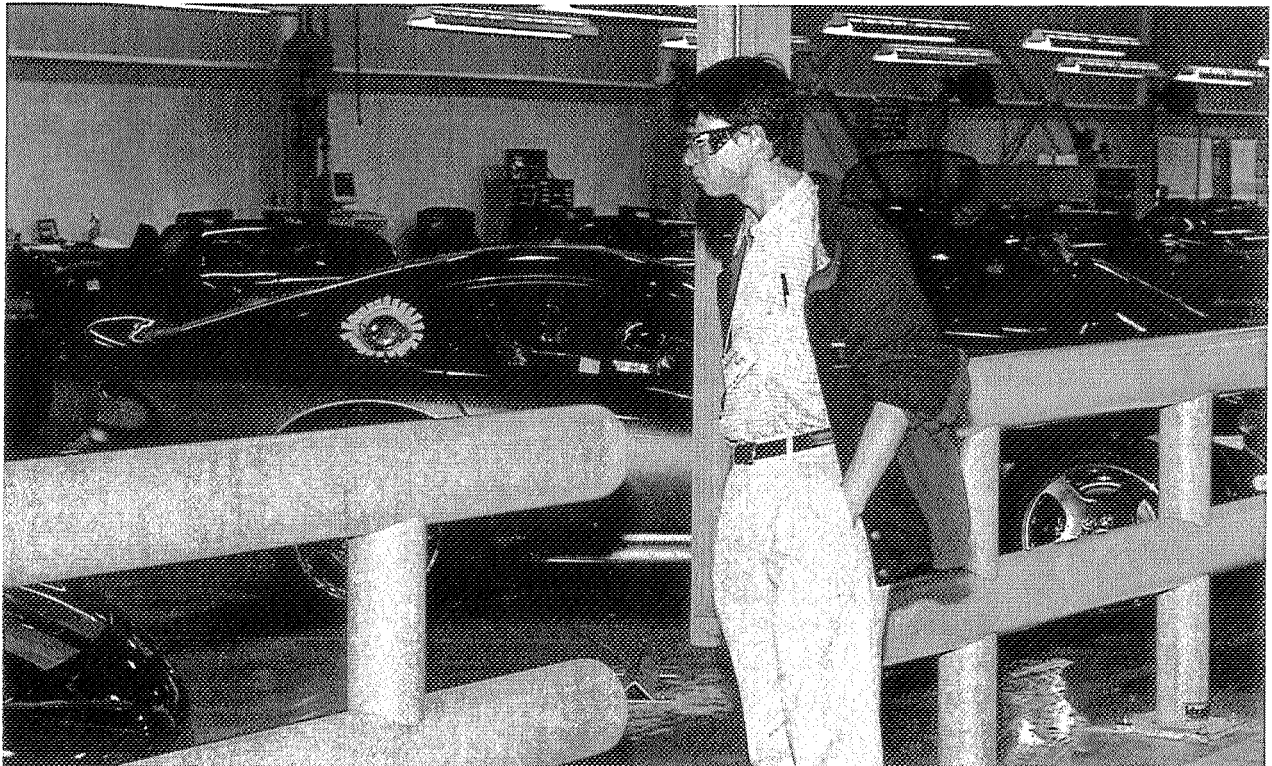
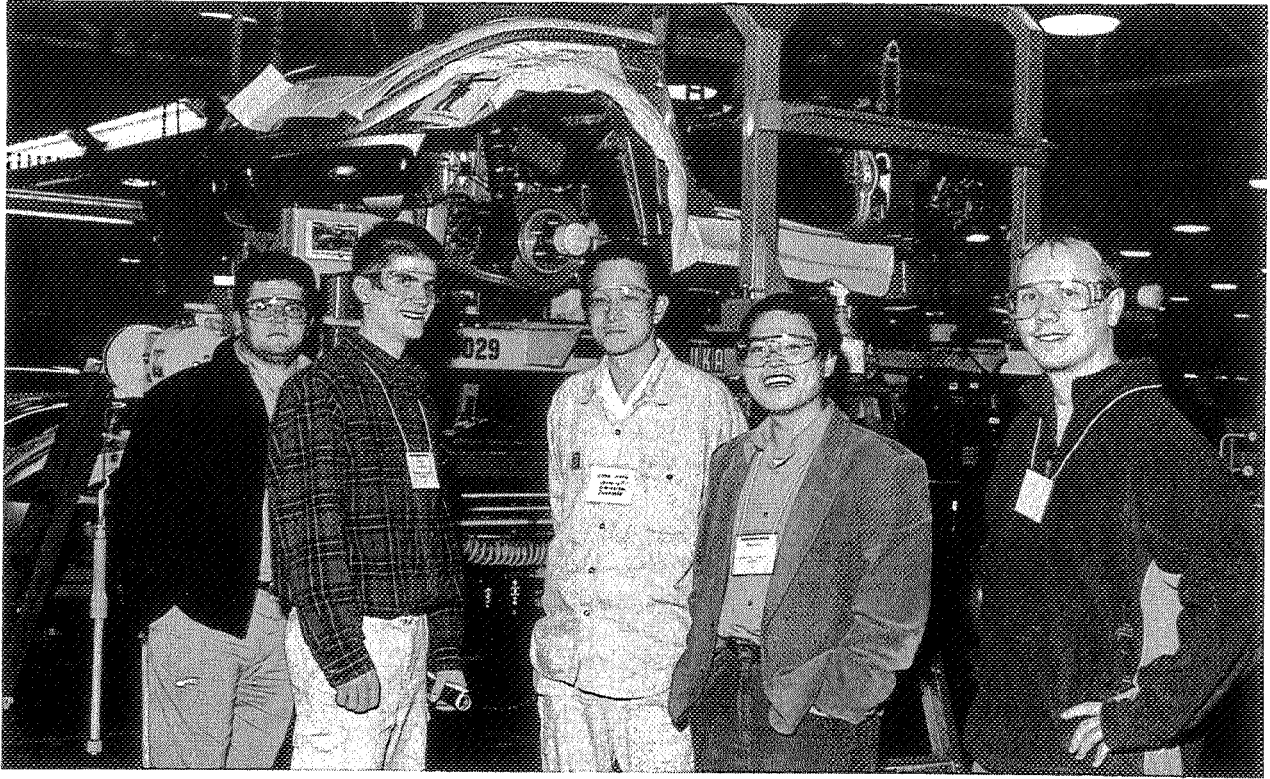
Automotive Design Systems – ULSAB Engineering:
Plan for the ultra light steel auto body and
Using CARS Computer Program: Designing
automotive components

FORD MOTOR COMPANY

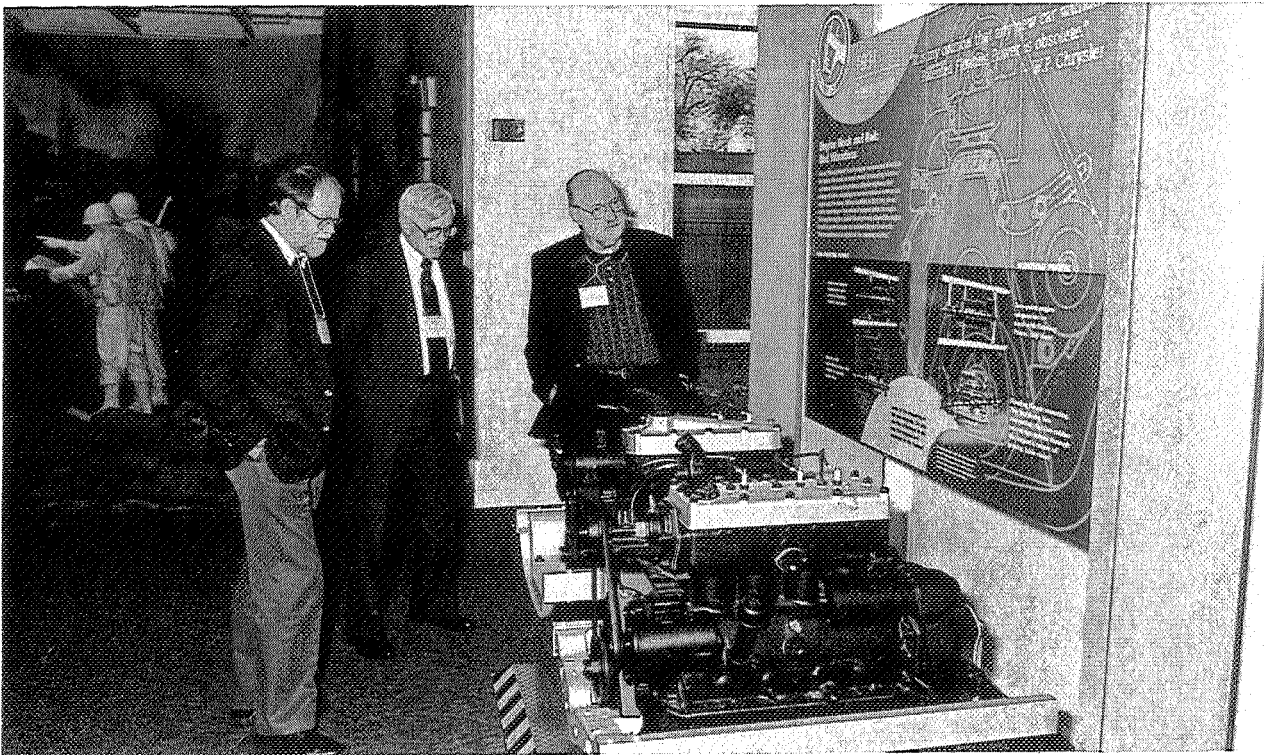
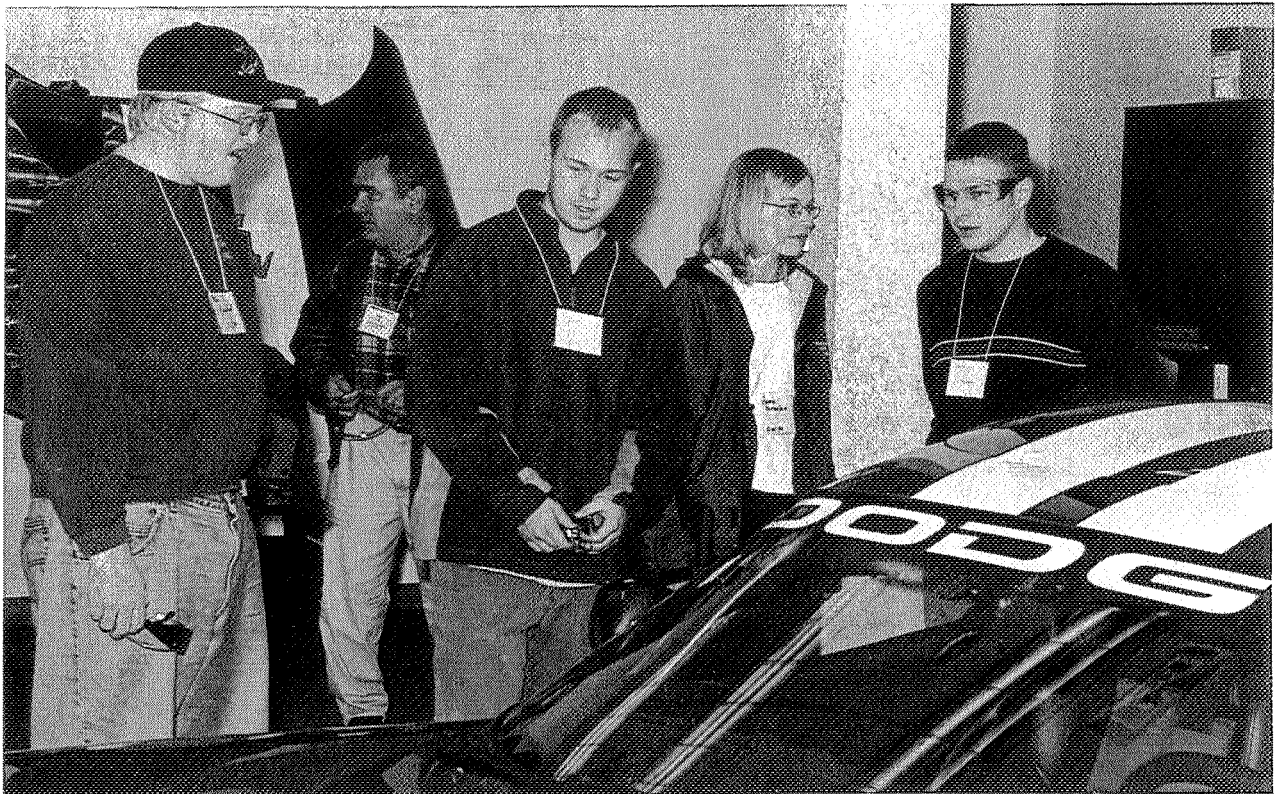
SCIENTIFIC RESEARCH LABORATORY

To include Microscopy (SEM) interesting topics on material properties;
Adhesives - different adhesives for different materials and use
of liquid nitrogen in testing;
Lightweight Materials such as SMC, RTM -
materials of future products;
Plastics - new materials and testing

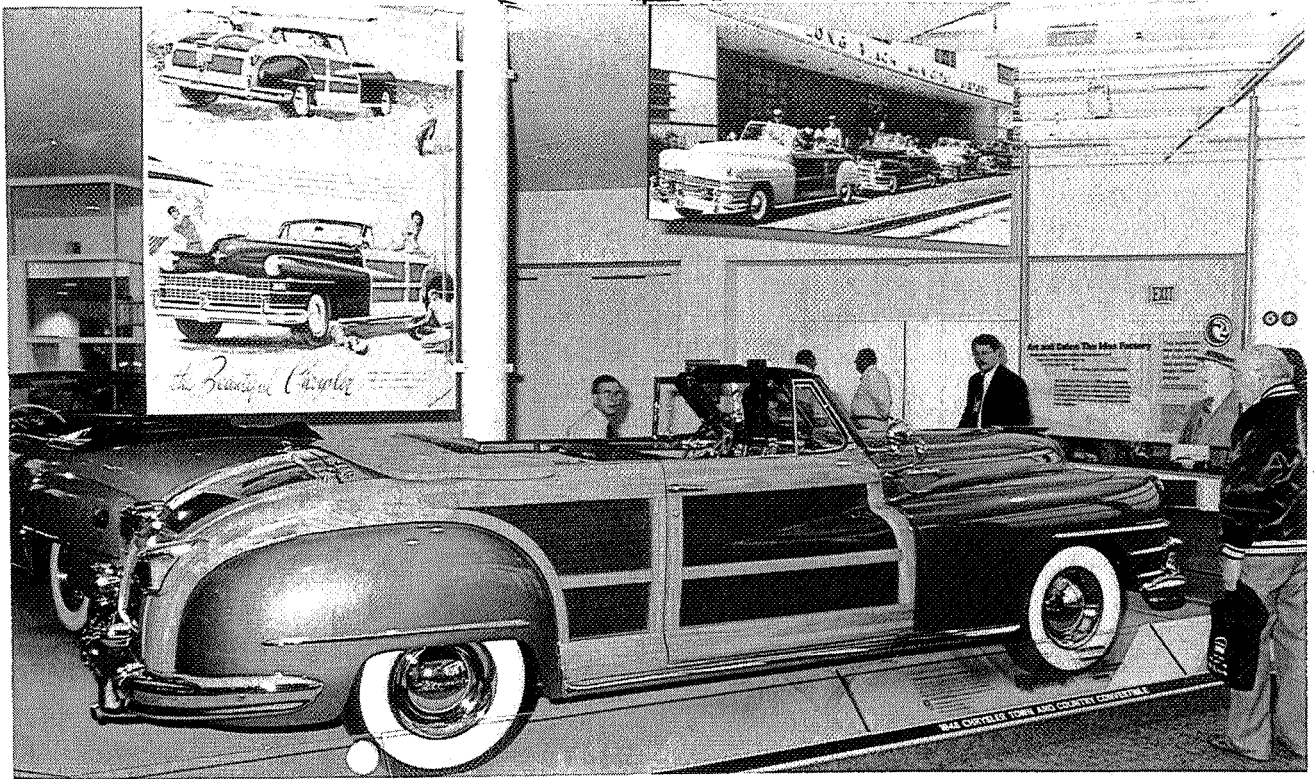
Mini Workshops



Mini-Workshops (Continued)



Mini-Workshops (Concluded)



CONTINUOUS LEARNING NETWORK (CLN)

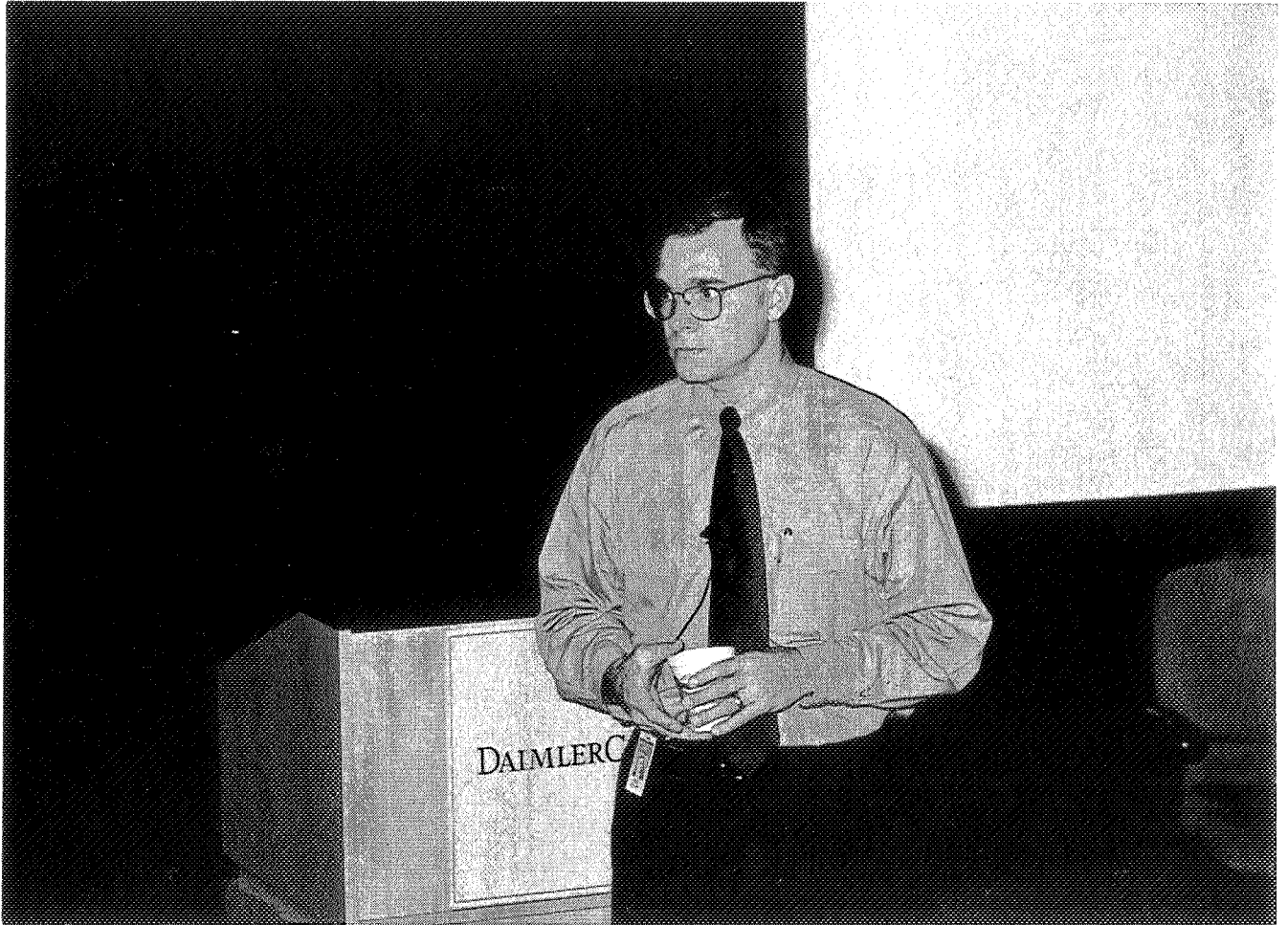
Robert Kleinhans

and

Marina Arizpe

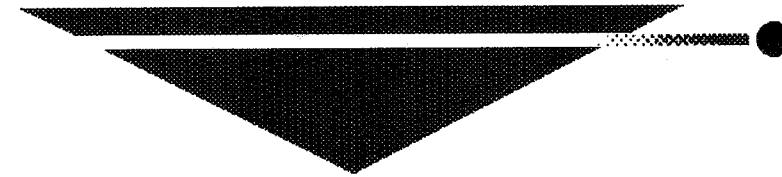
LightSpeed Technologies, Inc.
5987 Royal Country
St. Louis, Missouri 63129

Telephone 636-394-0012
e-mail rk@lightspeed-tech.com



Robert Kleinhans

L I G H T S P E E D



LigHtSpeed Technologies, Inc.

Continuous Learning Network (CLN®)

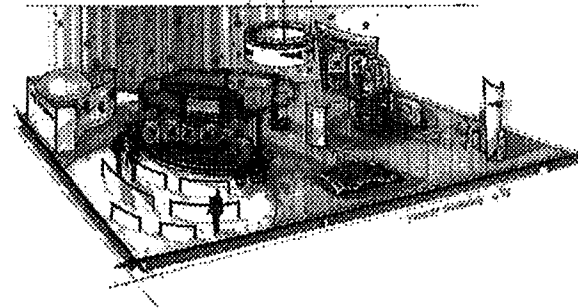
Presented By:

Marina Arizpe
Robert Kleinhans

November 2, 1999

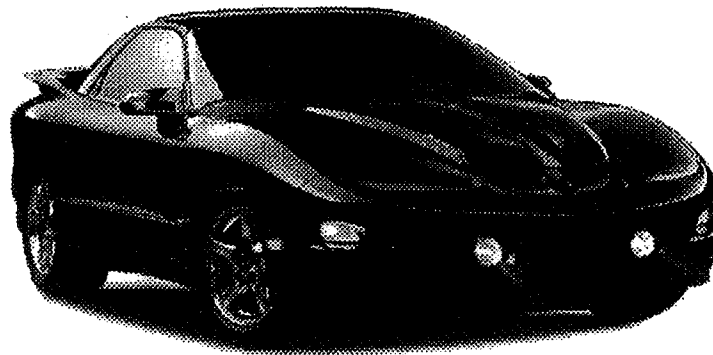
National Educator's Workshop

LightSpeed Technologies, Inc.
Continuous Learning Network (CLN®)



Today's Agenda

- * LightSpeed's Continuous Learning Network® (CLN®)
- * LightSpeed's CLN Demonstration



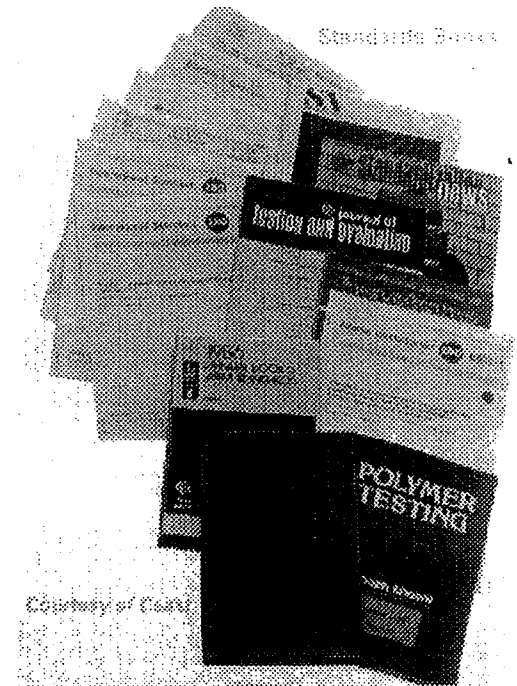
National Educator's Workshop

LIGHTSPEED



Scope of Demands on Today's Engineers

Today's Engineers must be cross-trained in numerous processes and technologies to effectively communicate with many diverse cross-functional design teams!



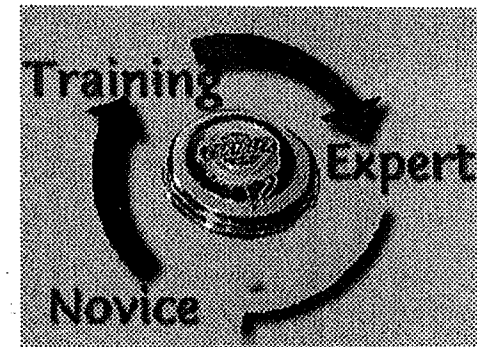
National Educator's Workshop

LIGHTSPEED

LightSpeed Technologies, Inc.
Continuous Learning Network (CLN®)

Continuous Learning Network® (CLN®)

*An online Engineering
Toolkit for “on-demand”
knowledge, utilizing
Intranet technologies for continuous
global availability over the network.*

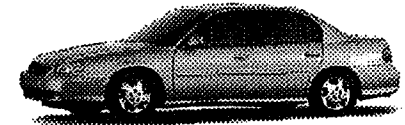


National Educator's Workshop

LIGHTSPEED

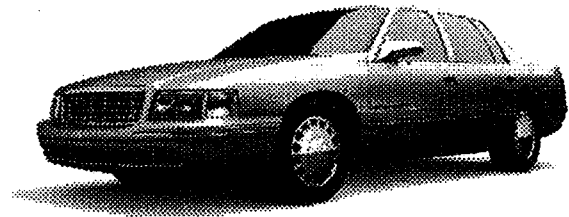
Training via the Intranet

- **Requires Netscape/Explorer Browser on PC**
- **Centrally supported architecture**
- **Knowledge shared across the Enterprise**
- **Designed for Engineers, Manufacturing, Purchasing & Management Personnel**
- **Allows for limitless number of students**
- **Education on demand -- anytime, any pace**
- **Minimizes travel costs & employee down-time**
- **CLN reflects latest materials & processes**



Reference Materials via the Intranet

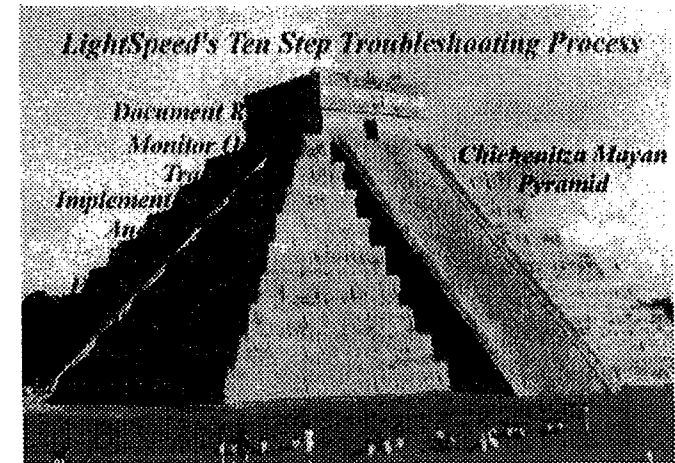
- *Technical information*
- *Design formulas*
- *Glossary*
- *Material & Equipment Suppliers*
- *Best Practices*
- *Case Studies*



**It's not just what you know that counts!
What also counts is knowing where to get the answers!**

Problem Solving Tool via the Intranet

- Design Checklist
- Design Tips
- Troubleshooting Guides
- Design Guides
- Case Studies
- Problem Solving Techniques
- Process Improvement Procedures
- Photos & Illustrations of Defects/Failures



“Find what you need, when you need it!”

CLN® for the Education Sector

- **Topics are Individually Packaged on CD's**
 - **Access CD as often as needed**
- **Consistent with Full Production Release**
- **Requires only Netscape or Microsoft Browser**
- **\$50 per Student fee for each Seminar**
- **Fees can be Bundled in with Price of Class**
- **Updates can be obtained for a Minimal Fee (\$15)**
- **Robust Training Programs**



10

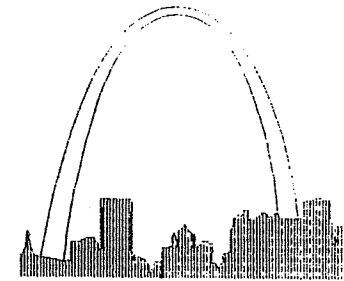
Typical Cost Factors for Engineering Seminars

	<u>Off-site Training</u>	<u>CLN® Training</u>
Seminar fees	\$650 - \$1,500 ea.	\$150 ea.
Day's Wages	\$300 - \$500 ea.	\$ - 0 -
Day's productivity Lost	Yes!	N/A
Travel Expenses	\$20 - \$1,250 ea.	\$ - 0 -
Knowledge Retrieval	20% after 30 days	Easy access to CLN!
Content Update/Refresh	N/A	Continuously!

LightSpeed Technologies, Inc.
Continuous Learning Network (CLN®)

LightSpeed Technologies, Inc.

- **Founded & Incorporated in 1991**
- **Headquartered in St. Louis, Missouri**
- **CLN is off-shoot from on-site Troubleshooting & Training Services**
- **Currently 34 Topics available**
- **14 Additional Topics under Development**



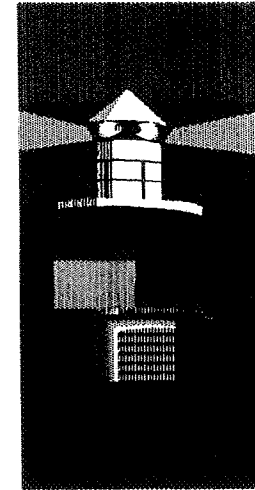
www.lightspeed-tech.com

National Educator's Workshop

LIGHTSPEED



Lighthouse Suppliers



- Lear
- Magna
- Nypro
- Textron
- TRW
- UTA

- DME
- Hobson Mould
- HS Die
- Husky
- Makino
- Melco
- Minco
- Mold Masters
- Progressive
- Snider Mold

- A. Schulman
- Allied Signal
- Bayer
- Dow
- DuPont
- GE Plastics
- Montell
- Ticona

Over 700 Suppliers

- AEC
- Barber Coleman
- Battenfeld
- Cincinatti Milacron
- Engel
- Husky
- Kistler
- Universal Dynamics
- Van Dorn/DeMaag

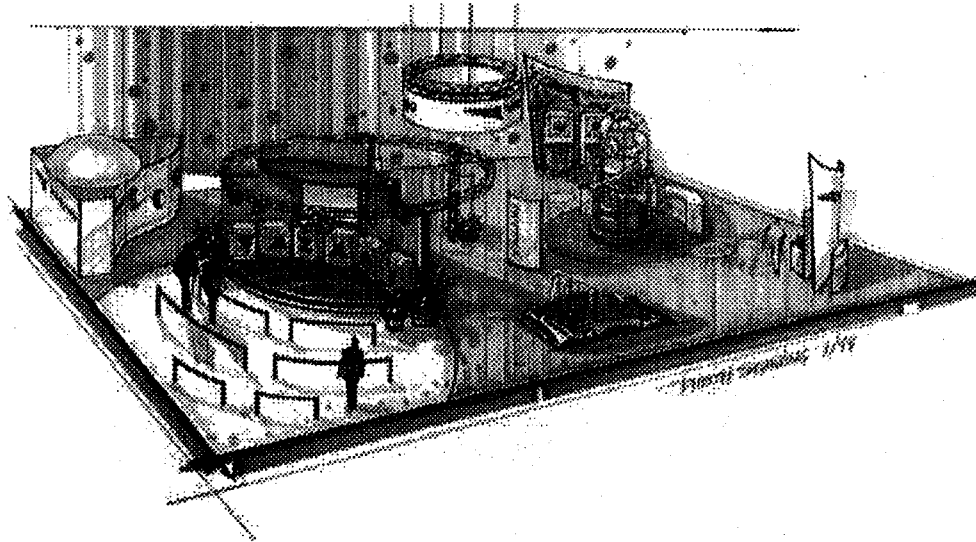
- Allied Signal
- Branson Ultrasonics
- Dow
- Dukane
- DuPont Plastics
- Lear

- Avery Dennison
- BASF
- CiMatrix
- DuPont Paints
- SDC Coatings
- Serigraph
- TampoPrint
- United Silicone

- C-Mold
- DTM
- Helisys
- MoldFlow
- NASA
- Stratasys
- Surfware
- Unigraphics
- Z-Corp

LightSpeed Technologies, Inc.
Continuous Learning Network (CLN®)

LightSpeed Technologies, Inc.
Continuous Learning Network® (CLN®)
“Demonstration”



14

National Educator's Workshop



LightSpeed Technologies, Inc.
1999 CLN® Seminar Price List

“Standard” List Price \$150/Seminar/User

Injection Molding

- Processing Essentials of Injection Molding
- Process Optimization for Injection Molding
- Injection Molding Process Troubleshooting
- Injection Molding & Testing of Colored Parts
- Cost Reduction of Plastic Parts
- Gas Assist Part & Mold Design Considerations
- Advanced Injection Molding Processes
- Multi-Color & Co-Injection Molding
- * Selection Criteria for Injection Molding Machines & Auxiliary Equip.
- * Automation of the Injection Molding Process
- * Insert Molding & Encapsulation

Plastics Engineering

- FEA, Virtual Prototyping & Validation
- Rapid Prototyping
- Rapid Tooling
- Testing & Specifications of Plastic Materials
- Weathering of Plastics & Colors
- * Noise, Vibration & Harshness (NVH) Testing

Materials

- Thermoplastic Materials
- Plastic Material Additives
- Foams: Insulating, Energy/Sound Absorbing, Structural

Plastics Design

- Design Concepts for Molded Parts
- Advanced Molded Part Design
- Assembly Designs for Plastic Parts

“Educational” Price \$50/Seminar/Student

Tooling

- Design Concepts for Injection Molds
- Mold Filling Analysis
- Selection & Preventative Maintenance for Injection Molds
- Hot Runner Systems
- Advanced Injection Mold Design

Plastics Processing

- Extrusion
- Recycling of Plastics Parts
- * Blow Molding
- * Compression Molding & Resin Transfer Molding
- * Reaction Injection Molding (RIM)

Plastics Finishing

- Plastic Parts Finishing Methods
- Paint Application & Troubleshooting
- Plastic Finishes Specifications
- Chrome Plating for Metals & Plastics
- * Off-line Painting of Interior & Exterior Parts

Quality Engineering

- Quality Engineering for Plastics Manufacturing

Metals - Materials and Processing

- Steel Materials & Processing Methods
- Aluminum Materials & Processing Methods
- * Sheet Metal Stamping
- * Corrosion

* Denotes availability within 6-months

L I G H T S P E E D



INJECTION MOLDING

CLN Seminars

Processing Essentials of Injection Molding

Description

Injection molding is a form of plastics processing that melts a thermoplastic polymer and injects the molten polymer into a mold. As the polymer cools in the mold, it takes the shape of the cavities and will retain this shape unless heat or mechanical forces change it.

The injection molding process can be described in four stages. In each stage, the temperatures and pressures, or the time, must be carefully and consistently controlled to produce high quality moldings (parts). A quality molding will reflect the tool surface and the cavity shape perfectly, will have minimum residual molding stress and will be free of flash around the edges or defects on visible surfaces. The technology that offers the most control and consistency is the reciprocating screw method. Maintaining consistency is the most important concept to employ to ensure quality and efficiency in the injection molding process.

This course provides a fundamental understanding of injection molding and is directed at engineering personnel. The course discusses the advantages and disadvantages of injection molding and reviews the equipment involved, the processing, and then finishes with Process Set-Up and Cycle Time.

Process Optimization for Injection Molding

Description

Injection molding of thermoplastic materials is a process that has many variables and must be set up carefully in order to produce high quality parts consistently. The main requirements for achieving high quality and consistency in production are:

Tooling - a well designed and well-built mold

Equipment - molding & auxiliary equipment which is capable and repeatable

Staff - trained and empowered personnel in all disciplines

Material - produced to meet or exceed the specification, with consistent quality

Use of these factors makes it possible to mold parts within a predictable range of qualities, including dimensional, performance and appearance characteristics. A system must be devised to optimize the processing conditions for production of each part. It is equally important to implement a system to maintain control over the process after it is optimized.

This seminar details the parameters of injection molding, their effect on the flow of melted thermoplastic material and molded parts and how to control these parameters. It also describes the causes of variations in part dimensions, performance, appearance and advises on methods to optimize the plastics injection molding process. As with all LightSpeed Technologies, Inc. training seminars, focus is on practical methods of maintaining quality assurance in a production environment.

Injection Molding Process Troubleshooting

Description

The term "Troubleshooting" refers to the process of solving problems. Problems within an injection molding process will usually be detected when visible defects appear on the molded parts. Other problems, such as parts sticking in the mold, or flashing of lifters or core pins, may interrupt the molding cycle, causing down time or excessive cycle times. Sometimes a problem will not surface until parts begin to fail dimensional or performance tests. In any case, once a problem becomes evident, it must be solved.

This seminar is designed to utilize an understanding of the injection molding process (learned in the Process Optimization seminar) to solve problems quickly and permanently. There are multitudes of problems that can result from the injection molding process. Included in this seminar is a Troubleshooting guide to many of the common defects found in injection molding, detailing possible causes and practical solutions.

The seminar also proposes a "Ten Step Process" to be used as a checklist for troubleshooting. This checklist is designed to help solve problems fast and effectively. A ten-step process may seem imposing, but the process is essential to ensure the success of solutions and to prevent recurrence of molding problems. Understanding that these steps are necessary to achieve and maintain process control increases their acceptance as part of an improvement plan. Taking the time to follow the ten steps will yield permanent solutions with records of the results. The steps require people in different departments to work together to solve problems, implement changes, and track progress, thus encouraging teamwork. As is usually the case, the solutions will apply to problems in other areas of the plant. The Ten-Step process will make continuous improvement a natural progression of troubleshooting. The Ten Step Process is defined within the course.

Molding & Testing of Colored Parts

Description

Color is much more than the simple description of a molded plastic part. Color is really a material science and study of color must include subjects such as light and illumination and the interactions of light with materials. When considering color it is also necessary to have an understanding of visual evaluation and instrumental color measurement. Once an understanding of color measurement is gained it then becomes possible to establish tolerances for the appearance of a molded part.

Within this seminar, the coloring of plastics and use of special effect additives is explained and recommendations for the coloring of specific polymer families are made. The use of pigments, dyes and special effects are examined along with discussion of the handling of coloring agents including dispersion and compounding. This seminar closes with an examination of molding colored materials, covering an assortment of the problems that can be encountered and the techniques used to solve them.



INJECTION MOLDING

CLN Seminars

Cost Reduction of Plastic Parts

Description

Injection molding is a manufacturing process with several stages. Simplistically defined, it involves melting a thermoplastic material in an injection molding machine and injecting it into a mold. The injection molding machine operates in two main sequences: melting the plastic pellets in the injection unit, and injecting the melt into a mold held in the clamping unit (molding the parts). If you have any involvement with manufacturing, you are aware of the many variables that effect these two "simple" stages, including a number of processes dependent on operator set-up and several functions performed by auxiliary equipment. Reducing costs of this manufacturing process can be accomplished in increments by improving each aspect one at a time.

Part design and mold design will define the rules and the playing field for those attempting to improve a process. For this reason, this seminar is recommended not only for manufacturing and maintenance personnel, but for designers and product engineers as well. Also, anyone responsible for purchasing molds and equipment will find helpful information in this seminar, since various features and options may have a significant effect on overall piece costs. Some options discussed here will have a more immediate and profound effect than others, so the relative potential for cost reduction of each option will be indicated.

Gas Assist Part/Mold Design Considerations

Description

Although the earliest 'gas assist' patents date back to the mid-1970's, it is only since the early 1990's that the technology has gained widespread industry acceptance. Gas assist is one of the most innovative, enabling molding techniques to emerge in the last decade. Proliferation of gas assist technology during that time has been rapid as designers have continued to push the limits in developing new applications. Gas assist equipment manufacturers have responded with a continuous stream of developments in hardware and control technology.

Gas assist molding is most useful when a part has thick sections or where the part is large and difficult to fill without high levels of residual stress. This process forms hollow sections in parts, reducing part weight, cycle times and stress resulting from differential shrinkage. With gas assist, larger channels can be intentionally designed into a part to facilitate flow so that the stress typically induced by the long flow paths is reduced. Injected gas creates hollow sections in each channel eliminating thick sections.

This seminar offers insight into the hardware/components used in gas assist, the polymer parameters, the gas injection parameters, the mold parameters, as well as the gas assist injection techniques and design considerations.

Advanced Injection Molding Processes

Description

The injection molding industry is continually investigating new methods and technologies to drive the continuous improvement goals of improved quality, reduced cost, and greater speed. This seminar contains discussions on two process technologies that have the potential to achieve some of these goals. Also included are several Case Studies detailing applications that these processes are being used for.

The first technology discussed in the seminar is called Multi-Live-Feed Molding, more commonly referred to as the Scorim™ process (Scorim is an acronym for Shear Controlled ORientation Injection Molding). Scorim is designed to reduce or eliminate weldlines and increase orientation by oscillating the melt in the cavity and maintaining it in a molten state long enough to achieve a better knit of the two flow fronts across the weldline.

The second technology discussed is called Pulsed Mold Temperature Control. Pulsed Mold Temperature Control is a technique designed to maximize the efficiency of the cooling stage of the molding cycle while maintaining or in many cases improving product quality. The technology works by supplying heating or cooling to the mold in intermittent bursts, or "pulses," rather than on a continuous basis.

LIGHTSPEED



PLASTICS ENGINEERING

CLN Seminars

FEA, Virtual Prototyping & Validation

Description

In today's marketplace, there are strong pressures to decrease development time and costs. Perhaps the best method to meet these demands is through the use of technological tools to reduce the need for prototype iterations and testing. By getting the design right the first time, large blocks of time, as well as capital, can be removed from the development process. These tools fall under the broad description of virtual simulation.

Virtual Simulation implies the use of the computer to simulate the design for a variety of requirements. Through the use of these tools, an engineer can develop the geometry of the individual parts, check fit and function in an assembly, generate images of the final part that reflect colors, textures, and additional cosmetic features, and determine the response to the operating environment. All of this can be completed without generating a single physical prototype, and, due to the advances in computational power, this can be done in a matter of minutes or hours, as opposed to days or longer for the creation of prototypes.

Within this seminar, each of these techniques are discussed, with examples and common tools provided. In addition, this seminar discusses the two stages in the virtual design process. The first is the creation of the engineering design, and the second is the evaluation of the design. The tools for each are reviewed in this seminar.

Rapid Prototyping

Description

The ability to create a functioning prototype, or at least a three dimensional model, has always been considered critical to the product development process. Designers need to see their concepts in a physical form to verify aesthetics, dimensions, the ability to manufacture, and some aspects of the part's functional capabilities. Based on the information about these characteristics that are demonstrated by the prototype parts, design revisions are then made to improve these characteristics. Prototypes are also useful tools for marketing new products, allowing customers to see, feel, and sometimes test out models of the designs. This reduces uneasiness about new ideas, eliminating many unknowns that may be perceived as intangible risks to customers.

Prototype parts are valuable tools used to evaluate form, fit, and function of new product designs. RP expedites build times significantly over conventional prototyping methods. These technologies have been advanced over the past 10 years to provide more dimensional accuracy, smoother surface finishes and a larger selection of materials to better simulate the physical characteristics of the intended production materials. These improvements serve to make rapid prototyping more valuable and effective at reducing lead times to market.

This seminar discusses the advantages and limitations of rapid prototyping, and highlights many rapid prototyping technologies and concept modeling technologies that are available within the industry.

Testing & Specifications of Plastic Materials

Description

There are many different methods that may be used to analyze polymeric materials, ranging from a simple test like the notched Izod to a sophisticated analysis carried out before, during and after a year long exposure under glass. These test methods all have a common purpose: insuring that a material or a part design does not fail during the product service life. In order to avoid and eliminate potential failures it is important to have an understanding of what the different test methods measure and the types of instruments that are used in the tests. Equally important is how these tests are used in writing specifications and what variables affect the test results.

This seminar discusses the variety of methods used to test the properties of different plastic materials, as well as the material standards and specifications that are used in establishing procedures to insure that a material will meet the application service requirements.

Rapid Tooling

Description

As Rapid Prototyping technologies are becoming more widely used to produce first concept articles, a whole new field is opening up in which Rapid Prototyping is being used to produce molds for multiple production of components. This seminar will discuss the various facets of this "Rapid Tooling" initiative being taken on by Rapid Prototyping vendors and users alike.

This seminar will also review advancements in existing tooling methods that accelerate the build of molds for prototype and short run production. New methods of reducing the build time for metal molds will be discussed, including using rapid prototyped parts to make mold inserts and using high performance machining technology to CNC steel or aluminum molds.

Weathering of Plastics & Colors

Description

The phenomena known as weathering, is a complex mix of environmental and material characteristics that are continually changing as a material undergoes exposure. The degrading influence of ultraviolet light, temperature and humidity cycling result in significant changes for many polymeric materials. These changes may be minimal for materials such as the acrylic polymers or very severe as in the case of epoxies. Exposure to natural sunlight and actual environmental weathering conditions require significant time periods but are the most accurate methods for judging material performance and service life. Artificial weathering methods have been developed to reduce the time required for weathering exposure and to provide a uniform means of exposing materials under controlled conditions.

This seminar provides an insight into the processes by which a material degrades under a variety of environmental conditions. The seminar concludes by discussing the methods and instruments used to analyze the effects of weathering on a variety of materials.

LIGHTSPEED

MATERIALS

CLN Seminars

Thermoplastic Materials

Description

A plastic material that can be softened and processed using heat, and that solidifies when cooled, maintaining the desired molded shape is a thermoplastic material. Thermoplastics can be re-processed repeatedly, and can be easily recycled. There are a variety of thermoplastic materials available, so it is important to carefully select the type that will best meet all of the usage and assembly requirements specific to each individual application.

Thermoplastic materials all have their own distinctive physical properties that differentiates them from other polymers. The most important differences that determine their performance in a given application include stiffness, tensile strength, elongation, resistance to heat, impact, abrasion, and chemicals.

The objectives of this seminar are to provide the users with a grasp of the basic properties and appropriate usage's associated with each thermoplastic polymer type. Thermoplastic materials are available in a wide variety and each type has characteristics that will be presented in this seminar in a concise manner. Photos of familiar applications are intended to make the aesthetic and functional capabilities of each material easy to conceptualize and identify. Brief summaries of the methods of processing thermoplastics are also discussed and exemplified by photographs of common applications produced by each processing method.

Foams: Insulating, Absorbing, Structural

Description

Polyurethane foams' greatest advantage over other polymeric materials is their broad range of finished product properties and simplistic process requirements. The physical properties, which contribute to the performance for a given application, are density, hardness, compression strength, stiffness, elongation, and resiliency. The common automotive applications are as follows: seats, headliners, carpet backing, steering wheels, instrument panels, door trim panels, package shelf, acoustical body cavity barriers/sealers, impact energy absorbers, and acoustical absorbers & decouplers.

This seminar provides insight into the components of urethane foams, the formation, structure, and physical properties of foams, as well as the applications best suited for foams.

Plastic Material Additives

Description

The additives used in modern polymer formulations have played a key role in the enormous expansion of applications for these materials. Plastics have become engineering materials, with combinations of properties and processing advantages that are duplicated by no other material.

Additives may be examined from many perspectives; the approach taken in this seminar will examine them from the main purpose for using the additive, broadly separated into processing aids, property modifiers and protective materials. Each of these is discussed briefly below. The seminar also presents information on the additives that are blended with polymers to improve the balance of properties and optimize the polymer for specific applications.

Processing aids refer to materials like lubricants or plasticizers that improve the efficiency of processing. By improving the flow of molten polymer or aiding in the release of plastic from a metal surface, they increase cycle times and make processing much easier.

Property modifiers change many of the physical properties of a polymer. Impact modifiers and flame retardants allow plastics to be specified in applications previously not suitable for synthetic materials. The protective additives such as the antioxidants and light stabilizers improve the durability and resistance to deterioration of plastics. Many materials can be adversely affected by processing conditions or exposure to heat and light. These additives prevent degradation and extend the service life of the plastic part.

The expansion of polymers into difficult service conditions like under the hood applications has placed demand on the additives manufacturers for improved products. The additives used in these materials are also under continuous development, serving to insure polymeric products continue to meet the requirements and expectation of the end user.

LIGHTSPEED

PLASTICS DESIGN

CLN Seminars

Design Concepts for Molded Parts

Description

The process of designing a plastic part may be broken down into steps, and there are many factors to consider when making decisions regarding design features. Listed in this seminar is an outline of basic design factors and a brief comment about their significance to part function, cost, and reliability. Each of these factors is discussed in this seminar, providing concise design guidelines and illustrated examples. Descriptions of pitfalls associated with common design errors demonstrate that there is more to part design than achieving the desired appearance and fitting to mating parts.

To summarize the concepts in this seminar, a short list of the most critical concepts of part design is provided. The relationships between part design features and part performance in the field are also described in detail. It is important to follow the basic rules listed in the seminar when determining part dimensions and design, in order to maximize the performance of the material and the end product.

Advanced Molded Part Design

Description

In today's world of advanced materials and manufacturing processes, plastic part design is perhaps one of the most challenging fields of design. Variables such as design, materials, finishes, molding methods, assembly and packaging require experienced input to achieve an acceptable finished part.

Unlike a puzzle where pieces can be assembled in a random fashion, the plastic part design process requires a coordinated effort to put each piece in its place in the correct sequence. Without proper planning some aspect of the process usually suffers, such as part quality, manufacturing cost, performance or service life.

This seminar provides insight into the critical roles that people play in the success of a Simultaneous Engineering Project. It also highlights molded part tolerances, insert molding, and provides much detail on structural design, including useful design formulas.

Assembly Designs for Plastic Parts

Description

In a study conducted by The Institute for Competitive Design in Rochester, Michigan, the design stage represents just 5% of the overall product cost, yet design decides 70% of the products production cost. Designing parts for assembly and manufacturing is an important task for all involved in the evolution of a product.

This seminar provides an insight into the various assembly methods commonly used in plastic product assembly and manufacturing. Once the preliminary design is completed, the engineering stage begins which consists of detailed engineering design and analysis of the part and assembly. It is during this stage where an understanding of plastic behavior and its mechanical limits are essential to preventing failure. It must be understood that classical theories of strength of materials do not always apply as plastics have a lower strength level than most metals and experience a much higher degree of deformation in the elastic region, especially under elevated temperatures. Experience and a working relationship with the material supplier are key to developing the final dimensions to achieve the optimum fit of a fastener or the proper joint design.

L I G H T S P E E D



TOOLING

CLN Seminars

Design Concepts for Injection Molds

Description

The mold is the most important component of the injection molding process. The mold consists of two halves, the stationary (injection) half, and the moving (ejection) half, which are mounted to the platens of a molding machine. The molding machine injects melted thermoplastic material into a hollow section in the center of the mold, which is called the mold cavity. There may be multiple cavities in the mold which allow for molding many parts simultaneously, and they are typically in multiples of two to balance the pressure while the mold is filling.

This seminar discusses the critical features of a mold design, including cavity number and placement, gating and feed systems, parting line locations, cooling layout, and ejection methods. Several important factors that influence these mold design decisions are also covered, including part production volumes, part function and quality requirements, and the material selected for part production.

Mold Filling Analysis

Description

Mold filling analysis is the simulation of the injection molding process, one of the methods used to make plastic parts. This tool allows the engineer the ability to predict how the mold will create the part, and if the part produced will be acceptable. This is accomplished by mathematically approximating the mold and the plastic that fills it.

A mold, in its simplest form, is composed of two halves. One half is named the core, the other the cavity. When placed together, a volume is enclosed between these two halves that defines the shape of the part to be made. This volume is then filled with molten plastic, which cools and forms the part.

While this process sounds simple, the actual process is immensely complex, and an error in any one of hundreds of variables can cause the parts that are formed to be useless.

This seminar breaks down the mold filling analysis and how it uses the computer to simulate the physics of the injection molding process. The seminar also reviews the geometry of the part, the filling of the mold, the cooling analysis, and finishes with a review of several mold filling software tools. Within this seminar, one will find many case studies with valuable examples of the use of mold filling analysis.

Select & Prevent Maint. for Injection Molds

Description

In the modern production and manufacturing environment, a buyer is given a design from the designer and is directed to solicit bids. Often the project is behind schedule and the buyer is directed to place the job as quickly as possible in order to get the part into production. This seminar will explain why careful selection and preventative maintenance for injection molds is extremely important in the current production environment.

The price of the part will be a direct function of the manufacturability of the part design. The more intelligent the design, the more reliable the product and the lower its cost. Significant savings can be achieved if, prior to soliciting quotations, the design is sent to someone who is independent of the project for a critique of the part's manufacturability. Products with overly tight tolerances, 'zero draft,' unreasonable cosmetic requirements, or specifications that the material is only marginally capable of producing, will increase the scrap rate and therefore inflate the cost of the part and increase wear on the tool.

The seminar will also discuss the importance of defining "tooling standards" so that all suppliers will bid a comparable product. It addresses pricing and maintenance concerns, mold classifications, and the materials used to make molds, as well.

LIGHTSPEED



PLASTICS PROCESSING

CLN Seminars

Recycling of Plastic Parts

Description

One of the controversial issues surrounding the implementation of recycling programs in the automotive industry is the effect on quality when reclaimed plastic materials are re-introduced back into automotive components. In general, engineers and designers are unaware of the fact that many "virgin" thermoplastic materials available on the market today already contain a percentage of recycled resins, either from off-spec material or from reclaimed post consumer products. This is not done in secrecy or against customer agreements, since agreements with customers can be fully adhered to while including recycled materials in their formulas.

For applications with specific requirements that prohibit the use of reprocessed materials, such as medical, optical, or critically functioning parts, the materials suppliers are careful not to use any recycled product. However, the majority of automotive and consumer goods applications simply require consistent melt behavior and physical properties, which can be accomplished while incorporating reprocessed materials in a controlled manner.

The key to controlling the quality of recycled material is to maintain control over each critical phase of the process. This seminar provides insight into In-Process recycling, Mechanical recycling, and reviews several applications where recycled materials are used.

Extrusion

Description

Extrusion involves the conversion of a polymer melt into a profile with a precise cross section with consistent and continuous repeatability in the machine direction. This seminar provides insight into the Extrusion process and the equipment required to complete an Extrusion process, including:

- Dryer
- Hopper
- Extruder (components:)
- Screen changer
- Static mixer (optional)
- Die
- Calibration unit
- Puller and cutoff device

Higher line speeds have translated into the need for on-line inspection of the profile as it sets in its final geometry. Both camera inspection and laser measuring have improved in speed and have come down in price to provide the capability to continually measure a number of geometric parameters of the profile. The seminar concludes with a discussion on inspection and measurement of the profile as it sets in its final geometry.

LIGHTSPEED

PLASTICS FINISHING

CLN Seminars

Plastic Parts Finishing Methods

Description

The decorating and finishing of molded plastic materials is as varied as the materials themselves. The methods used for decorating range from simple pad printing done on a manually operated machine to sophisticated graphics produced by lasers on an automated production line.

This seminar reviews the variety of methods used in the decorating and finishing of plastic parts. We discuss In-mold decorating and how using inserts or films provide a means of producing a finished part without post molding operations. The seminar reviews Transfer pad printing as a method used to print graphics or images on the exterior of molded parts.

Another example covered in the seminar is Heat stamping and how it is used to give molded parts a colored surface by using a foil or film to carry the graphic image. The images can be quite complicated in appearance, yet very simple to apply to the finished part. Other examples covered are Laser decorating of plastics, Metallizing technologies, and vacuum metallizing. Functional decorating is also discussed, referring to post molding finishing operations, such as flocking, hard-coating and part identification.

Paint Application and Troubleshooting

Description

There are many different application methods used in the automotive coatings industry. These may vary from something as simple as a hand spray gun supplied from a pressure pot to the very sophisticated robotic arms equipped with automated spray bells and flow meters. This seminar reviews many different application methods, including stationary and reciprocating applications, which may use conventional or rotary atomizers. We'll also discuss the different coatings used on External and Internal parts.

The defects that may occur in coatings are as numerous as the application technologies, each of which has inherent issues. As with troubleshooting of any manufacturing process, experience is invaluable. The ability to properly identify defects and the many factors contributing to these defects comes more easily to the experienced, however, these answers may be attained with careful diligence even for new personnel. This seminar will provide knowledge and procedures essential for successful and consistent painting processing.

Plastic Finishes Specifications

Description

The finishes used on injection molds may range from extremely high gloss for optical applications, to the sand blasted matte finish. When designing a part it is wise to consider the type of surface needed for the application due to the costly and time-consuming nature of the finishing process.

This seminar provides much information on the different finishing techniques and the specifications that accompany the type of material, application and surfaces being finished. The seminar discusses Gloss and Matte Finishes, Mold Finishing, Textured Surfaces, as well as Painted Finishes Specifications. Finally, this seminar discusses the three other methods of finishing including Metallizing, Hot Stamping, and Printing.

Chrome Plating for Metals and Plastics

Description

Electroplating is not a new science. In fact, its origins can be dated back as far as Ancient Egypt. Amazing artifacts found from that ancient civilization show electricity, generated from acid batteries, was used to electroplate less precious metal with gold. From early on, man has had the desire to alter the appearance of many objects, rendering those objects more visually appealing and or environmentally durable.

Decorative plating, in general, is typically a thin layer of metal or metals applied to a substrate to achieve a visually improved appearance. This seminar will describe the decorative chrome plating process on plastics as it relates to products used in the automotive, appliance, and plumbing industries. The seminar covers the materials selection process and how it relates to metal and plastic materials. In addition, the seminar discusses the advantages and disadvantages of Selective plating, as well as the Plating process itself.

LIGHTSPEED

QUALITY ENGINEERING

CLN Seminars

Quality Engineering, Plastics Manufacturing

Description

Quality is actually a philosophy that one must be willing to embrace in order to implement a successful quality management system. Building quality into the product within each process should be a normal mode of operation at a manufacturing facility. Brand names such as Rolls Royce automobiles, Bosch lenses, Waterford crystal, and Lladro sculptures are synonymous with excellence. This is not by chance. It is due to their staunch commitment to and insistence upon quality. In the culture of these organizations, the thought of producing or shipping products that do not conform to their standards for excellence is totally unacceptable.

The topics discussed in this seminar, variation, tolerance and quality control are designed to assist you in understanding quality management in its various incarnations. The seminar goes on to define the many benefits that could be gained from improving quality processes within an organization, not to mention improved production, customer satisfaction and reduced scrap.

To understand "Quality" one must first have an understanding of the nature of "variation". Without process or material variations, there would be no need for quality programs, inspections, and tolerances, however, variation is an inescapable eventuality. This seminar starts out by exploring this very important natural phenomenon called variation.

LIGHTSPEED



METALS – MATERIALS & PROCESSING

CLN Seminars

Steel Materials & Processing Methods

Description

In general, all solid matters that are known and used as a material of construction can be recognized as either metals or non-metals. This seminar is concerned with metals only and focuses particularly on steel, however, emphasis will be placed on other selected metals.

Metals are usually extracted from ore minerals which are mined from the earth, crushed, melted in a furnace at high temperatures and metallurgically processed before they are formed into shapes and prepared for manufacturing. They are generally classified as ferrous or non-ferrous. Ferrous metals contain iron as the major element in their composition, while the non-ferrous metals do not. Ferrous metals are heavier than some non-ferrous metals because of their density. For example, steel is three times heavier than aluminum, which is a non-ferrous metal.

The production, application and manufacturing of each kind of metal will be covered in the seminar, in a broad but limited sense. A brief discussion of properties and behavior of the metals will be submitted for a better comprehension of the subject to aid with selection and use of materials. Finally, the seminar provides major classifications of steel and discusses several application uses of steel.

LIGHTSPEED

STUDY OF MOLECULAR DEGRADATION OF POLYMERS BY INTRINSIC VISCOSITY

Ping Liu

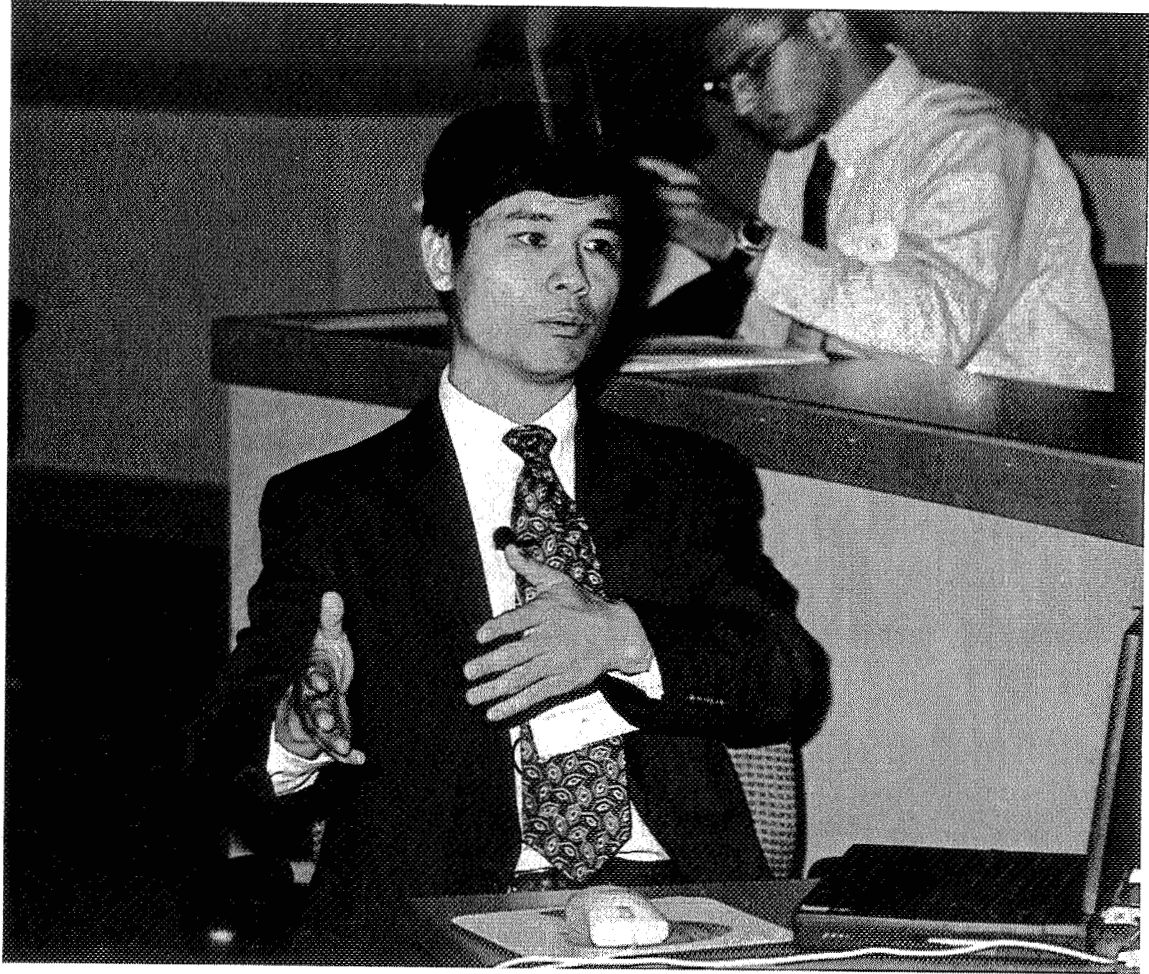
School of Technology
Eastern Illinois University
Charleston, Illinois 61920

Telephone: 217-581-6267

and

Danuta Ciesielska

Polymer Processing Laboratory
Institute of Materials Technology
Poznan University of Technology
Poland



Ping Liu

Study of Molecular Degradation of Polymers by Intrinsic Viscosity

Ping Liu
School of Technology
Eastern Illinois University
Charleston, IL 61920
USA

Danuta Ciesielska
Polymer Processing Laboratory
Institute of Materials Technology
Poznan University of Technology
Poland

Abstract:

Polymeric degradation causes deterioration in materials properties of polymers in various environments. Thus, understanding the degradation in molecular structure of polymers is of critical importance for many applications. This paper presents a method of evaluating molecular degradation of recycled polystyrene in terms of intrinsic viscosity. Fundamental relationship between molecular weight and intrinsic viscosity, as well as the experimental procedures are discussed.

Key Words: Polymers, Recycling, Degradation, Molecular Weight, Intrinsic Viscosity.

Prerequisite Knowledge: Basic knowledge of polymer degradation due to recycling. That is, polymeric chain scission occurs or polymeric chain length is reduced as a result of reprocessing. Polymeric chain length is expressed in terms of molecular weight.

Objective: To understand the experimental method of measuring molecular weight related to degradation caused by recycling or reprocessing.

Equipment and Materials:

1. Constant temperature bath
2. Glass thermometer
3. Viscometer (Ubbelohde type)
4. Solvent (Chloroform, 99.9%, ACS HPLC grade)
5. Timer or stop watch.

Safety Precautions:

1. Eye safety goggles are required.
2. Follow the Materials Safety Data Sheet (MSDS) for the chloroform in case of emergency.
3. After testing, do not pour the solution directly into any regular sink because the solvent will dissolve or severely corrode plastic plumbing parts.

Introduction:

Polymeric degradation causes deterioration in materials properties. Thus, understanding the degradation in molecular structure of polymers is of critical importance for many applications. One of the important measures for polymer structure is molecular weight, which is decreased as a result of polymer chain scission.

The molecular weight of a polymer is related to its intrinsic viscosity (limiting viscosity number) according to the following Mark-Houwink-Sakurada equation.

$$[\eta] = K(M_v)^a \quad (1)$$

where $[\eta]$ is intrinsic viscosity, which is also called limiting viscosity number. M_v is known as viscosity-average molecular weight since it is calculated from intrinsic viscosity. Empirical constants K and a are determined depending upon polymer type and experimental conditions. For example, for atactic polystyrene, K and a are 4.9×10^{-3} ml/g and 0.794, respectively.

A polymer can be dissolved into certain solvent to form a polymer solution at a specific concentration. Intrinsic viscosity $[\eta]$ of a polymer can be measured in terms of the solution viscosity. It is defined as

$$[\eta] = \lim_{c \rightarrow 0} \frac{\eta_c - \eta_o}{\eta_o c} \quad (2)$$

where η_o is solvent viscosity, η_c is the viscosity of solution, and c is the solution concentration of the polymer.

For molecular weight measurement, it is customary to employ dilute polymer solution and to use a glass viscometer. A typical glass viscometer, known as Ubbelohde viscometer, is shown in Fig. 1. The glass viscometer with solution is kept in a bath of constant temperature. Once the temperature of the solution is equilibrated at set point, the viscosity can be measured.

In measuring solution viscosity, the bulb A is filled with a solution of known concentration. Certain volume of this solution is then transferred to completely fill bulb

C between marks E and F by closing arm N and applying pressure in L. Upon simultaneously opening N and releasing pressure in L, excess liquid drains back into A. Thus, the pressure at point B at the bottom end of the capillary is atmospheric. The polymer solution is allowed to flow under gravity through the capillary. The time taken for the liquid level to move from mark F to mark E is called efflux time, which is recorded with a stopwatch. The efflux time can be measured several times in order to calculate average efflux time.

Based upon the efflux time, reduced viscosity can be calculated for a specific polymer solution. The reduced viscosity can be calculated from the following equation:

$$\eta_{red} = \frac{t_c - t_o}{t_o c} \quad (3)$$

where η_{red} is reduced viscosity, t_c is efflux time for polymer solution of specific concentration c , and t_o efflux time for solvent.

A graph of reduced viscosity versus polymer concentration can be plotted as in Fig. 2. The intrinsic viscosity $[\eta]$ can be obtained by extrapolating the straight line to zero concentration.

Experimental:

In a study of molecular degradation of polystyrene due to repeated recycling, recycled polystyrene was processed using a close-loop computer controlled injection molding machine (BOY 50M). After each cycle, the polymer was granulated into small pellets. The process was repeated up to six times to simulate repetitious recycling of the polymer.

Chloroform (99.9%, ACS HPLC grade) was used to dissolve the recycled polystyrene. The dilute solution concentrations were 0.002, 0.004, 0.006 and 0.008 g/ml. After the polymer was completely dissolved into the solvent, the solution was loaded into the glass viscometer. Then, glass viscometer was placed in the constant temperature bath, which was equilibrated at 30 °C.

Efflux time, the time for the liquid level to move from mark F to mark E in the capillary as shown in Fig. 1, was recorded for each solution and the pure solvent using a stopwatch. Ten readings on efflux time were taken for each solution. With the average efflux times for a specific solution and solvent, reduced viscosity can be calculated according to Eq. (3). Using the extrapolation shown in Fig. 2, intrinsic viscosity was obtained for the polystyrene at certain cycle. Viscosity-average molecular weight of the polymer was then computed according to Eq. (1).

Results:

Fig. 3 shows the viscosity-average molecular weight of recycled polystyrene as a function of injection molding cycles. As the number of injection molding cycles increased, the molecular weight of the recycled polystyrene was drastically reduced. For example, the molecular weight of recycled polystyrene was about 65,000 where the molecular weight was reduced to less than 10,000 after six cycles of repeated processing.

Conclusions:

1. The molecular weight of recycled polystyrene can be measured in terms of intrinsic viscosity using dilute concentration with chloroform.
2. The molecular weight of recycled polystyrene decreased drastically with increasing number of repeated processing cycles.

References:

1. A. Kumar and R. K. Gupta, Fundamentals of Polymers, The McGraw-Hill: New York (1998).
2. J. Brandrup, E. H. Immergut and E. A. Grulke (Editors), Polymer Handbook (4th ed.), J. Wiley and Son: New York (1999).
3. D. Ciesielska and P. Liu, Effect of processing on properties of recycled polystyrene, ANTEC'98, Society of Plastics Engineers (1998).
4. D. Ciesielska and P. Liu, Effects of reprocessing on structure and rheological behavior of recycled expanded polystyrene, to be published.

Acknowledgment

This work was performed at School of Technology, Eastern Illinois University with partial support from International Exchange Funds at Lumpkin College of Business and Applied Sciences, Eastern Illinois University.

Biographical Information:

Dr. Ping Liu obtained his B.S. degree in mechanical engineering from Nanchang University, China in 1982. He earned an M. S. degree in materials science and engineering from Zhejiang University, China in 1984 and completed a Ph.D. degree in mechanical engineering from Iowa State University in 1991. His major research interests rest on polymer recycling, polymer rheology, biomedical polymers, materials tribology, electrical sliding, corrosion, and failure analysis. He is a registered professional engineer (PE) in the State of Illinois, a certified quality engineer

(CQE) by American Society for Quality and a certified senior industrial technologist (CSIT) by National Association of Industrial Technology. He is currently a full professor at Eastern Illinois University, Charleston, IL, USA.

Dr. Danuta Ciesielska works in the Polymer Processing Laboratory of Poznan University of Technology in Poland. She earned a Doctor of Engineering degree in 1980 from Technical University of Poznan. Her specialty is the use of microscopic techniques for observation and study of the structure of interfacial surfaces as well as the examination of the rheological properties of polymers.

During Spring 1997 and again in Spring 1999, Dr. Danuta Ciesielska was invited to work at the Polymer Laboratories of Eastern Illinois University in Charleston, USA. Her research works were focused on the structure and properties of recycled polystyrene and its blends.

Dr. Danuta Ciesielska has received awards several times by the Rector of Technical University in Poznan for researches and activity. Dr. Danuta Ciesielska has authored 22 domestic publications, four international papers, and lectured at 18 scientific conferences.

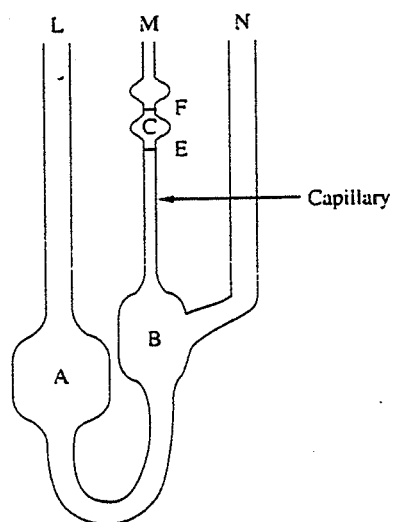


Figure 1. An ubbelhode viscometer.

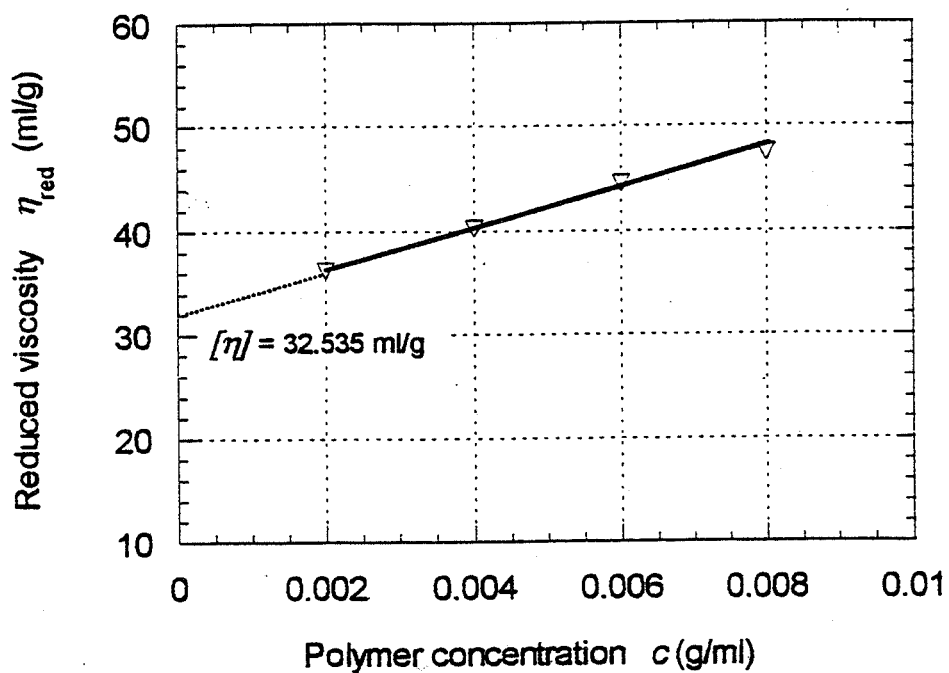


Figure 2. Typical plot of reduced solution viscosity of polystyrene as a function of concentration.

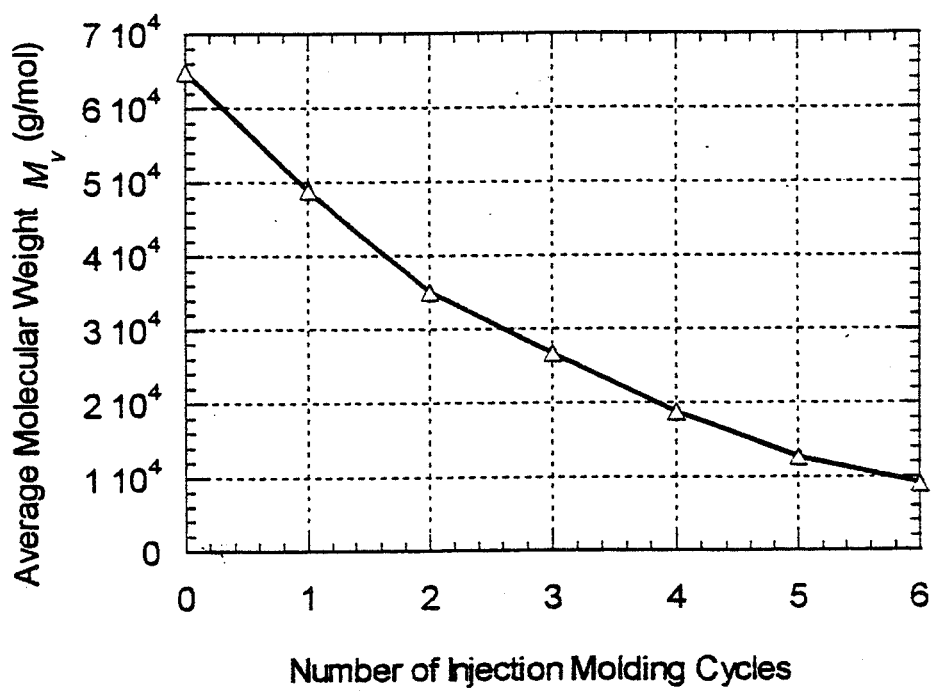


Figure 3. Variation of viscosity-average molecular weight of recycled polystyrene with number of injection molding cycles.

Dr. Danuta Ciesielska works in the Polymer Processing Laboratory of Poznan University of Technology in Poland. She earned a Doctor of Engineering degree in 1980 from Technical University of Poznan. Her specialty is the use of microscopic techniques for observation and study of the structure of interfacial surfaces as well as the examination of the rheological properties of polymers.

During Spring 1997 and again in Spring 1999, Dr. Danuta Ciesielska was invited to work at the Polymer Laboratories of Eastern Illinois University in Charleston, USA. Her research works were focused on the structure and properties of recycled polystyrene and its blends.

Dr. Danuta Ciesielska has received awards several times by the Rector of Technical University in Poznan for researches and activity. Dr. Danuta Ciesielska has authored 22 domestic publications, four international papers, and lectured at 18 scientific conferences.

Acknowledgment

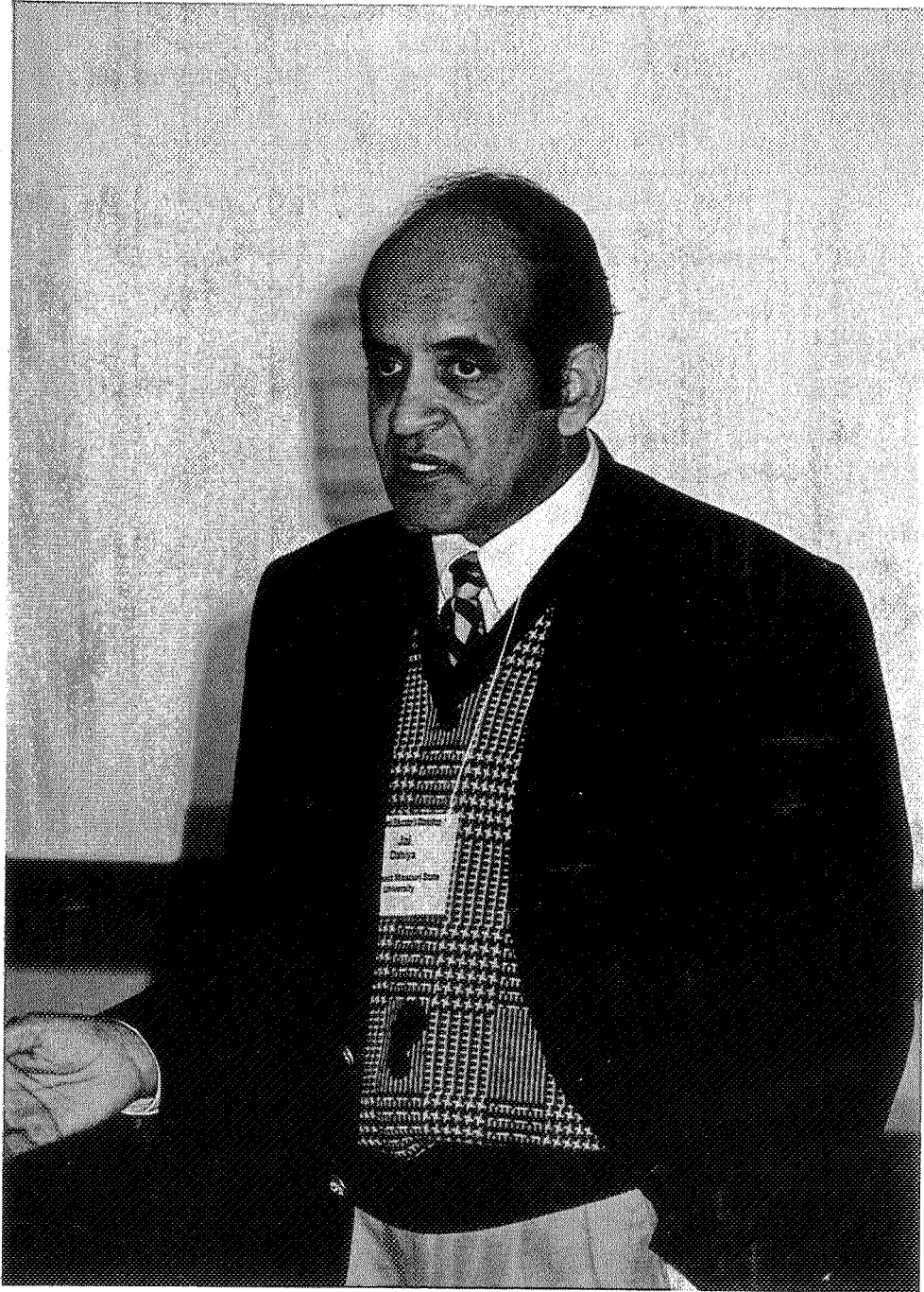
This work was performed at School of Technology, Eastern Illinois University with partial support from International Exchange Funds at Lumpkin College of Business and Applied Sciences, Eastern Illinois University.

MICROWAVE DIELECTRIC RESPONSE OF WATER AS A FUNCTION OF FREQUENCY

J. N. Dahiya

Physics Department
Southeast Missouri State University
One University Plaza
MS 6600
Cape Girardeau, Missouri 63701

Telephone: 573-651-2390
e-mail dahiya@physics.semo.edu



Jai Dahiya

MICROWAVE DIELECTRIC RESPONSE OF WATER AS A FUNCTION OF FREQUENCY

J.N. Dahiya
Physics Department
Southeast Missouri State University
One University Plaza, MS 6600
Cape Girardeau, MO 63701
dahiya@physics.semo.edu

Keywords

Microwave Resonant Cavity, Dielectric Response, Slater's Equations, Relaxation Time

Objectives

1. Set up a Microwave Spectrometer for temperature dependent studies.
2. Study dielectric relaxation in a sample of dionized distilled water as a function of temperature and frequencies.
3. Use computer interface for temperature dependent studies.
4. From the frequency dependent studies of water draw conclusions regarding the resonance behavior.

Introduction

In general materials expand when heated but there are a few exceptions and water is one of them. At 4°C the volume vs temperature curve shows a minima indicating a maximum density value for that temperature. It is very interesting to study the microwave dielectric response of water near this temperature of 4°C. The anomalous dielectric dispersion of water at various frequencies has been widely investigated [1-6]. There is no doubt in the main qualitative features of the phenomenon, but there are wide divergencies in the quantitative analysis of the problem. The fundamental importance of this problem lies in the theoretical analysis of the structure of water that is very significant in terms of its technical and biological interest. A detailed knowledge of the dielectric behavior of water at various microwave frequencies is needed for a partial solution of this problem.

A cylindrical resonant cavity in TE₀₁₁ mode is used in a microwave spectrometer to do the dielectric analysis of water. The dielectric relaxation studies of water are performed as a function of temperature at three different frequencies of 10.2, 10.6, and 11.4 GHz. A sensitive thermal bath is used to vary the temperature of the sample under study very precisely. A dramatic change in the dielectric response is seen near 4°C, the temperature at which density of

water is maximum rather than the phase transition temperature of 0°C. Slater's perturbation equations are used to calculate the real and imaginary parts of the dielectric constant. The activation energy of this molecule is calculated using Eyring's rate equations and Debye's theory of polar molecules is used to calculate the relaxation times at different frequencies used in this experiment.

Theory, Experiment and Results

According to Debye's theory of polar molecules [7] in terms of a single relaxation time, the dielectric permittivities are related to the relaxation time as shown below.

$$\varepsilon = \varepsilon_o + \frac{\varepsilon_s - \varepsilon_o}{1 + j\omega\tau} \quad (1)$$

where ε is the complex permittivity (dielectric constant) at angular frequency ω , ε_s is the static dielectric constant, ε_o is the contribution to the dielectric constant that is due to the atomic and electronic polarization and is independent of ω . In terms of the optical constants, equation (1) can be written as follows:

$$n^2 - k^2 = \varepsilon' = \varepsilon_o + \frac{\varepsilon_s - \varepsilon_o}{1 + \omega^2\tau^2} \quad (2)$$

or in terms of λ :

$$n^2 - k^2 = \varepsilon' = \varepsilon_o + \frac{\varepsilon_s - \varepsilon_o}{[1 + \lambda_s / \lambda]^2} \quad (3)$$

and

$$2nk = \varepsilon'' = \frac{(\varepsilon_s - \varepsilon_o)\omega\tau}{1 + \omega^2\tau^2} \quad (4)$$

or Equation (4) expressed in terms of λ :

$$2nk = \varepsilon'' = \frac{(\varepsilon_s - \varepsilon_o)\lambda_s / \lambda}{1 + [\lambda_s / \lambda]^2} \quad (5)$$

Where λ is the wavelength corresponding to a frequency ω and λ_s corresponds to $1/\tau$, n is the real part of the index of refraction, k is the absorption coefficient, ε' and ε'' are the real and imaginary parts of the complex dielectric constant.

Equations 1-5 indicate a drop in the dielectric constant from its value at low frequencies ε_s to optical frequency value ε_o . This drop in the dielectric constant is accompanied by a single broad absorption band near a characteristic wavelength λ .

The real and imaginary parts of the dielectric constant are related to the frequency shifts and Q-changes of a microwave signal through Slater's perturbation equations [8] shown below.

$$\frac{\Delta f}{f_0} = \frac{\epsilon' - 1}{2} \frac{\int \vec{E}_s \cdot \vec{E} dv}{\int \vec{E} \cdot \vec{E}_a dV} \quad (6)$$

and

$$\Delta \left(\frac{1}{Q} \right) = \epsilon'' \frac{\int \vec{E}_s \cdot \vec{E} dv}{\int \vec{E} \cdot \vec{E}_a dV} \quad (7)$$

where Δf and $\Delta(1/Q)$ are the frequency shifts and Q-changes of the resonant cavity, ϵ' and ϵ'' are the real and imaginary parts of the complex permittivity (dielectric constant), E_s , E and E_a are the fields of the sample, the unperturbed cavity and the field as applied to the cavity respectively, and v is the volume of the sample with V being the volume of the cavity.

A sample of dionized distilled water is placed in the resonant cavity through a capillary tube. The resonant cavity is used as a probe in a microwave spectrometer operating in the x-band of frequencies between 8.0 and 12.4 GHz. A condensed block diagram representation of the spectrometer is shown in Figure 1. The details of the spectrometer have been discussed elsewhere [4].

As the sample is inserted in the cavity a perturbation of electric and magnetic field takes place. For TE₀₁₁ mode the perturbations are mainly of the electric field. The perturbations of the electric field translate into a shift in frequency and Q-change of the signal. The frequency shifts and Q-changes are measured as a function of temperature. The real and imaginary parts of the dielectric constant are calculated using Slater's equations 6 and 7.

Figures 2-7 represent a response in the dielectric behavior of a sample of dionized distilled water at 10.2, 10.6, and 11.4 GHz. There seems to be a dramatic change in the real and imaginary parts of the dielectric constant near 4°C.

The results of this experiment indicate an extension of this study to higher frequencies. It will be very interesting to determine resonance behavior from frequency dependent dielectric studies of water.

References

1. Rusche, E.W. and W.B. Good, "Search for Discontinuities in the Temperature Dependence of the Dielectric Constant of Pure Water from -5° to $+25^{\circ}\text{C}$," J. Chem. Phys., Vol. 45, Number 12, 1966, p. 4667.
2. Kay, Robert L., G.A. Vidulich and Krishnahadi S. Pribadi, "A Reinvestigation of the Dielectric Constant of Water and its Temperature Coefficient," J. Phys. Chem., Vol. 73, Number 2, 1969, p. 445.
3. Roberts, J. and F. Wang, "Dielectric Relaxation in Water Over the Frequency Range $13 \leq f \leq 18$ GHz using a Resonant Microwave Cavity Operating in the TM_{010} Mode," J. Of Microwave Power and Electromagnetic Energy, Vol. 28, No. 4, 1993, p. 196.
4. Dahiya, J.N., S.K. Jani and J.A. Roberts, "Phase Transition Studies in Polar and Non-Polar Liquid at Microwave Frequencies," J. Chem. Phys. 74(6), 1981, p. 3609.
5. Johri, G.K. and J.A. Roberts, "Study of the Dielectric Response of Water using a Resonant Microwave Cavity as a Probe," J. Phys. Chem., 1994, p. 7386.
6. Hong, K.H. and J.A. Roberts, "Microwave properties of Liquids and Solids using a Resonant Microwave Cavity as a Probe," J. Appl. Phys., 1974, p. 2452.
7. Debye, P., "Polar Molecules," Chemical Catalog, NY, Chap. V, 1929.
8. Slater, J.C., "The Thory of Resonant Cavities," Microwave Electronics, Dover Publications, New York, 1969.

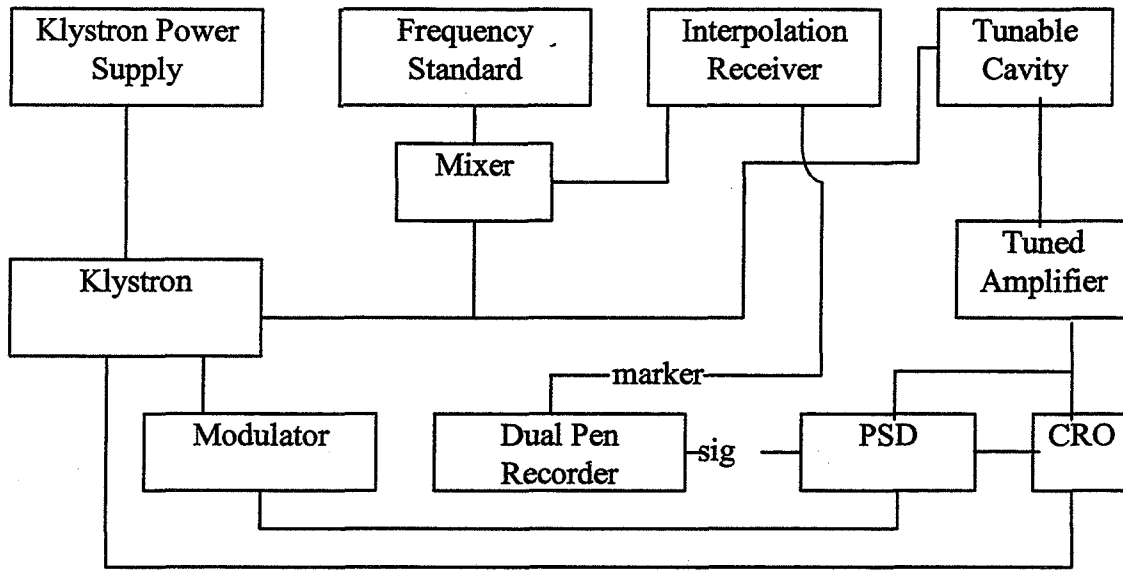


Figure 1. Condensed block diagram of the microwave spectrometer used in this experiment.

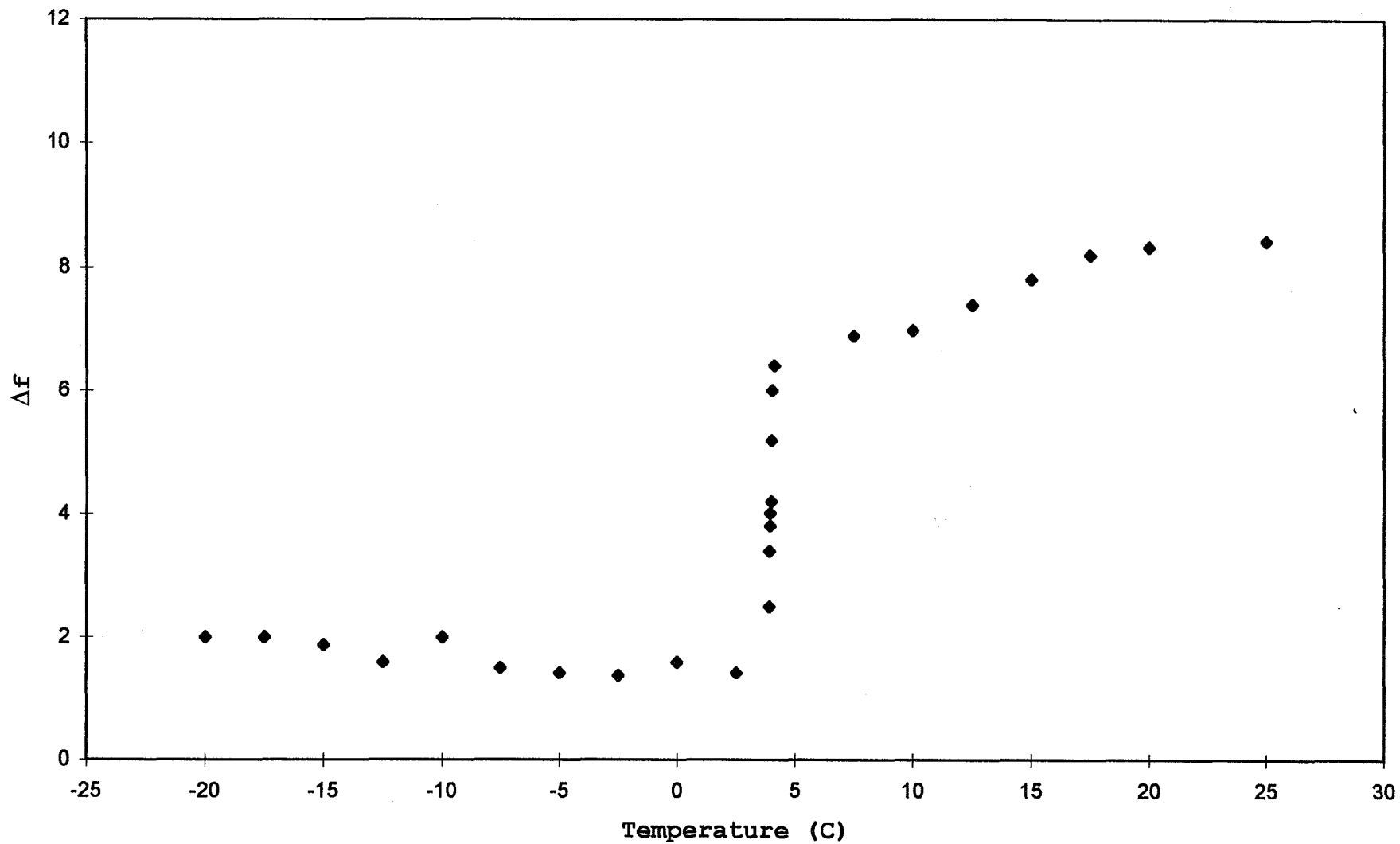


Figure 2. Change in frequency as a function of temperature for a sample of water at a resonant frequency of 10.2 GHz.

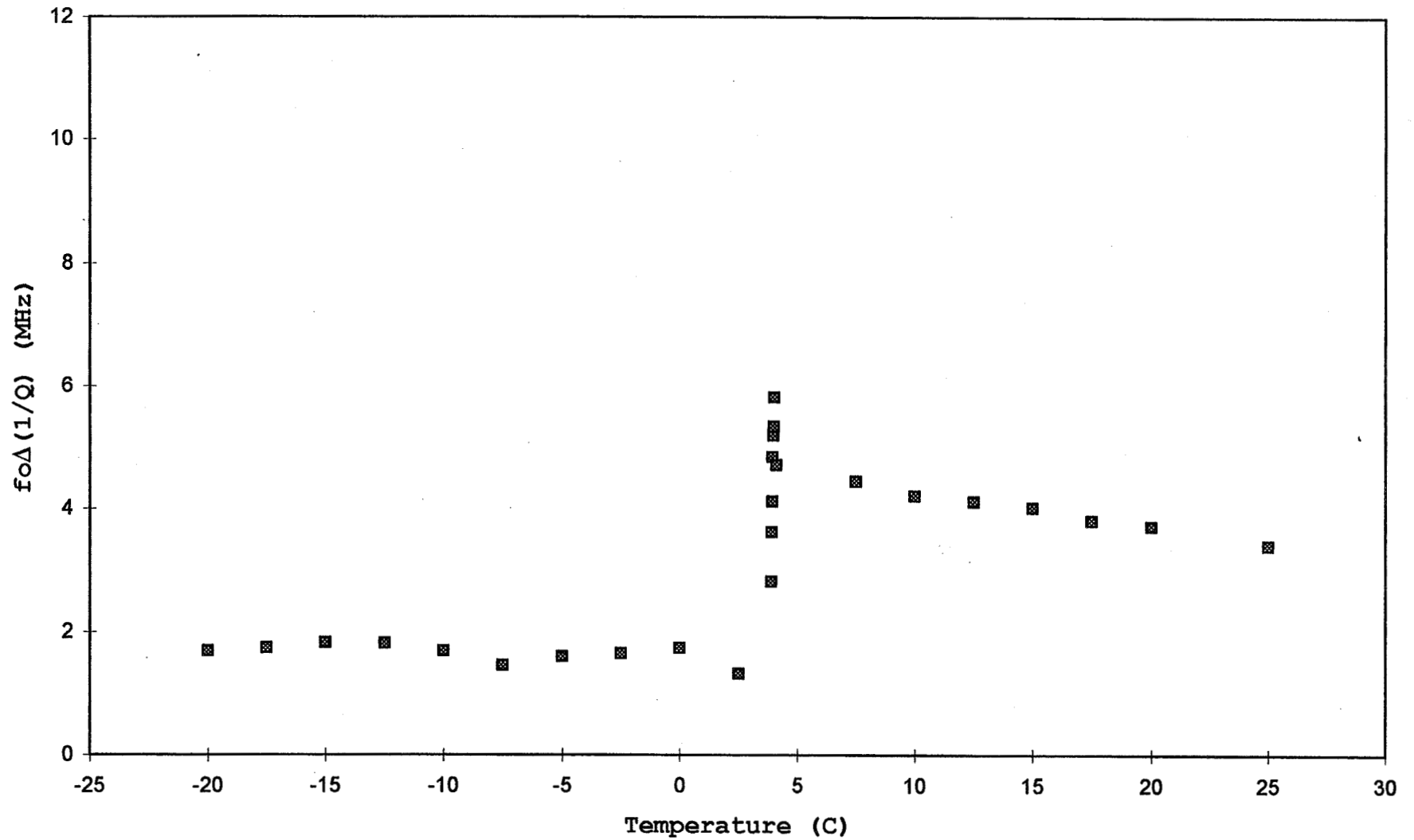


Figure 3. Change in $1/Q$ as a function of temperature for a sample of water at a resonant frequency of 10.2 GHz.

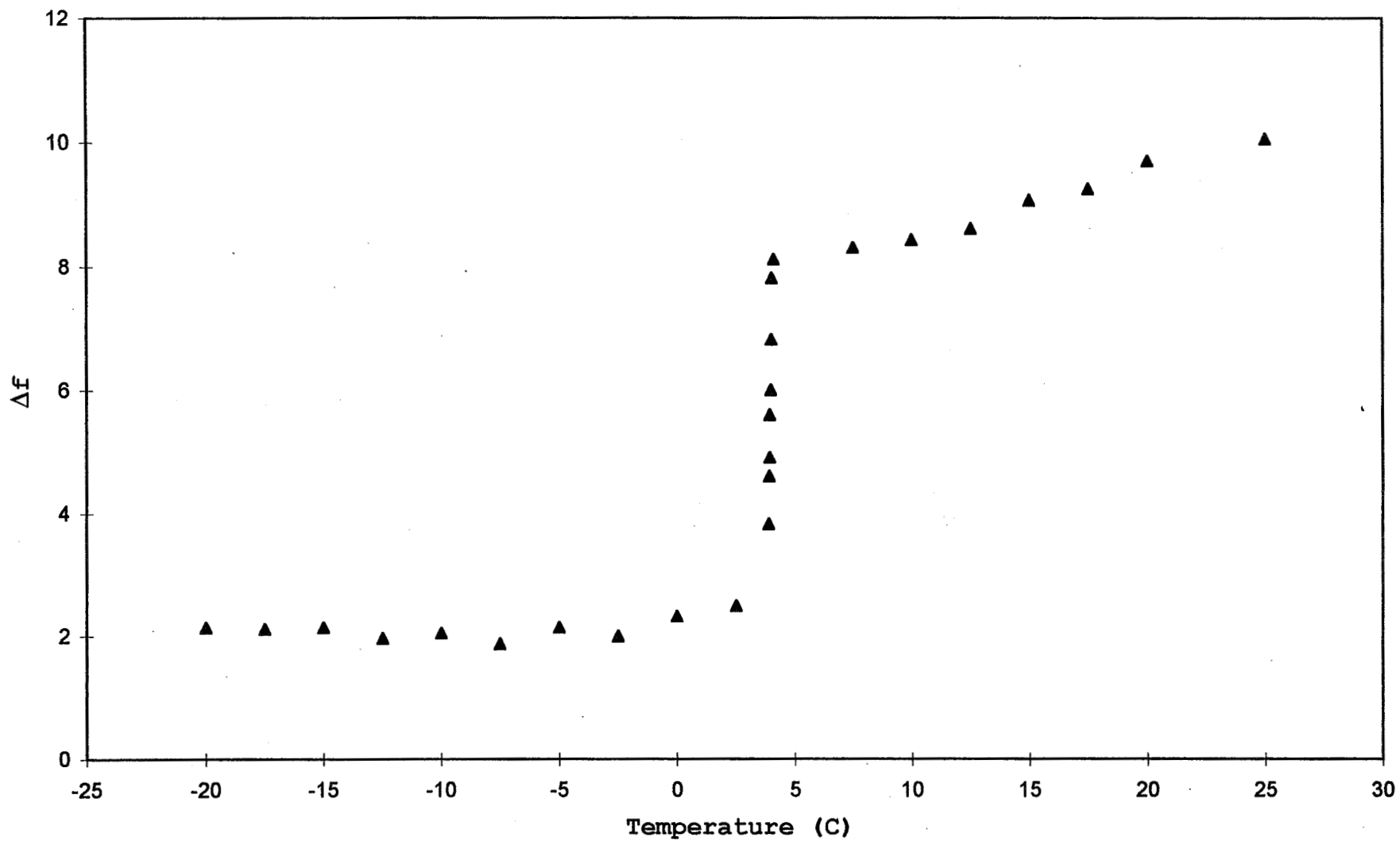


Figure 4. Change in frequency as a function of temperature for a sample of water at a resonant frequency of 10.6 GHz.

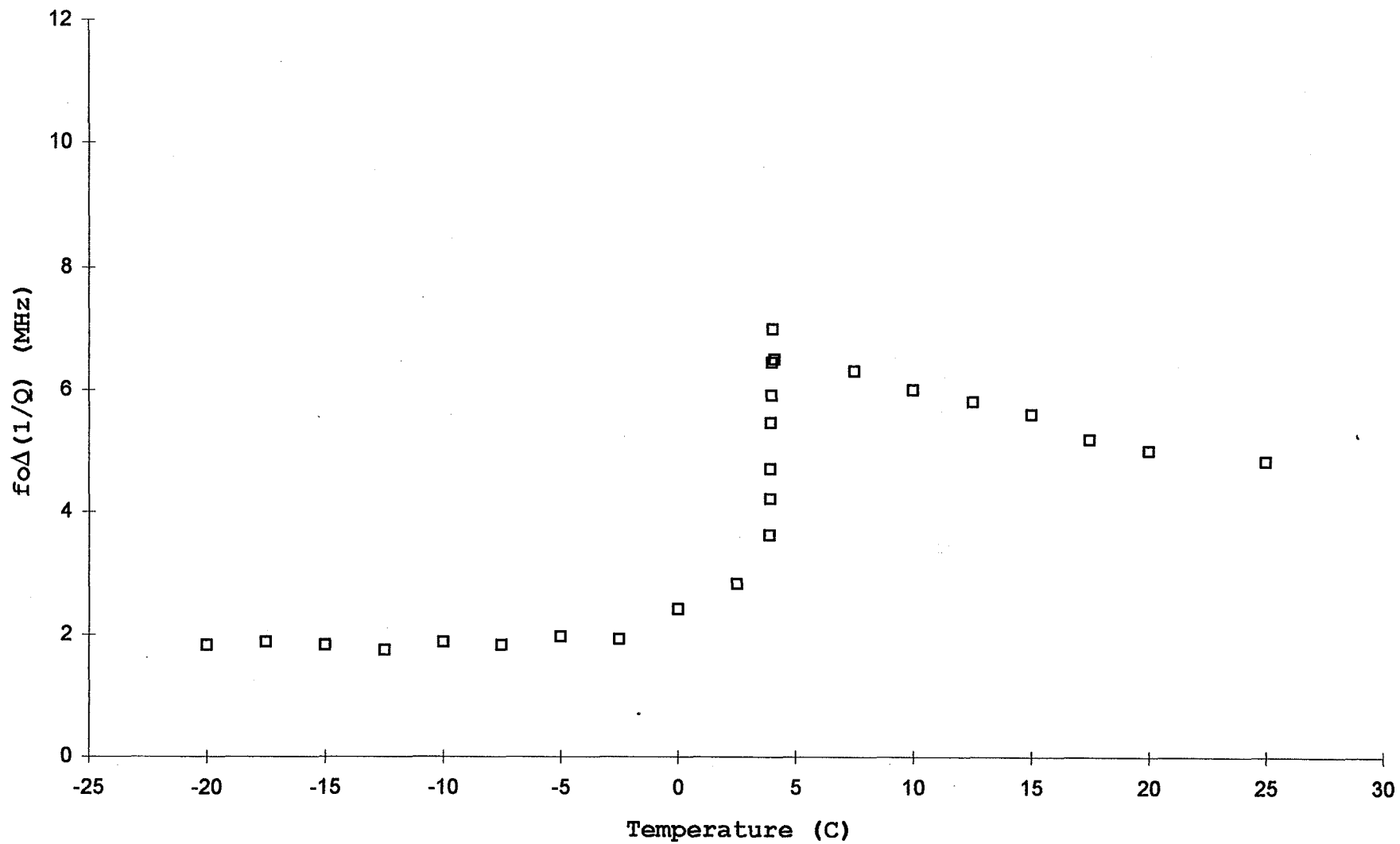


Figure 5. Change in $1/Q$ as a function of temperature for a sample of water at a resonant frequency of 10.6 GHz.

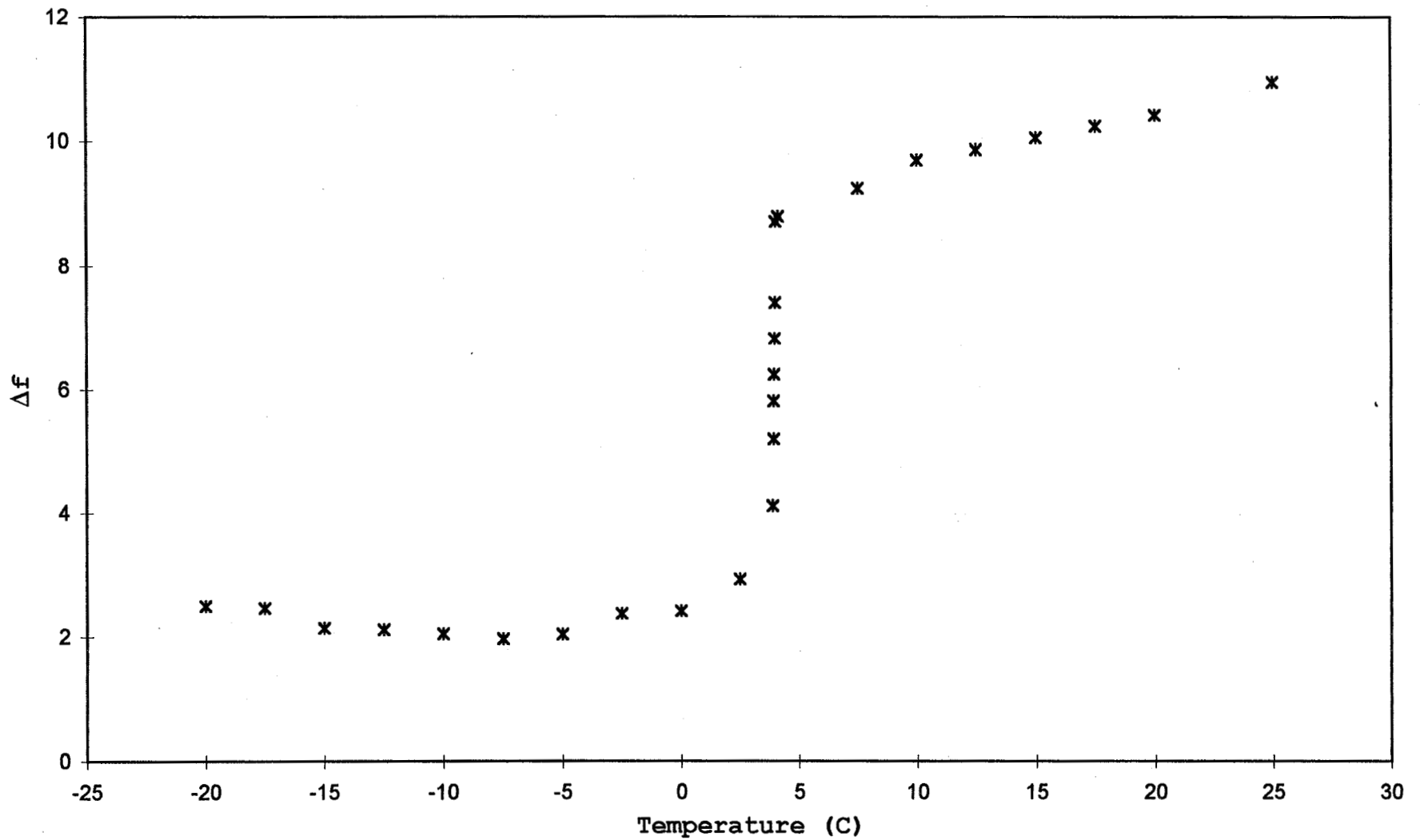


Figure 6. Change in frequency as a function of temperature for a sample of water at a resonant frequency of 11.4 GHz.

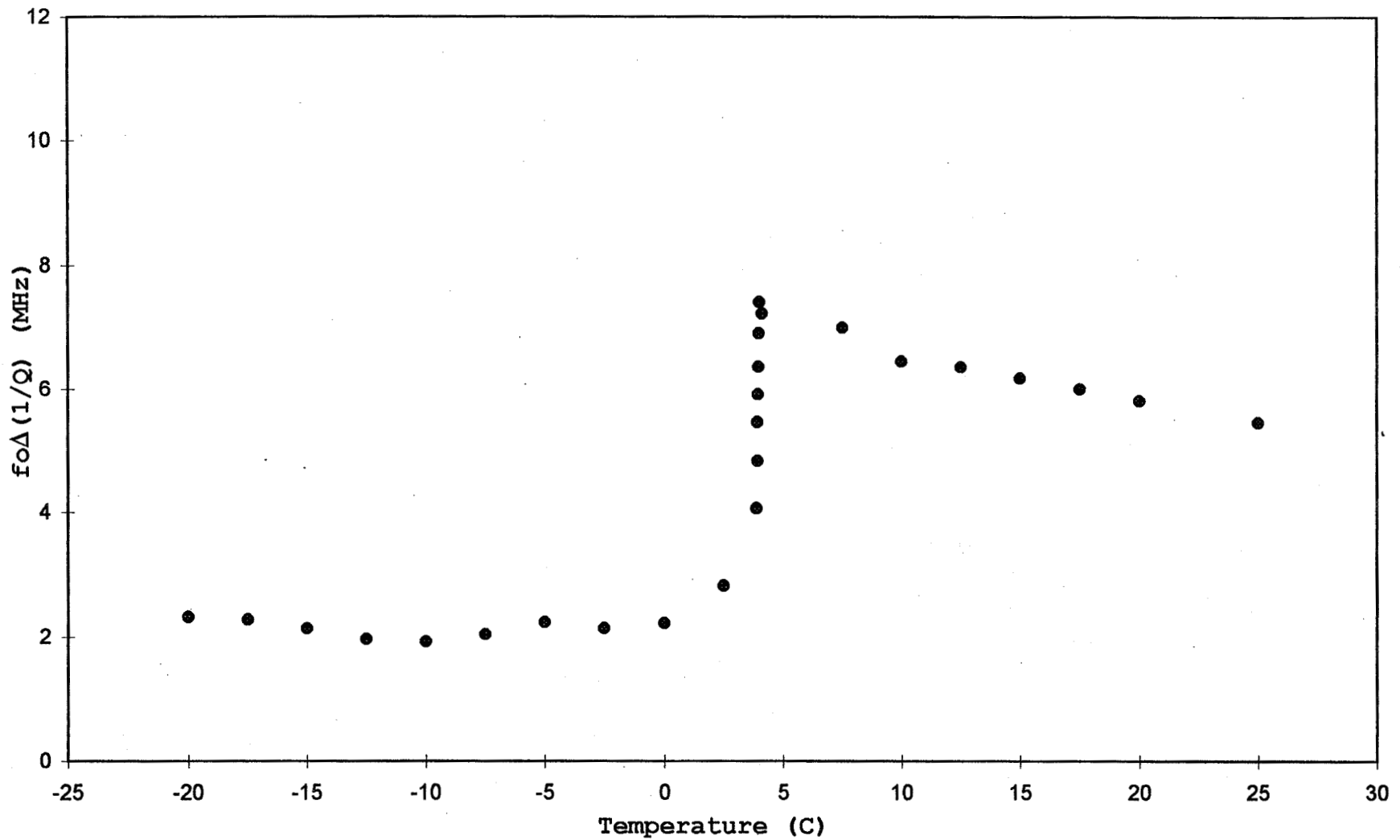


Figure 7. Change in $1/Q$ as a function of temperature for a sample of water at a resonant frequency of 11.4 GHz.

**CHALLENGES AND OPPORTUNITIES
FOR MATERIALS RESEARCH IN
THE AUTOMOTIVE INDUSTRY**

Christine S. Sloane

General Motors R&D Center and Advanced Technology Vehicles
MC: 483-619-409
1996 Technology Drive
Troy, Michigan 48007-7083

Telephone: 248-680-5754
e-mail christine.s.sloane@gm.com



Christine Sloane

Challenges and Opportunities
for Materials Research
in the Automotive Industry

Challenges for Weight Reduction

- Vehicle Body
- Powertrain

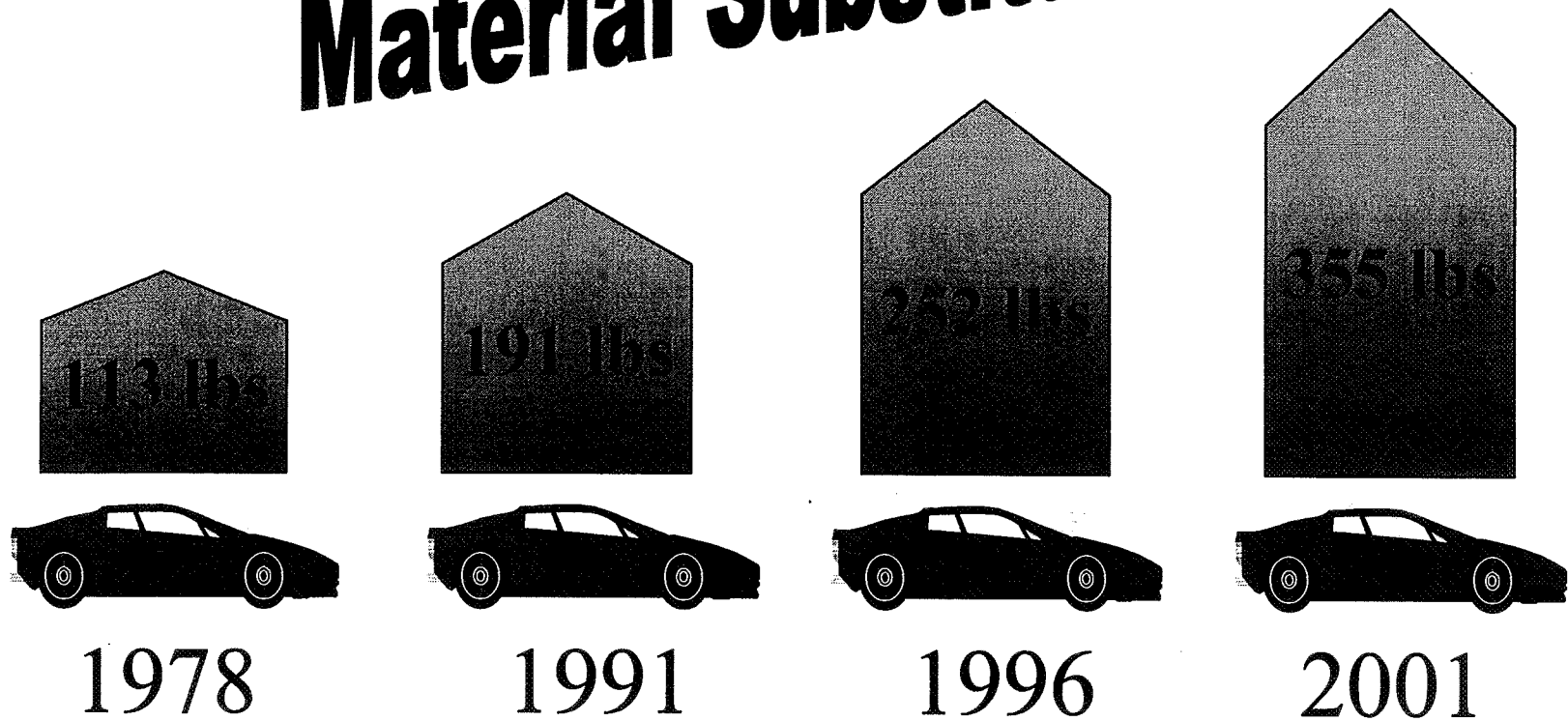
Means to Weight Reduction

Material Substitution

Parts Integration

Function Integration/ Elimination

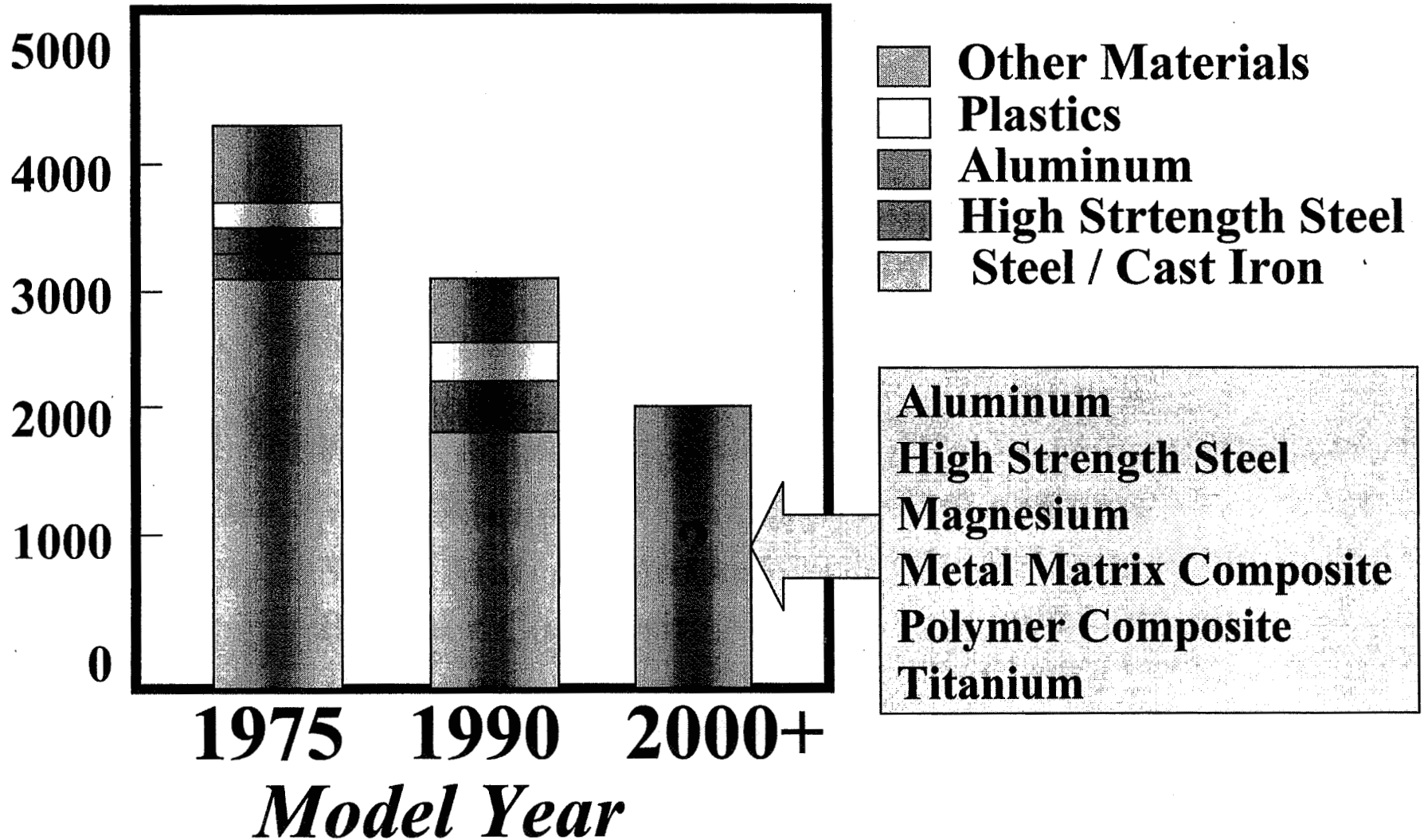
Material Substitution



**Average Amount of Aluminum in
North American Passenger Cars**

PNGV Changing Materials Usage

56



Light-weight Body Structural Materials

	Relative Raw Material Cost	Relative Component Cost	Weight Savings
Mild Steel	1.0		
HS Steel	1.1	1.0	15%
Aluminum	4.0	1.0	40-50%
Magnesium	6.0	2.0	50-65%
FR Polymer	3.0	0.8	25-35%
Gr FR Polymer	10-30	1.25-1.35	60-70%
<u>Castings</u>			
Cast iron	1.0	1.0	
Cast aluminum	2.0	1.0	50-60%
Cast magnesium	3.0	1.0	65-75%

Relative component costs can be comparable with more expensive raw materials

Reference: National Material Advisory Board

Materials Issues for Aluminum Body

- Sheet cost
- Forming complex shapes
- Joining (welding & adhesives)
- Galvanic Corrosion
- Alloy Composition
- Painting
- Dings and dents
- Recycling

Photo of aluminum
body structure

Integration of Parts and Function

- Elimination of connectors
- Compact design
- Reduced assembly cost
- Improved quality

Photos illustrating design integration

***Weight Reduction through Integration
of Parts & Function
requires
Molding of Complex Parts***

Photos of complex molds

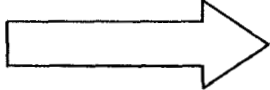
Advantages of Composites in Automobiles

- **Lower mass**
- **Damage and corrosion resistance**
- **Can be cost effective because of**
 - **parts consolidation**
 - **lower scrap rate**

Photos of large composite molds

Current Barriers to Wide Useage of Composites in Automobiles

- **Major change from current assembly methods**
- **Unknown durability as structural materials**
- **Understanding to design with composites**
- **Slow cycle times**

Flow  **Orientation**

Glass fiber reinforced polymers are anisotropic

Anisotropy is driven by process, materials and geometry

Graphic of flow in forming mold

Graphics illustrating forming effects

Powertrain Challenges

- Light weight materials**
- Fuels for efficient, low-emission combustion**
- Catalysts for emission control**
- Catalysts & membranes for fuel cells**

Lightweight Powertrain Materials

Key issue: Wear and Corrosion

Needed: Coating and surface treatment

Photo of thermalspraycoating

Catalysts for Exhaust Emission Control

- Key challenges:
1. Emission reduction
 2. On-board monitoring
 3. Lean NO_x catalysts

Photo of catalyst designs

Material Recycling

- manufactured scrap
- vehicles at end of life

67

Chart showing Breakout of material % recycled

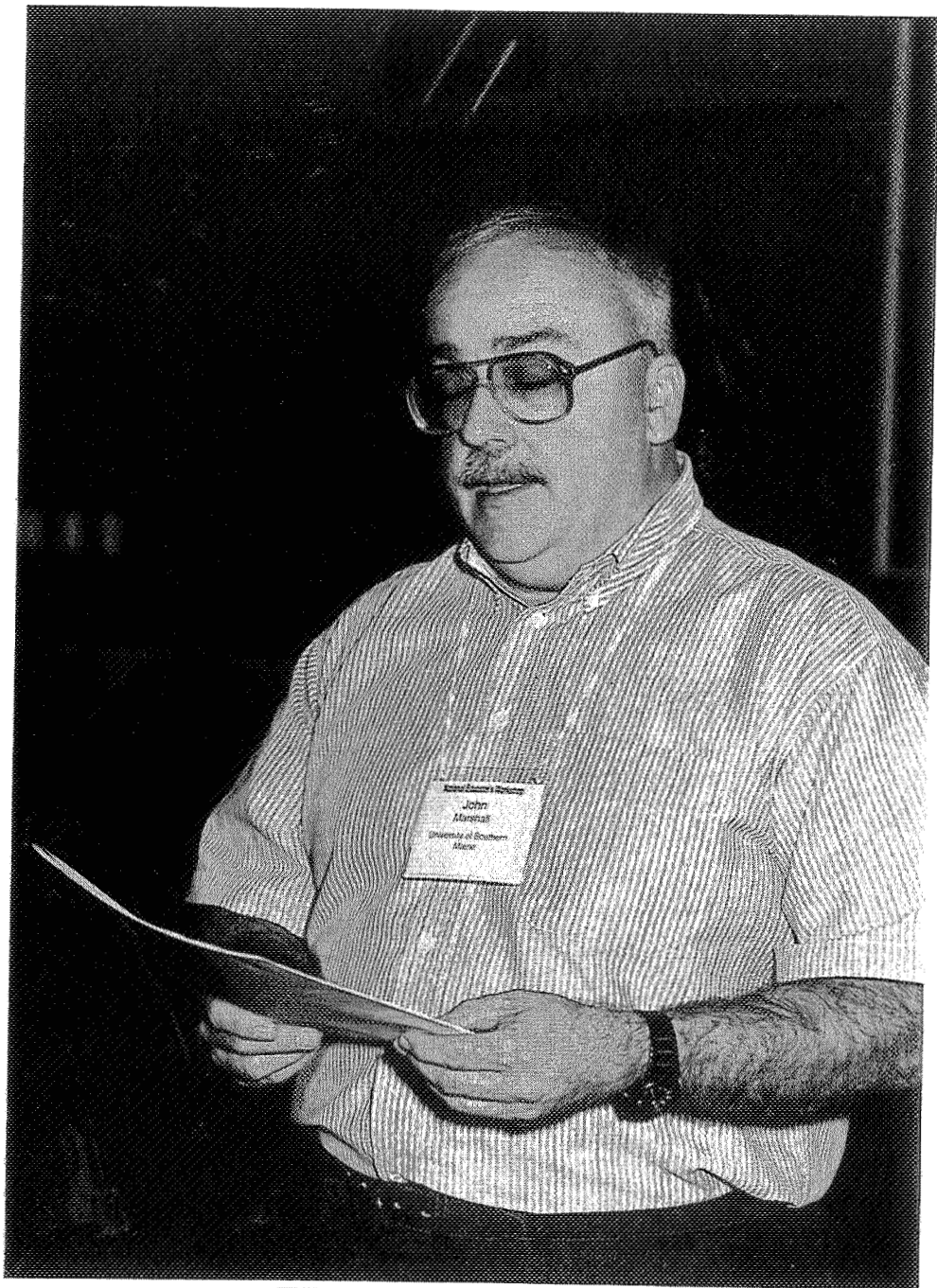
94% of vehicles retired from use are processed for recycling

SHAPE MEMORY ALLOYS

John A. Marshall

School of Applied Science
University of Southern Maine
Gorham, Maine 04038

Telephone 207-780-5447
e-mail jmarshall@usm.maine.edu



John A. Marshall

Shape Memory Alloys

John A. Marshall
School of Applied Science
University of Southern Maine
Gorham, Maine, 04038

Key Words: Shape Memory Alloys, Memory Metals, Nitinol

Prerequisite Knowledge: A basic understanding of electricity and materials

Objective: To observe and gain an understanding of an unusual crystal alloy that radically transitions to a different structure at a distinct temperature and recovers to the pre-deformation shape.

Equipment: Nitinol wire, mounting board, two AA batteries with holder and connecting wires, elastic band, two push pins, empty plastic milk jug.

Introduction:

Motors and solenoids are two very common ways to create motion from electricity. The majority of the machines and equipment used in industries and homes today make extensive use of these two devices. Both of these devices rely on magnetic fields to produce the mechanical motion that is utilized for linear and rotary power transmission.

Due to recent advancements in Shape Memory Alloys (SMAs), another method of creating motion has become available that does not rely on magnetic fields. SMAs are special metals that undergo changes in shape and hardness when heated or cooled, and do so with a great amount of force.

When made into wires, SMAs can be stretched from five to eight percent and will recover their original, shorter length when heated. This is formally referred to as the materials "deformation-to-recovery ratio.

Research during the 1960's and 70's was focused on devices such as: satellite antennas (NASA) that would unfold and expand when exposed to the heat of the sun; engines that would run on hot and cold water; automatic temperature-controlled greenhouse windows; and car fan clutches that would engage only when the engine warmed-up.

One of the primary applications of SMAs today are in the medical arena with devices such as filters that are inserted into a patient's vein or artery to trap stroke-causing blood clots. It is inserted cold, and as it warms, it opens to form a filter. Other applications include highly reliable coupling connections for aircraft hydraulic lines, air valves, fuse protectors, and even a six axis computer-controlled robotic arm!

Procedure:

1. Cut a strip of plastic from the milk jug that measures three-quarters of an inch by three and one-half inches to form the lever arm and make two holes in it with the pushpin. The first hole should be three-eighths of an inch from the end, and a second hole three-quarters of an inch from the same end.
2. Mount the lever arm on the cardboard by inserting the pushpin into the first hole. This is the pivot point of the lever.
3. Attach a four inch length of Nitinol wire to the second hole and, using the second pushpin, attach the other end of the Nitinol wire to the mounting board to position the lever slightly below horizontal.
4. The elastic band will serve as our "load" and is attached to the opposite end of the lever.
5. Connect the two "AA" batteries (in series) and briefly apply power to each of the ends of the Nitinol wire.
6. After observing the movement, remove the power quickly and observe the recovery.

Several forms of data collection are possible from this type of experiment. One data set can be the deformation-to-recovery ratios at various lengths of Nitinol wire. Other interesting data sets that can be collected and analyzed include mechanical advantages, loads, and lever calculations.

Deformation-To-Recovery Ratio			
	Inactivated	Activated	Ratio
	Length	Length	
Sample One			
Sample Two			
Sample Three			
Sample Four			

References: Gilbertson, R., Muscle Wires, Mondo-Tronics, Third Edition, San Anselmo, CA, 1994.

Biographical Information:

John Marshall is the Internship Coordinator for the Department of Technology at the University of Southern Maine. His areas of specialization include Power and Energy Processing, Electronic Control Systems, Plant Layout / Material Handling, and Industrial Distribution.

ACCELERATED AGING STUDY OF ABS COPOLYMER

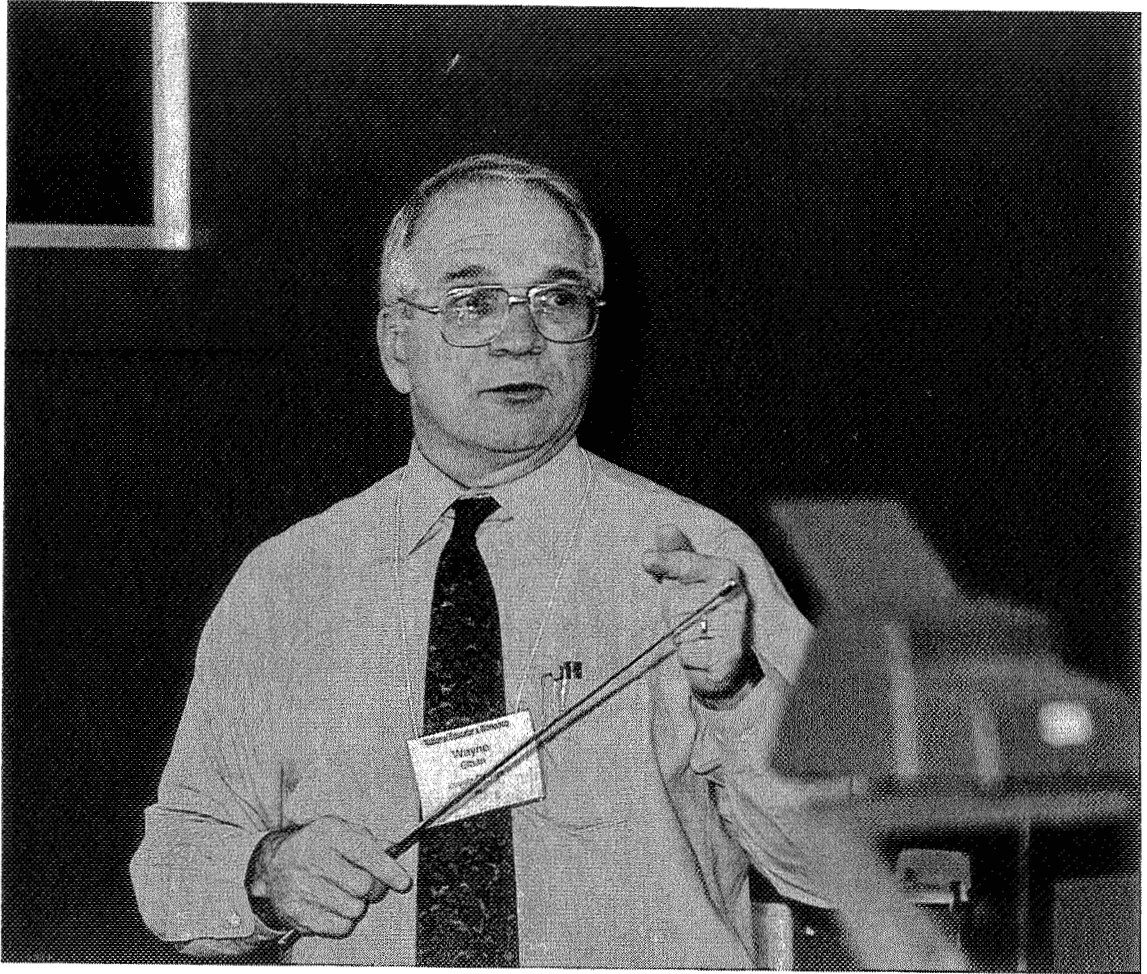
Wayne L. Elban

Scott N. Hornung

Matthew C. Reinhardt

Department of Electrical Engineering and
Engineering Science
Loyola College
4501 North Charles Street
Baltimore, Maryland 21210

Telephone: 410-617-2853
e-mail welban@loyola.edu



Wayne L. Elban

Accelerated Aging Study of ABS Copolymer

Wayne L. Elban, Scott N. Hornung, and Matthew C. Reinhardt
Dept. of Electrical Engineering and Engineering Science
Loyola College
Baltimore, Maryland 21210

ABSTRACT: A procedure is described for measuring the mechanical deformation/fracture properties and dimensional stability of tensile specimens of acrylonitrile-butadiene-styrene (ABS) copolymer exposed to several accelerated aging environments. A bench-top universal testing machine is used to obtain room temperature determinations of ultimate tensile and fracture strengths, and corresponding elongations, as a function of specimen conditioning/aging temperatures: 23 (room temperature), 50, 75, 90, and 105° C. Resultant fracture surfaces are visually inspected to determine brittle/ductile character. Subsequently, the exterior specimen surfaces immediately behind the fracture surfaces are examined using a reflected light microscope. Experimental determinations of mechanical properties are compared to values appearing in the literature. Dimensions of recovered specimens are measured, using a dial caliper, to study their dimensional stability for the same temperatures.

KEY WORDS: Uniaxial tensile testing, mechanical deformation properties, fracture, dimensional stability, stress whitening, accelerated aging, thermoplastic polymers, acrylonitrile-butadiene-styrene (ABS) copolymer.

PREREQUISITE KNOWLEDGE: upper-level undergraduate laboratory experiment requiring basic knowledge of thermoplastic polymers and their mechanical deformation/fracture behaviors and mechanical property testing as described in an introductory materials science course and accompanying laboratory course.

OBJECTIVES:

(a) Experimental Goals:

1. to measure the uniaxial tensile mechanical properties to fracture of a representative thermoplastic polymer having undergone accelerated aging at various elevated temperatures;
2. to measure the room temperature dimensions of tensile specimens of a thermoplastic polymer exposed to various temperatures in order to assess their dimensional stability; and
3. to examine the resultant fracture surfaces to assess their brittle-ductile character and the occurrence of stress whitening.

(b) Learning Goals:

1. to become familiar with uniaxial tensile testing, a prominent technique for characterizing the mechanical response of materials;
2. to become familiar with the distinctive features of brittle and ductile fracture; and
3. to become familiar with the effect of temperature on the aging behavior of a representative thermoplastic polymer.

EQUIPMENT AND MATERIALS: (1) Chatillon model LRX universal testing machine (bench top model with 500 pound capacity); (2) Wedge-action grips (model TG15N); (3) Metric universal dial caliper (Brown and Sharpe 559-579-13); (4) Zeiss model ICM 405 bench metallograph; (5) Conditioning ovens; (6) Injection molded tensile test specimens (ASTM Type I for sheet, plate, and molded plastics).

SAFETY PRECAUTIONS: Care must be taken to avoid having eye contact with or ingesting ABS debris that results from sanding specimen tabs. During this operation, it is recommended that safety glasses or laboratory goggles be worn along with a laboratory coat. Hands and specimens should be cleaned with a shop vacuum and then thoroughly washed in ambient-temperature water and dried before commencing tensile testing. (Instructor Note 1)

INTRODUCTION:

Problem Statement: You have recently been hired as a materials scientist by a company that is interested in starting up a testing effort to investigate the plastic deformation/fracture properties of various plastics that they manufacture. In an initial effort, it is of interest to investigate the aging behavior of acrylonitrile-butadiene-styrene (ABS) copolymer [1]. It is proposed to accomplish this by measuring the room temperature mechanical properties and dimensional stability of specimens exposed to several accelerated aging environments. Subsequently, it is desired to examine the specimens and relate observations to the measurements. Your company recently acquired a new universal testing machine (Chatillon model LRX) equipped with wedge-action grips (model TG15N). It is computer controlled and has computer data acquisition capabilities, and your boss requests that you use the new machine in your assessment of mechanical properties.

Thermoplastic polymers usually have a linear structure, although branching is possible. One prominent example is ABS, which is a two-phase material involving a brittle styrene-acrylonitrile copolymer matrix with rubbery styrene-butadiene copolymer inclusions. [2] Typical uses include luggage and telephones. [3] Upon heating above room temperature, thermoplastic polymers undergo significant changes in their elevated temperature mechanical properties as determined, for example, by uniaxial tensile testing, including decreases in elastic (Young's) modulus, ultimate tensile strength, and fracture strength and increase in elongation at break. (Instructor Note 2) However, chemical decomposition is minimal.

The effect of temperature on thermoplastic polymers is also exhibited by changes in dimensions that occur in specimens subjected to sufficiently elevated temperatures. This material behavior is important to design engineers who must select materials with good dimensional stability for end-products that experience a range of temperatures during their service lives.

The purpose of this experiment is to investigate the room temperature mechanical deformation/fracture behaviors of ABS copolymer having undergone accelerated aging. To this end, a quantitative evaluation of ultimate tensile and fracture strengths, and their corresponding elongations, as a function of aging temperature will be made from uniaxial tensile testing measurements. Subsequently, a visual inspection of each resultant fracture surface will be made to determine its character (i.e., degree of brittle versus ductile fracture). The regions immediately behind the fracture surfaces will also be examined using light microscopy. To verify determinations of strength and elongation for the room temperature specimens, the experimental values will be compared with those values for ABS appearing in the literature. Further, the dimensions of recovered samples will be measured allowing the dimensional stability of ABS to be studied for the same aging conditions.

PROCEDURE:

A. TENSILE TESTING (Instructor Note 1)

1. Development of Experimental Procedure: Referring to ASTM Standard Tensile Test Method [4] and Holman [5], specify what measurements need to be made and how they will be accomplished. The tensile testing machine will be operated at a constant crosshead speed (CHS) of 2.0"/min.
2. Preparatory Reading Assignment:
 - (a) Read Ref. [6] providing brief descriptions of aging at elevated temperatures and temperature index.
 - (b) Lightly read Ref. [7] providing background information on the aging of polymers.
 - (c) Read Ref. [8] providing detailed information on the yield behavior of polymers.

Not all of the material contained in Refs. [7,8] will be totally understandable, and results for many polymers are presented. However, becoming familiar with polymers and their mechanical and aging properties is very worthwhile since these materials are now widely used, and there is not time to cover this important topic in class. Further, reading and understanding technical survey articles are important skills to develop in preparation for your engineering careers.

3. Measurements (as developed according to Item #1 above):
 - (a) Measure the thickness and width of each specimen using a dial caliper prior to tensile testing.
 - (b) Perform room temperature tensile testing on five (5) specimens minimum for the following ABS copolymer:
 - (i) as-received to serve as a control;
 - (ii) exposed to 50° C for four (4) hours;
 - (iii) exposed to 75° C for four (4) hours;
 - (iv) exposed to 90° C for four (4) hours; and
 - (v) exposed to 105° C for four (4) hours. (Instructor Note 3)
4. After testing, place handwritten identification labels near both tab ends of each specimen.
5. Retain all specimen pieces for subsequent dimension measurements and examination.
6. Record your measurements and any relevant observations in your laboratory notebook with one or more drawings as appropriate.

B. DIMENSION MEASUREMENTS OF RECOVERED SPECIMENS

1. Using a dial caliper, measure the thickness and width of each tensile specimen in its gage length a few millimeters away from the fracture surfaces.
2. Record your measurements and any relevant observations in your laboratory notebook with one or more drawings as appropriate.

C. VISUAL/MICROSCOPIC EXAMINATION OF RECOVERED SPECIMENS

1. Ascertain how well the pieces from each tensile specimen fit back together as a preliminary check on whether the failure was brittle or ductile.
2. Examine a representative fracture surface from each tensile specimen type tested. Pay particular attention to the degree of surface roughness and whether the fracture surface appears to have undergone brittle or ductile fracture [9].
3. Examine the fracture surface and the region immediately behind it for a phenomena known as stress whitening. (Instructor Note 4)
4. Record any relevant observations in your laboratory notebook with one or more drawings as appropriate.

5. Using a Zeiss model ICM 405 bench metallograph, examine a representative specimen for each sample type tested, looking in the vicinity of the fracture surfaces.

D. ANALYSIS

Perform the following analyses and respond to any questions as completely as possible, being sure to show all of your work and reasoning as partial credit can be earned.

1. Tensile testing measurements:

- a. Calculate (ultimate) tensile strength (σ_{\max}), fracture strength (σ_f), elongation at maximum strength (e_{UTS}), and elongation at break (e_b) for each specimen using engineering stress-strain relationships (e.g., Eqn. (1-1a,b) in Ref. [10]) -- (Instructor Note 5):

$$\sigma_{\max} = F_{\max}/(t \times w), \quad (1)$$

where F_{\max} = maximum force in force-displacement curve, lbf,
 t = specimen thickness in gage length prior to testing, in., and
 w = specimen width in gage length prior to testing, in.;

$$\sigma_f = F_f/(t \times w), \quad (2)$$

where F_f = fracture force in force-displacement curve, lbf;

$$e_{\text{UTS}} = \Delta l_{\text{UTS}}/l_g, \quad (3)$$

where Δl_{UTS} = corresponding displacement at maximum force in force-displacement curve, in.,
 l_g = specimen gage length prior to testing, in.; and

$$e_b = \Delta l_b/l_g, \quad (4)$$

where Δl_b = corresponding displacement at fracture (break) in force-displacement curve, in.

- b. Calculate [11] the average and standard deviation, σ , of these determinations (Instructor Note 6) for each sample type.
2. Discuss the effect that aging temperature has on the mechanical properties of the copolymer specimens.

3. Compare the room temperature mechanical property values obtained with those given in the literature. Give one or more reasons why differences may exist.

4. Specimen dimension measurements:

a. Calculate the change in thickness, Δt , in units of mm, for each specimen using:

$$\Delta t = t_T - t_{RT}, \quad (5)$$

where t_T = thickness of specimen exposed to a given aging temperature, mm,
and

t_{RT} = room temperature specimen thickness, mm.

b. Calculate the change in width, Δw , in units of mm, for each specimen using:

$$\Delta w = w_T - w_{RT}, \quad (6)$$

where w_T = width of specimen exposed to a given aging temperature, mm,
and

w_{RT} = room temperature specimen width, mm.

c. Calculate [11] the average and standard deviation, σ , of these determinations for each sample type.

6. Discuss the effect that aging temperature has on the dimensional stability of the copolymer specimens.

7. Based on visual and microscopic observations, discuss the brittle versus ductile character of the fracture surfaces that resulted for each sample type. Also, discuss the occurrence of stress whitening as a function of aging temperature.

COMMENTS with Data Sheets and Plots:

All of the experimental steps were performed a number of times to verify that the results were reasonably reproducible. The data sets appearing in this section are considered to be representative.

Effect of Aging Temperature on Uniaxial Tensile Testing Response: Force and displacement measurements taken from experimental curves (e.g., Figure 1) are given in Table I as a function of aging temperature for the ABS specimens. The resultant strength and elongation determinations appear in Table II. Referring to the average values in Table II, the aged specimens did not exhibit large changes in their mechanical properties. Tensile strength increases slightly (1.1%) in going from 23 to 50° C, and then undergoes a modest decrease (6.3%) as temperature rises to 105° C. A similar trend occurs for fracture strength. The elongation at maximum strength values are nearly constant with temperature except for 105°

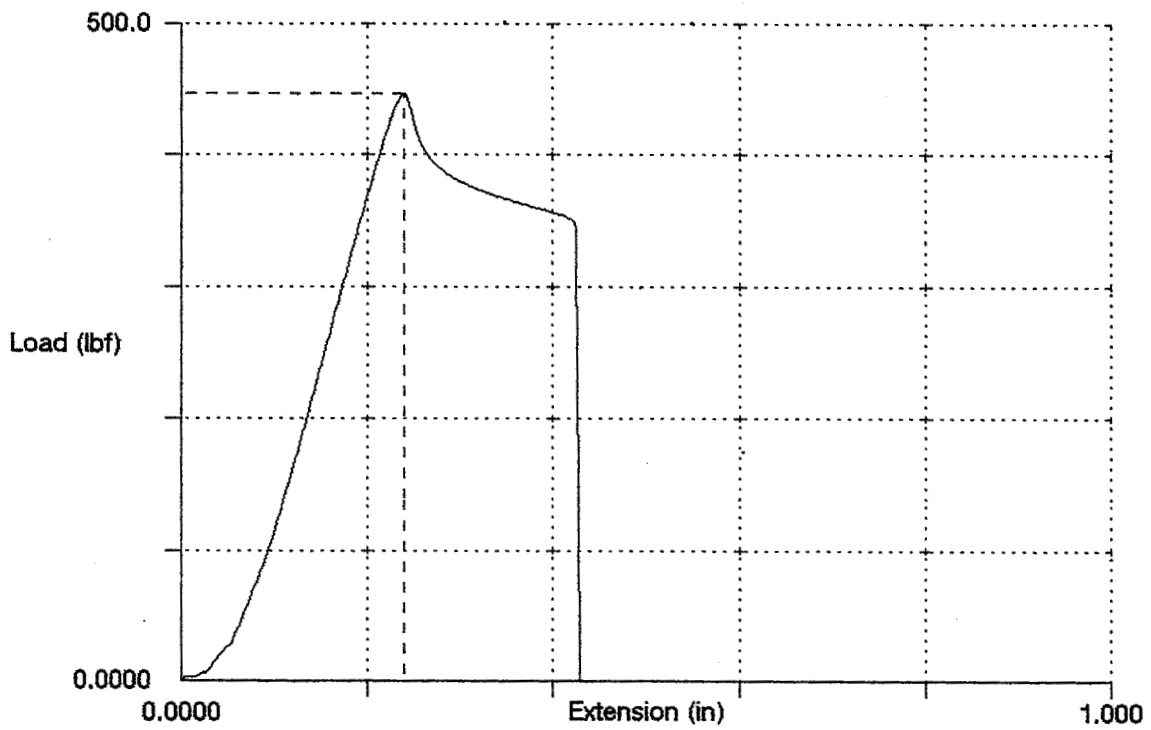


Figure 1. Force-displacement curve for as-received ABS copolymer (specimen CY5998) tested at room temperature in uniaxial tension.

Table I. Force and Displacement Measurements (23° C) for ABS Exposed to Various Aging Temperatures

Specimen Designation	Temperature (°C)	Maximum Force* (lb _f)	Displacement at Max.* (in.)	Fracture Force** (lb _f)	Displacement at Break** (in.)
CY5898	23	448.3	0.2303	369	0.340
CY5998	23	447.2	0.2383	351	0.398
CY6098	23	453.6	0.2283	364	0.427
CY6198	23	439.5	0.2561	357	0.344
CY6298	23	453.1	0.2398	368	0.406
CY6398	23	444.6	0.2291	347	0.388
CY3498	50	460.3	0.2294	378	0.448
CY3598	50	448.8	0.2727	378	0.315
CY3698	50	447.7	0.2351	352	0.476
CY3798	50	459.7	0.3030	360	0.515
CY3898	50	459.5	0.2360	382	0.348
CY3998	50	445.9	0.2618	428	0.273
CY4098	75	437.8	0.2549	355	0.441
CY4198	75	447.3	0.2142	371	0.436
CY4298	75	440.8	0.2689	363	0.423
CY4398	75	431.0	0.2172	367	0.249
CY4498	75	439.8	0.2636	351	0.564
CY4598	75	433.1	0.2696	347	0.439

Table I. Force and Displacement Measurements (23° C) for ABS Exposed to Various Aging Temperatures, Cont'd.

Specimen Designation	Temperature (°C)	Maximum Force* (lb _f)	Displacement at Max.* (in.)	Fracture Force** (lb _f)	Displacement at Break** (in.)
CY4698	90	436.6	0.2329	361	0.322
CY4798	90	456.3	0.2258	359	0.526
CY4898	90	459.6	0.2164	366	0.611
CY4998	90	444.2	0.2219	361	0.322
CY5098	90	448.5	0.2502	390	0.292
CY5198	90	451.1	0.2215	417	0.237
CY5298	105	481.6	0.2287	388	0.330
CY5398	105	483.0	0.2258	375	0.424
CY5498	105	476.6	0.2337	368	0.475
CY5598	105	464.9	0.2273	358	0.350
CY5698	105	456.1	0.2687	378	0.366
CY5798	105	468.9	0.2686	368	0.352

* Obtained from computer analysis of force-displacement curve.

** Determined from graphical analysis of force-displacement curve.

Table II. Mechanical Property Results (23° C) for ABS Exposed to Various Aging Temperatures

Specimen Designation	Temperature (°C)	Tensile Strength (psi) [MPa]	Elongation at Max. (%)	Fracture Strength (psi) [MPa]	Elongation at Break (%)
CY5898	23	7280 [50.2]	12	6000 [41.4]	17
CY5998	23	7260 [50.1]	12	5700 [39.3]	20
CY6098	23	7370 [50.8]	11	5910 [40.7]	21
CY6198	23	7120 [49.1]	13	5780 [40.0]	17
CY6298	23	7340 [50.6]	12	5960 [41.1]	20
CY6398	23	7210 [50.0]	12	5630 [38.8]	19
	Avg.:	7260 [50.1]	12	5830 [40.2]	19
	σ:	82 [0.56]	1	140 [0.95]	2
CY3498	50	7430 [51.2]	12	6110 [42.1]	22
CY3598	50	7240 [49.9]	14	6100 [42.1]	16
CY3698	50	7240 [49.9]	12	5700 [39.3]	24
CY3798	50	7460 [51.4]	15	5850 [40.3]	26
CY3898	50	7430 [51.3]	12	6190 [42.7]	17
CY3998	50	7240 [49.9]	13	6960 [48.0]	14
	Avg.:	7340 [50.6]	13	6150 [42.4]	20
	σ:	100 [0.69]	1	400 [2.8]	4
CY4098	75	7060 [48.7]	13	5720 [39.4]	22
CY4198	75	7210 [49.7]	11	5980 [41.3]	22
CY4298	75	7100 [49.0]	13	5840 [40.3]	21
CY4398	75	6970 [48.0]	11	5930 [40.9]	13
CY4498	75	7090 [48.9]	13	5660 [39.0]	28
CY4598	75	6990 [48.2]	14	5590 [38.5]	22
	Avg.:	7070 [48.8]	12	5790 [39.9]	21
	σ:	82 [0.56]	1	140 [1.0]	5

Table II. Mechanical Property Results (23° C) for ABS Exposed to Various Aging Temperatures, Cont'd.

Specimen Designation	Temperature (°C)	Tensile Strength (psi) [MPa]	Elongation at Max. (%)	Fracture Strength (psi) [MPa]	Elongation at Break (%)
CY4698	90	6730 [46.4]	13	5570 [38.4]	17
CY4798	90	7030 [48.5]	12	5530 [38.2]	28
CY4898	90	7070 [48.7]	12	5630 [38.8]	33
CY4998	90	6870 [47.4]	12	5580 [38.5]	17
CY5098	90	6940 [47.9]	14	6040 [41.6]	16
CY5198	90	6980 [48.1]	12	6450 [44.5]	13
	Avg.:	6940 [47.8]	12	5800 [40.0]	21
	σ:	110 [0.78]	1	340 [2.3]	7
CY5298	105	6700 [46.2]	13	5390 [37.2]	19
CY5398	105	6970 [48.1]	13	5410 [37.3]	25
CY5498	105	6920 [47.7]	14	5350 [36.9]	28
CY5598	105	6620 [45.6]	13	5100 [35.1]	20
CY5698	105	6810 [47.0]	16	5640 [38.9]	21
CY5798	105	6810 [46.9]	16	5350 [36.9]	20
	Avg.:	6810 [46.9]	14	5370 [37.0]	22
	σ:	120 [0.83]	1	160 [1.1]	3

C where the average elongation is higher. The average elongation at break values increase with temperature with the highest value also being obtained for the specimens exposed to the highest aging temperature. Significantly higher standard deviations are associated with fracture elongation.

Literature Comparison: There is reasonable agreement between experimental room temperature mechanical properties of unaged ABS specimens (Table II) and those appearing in the literature. Average values of 7260 and 5830 psi (50.1 and 40.2 MPa) were obtained for tensile strength and fracture strength, respectively, versus a value of 6000 psi (41 MPa) reported [1] for yield strength (essentially tensile strength based on the force-displacement curve in Figure 1) for a commercial-grade material, designated as Cycolac T resin, that is like what was used in the experiment. An average value of 19% elongation at break was obtained compared with reported [3] values ranging from 20 to 80%.

Dimensional Stability Assessment: Thickness and width measurements as a function of aging temperature for ABS specimens appear in Tables III and IV, respectively. Changes in thickness and width are also provided in these tables. Although ABS retained much of its strength and all of its strain capacity for the aging conditions selected, this was not the case for its dimensional stability, which differed markedly in heated specimens over the range of aging temperatures. Up to 75° C, the dimensional stability of ABS was excellent; at and above 90° C, significant changes in thickness and width were obtained with stability worsening as the temperature increased to 105° C, as expected. The loss of dimensional stability at 105° C is anisotropic with a strain of +8.3% occurring for specimen thickness compared to +3.5% for specimen width.

Visual and Microscopic Observations: A compilation of visual observations for the resultant fracture surfaces of ABS tensile specimens is given in Table V. Essentially brittle fracture occurred in specimens exposed to the entire range of conditioning/aging temperatures. In each instance, the fracture surfaces have a light appearance, and little or no necking occurred. The degree of surface roughness did change with the general tendency of smoother surfaces occurring for the specimens exposed to the higher temperatures. There is a similar trend for the occurrence of stress lightening (whitening).

Microscopic examination of specimen surfaces immediately behind the fracture surfaces revealed that numerous sub-critical cracks are present (Figures 2-5). The cracking is least prominent for specimens exposed to 50° C (Figure 3), which is consistent with having the highest average strength values (Table II). Less microcracking developed in specimens heated at 90° C (Figure 5), but large, relatively straight secondary cracks occurred. There was even less microcracking in specimens heated to 105° C; instead, a relatively fine-scale surface texture formed that caused the light to scatter, yielding poor quality photographs.

INSTRUCTOR NOTES:

1. A brief discussion of this test is provided [12] in another manual that is available in photocopied form. Students should be shown how to operate the testing machine and to position specimens in the machine prior to actual testing. Using 80 grit garnet paper on

Table III. Specimen Thickness Stability Results (23° C) for ABS Exposed to Various Aging Temperatures

Specimen Designation	Temperature (°C)	Initial Thickness (mm)	Final Thickness (mm)	Change in Thickness (mm)
CY5898	23	3.12	3.12	0.0
CY5998	23	3.12	3.12	0.0
CY6098	23	3.12	3.12	0.0
CY6198	23	3.13	3.13	0.0
CY6298	23	3.13	3.13	0.0
CY6398	23	3.13	3.13	0.0
			Avg.:	0.0
			σ:	0.0
CY3498	50	3.14	3.14	0.0
CY3598	50	3.13	3.14	0.01
CY3698	50	3.14	3.13	-0.01
CY3798	50	3.13	3.12	-0.01
CY3898	50	3.14	3.13	-0.01
CY3998	50	3.14	3.12	-0.02
			Avg.:	-0.01
			σ:	0.01
CY4098	75	3.14	3.14	0.0
CY4198	75	3.14	3.14	0.0
CY4298	75	3.14	3.14	0.0
CY4398	75	3.13	3.13	0.0
CY4498	75	3.14	3.14	0.0
CY4598	75	3.13	3.14	0.01
			Avg.:	0.0
			σ:	0.0

Table III. Specimen Thickness Stability Results (23° C) for ABS Exposed to Various Aging Temperatures, Cont'd.

Specimen Designation	Temperature (°C)	Initial Thickness (mm)	Final Thickness (mm)	Change in Thickness (mm)
CY4698	90	3.13	3.24	0.11
CY4798	90	3.13	3.23	0.10
CY4898	90	3.14	3.24	0.10
CY4998	90	3.13	3.22	0.09
CY5098	90	3.13	3.22	0.09
CY5198	90	3.14	3.22	0.08
			Avg.:	0.10
			σ:	0.01
CY5298	105	3.14	3.46	0.32
CY5398	105	3.14	3.39	0.25
CY5498	105	3.13	3.38	0.25
CY5598	105	3.13	3.42	0.20
CY5698	105	3.13	3.33	0.20
CY5798	105	3.14	3.38	0.24
			Avg.:	0.26
			σ:	0.04

Table IV. Specimen Width Stability Results (23° C) for ABS Exposed to Various Aging Temperatures

Specimen Designation	Temperature (°C)	Initial Width* (mm)	Final Width (mm)	Change in Width (mm)
CY5898	23	12.73	12.73	0.0
CY5998	23	12.73	12.73	0.0
CY6098	23	12.73	12.73	0.0
CY6198	23	12.72	12.72	0.0
CY6298	23	12.73	12.73	0.0
CY6398	23	12.72	12.72	0.0
			Avg.:	0.0
			σ:	0.0
CY3498	50	12.73	12.73	0.0
CY3598	50	12.73	12.74	0.01
CY3698	50	12.73	12.74	0.01
CY3798	50	12.73	12.74	0.01
CY3898	50	12.73	12.74	0.01
CY3998	50	12.73	12.73	0.0
			Avg.:	0.01
			σ:	0.0
CY4098	75	12.73	12.74	0.01
CY4198	75	12.73	12.74	0.01
CY4298	75	12.73	12.75	0.02
CY4398	75	12.73	12.75	0.02
CY4498	75	12.73	12.74	0.01
CY4598	75	12.73	12.74	0.01
			Avg.:	0.01
			σ:	0.0

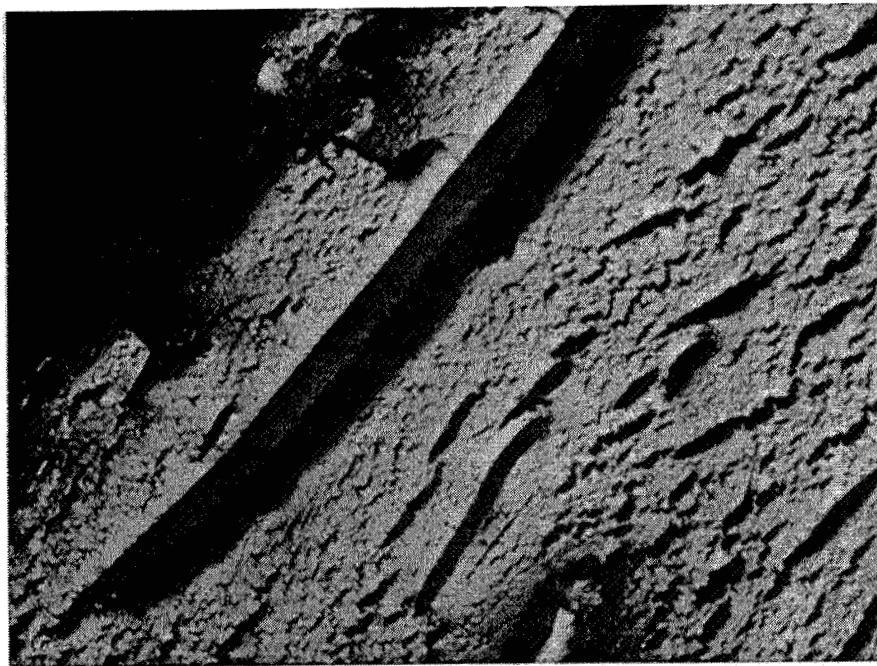
Table IV. Specimen Width Stability Results (23° C) for ABS Exposed to Various Aging Temperatures, Cont'd.

Specimen Designation	Temperature (°C)	Initial Width* (mm)	Final Width (mm)	Change in Width (mm)
CY4698	90	12.73	12.92	0.19
CY4798	90	12.73	12.96	0.23
CY4898	90	12.73	12.95	0.22
CY4998	90	12.73	12.96	0.23
CY5098	90	12.73	12.94	0.21
CY5198	90	12.73	12.95	0.22
			Avg.:	0.22
			σ:	0.01
CY5298	105	12.73	13.40	0.67
CY5398	105	12.73	13.19	0.46
CY5498	105	12.73	13.14	0.41
CY5598	105	12.73	13.25	0.52
CY5698	105	12.73	12.97	0.24
CY5798	105	12.73	13.15	0.42
			Avg.:	0.45
			σ:	0.13

* Initial width measurements were inadvertently not made for any specimens exposed to temperatures above 23° C. A value of 12.73 mm was chosen for all specimens exposed to elevated temperatures based on the rather consistent values obtained for the six room temperature specimens.

Table V. Fracture Surface Appearance of Recovered ABS Tensile Specimens

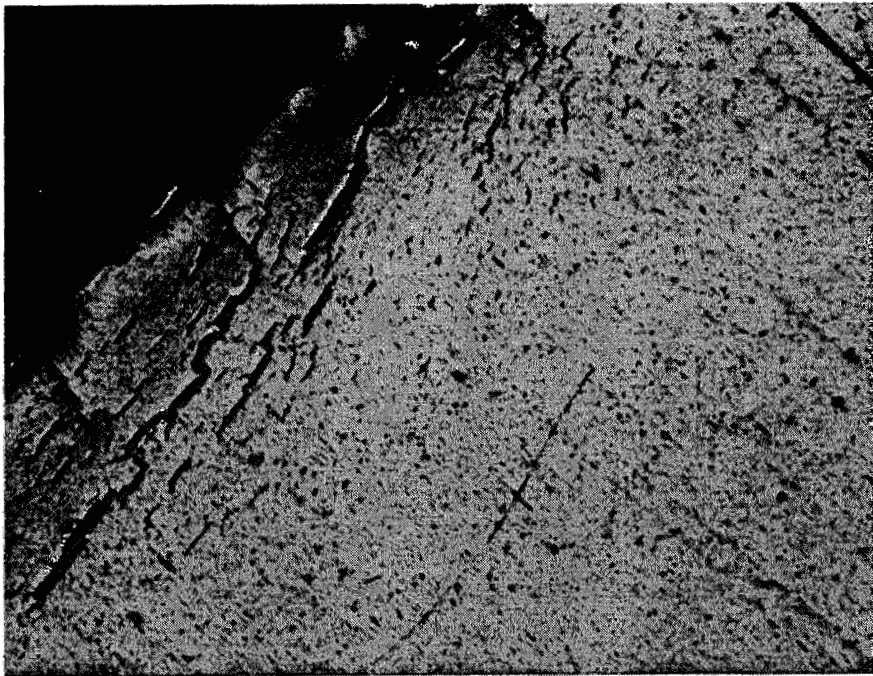
Temperature (°C)	Visual Observations
23	Mostly brittle with small reduction in cross-sectional area; light surface; somewhat rough; slight necking; slight stress lightening (whitening)
50	Brittle; light surface; somewhat rough; no necking
75	Brittle; light surface; smoother; no necking; slight stress lightening (whitening)
90	Brittle; light surface; smooth; no necking; slightly more stress lightening (whitening)
105	Less brittle; light surface; mostly smooth; very slight necking; more stress lightening (whitening)



200 μm



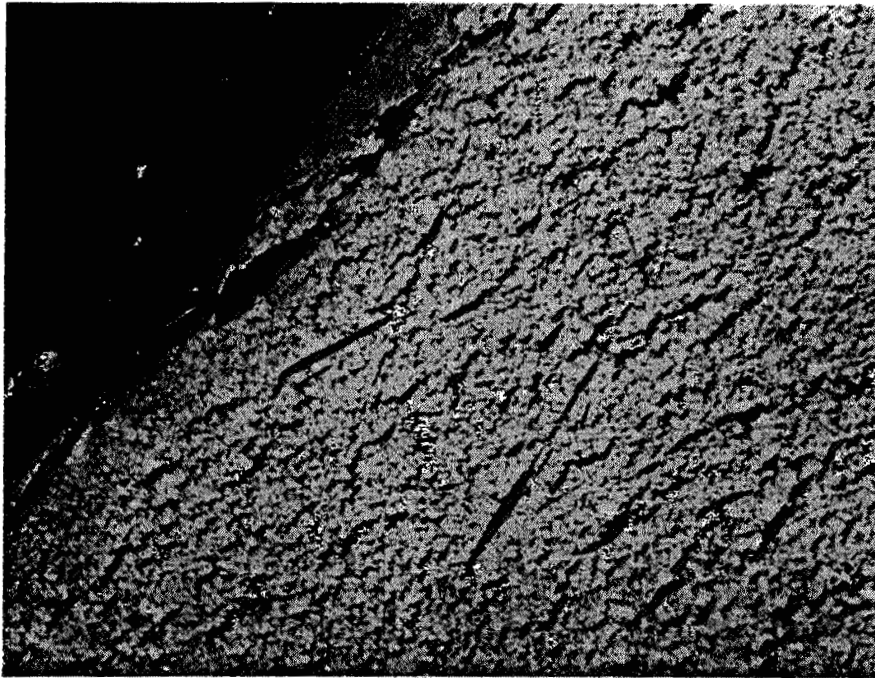
Figure 2. Photomicrograph of near-fracture surface region of ABS copolymer (specimen CY5998) conditioned at 23° C.



200 μm



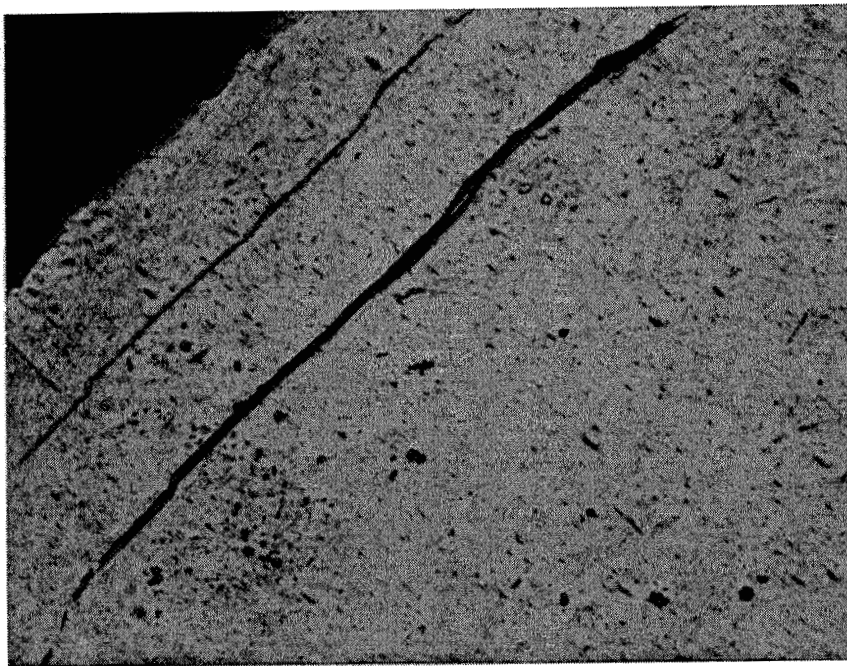
Figure 3. Photomicrograph of near-fracture surface region of ABS copolymer (specimen CY3598) aged at 50° C for 4 hrs.



200 μm



Figure 4. Photomicrograph of near-fracture surface region of ABS copolymer (specimen CY4098) aged at 75° C for 4 hrs.



200 μm
┌──┐

Figure 5. Photomicrograph of near-fracture surface region of ABS copolymer (specimen CY5098) aged at 90° C for 4 hrs.

specimens tabs (coarse scratches oriented orthogonal to pulling direction) reduces/eliminates slippage in grips. See **SAFETY PRECAUTIONS**.

2. A very nice discussion of various thermal properties of polymers is provided [13] in a manual that is available free for distribution to students.

3. The aging time was selected after performing a preliminary study of the effect of time on the maximum tensile force for various times up to 16 hours at 50° C. The greatest change occurred for specimens exposed for 4 hours. Specimens exposed to elevated temperatures were placed on glass plates in the conditioning ovens in order to retain specimen flatness. The specimens tend to stick to glass; this can be greatly alleviated by lightly coating the glass plates with silicone spray before switching on the ovens. The aging temperatures are all below the glass transition temperature (120° C) based on heat capacity measurements [14] obtained for commercial-grade material, designated as Cylolac T resin, that is like what was used in this experiment.

4. Stress whitening [15], sometimes referred to as blushing, can occur because of the formation of numerous small cracks causing a change in reflected light. Stress whitening can also result when polymer molecules become highly oriented upon experiencing large local stresses that alter the degree of crystallinity and cause internal micro-porosity (voids). The particular specimens used in this experiment contained a brown pigment (additive) which changed the observations to stress "lightening".

5. As an additional data analysis exercise, tensile toughness can be determined using Eqn. (1-25) in Ref. [16].

6. The uncertainty in the elongation determinations is large because displacement was obtained indirectly from constant CHS rather than using the preferred technique of affixing an extensometer to the specimen, thus providing a direct measurement.

REFERENCES:

[1] "Properties Guide: GE Engineering Thermoplastics," Publication PBG-140H (August 1992/Reprinted December 1996), General Electric Company, One Plastics Avenue, Pittsfield, Massachusetts 01201, pp. 6-7.

"Cylolac Resin Properties Guide," Publication CYC-300B (December 1993), General Electric Company, One Plastics Avenue, Pittsfield, Massachusetts 01201, pp. 1-2.

[2] Billmeyer, Jr., F.W.: Textbook of Polymer Science, 2nd Edn., Wiley-Interscience, 1971, p. 408.

[3] Flinn, R.A.; and Trojan, P.K.: Engineering Materials and Their Applications, 4th Edn., Houghton Mifflin Co. (now John Wiley and Sons, Inc.), 1990, pp. 560-561.

- [4] "Standard Test Method for Tensile Properties of Plastics," ASTM Designation D638-89, in 1989 Annual Book of ASTM Standards, Section 8: Plastics, Vol. 08.01, American Society for Testing and Materials, Philadelphia, pp. 156-167.
- [5] Holman, J.P.: Experimental Methods for Engineers, 6th Edn., McGraw-Hill Book Co., 1994, pp. 35-38.
- [6] "Designing with Plastic: The Fundamentals," Design Manual TDM-1 (1996), Hoechst Celanese Corporation, 90 Morris Avenue, Summit, New Jersey 07901, p. 4-3.
- [7] Struik, L.C.E.: "Physical Aging: Influence on the Deformation Behavior of Amorphous Polymers," in Failure of Plastics, W. Brostow and R.D. Corneliusen (Eds.), Hanser Publishers, 1986, pp. 209-234.
- [8] Brown, N.: "Yield Behavior of Polymers," in Failure of Plastics, W. Brostow and R.D. Corneliusen (Eds.), Hanser Publishers, 1986, pp. 98-118.
- [9] Hertzberg, R.W.: Deformation and Fracture Mechanics of Engineering Materials, 4th Edn., John Wiley and Sons, Inc., 1996, pp. 298-303.
- [10] Hertzberg, R.W.: op. cit., p. 3.
- [11] Holman, J.P.: op. cit., p. 58.
- [12] "Standard Tests on Plastics," Bulletin 1GC (1988), Hoechst Celanese Corporation, 90 Morris Avenue, Summit, New Jersey 07901, p. 4.
- [13] "Designing with Plastic: The Fundamentals," op. cit., pp. 4-1 to 5.
- [14] "Specific Heat," Materials Technology Notes, Number 1, MTD-ATN-001B (1993), General Electric Company, One Plastics Avenue, Pittsfield, Massachusetts 01201 (available in a packet entitled "Applied Technology Notes").
- [15] Strong, A.B.: Plastics: Materials and Processing, 2nd Edn., Prentice-Hall, Inc., 2000, pp. 168-169.
- [16] Hertzberg, R.W.: op. cit., p. 28.

SOURCES OF SUPPLIES: See Acknowledgements. It is also possible that plastics manufacturers will supply specimens and accompanying material property data sheets, thus allowing a more appropriate literature comparison to be made.

ACKNOWLEDGEMENTS: Dr. Jerry L. Wickman, Director, Plastics Research and Education Center, Ball State University, Muncie, IN, kindly provided the ABS tensile specimens with useful material description/properties. Special thanks to Mark A. Elban for re-analyzing all of the experimental data leading to preparation of Tables I to IV. Dr. John

D. Williams, Lab Manager, Mechanical Testing Instructional Laboratory, University of Illinois, Urbana-Champaign, provided helpful insights into tensile testing, especially specimen displacement measurements.

Wayne L. Elban

Since 1985, Professor Elban has taught engineering science courses at Loyola College, including introductory materials science, materials science lab, mechanical properties of materials, and transformations in solids. He received a BChE with distinction ('69) and a PhD in Applied Sciences: Metallurgy ('77) from the University of Delaware and a MS in Engineering Materials ('72) from the University of Maryland, College Park. From 1969-1985, he was a research engineer at the Naval Surface Warfare Center, White Oak Laboratory, Silver Spring, Maryland. He is a member of ASM International.

**FRICITION AND LUBRICATION OF HIGHLY
DEFORMABLE POROUS BEARINGS:
LEARNING FROM THE ARTICULAR
CARTILAGE OF HUMAN JOINTS**

Michael A. Soltz

and

Gerard Ateshian

Columbia University in the City of New York
Department of Mecanical Engineering
500 West 120th Street
New York, New York 10027



Michael A. Soltz

Friction and Lubrication of Highly Deformable Porous Bearings: Learning From Articular Cartilage of Human Joints

Michael A. Soltz and Gerard A. Ateshian
Department of Mechanical Engineering
Columbia University
New York, NY

Diarthrodial joints such as the knee, hip, or elbow provide the wide range of motion between body segments required for activities of daily living. Diarthrodial joints share a common structure (Figure 1) with a joint cavity surrounded by capsular ligaments that provide stability to the joint. The inner lining of the capsule secretes synovial fluid as well as absorbs waste products from cellular activity. The synovial fluid is a clear, yellowish, viscous fluid which aids in the nutrition of the avascular articular cartilage which is the bearing material lining the end of the bones; it is also believed to act as a lubricant for the joint. Articular cartilage is a deformable porous hydrated connective tissue, 1 to 6 mm in thickness, able to provide smooth, nearly frictionless motion under large time-varying loads (upwards of 3 to 5 times body weight) at low sliding speeds. Despite the harsh loading conditions of diarthrodial joints, cartilage normally remains functional for nearly seventy to eighty years in humans, due its remarkable tribological properties. When mechanical breakdown of the cartilage does occur, the joint progresses toward osteoarthritis, which is a common joint degenerative disease. Thus, understanding the tribology of diarthrodial joints provides insight into the osteoarthritic process which can potentially improve existing clinical treatment modalities. A number of theories have been proposed over the past several decades to explain the frictional properties of articular cartilage, though the precise mechanism of cartilage lubrication has not been fully elucidated. This paper briefly reviews the previous literature and summarizes some of our advances in this field which can provide a clearer understanding of the mode of lubrication inside our joints.

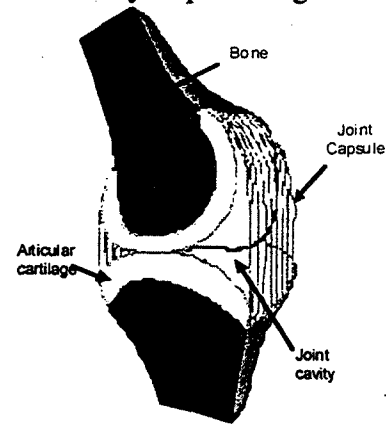


Figure 1. Generic articular joint

For nearly seven decades researchers have hypothesized various modes of lubrication in diarthrodial joints in order to explain the particularly low measured friction coefficient of articular cartilage. The earliest hypothesis proposed was that diarthrodial joints operate in the hydrodynamic lubrication mode, whereby the opposing articular surfaces are separated by a thin film of synovial fluid lubricant; as the fluid is entrained into the narrow gap separating the surfaces, it would pressurize and support the load acting across the joint (MacConaill, 1932). However, for this mode to be viable, the thickness of the fluid film would have to exceed the surface roughness of articular cartilage, which varies from 1 to 6 μm , and standard analyses demonstrated that this would not be possible given typical values of the sliding speeds, joint loads, and viscosity

of synovial fluid. Therefore this mode of lubrication may only be realistic if the loads are small and the relative sliding velocities are high, as may happen in lower extremity joints in the swing phase of walking. As a refinement to this theory, Dintenfuss (1963) proposed that the hydrodynamic pressure in the lubricant would cause deformation of the articular surfaces that may promote a sufficiently thick lubricant film; using this elastohydrodynamic model however, subsequent calculations demonstrated that the film thickness would still remain below the cartilage surface roughness. To address this limitation, Dowson and Jin (1986) proposed that micro-elastohydrodynamic lubrication may prevail in joints, whereby the articular surface asperities would be flattened under the hydrodynamic pressure, making this mode of lubrication viable. While this model appeared promising, theoretical calculations demonstrated that the predicted cartilage friction coefficient under this mode of lubrication would be much smaller than that measured from experiment, suggesting that another mode may prevail in joints.

In contrast to these previous authors, Charnley (1959, 1960) argued that the high loads, low sliding speeds and reciprocating motion of diarthrodial joints provided inadequate conditions for fluid film lubrication; he proposed that the more likely mode would be that of boundary lubrication and he experimentally demonstrated friction coefficients in the range 0.005-0.023. Further evidence refuting hydrodynamic lubrication was also provided by McCutchen (1966) and others. Since hydrodynamic lubrication is dependant upon the viscosity of the lubricant, this author used hyaluronidase to decrease the viscosity of the synovial fluid and he observed no noticeable changes in the friction coefficient of articular cartilage when compared to the untreated synovial fluid. He hypothesized that synovial mucin, a component of synovial fluid, may act as a boundary lubricant under small loads; similarly, Radin and coworkers (1970) and Swan and coworkers (1981) extracted a glycoprotein which they called lubricin and which they proposed as the candidate boundary lubricant of cartilage. Instead, Hills and Butler (1984) suggested that a phospholipid (dipalmitoyl phosphatidylcholine or DPPC) was the boundary lubricant of synovial fluid and that DPPC contaminated the lubricin extracted by Swann et al. Several studies on synthetic surfaces confirmed that either lubricin or DPPC could reduce the friction coefficient under boundary lubrication, though not to the low values observed experimentally in cartilage.

Further experimentation on the frictional properties of cartilage revealed a time dependant response of the friction coefficient. After initial loading of the tissue the friction coefficient could increase from a value as small as 0.002 up to 0.15 in 30 minutes, suggesting that cartilage maintains good frictional properties only under transient conditions. McCutchen (1959) attributed this phenomenon to a hydrostatic pressure developing within the cartilage interstitial fluid which drives fluid into the gap between the articular surfaces, thus acting as a "self-pressurized" hydrostatic bearing. Under this proposed mode of lubrication, only a small component of the contact stress would be borne by the solid matrix resulting in a small friction coefficient. As the pressure decreases the friction coefficient would increase. McCutchen termed this new mechanism "weeping lubrication". Conversely, Walker and coworkers (1968) attributed the time varying friction coefficient to another proposed mode termed "boosted lubrication" where

pools of synovial fluid would be trapped between the contacting micro-asperities of the opposing articular surfaces. These pools would pressurize when loaded, supporting the majority of the applied stress and reducing the friction. Over time the low-viscosity components of the fluid would filter into the tissue leaving behind a viscous gel of hyaluronan which may then act as a boundary lubricant. However, subsequent theoretical squeeze-film lubrication analyses performed by Hou and coworkers (1992) suggested that the transient response for such a mechanism has a time constant of a few seconds and could not explain the much longer transient response of the friction coefficient observed experimentally.

In parallel to the progress reported on the measurement and analysis of cartilage lubrication, major advances have taken place in the last two decades in understanding the complex mechanics of articular cartilage. Through the work of Mow and coworkers (1980, 1992) it has been shown that porous media theories can successfully predict the experimentally measured response of articular cartilage under various loading conditions, thereby attributing the viscoelasticity of this tissue to the viscous drag of the interstitial fluid flowing within the porous-permeable solid matrix. From theoretical analyses of contacting articular layers modeled using solid-fluid mixture theory, it has been confirmed that the interstitial water of articular cartilage pressurizes considerably under loading and that the time constant for the duration of this pressurization under a prescribed load is on the order of 1,000 seconds or greater (Ateshian et al., 1994; Ateshian and Wang, 1995; Kelkar and Ateshian, 1999). From these same studies it has been observed that even in the absence of a synovial fluid film separating the articular surfaces, the interstitial fluid pressure at the contact interface still contributes in excess of 90% of the total applied load for physiological durations of loading (up to a few hundred seconds). (In contrast, in fluid film lubrication, 100% of the load would be supported by the pressurized fluid film lubricant.) Therefore, from these studies, we concluded that the porous-permeable cartilage naturally imparts a form of mixed lubrication at the contacting interface of articular layers where the fluid pressure supports most, but not all, of the load transmitted across the joint; unlike squeeze-film lubrication which may last for only a few seconds, the very low permeability of articular cartilage prevents a rapid loss of the fluid pressurization thereby maintaining favorable conditions for much longer durations. This interpretation is closest in agreement with the mechanism proposed by McCutchen (1959) and later by Malcom (1976) where the time dependent behavior of the friction coefficient relies on the developed interstitial fluid pressure. Importantly however, our proposed mechanism functions regardless of the direction of fluid flow at the contact interface; thus, in our model, there is no need to appeal to a "weeping" or "boosted" lubrication mechanism to explain the frictional response of cartilage.

A theoretical formulation of this new friction model was developed and was demonstrated to provide predictions of the cartilage frictional response consistent with previously reported experimental findings (Ateshian, 1997). Subsequently we performed our own experimental friction measurements and demonstrated direct agreement between theory and experiment (Ateshian et al., 1998). The formulation of this model employed the theory of mixtures, recognizing that the contact of biphasic (solid-fluid mixture)

materials involves solid-solid, solid-fluid, and fluid-fluid interactions at the contacting surfaces when in the absence of a fluid film lubricant. Because of the paramount role of interstitial fluid pressurization in the formulation of this theory, we performed parallel experiments of cartilage loading to demonstrate that the predictions of interstitial fluid pressurization from the biphasic theory of Mow et al. (1980) indeed agreed accurately with experimental measurements. Thus, we used a novel approach to measure the cartilage interstitial fluid pressure (Soltz and Ateshian, 1998, 1999) in a one-dimensional loading configuration, during static and dynamic loading. Remarkably we found nearly 100% of the applied load to be supported by fluid pressure for several hundred seconds after load application in the static tests (Figure 2); we also observed that under dynamic loading, the fluid pressure does not subside even over four decades of loading frequencies (Figure 3). These results clearly demonstrate the significance of the fluid pressurization in supporting the applied load and its role in shielding the solid matrix from damaging stresses. Using our friction model we have been able to successfully predict the measured friction coefficient of cartilage in the configuration of unconfined compression stress-relaxation as shown in Figure 4. From both theory and experiment, it can be observed that the friction coefficient achieves its lowest value when the fluid pressure is at its peak; as the fluid pressure subsides and a greater portion of the applied load shifts to the solid collagen-proteoglycan matrix, the friction coefficient increases, confirming that interstitial fluid pressurization regulates the frictional response of articular cartilage. These results not only help validate our theoretical cartilage friction model but also demonstrate an appreciable advance in our understanding of the tribology of articular cartilage. While it had long been recognized that fluid pressurization occurs within the tissue under loading, it now has been verified from our studies that it is a fundamental mechanism essential for the normal function of articular cartilage.

Acknowledgement: This study was supported by a grant from the National Institutes of Health (AR43628).

References:

1. Ateshian, G.A., Wang, H., Lai, W.M. (1998) The role of interstitial fluid pressurization and surface porosities on the boundary friction of articular cartilage. *J. Tribology, ASME*, 120:241-251.
2. Ateshian, G.A., (1997) A theoretical formulation for the boundary friction in articular cartilage. *J. Biomech. Eng.*, ASME, 119:81-86.

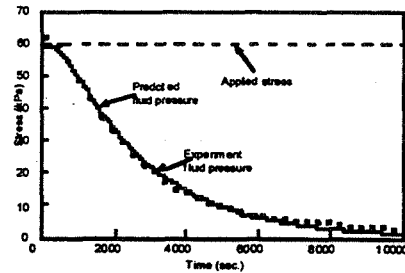


Figure 2. Experiment and predicted fluid pressure under constant applied stress

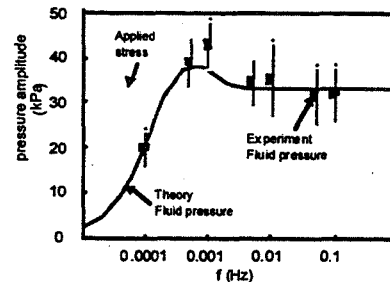


Figure 3. Frequency spectrum of interstitial fluid pressure

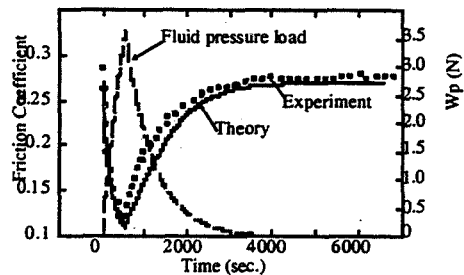


Figure 4. Experimental and predicted friction coefficient with predicted fluid pressure.

3. Ateshian G.A., Lai, W.M., Zhu, W.B., Mow, V.C. (1994) An asymptotic solution for two contacting biphasic cartilage layers. *J. Biomech.*, 27:1347-1360.
4. Ateshian G.A., Wang H. (1995) A theoretical solution for the rolling contact of frictionless cylindrical biphasic cartilage layer. *J. Biomech.* 28:1341-1355.
5. Charnely, J., (1959) The lubrication of animal joints. In: *Symposium on biomechanics IMechE*, London, pp. 12-22.
6. Charnely, J. (1960) The lubrication of animal joints in relation to surgical reconstruction by arthroplasty. *Ann. Rheum. Dis.* 19:10-19.
7. Dintenfuss, L. (1963) Lubrication in synovial joints: A theoretical analysis. *J. Bone Joint Surg.* 45A:1241-1256.
8. Dowson D. and Jin, Z.M. (1986) Micro-elastohydrodynamic lubrication of synovial joints. *Eng. Med.* 15:63-65.
9. Hills, B.A., Butler B.D. (1984) Surfactants identified in synovial fluid and their ability to act as boundary lubricants. *Ann Rheum. Dis.* 43:641-648.
10. Hou, J.S., Mow, V.C., Lai, W.M. and Holmes, M.H. (1992), Squeeze film lubrication for articular cartilage with synovial fluid. *J. Biomech.* 25:247-259.
11. Kelkar R., Ateshian, G.A. (1999) Contact creep of biphasic cartilage layers: Identical layers. *J. App. Mech.*, ASME, 66:137-145.
12. MacConaill, M.A., (1932) The function of intra-articular fibrocartilages, with special references to the knee and radio-ulnar joints. *J. Anat.* 66:210-227.
13. Malcom, L.L., (1976) An experimental investigation of the frictional and deformational response of articular cartilage interface to static and dynamic loading. PhD, University of California, San Diego.
14. McCutchen, C.W., (1959) Sponge-hydrostatic and weeping bearing. 184:1284.
15. McCutchen, C.W., (1966) Boundary lubrication by synovial fluid: demonstration and possible osmotic explanation. *Fed. Proc.* 25:1061.
16. Mow, V.C., Kuei, S.C., Lai, W.M., Armstrong, C.G. (1980) Biphasic creep and stress relaxation of articular cartilage in compression: Theory and experiments. *J. Biomech. Eng.*, ASME 102:73.
17. Mow, V.C., Ratcliffe, A., Poole, A.R. (1992) Cartilage and diarthrodial joints as paradigms for hierarchical materials and structures. *Biomaterials* 13:67-97.
18. Radin, E.L., Swan D.A. and Weisser, P.A., (1970) Separation of a hyaluronate-free lubrication fraction from synovial fluid. *Nature* 228:377-378.
19. Soltz M.A., Ateshian, G.A. (1998) Experimental verification and theoretical prediction of cartilage interstitial fluid pressurization at an impermeable in confined compression. *J. Biomech.*, 31:927-934.
20. Soltz M.A., Ateshian, G.A. (1999) Interstitial fluid pressurization during confined compression cyclical loading of articular cartilage. *Ann. Biomed. Eng.*, In Press.
21. Swann D.A., Hendren, R.B., Radin, E.L., Sotman, S.L., Duda, E.A. (1981) The lubricating activity of synovial fluid glycoproteins. *Arthritis and Rheumatism* 24:22-30.
22. Walker, P.S., Dowson, D., Longfield, M.D., and Wright, V. (1968) "Boosted lubrication" in synovial joints by fluid entrapment and enrichment. *Ann. Rheum Dis.* 27:512-520.

**EXPERIMENTS IN MAGNETICS
FOR TELECOMMUNICATIONS:
ORGANIC AND SOL-GEL**

James V. Masi

Northeast Center for Telecommunications Technologies
1 Armory Square
Springfield, Massachusetts 01105

Telephone 413-731-3155
e-mail masi@stcc.mass.edu



James V. Masi

EXPERIMENTS IN MAGNETICS FOR TELECOMMUNICATIONS: ORGANIC AND SOL-GEL

James V. Masi
Northeast Center for Telecommunications Technologies
Springfield, MA 01105
(413)731-3155, FAX (413)734-0515
masi@stcc.mass.edu

KEY WORDS: Sol-gel, polymers, magnetics, nanoparticles.

PREREQUISITE KNOWLEDGE: The student should be familiar with the basics of materials science, metallography, and chemistry. Levels at which these experiments are performed are second semester junior year and either semester senior year. The students are first given lectures the properties of materials produced by sol-gel methods and one lecture on organic magnetic and conducting polymers. They should have already had a laboratory experiment on metallography and sample preparation.

OBJECTIVES: The objectives of these experiments are to show the area of fabrication of sol-gel magnetic ceramic materials and magnetic polymer (organic molecular materials), especially the similarities associated with the apparently disparate materials. These experiments contain all of the elements of good design, with the caveat that a novelty in structure is sometimes a part of design. The students learn the process of designing materials for the world of telecommunications, analyze those already used, and suggest possible solutions to the problems involved with present technology.

EQUIPMENT AND SUPPLIES:

- (1) Metallurgical preparation and polishing apparatus (eg. Buehler Co.).
- (2) Chlorides of nickel, iron, and zinc; ammonium hydroxide; nitric acid; ethylene-diamine-tetra acetic acid salt; hydrochloric acid; phenylene vinylene monomer; (eg. Fisher Scientific).
- (3) Miscellaneous graduates, glassware, alumina firing boats, and furnaces(Fisher Scientific),
- (4) Magnets (Edmund Scientific).
- (5) Alumina substrates (Kyocera); miscellaneous meters and power supplies.
- (6) Metallurgical microscope (Olympus, Zeiss, etc.).
- 7) SEM with EDAX (optional).

INTRODUCTION:

New organic and sol-gel technologies have allowed the experimenter to turn designs into a world of size control, materials properties, and new materials hard to realize by other more arduous methods. The importance of size and crystallite perfection with respect to properties of finished devices has, only recently, been shown to be one of many critical parameters vital to high performance magnetic devices. The realm of very high and very low frequency devices seem to benefit most from the unique properties attainable from these sol-gel methods. Low temperature scenarios seem to benefit most from the use of the new organic materials. The advent of creating organic electromagnetic materials has raised the challenge of finding polymer (organic) materials in which there is sufficient electronic exchange as well as stability in both the thermal and chemical arena. This experiment gives an overview of how to build and synthesize promising new complex polymer building blocks and sol-gel nanoscale materials which can yield superparamagnetic materials for devices of the future in power, storage, displays, and communications devices. The underlying principles and formulations of molecular and sol-gel structures which either imitate conventional ferromagnetic materials or uniquely take advantage of the very small and very complex magnets offered by organic materials and sol-gel formulations. A wide variety of properties may be obtained, dependent on pH, concentrations, impurities, polymer type, dopants, etc. Applications of these materials to transformers and inductors are detailed, and the underlying principles and formulations of both equilibrium and non-equilibrium materials are explained. The experiments are simple to perform and make great demonstrations of ferro-, ferri, and molecular magnetism.

EXPERIMENTS:Sol-gel materials

There are few materials which capture the essence and the mystery of materials science as those which can be fabricated by gel and sol-gel methods. The unique properties and the control of the chemistry

leading to these properties make these methods excellent teaching, research, and learning tools. Certain of these synthetic materials are now deemed potentially useful as magnetic materials for such applications as magnetic devices (transformers, inductors, etc.), high frequency magnetic and electromagnetic devices, shielding materials, and magneto-optic devices. The development of sol-gel methods for the production of nanoscale materials allows the scientist to tailor both properties and physical characteristics in fabrication by thick film, casting, firing or baking, dipping, or spraying. These methods produce nanoparticulate materials which have properties different from those formed by conventional chemical and calcining techniques. Tests involving SEM, conventional optical microscopy, and x-ray diffraction techniques are employed. A section on background theory¹ is given in the Appendix for use as a reference for the researcher. There are different forms of sol-gel technology (See Appendix A). The one chosen for these experiments involves the use of an organic compound as the complexing agent. The organic compound is ethylene-diamine-tetra acetic acid (EDTA). One of the reasons EDTA was chosen is because it bonds well with most metallic elements and that it is comprised of an amine and an acid, fundamental for the gel.

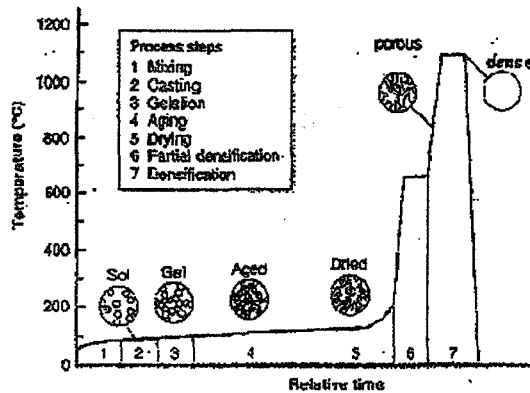


Figure 1
Stages of sol-gel

Figure 1 shows a typical depiction of the stages of the sol-gel process. Nanoparticles (particles with sizes in the range of a tens of nanometers) form up to and including step five. Some growth occurs in step six, and even larger particles result from firing (sintering) in stage 7. In this experiment, the regions 1 through 6 are pertinent to the unique properties obtained by sol-gel processes. It is these regions which we will use for most of the materials described.

The change in properties for magnetic materials at the nanocrystalline size scale are the following: (a) Initially there is an increase in the magnetic coercivity down to a critical crystallite size in the nanoscale size regime; and (b) below a critical crystallite size, there is a decrease in coercivity leading to superparamagnetic behavior, high frequency response, and higher than expected permeabilities at these frequencies¹¹. This approach initially involves the complexing of aqueous solutions of iron, nickel, and zinc cations in complex nitrate gels. This method consists of complexing the solution with two mole citric acid/mole of cation and adjusting the pH of the mixture with ammonium hydroxide in the range of 7 to 11, dependent on the morphology of the powder desired. The solutions used FeCl_3 , NiCl_2 , and ZnCl_2 in an aqueous solution. Ethylene diamine tetraacetic acid salt (EDTA) are added to obtain the sol-gel, typical of that shown in Figure 2. The pH is adjusted upward and downward using aqueous NH_4OH and HCl respectively. The compounds formed are $\text{Fe}_2(\text{Ni}_x\text{Zn}_{(1-x)})\text{O}_4$ with $x = 0.8$.

Once processed, all of the above yields are added together to form one mixture, which is then ready to be processed further. The metal and nitrate mixtures are combined are then heated at 220°C until a dark, reddish brown foam (the oxide) forms from the gel (approximately 15 minutes). The "foam" is ground to obtain a very fine powder, shown in Figure 2.

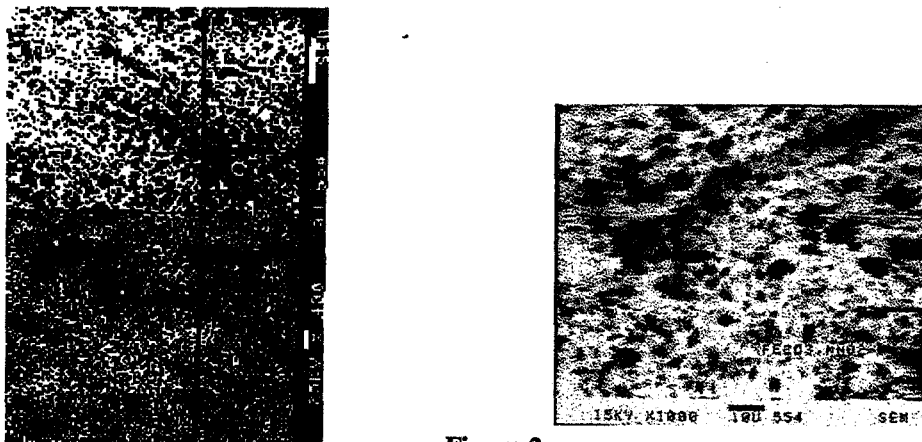


Figure 2
First fired foam/powder

The powder is then fired in an aluminum oxide crucible according to a schedule, shown in Figure 1 up to step 5. The powder is then either pressed into bulk forms or processed in polymer binder (>80w/o powder to polymer) for thick film screening onto alumina. The vehicle/polymer is composed of polyimide or epoxy. Using a screen printer and using alumina or printed circuit board substrates, the films are printed 150 microns off contact with 3 psi squeegee pressure through a 200 mesh screen. This produces films ranging in thickness from 3 to 27 microns. The disks or thick films are then fired according to a schedule shown in Figure 1 up to step 5 (on a printed circuit board) or up to step 7 (on alumina) or cured (if polymer binder remains) at 150° C. Variations on the samples produced can range from solids to "packed" powders.

Tests involving SEM, conventional optical microscopy, and x-ray diffraction techniques are employed. A section on background theory¹ is given in the Appendix for use as a pre-lab lecture or as reference for the student and laboratory instructor.

Organic Magnetic Materials

The experiments in this section are for reference only. They are advanced in both preparation and concept and should be given at the discretion of the instructor. An overview is given in Appendix 2.

New Organic Magnetic Materials Design

Since standard stand-alone materials gave way to polymeric techniques, the possibilities of cooperative phenomena became more feasible. Since magnetic materials are only useful below their Curie temperature, this temperature should be substantially above room temperature. In fact, to obtain these higher Curie temperatures, one must induce some order (local disorder leads to random and inconsistent interactions). In 1985, the first molecule based magnetic materials were reported.^{5,6} These materials were ionic salts (containing alternating donors and acceptors, of tetracyanoethylene and tetracyanoquinodimethane, TCNE and TCNQ in a "...DADA..." configuration, producing high multiplicity spin radicals. A ferromagnetic $[\text{FeCp}^*_2]^+ [\text{TCNE}]^-$ forming chains of alternating donors (cations) and acceptors (anions) can be modified from ferromagnetic to metamagnetic by replacing TCNE with TCNQ or when $[\text{C}_3(\text{CN})_3]^-$ is added magnetic coupling is no longer effective. (Cp^* is pentamethylcyclopentadienide). A symbolic representation is shown in Figure 3.⁹

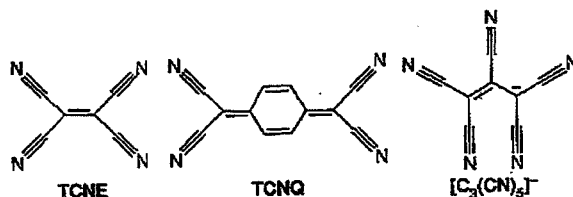


Figure 3
TCNE and TCNQ salts with ...DADA...

Up to 1991, the Curie temperatures were low, only in the tens of degrees Kelvin. Though the performance in magnetization in all forms of magnetic behavior seem to degrade with increasing temperature, a few materials show promise for the future.⁹ Some of these are shown in Figures 4 and 5.

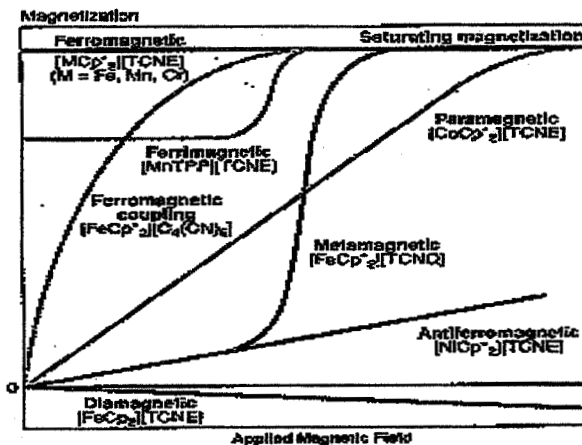


Figure 4
Magnetization vs applied magnetic field for some materials

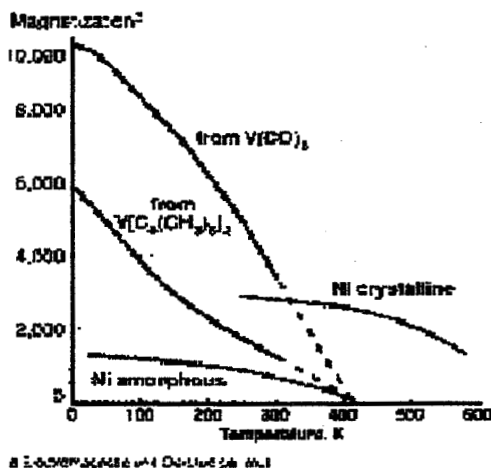


Figure 5
Vanadium salt $V(TCNE)_x \cdot y(CH_2Cl_2)$
prepared from $V(CO)_6$

As can be seen from the figures above, the magnetic behavior, magnetization, and temperature profile vary greatly with host (TCNE, TCNQ, etc.), salt (vanadium, iron, cobalt, nickel, etc.) and precursor. These polymers, especially the $V(TCNE)_x \cdot y(CH_2Cl_2)$, can be formed from the monomer and initiated with a peroxide initiator. Standard safety common to other cyano organic compounds should be observed. As mentioned previously in this paper, these are experiments which are both advanced and should be given at the discretion of the instructor.

Electrical Measurements

Electrical measurements are made with screened contacts in a 4-point probe arrangement. Early measurements^{11, 12} indicate that these materials are semiconductor-like in their. Devices are also made by immersing a coil, as shown in Figure 6, in a polymer sol-gel or molecular magnetic mixture. It should be noted that "planar magnetic" devices are made with similar coil structures but have prefired, large crystallite materials as their core and the coils are not "immersed in the "core". Due to the conductive nature of some of these materials, insulating coatings are necessary to prevent losses due to shunting the metallic coil.

(Courtesy of Philips Magnetics)

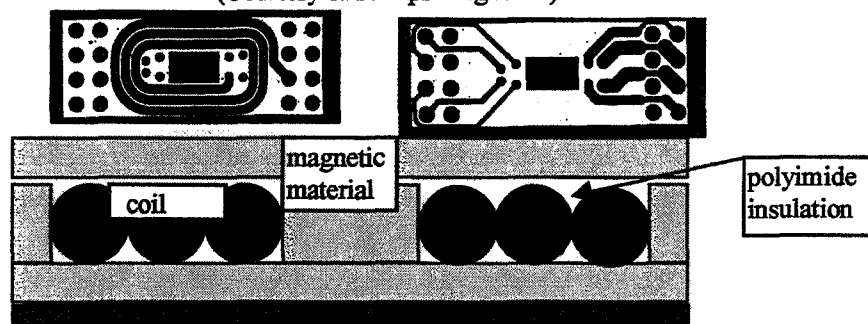


Figure 6
Coil Configurations for Test

Magnetic Testing

Impedance measurements, giving the relative permeability and dielectric constant as well, and multi-port tests on the materials can be made on an 8700 series HP Network analyzer as shown in Figure 7. "Donuts" were 3 mm thick, made to fit in the coaxial air line.

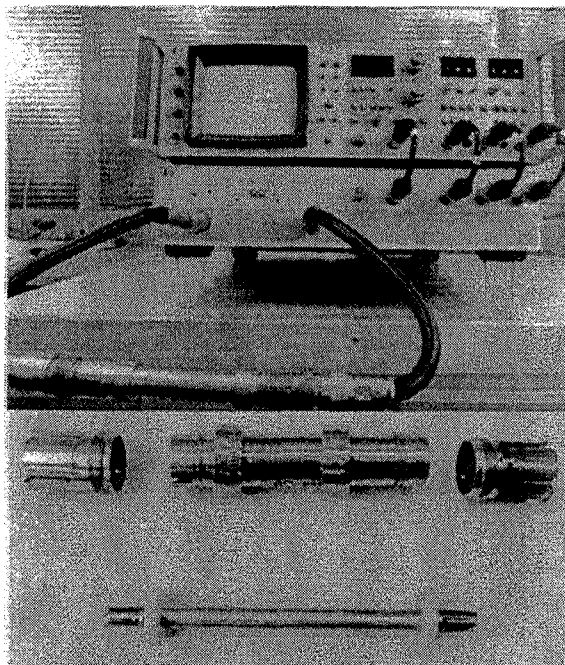


Figure 7
Network Analyzer/Coaxial Setup

High frequency measurements vary on the molecular materials with the vanadium salts showing permeabilities of 30 at room temperature at 100 MHz. More work needs to be performed on these materials at high frequencies to determine what models are justified by these measurements. Permeabilities in excess of 80 have been measured for sol-gel materials at 250 MHz, as shown in Figure 8.

Wt.% Sol-Gel Ferrite in Polymer vs Permeability

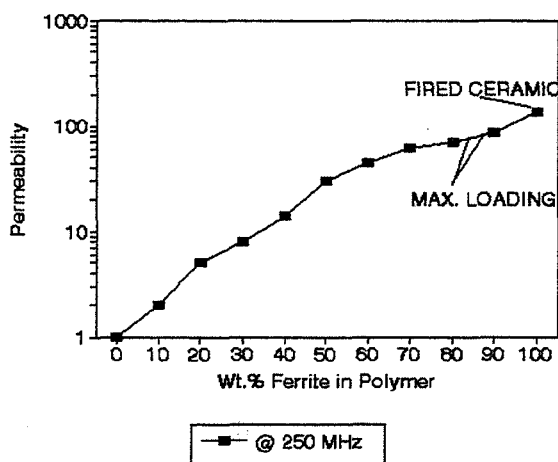


Figure 8
Polymer/Ferrite Loading

As with the molecular materials, much work needs to be done to further characterize and exploit the unique properties of these new magnetic materials. Students should suggest methods of both materials fabrication and device testing. These suggestions should be incorporated into future experiments.

REFERENCES:

1. A. B. Ellis, et al., "Teaching General Chemistry: A Materials Science Companion", A.C.S. Books, 1993. pp.463-472.
2. H. B. Weiser, A Textbook of Colloid Chemistry, John Wiley, New York, 1949. pp. 2-4.
3. C. W. Turner, Atomic Energy of Canada Rept. No. AECL-8062. Chalk River Labs, Chalk River ONT., Canada, 1986.
4. R. L. Beatty, et al., Oak Ridge Nat'l Labs Rept. No. ORNL-5469, Oak Ridge, TN, 1979.
5. J. S. Miller and A. J. Epstein, *J. Am. Chem. Soc.*, **109**, 3850 (1987).
6. J. M. Williams *et al.*, *Acc. Chem. Res.*, **18**, 261 (1985).
7. G. Allinson *et al.*, *J. Mat. Sci.: Mat'ls in Electr.*, **5**, 67 (1994).
8. D. Gatteschi, *Adv. Mat.*, **6**, 635 (1994).
9. J. S. Miller and A. J. Epstein, ed. "Proceedings of the Conference on Molecule-Based Magnets," *Molec. Cryst., Liq. Cryst.*, 271-274 (1995).
10. A. Lukasiewicz, *et al.*, *Mat. Lett.*, **14**, 127 (1992).
11. J. V. Masi and W. Thibault, *New, High Frequency Transformer Topologies*, in Proc. of the EMCWA, IEEE Press, N.J., 1995, pp 157-162.
12. J. S. Miller and A. J. Epstein, *C & EN*, 30, Oct. 2, (1995).

APPENDIX A1 Sol-Gels

Introduction¹

Sols are dispersions of colloidal (solid) particles (size 1-100 nm) in a liquid phase where the particles are small enough to remain suspended, almost indefinitely, by Brownian motion⁴. For aqueous sols this implies a particle size of under 1 mm. Sols are called lyophobic (weak solvent-particle interaction) and

lyophobic (relatively strong interaction). A gel is an interconnected, rigid network with pores of submicrometer dimensions and polymeric chains whose average length is greater than a micrometer and the solid and liquid are in a highly dispersed state. One of the most important conditions for gel formation is that a strong solvent-particle interaction exists, in order to bind a large amount of the solvent.

The sol-gel process is the name given to any one of a number of processes that involve a solution or sol that undergoes a transition to a rigid, porous mass, a gel. These processes can be divided into two categories: aqueous-based processes that start from a solution of a metal salt^{2,3} and the alcohol based processes that initiate from metal aloxides.⁴ A Typical schematic diagram of the metal aloxide process is shown in Figure A1.

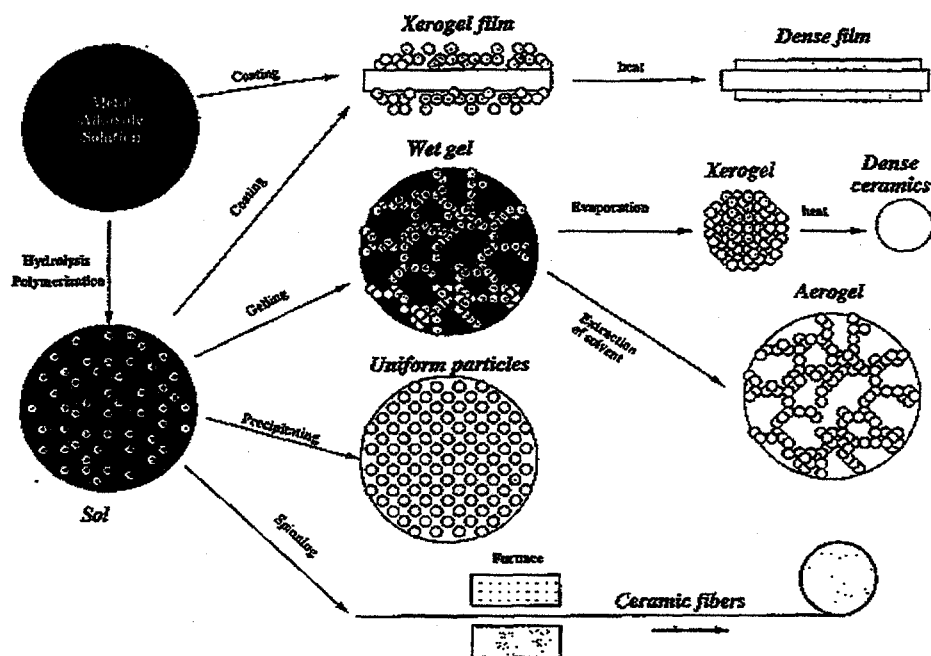


Figure A1-1

Sol-Gel Schematic and Typical Products

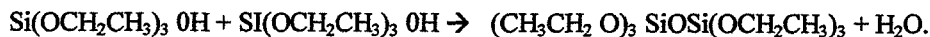
A particular example of a sol-gel process which is easier to understand than the magnetic oxide reaction is the reaction of $\text{Si}(\text{OCH}_2\text{CH}_3)_4$, ethanol, and water. These three reactants form a one-phase solution that goes through a sol-gel transition to a rigid, two-phase system of solid silica (SiO_2) and solvent-filled pores. The fundamental reaction of the sol-gel process is hydrolysis and polymerization of a silicon alkoxide. Hydrolysis occurs when $\text{Si}(\text{OCH}_2\text{CH}_3)_4$ and water are mixed in a mutual solvent, generally ethanol:



The intermediates that exist as a result of partial hydrolysis include molecules with Si-OH groups, which are called silanols. Complete hydrolysis of $\text{Si}(\text{OCH}_2\text{CH}_3)_4$ to $\text{Si}(\text{OH})_4$ would yield silicic acid, but complete hydrolysis does not occur. Instead, condensation may occur between either two silanols or a silanol and an ethoxy group to form a bridging oxygen or a siloxane group

(-Si-O-Si-), and a water or ethanol molecule is eliminated. An example of the condensation

between two silanols with the elimination of water is

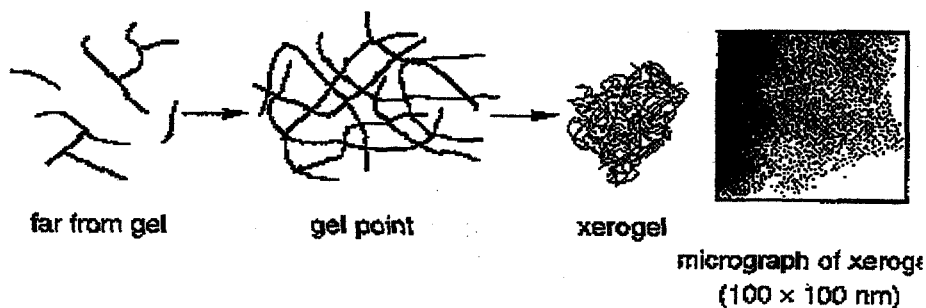


Then hydrolysis of $(\text{CH}_3\text{CH}_2\text{O})_3\text{SiOSi}(\text{OCH}_2\text{CH}_3)_3$ will produce, as one possibility, $(\text{CH}_3\text{CH}_2\text{O})_3\text{Si}(\text{OH})\text{OSi}(\text{OCH}_2\text{CH}_3)_3$ that can undergo further polymerization. When a sufficient number of interconnected

Si-O-Si bonds are formed in a region, they interact cooperatively to form colloidal particles or a sol. With time, the colloidal particles and condensed silica species link together to form a three-dimensional network. At gelation, the viscosity increases sharply, and a solid object in the shape of the mold results. The product of this process at the sol-gel transition is called an *alcogel*. Once through the sol-gel transition, the solvent phase can be removed. If it is removed by conventional drying, such as evaporation, *xerogels* result. If it is removed via supercritical (high-temperature) evacuation, *aerogels* result.

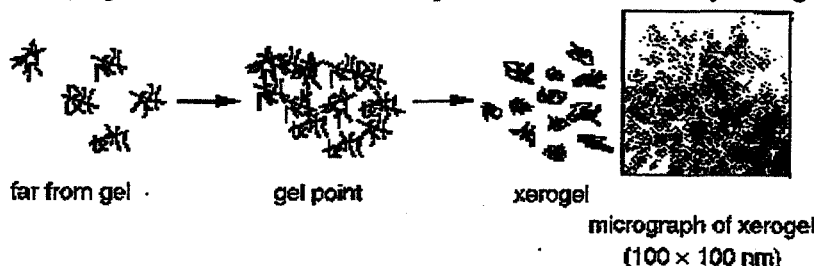
Acid-Catalyzed Reaction

At low pH levels, that is, acidic conditions (slow hydrolysis), the silica tends to form linear molecules that are occasionally cross-linked. These entangle and form additional branches, resulting in gelation.



Base-Catalyzed Reaction

Under basic conditions (faster hydrolysis), more highly branched clusters form that do not interpenetrate prior to drying and thus behave as discrete species. Gelation occurs by linking of the clusters.



Some advantages of sol-gel processing over conventional ceramic processing are:

1. Increased chemical homogeneity in multicomponent systems;
2. High surface area of the gel/powders, leading to relatively low sintering
3. Relatively high chemical purity is possible due to the absence of grinding and pressing; and
4. Product in the form of powders, fibers, coatings, and spheres are possible with simple solution controls, such as pH, temperature, aging, etc.

APPENDIX 2 Organic Magnetic Materials

When the early civilizations made the discovery that iron was indeed attracted to lodestone, the era of magnetism and its devices and effects was launched. After that time, the earliest device recorded was the compass, an invention of the Chinese. Since then, ferromagnetic (Fe, Ni, Co, etc.), ferrimagnetic (eg. F_3O_4), and paramagnetic materials have been used in technology applications such as magnets, magnetic tapes and disks, magnetic resonance imaging contrast enhancers, and magneto-optic memories, to name a few. Organic/molecular based materials, with *p* or *d* orbitals aiding the magnetic properties, have been a source of scientific curiosity for a number of years^{5,6}, but only recently have such materials become a reality^{7,8,9}.

This new class of magnetic materials is, for the most part, non-metallic, being made from simple to complex organic molecules. Their structure can be uni- or bi-dimensional and need not have the three-dimensional format necessary for conventional ferromagnetic, ferrimagnetic, paramagnetic, and antiferromagnetic materials. These materials can be simply fabricated from a variety of solvents at or near

room temperature. These should not be confused with bimetallic complexes such as those formed by pyrolysis or partial oxidation.¹⁰ Other work postulated the use of a new class of pi-biradicals called the non-Kekule polynuclear aromatics, shown in Figure A2-1 below.⁷ The high spin nature of these systems should drive ferromagnetic coupling in charge transfer complexes. This is best served by having the centers covalently bonded together, namely, a polymer system made up of repeating molecular segments sharing the framework of the high-spin systems, quinodimethanes based on the benzene, naphthalene, and biphenyl nuclei.

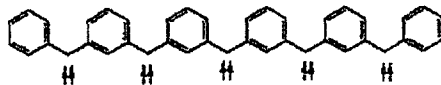
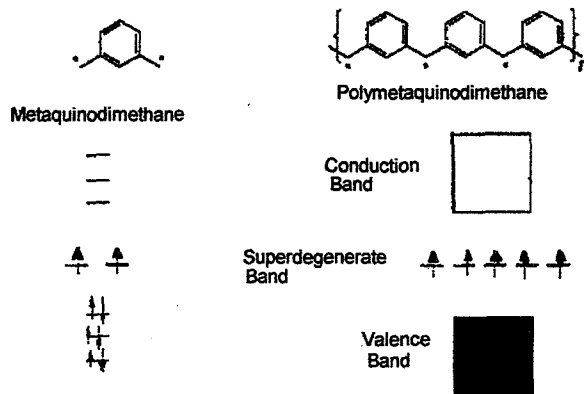


Figure A2-1

Representation of pi-molecular of metaquinodimethane, the associated spins, and an oligomer

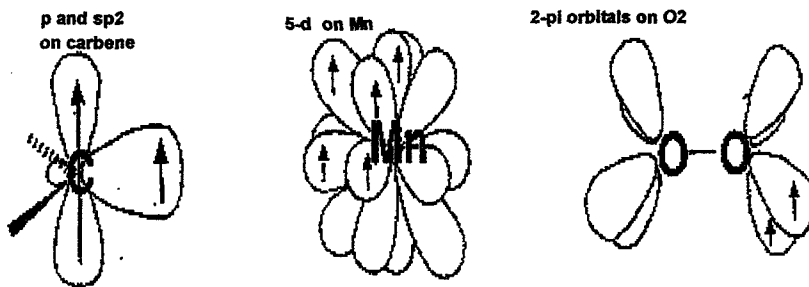


Figure A2-2

Possible model for magnetic spin coupling

Figure A2-2 shows a possible model for magnetic spin coupling where spins align in orthogonal orbitals in a small spatial region.³ Figure A2-3 shows six possible configurations of parallel and anti-parallel spins, along with canted ones for reference, to describe paramagnetic, ferromagnetic, antiferromagnetic, ferrimagnetic canted ferromagnetic, and correlated spin glass (disordered structure previously mentioned).

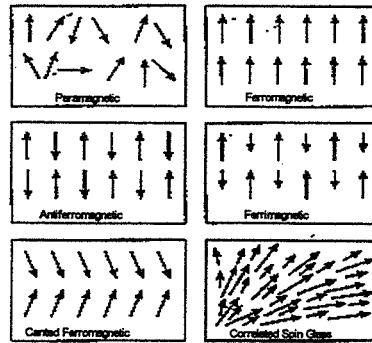


Figure A2-3
Spin configuration directions for magnetic types

**EFFECT OF TEMPERATURE ON THE IMPACT
BEHAVIOR AND DIMENSIONAL STABILITY
OF THERMOPLASTIC POLYMERS**

Wayne L. Elban

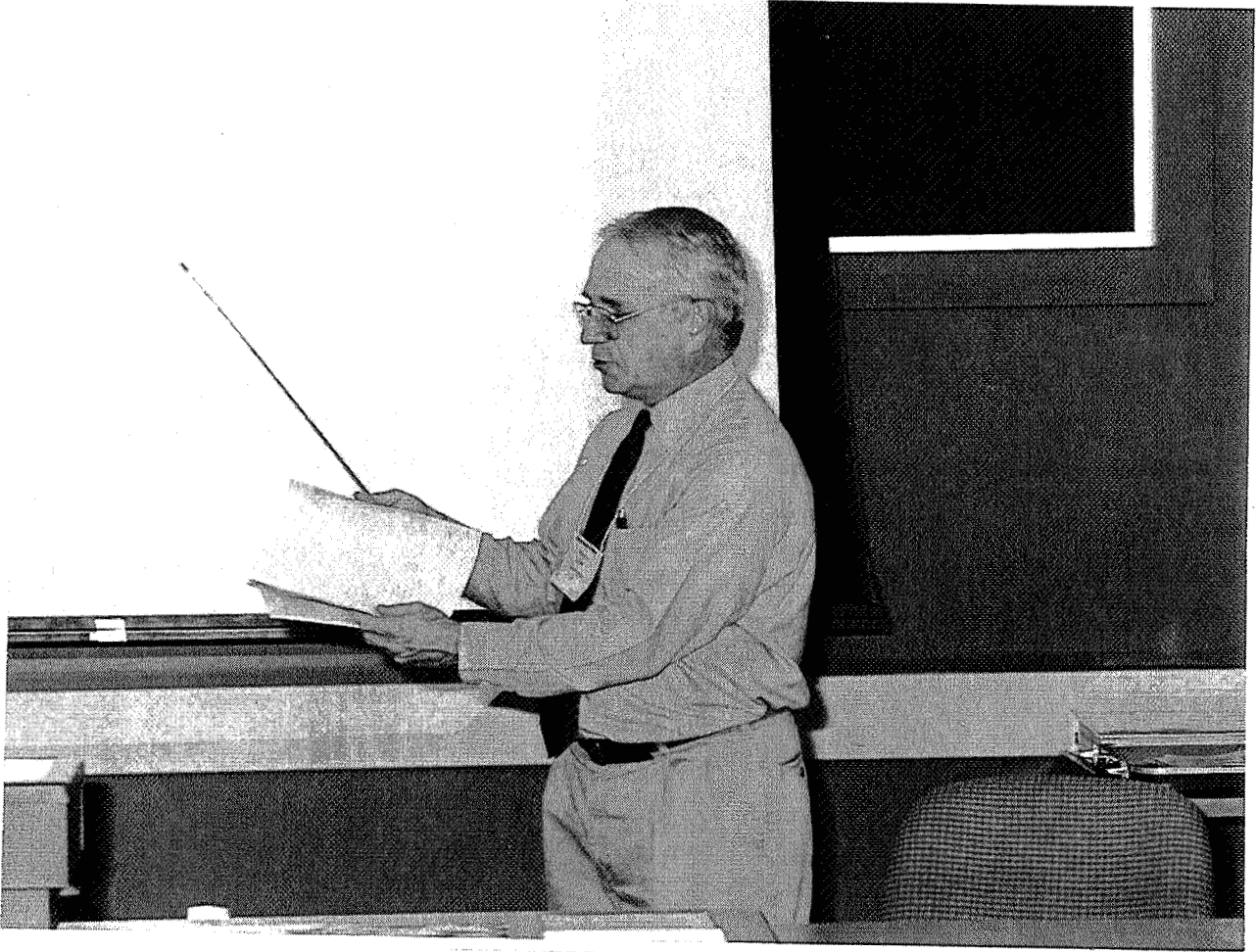
Department of Electrical Engineering and
Engineering Science
Loyola College
4501 North Charles Street
Baltimore, Maryland 21210

Telephone: 410-617-2853
e-mail welban@loyola.edu

and

Matthew J. Elban

Carroll Christian High School
Westminster, Maryland 21157



Wayne L. Elban

Effect of Temperature on the Impact Behavior and Dimensional Stability of Thermoplastic Polymers

Wayne L. Elban
Dept. of Electrical Engineering and Engineering Science
Loyola College
Baltimore, Maryland 21210

Matthew J. Elban
Carroll Christian High School
Westminster, Maryland 21157

ABSTRACT: A procedure is described for evaluating the brittle-ductile transition behavior of two thermoplastic polymers: acrylonitrile-butadiene-styrene (ABS) copolymer and recycled high density polyethylene (HDPE). A bench-top Charpy impact tester is used to make a quantitative evaluation of impact strength as a function of specimen conditioning (testing) temperature, which ranged from -196 to 120° C for ABS and to 135° C for HDPE. Additionally, the notch sensitivity of both materials is assessed by determining the impact strength of room temperature specimens with and without standard V-notches. The resultant fracture surfaces are visually inspected to determine its brittle/ductile character. The fracture surface and region immediately behind it are examined for stress whitening. The experimental determinations of impact strength are compared to values appearing in the literature for both materials. Thicknesses of recovered samples are measured, using a dial caliper, to study the dimensional stability of both polymers for the same temperature ranges.

KEY WORDS: Charpy impact testing, brittle-ductile transition behavior, notch sensitivity, dimensional stability, fracture, stress whitening, thermoplastic polymers, acrylonitrile-butadiene-styrene (ABS) copolymer, high density polyethylene (HDPE).

PREREQUISITE KNOWLEDGE: sophomore-level undergraduate laboratory experiment requiring basic knowledge of thermoplastic polymers and brittle versus ductile fracture behaviors as described in an introductory materials science course and accompanying laboratory course.

OBJECTIVES:

(a) Experimental Goals:

1. to measure the Charpy impact energies of V-notched specimens of two representative thermoplastic polymers as a function of temperature;
2. to measure the Charpy impact energies of specimens with and without standard V-notches for the same polymers;

3. to measure the room temperature thicknesses of impact specimens of two thermoplastic polymers exposed to various temperatures in order to assess their dimensional stability; and
4. to examine the resultant fracture surfaces to assess their brittle-ductile character and the occurrence of stress whitening.

(b) Learning Goals:

1. to become familiar with Charpy impact testing, a prominent technique for characterizing the dynamic mechanical response of materials;
2. to become familiar with the distinctive features of brittle and ductile fracture;
3. to become familiar with the effect of temperature on the properties of thermoplastic polymers, including transition temperature phenomena; and
4. to become familiar with notch sensitivity, an important material property relating to machining and fabrication processes.

EQUIPMENT AND MATERIALS: (1) Tinius Olsen Charpy impact tester (bench top model with 50 inch-pound capacity); (2) Metric universal dial caliper (Brown and Sharpe 559-579-13); (3) Liquid nitrogen contained in cylindrical Dewar flask; (4) Conditioning ovens; (5) Injection molded Charpy impact specimens: (i) Un-notched ABS; (ii) Un-notched HDPE; (iii) ABS with V-notch; and (iv) HDPE with V-notch.

SAFETY PRECAUTIONS: It is required that the same person both position the specimen and operate the Charpy impact tester; extreme care must be taken to have both hands away from the sample prior to releasing the pendulum. Everyone else must stay in back of the operator so that they are not struck by flying specimen pieces.

Handling specimens at temperatures other than room temperature also requires care that frost bite and burns do not occur. Normal safe laboratory practice for working with liquid nitrogen should be followed. Specimens can be safely immersed in liquid nitrogen with long-handled tongs, taking care to use an insulated glove and to extend arm fully. Depending on stand-off distance determined by the size of the tongs, safety glasses or laboratory goggles should be worn. Rapid retrieval of specimens from the conditioning ovens can be safely accomplished with large, blunt tweezers. (Instructor Note 1)

INTRODUCTION:

Problem Statement: You have recently been hired as an entry-level materials engineer in a company that molds plastic parts using both newly formulated and recycled/scrap materials. For your first assignment, you are asked to study the influence that temperature has on the properties of injection molded beam specimens of two thermoplastic polymers: ABS and

HDPE. Secondly, it is of interest to assess the notch sensitivity of these polymers. The material phenomena of interest and specimen geometry are amenable to pendulum impact testing, and the quality of specimens is representative of parts that your company manufactures. As such, their characterization provides important materials science insights to your company's design and applications engineers.

Thermoplastic polymers usually have a linear structure, although branching is possible. Two prominent examples are ABS and HDPE. ABS is a two-phase material involving a brittle styrene-acrylonitrile copolymer matrix with rubbery styrene-butadiene copolymer inclusions. [1] Typical uses include luggage and telephones. [2] HDPE has a linear carbon backbone and reasonably high degree of crystallinity, referred to as being semicrystalline. It has a sizable use percentage that includes film, sheet, and bottles/containers [3] together with wire/cable insulation, pipe, and conduit [4]. Upon heating above room temperature, thermoplastic polymers undergo significant changes in mechanical properties as determined, for example, by uniaxial tensile testing, including decreases in elastic (Young's) modulus, ultimate tensile strength, and fracture strength and increase in elongation at break. (Instructor Note 2) However, chemical decomposition is minimal.

A V-notched Charpy specimen and associated standard ASTM procedure [5] provide a laboratory evaluation of fracture toughness in order to simulate actual service conditions. This destructive, single-blow impact test involves a bar or beam specimen, supported at both ends, having a transverse load applied at high strain rate in the center with a pendulum striker (Fig. 3.6(a), Ref. [6]). [7,8] The amount of energy absorbed by the specimen on impact is inversely related to the maximum height the pendulum rises after it passes through the specimen. A wide range of metallic and non-metallic materials, including steels and plastics, have been studied using this technique. For plastics, the specimen is specified to be 5 in. long, 1/2 in. wide and 1/2 in. or less thick with a 22.5° notch machined in the thin dimension. A specimen with 1/8 in. thickness is often tested because this corresponds to the nominal thickness for molded commercial plastic parts. [9]

By performing Charpy impact tests on thermoplastic polymer specimens above and below room temperature, with follow-up examination of the resultant fracture surfaces, it is possible to assess transition temperature behavior. The effect of temperature on the energy to fracture is related to a change in the fracture mechanism at the micron/nanometer level. At sufficiently low temperature, fracture occurs at low energy and is said to be brittle. In contrast, high energy or ductile fracture occurs at a sufficiently elevated temperature. A transition from brittle to ductile fracture manifests itself in the portion of the plot of impact energy (or stress) versus temperature where a sizable change in energy occurs over a narrow temperature range (Fig. 3.6(b), Ref. [6]).

Notch sensitivity can be evaluated by performing Charpy impact tests on specimens with and without notches at a given temperature (e.g., room temperature). If there is a significant difference in the absorbed energies for the two specimen types, the material is said to be notch sensitive. The energy level is much lower, and fracture propagation is more controlled and reproducible for a specimen with a notch.

The effect of temperature on thermoplastic polymers is also exhibited by changes in dimensions that occur in specimens subjected to sufficiently elevated temperatures. Like brittle-ductile transition and notch sensitivity behaviors, this phenomena is important to design engineers who must select materials with good dimensional stability for end-products that experience a range of temperatures during their service lives.

The purpose of this experiment is to investigate the brittle-ductile transition and notch sensitivity behaviors of both polymers using Charpy impact testing. To this end, a quantitative evaluation of impact energy as a function of specimen conditioning temperature (taken also to be the specimen testing temperature) will be made using standard V-notch specimens. Impact energy measurements will also be obtained for room temperature specimens with and without V-notches. Subsequently, a visual inspection of each resultant fracture surface will be performed to determine its character (i.e., degree of brittle versus ductile fracture). To verify the measurements, experimental values of impact strength will be compared with those values appearing in the literature for both materials. Further, the thicknesses of recovered specimens will be measured allowing the dimensional stability of both polymers to be studied for the same temperature range.

PROCEDURE:

A. CHARPY IMPACT TESTING (Instructor Notes 1,3)

1. Preparatory to testing, place handwritten identification labels (Instructor Note 4) near both ends of two (2) specimens of each of sample type listed below:
 - (1) un-notched ABS at room temperature ($23 \pm 2^\circ \text{C}$);
 - (2) un-notched HDPE at room temperature ($23 \pm 2^\circ \text{C}$);
 - (3) V-notched ABS at room temperature ($23 \pm 2^\circ \text{C}$);
 - (4) V-notched HDPE at room temperature ($23 \pm 2^\circ \text{C}$);
 - (5) V-notched ABS kept at liquid nitrogen temperature (-196°C) until boiling stops;
 - (6) V-notched HDPE kept at liquid nitrogen temperature (-196°C) until boiling stops;
 - (7) V-notched ABS kept at $80 \pm 2^\circ \text{C}$ for 30 minutes;
 - (8) V-notched ABS kept at $100 \pm 2^\circ \text{C}$ for 30 minutes;
 - (9) V-notched HDPE kept at $100 \pm 2^\circ \text{C}$ for 30 minutes;
 - (10) V-notched ABS kept at $110 \pm 2^\circ \text{C}$ for 30 minutes;
 - (11) V-notched ABS kept at $120 \pm 2^\circ \text{C}$ for 30 minutes;
 - (12) V-notched HDPE kept at $120 \pm 2^\circ \text{C}$ for 30 minutes;
 - (13) V-notched HDPE kept at $127 \pm 2^\circ \text{C}$ for 30 minutes; and
 - (14) V-notched HDPE kept at $135 \pm 2^\circ \text{C}$ for 30 minutes.
2. Measure the thickness in several places near the center with a dial caliper.
3. Perform impact testing by measuring the apparent impact energy from the large dial.

4. Recover all of the fractured pieces and retain for subsequent thickness measurements and examination.
5. Correct the apparent impact energy values to account for the center location of the pendulum. (Instructor Note 5)
6. Record your measurements and any relevant observations in your laboratory notebook with one or more drawings as appropriate.

B. THICKNESS MEASUREMENTS OF RECOVERED SPECIMENS

1. Using a dial caliper, measure the thickness of each impacted specimen several millimeters away from its fracture surfaces.
2. Record your measurements and any relevant observations in your laboratory notebook with one or more drawings as appropriate.

C. VISUAL OBSERVATION OF RECOVERED SPECIMENS

1. Ascertain how well the pieces from each impacted specimen fit back together as a preliminary check on whether the failure was brittle or ductile.
2. Examine a fracture surface from each impacted specimen. Pay particular attention to the degree of surface roughness and whether the fracture surface appears to have undergone brittle or ductile fracture.
3. Examine the fracture surface and the region immediately behind it for a phenomena known as stress whitening. (Instructor Note 6)
4. Record any relevant observations in your laboratory notebook with one or more drawings as appropriate.

D. ANALYSIS

Perform the following analyses and respond to any questions as completely as possible being sure to show all of your work and reasoning as partial credit can be earned.

1. Impact energy measurements:
 - a. Plot (#1) impact energy, in-lb, versus temperature, °C. Use different plotting symbols to distinguish the two polymers.
 - b. Calculate the Charpy impact strength, σ_I , in units of ft-lb/in, for each room temperature specimen of both polymers using:

$$\sigma_I = IEC/t_{RT}, \quad (1)$$

where IEC = corrected impact energy; and
 t_{RT} = room temperature specimen thickness.

Note: impact energy and specimen thickness measurements were obtained in units of in-lb and mm, respectively.

2. Discuss the effect temperature has on the impact behavior of both polymers.
3. Discuss what effect the presence of the V-notch has on the room temperature σ_I values of both polymers.
4. Compare the room temperature σ_I values obtained with those given in Refs. [10], [11]. Give one or more reasons why differences may exist.
5. Specimen thickness measurements:
 - a. Calculate the change in thickness, Δt , in units of mm, for each specimen of both polymers using:

$$\Delta t = t_T - t_{RT}, \quad (2)$$

where t_T = thickness of specimen exposed to a given conditioning temperature, mm.

- b. Plot (#2) Δt , mm, versus temperature, °C. For consistency, choose the same plotting symbols used in Plot #1 to distinguish the two polymers.
6. Discuss the effect temperature has on the dimensional stability of both polymers.
7. Based on visual observations, discuss the brittle versus ductile character of the fractures that resulted for both polymers over the temperature range used. Also discuss the occurrence of stress whitening as a function of temperature.

COMMENTS with Sample Data Sheets and Plots:

All of the experimental steps were performed twice to verify that the results were reasonably reproducible. The data sets appearing in this section are considered to be representative.

Effect of Temperature on Charpy Impact Energies: The measured impact energies as a function of temperature for ABS and HDPE specimens appear in Tables I and II, respectively, and are plotted in Figure 1. ABS and HDPE specimens tested at -196° C had the same Charpy impact energy, which was only slightly more than when no sample was present. Therefore, these materials offer very little impact resistance at cryogenic temperatures or even at room temperature for HDPE. As temperature increased, the impact energy values for both ABS and HDPE specimens increased, but the effect was more pronounced for HDPE. For ABS, there was a modest increase in impact energy up to 98° C.

Table I. Charpy Impact Results for ABS Copolymer for Various Temperatures

Specimen Designation	Temperature (°C)	Impact Energy (in-lb)
ABS T5	-196	1.5
ABS T6	-196	1.5
ABS T1	23	3.25
ABS T2	23	2.75
ABS T3	80	7.0
ABS T4	80	6.5
ABS T7	98*	4.75
ABS T8	98*	4.75
ABS T11	109**	7.5
ABS T12	109**	17.0
ABS T9	120***	6.25
ABS T10	120***	6.25

* Numerous very fine cracks were observed.

** More numerous small cracks were observed.

*** Apparently, temperature was too high and/or time duration was too long because samples were very soft, and larger cracks developed throughout, that are attributed to causing a decrease in impact energy.

Table II. Charpy Impact Results for HDPE Polymer for Various Temperatures

Specimen Designation	Temperature (°C)	Impact Energy (in-lb)
PE T5	-196	1.5
PE T6	-196	1.5
PE T1	23	1.5
PE T2	23	1.5
PE T3	98	3.25
PE T4	98	3.25
PE T7	120	6.25
PE T8	120	5.0
PE T11	127	10.25
PE T12	127	18.0
PE T13	128	19.0
PE T14	128	14.0
PE T9	135	Samples did not break.
PE T10	135	Samples did not break.

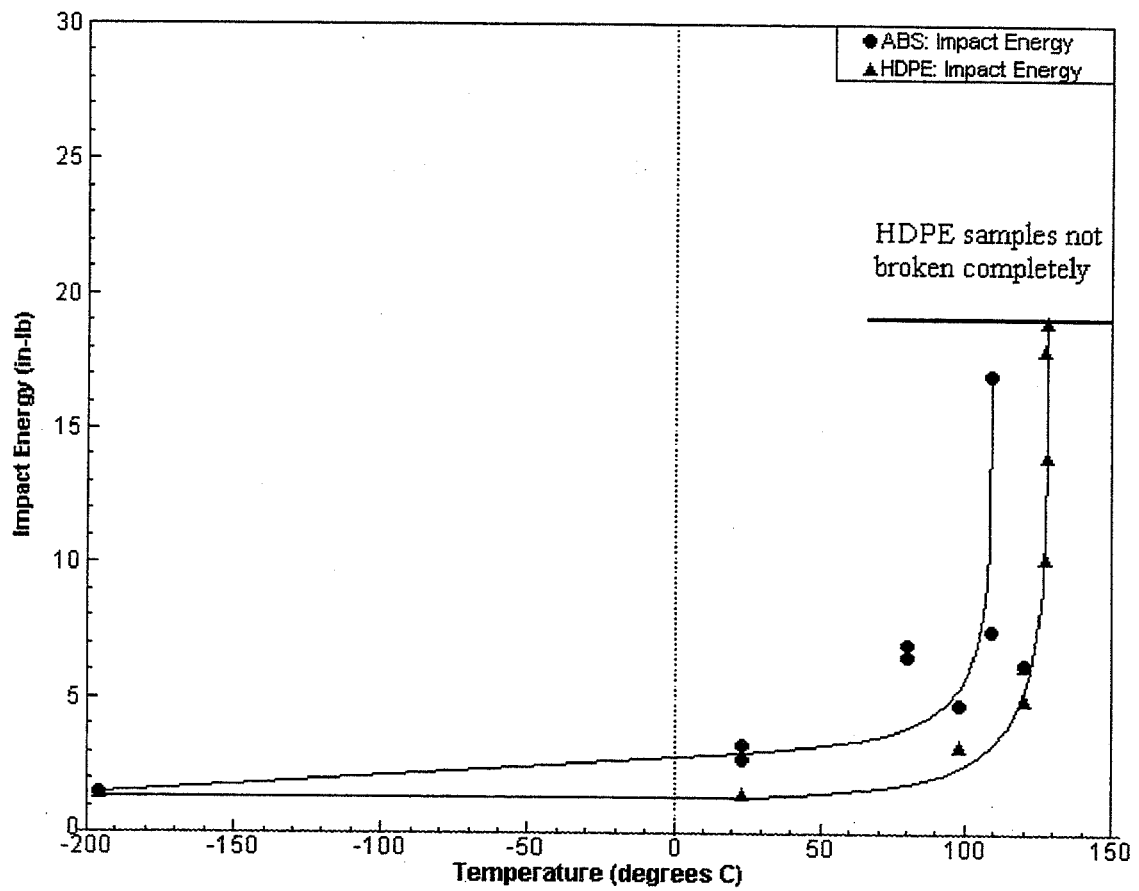


Figure 1. Charpy impact energy versus temperature for ABS copolymer and HDPE polymer.

At 109° C, a large difference in higher energy values was obtained, indicating that the temperature was at least close to the brittle-ductile transition temperature. Exposure to 120° C resulted in small cracks developing with a consequent (but unexpected) reduction in impact energy. For HDPE, the impact energy increased gradually up to 120° C. At 127-128° C, a large variation in significantly higher energy values was obtained, indicating that the brittle-ductile transition temperature had been reached.

Notch Sensitivity: For both plastics, the presence of the V-notch resulted in more than a 10X decrease in impact strength compared to when no notch was present (Table III). This indicates that both materials exhibit a strong notch sensitivity. Designers using these materials must be mindful to avoid specifying parts with high stress concentrations. [12]

Literature Comparison: There is reasonable agreement between measured room temperature Charpy impact strengths of notched specimens (Table III) and notched Izod impact strengths appearing in the literature. For ABS, values of 1.9 and 2.2 ft-lb/in were obtained versus a value of 6.5 ft-lb/in for a commercial-grade material, designated as Cycolac T resin [10], that is like what was used in the experiment. For HDPE, a value of 1.0 ft-lb/in was measured versus values ranging from 1.2 to 25 ft-lb/in depending on melt index for commercial-grade polyethylene with densities between 0.941 and 0.965 g/cm³ [11]. Material and processing variations probably explain the differences between measured and literature values for both materials. For HDPE, it is important to remember that recycled versus newly polymerized materials are being compared.

Dimensional Stability Assessment: Thickness measurements as a function of temperature for ABS and HDPE specimens appear in Tables IV and V, respectively, and change in thickness versus temperature is plotted in Figure 2. Dimensional stability of the heated specimens differed markedly. HDPE showed excellent stability over the complete temperature range, while at and above 98° C, a significant change in thickness was measured for ABS.

Visual Observations: A compilation of visual observations for the resultant fracture surfaces of ABS and HDPE impact specimens is given in Table VI. ABS underwent brittle fracture over the entire temperature range with the exception of one sample, tested at 109° C, exhibiting noticeable ductility. This is consistent with being close to the glass transition temperature (120° C) obtained for Cycolac T resin based on heat capacity measurements [13]. The occurrence of brittle fracture is consistent with the measured low impact energies. However, cracks developed in ABS specimens heated at or above 98° C which would at least partially explain the absence of a smoothly increasing trend above 80° C. In contrast, the observations reveal that HDPE clearly underwent brittle-ductile transition behavior with corresponding greater than 10X increase in impact energy over the temperature range where measurements could be obtained.

Referring to Table VI, stress whitening becomes prominent in HDPE once the ductile-brittle transition temperature is reached, indicating that stress whitening is associated with plastic deformation/ductile fracture.

Table III. Charpy Impact Results for ABS Copolymer and HDPE Polymer to Assess Notch Sensitivity at Room Temperature (23° C)

Specimen Designation	V-Notch Present	Impact Energy (in-lb)	Impact Strength (ft-lb/in)
ABS Copolymer			
ABS T1	Yes	3.25	2.2
ABS T2	Yes	2.75	1.9
ABS T13	No	28.0	18.8
ABS T14	No	29.0	19.5
HDPE Polymer			
PE T1	Yes	1.5	1.0
PE T2	Yes	1.5	1.0
PE T15	No	22.0	14.9
PE T16	No	20.0	13.6

Table IV. Dimensional Stability Results for ABS Copolymer for Various Temperatures

Specimen Designation	Temperature (°C)	Initial Thickness (mm)	Final Thickness* (mm)	Change in Thickness (mm)
ABS T5	-196	3.16	3.15	-0.01
ABS T6	-196	3.16	3.15	-0.01
ABS T1	23	3.15	3.15	0.0
ABS T2	23	3.15	3.15	0.0
ABS T3	80	3.15	3.16	0.01
ABS T4	80	3.16	3.18	0.02
ABS T7	98	3.15	3.29	0.14
ABS T8	98	3.15	3.29	0.14
ABS T11	109	3.15	3.49	0.34
ABS T12	109	3.15	3.43	0.28
ABS T9	120	3.15	3.62	0.47
ABS T10	120	3.15	3.60	0.45

* Average of single measurements on both fractured pieces.

Table V. Dimensional Stability Results for HDPE Polymer for Various Temperatures

Specimen Designation	Temperature (°C)	Initial Thickness (mm)	Final Thickness (mm)	Change in Thickness (mm)
PE T5	-196	3.16	3.14	-0.02
PE T6	-196	3.14	3.13	-0.01
PE T1	23	3.15	3.15	0.0
PE T2	23	3.14	3.14	0.0
PE T3	98	3.14	3.15	0.01
PE T4	98	3.14	3.15	0.01
PE T7	120	3.14	3.14	0.0
PE T8	120	3.13	3.16	0.03
PE T11	127	3.14	3.14	0.0
PE T12	127	3.16	3.16	0.0
PE T13	128	3.16	3.16	0.0
PE T14	128	3.15	3.15	0.0
PE T9	135	3.14	3.16	0.02
PE T10	135	3.12	3.15	0.03

* Average of single measurements on both fractured pieces.

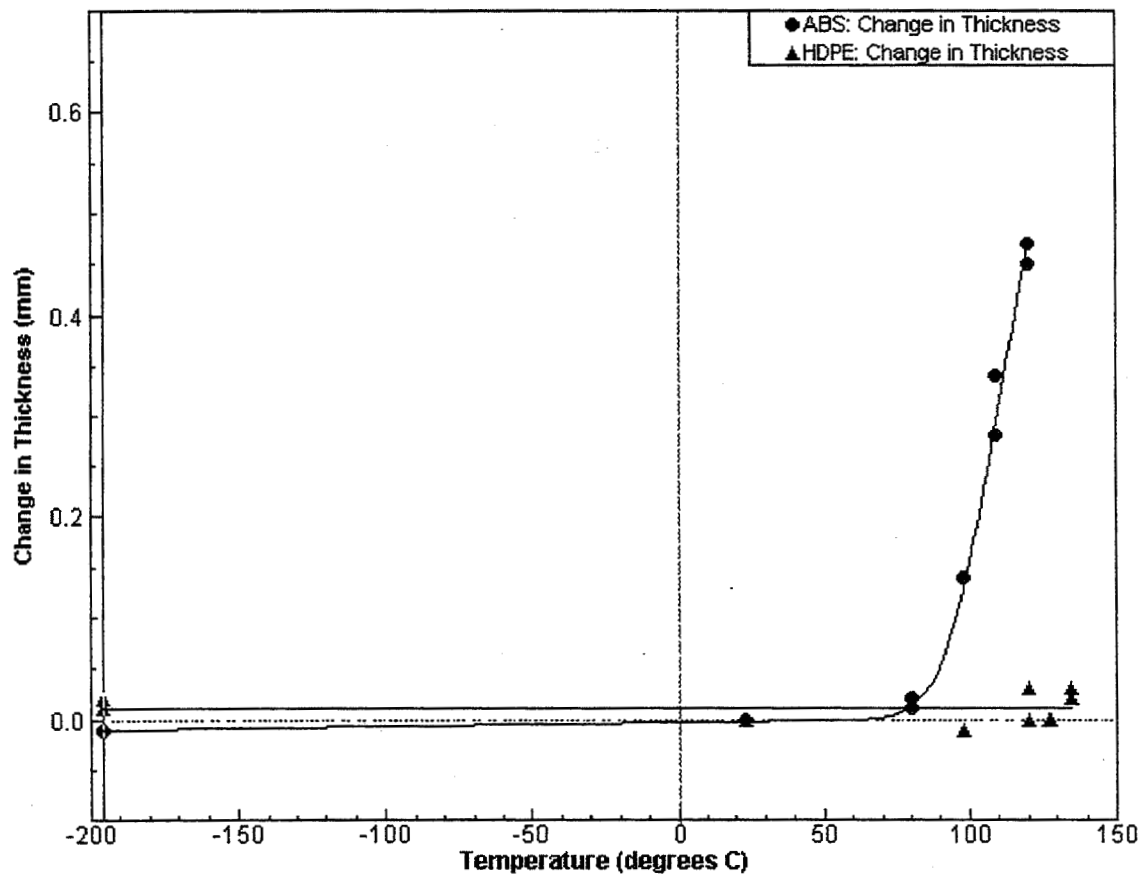


Figure 2. Change in impact specimen thickness versus temperature for ABS copolymer and HDPE polymer.

Table VI. Fracture Surface Appearance for Recovered Specimens of Impacted
ABS Copolymer and HDPE Polymer

Material	Temperature (°C)	Visual Observations
ABS	-196	Brittle; dark surface; somewhat rough
	23	Brittle; light surface; smooth
	80	Brittle; light surface; smooth
	98	Brittle; light surface; smooth
	109 (T11)	Brittle; light surface; smooth
	109 (T12)	Somewhat ductile; dark surface; a little rough
	120	Brittle; light surface; smooth
	23 (No notch)	Brittle; light surface; very rough
HDPE	-196	Brittle; rough; wavy surface
	23	Brittle; smooth; apparent "shear edge" (?)
	98	Brittle; smooth
	120	Brittle; smooth
	127 (T11)	A little ductile, rough, and stress whitening
	127 (T12)	More ductile; rougher; more stress whitening than T11
	128 (T13)	Very similar to T12
	128 (T14)	Slightly less ductile, etc. than T13
	135	Ductile; rougher; more stress whitening than T12/13; fracture not completely through specimens
	23 (No notch)	Brittle; very irregular

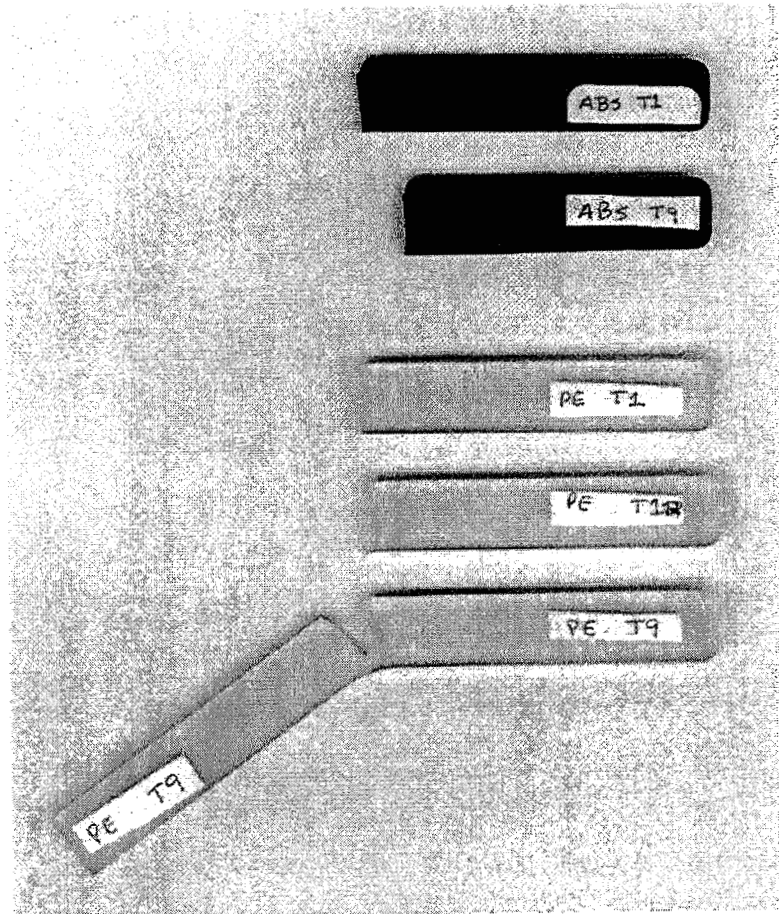
Optional Activity -- Scanned Images: Several of the recovered specimen pieces for both polymers were arranged on a Hewlett-Packard Scan Jet IICx flatbed scanner, and roughly one-to-one magnification images were obtained (Figures 3,4).

Referring to Figure 3, the fracture traces for both ABS specimens (T1,T9) were essentially identical, having relatively straight trajectories. However, the lack of dimensional stability in Specimen T9 (exposed to 120° C) is seen to be quite dramatic with its final length being significantly less than room temperature Specimen T1. Referring to the bottom three specimens of HDPE in Figure 3, the fracture traces for the two completely broken specimens show an important difference in trajectory: Specimen T1 exhibits a very straight fracture path of shortest length through the specimen. Whereas, the path through Specimen T12 is less direct, indicating that the fracture process was more ductile, which is consistent with it having a significantly higher impact energy value. Finally, the even greater fracture toughness of Specimen T9 is quite apparent since the fracture could propagate only part way through the material.

Referring to Figure 4, the absence of a V-notch in the impact specimens for both polymers causes the fracture path to be longer and more complicated that correlates well with the higher impact energy values measured for these specimens. Fracture of un-notched HDPE Specimen T15 resulted in the formation of at least one small fragment per specimen half.

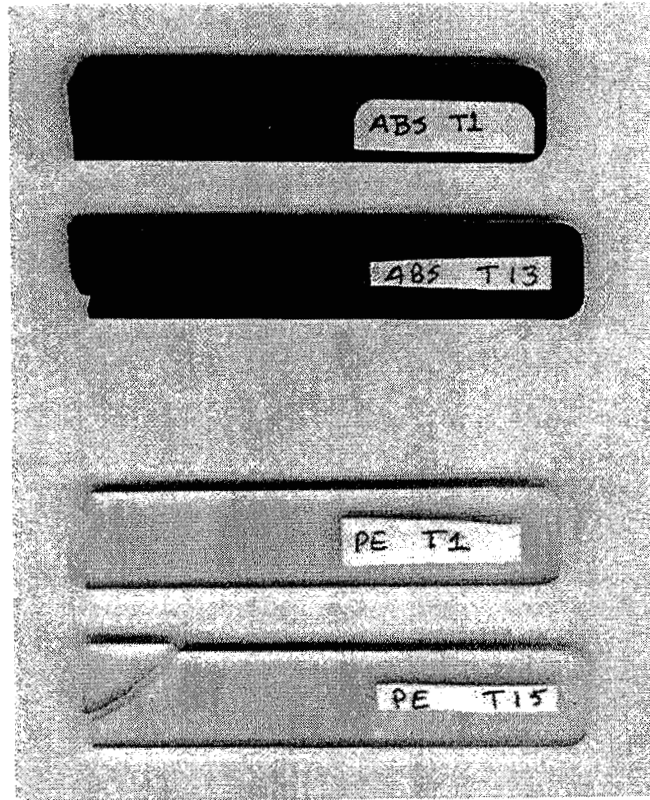
INSTRUCTOR NOTES:

1. It is important to demonstrate to students how to operate the Charpy impact tester and to position specimens in the machine prior to actual testing. The temperatures used in this experiment were selected in an effort to demonstrate brittle-ductile transition behavior for the polymers of interest, subject to the measurement limitation of the available impact tester and a serious heat distortion problem encountered for ABS at 120° C. Liquid nitrogen provided a convenient constant temperature medium that was below room temperature. Students also need to be shown how to handle specimens exposed to temperatures other than room temperature. The specimens exposed to elevated temperatures were placed on glass plates in the conditioning ovens in order to retain specimen flatness. ABS, in particular, tends to stick to glass; this can be greatly alleviated by lightly coating the glass plates with silicone spray before switching on the ovens. See **SAFETY PRECAUTIONS**.
2. An excellent background discussion of various thermal properties of polymers and the effect of temperature on their mechanical properties is provided [14] in a manual that is available free for distribution to students.
3. This part of the experiment relates to a previous year's National Educators' Workshop paper [15] describing temperature dependent impact results for steel.
4. Labeling both ends of each specimen facilitates keeping the recovered pieces organized for subsequent thickness measurements and visual examination.



1.3 cm
|---|

Figure 3. Scanned image of selected recovered ABS and HDPE Charpy impact specimens.



1.0 cm
|---|

Figure 4. Scanned image of selected recovered ABS and HDPE Charpy impact specimens with (top of each pair) and without V-notches.

5. The particular Charpy impact tester used in this experiment no longer has the pointer assembly used to make direct impact energy readings. The forward progress of the pendulum can be easily viewed and then corrected to give a value to correspond to the center of the pendulum tip. The reason and method for doing this is presented in lab. Hopefully, this will not be an issue for those who adopt this experiment.

6. Stress whitening [16], sometimes referred to as blushing, can occur because of the formation of numerous small cracks causing a change in reflected light. Stress whitening can also result when polymer molecules become highly oriented upon experiencing large local stresses that alter the degree of crystallinity and cause internal micro-porosity (voids).

REFERENCES:

- [1] Billmeyer, Jr., F.W.: Textbook of Polymer Science, 2nd Edn., Wiley-Interscience, 1971, p. 408.
- [2] Flinn, R.A.; and Trojan, P.K.: Engineering Materials and Their Applications, 4th Edn., Houghton Mifflin Co. (now John Wiley and Sons, Inc.), 1990, pp. 560-561.
- [3] Ibid.
- [4] Billmeyer, Jr., F.W.: op. cit., pp. 279-280.
- [5] "Standard Test Methods for Impact Resistance of Plastics and Electrical Insulating Materials," ASTM Designation D 256-88, in 1989 Annual Book of ASTM Standards, Section 8: Plastics, Vol. 08.01, American Society for Testing and Materials, Philadelphia, pp. 57-73.
- [6] Flinn, R.A.; and Trojan, P.K.: op. cit., p. 163.
- [7] "Mechanical Properties and Tests," Materials and Methods Manual 106, Compiled by J.B. Campbell, Compliments of Reihle Testing Machines, Reprinted from Materials in Design Engineering, July 1954.
- [8] "Designing with Plastic: The Fundamentals," Design Manual TDM-1 (1996), Hoechst Celanese Corporation, 90 Morris Avenue, Summit, New Jersey 07901, pp. 3-10 to 11.
- [9] "Standard Tests on Plastics," Bulletin 1GC (1988), Hoechst Celanese Corporation, 90 Morris Avenue, Summit, New Jersey 07901, p. 6.
- [10] "Properties Guide: GE Engineering Thermoplastics," PBG-140H (August 1992/Reprinted December 1996), General Electric Company, One Plastics Avenue, Pittsfield, Massachusetts 01201.

"Cyclocac Resin Properties Guide," CYC-300B (12/1993), General Electric Company, One Plastics Avenue, Pittsfield, Massachusetts 01201.

- [11] "Materials Selector 1992," Materials Engineering, December 1991, p. 184.
- [12] "Designing with Plastic: The Fundamentals," op. cit., pp. 8-10 to 11.
- [13] "Specific Heat," Materials Technology Notes, Number 1, MTD-ATN-001B (1993), General Electric Company, One Plastics Avenue, Pittsfield, Massachusetts 01201 (available in a packet entitled "Applied Technology Notes").
- [14] "Designing with Plastic: The Fundamentals," op. cit., pp. 4-1 to 5.
- [15] Bates, S.P.: Charpy V-notch Impact Testing of Hot Rolled 1020 Steel to Explore Temperature-Impact Strength Relationships, in National Educators' Workshop: Update 90, NIST Special Publication 822, 1991, pp. 129-135.
- [16] Strong, A.B.: Plastics: Materials and Processing, 2nd Edn., Prentice-Hall, Inc., 2000, pp. 168-169.

SOURCES OF SUPPLIES: See Acknowledgements. It is also possible that plastics manufacturers will supply specimens and accompanying material property data sheets, thus allowing a more appropriate literature comparison to be made.

ACKNOWLEDGEMENTS: Dr. Jerry L. Wickman, Director, Plastics Research and Education Center, Ball State University, Muncie, IN, kindly provided un-notched polymer impact specimens with useful material descriptions/properties. Michael Frankowiac, Johns Hopkins University, Baltimore, MD, machined standard V-notches in the impact specimens. Special thanks to Mark A. Elban for using computer graphics to prepare Figures 1,2.

Wayne L. Elban

Since 1985, Professor Elban has taught engineering science courses at Loyola College, including introductory materials science, materials science lab, mechanical properties of materials, and transformations in solids. He received a BChE with distinction ('69) and a PhD in Applied Sciences: Metallurgy ('77) from the University of Delaware and a MS in Engineering Materials ('72) from the University of Maryland, College Park. From 1969-1985, he was a research engineer at the Naval Surface Warfare Center, White Oak Laboratory, Silver Spring, Maryland. He is a member of ASM International.

Matthew J. Elban

Matt Elban is currently a high school junior and especially enjoys mathematics and science courses and writing. He is a member of the varsity soccer, basketball, and baseball teams. For the past two years, he has received honorable mention on the All-Carroll County soccer team. He has been the recipient of several ribbons for craft entries in the Maryland State Fair. His hobbies including fishing, playing guitar, and mountain biking. He is considering a career in criminal justice, forensics, or journalism.

**BIOSPHERE 2 CENTER
PAST, PRESENT AND FUTURE**

W. C. Harris

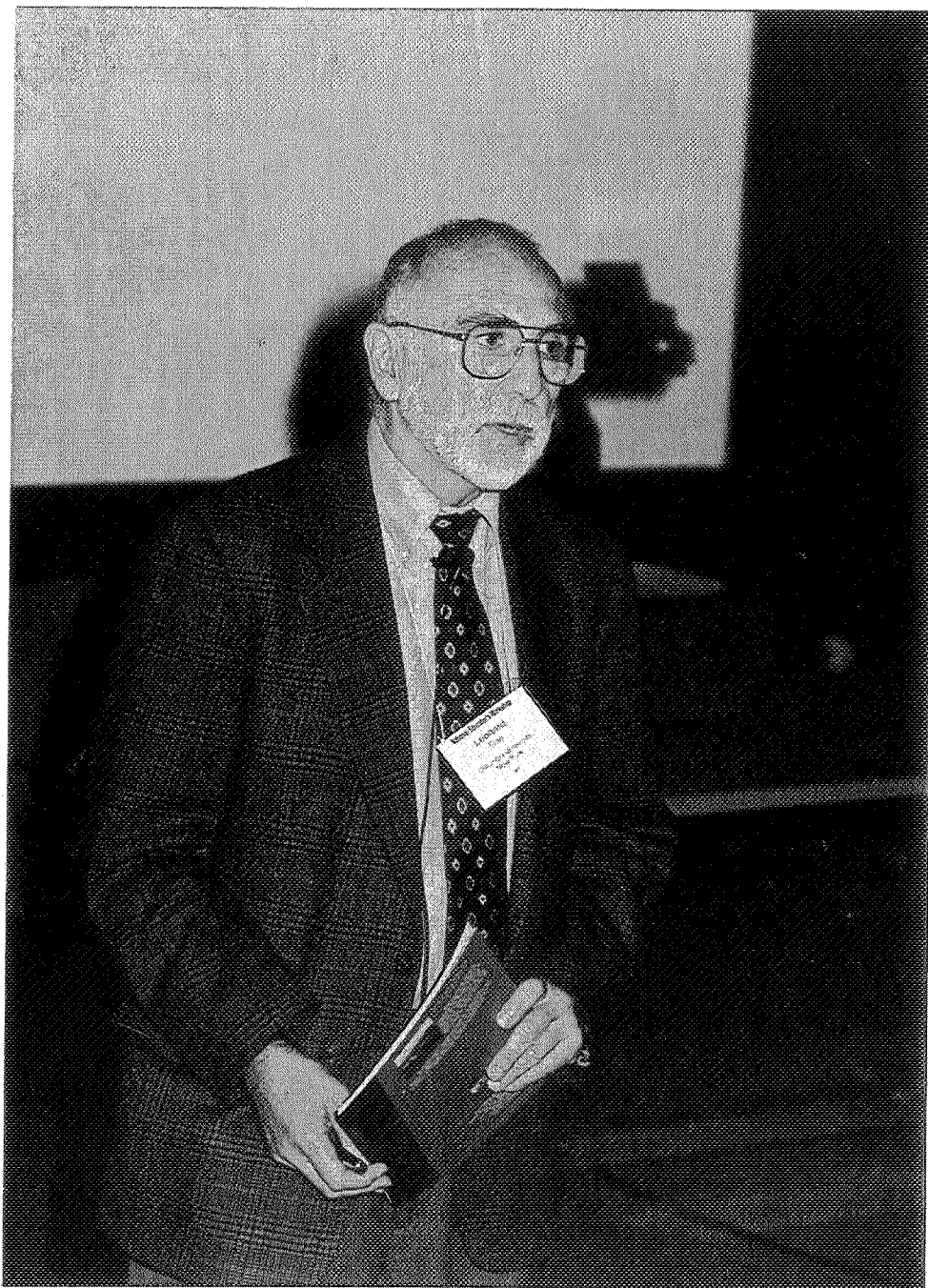
Columbia University
Biosphere 2 Center
32540 S. Biosphere Road
Oracle, Arizona 85623
Telephone 520-896-6453
e-mail wharris@bio2.edu

Leonard W. Fine

Columbia University in the City of New York
Department of Chemistry
Havemeyer Hall MC 3108
500 West 120th Street
New York, New York 10027
Telephone 212-854-2017
e-mail fine@chem.columbia.edu

Morton B. Friedman

Columbia University
School of Engineering and Applied Science
Office of the Dean, 510 Mudd
New York, New York 10027
Telephone 212-854-2986
e-mail friedman@columbia.edu



Leonard W. Fine

**Biosphere 2 Center
Past, Present and Future**

Columbia University assumed responsibility for the Biosphere 2 Center January 1, 1996 with the goal of building a new campus that focused on earth systems science, policy and management. Academic programs are now offered year round and we benefit by working with 25 university and college partners. **IN ADDITION, WE HAVE A WORKING PARTNERSHIP WITH VOLVO WITH RESPECT TO EDUCATION AND PUBLIC OUTREACH.** Our research effort is now receiving external funding, following a major investment in re-configuring the Biosphere 2 apparatus and converting into a laboratory for controlled studies to determine the impact of high CO₂ on oceans (coral reefs), agro-forestry systems (carbon sequestration) and a rain forest model. **THE UNIQUE NATURE OF THE BIOSPHERE 2 CENTER MAKES IT ESPECIALLY ATTRACTIVE FOR APPLIED RESEARCH AND ENGINEERING EDUCATION COURSES AND PROGRAMS.** How did Columbia University get involved in this new activity is a fascinating story - which will be outlined during the presentation.

William C. Harris
Columbia University
Biosphere 2 Center
32540 S. Biosphere Road
Oracle, AZ 85623
520-896-6453
email:<wharris@bio2.edu>

Leonard W. Fine
Columbia University
Department of Chemistry
Havemeyer Hall MC 3108
New York, NY 10027
212/854-2017
email<fine@chem.columbia.edu>

Morton B. Friedman
Columbia University
School of Engineering and Applied Science
Office of the Dean, 510 Mudd
New York, New York 10027
212/854-2986
email<friedman@columbia.edu>



Introduction

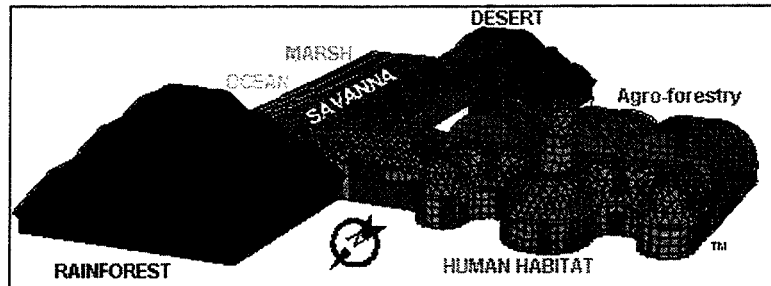


Figure 1: Locations of Biosphere 2 mesocosms.

Biosphere 2 consists of medium scale synthetic communities of plants and soils encased in a glass and metal shell. It includes a rainforest, desert, savanna, marsh, ocean and a separate agro-forestry area (Figures 1, 2). The structure covers 1.27 hectares (3.15 acres) and can be operated in a variety of configurations including 'flow-through' and 'closed system' modes. When operated as a 'closed system' the air leakage is estimated at a rate of 1.5% per day (as measured on 12-May-97). Operation as a 'flow-through' system means that the apparatus has external air flowing through it. In the wilderness area air can be brought into the desert and exhausted through the rainforest either with a TESCO fan (Figure 2) at a rate of up to 280 meters³/min (10,000 feet³/min) or by passive air movement in and out of the apparatus. The enclosure contains approximately 170,000 meters³ (6,000,000 feet³) of atmosphere, 1,500,000 liters (390,000 gallons) of freshwater, 3,800,000 liters (988,000 gallons) of saltwater, and 17,000 meters³ (600,000 feet³) of soil.

Located at an elevation of 1,200 meters (3,960 feet) above sea level at 32.5 north latitude in southern Arizona, Biosphere 2 is subject to the light regimes of a temperate desert region. The glass and structure components of the Biosphere 2 act as a filter for incoming solar radiation. Virtually all UV radiation is absorbed, and photosynthetically-active radiation (PAR) is cut by about 55%. However, because of the low-latitude location of this facility mean daily par levels inside the agro-forestry of about 15 mol m⁻² day⁻¹ in the winter and 25 mol m⁻² day⁻¹ in the summer are higher than typical greenhouse intensities and are acceptable for research purposes. The designers of Biosphere 2 used soils with high organic matter in the agro-forestry and the rainforest, resulting in a system that had experienced higher than ambient concentrations of carbon dioxide (CO₂). Heating, cooling, and electricity are supplied from an energy center external to the structure. Water is conserved inside Biosphere 2 wilderness mesocosm (desert, marsh, savanna, and rainforest). The major internal water cycling components for the wilderness are condensation (mainly in cooling coils of airhandlers), artificial rain or irrigation (by sprinkler systems), evapotranspiration, and soil sub-drainage (Figure 3). The agro-forestry water cycle unlike the wilderness mesocosms uses a single-pass water system.

The internal pressure is maintained close to external pressures by using two variable volume chambers, or 'lungs,' to avoid pressure-induced damage to the glass structure. The lungs are used only when the structure is operated as a closed system.

An array of sensors (CO₂ analyzers, temperature, relative humidity, and light) are housed inside the facility to monitor the atmospheric composition and climate. Mesocosm conditions are maintained to simulate the area they were modeled after and are tightly controlled (Figures 5, 7, 9-10).

Biosphere 2 Center strives to check data quality however, the nature of equipment is such that faults may develop. If this occurs during non-working times this often results in deviations present in the data (Figures 5, 7, 9-10).

Data acquisition and communication are fully automated. To allow maximum flexibility for research the Biosphere 2 facility is currently divided into four independent areas: wilderness (desert, savanna, ocean), rainforest, agro-forestry, and human habitat (Table 1, Figure 2), the last being open for interpretive visitor experiences.

Mesocosms	Volumes (air)	Areas		Dimensions		
	Cubic Meters	Square Meters	Hectare	N-S (Meters)	E-W (Meters)	Height (Meters)
Agro-forestry	35222*	2000	.022	41	54	24
Rainforest	26700^	2000	0.19	44	44	28
Savanna / Ocean	41500^	2500	0.26	84	30	27
Desert	18000^	1400	0.14	37	37	23

Table 1: Biosphere 2 facts. *(Silverstone and Nelson, 1995). ^Derived from mass balance calculations after SF₆ injection. (Van Haren, pers. comm.)

Biosphere 2 and a group of external scientists have been conducting a facility assessment to quantify current capabilities. Suggested changes necessary to implement fully controlled scientific experiments have been made in the rainforest and agro-forestry regions. Recent modifications include the installation of a CO₂ control system to adjust internal CO₂ levels to programmed set points, air circulation fans to help reduce thermal stratification, continuous trace gas monitoring system, and movable partitions to isolate the rainforest and divide the agro-forestry into three separate sections.

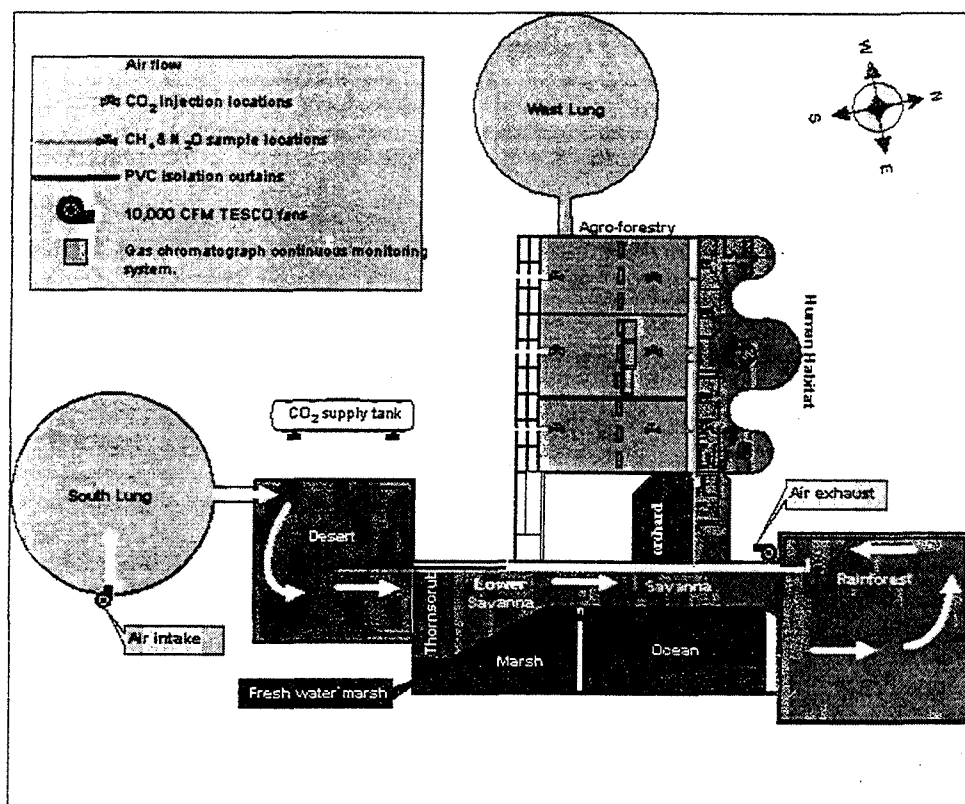


Figure 2: Airflow, trace gas sampling, CO₂ injection and partition placement with Biosphere 2 Center.

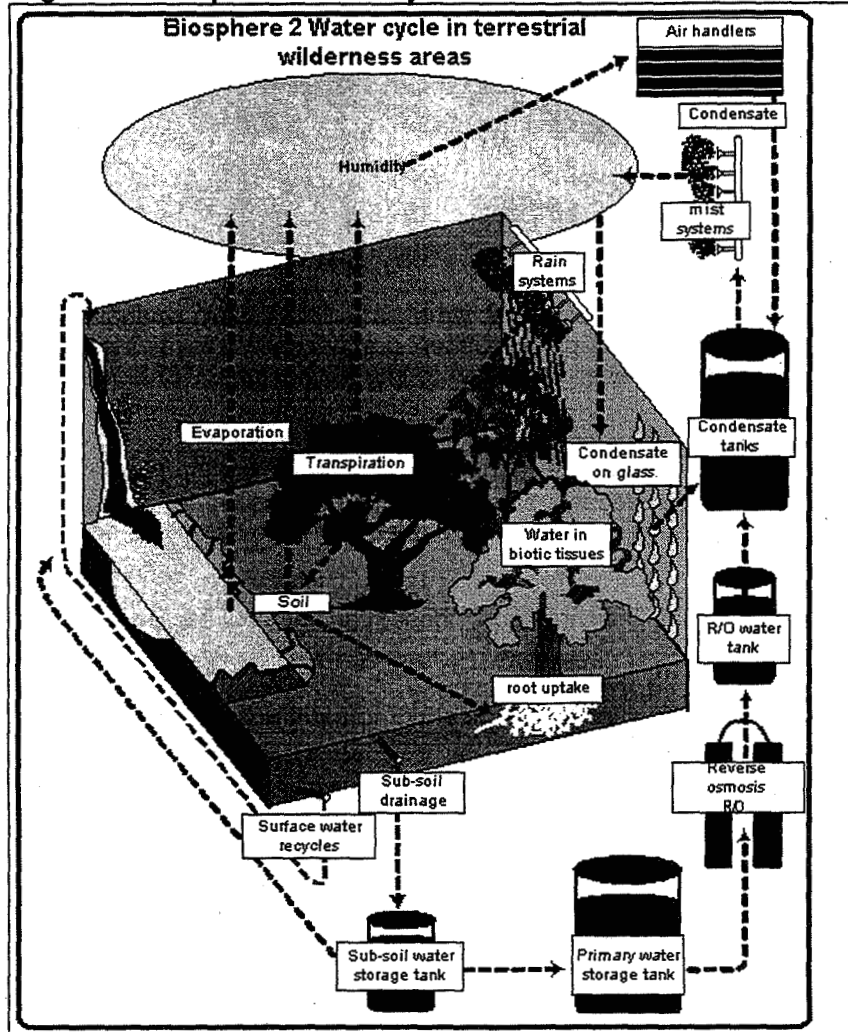
The continuous trace gas monitoring system (Figure 2) consists of an air sampling system and a gas analysis system. Air pumps draw air at approximately five liters per minute from the rainforest, savanna, desert, and agricultural areas in Biosphere 2 and from one external location through 3/8 inch bonded tubing. Currently, the system is set up for analyses of methane (CH₄) and nitrous oxide (N₂O) on a continuous basis and manual canister filling for other gas analyses (N₂/O₂ ratio, stable isotope analyses, etc.). CH₄ and N₂O are analyzed on a Gas Chromatograph using a FID (Flame Ionization Detector) and ECD (Electron Capture Detector) for CH₄ and N₂O, respectively. The gas sampling system allows future expansion of the analytical capabilities. We are developing a fully automated GC-IRMS (Gas Chromatograph _ Isotope Ratio Mass Spectrometer) system that will analyze the stable carbon, oxygen, and nitrogen isotope compositions of CO₂ and N₂O on a continuous basis. The system could also supply air samples for the analyses of other gases of interest; for example, isoprene,

carbon monoxide, hydrogen sulfide, and terpenes.

Lightweight curtains allow reversible closure of the rainforest and three agro-forestry sections (Figure 2). The curtains provide isolated 'system level' responses (e.g. net ecosystem carbon exchange, transpiration, trace gas production and isotope balances) to changing CO₂ and/or other climate factors, allowing comparisons between vegetation types under set experimental conditions. The isolated mesocosm acts essentially like a large static chamber in which fluxes of water, carbon and other compounds can be monitored precisely. The associated data are invaluable to validate models that scale up from leaf to canopy to ecosystem. The curtains also allow the Bio-Operations team better control of the environmental parameters necessary to maintain the biomes. When the rainforest curtain is sealed, the exchange of air occurs at a rate of approximately 1.4% per hour (as measured on 24-Nov-97).

These and future modifications will produce unique research opportunities to study 'system-level' responses to elevated CO₂ and climate changes.

Figure 3: Biosphere 2 water cycle in terrestrial wilderness areas.

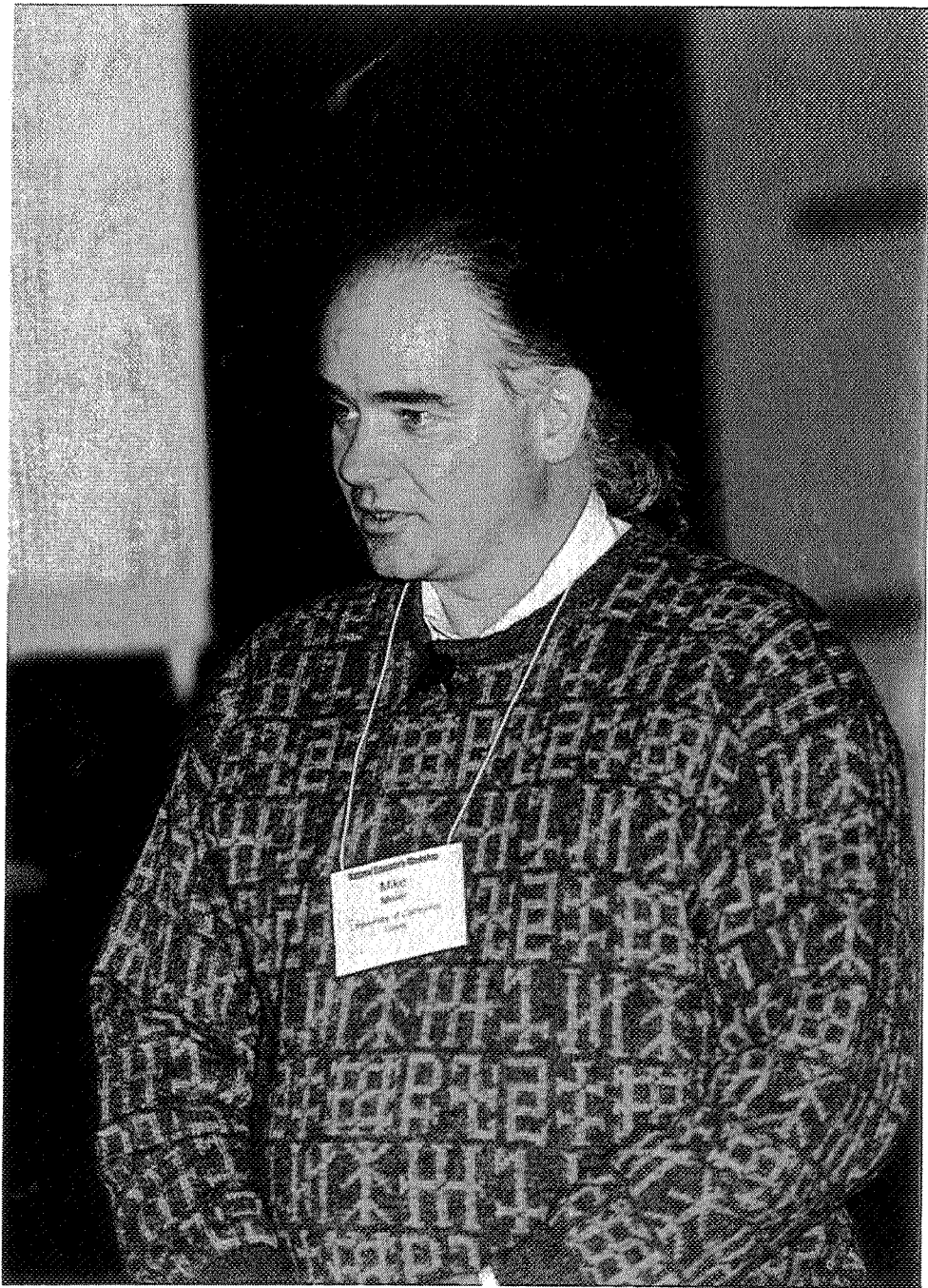


IONIC BONDING, AN INTRODUCTION TO MATERIALS AND TO SPREADSHEETS

Mike L. Meier

Department of Chemical Engineering and Materials Science
University of California, Davis
Davis, California 95616

Telephone: 916-752-5166
e-mail mlmeier@ucdavis.edu



Mike Meier

Ionic Bonding, An Introduction to Materials and to Spreadsheets

Mike L. Meier

Department of Chemical Engineering and Materials Science
University of California, Davis
Davis, CA 95616

Keywords

Ionic bonding, NaCl-type structure, halite, interatomic spacing, bulk modulus, shear modulus, Young's modulus, Poisson's ratio.

Prerequisite Knowledge

The student should be familiar with the basics of ionic bonding, including the attractive and repulsive energy terms, their relationship to interatomic forces, the relationships between bulk, shear and Young's elastic moduli and the effect of temperature on lattice energy. They should also be familiar with the basics of simple crystal structures, particularly the halite structure.

Objective

In this experiment the energies and forces involved in ionic bonding plus selected physical properties will be computed. The energy-spacing and force-spacing results will be graphed and the calculated properties will be compared to the values available in the literature. All calculations plus the graphing will be done using a spreadsheet. This spreadsheet program will be constructed using a logical, progressive approach which allows one to carefully examine each aspect of the program as it is being built. This spreadsheet will also be somewhat generalized, allowing one to calculate the bonding energies and forces for a number of ionic substances.

This exercise will involve first performing these calculations for KCl and, when you are sure your program works correctly, repeating the calculations for at least one of the other compounds listed in tables 1 and 2. The results will be compared to those compiled in table 2.

Equipment and Materials

1. Personal computers, at least one for every two students, running a spreadsheet program such as Quattro Pro, Excel, etc., and a printer
2. A quick-reference card covering basic spreadsheet commands and procedures (constants, formulas, formatting cells, copying cells, graphing, printing)
3. A model of the halite structure

Introduction

A good place to start the study of engineering materials is with the nature of the energies and forces involved in the bonding between atoms in a crystalline lattice. When we do we find that there are four principle types of bonds: ionic, metallic, covalent and Van der Waals. While bonding in most materials involves several of types of bonds it is still convenient to think of materials in terms of

their dominant type of bonding. For example, ceramics, whose bonding is primarily ionic but may also have covalent traits, tend to be brittle, chemically inert, poor electrical conductors and may be optically transparent while metals, due to their primarily metallic bonding, are ductile, shiny and have high thermal and electrical conductivities. Certain covalently bonded materials are among the hardest (diamond) and have the highest melting points. The chemical bonds in the well known semiconductors silicon and germanium are almost purely covalent.

Clearly when we know something about a material's bonding we are in a better position to predict and even control its structure and properties. Fortunately we can also make a number of generalizations regarding properties such as its melting point, stiffness and coefficient of thermal expansion even without having to consider the details of the band structure of inner and outer electron shells (the outer shells are most important in bonding and in the material's electrical properties). In fact, the methods of calculating these bonding energies and properties can be quite simple.

Lattice Energies

The chemical bonds in a crystal consists of two parts, an attractive component which acts over relatively large distances, and a repulsive component, which dominates at small interatomic spacings. For purely ionic bonds the energy of attraction is primarily due to the coulombic attraction between the outer shells of the oppositely charged ions. The equation for this energy is given by

$$E_a = \frac{Mz_1z_2q^2}{4\pi\epsilon_0r} \quad (1)$$

where M is the Madelung constant, r is the interatomic spacing, ϵ_0 is the permittivity in free space, q is the elementary charge and z_1 and z_2 are the valences of two ions. The energy of repulsion is due to the overlapping of the negatively charged electric fields of the inner shells and the positively charged nuclei. While the exact expression for this energy is difficult to derive a good approximation is given [2] by

$$E_r = b\lambda \exp\left(\frac{-r}{\rho}\right) \quad (2)$$

where b is the coordination number, λ is the repulsive energy coefficient and ρ is the repulsive range parameter. The total energy of the bond between the two ions is equal to the sum of the repulsive

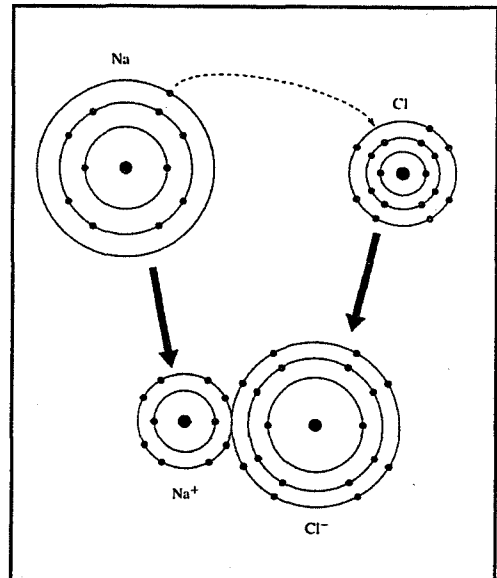


Figure 1. The formation of an ionic bond between a sodium and chlorine atom [1].

and attractive energies

$$E_{total} = E_a + E_r \tag{3}$$

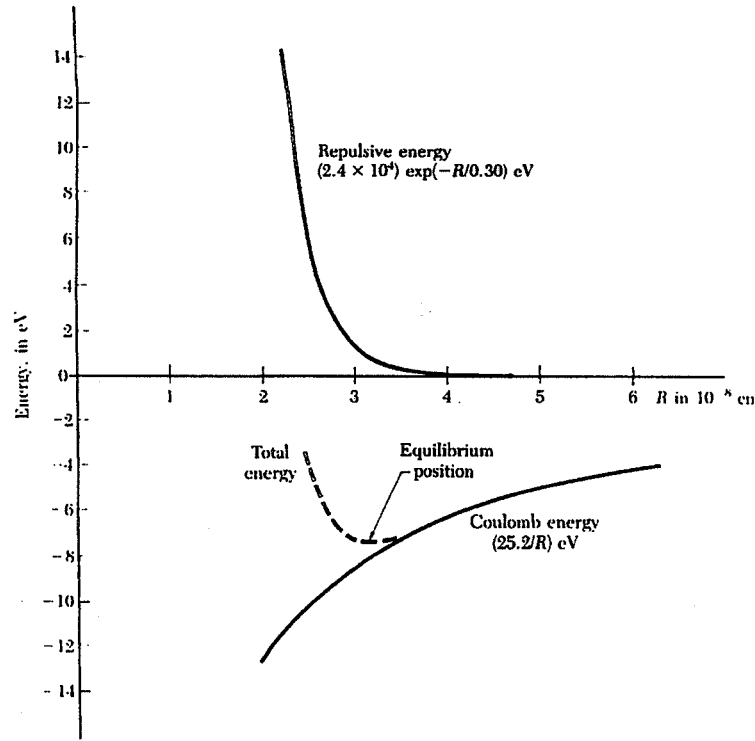


Figure 2. Energy per molecule in the KCl crystal [2].

Figure 2 shows the individual and combined lattice energies of NaCl as a function of interatomic spacing. Note that at large spacings there is still a small energy of attraction which increases ever more rapidly as the ions are brought closer together. On the other hand, the energy of repulsion is negligible at large spacings but when the ions are brought close enough together this term increases very quickly and soon dominates. Adding these two terms produces a minimum in the total lattice energy curve which defines both the equilibrium bond energy and interatomic spacing. The lattice energy at this point is given by:

$$E_0 = \frac{Mz_1z_2q^2}{4\pi\epsilon_0r_0} \left(1 - \frac{\rho}{r_0} \right) \tag{4}$$

where r_0 is the equilibrium spacing between nearest neighbor ions. A typical value for this equilibrium spacing is 0.3 nm and 6 eV is a typical value for the lattice energy.

Mechanical (Elastic) Properties

The forces that hold the lattice together are simply the first derivatives of lattice energies with respect to the interatomic spacing

$$F = \frac{dE}{dr} \approx \frac{\Delta E}{\Delta r} \quad (5)$$

Written this way we can better understand, and predict, certain mechanical properties. These are the elastic properties, one of which is the bulk modulus

$$K = \frac{1}{9r} \frac{1}{2} \frac{d^2E}{dr^2} \Big|_{r=r_0} = \frac{1}{9r} \frac{1}{2} \frac{dF}{dr} \Big|_{r=r_0} \approx \frac{1}{9r} \frac{1}{2} \frac{\Delta F}{\Delta r} \Big|_{r=r_0} \quad (6)$$

The bulk modulus describes the elastic behavior of a material subjected to hydrostatic pressures and is related to the mechanical force required to change the volume per ion. It is also related to the material's shear modulus, its resistance to elastic deformation by shear forces, by the equation

$$G = \frac{3K(1-2\nu)}{2(1+2\nu)} \quad (7)$$

and to Young's modulus, the material's stiffness in uniaxial tension and compression, by

$$Y = \frac{3K(1+\nu)(1-2\nu)}{(1+2\nu)} \quad (8)$$

where ν is Poisson's ratio. The value of Poisson's ratio ranges from 0.1 for ceramics to 0.3 for metals.

Thermal Properties

Calculations of lattice energies and spacing and the corresponding experiments are often done for temperatures at absolute zero but they are also done for other temperatures. When we examine the results for the different temperatures we find that as the temperature increases the magnitude of the lattice energy decreases and the equilibrium spacing between ions increases. This increase in spacing is what is commonly called thermal expansion and is one manifestation of the energy required to change the volume per ion. The decrease in the lattice energy leads to an understanding of why materials become softer as they are heated. We also know from experience that if the temperature continues to increase the material will eventually reach a point where the bonds are so weak that atoms can easily move to other lattice sites, the crystalline structure may break down, and the material either melts or vaporizes. The amount of thermal energy required to melt the material is also shown in figure 2. Once we locate this point on the graph we should be able to

estimate the melting point.

If the amount of thermal energy was equal to the energy of the bond the two atoms would separate completely. Merely melting the material, however, would require considerably less thermal energy. The energy level one must reach to cause melting is difficult to see in figure 2 but if we use the data to plot force versus distance one will find a maximum slightly to the right of the equilibrium spacing. This is an interesting point whose interpretation strongly suggests the material is in a fluid state. At this point a significant restoring force exists (the force is quite high) so the material is not yet a gas. But if an applied force equal to the maximum is removed it is just as likely that the atom would return to its original position as it is to move further away. If thermal energy alone had brought us close to this maximum then very little additional force would be required to move the atoms past the maximum, or back again, and if even more thermal energy was present then we would be to the right of the maximum where only a small restoring force is holding the atoms together. The material would be fluid.

The maximum on the $F-r$ curve corresponds to the inflection point on the $E-r$ curve. Once this energy E_l has been found one can then estimate the melting point of the material. The energy required to raise the temperature of the material to its melting point is given by

$$\frac{\Delta E}{n} = c\Delta T \approx 3k_B\Delta T \quad (9)$$

where c is the material's heat capacity, which can be approximated as $3k_B$ (k_B is Boltzmann's constant), and n is the number of lattice sites in the unit cell. The melting point can now be estimated using the following equation

$$T_{mp} \approx \frac{\Delta E}{n3k_B} + T_0 \quad (10)$$

where T_0 is the temperature for which E_0 was calculated.

Procedure

Start these computations by defining all terms, parameters and constants that are using in these equations and make sure the units of measure for each are consistent. Next, define the parameters for the particular material whose bonding behavior is being modeled. Once this has been done it will be possible to compute the attractive, repulsive and total lattice energies and then, taking the first derivative to be the central difference of these $E-r$ data, one can compute the $F-r$ curves. When this is done one will be able to extract several results, specifically:

Interatomic Spacing Locating the minimum in the $E-r$ data one can determine the interatomic (interionic) spacing.

Bond Strength	The minimum on the $E-r$ curve gives the strength of the bonds in the lattice.
Elastic Moduli	The bulk modulus (compressibility) can be computed using equation 8. Provide your own estimate of Poisson's ratio and compute the tensile and shear moduli.
Melting Point	Determine the amount of thermal energy required to reach melting point and then estimate the melting temperature.

After successfully completing these calculations for potassium chloride repeat them for other materials listed in table 2.

The remainder of this procedure will guide a person new to spreadsheets through the process of building an organized, readable, reusable spreadsheet, one that can be used to model the bonding behavior of all of the ionic materials listed in table 2. Immediately following table 2 is a printout of the interesting part of a spreadsheet like the one you will be making.

Necessary Preparations

1. Go to the various reference books and look up the interatomic spacing, lattice energy, melting point, bulk modulus and Young's modulus for a number of inorganic compounds. Your objective here is to find the typical range of values for these properties.
2. Obtain the relevant data for the specific material for which you will be calculating the bonding energies.
3. Sketch the unit cell for this material. Label the positions of each ion and determine the spacing between nearest neighbor atoms.
4. Decide on which units you will be using and obtain the necessary conversion factors.
5. The calculations you will be doing may produce divide-by-zero errors or, if you attempt to divide a very large number by a very small number, you may get an overflow error. Which equations are most likely to produce these errors and how do you plan to deal with these situations?
6. The numerical method you will be using to calculate the lattice energies and their derivatives involves an approximation of a curve with a series straight line segments. Comment on the errors you will be introducing into these calculations and how you plan to minimize their effects in your results.

General Layout of the Spreadsheet

The process of building this spreadsheet involved four basic steps. They are:

1. Put All Constants and Parameters in a Separate Block of Cells

As a general rule it is best to define all constants and parameters used by the equations in a separate block of cells. This makes it easier to debug the program, to change the units used and to experiment

with the equations. It also makes constructing the spreadsheet simpler since it is easier to reference a particular cell than it is to memorize a parameter's value and enter it into each equation. Besides, later you may want to replace a particular parameter with an equation, for instance, replacing a fixed value with an equation to this parameter a temperature-dependent variable.

2. Enter the Equations for Lattice Energies and Forces in Columns

The main part of the spreadsheet will be a series of columns containing the values and equations for the interatomic spacing, the energy of attraction, the energy of repulsion and the total lattice energy. One could put all this into one large equation for the energy of the lattice but long equations are difficult to enter and even more difficult to debug. It is best to keep all equations to a reasonable length.

3. Analyze the Results

Create a table where you list the reference values of the interatomic spacing, lattice energy, moduli, etc. and where you calculate these properties based on the $E-r$ and $F-r$ data. This is also a good place to show the differences in the two sets of numbers.

4. Define the Graphs

The graphs will be standard x-y graphs with interatomic spacing as the x axes and the lattice energies and forces plotted along the y axes. The line colors and styles and the legend will be used to identify the attractive, repulsive and total energies and forces.

Construct the Spreadsheet

1. Create the Header

Start by entering the basic details about this spreadsheet, such as the file name, title, owner, and the dates it was created and last revised, at the top. Next, enter a brief description of the purpose or function of this spreadsheet plus any literature citations that might be important. This header can be very useful when sharing the spreadsheet with others or when referring to it in the future.

2. Define the Physical Constants, Conversion Factors and Parameters for the Equations for Bonding Energies and Forces

Enter the values for every parameter used by all equations in cells just below the spreadsheet's header. Include their names and the units you are using. If the original units are not those you will be using in the equations then include a cell with the value of this parameter given in the correct units. Your equations will then reference these cells, saving you the trouble of including the units conversion factors in the equations.

3. Define the Parameters for the Material

Use a block of cells to define all details about the material that the lattice energy and force equations will require. You might also want to include additional information such as the mineral name, lattice-type and references to your sources of information.

4. Define the Values for the Interatomic Spacing

The first column in your spreadsheet will contain the values for the interionic spacing which the equations for lattice energy and force will use. The equation which generates these values will

require only an initial value and an increment. Both of these parameters should be located in the parameter section of your spreadsheet. This approach will allow you to easily adjust the value of the increment to change the range and resolution of interionic spacing and to adjust the initial value to shift the curves to the left and right on the graphs. This can be useful when fine tuning the spreadsheet to obtain the best estimate of the energy minimum.

At the top of the first column you will reference the cell containing the initial value of the interionic spacing. In the next cell you will add the predefined increment to the value in the first cell. Finally, you will replicate this second cell, say 300 times, to generate a column containing all of the values for the interionic spacing.

5. Calculate the Attractive, Repulsive and Total Lattice Energies and Forces

In the adjacent columns enter the equations for the attractive and repulsive energies. Enter them at the top of the columns and then replicate them so that these two columns are as long as the first column. Add these two columns together in column 4 to obtain the total lattice energy. Next, add three more columns containing the calculated coulombic, repulsive and total lattice forces. The equations for these columns will be simply the slopes (first derivative) of the corresponding bond energy values. Finally, add one last column which will contain the dF/dr data, calculated from the slope of the $F-r$ curve.

6. Create the Results Section

Construct a table-style summary of the reference and calculated properties. If this is done well it will make debugging, using and improving the accuracy of your spreadsheet much easier.

7. Annotate the Spreadsheet

Label each column, parameter, physical constant and result in the spreadsheet. Don't forget to include the units, to center the text, etc.

8. Construct the Graphs

Construct xy graphs for both the $E-r$ and $F-r$ results. In this spreadsheet column 1 contains the values for the x axis for both graphs, columns 2 through 4 contain the values for the first 3 series of the y axis in the $E-r$ graph and columns 5 through 6 contain the values for the data for the y axis on the $F-r$ graph. Label the axes appropriately and include a legend. Insert the graph into the spreadsheet, above the columns and to the right of the parameters. Optionally, save these graphs as TIFF or JPEG files so that you can insert them into your report or you can copy them to the clipboard then paste them directly into your laboratory report.

9. Add Data Symbols and Labels

Enter the values of the energy minimum and the force maximum in column 9 and in the same row the values are found in columns 4 and 7. Add this column to your graph but specify plotting symbols without lines.

Enter text into column 9 and in the same row as the energy minimum and the force maximum. Make this column the data label column for the total lattice energy and total force data. This text will be displayed on the graph next to the symbols.

10. Print the Spreadsheet

Print each graph separately and then print the top portion of the spreadsheet which includes the parameters, results, the first dozen or so values in the columns and possibly the inserted graphs. This can be placed in the appendix to show the reader how you set up and solved this problem using a spreadsheet.

Analyzing the Results of these Calculations

You might want to start with a brief description of the curves you calculated, noting the similarities and differences to those shown in figure 2 and the correspondence of key features in your $E-r$ and $F-r$ curves. Next, you will probably want to compare your results with those measured and calculated by others. In general, the differences between measured and calculated values of the lattice energy are usually around 1% or 2%. Some of the other results will be within these limits while others will not. Can you account for this and can you think of ways to improve on these results?

Optionally, plot dF/dr versus r for values of r within a few percent of the equilibrium spacing. Is the line straight? What does this say about the elastic moduli? Refer to these results again when you do the tensile tests in another experiment.

Discussion of the Results

The reader would probably like for you to start your discussion by confirming that your results are consistent with the description of ionic bonding given above. If everything looks OK up to this point you might want to comment on the possibility of using your spreadsheet to model the bonding and properties of the other materials listed in table 2. You might even want to take this to the next level and show that the equations you have used, the results of your calculations and the data in table 2 prove that there is a well-defined relationship between the nature of the chemical bond and certain physical properties. You might even think of other properties which one might be able to calculate using your spreadsheet. Finally, would it be possible to modify this spreadsheet to model other types of bonding?

Conclusions

If all has gone well your results will be very close to those measured and calculated by others. Looking back on this experiment you may also find that this exercise has provided you with both a valuable new set of skills which you can use to solve other engineering problems and also a good lesson on the fundamental aspects of chemical bonding which will help you understand something about the nature of all materials and the origins of many of their properties.

Comments

The author has used this experiment for several years in an introductory materials science course. It is the first of four experiments and as such is both a good introduction to materials science and an introduction to modeling using spreadsheets. As an introduction to spreadsheets this experiment has become a valuable asset in our laboratory teaching program. Without requiring it, the students use these new skills in the other three experiments, for example, compiling data from group experiments or importing data from a tensile test to analyze the mechanical properties and plot the stress strain curve. It is also our most successful experiment in terms of the quality and completeness of the

results the students obtain and in the amount of out-of-class time they devote to this experiment. We believe that the sense of ownership of their work, the creative outlet this experiment provides, the fun of making/building something, and addictive quality of programming are what has made this experiment work.

References

1. J.F.Shackelford, Introduction to Materials Science for Engineers, 4th edition, Prentice Hall, New Jersey, pp. 26-36, (1996).
2. C. Kittel, Introduction to Solid State Physics, 7th edition, John Wiley and Sons, New York, pp.66-73, (1996).
3. Handbook of Chemistry and Physics, R.Weast, ed., 65th edition, CRC Press, Inc, Boca Raton, FL, pp. F190-F191, (1984).
4. J.Shermon, Chemical Reviews, vol. 11, pp.93-170, (1932).
5. H.H.Sisler, Electronic Structure, Properties and the Periodic Law, 2nd edition, D.Van Nostrand, New York, pp.65-69, (1973).
6. G.Simmons and H.Wang, Single Crystal Elastic Constants and Calculated Aggregate Properties, A Handbook, 2nd edition, The M.I.T. Press, Cambridge Massachusetts, (1971).
7. O.H.Wyatt and D.Dew-Hughes, Metals, Ceramics and Polymers, Cambridge University Press, pp.67-69, (1974).
8. L.Pauling, The Nature of the Chemical Bond, 3rd edition, Cornell University Press, Ithaca, NY, pp. 505-510, (1960).
9. C.Giacovazzo, H.L.Monaco, D.Viterbo, F.Scordari, G.Gilli, G.Zanotti, M.Catti, Fundamentals of Crystallography, International Union of Crystallography, Oxford University Press, pp.410-413, (1992).
10. ICDD-JCPDS Powder Diffraction Database, Sets 1-46, (1997).

Biographical Information

Michael L. Meier received his B.S. in Materials Engineering from North Carolina State University in 1979 and his M.S. (1986) and Ph.D. (1991) in Materials Science and Engineering from the University of California, Davis. After a two-year post-doctorate position at the Universität Erlangen-Nürnberg in Erlangen, Germany he returned to UC Davis where he is the director of Materials Science Central Facilities and teaches many of the laboratory courses.

Physical Constants

Avogadro's Number	N_A	$6.022045 \times 10^{23} \text{ mol}^{-1}$
Boltzmann's Constant	k_B	$1.380662 \times 10^{-23} \text{ J K}^{-1}$
Elementary Charge	q	$1.6021892 \times 10^{-19} \text{ C}$
Permittivity of Free Space	ϵ_0	$8.85418782 \times 10^{-12} \text{ C}^2 \text{ N}^{-1} \text{ m}^{-2} \text{ or } \text{C}^2 \text{ J}^{-1} \text{ m}^{-1}$

Conversion Factors

1 eV	$1.6021917 \times 10^{-19} \text{ J}$
1 MPa	145 psi
1 calorie	4.184 J

Distance Between Any Two Points

The following equation gives the distance between point 1 and point 2 where their coordinates x, y, z are defined for any of the seven crystal systems where a, b and c and α, β and γ have their usual meanings.

$$d_{12}^2 = (x_1 - x_2)^2 a^2 + (y_1 - y_2)^2 b^2 + (z_1 - z_2)^2 c^2 + 2(x_1 - x_2)(y_1 - y_2) ab \cos \gamma + \\ 2(y_1 - y_2)(z_1 - z_2) bc \cos \alpha + 2(z_1 - z_2)(x_1 - x_2) ca \cos \beta \quad (11)$$

Table 1. Crystallographic Data for Selected Inorganic Compounds [2,3,4,10]

Substance	Mineral Name	Crystal Lattice	Lattice Constants, nm	Madelung Constant
Al ₂ O ₃	Corundum	Rhombohedral	a=0.47587, c=1.29929	4.171900
CaF ₂	Fluorite	Cubic	a=0.546305	2.3650
CaO	Lime, Calcia	NaCl-type	a=0.481059	1.747565
CdI ₂	-	Hexagonal	a=0.42481, c=1.37265	2.355
CsCl	-	Cubic	a=0.41230	1.762670
Cu ₂ O	Cuprite	Cubic	a=0.42696	2.221240
KBr	-	NaCl-type	a=0.66005	1.747565
KCl	Sylvite	NaCl-type	a=0.62917	1.747565
KF	Corobbiite	NaCl-type	a=0.534758	1.747565
KI	-	NaCl-type	a=0.70655	1.747565
LiBr	-	NaCl-type	a=0.55013	1.747565
LiCl	-	NaCl-type	a=0.51396	1.747565
LiF	Griceite	NaCl-type	a=0.40270	1.747565
LiI	-	NaCl-type	a=0.600	1.747565
MgF ₂	Sellaite	Tetragonal	a=0.46200, c=0.30509	2.3810
MgO	Periclase	NaCl-type	a=0.42112	1.747565
NaBr	-	NaCl-type	a=0.597353	1.747565
NaCl	Halite	NaCl-type	a=0.56402	1.747565
NaF	Villiaumite	NaCl-type	a=0.463329	1.747565
NaI	-	NaCl-type	a=0.6473	1.747565
RbBr	-	NaCl-type	a=0.6889	1.747565
RbCl	-	NaCl-type	a=0.65810	1.747565
RbF	-	NaCl-type	a=0.56516	1.747565
RbI	-	NaCl-type	a=0.7342	1.747565
SiO ₂	β-Quartz	Hexagonal	a=0.511, c=0.537	4.1719
TiO ₂	Rutile	Tetragonal	a=0.45933, c=0.29592	2.248037
TiO ₂	Anatase	Tetragonal	a=0.37852, c=0.95139	2.400000
ZnO	Zincite	Hexagonal	a=0.324982, c=0.520661	1.4985
ZnS	Sphalrelite (Zinc Blend)	FCC	a=0.54060	1.638060
ZnS	Wurtzite	Hexagonal	a=0.382098, c=0.62573	1.641320

Table 2. Selected calculated and measured room temperature properties of materials having the NaCl-type structure [2,3,6].

Substance	Interionic Spacing nm	Repulsive Energy Parameter eV	Repulsive Range Parameter nm	Measured Lattice Energy eV	Calculated Lattice Energy eV	Gibb's Free Energy kJ/mol	Melting Point K	Bulk Modulus GPa	Poisson's Ratio	Shear Modulus GPa	Young's Modulus GPa
KBr	0.3298	2392.6	0.0336	-6.886	-6.908	-380.8	1007	15.1	0.254	8.9	22.2
KCl	0.314655	2132.5	0.0326	-7.190	-7.008	-409.2	1043	17.4	0.249	10.5	26.2
KF	0.2674	1362.7	0.0298	-8.230	-8.200	-537.8	1131	31.1	0.260	17.8	44.9
KI	0.3533	2964.7	0.0348	-6.500	-6.266	-324.9	954	11.7	0.251	7.0	17.5
LiBr	0.2751	614.8	0.0340	-8.230	-7.849	-342.0	823	25.7	0.248	15.6	38.9
LiCl	0.2570	509.7	0.0330	-8.621	-8.365	-384.4	878	31.8	0.238	20.2	50.0
LiF	0.2014	307.9	0.0291	-10.507	-10.503	-587.7	1118	66.6	0.198	50.5	120.9
LiI	0.3000	623.1	0.0366	-7.706	-7.203	-270.2	722	17.1	0.200	10.99	26.38
NaBr	0.2989	1383.5	0.0328	-7.528	-7.337	-348.9	1020	19.9	0.250	11.9	29.8
NaCl	0.282010	1092.3	0.0321	-7.918	-7.745	-384.2	1074	23.9	0.249	14.4	36.0
NaF	0.231710	666.8	0.0290	-9.297	-9.332	-543.5	1266	48.1	0.231	31.6	77.7
NaI	0.3237	1643.6	0.0345	-7.077	-6.791	-286.1	934	16.1	0.274	8.6	21.9
RbBr	0.3445	3151.9	0.0338	-6.617	-6.431	-381.8	966	13.8	0.268	7.6	19.2
RbCl	0.3291	3318.4	0.0323	-6.908	-6.739	-407.8	991	16.2	0.268	8.9	22.6
RbF	0.2815	1851.6	0.0301	-7.866	-7.823	-	1068	27.3	0.276	14.4	36.9
RbI	0.3671	4150.6	0.0348	-6.283	-6.054	-328.9	920	10.8	0.262	6.1	15.5
MgO	0.2110	-	-	-	-42.405	-569.4	2852	153.3	0.172	128.6	301.5
CaO	0.2100	-	-	-	-37.437	-604.0	2614	-	-	-	-

File: Ionic Bonding.WB3
 Owner: Mike Meier
 Created: June 19, 1997
 Revised: June 15, 1999
 Description: Calculation of ionic bonding energies, forces and related properties for materials with the NaCl-type structure.

Conversion Factors

From	To	Value	Units
Joules	eV	6.242E+18	eV/J
Coulombs	eV s	6.242E+18	eV s/C
GPa	ksi	145	ksi/GPa
Calories	Joules	4.184	J/cal

Physical Constants

Avogadro's Number:	6.022E+23	per mole	
Boltzmann's Constant:	1.381E-23	J/K	8.618E-05 eV/K
Proton Charge:	1.602E-19	C	
Velocity of Light:	2.998E+08	m/s	
Permittivity:	8.854E-12	C ² /Nm ²	

Environmental Parameters

Temperature:	298	K
Pressure:	1	atmospheres

Material

Substance:	KCl
Mineral Name:	Sylvite
Melting Point:	1043 K
Crystal Lattice:	NaCl type
Lattice Constants:	0.629310 0.629310 0.629310 a,b,c in nm
Lattice Angles:	90.000 90.000 90.000 degrees
Equivalent Sites:	4
Reference Ion:	0 0 0 u,v,w
Nearest Ion:	0 0 1/2 u,v,w
	Type Number Valence CN
Cation:	K+ 1 1 6
Anion:	Cl- 1 -1 6

Interionic Spacing (independent variable)

Initial Value:	0.061895 nm
Increment:	0.002500 nm

Repulsive Energy

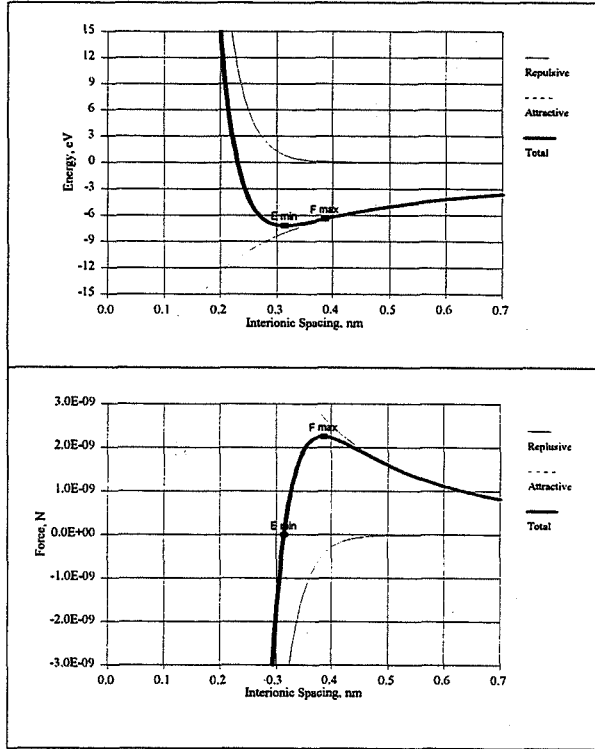
Energy Parameter:	2132.5 eV
Range Parameter:	0.032600 nm

Coulombic Attraction

Madelung Constant:	1.747565
--------------------	----------

Results

Property	Reference	Calculated	Units	Calculated	Units	Difference	Note
Cell Containing E min:	[F:\National Educator's Workshops\NEW-Update 99\Ionic Bonding.WB3]Kittel:D17						Uses the Quattro Pro @MinLookup function on column D
Cell Containing F max:	[F:\National Educator's Workshops\NEW-Update 99\Ionic Bonding.WB3]Kittel:G20						Uses the Quattro Pro @MaxLookup function on column G
Equilibrium Spacing:	0.314655	0.314395	nm	3.14395	Angstroms	-0.08%	Ionic spacing at the minimum for column D
Energy Minimum:	-7.190	-7.176	eV	-692.3	kJ/mole	-0.20%	Minimum, column D
Total Lattice Energy:	-7.190	-7.175	eV	-692.2	kJ/mole	-0.21%	Equation 4
Force at Emin:	n/a	2.607E-14	N	-	-	-	Minimum, column G, absolute value
dF/dr at F=0:	n/a	99.299	N/m	-	-	-	dF/dr at E min
Bulk Modulus:	17.40	17.55	GPa	2.54	1e6 psi	0.84%	Equation 6
Poisson's Ratio:	0.249	0.215	-	-	-	-	(Adjust Poisson's ratio to get the correct value for the shear modulus.)
Shear Modulus:	10.50	10.49	GPa	1.52	1e6 psi	-0.08%	Equation 7
Young's Modulus:	26.20	25.49	GPa	3.70	1e6 psi	-2.70%	Equation 8
Maximum Force:	n/a	2.252E-09	N	-	-	-	Maximum, column G
Energy at F max:	n/a	-6.415	eV	-	-	-	Energy at maximum for column G
delta E:	n/a	0.760	eV	73.4	kJ/mole	-	-
Melting Point:	1043.0	1033.4	K	760.4	C	-0.92%	Equation 10



Ionic Spacing nm	Repulsive Energy eV	Attractive Energy eV	Total Energy eV	Repulsive Force Newtons	Attractive Force Newtons	Total Force Newtons	dF/dr N/m	Energy Data		Force Data	
								Symbols	Labels	Symbols	Labels
0.061895	1916.374	-40.660	1875.714								
0.064395	1774.906	-39.082	1735.825	-8.731E-06	9.738E-08	-8.634E-06					
0.066895	1643.882	-37.621	1606.261	-8.086E-06	9.022E-08	-7.996E-06			2.456E+05		
0.069395	1522.530	-36.266	1486.264	-7.490E-06	8.383E-08	-7.406E-06			2.275E+05		
0.071895	1410.136	-35.005	1375.132	-6.937E-06	7.810E-08	-6.859E-06			2.108E+05		
0.074395	1306.039	-33.828	1272.211	-6.425E-06	7.293E-08	-6.352E-06			1.953E+05		
0.076895	1209.627	-32.729	1176.899	-5.950E-06	6.826E-08	-5.882E-06			1.809E+05		
0.079395	1120.332	-31.698	1088.634	-5.511E-06	6.402E-08	-5.447E-06			1.676E+05		
0.081895	1037.629	-30.730	1006.898	-5.104E-06	6.017E-08	-5.044E-06			1.553E+05		
0.084395	961.030	-29.820	931.210	-4.727E-06	5.666E-08	-4.671E-06			1.438E+05		
0.086895	890.087	-28.962	861.125	-4.378E-06	5.344E-08	-4.325E-06			1.332E+05		
0.089395	824.380	-28.152	796.228	-4.055E-06	5.049E-08	-4.005E-06			1.234E+05		
0.091895	763.524	-27.386	736.138	-3.756E-06	4.778E-08	-3.708E-06			1.143E+05		
0.094395	707.160	-26.661	680.499	-3.479E-06	4.528E-08	-3.433E-06			1.058E+05		
0.096895	654.958	-25.973	628.984	-3.222E-06	4.297E-08	-3.179E-06			9.804E+04		
0.099395	606.608	-25.320	581.289	-2.984E-06	4.084E-08	-2.943E-06			9.080E+04		
0.101895	561.828	-24.699	537.130	-2.764E-06	3.886E-08	-2.725E-06			8.410E+04		
0.104395	520.354	-24.107	496.247	-2.560E-06	3.702E-08	-2.523E-06			7.788E+04		
0.106895	481.941	-23.543	458.398	-2.371E-06	3.530E-08	-2.335E-06			7.213E+04		
0.109395	446.364	-23.005	423.359	-2.196E-06	3.371E-08	-2.162E-06			6.680E+04		
0.111895	413.413	-22.491	390.922	-2.034E-06	3.222E-08	-2.001E-06			6.187E+04		
0.114395	382.895	-22.000	360.895	-1.884E-06	3.082E-08	-1.853E-06			5.729E+04		
0.116895	354.629	-21.529	333.100	-1.744E-06	2.952E-08	-1.715E-06			5.306E+04		
0.119395	328.515	-21.078	307.437	-1.616E-06	2.830E-08	-1.587E-06			4.913E+04		
0.121895	304.204	-20.646	283.558	-1.496E-06	2.715E-08	-1.469E-06			4.550E+04		
0.124395	281.748	-20.231	261.517	-1.386E-06	2.607E-08	-1.360E-06			4.214E+04		
0.126895	260.949	-19.833	241.116	-1.284E-06	2.505E-08	-1.259E-06			3.902E+04		
0.129395	241.686	-19.449	222.236	-1.189E-06	2.409E-08	-1.165E-06			3.613E+04		
0.131895	223.844	-19.081	204.764	-1.101E-06	2.318E-08	-1.078E-06			3.346E+04		
0.134395	207.320	-18.726	188.594	-1.020E-06	2.233E-08	-9.975E-07			3.098E+04		

TABLETOP EXPERIMENTS FOR MATERIAL PROPERTIES DETERMINATION

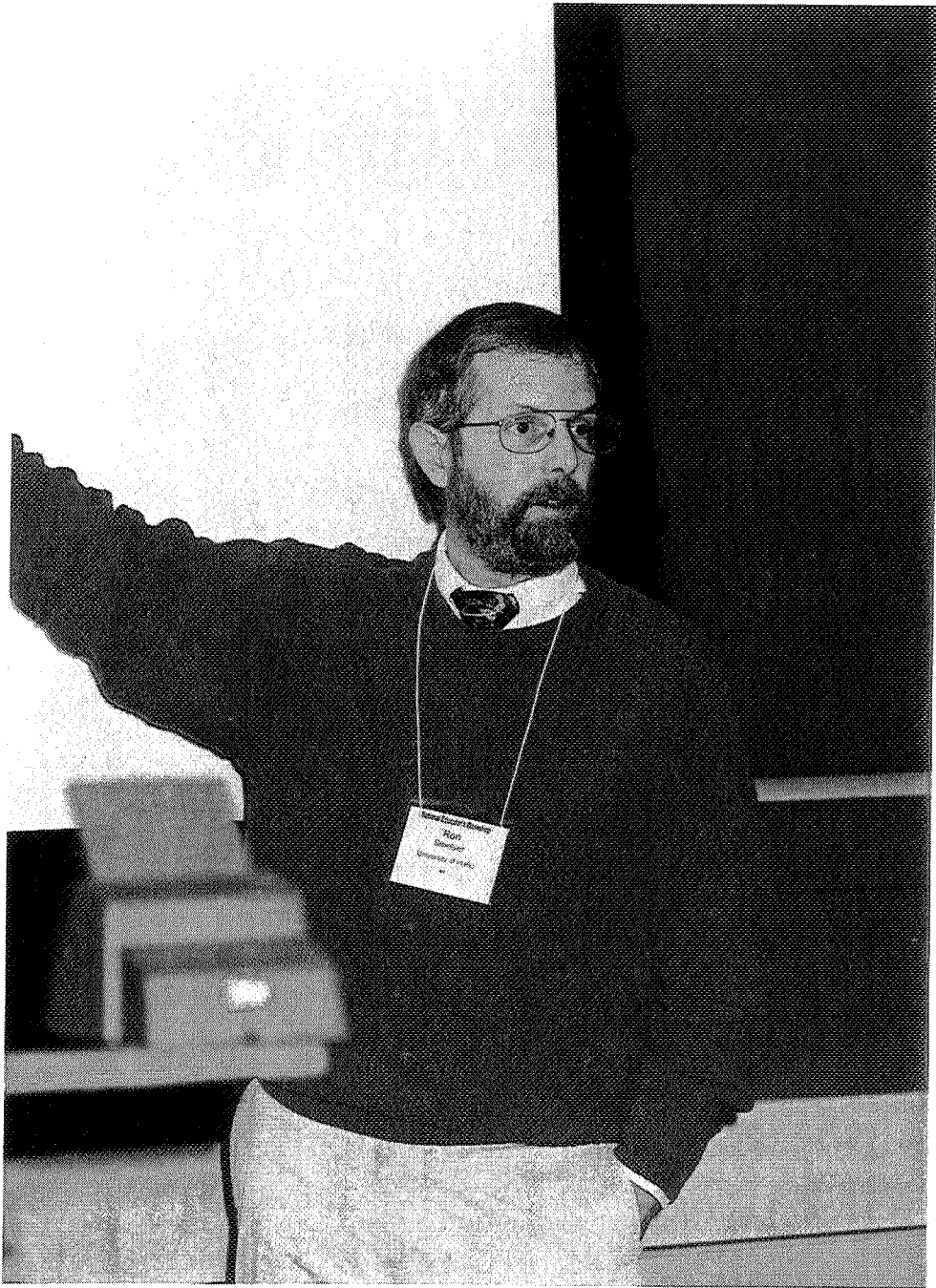
R. E. Smelser

E. M. Odom

S. W. Beyerlein

Mechanical Engineering Department
University of Idaho
Moscow, Idaho 83844-0902

Telephone: 208-885-4049
e-mail rsmelser@uidaho.edu
eodom@uidaho.edu



Ron Smelser

TABLETOP EXPERIMENTS FOR MATERIAL PROPERTIES DETERMINATION

R. E. Smelser, E. M. Odom, and S. W. Beyerlein
Mechanical Engineering Department
University of Idaho
Moscow, ID 83844-0902

Key Words: Elastic Modulus, Shear Modulus, Poisson's Ratio, Stress-Strain Curves

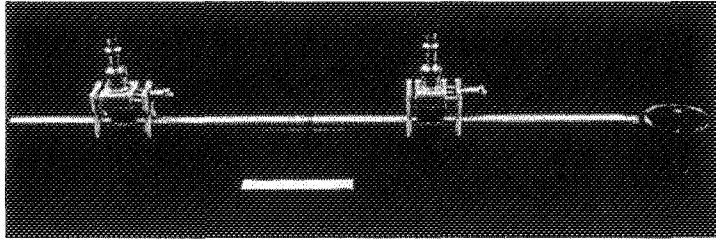
Prerequisite Knowledge: A knowledge of statics and a curiosity to understand how materials respond when subjected to various loadings.

Objectives: The determination of mechanical properties of materials can be a dull and sterile activity. Specimens are instrumented and loaded into testing machines. Machine parameters are set, buttons are pushed, and data are recorded. The data are subsequently analyzed and material properties are determined. This process removes the student from interaction with the material and a connection to the equipment. To increase student involvement and engage the student in the laboratory experience, we have designed a series of tabletop experiments to determine the elastic modulus, the shear modulus, Poisson's ratio, and the plastic response of engineering materials.

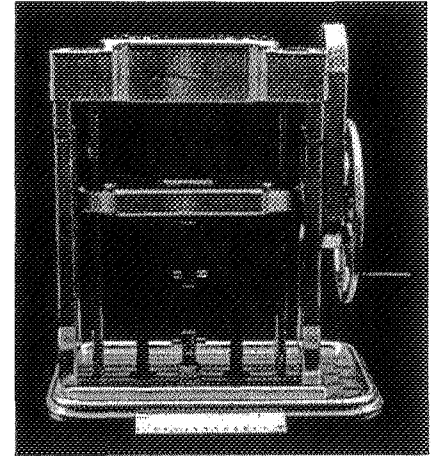
These experiments are part of the introductory course in the laboratory sequence in the Mechanical Engineering Department at the University of Idaho. The experiments are designed to introduce the student to the fundamental behavior of materials and structures through experiential learning. The experiments are also designed to help the student bridge the gap between the materials science courses and mechanics of materials courses. The laboratories also move the student from the prescribed experiments found in chemistry and physics courses to defining the experimental procedures that will be required in an engineering environment.

Equipment and Materials: The equipment used for these laboratories is a unique feature of the laboratory experience. Each of the experimental devices is simple, self-contained, portable, and of professional quality. Students design and construct the devices in the capstone design sequence under the mentoring of graduate assistants from the Idaho Engineering Works (IEW). The IEW is a program designed to foster leadership in engineering through an atmosphere of individual ownership and valuing of the person [Odom et al., 1999].

The tensile response of materials is determined by using a variant of the experiments that Robert Hooke employed to establish the elastic modulus [Timoshenko, 1953]. Figure 1(a) shows the device. A tabletop electromechanical load frame is used to determine the plastic properties of materials. Figure 1(b) shows a prototype of the tensile load frame. The load frame allows the students to feel the plastic response of a material as the deformation occurs under their control. The current load frame records the data from the experiment. The data can subsequently be downloaded to a personal computer for data analysis. A miniature R. R. Mohr device is currently under design and construction to allow the determination of the fatigue properties of metals.

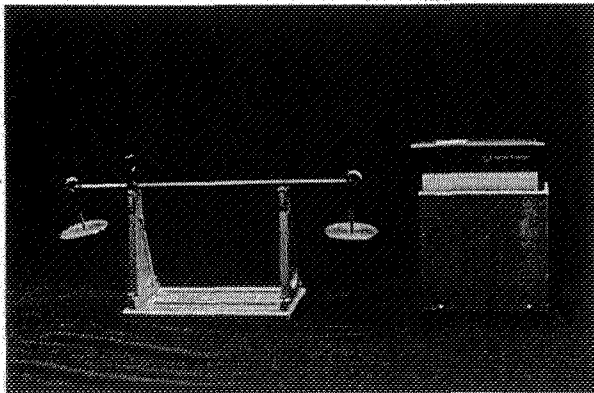


(a)

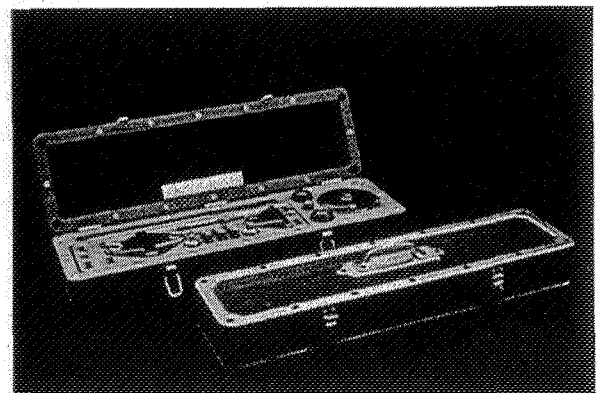


(b)

Figure 1. Experimental apparatus for tensile deformation (a) and stress-strain response (b).



(a)



(b)

Figure 2. Experimental apparatus for four point bending (a) and torsional response (b).

The elastic material properties are accurately determined from a four-point bend experiment and a simple torsion experiment, Figure 2. An optical system incorporating a low-power laser and a reflecting mirror allows the accurate determination of the specimen deflections. Several loads are applied to the system. This produces a series of data as a function of load. Elementary laws of optics and mechanics of materials formulae allow the determination of the elastic properties from this data. The computed elastic properties are typically within five per-cent of the accepted handbook value. The authors are exploring ways to make the designs for this equipment available for others.

Axial Loading - Tensile Tests

Introduction

In a standard tensile test, a uniaxial, increasing monotonic load is applied to a specimen until failure. Prior to specimen testing, the cross-sectional dimensions and the gage length of the specimen are measured. During the test, two transducers, a load cell and an extensometer, measure the load applied to the specimen and the elongation of the gage length, respectively. A load-elongation plot is generated as the test progresses from these transducer signals. More commonly, the data are stored in a computer for subsequent analysis. Some tensile tests are performed for strength determination only. In this case, only the maximum load prior to failure is required. Other tensile tests are performed to obtain strength, Young's modulus (the slope of the linear portion of the stress-strain curve), and percent elongation at failure.

Stress-strain data are typically generated from the load-elongation data by using the following equations:

$$\sigma = \frac{P}{A_i} \qquad \varepsilon = \frac{\delta}{L_i} = \frac{(L_f - L_i)}{L_i}$$

where σ is the tensile stress, P is the applied load, A_i is the initial cross-sectional area, ε is the strain, δ is the change in length, and L_i and L_f are the initial and final specimen gage lengths.

Objectives

The objectives of this experiment are:

- a) To observe and measure the axial loading response of various engineering materials.
- b) To determine the desired material properties for the given materials.
- c) To develop a general understanding of the behavior of various engineering materials.

Laboratory Equipment

- 1.) UI electromechanical test frame
- 2.) Hanging scales/hanging apparatus
- 3.) UI Wire tension apparatus

Procedure

Conduct various axial tension tests, one each for the nickel-chromium wire, the aluminum, brass or steel tensile specimens, and a rubberband. This means that you will need to observe the applied load for all cases and the change in length of the gage section (elongation). For the aluminum, brass or steel specimens, you will obtain digital output of the load vs. elongation from the UI electromechanical test frame. Your Lab Assistant will instruct you in the proper experimental procedure for these experiments. Before taking data, you should inspect and understand how the apparatus that you are going to use works. A brief explanation of each device is expected in your report. Some tables/needed information are provided as a guide to aid you in the data that you need to collect.

Laboratory Write-up

Your laboratory write-up should include all the sections outlined in the Laboratory Report requirements. Tables, graphs, answers to questions, and conclusions will be evaluated quite

thoroughly. A graph of the data observed and a sample calculation of the results for each material is required. A regression fit of the data where appropriate is also appropriate.

Questions/Exercise

Perform a regression fit of the stress-strain data that you collected for the two different gauge lengths to find Young’s modulus for the Ni-Cr wire. How do your “two” fits compare?

After you plot the stress-strain curve for rubber, can you calculate Young’s modulus for this material? If not why not? Can you explain how the behavior of the rubberband is similar to the “balloon” behavior in your PC exercise? While you are on the computer making graphs, graph the stress-strain responses for rubber and the nickel-chromium wire on the same graph. Include this plot if you feel it is relevant. If you do not feel that it is relevant, do not include the graph but explain why it was not included.

For the tensile specimens (aluminum, steel and brass) that were pulled apart,

1. Calculate the percent elongation (% elong) at failure of the smooth part of the gage section,
2. Calculate the percent reduction in area (% red area) at failure of the gage section,
3. Reflect on the difference of the values above for the two materials, and what these values conceptually mean.
4. How is δ_{max} from your tensile information different from your percent elongation at failure? What is that difference (calculation)?
5. What can be said about the “stiffness” of the metal specimen tested? How about strength?
6. Can you determine when the two metals tested began to yield? Estimate the yield strength of each material if you can.
7. What happened to the cross section of the specimens once the maximum strength (stress) was applied to the specimens?
8. Include a plot of the curves generated from the metal specimens and label the axes appropriately. Identify the point where the maximum stress was observed and where the specimen failed. If energy is measured as area under the curve (remember Experiment 1), which specimen had more stored energy?

Comment on the accuracy and adequacy of each apparatus used. What could be done to improve the accuracy of each portion of the experiment?

Data Tables

Load Versus Change in Length Data (Rubberband)					
$L_{initial} =$ _____ in		(width = _____ in, thickness = _____ in)			
P (lb.)	$L_{instantaneous}$ (in)	δ (in)	P (lb.)	$L_{instantaneous}$ (in)	δ (in)

Load Versus Change in Length Data (Nickel-Chromium Wire)					
Force on wire = $2.5 \times$ force due to weight of water					
Position #1 $L_{\text{initial}} = 14.125$ in			Position #2 $L_{\text{initial}} = 29.5625$ in		
Volume of water (ml)	micrometer reading (in)	δ (in)	Volume of water (ml)	micrometer reading (in)	δ (in)
0	0.3075	0.0	0	0.1952	0.0
20	0.3110	0.0035	20	0.2005	0.0053
40	0.3135	0.006	40	0.2050	0.0098
60	0.3157	0.0082	60	0.2085	0.0133
80	0.3172	0.0097	80	0.2135	0.0183
100	0.3207	0.0132	100	0.2202	0.0250
120	0.3221	0.0146	120	0.2231	0.0279

Wire diameter = 0.006 in

Tensile Information			
Steel Specimen		Brass Specimen	
$d_{\text{initial}} =$	$d_{\text{final}} =$	$d_{\text{initial}} =$	$d_{\text{final}} =$
$L_{\text{initial}} =$	$L_{\text{final}} =$	$L_{\text{initial}} =$	$L_{\text{final}} =$
$P_{\text{max}} =$ (from UI Load Frame)	$\delta_{\text{max}} =$ (from UI Load Frame)	$P_{\text{max}} =$ (from UI Load Frame)	$\delta_{\text{max}} =$ (from UI Load Frame)

Comments:

1. Example data is provided in the data table for the Ni-Cr wire experiment. This data is plotted in Figure 3.
2. The Ni-Cr wire experiment reinforces the ideas learned from statics that the load and hence the stress in the wire is the same for all locations.
3. The apparatus allows the deformation to be measured with an eyepiece micrometer at two locations. The reduction of the resulting data demonstrates that the strain at these locations is the same.
4. The question concerning the plotting of results for the rubberband and metals on a single graph requires the student to think about what is being plotted. The rubberband has a large strain but a small stress. The metals have small strains but substantial stresses. These two behaviors are incompatible on a single plot.
5. The data acquisition for the rubberband requires the students to consider the free body diagram of the loading devices. The total force is measured but is divided over two strands of the rubberband. Care must be used to assure that the appropriate forces and areas are used to compute the stresses.
6. Data are graphically displayed for the tensile tests conducted on the metal specimens. The data table has also been filled in for the tests.

7. The questions relating to these tests are to encourage the student to reflect on what the data is showing about the behavior of the materials and to make connections to descriptions in the course text [Gordon, 1978].
8. Figure 4 shows plots of typical load - elongation responses obtained from the UI electro-mechanical test frame.

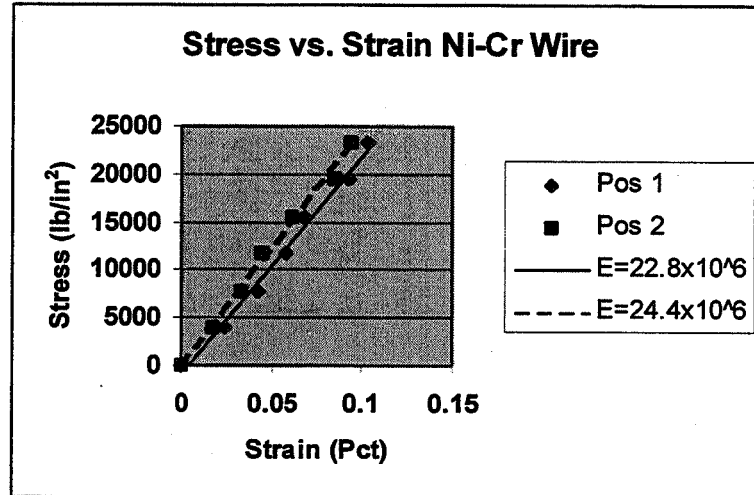


Figure 3. Stress-strain curve for the Ni-Cr wire using the UI wire tension apparatus.

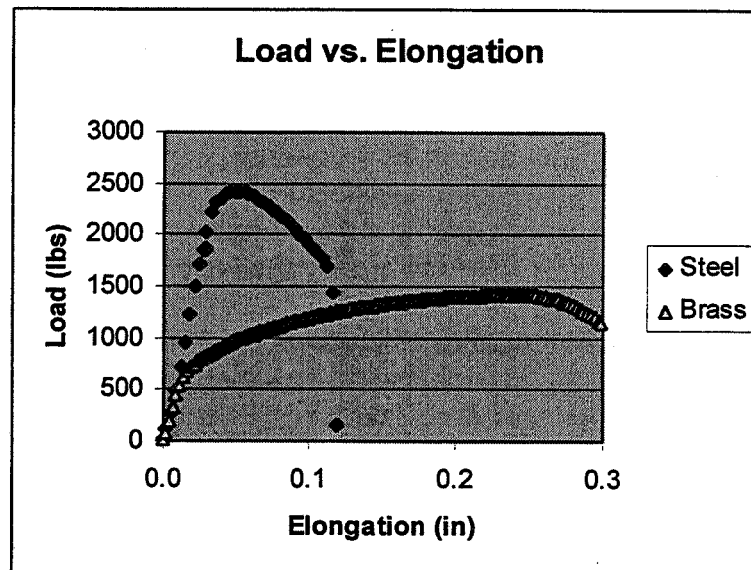


Figure 4. Load Elongation data for the steel and brass specimens.

Beam Deflections and Material Properties

Introduction

Probably the most common type of structural member is the beam. A beam may be defined as a member whose length is relatively large in comparison with its thickness and depth, and it is loaded with transverse loads that produce significant bending effects as opposed to twisting or axial effects (Remember the Axial Load Experiment?). Whenever a real beam is loaded in any manner, the beam will deform such that an initially straight beam will assume some deformed shape. Remember that in statics we assumed a beam was rigid. This is not actually the case. In Mechanics of Materials, many relationships for beams will be developed. We will explore several of them in this laboratory. The first is:

$$\frac{1}{\rho} = \frac{M}{EI}$$

where ρ is the radius of curvature of the deflected beam at the point of interest. In addition, from your statics background, M is the internal bending moment, E is Young's modulus, and I is the moment of inertia of the cross sectional area of the beam about the neutral axis perpendicular to the direction of the applied load on the beam. The moment of inertia I is given by the expression below:

$$I = \frac{1}{12}bh^3$$

where b is the width of the beam and h is the height or thickness of the beam.

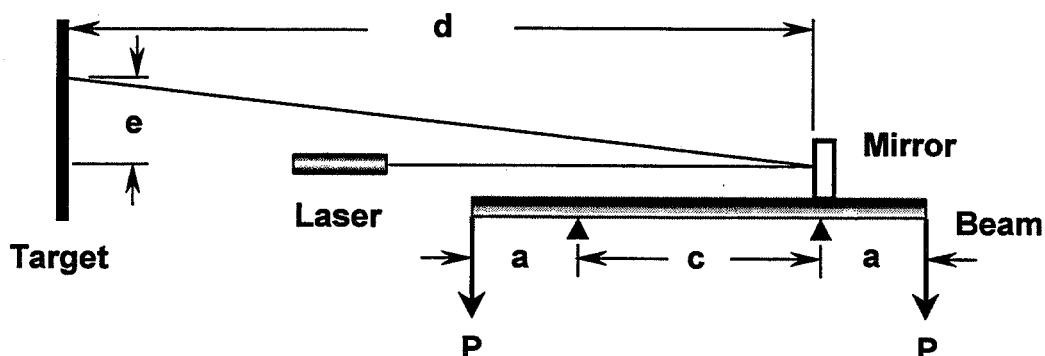
Objectives

The objectives of this experiment are:

- To explore beam deflections that result from externally applied loads. To accomplish this, we will measure the Young's modulus of aluminum, brass, and steel.
- To experimentally measure beam deflections and compare them to analytical predictions.

Procedure

This experiment involves using a simply supported beam loaded as shown in the next figure. This beam is loaded in such a manner that the *radius of curvature*, ρ , is constant between the two supports. A mirror mounted to the beam changes angle as the beam is loaded. By reflecting a laser beam off of the mirror and measuring the change in height of where the beam strikes a vertical



plane, we can determine the radius of curvature (ρ). Knowing the moment (M) and the moment of inertia (I) we can perform a calculation to find Young's Modulus (E).

Part A (Determining Young's Modulus)

The following information should help you in understanding the fundamentals of beam deflection and should also allow you to make the proper calculations to determine Young's Modulus for the various beam materials.

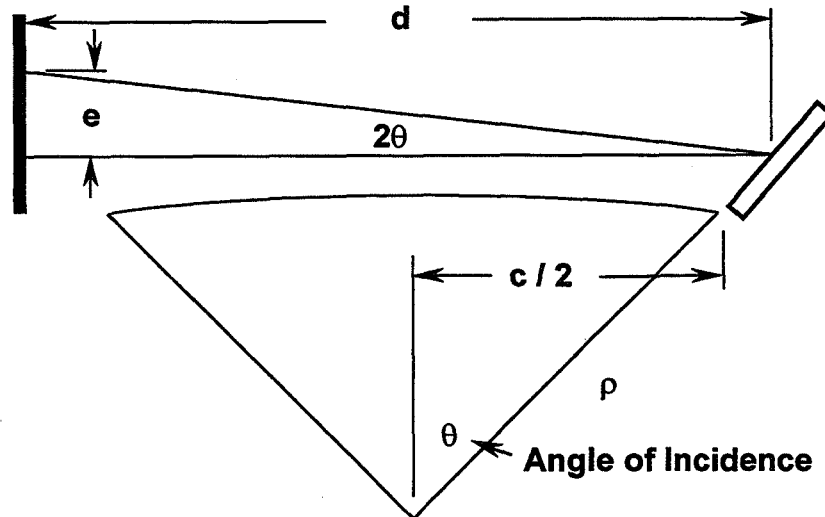
For the above loading condition on the beam, the moment, M , is determined to be:

$$M=Pa$$

From the following figure two more relationships can be found as shown below:

$$e/d = 2\theta$$

$$\rho \theta = c/2$$



If the last two relationships are combined, the result is:

$$\rho = dcle$$

Putting all these relationships into the radius of curvature relationship leads to the following:

$$\frac{l}{\frac{dc}{e}} = \frac{Pa}{E \frac{bh^3}{12}}$$

This can be rearranged to give the following:

$$P = \frac{Eb h^3}{12dca} e$$

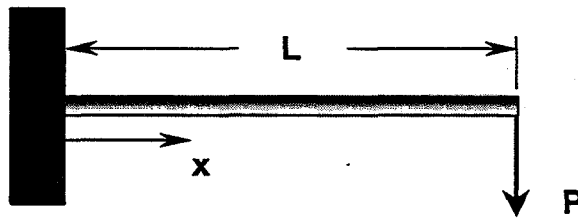
The expression has the form of a straight line, $y = mx + b$ where $y = P$ and $x = e$. In Part A, you will apply a load P and measure an elevation \hat{e} . You then will do a regression fit to find the slope m from which you can calculate Young's Modulus E . The data that you will need to take is to be found in the Data Sheets.

Part B (Comparison of Values)

In this part of the experiment, you will take measurements of beam deflections and compare them to an analytical prediction. The following equation applies to a cantilever beam as shown in the next figure.

$$v = \frac{P x^2}{6EI} (3L - x)$$

where (v) is the vertical deflection of the beam at any point along the length of the beam (x) The Laboratory Assistant will demonstrate the experimental apparatus. See the Data Sheets for the data that needs to be taken.



Part C (Deviation of Curvature Equation)

One of the main assumptions related to beam deflections is that the deflections are small. From this comes the simplification that when θ is small, $\cos\theta \approx 1$. However, when beams are exposed to large deflections, this assumption breaks down. This part of the laboratory addresses the breakdown of the moment-curvature equation presented in Part A. For the cantilever beam similar to Part B, the deflection equation for the "end" of the beam is

$$v = \frac{PL^3}{3EI}$$

Now apply loads in increments of 10 grams up to 100 grams and measure the deflections. See the Data Sheets for the required data.

Laboratory Write-up

Follow the laboratory report instructions previously provided. For Part A, do the values for Young's modulus compare well with the values provided in Gordon [1978] on page 54? Also find two other sources for Young's modulus. Are the various sources consistent? How well should they compare? You measured a, c, d, b, h, e, P during this experiment. An error in which of these would cause the most error in the resulting calculation of Young's Modulus? Why? Draw the

general profile of the “Shear and Moment Diagram” for the loading conditions of Part A. Explain why the radius of curvature is constant over the range of “ c ” from the first figure in this laboratory.

For Part B, prepare a plot of P (x-axis) versus v (y-axis) with the analytical expression indicated as a solid line and the experimental data as points. How well do the two compare? What is your definition of well in this case?

For Part C, prepare a plot of P versus v with the analytical expression indicated as a solid line and the experimental data as points. How well do the two compare? At what load does it appear that the experimental results start to diverge from the analytical expression? If the equation for the slope of the beam at the point of loading is $\theta = PL^2/3EI$, what is the angle θ at the maximum load applied? What is value of θ where the analytical and experimental results diverge? What is the value of $\cos \theta$ at the angle you chose? Is it close to 1? Also, in looking at the deflection of the beam at the higher loads, what geometrical changes are occurring to the loading configuration that could influence the deflection results?

Data Sheets

Part A:

Data you will need before beginning the experiment is as follows:

Distance from target to mirror (d)= 118.625 in
 Distance between supports (c)= 9 in
 Distance from load to support (a)= 3.5 in
 Width of beam (b)= 0.501 in
 Height of beam (h)= 0.252 Al, 0.254 Steel, 0.253 Brass (in)
 Initial height mark of laser = 0 in

Young's Modulus for aluminum is 10.3×10^6 lb/in²
 Young's Modulus for brass is 15.4×10^6 lb/in²
 Young's Modulus for steel is 30.0×10^6 lb/in²
 Young's Modulus for stainless steel is 27.8×10^6 psi

The following table may be useful for taking data.

Load P Versus Elevation e					
Aluminum		Steel		Brass	
Load (lb)	Elevation (in)	Load (lb)	Elevation (in)	Load (lb)	Elevation (in)
0.5	0.248	1.0	0.183	4.5	1.890
1.5	0.804	3.0	0.561	3.5	1.478
3.5	1.881	5.0	0.953	2.5	1.054
2.5	1.358	7.0	1.354	1.5	0.622
4.5	2.435	4.5	0.805	0.5	0.201

Part B:

Before starting this experiment you need to measure the following quantities:

- The beam width (b) = _____
- The beam height (h) = _____
- The beam length ($L+h$) = _____
- The distance ($x+h$) to where
you are measuring the deflection = _____
- The initial micrometer reading ($D_{initial}$) = _____

The following table may be useful for data collection.

Load P versus Deflection (v)					
Load (lb)	D_{final} (in)	v^* (in)	Load (lb)	D_{final} (in)	v^* (in)

* $v = D_{initial} - D_{final}$

Part C:

Before starting this experiment you need to measure the following quantities:

- The beam width (b) = 1.244 in
- The beam height (h) = 0.030 in
- The beam length ($L+h$) = 8 in
- The initial deflection of the beam due to its own weight ($v_{initial}$) = 0.140 in

The following table may be useful for data collection.

Load (grams)	Deflection (in)	Load (grams)	Deflection (in)
10	0.192	60	0.416
20	0.246	70	0.464
30	0.277	80	0.508
40	0.321	90	0.559
50	0.369	100	0.602

Comments:

1. The data tables have been completed for the determination of the modulus. The data are plotted in Figure 5. The regression of the data is shown, and the resulting moduli are as follows:

$$E_{Al} = 10.3 \times 10^6 \text{ lb/in}^2$$

$$E_{Steel} = 28.0 \times 10^6 \text{ lb/in}^2$$

$$E_{Brass} = 13.1 \times 10^6 \text{ lb/in}^2$$

2. The modulus of brass is highly composition dependent. The student learns this from the exploration of the literature to find handbook values for this quantity.

3. The data is randomly collected to avoid systemic errors that may occur in data collection.
4. In Part B, the length of the beam is specified as $L+h$. This is an empirical relationship. The relationship evokes student questions and facilitates a discussion of actual constraints in experimental development versus idealized constraints in models.
5. The large deflection of the cantilever beam is included to demonstrate the limitations of theories for beam deflection. The data table has been completed for this experiment and the graph of the data is shown in Figure 6.
6. The plot in Figure 6 forces students to recognize the mixed units in the plot. It also causes them to think about when a plot begins to deviate from the expected relationship and how to they might quantify such a deviation.
7. The class discussion that follows the laboratory explores the reasons why the linear theory does not fit the data. The students are shown the analytical result of Bisshopp and Drucker [1945] for this problem.

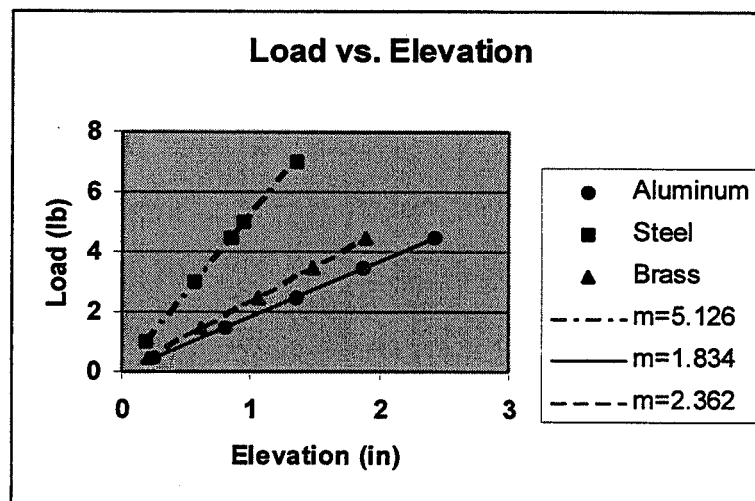


Figure 5. Plot of load vs. elevation for a beam in bending. The slope m is the elastic modulus

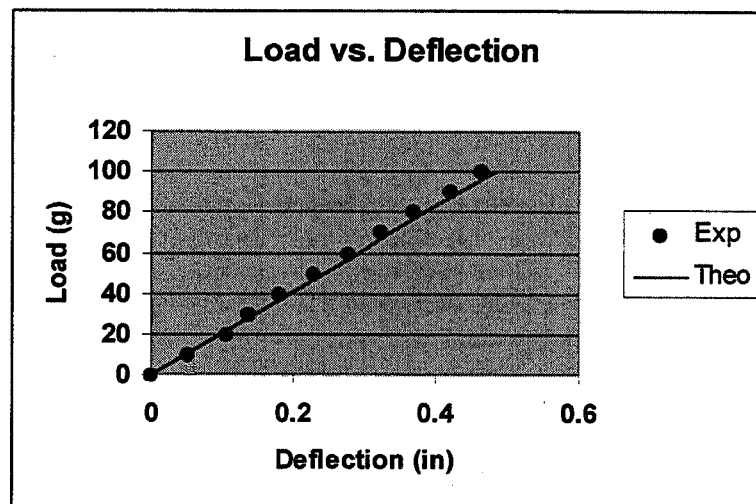


Figure 6. Plot of load vs. deflection for a large deflection cantilever beam.

Torsion of Shafts

Introduction

In the design of machinery (as well as structures) the problem of transmitting a torque (a couple) from one plane to a parallel plane is frequently encountered. The simplest device for accomplishing this function is a circular shaft. An example of a shaft is the connection of an electric motor with a pump, compressor, or other mechanism. In statics you saw several problems where shafts were subjected to torsional loads. In Mechanics of Materials, several analytical relationships for shafts subjected to torsion will be derived. Most of these will be related to deformation and load characteristics. One of these follows:

$$\theta = \frac{TL}{JG} \left(\frac{360^\circ}{2\pi} \right)$$

θ = angle of twist in degrees

T = torque

L = length of shaft

$J = \pi r^4/2$ (polar moment of inertia for circular cross section)

G = shear modulus

For the loading condition on the beam, the angle 2θ is:

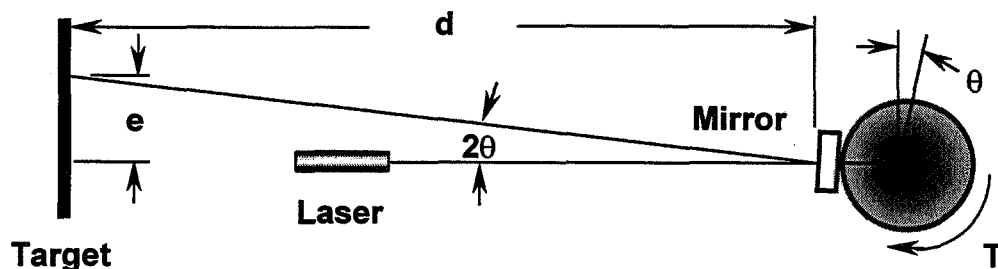
$$2\theta = e/D \text{ (for small angles, in radians)} \quad \text{or} \quad 2\theta = \tan^{-1} e/D \text{ (actual, in degrees)}$$

The angle of twist, θ , can then easily be determined.

Objectives

The objectives of this experiment are:

- To explore the relationship between the applied torque and the resulting angle of twist of a shaft.
- To measure the shear modulus of various engineering materials.
- To observe deformation characteristics of torsional members.



Part A (Torque vs. Angle of Twist)-Dial Apparatus

First, rewrite the above relationship as:

$$\theta = \left(\frac{T}{JG} \right) \left(\frac{360^\circ}{2\pi} \right) L$$

This equation has the form of $y = mx + b$, where $\theta = y$, $m = (T/JG)(360^\circ/2\pi)$, $x = L$, and $b = 0$. To verify this relationship, first place a shaft into the torsion test device and make the measurements as indicated in the data table. Plot the angle of twist versus the length for each of the applied torque's. If appropriate draw a straight line through the data.

Part B (Determining Torsional Properties)

In this experiment, you will measure the shear modulus of aluminum, brass, and steel. This will be accomplished by first rewriting the previous equation as follows:

$$T = \left(\frac{JG}{L}\right)\left(\frac{2\pi}{360^\circ}\right)\theta$$

In this case the slope $m = (JG/L)(2\pi/360^\circ)$. By selecting one rod of aluminum, brass, and steel, applying at least three torque's (T 's), and measuring the resulting angles of twist (θ 's), the slope m can be calculated using a regression fit. Since the length L and the radius r can be measured before the test, the only value to be determined is the shear modulus G .

Laboratory Write-up

Answer the following questions for each of the parts of the experiments where appropriate. Perform a regression fit between the angle of twist versus length data for each applied torque. Does a straight line represent the data? Does the regression fit give an intercept of zero. Should it? Any ideas? After determining the slope m for Part B, calculate the shear modulus G for both procedures. How do the results compare? Which appears more accurate (for actual values-see last question)? List some of the experimental errors for both experimental set-ups. How might the errors introduced be reduced or eliminated? In your experiments, how would you know if you accidentally exceeded the elastic limit of the rods? Assuming a Poisson's ratio of 0.3, a value for Young's modulus E as stated on page 54 of Gordon [1978], and the equation on the bottom of page 249 of Gordon [1978], calculate the shear modulus G . Compare G from the experiments to these values. In addition, list and briefly describe three components that experience torsional loads (try and be creative).

Data Tables

(Part A)

Angle of Twist θ versus Length L				
Material:	Length (in)	$\alpha_{initial}$ ($^\circ$)	α_{final} ($^\circ$)	$\theta = \alpha_{final} - \alpha_{initial}$ ($^\circ$)
$T_1 = (\text{force X moment arm}) = (\text{X}) =$				
L_1				
L_2				
$T_2 = (\text{force X moment arm}) = (\text{X}) =$				
L_1				
L_2				
$T_3 = (\text{force X moment arm}) = (\text{X}) =$				
L_1				
L_2				

The radius of the pulley, r , is 3 in

(Part B)-ALL THREE MATERIALS

Torque = load x moment arm = P x r					
Load P vs. elevation e					
Aluminum		Brass		Steel	
load(P) (grams)	Elevation(e) (in)	load (grams)	Elevation (in)	load (grams)	Elevation (in)
1000	4.125	500	2.8375	500	6.7125
2000	9.625	1000	5.75	1000	13.363
3000	15.8125	1200	7.125	1200	16.125
L = 7.81 in,		L = 7.25 in,		L = 7.25 in,	
diameter = 0.2506 in		diameter = 0.1878 in		diameter = 0.1251 in	
D = 115 in		D = 115 in		D = 114.25 in	

The radius of the pulley, r, is 2 in

(Part B)-TWO OF THE THREE MATERIALS

Torque = load x moment arm = P x r			
Material	Length	shaft diameter	
Load (lb)	$\alpha_{initial}$ (°)	α_{final} (°)	$\theta = \alpha_{final} - \alpha_{initial}$ (°)
Material	Length	shaft diameter	

The radius of the pulley, r, is 3 in

Comments:

- The data table for Part B has been completed. The resulting plots are shown in Figure 7. The resulting shear moduli are
 - $G_{Al} = 3.8 \times 10^6 \text{ lb/in}^2$
 - $G_{Steel} = 11.3 \times 10^6 \text{ lb/in}^2$
 - $G_{Brass} = 5.1 \times 10^6 \text{ lb/in}^2$
- The shear modulus from this experiment can be used with the tensile modulus from the beam bending experiment to compute Poisson's ratio.
- The combination of these two experiments to compute Poisson's ratio is a natural way to introduce the subject of error propagation in experiments. This topic is discussed in detail in later laboratory courses.

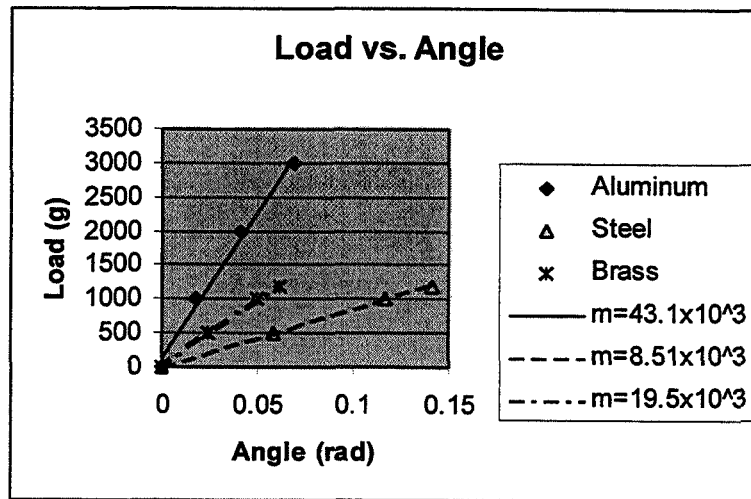


Figure 7. Load vs. angle of elevation for determining the shear modulus for Aluminum, steel, and brass.

References:

K. E. Bisshopp and D. C. Drucker, 1945, Large Deflection of Cantilever Beams, *Quarterly of Applied Mathematics*, 3, 272-275.

J. E. Gordon, 1978, *Structures, or Why Things Don't Fall Down*, Da Capo Press, New York.

Edwin M. Odom, Steven W. Beyerlein, Blaine W. Tew, Ronald E. Smelser, and Donald M. Blacketter, 1999, Idaho Engineering Works: A Model for Leadership Development in Design Education, *Frontiers in Education Conference*, San Juan, Puerto Rico, 1999 November 10-13.

Stephen P. Timoshenko, 1953, *History of Strength of Materials*, McGraw-Hill Book Company, New York.

Ronald E. Smelser

Ronald E. Smelser is an Associate Professor of Mechanical Engineering at the University of Idaho. He holds a Bachelor's degree from the University of Cincinnati, a Master's Degree from MIT, and a Ph. D. from Carnegie Mellon University. Prior to joining the faculty at the University of Idaho, he worked for fourteen years at U. S. Steel, Alcoa, and Concurrent Technology Corporation. He currently teaches the Sophomore Laboratory, is involved with the Idaho Engineering Works, and leads the effort to develop the Sophomore Laboratory for distance delivery. His interests include materials process modeling, structure-property relations of materials, and material failure and fracture. He is a member of ASME, ASEE, and AAM. He has published numerous papers on materials processing and fracture and has contributed to the ASEE Annual Conference.

Edwin M. Odom

Edwin M. Odom, an Associate Professor of Mechanical Engineering at the University of Idaho, obtained his undergraduate and graduate degrees from the University of Wyoming. His interests include experimental mechanics and the design process. Dr. Odom joined the University of Idaho eight years ago and takes an active interest in the ME Machine Shop as a key element in design education. The ME department benefits enormously from his experience in the US Army at the Material Test Directorate as well as his experience as a gas turbine design engineer for the General Electric Company. Dr. Odom developed the Sophomore Laboratory. He also maintains an avid interest in the subject of creativity and management and is a recognized leader in the areas of team dynamics and leadership styles. He was recognized for his role in development of the Senior Design program and the Idaho Engineering Works by a university teaching award in 1998.

Steven W. Beyerlein

Steven W. Beyerlein is an Associate Professor of Mechanical Engineering at the University of Idaho. He has a Bachelor's degree from the University of Massachusetts, a Master's degree from Dartmouth University, and a Ph. D. from Washington State University. Dr. Beyerlein is a leader in the design and implementation of process-oriented engineering curricula that stresses cooperative learning, computer technology, and mini-projects. Since joining the University of Idaho eleven years ago, he has regularly taught introductory courses to freshman and sophomores and has shaped the Senior Laboratory course. Implementation of Process Education techniques in these courses significantly improved student preparation for the ME capstone design experience. Over the last four years, he has led interactive faculty workshops on Process Education at the University of Idaho, Washington State University, Boise State University, and Ricks College. He has also been active in the local section of ASEE.

ACCELERATED FATIGUE TEST

Yulian Kin

and

Dennis Holler
Graduate Student

Purdue University Calumet
Hammond, Indiana 46323

Telephone: 219-989-2684
e-mail kin@hwi.calumet.purdue.edu



Yulian Kin

ACCELERATED FATIGUE TEST

Yulian Kin
Dennis Holler
Purdue University Calumet

Key Words: Fatigue, endurance limit, fatigue life, fatigue tests.

Prerequisite Knowledge: Knowledge of basic fatigue concepts and fatigue experimentation is helpful.

Objective: Conduct a conventional fatigue test using 16-20 standard specimens, plot S-N curve, plot family of fatigue curves with 5%, 50% and 95% probability of failures and determine necessary parameters for the accelerated fatigue test. Then conduct an accelerated fatigue test. Compare the endurance limits determined from conventional and accelerated tests.

Equipment:

1. Rotating beam fatigue machine.
2. Standard round fatigue specimens.

Introduction:

A long-term conventional fatigue test procedure requires the breaking of 30 to 60 identically prepared specimens and 15 days to 1 month to complete. Thus, manufacturers are often reluctant to perform a conventional fatigue test in spite of its obvious utility. Therefore, there is a definite need for an accelerated test that can be completed in approximately one shift. The accelerated fatigue test is also very useful to control technological process and in preliminary evaluation of the new designs.

The Locaty's accelerated procedure was used in this experiment. This method is based on the concept of cumulative fatigue damage [1] and we assumed that fatigue limit corresponds to sum of relative lives $\Sigma (n_i/N_i) = 1$, where n_i is the number of cycles which a specimen worked in the specified testing regime, and N_i is the number of cycles which a specimen could potentially work in accordance with the fatigue curve received from the long-term fatigue tests of the same type of specimens. The loading program and treatment of the results are given in details later.

Specimens:

The testing specimens were machined from 1018 cold finished steel and their configuration is given in Figure 1.

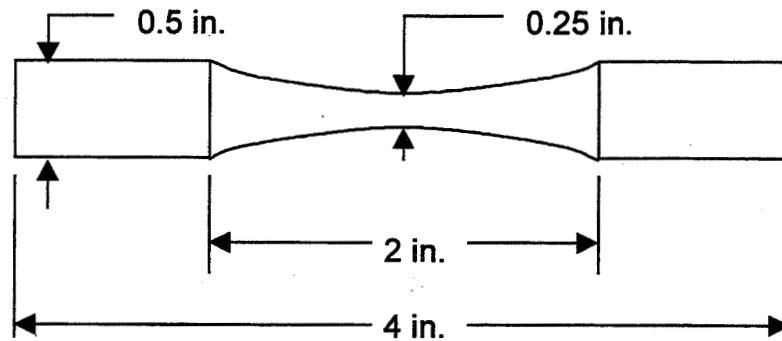


Figure 1. Specimen Configuration.

Experimental Set-up:

A bending fatigue testing machine sketch with an installed specimen is shown in Figure 2. The bending moment varies along the beam and the critical stress was determined at section "A".

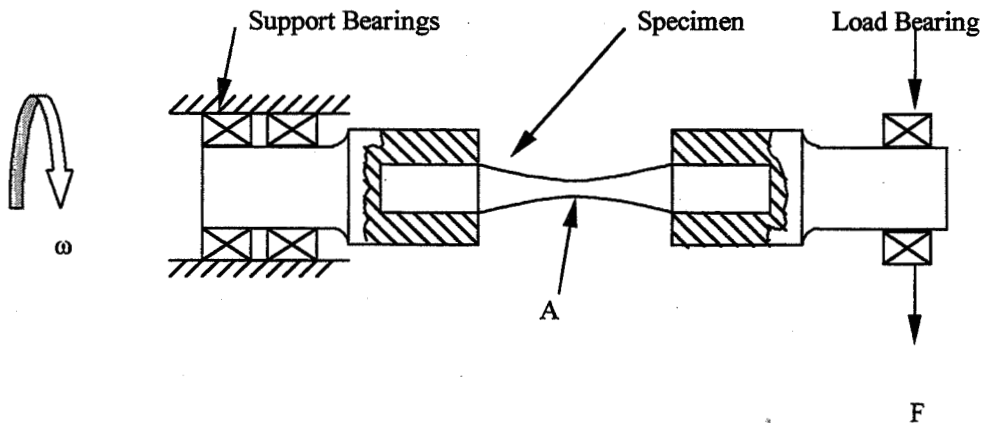


Figure 2. Experimental set-up.

Conventional Fatigue Test Procedure and Results:

61 identical specimens were tested to accumulate data for the S-N curves. Load levels and corresponding fatigue lives are given in the Table 1. They were ordered by load and cycles to failure for ease of use in the Excel program. While an equal number of specimens per stress level is desirable, it is not necessary. The difference in specimen number per stress level is due to the limited amount of testing time.

TABLE 1. Conventional Fatigue Test Results

Specimen number	Amplitude Stress, psi	Number of cycles	Specimen number	Amplitude Stress, psi	Number of cycles
1	55,411	160000	32	50,522	800000
2	55,411	178700	33	50,522	920000
3	55,411	190000	34	50,522	980700
4	55,411	205800	35	50,522	1553000
5	55,411	207400	36	48,892	611700
6	55,411	210000	37	48,892	630000
7	55,411	210100	38	48,892	639400
8	55,411	224000	39	48,892	733300
9	55,411	224000	40	48,892	797600
10	55,411	238000	41	48,892	809200
11	55,411	250000	42	48,892	914200
12	55,411	260000	43	48,892	950000
13	55,411	280000	44	48,892	1169500
14	52,151	339400	45	48,892	1326300
15	52,151	360000	46	48,892	1801100
16	52,151	418300	47	48,892	1 x 10 ⁷
17	52,151	420000	48	45,632	1871100
18	52,151	541600	49	45,632	2480000
19	52,151	620000	50	45,632	3738600
20	52,151	860000	51	45,632	4092800
21	52,151	946700	52	45,632	5545400
22	52,151	965500	53	45,632	7472500
23	52,151	990000	54	45,632	1 x 10 ⁷
24	50,522	204800	55	45,632	1 x 10 ⁷
25	50,522	350000	56	45,632	1 x 10 ⁷
26	50,522	400000	57	45,632	1 x 10 ⁷
27	50,522	447300	58	45,632	1 x 10 ⁷
28	50,522	520000	59	39,113	1 x 10 ⁷
29	50,522	603100	60	39,113	1 x 10 ⁷
30	50,522	623100	61	39,113	1 x 10 ⁷
31	50,522	626500			

Fatigue data for constant stress level with 50% probability of survival plotted on standard S-N plot are given in Figure 3 and curves with 5% and 95% probability of survival are shown in Figure 4. The vertical portion of the curves is formed based on a plot of the probability of failure of each specimen at a given life on log-normal probability paper. At the same time, the horizontal portion of the curves is based on the probability of survival at the load level. From these data we can conclude that 50% fatigue limit = 45,632 psi, 5% fatigue limit = 48,240 psi, and 95% fatigue limit = 41,721 psi.

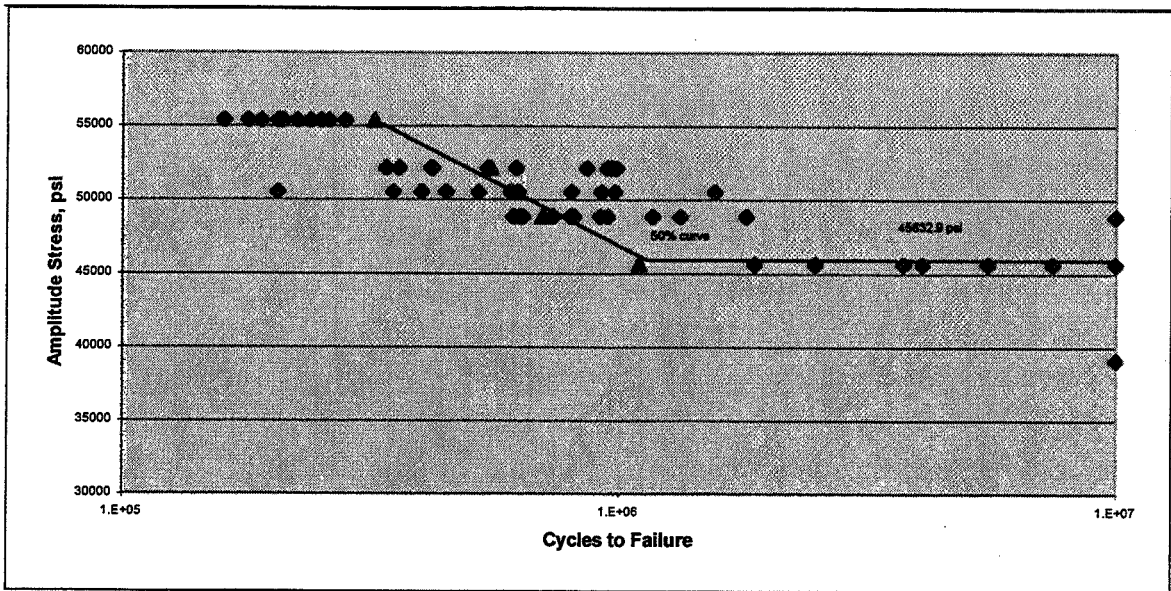


Figure 3: 50% probability fatigue curve

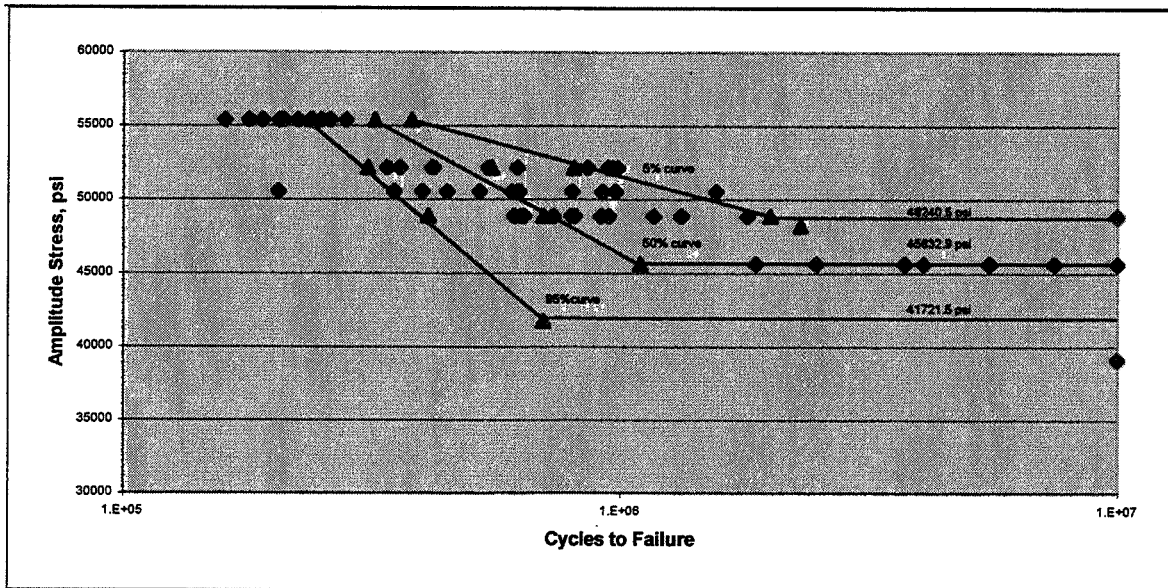


Figure 4: Family of Fatigue Curves (5%, 50%, 95% probability of survival)

Accelerated Fatigue Test Procedure and Results:

Program and results of accelerated fatigue test are given in Figure 5 and 6. The load increment and constant number of cycles on one load level were determined by trials to get at least 6 loading increments before fracture of the specimen.

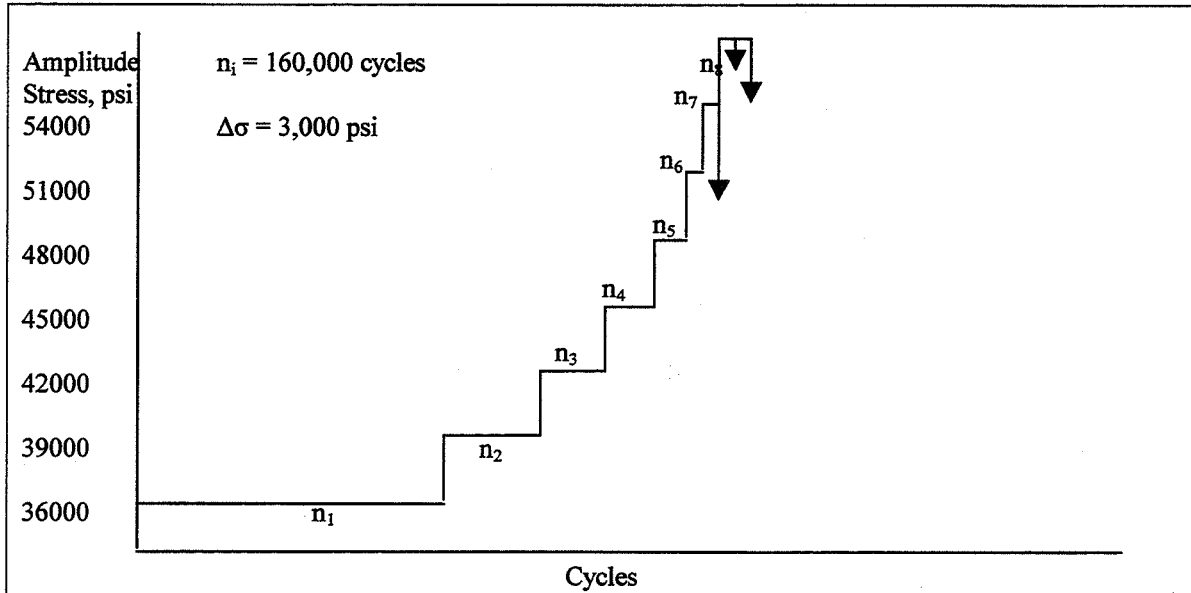


Figure 5: Program of Accelerated Fatigue Test. Load increment = 3000 psi; Number of cycles at each load level before fracture = 160,000 cycles.

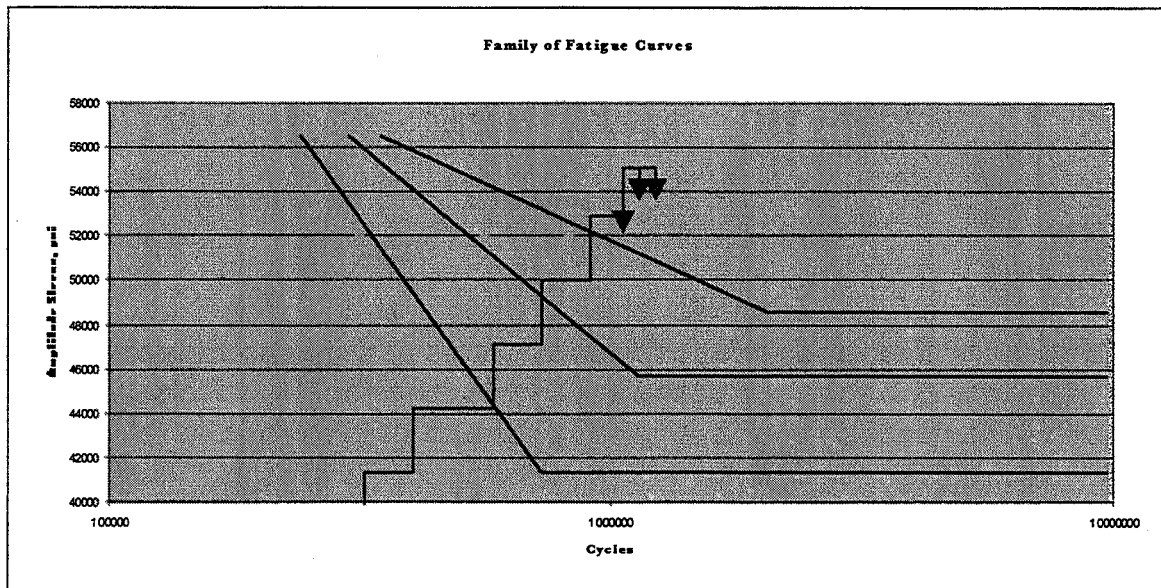


Figure 6: Probability S-N curves and accelerated fatigue test results. This diagram is used to determine relative lives at each load level for each curve.

The accelerated fatigue test results are given also in table 2, and treatment of the results is shown in table 3.

Table 2. Accelerated Test Results

Specimen number	Stress increment, psi	Number of cycles at one load level	Number of steps until failure	Number of cycles until failure
1	3000	160,000	8	1,146,100
2	3000	160,000	8	1,162,700
3	3000	160,000	7	1,021,800

Table 3. Accelerated Test Results Treatment

Amplitude Stress, psi	Curve A (95%)		Curve B (50%)		Curve C (5%)	
	N_i	n_i/N_i	N_i	n_i/N_i	N_i	n_i/N_i
36,000	1×10^7	0.016	1×10^7	0.016	1×10^7	0.016
39,000	1×10^7	0.016	1×10^7	0.016	1×10^7	0.016
42,000	1×10^7	0.016	1×10^7	0.016	1×10^7	0.016
45,000	1×10^7	0.016	1×10^7	0.016	550,000	0.291
48,000	1×10^7	0.016	1,010,000	0.158	480,000	0.333
51,000	1×10^6	0.016	700,000	0.229	310,000	0.516
54,000	550,000	0.291	400,000	0.400	290,000	0.552

$$\Sigma (n_i/N_i)_A = 0.531 \quad \Sigma (n_i/N_i)_B = 0.851 \quad \Sigma (n_i/N_i)_C = 1.74$$

Where: N = number of cycles possible for defined infinite life of specimen
 n = number of cycles completed by specimen at the particular stress level.

The Treatment of the Accelerated Test Results is a sum of the cycles completed at each load level compared to the cycles at infinite life of the specimen. These values were then plotted versus the endurance limit for each of the fatigue curves (5%, 50%, 95%). The resulting amplitude stress that corresponds to one is the endurance limit of the material. The Graphical Determination of Fatigue Strength (Figure 7) shows how the accelerated test results treatment (Table 3) is used to find the Endurance Limit of the material.

Graphical representation of the accelerated fatigue test results is given in Figure 7. Fatigue limit corresponds to the sum of relative lives equal unity which is indicated on the plot by the lines with arrows

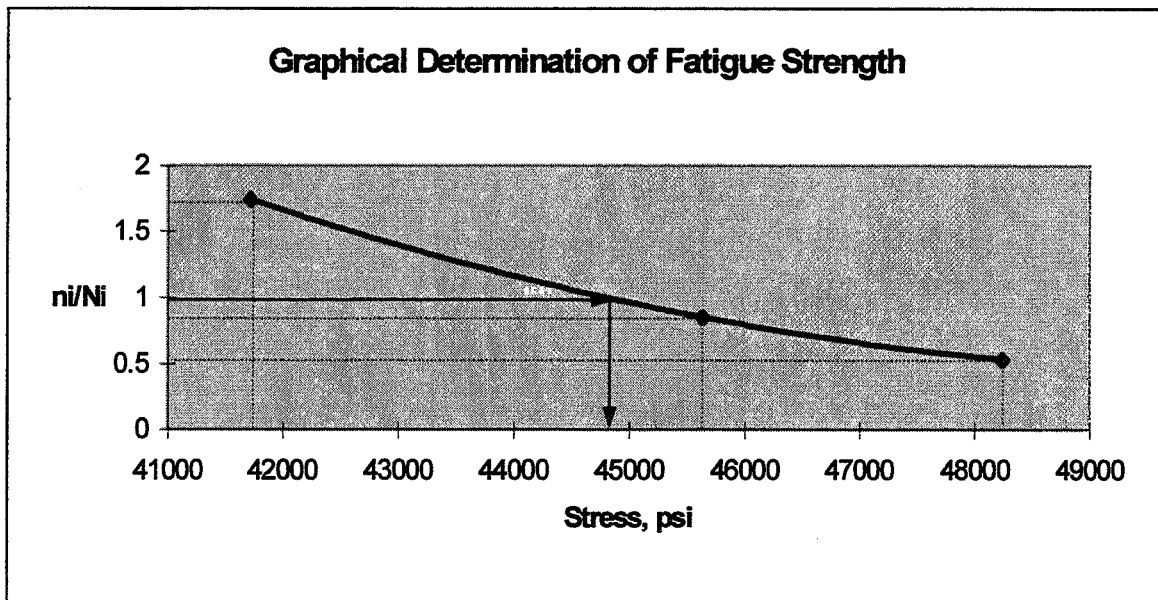


Figure 7.

Comments:

1. Comparing fatigue limits determined from the accelerated and conventional tests we can see that the difference is not more than 5% which is very good for the fatigue experimental results.
2. Time spent for the accelerated fatigue test was four hours.
3. Time spent for the conventional fatigue test was fifteen days.
4. Number of specimens used in the conventional procedure was (lots).
5. Number of specimens used in the accelerated procedure was three.

Acknowledgement:

Sponsorship by the Indiana Space Grant Consortium is gratefully acknowledged.

References:

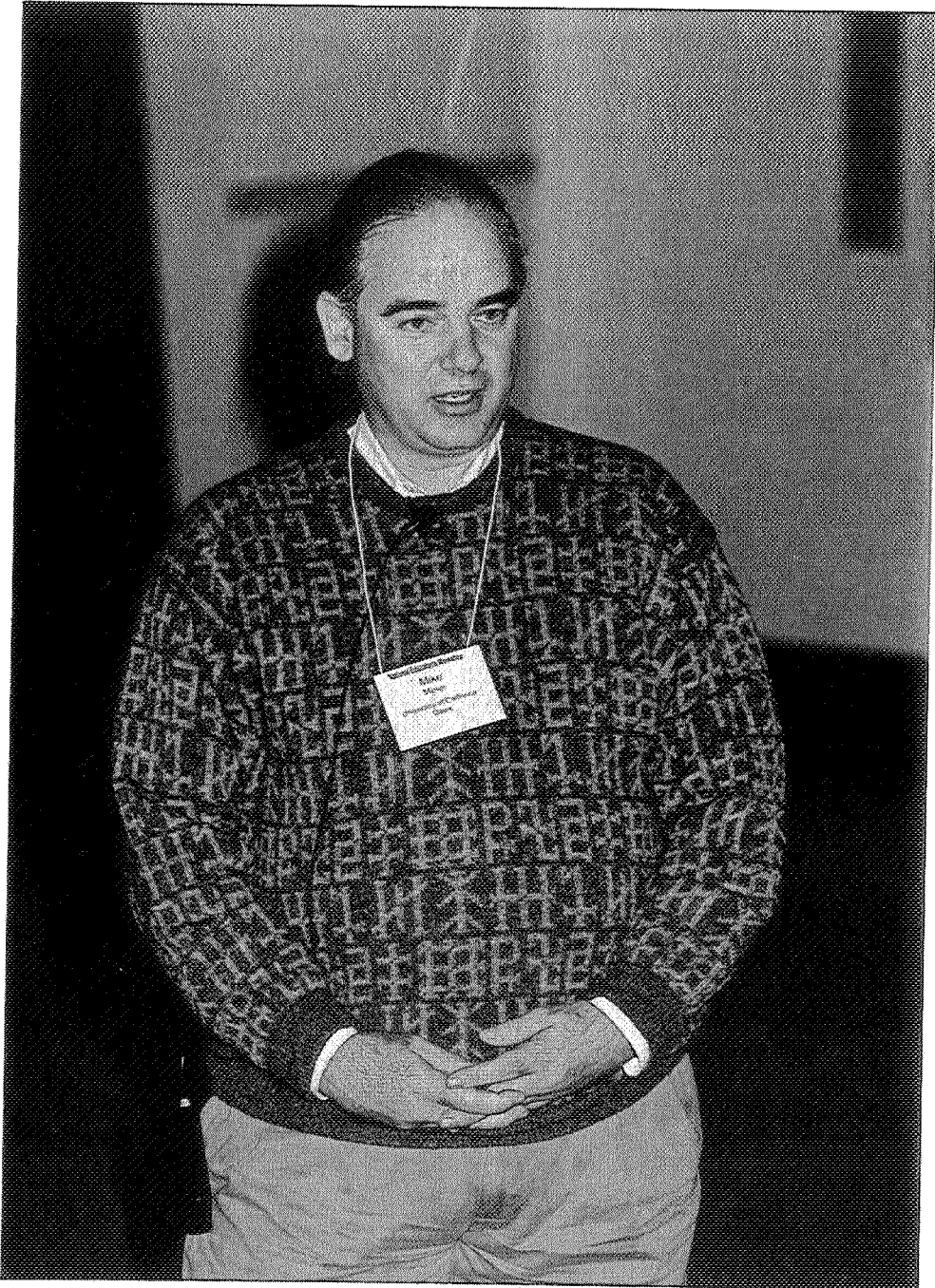
1. A. Palmgren, "Die Lebensdauer von Kugellagern", ZVDI, Vol. 68, pp. 339-341, 1924, M. A. Miner, "Cumulative Damage in Fatigue", J. Appl. Mech., Vol. 12, Trans. ASME, Vol. 67, pp. A159-164, 1945

FOUR WINDOWS PROGRAMS FOR THE MATERIALS SCIENCE LABORATORY

Mike L. Meier

Department of Chemical Engineering and Materials Science
University of California, Davis
Davis, California 95616

Telephone: 916-752-5166
e-mail mlmeier@ucdavis.edu



Mike Meier

Four Windows Programs for the Materials Science Laboratory

Mike L. Meier
Department of Chemical Engineering and Materials Science
University of California, Davis
Davis, CA 95616

Keywords

Software, grain size, mean lineal intercept, volume fraction of phases, point count method, Jominy end-quench, heat treating of steels, hardness, hardenability, data acquisition, WAV files.

Prerequisite Knowledge

The prerequisite knowledge for each of the programs is listed below.

- *Heyn's Method* - basic metallography and stereology, grain size, mean lineal intercept
- *Point Count* - basic metallography and stereology, volume fraction of phases, point count method
- *Jominy* - Jominy end-quench, heat treating of steels, hardness, hardenability
- *Audio Scope* - data acquisition, WAV files

Objective

This article does not describe an experiment, but rather several computer programs that may be useful in laboratory experiments many of us already perform. The functions and features of each program are summarized along with comments on how we use these programs in the classroom.

Equipment and Materials

All of these programs run under Window 95 and NT, so all one needs is a PC running one of these operating systems. To use *Audio Scope* in the laboratory one may also need an external amplifier to condition the signal for the ± 1 volt sound card inputs.

Introduction

As microcomputers become more powerful, less expensive and easier to use they are finding their way into almost every aspect of education. In the laboratory they have long been used for data collection and analysis. Currently there are also many large and often expensive programs on the market that will do what would have been extremely impractical, if not impossible to do by hand. In our small department, for instance, we use major software packages that perform finite element modeling, molecular dynamics modeling, crystallographic calculations, image processing and analysis, thermodynamic calculations and data retrieval from large databases. Still, we are in constant need of simpler and smaller software tools that do tedious work that we somehow still find ourselves doing manually. Many of us can think of operations that we wish the computer could do for us, or which would help ensure success in our teaching experiments, or something that has been sitting in our heads for years, or staring back at us from a text book, whose time has come to be

“animated” as computer code. Fortunately programming tools such as Microsoft’s VisualBASIC and Borland’s Delphi make it relatively easy for intermittent programmers such as engineering students and instructors to write useful programs that can run in the rich but very complicated Windows environment. With the availability of such tools the desire to code finally got the best of me and I ended up writing several modest but useful computer programs that we regularly use in our laboratory courses.

Heyn’s Method

Heyn’s method, better known as the mean lineal intercept method, is widely used for estimating the average grain size in polycrystalline materials. ASTM standard E 112-88 describes this method in detail along with the procedure for converting the mean lineal intercept length to an equivalent ASTM grain size.

Basically, the method involves laying a test line over a field of view and counting either the number of grain boundary intersections or the number of grain intercepts. The length of the test line divided by the number of intersections, or intercepts, gives a mean lineal intercept length. After repeating this procedure a number of times basic sampling statistics can be used to produce an overall average value plus the confidence interval for a specified confidence level. The math is simple enough, but tallying the counts and doing the calculations while observing the microstructure is tedious and likely to lead to errors, especially for the student who is doing this for the first time.

The program *Heyn’s Method* (Figure 1) makes tallying the counts and calculating the results painless and easy. To use it, one presses the *New* button to start a new measurement. After entering the test line length, magnification and confidence level one can start entering the counts into a spreadsheet-style grid. After five entries have been made, the program will calculate and display the mean value, the relevant statistics and the ASTM grain size. To aid in data entry one can bring up the keypad tool which will allow one to click-in the intercepts while observing them in the microscope. Finally, the results can be printed and saved as a text file.

One final feature, the graph, was added to help the student see the data plotted as a histogram plus the normal distribution for the current values of the mean and standard deviation. This graph will automatically rescale itself to center the data along the x-axis and to fit it within the range of the y-axis.

This has been a very useful program in several of our laboratory courses. We give it to the students to take home and perform several grain size measurements on real and artificial microstructures [1]

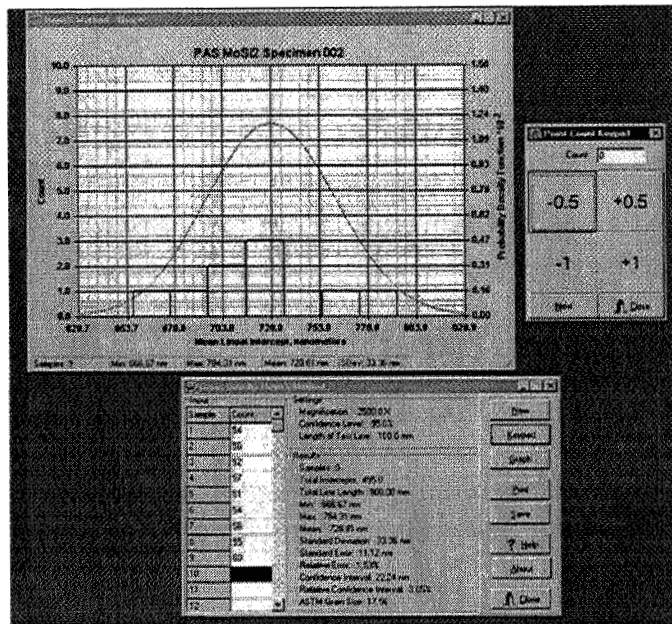


Figure 1 Screen shot of the Heyn’s Method program.

after we have spent sufficient time together discussing the technique and the statistical functions involved. Several of our graduate researchers have also taken copies to their lab and use it to analyze their optical and TEM images.

Point Count

The point count method is widely used to estimate the volume fraction of phases in a multi-phase material. This method, described in detail in reference 2, involves laying a grid over the field of view and counting the number of grid intersections which fall on the phase of interest. The volume fraction of phases is calculated by simply dividing this count by the total number of intersections in the grid.

The program *Point Count* (Figure 2) is nearly identical to *Heyn's Method* except for minor changes in how it handles the counts, and the fact that it is used to estimate the volume fraction of phases. The statistics are identical.

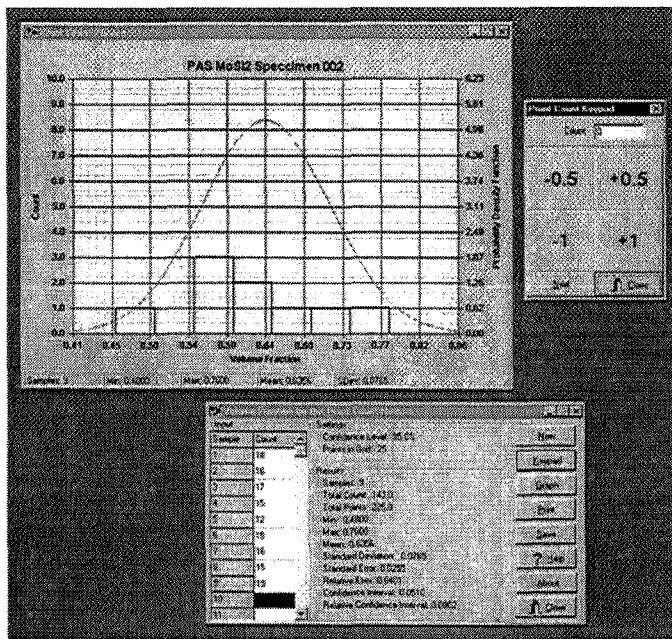


Figure 2 Screen shot of the Point Count program.

The utility of this program in our laboratories is similar to that of the *Heyn's Method*. Student's and researchers alike have found it to be a handy program to have on a computer next to the microscope or a collection of micrographs.

Jominy End-Quench

The Jominy end-quench (ASTM A 255-89) is widely used in industry to gage the heat treatability of steels. In the classroom it may be used to teach the principles of the kinetics of phase transformations, of strengthening mechanisms, and of the heat treatment of steel. Among these lessons is the fact that it is the carbon in steel which is primarily responsible for the maximum hardness of the martensite while the other alloying elements may increase or decrease the rate of martensite formation and therefore the amount of martensite that forms for a given cooling rate. Appendix X2 of ASTM A 255-

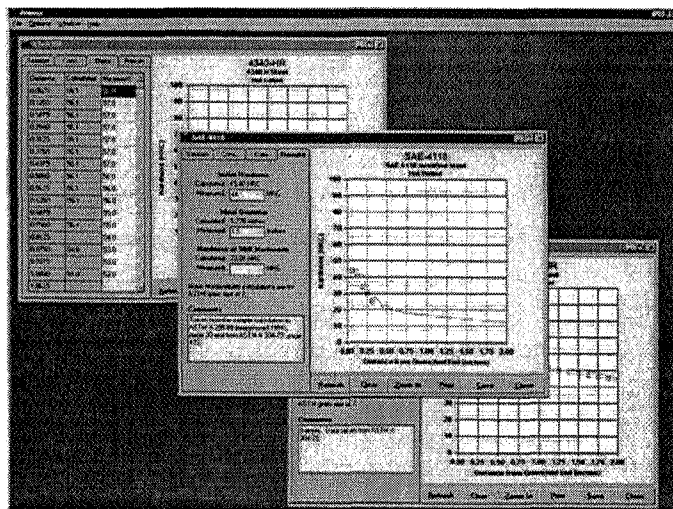


Figure 3 Screen shot of the Jominy End-Quench program.

89 describes how to calculate the maximum hardness and the hardness as a function of distance from the quenched end of the Jominy specimen. These calculations involve a number of polynomials, each of which is valid over various ranges of composition and distance from the quenched end; the

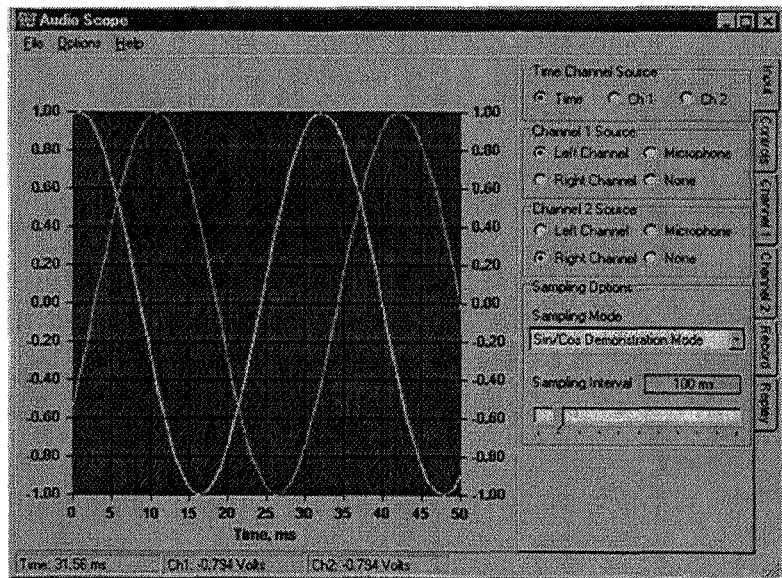
calculations which are tedious when done manually but are easy to code.

The *Jominy* program (Figure 3) allows one to calculate the Jominy curve for whatever steel is being tested (within the limits specified in the ASTM standard); this curve may also be plotted on the same graph as the measured hardness values. To use this program one creates a new job and after entering data on the steel and the end-quench procedure, the user can enter the composition of the steel and the measured hardness values. When this is complete, the program will calculate the initial hardness, the ideal diameter, and the hardness at a point in the Jominy specimen (along the length or in from the outer diameter) where the microstructure consists of 50% martensite. The graph can be rescaled and the results printed, saved in a file and reloaded at a future time. It is an MDI-type program, meaning that within the main (parent) window one can open any number of child windows, each for a different Jominy specimen.

We have used an earlier version of this program in our courses. It was well received and added much to the success of the experiment. The students could share their printouts and their files with each other, allowing them to very efficiently pool the results from a number of quenches of different steels.

Audio Scope

Audio Scope was written to avoid having to purchase expensive data acquisition boards or oscilloscopes for up to three laboratory stations where students could observe B-H curves. This experiment [3] uses 60 Hz excitation and our current DMM/scanner setups could not provide the necessary data acquisition rates and they do not offer simultaneous sample-and-hold for the two channels of input. All we needed were two channels of input, simultaneous sample-and-hold, and moderate data acquisition rates. In Figure 4 Screen shot of the Audio Scope program. fact we could have used low data acquisition rates and collected data over a period of time since the signal was periodic, but we definitely needed simultaneous sample-and-hold.



The solution to this problem was to use the sound card which comes with most PCs. Sound cards provide two channels of input through their line-in ports plus a third channel through the microphone input. Sound cards offer sampling rates ranging from 8 kHz to 44.1 kHz, monaural or stereo, and 8 or 16-bit resolution. Input to the line-in ports has a full-scale range of ± 1 volt, which normally is adequate; and when it is inadequate one can use amplifiers to strengthen or other devices to attenuate the signals.

Audio Scope offers many of the features one would expect to see on an oscilloscope. You can scale and attenuate the signals from each channel, adjust their zero positions independently, and shift them left and right. It even offers a triggering feature plus the ability to plot the signal from one channel versus the signal from the other one. The data can be saved to disk, and, if desired, the data can be saved directly to disk as a WAV file and replayed later.

Audio Scope is a much more ambitious program than the previous three. It has many more features and it must interact with Windows on a more intimate level. It makes many calls to Window's multimedia API functions [4] to get the data from the sound card and the data must be decoded from its native WAV file format [5] before it can be plotted. *Audio Scope* is also a much more active program since it must get the data from the sound card, translate it into x-y coordinates, plot it, and handle all user requests; it must do this quickly enough to present a smooth display. Unless your computer is reasonably fast you may not get the quick oscilloscope-like performance you were expecting. Also, if one can manage to make less demand on the system's resources -- for instance by sampling for shorter time periods -- the performance should be adequate. Even if the display is not smooth, it will still acquire data at audio rates.

This program is new. I haven't had a chance to thoroughly test it or to use it in our courses, but I am anxious to implement it with Furguson and Stoebe's magnetic properties experiment that was presented at NEW:Update 96 in Los Alamos [3].

Comments

Three of the four programs described here have been used in our laboratory courses for up to two years. They have been worthwhile additions to our experiments and have helped to improve the quality of and the student's understanding of the results. The fourth program, *Audio Scope*, will be used for the first time this year. Before using it we will do additional testing to ensure accuracy and reliability. We plan to test it on every sound card we can find and if the results vary appreciably between sound cards it may be necessary to add a calibration feature. One feature that each program needs, however, is an extensive help utility. These help utilities would explain how to use the program and how the technique works; use of a tutorial is a possibility. This would give the programs an additional instructional component.

All four programs can be downloaded from our department's web site at www.matsci.ucdavis.edu. Go to the laboratory teaching section where you will find the link to the NEW:Update 99 page. All files are zipped so you will need a Pkunzip-type utility to extract them.

References

1. M.L.Meier, Artificial Microstructures, NEW:Update 98.
2. R.T. Dehoff and F.N. Rhines, Quantitative Microscopy, McGraw-Hill, New York, (1968).
3. M.Furguson and T.Stoebe, Hysteresis Loops and Barkhausen Effects in Magnetic Materials, NEW:Update 96.
4. Wotsit's Format, The Programmer's Reference, www.wotsit.org
5. A.Moore, The Tomes of Delphi 4: Win32 Multimedia API, Wordware Publishing, Inc., Plano, Texas, (1999).

Biographical Information

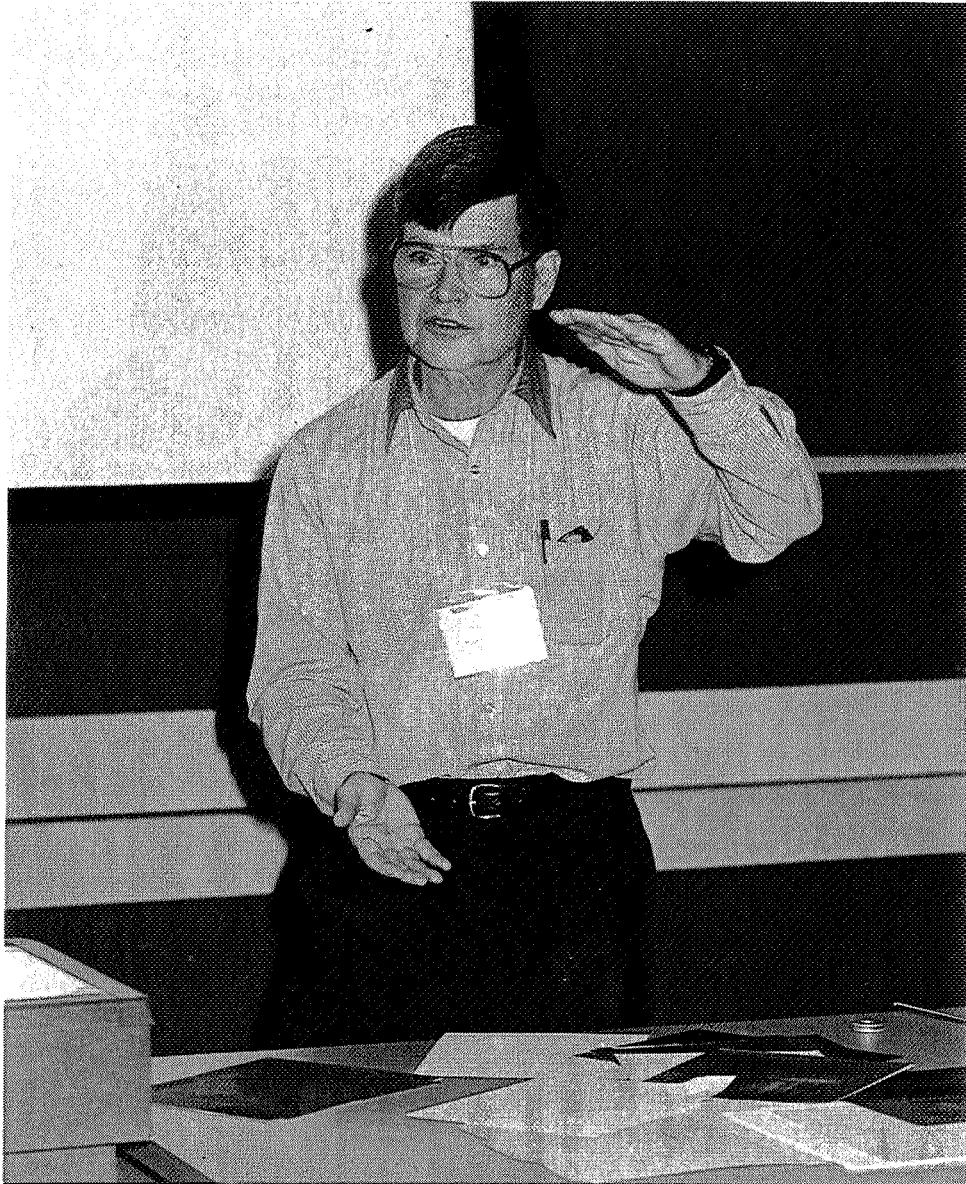
Michael L. Meier received his B.S. in Materials Engineering from North Carolina State University in 1979 and his M.S. (1986) and Ph.D. (1991) in Materials Science and Engineering from the University of California, Davis. After a two-year post-doctorate position at the Universität Erlangen-Nürnberg in Erlangen, Germany he returned to UC Davis and is the director of Materials Science Central Facilities and teaches many of the laboratory courses.

EGG BUNGEE CORD DROP

Robert A. McCoy

Mechanical Engineering Department
Youngstown State University
Youngstown, Ohio 44555

Telephone 330-742-1736
e-mail ramccoy@cc.ysu.edu



Robert A. McCoy

Robert A. McCoy is a Professor of Materials and Mechanical Engineering at Youngstown State University, Youngstown, Ohio. He has bachelor's and master's degrees from Ohio State University and a Doctor of Engineering degree from University of California at Berkeley. At YSU, he teaches freshmen engineering, mechanical engineering, manufacturing processes, and materials engineering courses. He is also a failure analysis consultant and a member of ASM and ASEE.

Egg Bungee Cord Drop

Robert A. McCoy
Youngstown State University
Youngstown, OH 44555

Key Words: Bungee cord, spring, gravitational potential energy, spring potential energy

Prerequisite Knowledge: The students need a basic understanding of how a linear spring behaves and how gravitational potential energy can be converted into spring potential energy.

Objectives:

1. The students gain practical experience of working together on a group design project that is both educational and fun.
2. The students learn how a real bungee cord behaves as compared with an ideal linear spring.
3. The students discover the large difference between the cord behavior when statically loaded as compared with the same cord dynamically loaded.
4. The students learn how to use the computer program Excel to record, mathematically manipulate, and plot experimental data.
5. The students learn how to apply experimental data from a small test piece of cord to their full-scale egg-drop apparatus.

Equipment and Materials:

1. A 1000-ft spool of 31 gauge latex bungee cord.
2. Large steel washers weighing about 17 grams each. Each group needs about ten.
3. Small resealable freezer plastic bags, three or four per group.
4. Eggs, one or two per group.
5. Tape measure, yardstick, or meter stick.
6. Scissors, stapler, binder clips, and white correction fluid.
7. Scale, 0-1 lb. or 0-500 g.
8. Adjustable stand up to six feet high with a horizontal bar.
9. A balcony with about a twenty-foot drop.
10. A computer with the program Excel.
11. A videocamera to tape the competition drops.

Introduction:

This paper describes a freshman engineering design project and competition. Groups of about five students each design, build, and test a bungee cord apparatus such that when an attached egg is dropped from a height of twenty feet, the egg will come close to hitting the floor. The group whose egg comes closest to the floor without actually hitting it and breaking the egg wins the competition. Before building their egg-drop apparatus, the students must first figure out what unstretched cord length to use so their egg will just miss hitting the floor in the competition. They are not allowed to have a full-scale practice drop. Instead they must analyze static stretch data and dynamic drop data on a short test piece of cord in the range of 0.25 to 0.5 m (10 to 20 in) long to be assigned by the instructor to determine their unstretched cord length.

Procedure for Static Testing:

Each group must devise a way to securely fasten the cord to the plastic bag by using a combination of square knots, staples, binder clips, etc. Knots alone will probably slip when the cord is stretched. Prior to securing the other cord end to a horizontal bar of an adjustable stand, the plastic bag, knots, staples, clips, and about one-third of the test-piece length of cord are weighed on a scale. This tare weight must be included in the weight versus stretch data. Care must be taken while securing the cord to the bar that the cord length between bar and the top of the plastic bag where it is attached is the assigned unstretched length when the cord is unloaded. The two cord ends should be marked with white correction fluid to aid in obtaining stretch data. The following parameters are defined:

L_0 = unstretched cord length with no weight added, not even the tare weight

L = cord length with weight added

S = stretch = $L - L_0$

W = cumulative weight including tare weight acting on the cord

H = drop height = distance from top cord end to bottom cord end where it attaches to the bag at the moment the bag reaches its lowest point in a drop. The bag height is not included.

If S.I. units are used, the weights should be converted from grams (unit of mass) to newtons (unit of force).

Using preweighed steel washers as weights, each group slips the washers, one by one, into their plastic bag and measures the new cord length after each addition. W and S should be calculated for each increase in weight and this data is entered into an Excel spreadsheet, as shown in Figure 1. A weight versus stretch curve is plotted using the Excel plotting capability, as shown in Figure 2. Clearly this curve is not linear so the students should realize that the bungee cord will not behave as a linear spring. Since W (a force) acts through S (a distance), the area under the curve up to some specific S represents the work stored by the cord, i.e. the spring potential energy, SPE.

To find SPE values for each data point, the trapezoidal method can be applied to the data in Figure 1 as follows:

1. ΔS finds the difference in S between two adjacent data points.
2. W_{av} finds the average weight between two data points.
3. W_{av} times ΔS is the increase in potential energy in going from one data point to the next.
4. The column labeled SPE is the cumulative potential energy up to a particular weight and is plotted versus S in Figure 3.

Procedure for Dynamic Testing:

The gravitation potential energy of a weight W about to be dropped from a height H equals $W \times H$. Theoretically at the bottom of the drop when all motion momentarily stops and kinetic energy is zero, the gravitational potential energy is completely transformed into spring potential energy. The students check this idea by performing a dynamic test dropping a weight close to their egg weight and using their short test piece. In this test, the weighted bag is raised to the height of the top end of the cord where it is secured to the horizontal bar and then released. The bag freefalls for a height L_0 and then the cord starts to stretch converting kinetic energy into

spring potential energy. After the group measures the drop height, $W \times H$ is compared with the SPE from the SPE vs. S curve. The ratio of the $W \times H$ value to the SPE value will be called the static-to-dynamic factor F_{SD} since the $W \times H$ was obtained from the dynamic test and SPE was obtained from static testing.

$$F_{SD} = \frac{W \times H}{SPE(\text{static})}$$

The students may be surprised to find this factor to be around five. This relatively large factor results from the basic difference between the two tests. The static test depends only on balancing the forces, i. e., establishing an equilibrium between the weight and the spring force. This equilibrium is independent of the initial height of the weight and occurs when the weight is motionless. On the other hand, the dynamic test, the drop, is greatly affected by the height of the weight and the weight descends far lower than where the weight is balanced by the spring force. At the bottom of the drop, the spring force exceeds the weight and this net upward force causes the weight to accelerate upward. Although there may be a mathematical correlation between the two types of tests if the system could be approximated by an ideal linear spring, the correlation involving F_{SD} had to be empirically determined for the actual bungee cord for the following reasons:

1. The actual bungee cord was shown to behave nonlinearly.
2. During static testing, the cord was found to creep and the amount of stretch was affected by how long the weight was applied.
3. Dynamic testing may involve nonuniform stretching.

Analysis of Test Data:

After comparing the W vs. S curves for different test cord lengths, the groups should conclude that for supporting the same weight, stretch is directly proportional to unstretched length. Hence, a scale factor applies such that

$$F = \frac{L_{o2}}{L_{o1}} = \frac{S_2}{S_1} \quad \text{for the same weight}$$

Also the groups should compare their F_{SD} values and arrive at an average value to be used in calculations. The following is an example of how the groups could use the test data to select the unstretched cord length for their drop.

Let $W = 1.34 \text{ N}$ (approx. weight of 2 eggs)

Let $H = 5.86 \text{ m}$ (assigned by the instructor)

From Fig. 2, $S = 0.58 \text{ m}$ for a 0.5-m test cord with static load

From Fig. 3, $SPE(\text{static}) = 0.47 \text{ J}$

$SPE(\text{dyn}) = F_{SD} \times SPE(\text{static}) = 5 \times 0.47 \text{ J} = 2.35 \text{ J}$ for 0.5-m test cord

Grav. Pot. Energy = $W \times H = 1.34 \text{ N} \times 5.86 \text{ m} = 7.85 \text{ J}$ for drop.

Length scale factor = $F = \frac{\text{Grav. Pot. Energy}}{SPE(\text{dyn})} = \frac{7.85 \text{ J}}{2.35 \text{ J}} = 3.34$

Therefore $L_o(\text{drop}) = F \times L_o(\text{test}) = 3.34 \times 0.5 \text{ m} = 1.67 \text{ m}$

Comments:

Prior to the competition, each group should use their drop weight and height to determine their unstretched cord length following the procedure outlined above which they should figure out on their own aided by guidance from the instructor only when needed. For a drop area, the instructor must select a safe balcony and provide a stable horizontal bar to which the top ends of the cords may be securely attached. On the ground floor, the instructor should tape a scale on a wall near the drop area floor indicating the height above the floor. The use of a videocamera to tape each drop of the competition is very helpful. By replaying the videotape in slow motion, one can easily judge the minimum height that each group's bag comes to hitting the floor. To do this successfully, the camera, the bag, and the height scale must all be aligned. The group whose bag comes closest to the floor without hitting it should be given special recognition, a prize, or extra credit. After the competition, each group should be required to write a design project report. Ask that they include in their report a listing of what all they learned from their project. This could be quite a list.

Bungee Cord Source:

The bungee cord used by this author was a 31-gauge latex cord bought as a 1000-ft. spool for \$175 from:

Ross Mathews Mills, Inc.
P.O. Box 27, 372 Kilburn St.
Fall River, MA 02724
(508) 677-0601

This cord had a diameter of 1.12 mm (0.044 inch) and weighed about 1 g/m. It could be stretched at least 500% before breaking at a load of about 2.4 kg (3.3 lbs).

Reference:

Paul G. Menz, "The Physics of Bungee Jumping," *The Physics Teacher*, Vol. 31, No. 8, 483-487, Nov., 1993

Biography:

Robert A. McCoy is a Professor of Materials and Mechanical Engineering at Youngstown State University, Youngstown, Ohio. He has bachelor's and master's degrees from Ohio State University and a Doctor of Engineering degree from University of California at Berkeley. At YSU, he teaches freshmen engineering, mechanical engineering, manufacturing processes, and materials engineering courses. He is also a failure analysis consultant and a member of ASM and ASEE.

	<u>S (m)</u>	<u>W (g)</u>	<u>S (m)</u>	<u>W (N)</u>	<u>Delta S(m)</u>	<u>W_{av} (N)</u>	<u>Area(J)</u>	<u>SPE(J)</u>
1	0.025	15.55	0.025	0.152	0.025	0.0762	0.0019	0.0019
2	0.072	34.15	0.072	0.335	0.047	0.2437	0.0115	0.0134
3	0.127	51.75	0.127	0.507	0.055	0.4212	0.0232	0.0365
4	0.201	69.69	0.201	0.683	0.074	0.5954	0.0441	0.0806
5	0.292	87.1	0.292	0.854	0.091	0.7687	0.0700	0.1505
6	0.391	104.45	0.391	1.024	0.099	0.9392	0.0930	0.2435
7	0.505	123.07	0.505	1.207	0.114	1.1155	0.1272	0.3707
8	0.616	142.19	0.616	1.394	0.111	1.3006	0.1444	0.5151
9	0.704	159.36	0.704	1.563	0.088	1.4785	0.1301	0.6452
10	0.795	175.34	0.795	1.719	0.091	1.6410	0.1493	0.7945
11	0.886	190.64	0.886	1.869	0.091	1.7944	0.1633	0.9578
12	0.991	210.64	0.991	2.066	0.105	1.9675	0.2066	1.1644
13	1.078	230.64	1.078	2.262	0.087	2.1636	0.1882	1.3526
14	1.125	239.65	1.125	2.350	0.047	2.3058	0.1084	1.4610

Figure 1. Weight and Stretch Data for $L_0 = 0.5$ m Cord

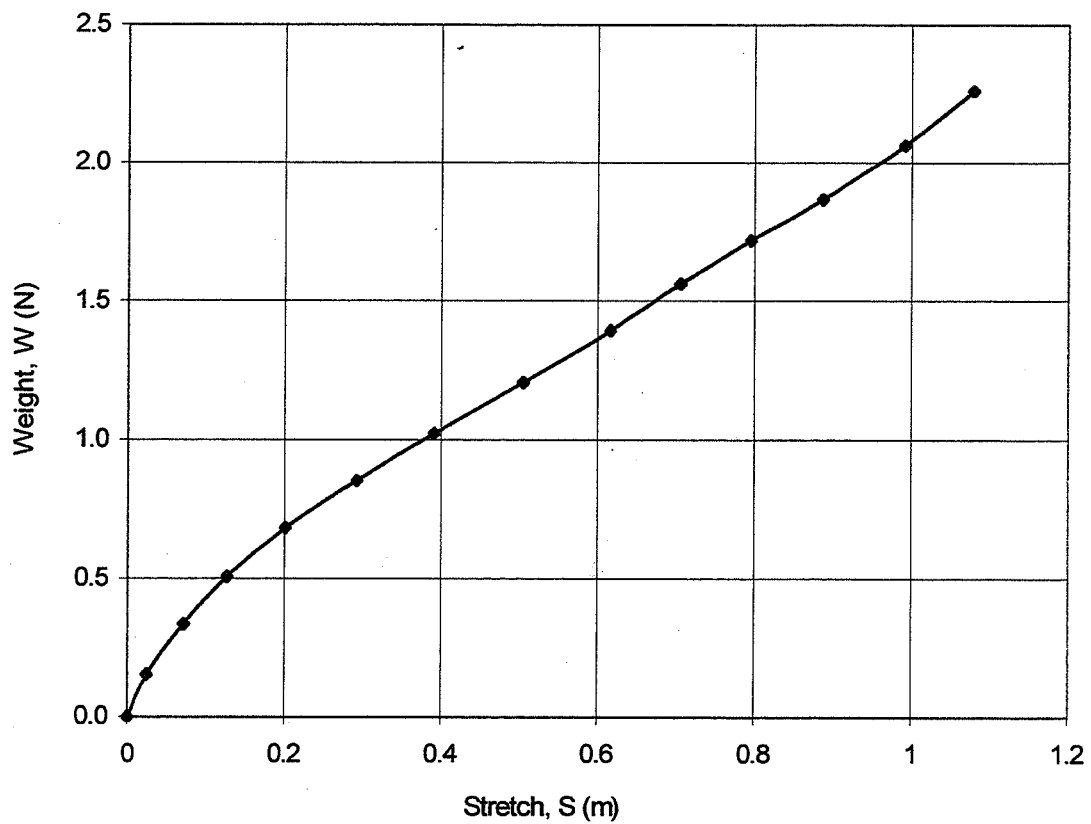


Figure 2. Weight vs. Stretch for $L_0=0.5$ m Cord

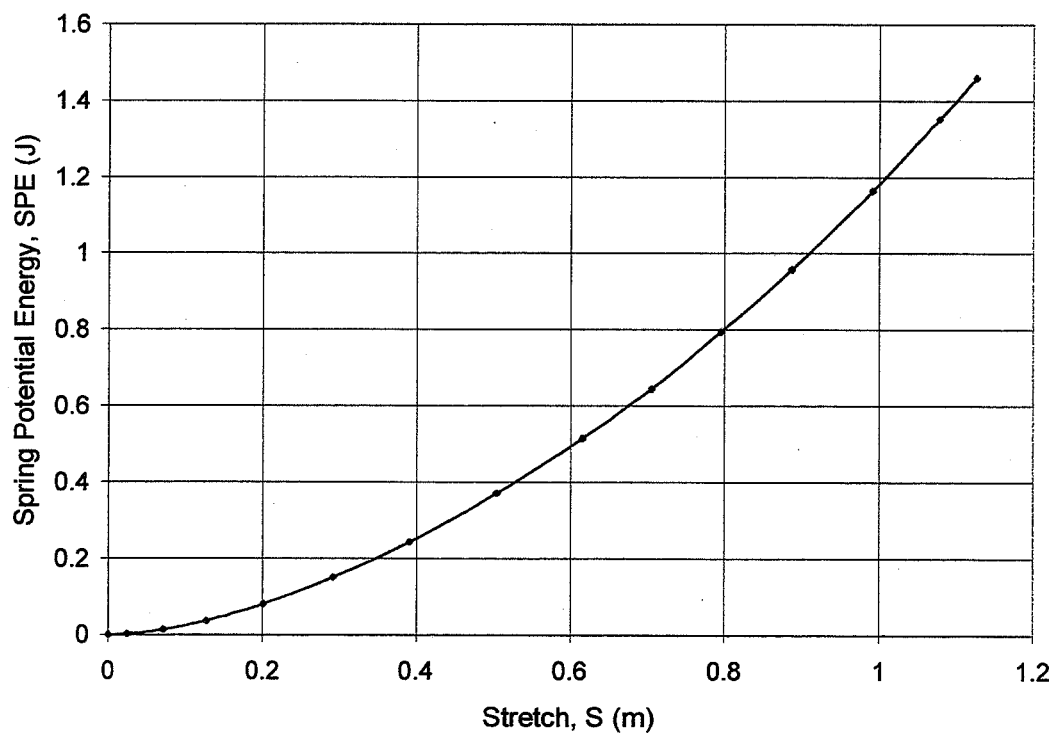


Figure 3. Spring Potential Energy vs. Stretch for $L_0=0.5$ m Cord

DESIGN PRACTICES FOR AUTOMOTIVE AND LIGHT TRUCK ALUMINUM BODIES

M. J. Wheeler

Alcan Global Automotive Products
136 Bagot Street
Kingston, Ontario K7L 3E5
Canada

Telephone:
e-mail Mike.Wheeler2@sympatico.ca



Michael Wheeler

Design Practices for Automotive and Light Truck Aluminum Bodies

M.J. Wheeler on behalf of Alcan Global Automotive Products
and the Aluminum Association

1 Introduction

Aluminum has about one third the density of steel and about one third its elastic modulus so that both materials have essentially the same mass-specific elastic modulus. On the face of it therefore, for passenger car and truck body structures, where stiffness—and particularly torsional stiffness—is critical for achieving predictable handling and good driveability, there is little to be achieved in terms of weight saving by substituting aluminum for steel. However, in designing vehicles, we are concerned with three dimensional structures of beams and panels rather than just the material properties. What we need to examine and understand in looking at aluminum for vehicle structures is how the overall stiffness is governed by the dimensions and configuration of these beams and panels.

In this plenary session therefore, I am going to cover briefly the material property and mechanical design aspects that govern the use of aluminum in achieving vehicle structures. I will then go on to illustrate how these principles have been applied in developing both sheet-based monocoque (body-frame integral) and space frame vehicle structures in aluminum.

Before embarking on this, however, there are some related aspects that need to be appreciated. First, it should be remembered that elastic modulus, Poisson's ratio and density are essentially inherent material properties, and are not significantly changed by alloying additions. This is not rigorously true for aluminum alloys since there are now some Al-Li alloys which have a 10-15% higher modulus and a lower density than conventional aluminum alloys, and have found some specialized applications in advanced passenger jet aircraft. There are also aluminum metal matrix composites such as Duralcan™ which contain small ceramic particles such as alumina or silicon carbide, which increase the modulus by up to 20%. However, these have been developed for specialty applications (e.g. Duralcan™ MMC for cast brake rotors, where its wear resistance and thermal stability are unique advantages). These materials are not available at costs, or in volumes, or—in the case of the metal matrix materials—in product forms that make them at all feasible for manufacturing high volume autobody structures.

In the same vein, you may have heard of “light weight steel,” but in fact there is no such material as a reduced density steel. There are high strength steels where this higher strength allows thickness and hence weight to be reduced, but advantage of this can only be taken when stiffness is not the design-limiting factor.

Finally, it should be noted that the overall stiffness of a vehicle structure is one of its key performance attributes and the way that the sub-components of a structure are joined together is critical to its overall structural stiffness. Thus joining technology is as critical as materials and mechanical design in achieving lightweight, structurally efficient vehicle structures. This will be illustrated for an aluminum monocoque structure and also for a truck frame.

2.1 Material Characteristics – Sheet Materials

For formed structural components, the main material requirements are for formability, stiffness and strength. Stability in the elevated temperature environments anticipated under the hood and close to the exhaust system, as well as crashworthiness and good corrosion resistance, are additional considerations. Probably the first requirement is for good formability. Fatigue strength, impact strength and ductility for collapse members, and high yield strength for the supporting structure are all important, as is the stability of the material properties over the life of the vehicle.

For these requirements, the AA5xxx series aluminum-magnesium alloys offer the best all round performance, and AA5754, where its performance has been optimized to maximize strength and formability while eliminating the risk of stress-corrosion, has become the alloy of choice for sheet structural applications. The excellent ductility for this alloy also means that structural beams in this alloy perform well for the front and rear end crash energy absorbing members of vehicle structures.

External closure panels have different property requirements. Here the strength of the panel is key since that determines the denting resistance for a particular geometry. The AA6xxx aluminum-magnesium-silicon series of alloys are attractive since they can be supplied in the

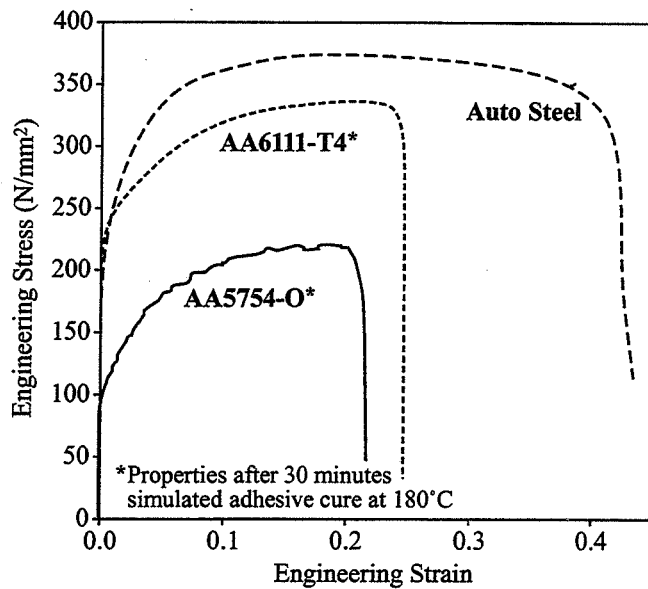


Figure 1. Stress/strain curves for two aluminum alloys and auto steel.

solutionized and quenched condition (T4 temper) where their yield strength, and hence springback, is low and their formability is high. This enables intricate external panel shapes to be formed and then, when the panels are subsequently heated during the E-coat cure step in the vehicle assembly process, a precipitation reaction occurs and the strength of the panels increases. The final strength is a function of the composition (alloy) and the strain and heating cycle imposed by the vehicle builder.

A number of alloys are used in current applications, but the major one is the alloy AA6111 which has an Al-Mg-Si-Cu composition and offers the strongest properties after painting. However, care must be taken with alloys of the AA6xxx family when used for structural applications because they are not as thermally stable as the 5xxx alloys. For example, the 6xxx alloys should not be used for crash-energy management structural members that will be constantly exposed to elevated temperatures dur-

Alloy and temper	Yield stress (MPa)	Tensile strength (MPa)	Elongation (%)
AA5754-O	110	220	23
AA6111-T4	160	305	25
AA6111-T8X	230	325	20
Auto Steel	220	370	39

Table 1. Material structural properties.

**Simulated paint bake conditions (2% strain plus 30 min at 177°C)*

ing vehicle service, unless a special aging treatment has been applied to stabilize the material and ensure good ductility. Typical mechanical properties and, for comparison purposes, those for a typical automotive steel, are shown in Table 1. Stress-strain curves for these materials are shown in Figure 1.

2.2 Material Characteristics – Extruded Shapes

The aluminum AA6xxx (Al-Mg-Si) alloys are the preferred ones for extrusions for thin-walled (and solid) beam structural members, and particularly for space frame structures. This is due to ease of extrusion, good formability, excellent corrosion resistance and good weldability. These alloys provide good strength at low cost, are readily formed in the T4 temper and can be used in this temper or can be artificially aged to the T5 or T6 temper to give higher strengths. Of the alloys used in space frames, AA6063 has the lowest strength and highest formability, followed by the medium strength AA6061, AA6005 and AA6005A alloys and the high strength AA6082. Typical mechanical properties for these alloys are given in Table 2. The AA7xxx series of alloys (Al-Mg-Zn) are used for bumper support beams but are not as corrosion resistant, are not as easy to weld and are not therefore favored for body structures. The Al-Mg alloys are not readily extruded and therefore are not available as extrusions, but seam-welded tube in Al-Mg alloys such as AA5754 can be effectively used instead of

Alloy	Elastic modulus (MPa x 10 ³)	Density (kg/m ³ x 10 ³)	Yield strength (MPa)	UTS (MPa)	Elongation (%)
6063-T4			90	172	23
6063-T5	69	2.7	145	185	12
6063-T6			215	240	12
6005A-T4			115	215	22
6005A-T5	69	2.7	265	290	12
6005A-T6			265	290	12
6061-T4			145	240	22
6061-T5	69	2.7	270	300	10
6061-T6			275	310	12
6082-T4			150		21
6082-T6			310	330	8

Table 2. Typical mechanical properties of automotive extrusion alloys.

Structural criterion	Aluminum to steel beam wall Thickness ratio		Aluminum to steel beam wall Mass ratio	
	AA5754-O	AA6111-T8X	AA5754-O	AA6111-T8X
Bending stiffness	3.00	3.00	1.03	1.03
Bending strength	1.64	0.78	0.56	0.27
Buckling stability	1.44	1.44	0.49	0.49
Vibration frequency	1.03	1.03	0.35	0.35

Table 3. Structural performance of thin-walled beams for two aluminum alloys compared to auto steel.

extruded tube in an AA6xxx alloy, and especially for making hydroformed shapes.

The 6xxx alloys commonly used in vehicle structures for crash energy absorption are 6063, 6005A and 6061. As with the 6xxx sheet materials, some consideration must be given to the material temper that is employed, particularly where these components will be exposed to elevated temperature during vehicle service. One recommended treatment is overaging to the T7 temper, typically using 8 hrs. at 210° C, to improve the ductility and reduce and stabilize the strength..

3.1 Aluminum in Automotive Structures – General

Vehicle structures can be regarded as an assembly of three types of components namely:

- Thin walled beams
- Panels
- Solid beams

The performance of aluminum materials in each of these types of components depends on the yield strength of the material (σ_y) and three critical material parameters namely Young's modulus, Poisson's ratio and density, all three of which as noted above are essentially constant for the alloys used in automotive structures. The value of these parameters at room temperature are:

- Young's modulus: (E) 70,000 MPa
- Poisson's ratio (ν) 0.33
- Density (ρ) 2700 kg/m³

The consequences of these material parameters in developing passenger car structures and truck frames when compared with steel, the conventional and well-proven material for automotive structures, are developed in the next three sections.

3.2 Structural Performance of Thin-walled Beams

Thin walled beams are the predominant structural elements in vehicle structures, whether these are fabricated

from sheet as in monocoque body-in-white (B-I-W) structures or, in the case of aluminum space frame structures, from hollow extrusions. Structural criteria for thin-walled beams for two different materials for beams with fixed outer dimensions are presented in Appendix A.

Numerical results for two different alloys, AA5754-O and AA6111-T4, compared to a typical automotive steel are given in Table 3.

The above results need some clarification. Namely, from the stiffness criterion, it looks as if there is no weight saving to be achieved by substitution of aluminum. This, however, will only be the case when the outer dimensions of the beam are fixed. In this case, the aluminum beam, with three times the wall thickness of the steel beam will be over-designed for all other criteria. When an increase in the outside dimension of the beam is permitted, however, aluminum substitution can achieve a balance of properties with equal wall buckling resistance and stiffness in bending, and with a mass ratio to a steel

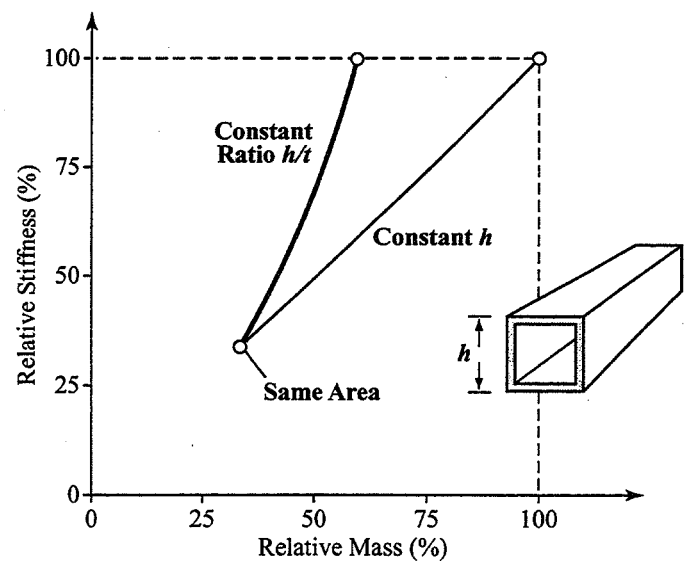


Figure 2. Comparative box section bending stiffness of aluminum as a percentage of steel.

Structural criterion	Aluminum to steel beam wall Thickness ratio		Aluminum to steel beam wall Mass ratio	
	AA5754-O	AA6111-T8X	AA5754-O	AA6111-T8X
	Bending stiffness	1.44	1.44	0.50
Bending strength	1.28	0.88	0.44	0.30
Buckling strength	1.44	1.44	0.49	0.49
Denting resistance	0.94	0.45	0.32	0.16
Vibration frequency	1.03	1.03	0.35	0.35

Table 4. Structural performance of panels for two aluminum alloys compared to auto steel.

beam of 0.67. In that case, the thickness ratio t_A/t_S is 1.65 and the beam height ratio h_A/h_S is 1.22, where the subscripts A and S refer respectively to aluminum and steel. The effect of changing the beam dimensions and material thickness on the stiffness and mass of an aluminum beam relative to a steel one is shown in Figure 2.

3.3 Structural Performance of Panels

The bending stiffness of a flat panel of a unit length is proportional to the cube of its thickness and the Young's modulus of the material. Again, designating steel and aluminum properties with subscripts S and A respectively, the thickness ratios and mass ratios of components made of two materials for equal stiffness can be expressed as:

$$\frac{t_A}{t_S} = \left[\frac{E_S}{E_A} \right]^{1/3} \quad \frac{m_A}{m_S} = \frac{\rho_A}{\rho_S} \left[\frac{E_S}{E_A} \right]^{1/3}$$

Substituting properties of aluminum as $E_A = 70,000$ MPa, $\rho_A = 2700$ kg/m³ and of steel as $E_S = 210,000$ MPa, $\rho_S = 7850$ kg/m³ gives

$$\frac{t_A}{t_S} = 1.442 \quad \frac{m_A}{m_S} = 0.496$$

Therefore, in order to achieve the same bending stiffness, an aluminum panel will require to have 1.442 times the thickness of a steel panel. Its mass (and consequently weight) will be just under half of that of the steel one.

It is also possible to calculate thickness and mass ratios for two materials for bending strength, buckling strength, denting resistance and vibration frequency and the relationship for various performance criteria are given in Appendix B.

Numerical results for two different alloys, AA5754-O and AA6111-T8X, compared to a typical automotive steel are presented in Table 4.

It is apparent from the table that a mass reduction of 50% compared to a typical automotive steel is achievable in aluminum panels for all criteria. Furthermore, if denting resistance or the frequency of natural vibration are the dominant criteria, an alloy such as AA6111-T8X that attains high strength in the paint-baked condition, has the potential to reduce the mass even more.

3.4 Structural Performance of Solid Section Beams

Solid section beams rarely occur as structural components in passenger vehicles, but are dealt with here for completeness. It is assumed that the cross section is of a fixed shape (fixed ratio between width and height), but that it can vary in overall dimension. Structural criteria for two different materials for beams with fixed outer dimensions are presented in Appendix C.

Numerical results for two different alloys, AA5754-O and AA6111-T8, compared to a typical automotive steel are given in Table 5.

Structural criterion	Aluminum to steel beam wall Outer dimension ratio		Aluminum to steel beam wall Mass ratio	
	AA5754-O	AA6111-T8X	AA5754-O	AA6111-T8X
	Bending stiffness	1.32	1.32	0.45
Bending strength	1.18	0.92	0.41	0.32
Vibration frequency	1.01	1.01	0.35	0.35

Table 5. Structural performance of solid section beams for two aluminum alloys compared to auto steel.

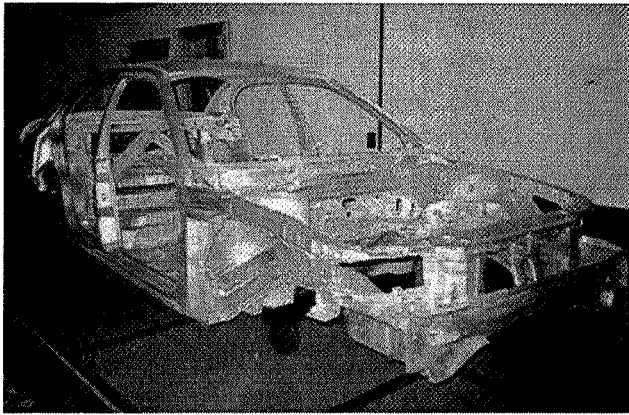


Figure 3. Ford P2000 aluminum body-in-white.

4.1 Passenger Car Body Structures

Figures 3 and 4 illustrate two good but very different approaches to the use of aluminum for passenger car body structures. The former shows the aluminum stamped sheet body-in-white (B-I-W) structure for Ford's P2000 PNGV (Partnership for a New Generation of Vehicles) prototype family sedan, while Figure 4 shows the structural space frame of the production Audi A8, a large luxury sedan. However, both represent excellent examples of the structural use of aluminum for automotive applications.

The P2000 structure is essentially built using stampings in AA5754-O aluminum sheet material, joined in stiffness critical regions by weld bonding and otherwise by conventional spot welding. Weld bonding is a combination of structural adhesive bonding with spot welding and the continuous nature and the geometric configuration of such joints results in significant increases in joint stiffness and fatigue endurance compared with just spot welding. As a result, the amount of aluminum gauge increase necessary to obtain global structural stiffness compared with an equivalent all spot welded steel structure can be limited to about 50%. However, in new designs, selected increase in "beam" sections can reduce the amount of gauge increases that are necessary. The B-I-W weight for the P2000 is just 299 lb. (135.6 kg) compared with 632 lb. (286.8 kg) for the current Ford Taurus, an equivalent sized family sedan.

The benefit in terms of stiffness improvement that comes from using continuous rather than spot joining is illustrated in Figure 5. This shows as a result how the material thickness can be reduced and also how then the materials gauges can be optimized to further reduce the weight.

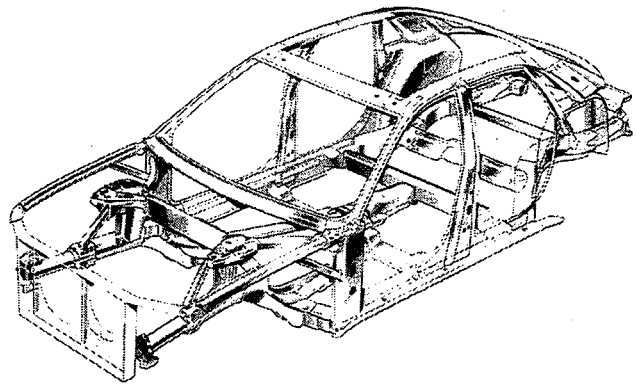


Figure 4. Aluminum space frame for the Audi A8.

The main structural members in the Audi A8 structure are derived from hollow aluminum extrusions in a medium strength AA6xxx alloy of the 6063 type. These have been formed using either stretch bending or other forming techniques as appropriate, and they are joined together by fusion welding to cast, high ductility connector nodes in an Al-Si alloy. Again the thickness and the sections of the beams have been designed to provide a high stiffness and this is helped by the fact that the main beams are closed sections and that they are joined together efficiently at the nodes by the welding. The body structure is completed with sheet stampings, which act as shear panels. Audi has estimated that this structure is some 40% lighter than a similar sized steel structure and yet provides enhanced structural stiffness and exceptional crashworthiness.

Several other aluminum space frame vehicles have been successfully developed using formed extrusions, some with different joining techniques such as compression

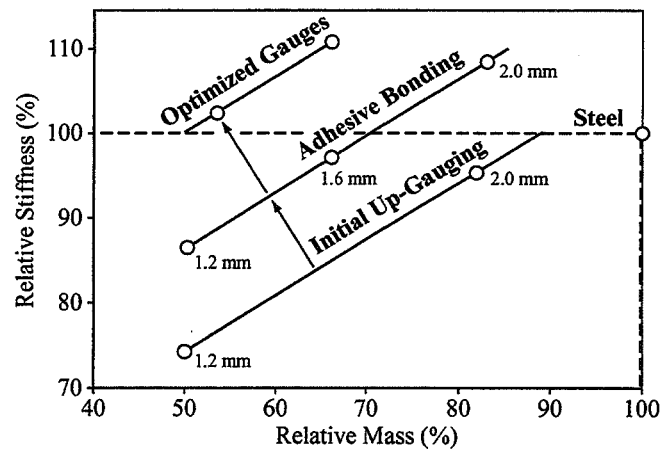


Figure 5. Impact of adhesive bonding and gauge optimization on body structure stiffness.

fit forming or structural adhesive bonding coupled with self tapping mechanical fasteners.

4.2 Truck body Frames

The next example of aluminum for automotive structures comes from a study to examine the replacement of a steel truck frame with an aluminum one. Again this illustrates the use of section changes and the importance of joining for achieving both stiffness and weight saving. A typical ladder type frame, as is commonly used for pick-up trucks and some sports utility vehicles, was studied. The design options examined for substituting aluminum were as follows:

- Uniform up-gauge from steel
- Selective up-gauge (optimization)
- Increase in sections' outer dimensions
- Improvements in connections
- Modification of cross sections

Up-gauging alone would allow the bending and torsional stiffness targets to be met with a gauge increase of some 2.25, giving a weight saving of only 17%. However, up-gauging by 1.8 and increasing section height by 20% allowed the bending stiffness target to be met and the torsion stiffness target to be exceeded, giving a projected weight saving of 34%. And with up-gauging optimization, this could be increased to a 36% weight saving.

Next the stiffness of the joints between the longitudinal and cross beams was examined, and by making these more efficient, the weight saving over the steel frame could be increased to 47%. Finally, replacing some open beams with closed sections showed the potential for a greater than 50% weight saving. These various scenarios are summarized in Table 6.

Scenario	Relative mass reduction (%)
Uniform up-gauge from steel	17
Section size increase and selective up-gauge from steel	36
Improvement of connections, expansion of sections by 20%, selective up-gauge	47
Re-design with closed sections and efficient connections	> 50

Table 6. Summary of potential design optimizations for an aluminum truck frame.

Of necessity, the study also addressed fatigue durability and impact performance. In both cases it was concluded that, with the optimized gauges and sections required to achieve the stiffness targets, meeting the fatigue endurance and the impact collapse requirements to provide crashworthiness would not be an issue.

It should be noted here, however, that the above study could only be carried using finite element analysis methods. Today, this has become a necessity for the detailed analysis and optimizations routines that are required to make optimum use of materials for establishing weight-efficient vehicle structure designs.

5. Summary

The above study essentially captures all the factors that have to be considered in designing automotive structures in aluminum. In particular, it illustrates the importance of maximizing the section properties of structural members, of optimizing gauge depending upon the structural function of each component, and of employing efficient joints between the structural members and between these and the structural shear panels.

With a range of alloys for both structural and closure panel materials—which are available in a variety of product forms including sheet, extruded shapes and seam welded tube—and proven joining methods such as fusion welding and weld bonding, aluminum is well placed to meet the need of the automotive industry for building light weight, structurally efficient vehicles.

6. Acknowledgment

The author wishes to acknowledge the input of Dr. D.M. Moore and Mr. A.S. Warren of Alcan Global Automotive Products, and access to Alcan's automotive technology database.

Duralcan™ is a trademark of Alcan Aluminum Corporation

Appendix A
Structural Criteria for Thin Walled Beams

Structural Criterion	Wall Thickness Ratio	Mass Ratio
Bending Stiffness	$\frac{E_s}{E_A}$	$\frac{\rho_A}{\rho_s} \frac{E_s}{E_A}$
Bending Strength	$\frac{\sigma_{ys}}{\sigma_{ya}}$	$\frac{\rho_A}{\rho_s} \frac{\sigma_{ys}}{\sigma_{ya}}$
Buckling Stability in Bending	$\left[\frac{(1-\nu_A^2) E_s}{(1-\nu_s^2) E_A} \right]^{1/3}$	$\frac{\rho_A}{\rho_s} \left[\frac{(1-\nu_A^2) E_s}{(1-\nu_s^2) E_A} \right]^{1/3}$
Vibration Frequency	$\frac{E_s}{E_A} \frac{\rho_A}{\rho_s}$	$\left(\frac{\rho_A}{\rho_s} \right)^2 \frac{E_s}{E_A}$

Appendix B
Structural Criteria for Panels

Structural Criterion	Thickness Ratio	Mass Ratio
Bending Stiffness	$\left(\frac{E_S}{E_A}\right)^{\frac{1}{3}}$	$\frac{\rho_A}{\rho_S} \left(\frac{E_S}{E_A}\right)^{\frac{1}{3}}$
Bending Strength	$\left(\frac{\sigma_{YS}}{\sigma_{YA}}\right)^{\frac{1}{2}}$	$\frac{\rho_A}{\rho_S} \left(\frac{\sigma_{YS}}{\sigma_{YA}}\right)^{\frac{1}{2}}$
Buckling Strength	$\left[\frac{(1-\nu_A^2) E_S}{(1-\nu_S^2) E_A}\right]^{\frac{1}{3}}$	$\frac{\rho_A}{\rho_S} \left[\frac{(1-\nu_A^2) E_S}{(1-\nu_S^2) E_A}\right]^{\frac{1}{3}}$
Denting Resistance	$\frac{\sigma_{YS}}{\sigma_{YA}} \left(\frac{E_A}{E_S}\right)^{\frac{1}{2}}$	$\frac{\rho_A}{\rho_S} \frac{\sigma_{YS}}{\sigma_{YA}} \left(\frac{E_A}{E_S}\right)^{\frac{1}{2}}$
Vibration Frequency	$\frac{E_S}{E_A} \frac{\rho_A}{\rho_S}$	$\left(\frac{\rho_A}{\rho_S}\right)^2 \frac{E_S}{E_A}$

Appendix C
Structural Criteria for Solid Section Beams

Structural Criterion	Outer Dimension Ratio	Mass Ratio
Bending Stiffness	$\left(\frac{E_S}{E_A}\right)^{\frac{1}{4}}$	$\frac{\rho_A}{\rho_S} \left(\frac{E_S}{E_A}\right)^{\frac{1}{2}}$
Bending Strength	$\left(\frac{\sigma_{YS}}{\sigma_{YA}}\right)^{\frac{1}{3}}$	$\frac{\rho_A}{\rho_S} \left(\frac{\sigma_{YS}}{\sigma_{YA}}\right)^{\frac{2}{3}}$
Vibration Frequency	$\left(\frac{E_S}{E_A} \frac{\rho_A}{\rho_S}\right)^{\frac{1}{3}}$	$\left(\frac{\rho_A}{\rho_S}\right)^{\frac{5}{3}} \left(\frac{E_S}{E_A}\right)^{\frac{2}{3}}$

ALUMINUM MATERIALS FOR ENVIRONMENTALLY FRIENDLY VEHICLES

M. J. Wheeler

Alcan Global Automotive Products
136 Bagot Street
Kingston, Ontario K7L 3E5
Canada

Telephone:
e-mail Mike.Wheeler2@sympatico.ca

Aluminum Materials for Environmentally Friendly Vehicles

M.J. Wheeler

Alcan International Limited

ESD/SAE Conference and Exposition (ENV'98)
on Environmental Vehicles and Alternative Fuels

Ypsilanti, MI - June 15-17 1998

ABSTRACT

The energy consumption of vehicles is largely determined by their weight. Therefore, reduction in weight for environmentally friendly vehicles is particularly important, not only for conventionally powered vehicles which generate exhaust emissions but also for electric and alternative energy powered vehicles since their range is critically dependent on weight.

Aluminum, because of its low density and availability in a wide range of product forms, is already an important automotive material for saving weight. However, by using aluminum for the body structures and frames of vehicles, significantly more weight can be saved.

This paper will describe the aluminum materials and enabling technologies that have been developed for building aluminum intensive vehicles and will illustrate the application of aluminum for vehicle structures through the prototype and production vehicles that have been developed by the auto companies during the last few years. The paper will conclude on the activities of the aluminum industry to ensure an appropriate supply of material for the automotive industry.

INTRODUCTION

The carbon dioxide generated by transportation vehicles accounts for a very significant part of the greenhouse gases generated by industrialized countries and one statistic here, for example, is that one-third of the United States' carbon dioxide emissions comes from the transportation sector and primarily from passenger vehicles⁽¹⁾. The fuel consumption and hence the CO₂ emissions of these vehicles is directly related to their weight and thus weight reduction is a very key requirement for the development of environmentally friendly vehicles powered by conventional fossil fuel engines. However, weight reduction is also very important for an alternative energy powered vehicles since this again lowers their energy consumption, reducing, in turn, the size and output requirement of the power train and extending their range, this being a common limitation of most of the alternative fueled vehicles which have been introduced to date.

Another important consideration for the development of environmentally friendly vehicles is that the materials used for their manufacture must themselves be environmentally friendly, especially in regard to recycling. This is so that as vehicles reach the end of their useful life, the materials can be recycled into new vehicles and done so without the generation of significant quantities of greenhouse gases.

ALUMINUM AS A MATERIAL FOR ENVIRONMENTALLY FRIENDLY VEHICLES

Aluminum, because of its low density, high strength to weight ratio, corrosion resistance, ready availability in a wide range of product forms and its recyclability, is already an important material to the automakers for weight reduction. In 1996, for example, some 3.6 billion lbs. of aluminum were used in North American cars and light trucks, saving about this same weight of heavier materials⁽²⁾. However, by extending its use to the main body structure of vehicles and for all the exterior panels, much more weight could be saved both as primary weight saving and also through the secondary weight saving which can be achieved when the primary weight is reduced.

As I will describe in this presentation, aluminum can typically replace twice its weight in steel and the benefit of this for developing environmentally friendly vehicles is very significant, and especially so when recycling is involved. For a typical family-sized, six passenger sedan with a gasoline internal combustion engine, the accepted number for the impact of weight saving on fuel consumption is 0.88 US gal. per lb. of weight saving over a typical lifetime mileage of 100,000 miles. Some 2.88kg of CO₂ is generated from each liter of gasoline used, giving a reduction of 21 tonnes of CO₂ when 2 tonnes of steel are replaced by 1 tonne of aluminum. This is offset by the CO₂ generated in the production chain of aluminum from bauxite and, for smelting in North America, this amounts today to about 12.6 tonnes of CO₂ per tonne of aluminum. However, there are the savings in CO₂ generation from not producing the steel.

If the aluminum is supplied from recycled material, the CO₂ generated comes down from 12.6 to 1.6 tonnes per tonne of aluminum, thereby significantly enhancing the environmental impact of using aluminum and emphasizing the importance of using a material which is readily recyclable and at minimum "cost" in terms of energy use and CO₂ generation. As a matter of record, the study on the aluminum usage in the automotive and light truck market for 1996 conducted on behalf of the Aluminum Association⁽³⁾ showed that some 2.0 billion lbs. of the 3.6 billion lbs. of aluminum used by the North American auto industry in cars and light trucks in 1996 was secondary (recycled content) metal. Finally, it is perhaps worth noting that, should trading permits for CO₂ emissions develop as a result of the Kyoto Protocol, then the improvement in gas mileage and reductions in CO₂ emissions that will result from the greater use of aluminum in vehicles could flow through to the auto companies and to their customers in terms of some significant dollar value credits.

There are thus some compelling reasons for using aluminum in the production of environmentally friendly vehicles but what materials and manufacturing systems have been developed to enable the environmental benefits of aluminum to be attained?

MATERIALS AND ALUMINUM VEHICLE DESIGN SYSTEMS

STAMPED SHEET STRUCTURES

The stamped sheet or unibody approach for aluminum structured vehicles is based on the approach used today with steel for essentially all high volume production vehicles where designs have been gradually optimized to reduce mass and enhance structural stiffness, the latter being key for good handling and drivability characteristics. Honda⁽⁴⁾ employed the stamped sheet approach for their aluminum intensive NSX, using a combination of spot and MIG spot welding to join the structure together but, due to the lower modulus of aluminum, the body structure weight saving was limited to 40% compared with an equivalent steel design. However, a breakthrough came for aluminum with the development by Alcan of its Aluminum Vehicle Technology (AVT) structural bonding system using an Al-3%Mg structural sheet material (AA5754-0)⁽⁵⁾. The structural bonding significantly increases the body structure stiffness, particularly the torsional stiffness. In turn, this enables



Figure 1. Ford's P2000 PNVG prototype

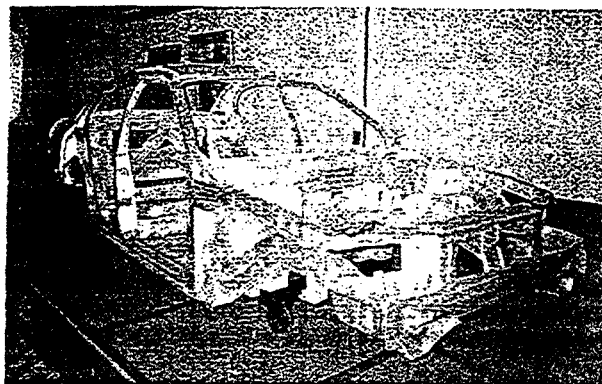


Figure 2. Aluminum body structure of Ford's P2000

the weight saving compared to steel to be increased to over 50%, thereby improving the economics for using aluminum by reducing the weight used and also giving enhanced torsional stiffness compared to spot welded steel, exceptional fatigue endurance and enhanced impact energy absorption (which will be discussed later).

The AVT system was first used in a production vehicle for the front longitudinal crash energy management beams for the Jaguar Sport XJ220, a limited production, high performance sports car. The major applications to date are for General Motors' EV1 production electric car, for Ford's AIV and, most recently, for Ford's P2000 PNVG prototype which is shown in Figure 1. The road behaviour of all of these vehicles has proved to be outstanding particularly in terms of road holding, improved NVH characteristics and enhanced acceleration and braking performance. Table 1 shows the weight savings that were achieved with aluminum in Ford's AIV compared with the then current DN5 Ford Taurus on which the design was based.

The weld-bonded aluminum body-in-white structure of the Ford P2000 is shown in Figure 2. Table 2 shows the weight reduction for the aluminum body-in-white and closure panels for the P2000 compared with the current (DN101) Taurus. In total, some 733 lbs. of aluminum, which represents some 36.9% of the vehicle weight, is used in the P2000 and the total weight reduction for this vehicle compared with the DN101 Taurus is 1318 lbs or 40%, much of which stems from the substitution of aluminum for heavier materials⁽⁶⁾.

	lb			% saved
	Steel	Al	Wt saved	
Body structure	596	320	276	46
Hood, deck and fenders	90	38	52	58
Front and rear doors	132	79	53	40
Total body and closures	818	437	381	47
Total vehicle	3275	2894	381	12

Based on published Ford information

Table 1. Weight and weight saving for the Ford AIV

	P2000	DN101	Weight reduction	
	(lb)	Taurus (lb)	lb	%
Body-in-white	299	632	333	53
Closures	102	243	141	58
Total	401	875	474	54

Table 2. Body-in-white and closure panel weight reductions for P2000 versus 1997 (DN101) Taurus

In the AVT system, essentially only one sheet material, the Al-Mg alloy AA5754 in the 0 temper is used. This is supplied with a surface pretreatment to provide good long-term bond strength durability and with a system compatible pre-applied press-forming lubricant to facilitate forming and to protect the pretreatment during forming and handling. Honda uses 5182-0 in the body structure of the NSX but this material can be susceptible to stress corrosion cracking and must have appropriate surface protection. However, it has an excellent combination of strength and formability and is an excellent material for semi structural parts and inner closure panels. It is susceptible to Luders lines on forming and thus is not suitable for visually critical outer panels.

While the use of aluminum for the body structure can provide weight savings of over 300 lbs in a typical mid-sized sedan, the outer body panels also represent a significant opportunity for weight saving. Aluminum is already a well established material for exterior closure panels such as hoods and deck lids and Table 2 shows that the adoption of aluminum for all the closure panels in the Ford P2000 resulted in a weight of just 102 lbs. compared 243 lbs. for closure panels of the current Ford Taurus.

Today, the predominant closure panel alloy is AA6111 and is used, for example, for all the hoods on the Ford F150 pickups where the annual volume is in excess of 600,000 units. It is an Al-Mg-Si-Cu alloy which is highly formable in the as-supplied T4 temper and strengthens to give a yield strength of >200 MPa on paint baking. A roping-free version (T41 temper) and enhanced paint bake response variants (eg. T4P temper) which can also be roping-free, are now available where the latter can develop a yield strength of up to 270 MPa on paint baking following forming. This strength is comparable with that of some of the bake-hardening steels used today for closure panels and gives comparable dent resistance⁽⁷⁾. Another 6000 series alloy, AA6022, has also recently been introduced with somewhat similar properties to AA6111 and is used for some of the body panels of the Plymouth Prowler.

Typical properties for the above structural and closure sheet materials are given in Table 3.

SPACE FRAME STRUCTURES

The space frame approach for developing light weight vehicle structures was pioneered by Alcoa⁽⁸⁾ and Norsk Hydro⁽⁹⁾ and, more recently, has been further evolved by Alumax⁽¹⁰⁾ and by Lotus Cars⁽¹¹⁾. In this approach, structural frames are built using shaped or formed aluminum extrusions which are joined together by a variety of methods such as fusion welding to cast connecting nodes (Alcoa), sectioning and direct fusion welding (Norsk Hydro), compression fit forming (Alumax), and

Alloy/ temper	Elastic modulus (MPa x 10 ³)	Density (kg/m ³ x10 ³)	Yield strength (MPa)	UTS (MPa)	Elong- ation (%)
5754-O	70	2.67	95	220	26
5182-O	71	2.65	130	275	21
6111-T4	69	2.71	150	290	26
2% ε + PB*			205	315	22
6111-T4P	69	2.71	145	288	25
2% ε + PB			270	345	20
6111-T41	69	2.71	165	290	25
2% ε + PB			215	295	19
6062-T4	69	2.69	150	255	26
2% ε + PB			215	285	24

*2% tensile strain plus 30 min at 177°C

Table 3. Typical mechanical properties for aluminum automotive sheet materials

adhesive bonding supplemented by mechanical fasteners (Lotus Cars).

The first aluminum space frame production car is the Audi A8, and Figure 3 shows the space frame of this vehicle. The major structural members, which are made from medium strength Al-MgSi alloy extrusions, are joined together by fusion welding to cast nodes in an Al-Si alloy, the latter being produced using a "high ductility" casting process. Much of the welding is carried out robotically. The body structure is completed with stamped panels in an aluminum 6000 series alloy and the exterior closure panels are also in aluminum, using the European AA6016 Al-MgSi alloy. As a result, sheet is the predominant material in the vehicle although structural integrity and energy absorption for crashworthiness is mainly provided by the space frame.

Other examples of space frame vehicles are the Renault Spider with the Norsk Hydro approach, the Lotus Elise, the Plymouth Prowler (Alcoa) and the Panoz Roadster (Alumax). The latter is a very low volume production vehicle and interestingly its outer panels are formed from superplastic aluminum sheet. Another space frame vehicle is Nissan's AL-X

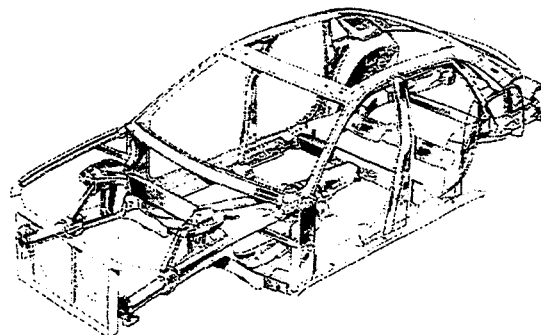


Figure 3. Audi's A8 aluminum space frame

hybrid gasoline/electric powered vehicle and Chrysler has also taken advantage of the weight saving that can be achieved with aluminum in its ESX 1 and 2 PNGV prototypes.

The aluminum 6000 series (Al-Mg-Si) alloys are the preferred ones for space frames due to ease of extrusion and good formability, corrosion resistance and weldability. They are readily formed in the as-extruded and naturally aged condition (T4 temper) and can be used in this condition or can be artificially aged to the T5 or T6 temper to give increased strength. The alloys most commonly used are AA6063, AA6005A and AA6061, with the T4 or the overaged T7 tempers preferred, due to their good fracture toughness, for members designed for the crash energy absorption structure of vehicles⁽¹²⁾. Table 4 lists typical properties for these alloys.

CRASHWORTHINESS

The various aluminum intensive vehicles that have been developed provide adequate demonstration that the weight savings required for environmentally friendly vehicles can and are being achieved. However, this is not by itself sufficient to prove that such vehicles will also be crashworthy.

While it is obvious that no car manufacturer would build and sell or release for road use any vehicle that does not meet or exceed the accepted standards for occupant safety, there is nevertheless a concern that vehicles with reduced weight also have reduced crashworthiness. In fact, aluminum vehicle structures absorb kinetic energy in a crash by concertina folding or bending collapse in just the same way as for steel structures and very similar design approaches are used for both materials. Thus, the front and rear end extensions to the occupant "safety cage" are designed to collapse in major impacts by concertina folding. Aluminum, which typically is used at 50% thicker gauge than steel and hence at about half the weight, has an advantage in that the greater thickness results in more of the metal being deformed by the folding collapse, thereby enhancing its energy absorption. This compensates for the

	AIV	Steel (DN5)	FMVSS 208 Req.
Dynamic crash (in)	30.8	28.4	—
Head Injury Criteria (HIC)	549	524	1000
Chest acceleration (g)	37	53	60
Chest displacement (in)	1.4	1.4	3.0
Torso belt load (lb)	1219	1686	—
Left femur load (lb)	697	1644	2250
Right femur load (lb)	906	1092	2250

Table 5. Frontal barrier crash results for Ford AIV and DN5 Taurus

Alloy	Elastic modulus (MPa x 10 ³)	Density (kg/m ³ x 10 ³)	Yield strength (MPa)	UTS (MPa)	Elongation (%)
6063-T4			90	172	23
6063-T5	69	2.70	145	185	12
6063-T6			215	240	12
6063-T7*			115		13
6005A-T4			115	215	22
6005A-T5	69	2.70	265	290	12
6005A-T6			265	290	12
6005A-T7*			176		14
6061-T4			145	240	22
6061-T5	69	2.70	270	300	10
6061-T6			275	310	12

*8 hrs at 210°C

Table 4. Typical mechanical properties for automotive extrusion alloys.

higher strength of steel and the net result is that an aluminum structure will absorb about the same amount of energy as an equivalent steel one at half the weight. Another advantage for aluminum is that longer front and rear crumple zones can be maintained without incurring a severe weight penalty. Information on the crash behaviour of aluminum vehicle structures can be found in references (12), (13) and (14).

Definitive impact crash information has been released for both Ford's AIV and Audi's A8 and this demonstrates that well designed aluminum vehicle structures can comfortably exceed the US FMVSS 208 occupant safety requirements for 30mph impact, even when crashed at 35mph. This represents a 36%

	Driver	Passenger	Low Risk Injury Values
Head Injury Criteria (HIC)	531	424	< 1250
Head acceleration (g)	61	54	≤ 90
Head pitch angle (°)	40	50	—
Chest acceleration (g)	56	57	≤ 60
Pelvis acceleration (g)	61	66	≤ 55 (56 - 75*)
Force on thighs (lb)	530	587	≤ 1349

Table 6. Frontal crash barrier data for 54.8 km/h impact for Audi A8 (*medium risk)

increase in the impact energy over what is required for the 208 regulations. The crash data for the AIV and the A8 are given in Tables 5 and 6. Table 5 also includes corresponding data for a regular production steel DN5 Taurus and it can be seen that the AIV generally meets or improves on the performance of the production steel vehicle.

OTHER AUTOMOTIVE ALUMINUM DEVELOPMENTS

Today, the automotive use of aluminum is dominated by castings for engine and transmission components, and for wheels where now over 40% of new vehicles have aluminum wheels, most of which are cast. The other major use of aluminum is for heat exchangers, i.e. radiators, evaporators and condensers for air conditioning systems and oil coolers where aluminum in the form of brazed and/or mechanically assembled units has essentially eliminated copper from this sector of the automotive market. However, there are several new and significantly large market opportunities developing for aluminum in addition to the closure sheet market and the emerging body structure market. These are described briefly in the following sections:-

CHASSIS AND SUSPENSION COMPONENTS

Components for chassis and suspension components produced as structural castings or a semi-solid forgings (SSF) for engine brackets, control arms, steering knuckles and suspension components represent the next near term major growth opportunity for auto aluminum.

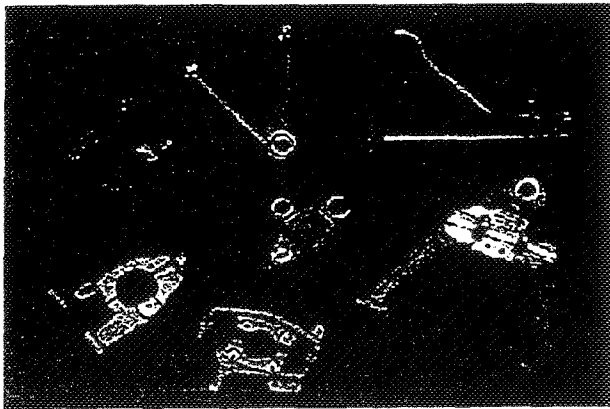


Figure 4. SSF suspension components for the Plymouth Prowler

Figure 4 illustrates some of the suspension components made by the SSF process for the Plymouth Prowler. Cast brake rotors and brake drums in DURALCAN™ materials, a family aluminum metal matrix composites developed by Alcan, are penetrating the market, presently for in low volume vehicles such as the Prowler. GM's EV1 and Toyota's electric version of the RAV4, and high volume applications are under active development. Figure 5 shows some examples for DURALCAN brake components. DURALCAN material in the extruded form is also being used instead of steel for driveshafts such as in the current Chevrolet Corvette.

DURALCAN™ - Owned by Alcan Aluminium Ltd.

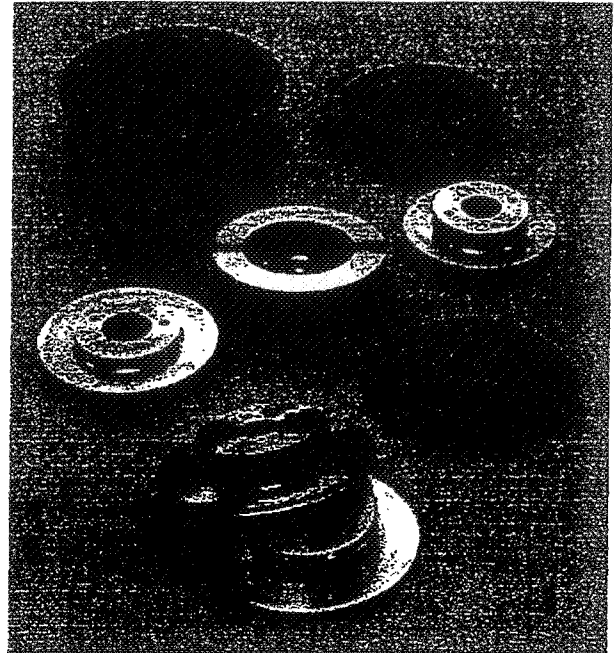


Figure 5. DURALCAN aluminum metal matrix brake components

All of these aluminum applications have the advantage that they reduce the weight of unsprung components and thus provide an additional bonus in improving ride characteristics. In fact, it is necessary to do this to maintain good ride characteristics whenever the sprung weight of a vehicle is reduced such as when a cast-iron engine block is replaced by an aluminum one.

TAILOR WELDED BLANKS

Tailor welded blanks in steel are now becoming commonplace due to improvement these give in terms of dimensional accuracy for the final stamped part as well as to the reductions in material stamping offal and in the sets of stamping tooling required. These advantages will also apply to aluminum, first, as it further penetrates into closures and then into body structures. Much progress has been made in the last two years in developing welding techniques for producing tailor welded blanks in aluminum, helped by the development of improved laser beam power sources, and particularly, YAG lasers. What I believe to be the first application for an aluminum tailor welded blank in an automotive development is shown in Figure 6. This is the rear body side inner stamping for Ford's P2000 prototype produced in 1.0mm joined to 2.00mm 5754 sheet material. The technology has now progressed to the point where components incorporating an aluminum tailor welded blank are being actively pursued.

HYDROFORMING

Hydroforming of tubes to replace stamped and spot welded sub-components is growing rapidly for steel and is also being adopted for some aluminum components. For example, the current 5 series BMW sedan has an aluminum rear sub-frame assembled from hydroformed tubes in an Al-Mg alloy, the

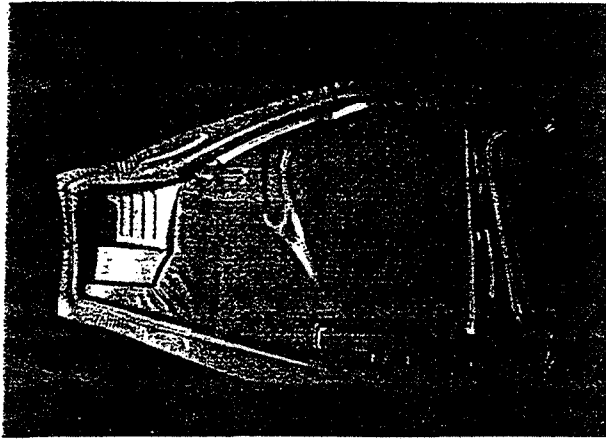


Figure 6. Aluminum body side inner stamping from a tailor-welded blank

tubing being made from sheet formed into tube and joined by high-speed induction welding⁽¹⁵⁾. The P2000 has a front sub-frame made, in this case, from hydroformed 6000 series extruded aluminum tubes and joined together by fusion welding to cast connectors⁽⁶⁾.

Volvo has also explored the use of hydroformed aluminum members for the construction of a front end structure for the current S70 (formerly the 850) model⁽¹⁶⁾. Combined with some aluminum sheet stampings and an extruded/stretched-bent part, they demonstrated a weight saving of 50% or 121lb compared with the steel monocoque structure of the production vehicle. The part count was also reduced by 50%.

SOURCING SHEET MATERIALS BY CONTINUOUS CASTING

Concern has been expressed by the auto companies on the capacity of the aluminum industry to meet the sheet supply requirement needed for the high volume production of aluminum intensive vehicles. While this is certainly not an issue today or in the near future, there is a recognition that continuous strip casting integrated with rolling would be a way to add a new capacity when needed and in increments that match the market growth. Typical capacity increments for a suitable continuous casting plant would be 100 to 150,000 tonne/annum and would therefore avoid the high up-front costs for installing a DC ingot-

	Yield Strength (MPa)	UTS (MPa)	Uniform El. (%)	r (at 10% ε)	n
6111-T4 CC	174	305	22	.74	.24
(0.9 mm) DC	171	312	22	.78	.25
5754-O CC	94	224	18	.66	.25
(1.0 mm) DC	102	231	20	.84	.24

from Friedman and Sherman

Table 7. Mechanical properties for aluminum automotive sheet from continuous-cast and DC cast stock (rolling direction)

hot mill/cold mill production complex. Potentially, it could also reduce the overall production costs for sheet.

Alcan has been exploring this possibility, both through laboratory simulation and through trials at the continuous strip casting/rolling plant it operates in the Saguenay region of Quebec. Finished sheet of both AA5754 and AA6111 has been produced and encouraging results from the evaluation of some of this material were reported by Ford at this year's TMS conference in San Antonio⁽¹⁷⁾. A sample of these results is given in Table 7. While not quite matching the performance of today's conventionally produced materials, the results indicate that it should be possible to develop acceptable products by the continuous strip casting route.

SUMMARY

Since the fuel consumption of vehicles is closely related to their weight, weight reduction is the key for developing environmentally friendly vehicles, and especially those that derive their power from fossil fuels.

Aluminum, due to its low density, high strength to weight ratio, corrosion resistance and availability in a wide range of product forms is an ideal material for many automotive applications including vehicle construction. Typically today, passenger cars contain ~8.5% aluminum and in 1996 the auto industry used 3.6 billion lbs. of aluminum in passenger vehicles, of which some 2 billion lbs. was secondary metal.

Aluminum is a particularly effective material for body structures and closure panels which together comprise a large part of the primary weight of vehicles. Here, materials and enabling technologies have been developed to give weight reductions of over 50% compared with today's vehicles while yet maintaining vehicle crashworthiness. In turn, the primary weight reduction allows the weight of many other components including the power train to be reduced.

In body structures, closure panels and many other components, aluminum can replace twice its weight of steel, thereby saving during the lifetime of typical family sedans at least 8 tonnes of CO₂ for each one tonne of aluminum that has replaced two tonnes of steel, and almost 20 tonnes of CO₂ when secondary aluminum is used.

Several aluminum intensive environmentally friendly prototypes and production vehicles have been developed, notably, GM's EV1 and Ford's P2000 PNGV prototype, providing vehicles that have excellent road holding, that are exciting to drive and amply demonstrate that environmentally friendly vehicles can be very attractive and desirable vehicles.

REFERENCES

- [1] President Clinton Announces the United States Climate Change Policy, Oct. 22, 1997 - Fact Sheet.
- [2] Drive Aluminum and Drive Our Future - The Aluminum Association, Washington, DC, 1997.
- [3] Study to Determine Aluminum Content in North American Vehicles in 1996. The Aluminum Association, Washington, 1996.
- [4] Y. Komatsu et al., SAE Technical Paper Series 910548,

1991.

- [5] M.J. Wheeler et al., SAE Technical Paper 870416, 1987.
- [6] Ford P2000 Ford Motor Company Press Release, May 1997.
- [7] H. Thorburn, Proceeding of the International Body Engineering Conference (IBEC '94) Vol. 7, Automotive Body Materials, p. 105.
- [8] E.F.M. Winter et al., Paper 905178 XXIII FISITA Congress Italy, Vol. II, pgs. 465-471.
- [9] W. Ruch, Hydro Aluminium, Private Communication.
- [10] J.C. Benedyk, Light Metal Age, pgs. 8-10, Oct. 1996.
- [11] Automotive Innovation, Materials World Vol. 3, pg. 584, 1995.
- [12] M.J. Wheeler, Paper 98SAF042 ISATA Dusseldorf 1998.
- [13] I.J. McGregor et al., Structural Crashworthiness and Failure, Chapter 10 pgs. 385-421, Chapman and Hall, N.York, 1993.
- [14] "Crash Energy Management in Aluminum Alloy Automotive Structures", The Aluminum Association, Washington (to be published 1998).
- [15] Thorsten Schulze VAW alutubes GmbH, 2nd International Conference on Innovations in Hydroforming Technology, Sept. 1997, Columbus, Ohio.
- [16] Gunnar Lassi et al., IBEC '97 Advanced Technologies and Processes, pgs. 11-20.
- [17] P.A. Friedman and A.M. Sherman, Automotive Alloys II TMS Annual Meeting, San Antonio, 1998, pgs. 147-160.

THE DRIVE FOR LIGHT WEIGHT VEHICLES IN NORTH AMERICA

M. J. Wheeler

Alcan Global Automotive Products
136 Bagot Street
Kingston, Ontario K7L 3E5
Canada

Telephone:
e-mail Mike.Wheeler2@sympatico.ca

THE DRIVE FOR LIGHT WEIGHT VEHICLES IN NORTH AMERICA

Dr. M.J. Wheeler*, Alcan International Limited

ABSTRACT

This paper will summarize the underlying reasons for the drive for lighter weight passenger vehicles in North America and the response of the major North American vehicle manufacturers to government-imposed regulations and also to the joint government-industry initiative to develop light weight, high mileage passenger cars under the so-called clean car or PNGV (Partnership for a New Generation of Vehicles) program. Some of the aluminium intensive vehicles that have been developed under the various programs and the respective materials and technologies will be described. In addition, a summary will be presented of the efforts being undertaken by the North American aluminium companies, working jointly through the Automotive and Light Truck Committee of the Aluminum Association, to highlight the value of aluminium for light weighting vehicles and also to remove the real and/or perceived barriers to the high volume use of aluminium in aluminium intensive vehicles.

THE UNDERLYING REASONS FOR VEHICLE WEIGHT REDUCTION

In North America, the major concerns about vehicle fuel consumption are the exhaust emissions that vehicles create, particularly CO₂, the consumption of oil reserves and dependence on oil imports. This became highlighted in 1973 at the time of the OPEC oil crisis when the United States was importing some 35% of its crude oil needs and cars were only achieving 14.2mpg(US) (16.6ℓ/100km). These concerns led to the introduction of the CAFE or corporate average fuel economy regulations in 1978 which required each of the Big Three's car makers fleet of domestically produced cars (US and Canada) to achieve 18.0mpg(US) (13.1ℓ/100km). This target has been progressively increased to the present 27.5mpg (8.57ℓ/100km) and there are financial penalties imposed by the government if a car company's fleet does not reach this value.

It was recognized that a vehicle's weight was the main factor in determining its fuel consumption and the impact of the OPEC oil crisis and then the CAFE legislation led to the introduc-

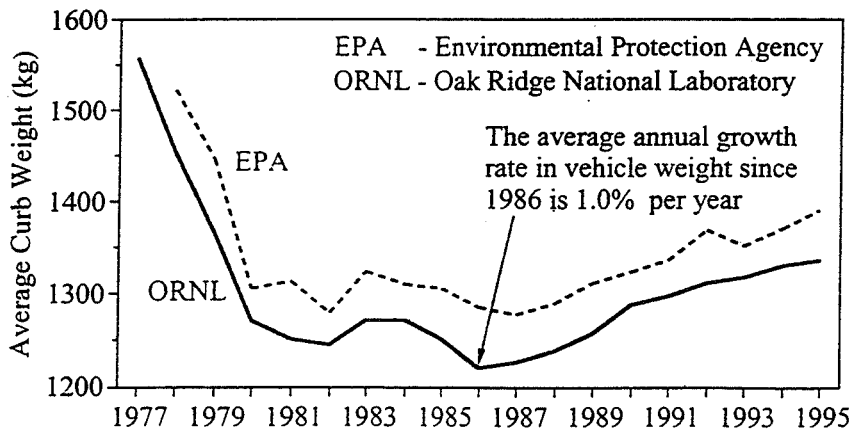


Figure 1. Average weight of new North American passenger cars 1977–1995

*Dr. M.J. Wheeler, Director of Research, Alcan International Limited

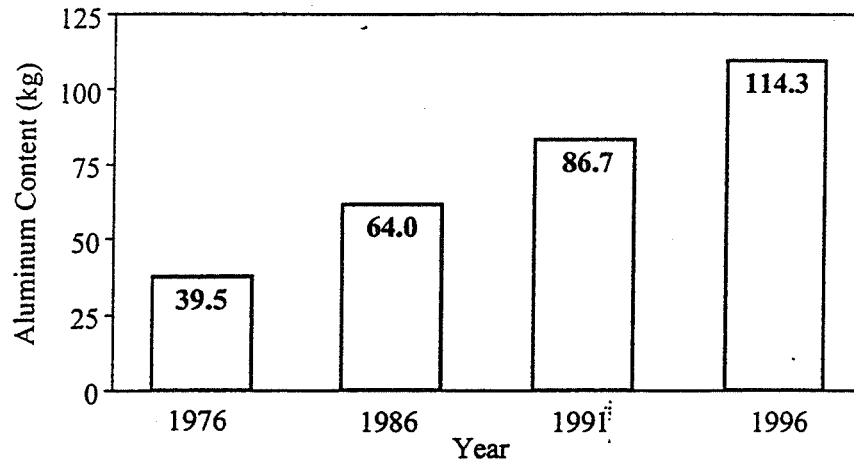


Figure 2. Average aluminium content in North American passenger cars from 1976 to 1996

tion of unibody or monocoque construction, the progressive adoption of front wheel drive and a general downsizing of vehicles to save weight. As a result, the average weight of new vehicles dropped rapidly from 1977 to 1980, reached a low in 1986 but has been increasing by about 1% per annum for each new car since then (see Figure 1) due to the combination of government imposed safety requirements, and market demands and competition to provide added vehicle content and performance. However, the car makers have only been able to contain weight increases by gradually substituting aluminium for heavier materials in their vehicles, the aluminium content on average increasing from 39.5kg in 1976 to 114.3kg per car last year, a compound annual growth rate of ~ 6% (Figure 2)⁽¹⁾. Currently, Chrysler and General Motors (GM) are meeting the passenger car CAFE requirement but Ford is just under the target at 27.4mpg (8.60l/100km) (Table1).

Light trucks which includes mini vans and sports utility vehicles as well as the ubiquitous N. American pick up, were made subject to a CAFE target of 17.5mpg (US) (13.5ℓ/100km) in 1982 and now have to meet a target of 20.7mpg (11.38ℓ/100km). This market sector has become almost as large as the passenger car market but today none of the producers are meeting the CAFE target (see Table 1), even though they are using on average 109.3kg of aluminium per vehicle.

As a result of the growth of the light truck market sector and the lower CAFE requirement for these vehicles, the net fuel consumption and exhaust emissions for passenger vehicles are now increasing again in N. America and its also interesting to note that the US now imports some 45% of its crude oil needs!

	Cars		Light Trucks	
	mpg	(L/100 km)	mpg	(L/100 km)
Required	27.5	8.57	20.7	11.38
Chrysler	27.9	8.44	20.4	11.55
Ford	27.4	8.60	19.9	11.84
General Motors	28.1	8.38	20.4	11.55

Table 1. CAFE requirements and actuals

An obvious way to reverse these trends is to raise the CAFE requirements but recent US administrations have been reluctant to impose tighter standards. As an alternative, non-confrontational approach, the Clinton administration in the early part of its first term initiated a dialogue with the Big Three US car makers on ways to radically reduce vehicle fuel consumption and to improve air quality by the reduced exhaust emissions. This resulted in the PNGV or Partnership for a New Generation of Vehicles program between the government and the Big Three car companies where the major aim is to develop by 2004 production ready prototypes of mid-sized sedans (saloons) which achieve 80mpg (US) (2.95ℓ/100km) and which will cost at that time no more than conventional vehicles of the same size. Two other goals of the program are to increase material competitiveness in manufacturing and to implement technologies as they are developed to improve the gas mileage of conventional vehicles⁽²⁾.

It was immediately recognized that the 80mpg goal would require power trains with much improved thermal efficiency compared with even the best of today's vehicles and also very significant weight reductions, especially in the body and the chassis. However, in 1995 when the partnership was started, all three of the car companies had some experience in using aluminium in body structures to reduce vehicle weight. Ford had built and tested its AIV and Synthesis 2010 vehicles, aluminium intensive cars derived from the Taurus/Sable model, GM had developed an aluminium structure for the Impact, the prototype of its EV1 electric car, and Chrysler had built the Neon Lite, an aluminium replica of the Neon sedan production car.

Other factors driving weight reduction are the existence of various clean air acts and the slowness in the development of high storage capacity batteries for electric cars. Even though the GM EV1 and other electric vehicles are now available, the short range of these vehicles has limited their growth and the few that are in use are insufficient to provide any relief from vehicle air pollution effects in cities such as Los Angeles where they are being marketed.

CURRENT APPLICATIONS OF ALUMINIUM

In a very detailed survey carried out on behalf of the Aluminum Association⁽¹⁾, it was estimated that some 1.63M tonne of aluminium would be used in passenger cars and light trucks in N. America in 1996, some 0.9M tonne of which would be recycled metal. The dominant product form was castings (77%) followed by rolled products (12%) and extrusions (10%).

The use by vehicle system is shown in Figure 3 where the major uses are for engine systems (32%) (cylinder heads, pump housings, and increasingly, cylinder blocks), transmission system (24%) (automatic transmission components, transmission cases, drive shafts, etc.), heat exchangers (19%) and wheels (14%). Almost all heat exchangers—radiators, oil cooler and air conditioning evaporator and condenser units—are now made in aluminium, most being brazed assemblies for reduced weight and increased thermal efficiency. Increasingly, some suspension components are now made by casting or by the semi-solid forging (SSF) process and brake components, particularly brake rotors and drums, are beginning to be made from aluminium metal matrix materials including the DURALCAN™ material developed by Alcan. These applications fall within the other applications sector (11%) which also includes closure sheet applications and body structures. It is these two where weight reduction from using aluminium can have the biggest impact and they represent major opportunities for aluminium that could grow to be bigger than the total of all of the aluminium applications in today's vehicles.

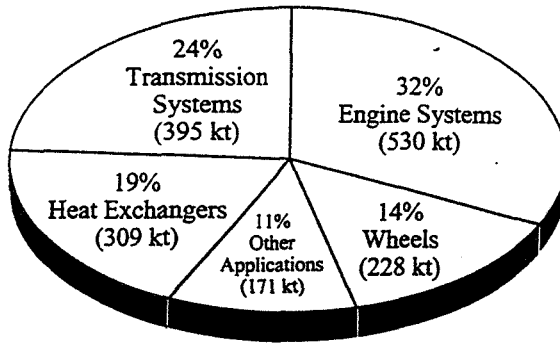


Figure 3. Aluminium applications in vehicle systems for 1996

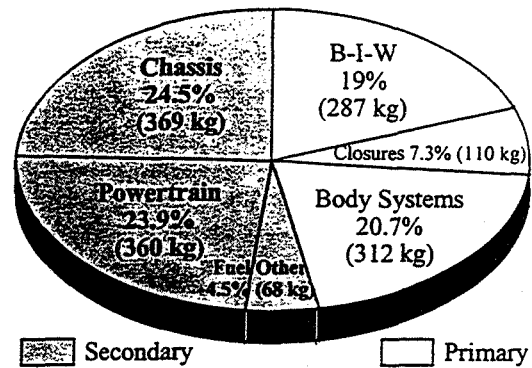


Figure 4. Primary and secondary weights in a typical N. American sedan (1997 Ford Taurus)

Aluminium is an obvious material for these and other automotive applications. Its density is about one-third that of steel (2.7kg/m^3 versus 7.8kg/m^3 for steel), it has a higher strength to weight ratio than steel, and although its stiffness modulus is lower, it has specific modulus equal to that of steel. It is available in volume as sheet, extrusions, castings, forgings and now as metal matrix composites, is corrosion resistant and 100% recyclable.

PRIMARY AND SECONDARY WEIGHT SAVING

In order to reduce the overall weight of a vehicle, it is important to appreciate the significant of saving weight in the body structure and to a lesser extent in the exterior closure panels. The various system weights for a typical N. American mid-sized sedan, the current Ford Taurus, is shown in Figure 4. The body structure or body-in-white is the single heaviest component in all cars and is structurally the most important, providing the safety cage to house and protect the occupants, front and rear crumple zones to absorb energy in the event of a major collision and a rigid structure to support the power train and the vehicle's suspension.

It is the weight and size of the body structure and the weight of the closure panels that surrounds it that determine size of the power train required, the performance required of the suspension and brakes and the size of the fuel system. Thus, the body structure and closure panels form part of what is known as the primary vehicle weight and major reductions in their weight allows for corresponding weight reductions in the secondary vehicle systems. Another paper in this conference, shows, in fact, that secondary weight savings can be almost equal to the primary weight saving. In the following section, some of the vehicles with aluminium body structures and the materials and enabling technologies that have been used to build them will be briefly described.

ALUMINIUM SPACE FRAME VEHICLES

The space frame approach for developing light weight aluminium vehicle structures was pioneered by Alcoa⁽³⁾ and Norsk Hydro and, more recently, has been further developed by Alumax⁽⁴⁾ and by Lotus Cars in the UK⁽⁵⁾. In this approach, structural frames are built using shaped or formed aluminium extrusions which are joined together by a variety of methods such as fusion welding to cast connecting nodes (Alcoa), sectioning and direct fusion welding (Norsk Hydro), compression fit forming (Alumax), and adhesive bonding supplemented with mechanical fasteners (Lotus Cars). The compression fit forming approach is particularly attractive in that there is no heat-affected zone from welding and only relatively simple tooling is required.

The first aluminium space frame production car was the Audi ASF A8 which is now sold in North America as well as in Europe, see Figure 5. Other examples are the Renault Spider with the Norsk Hydro approach, the Lotus Elise, the Panoz Roadster (Alumax) and the Plymouth Prowler (Alcoa). In the latter two examples, the space frame is really more of a basic ladder frame since the vehicles are open-topped sports cars.

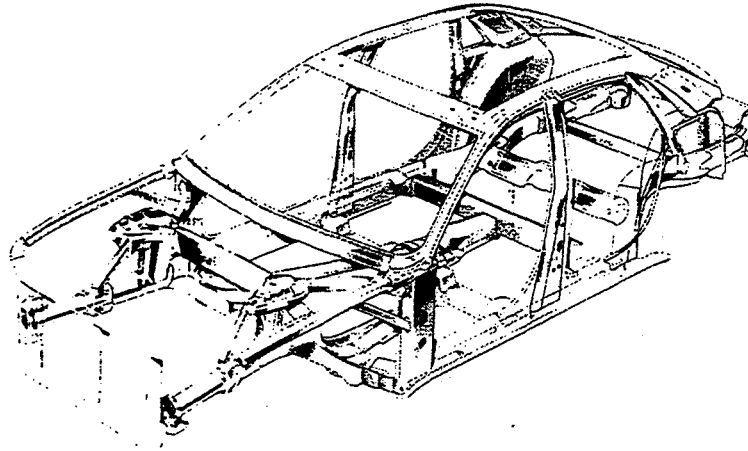


Figure 5. Aluminium space frame for the Audi A8

The space frame approach does not save as much weight as the unibody approach but is more cost efficient at low production volumes, even in comparison with the conventional steel unibody design. This is because extrusion dies are less expensive than sheet stamping dies and the part integration opportunities with extrusions allows for the reduction in the number of parts and in the assembly costs.

Space frames have to be completed with sheet stampings and, typically, there can be more sheet than extrusions in a completed body; for instance, in the Audi A8 there is 110kg of sheet compared with 61kg of extrusions. The major advantages for the aluminium space frame approach are:

- Lower part making investment costs.
- Reduced part count due to part integration provided by extrusions and castings.
- Adaptable to a variety of low volume vehicle design approaches and methods for assembly.
- An enabling approach for the development of low volume specialty vehicles.

ALUMINIUM UNIBODY VEHICLES

Almost all the high volume cars produced today have steel unibodies made from stamped sheet, spot welded together. This approach has been gradually optimized to reduce the mass and enhance the structural stiffness, the latter being key for obtaining good handling and drivability characteristics. The aluminium unibody is based on the same approach and an early example was the Dyna Panhard of circa 1954⁽⁶⁾, where spot welding was used to assembly the panels. A much more recent example is the Acura NSX where Honda used a combination of spot and MIG spot welding⁽⁷⁾. However, due to the lower modulus of aluminium, the weight saving was limited to about 40% compared with steel but a breakthrough for aluminium came with the development by Alcan of its Aluminium Vehicle Technology (AVT) structural bonding approach

using AA5754 (Al-3%Mg) structural sheet⁽⁸⁾ (Figure6). This enables the weight saving compared with steel to be increased to over 50%, thereby reducing the weight of the aluminium and hence the cost as well as giving enhanced structural stiffness compared with spot welded steel and exceptional fatigue endurance as a result of eliminating the stress concentrations at spot welds.

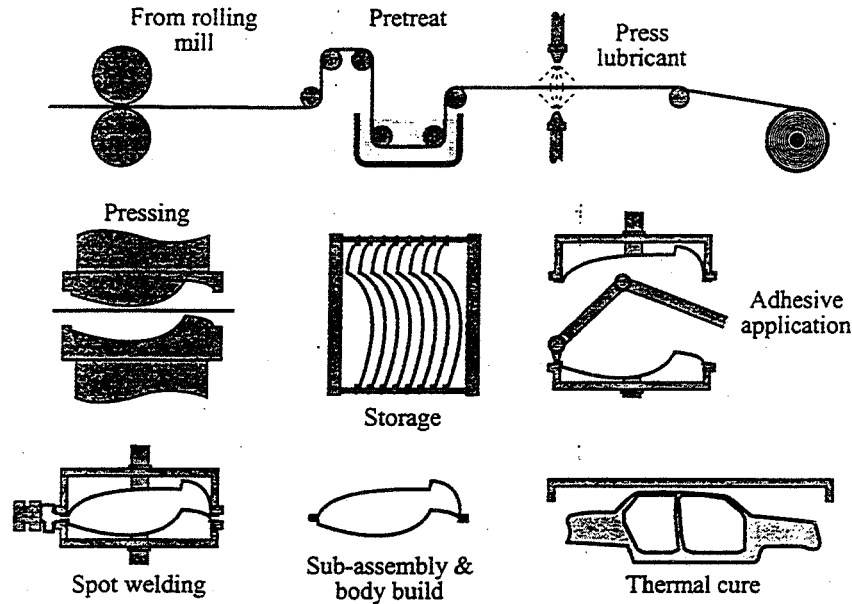


Figure 6. Alcan AVT system for bonded body structures

Ford employed the AVT system for its Aluminium Intensive Vehicle (AIV) program where some 40 AIV's were built, based on the geometry and mechanicals of the then current DN5 Taurus/Sable models. The aims of this program were to confirm the weight savings that could be achieved, to test the drivability, durability and crashworthiness of the vehicles and to explore the suitability of the system for high volume manufacturing. The AIV body-in-white structure is shown in Figure 7 and the car body was completed with AA6111 aluminium alloy closure panels. The net weight saving was 173kg and the cars proved to have excellent handling and NVH characteristics, durability and crashworthiness. Had secondary weight savings been adopted, it is estimated that a total weight reduction of almost 318kg could have been achieved⁽⁹⁾.

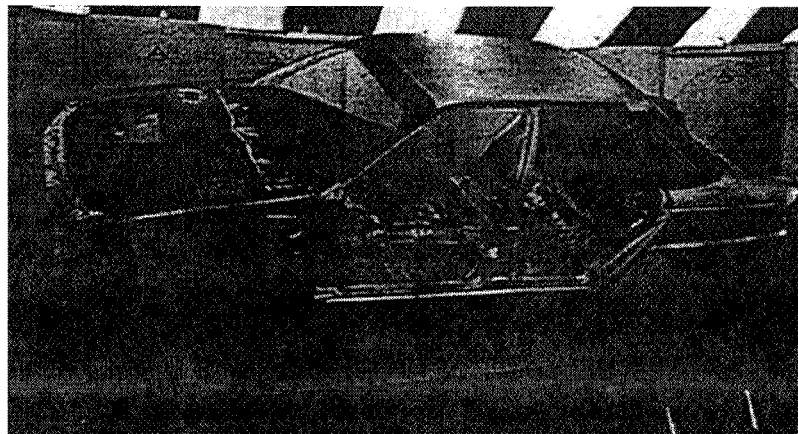


Figure 7. Ford AIV body-in-white

GM also adopted the AVT system for the body structure of its electric car prototype, the Impact which has since become its EV1 production car. Here, to reduce tooling costs for low volume production, some stamped sub-assemblies were replaced with either extrusions or castings and this also provided some part integration, reducing the part count from a typical 200 plus to 168⁽⁹⁾.

The advantage of the AVT system for unibody structures are:

- Use of structural adhesive bonding to minimize weight, enhance fatigue endurance and structural rigidity.
- Its compatible with existing volume manufacturing facilities of the auto companies.
- Adaptable to low volumes by incorporating extrusions and casting.

The Chrysler Corporation has explored the replacement of steel by aluminium in the body structure and closure panels in its Neon vehicle to produce the Neon Lite⁽¹⁰⁾ and subsequently developed an aluminium body structure for its Intrepid ESX PNGV prototype which is powered by a hybrid diesel-electric power system⁽¹¹⁾.

The most recent application of Alcan's AVT system is for Ford's P2000, their first purpose designed PNGV prototype where they have fully exploited the weight savings that can be achieved with aluminium in both the primary and secondary vehicle systems to achieve a projected weight of just 908kg (2000lb)⁽¹²⁾. The major aluminium applications are as follows:-

- A weld bonded AA5754 sheet body-in-white structure weighing 135.7kg and featuring two tailor welded blanks
- Sheet closure panels in paint bake hardening 6000 series alloys (AA6111, with the deck lid in AA6022), weighing 46.3kg
- Cast front and rear shock towers in A356 alloy
- Fabricated front-sub-frame using hydroforms and castings weighing 14.4kg
- DURALCAN™ front brake rotors and rear brake drums
- Engine cylinder block for a 1.2 liter CIDI engine

There is a total of 333kg aluminium in the P2000 and this comprises some 37% of the total vehicle weight. The full mix of materials compared with the materials used in the current Ford Taurus is shown in Table 2. The Figure 8 shows the weight reductions for the various vehicle

	P2000		Ford Taurus	
	(kg)	(%)	(kg)	(%)
Ferrous	218	24.0	978	65.0
Aluminium	333	36.6	129	8.6
Magnesium	39	4.3	4	0.3
Plastic	122	13.4	173	11.5
Other	196	21.6	221	14.7
TOTAL	908		1505	

Table 2. Materials usage in Ford P2000 and Ford Taurus

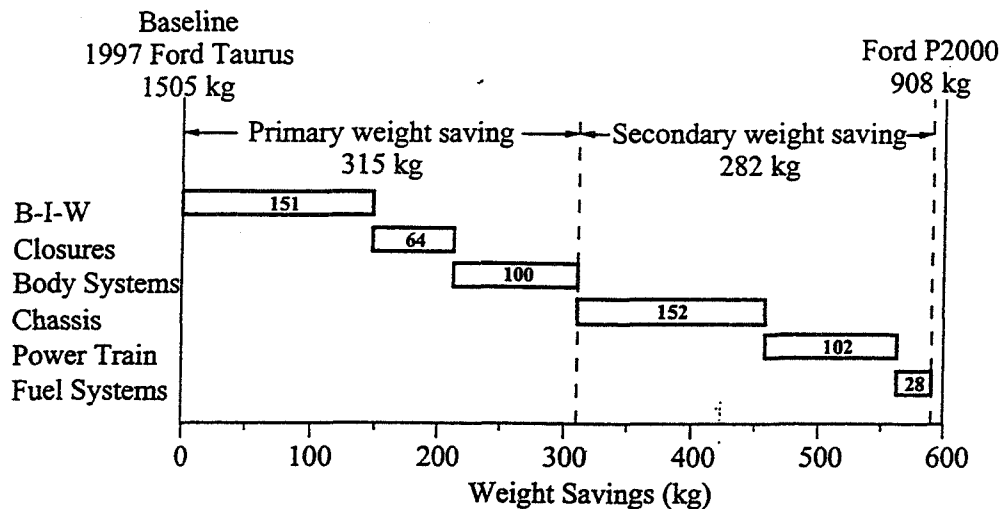


Figure 8. Primary and secondary weight reductions in the P2000 and Ford Taurus

systems in the P2000 compared with those for the Taurus. The secondary weight saving is 282kg which is some 0.9 of the primary weight saving of 315kg and is a significant achievement. The projected fuel consumption of the vehicle for highway driving is expected to be at or above 70mpg (US) (3.37ℓ/100km)⁽¹²⁾.

ALUMINIUM CLOSURE PANELS

The closure panels on a car, while weighing considerably less than the body structure, still form part of the primary weight and the replacement of steel panels by aluminium can save considerable weight as is evident from the weight reduction data for the P2000. In fact, aluminium closure panels are already a reality, especially in the North American market where 1 in 11 new vehicles produced today has one or more such panels. They are being produced at an annualized rate of about 1.7 million units and the key to this success has been the adoption of 6000 series aluminium alloys which are supplied in a solution-treated/formable condition but which harden during the normal automotive paint bake treatment to provide high strength and dent resistance. The highest volume use today is for the hood of the Ford F150 light truck and its derivatives where the production rate is expected to reach approximately 600,000 units per annum. The dominant alloy today is AA6111, an Al-Mg-Si-Cu heat-treatable alloy developed by Alcan, which typically reaches a strength of 230MPa following forming and paint baking or up to 280MPa in a recently-introduced preaged version. This is comparable in strength to the bake hardening steels used today. With this strength, weight savings exceeding 50% compared with steel are being achieved. Table 3 lists the current N. American vehicles which have one or more aluminium closure panels.

SUPPORTING TECHNOLOGY

While individual aluminium companies are developing specific materials and technologies and introducing these to the various car companies, the aluminium producers are also working together through the Aluminum Association in Washington to address those issues which are generic and which must be resolved for aluminium to penetrate the market for high volume production vehicles. In some cases, these activities also involve cooperative program with the car companies. Some of the more important projects are:-

Lincoln Town Car	Hood
Mercury Marquis	Deck lid* and hood
Ford Crown Victoria	Deck lid* and hood
1996 Ford Taurus	Deck lid*
1996 Mercury Sable	Deck lid*
Oldsmobile Aurora	Hood*
Buick Riviera	Hood*
1996 Ford F-150 Pickup	Hood*
1997 GM APV	Hoods*
1997 Lincoln Mark VIII	Hood*
1997 Buick Park Avenue	Hood*

Table 3. Current N. American vehicles with aluminium closure panels
*exterior panels in AA6111

- Modelling to predict the aluminium composition that would result from recycling aluminium intensive vehicles such as Ford P2000 PNGV prototype.
- Evaluation of alloy sorting techniques for separating individual alloys or alloy families from mixed shredded scrap.
- Life cycle analysis for vehicles based on the mix of the major materials. This is a joint activity between the United States Automotive Materials Partnership (USAMP), the Aluminum Association, the American Iron and Steel Institute and the Plastics Consortium.
- Resolution of environmental issues and particularly a US Federal Environmental Protection Agency's regulation that wrongly identifies the sludge from automotive finishing lines processing aluminium as toxic.
- The preparation and publication of technical manuals and, most recently, the distribution of a CD ROM promoting aluminium automotive technology and applications.

In addition to these industry efforts, Alcan has pursued and/or encouraged the development of related technologies which are key to establishing and then maintaining the long-term economic availability of aluminium for vehicle-structures. Briefly, these are:-

- Evaluation of welding methods for producing tailor-welded blanks in aluminium.
- Production of automotive structural sheet by continuous slab casting integrated with rolling.
- Use of laser induced optical emission spectroscopy for the alloy identification of shredded scrap⁽¹³⁾.
- Pollution-free decoating of painted automotive scrap prior to remelting by the use of fluidized bed decoating⁽¹⁴⁾.

Not all of these technologies are needed today but their technical feasibility has been established to the point where industrial scale facilities could be developed when they are needed to sustain the economic production and recycling of aluminium automotive materials.

SUMMARY

- Today, the passenger cars produced by the Big Three automakers in N. America are just meeting the US government's CAFE (fuel economy) requirements but none of their light trucks fleets meet the CAFE target for this class of vehicle.
- The weight of new passenger cars is still increasing at about 1% per annum, even though the use of aluminium to replace heavier materials is increasing at about 6% per annum and is now at an average of 112kg per vehicle for the combined fleet of cars and light trucks.
- Aluminium external closure panels are becoming relatively commonplace with one in eleven new vehicles with one or more such panels. Aluminium hoods for one vehicle, the Ford F150 light truck, are being produced at a rate approaching 600,000 units/annum.
- There are now proven technologies for light weight, aluminium intensive vehicles using either the space frame technique with extrusions or the unibody approach with the structural bonding technique pioneered by Alcan. This latter approach is being favoured for the development of the high volume, light weight body structures needed to meet the weight reduction targets of the PNGV (Partnership for a New Generation of Vehicles) program.
- The PNGV program is now providing the driving force in N. America for the development of light weight but structurally efficient and crashworthy vehicles.
- The real and/or perceived barriers to use of aluminium for high volume production cars, including the eventual recycling of aluminium from end-of-life vehicles are being addressed and resolved by the aluminium producers working either independently or, when appropriate, through the Washington DC based Aluminum Association.

References

- (1) *Study to Determine Aluminum Content in North American Vehicles in 1996* - The Aluminum Association, Washington, 1996.
- (2) *Partnership for a New Generation of Vehicles - Program Plan* - PNGV Secretariat, US Dept. of Commerce, Washington, 1995.
- (3) E.F.M. Winter et al, Paper 905178, XXIII FISITA Congress Italy Vol II pp 465-471.
- (4) J.C. Benedyk, *Light Metal Age*, pp 8-10, October 1996.
- (5) *The Engineer Report* - Engineer Nov 2, p 30, 1995.
- (6) J.J. Baron, *Aluminium* Vol 30, No. 5, 1954.
- (7) Y. Komatsu et al, SAE Technical Paper Series 910548, 1991.
- (8) M.J. Wheeler et al, SAE Technical Paper Series 870416, 1987.
- (9) *Aluminum Auto Design Review*, Vol 3 No. 2, The Aluminum Association, Washington, 1995.
- (10) Saad M. Abouzahr et al, *Automotive Body Design and Engineering* pp 12-16, IBEC, 1994.
- (11) *PNGV Technical Accomplishments* - United States Council for Automotive Research, 1996.
- (12) Ford P2000 Press Release, May 1997.
- (13) A.J. Gesing and A. Rosenfeld, SAE Technical Paper Series 960163, 1996.
- (14) F. Tremblay et al, *Proc 3rd International Symposium on Recycling of Metals. The Minerals, Metals and Materials Society*, pp 19-30, 1995.

THE DRIVE FOR LIGHT WEIGHT VEHICLES IN NORTH AMERICA

M. J. Wheeler, Alcan International limited

Paper presented at the Institute of Materials' conference on "Materials for Lean Weight Vehicles" at Gaydon in the United Kingdom in November 1997 and subsequently published in the conference proceedings.

STRUCTURAL DESIGN OF ALUMINUM COMPONENTS WITH ADS SOFTWARE

J. Randolph Kissell

The TGB Partnership
1325 Farmview Road
Hillsborough, North Carolina 27278

Telephone: 919-644-8250
e-mail tgb@mindspring.com

Structural Design of Aluminum Components with ADS Software

Prepared by J. Randolph Kissell, *The TGB Partnership*

ABSTRACT – The Aluminum Association recently released software called the Aluminum Design System (ADS) based on *Specifications for Aluminum Structures*, a structural design code for aluminum components. *Specifications for Aluminum Structures* includes equations for the strength of aluminum members, but is complicated to understand and apply, often involving many calculations. The ADS software performs these calculations automatically to check the structural adequacy of aluminum parts subjected to various loads. The software also includes several data bases - one for various aluminum cross sections and one for aluminum alloys, both of which may be customized by the user. This paper describes the main features of the software for potential users.

INTRODUCTION

The structural design of many aluminum components is performed according to the rules in the Aluminum Association's *Specifications for Aluminum Structures*^[1], hereafter referred to as the aluminum *Specifications*. This design process has been automated in the Aluminum Design System (ADS) software. This paper describes the capabilities of the software.

STRUCTURAL DESIGN OF COMPONENTS

The dimensions of many aluminum components are dictated by requirements that the part perform adequately as a structural component. These requirements might include a limit on its deflection or the ability to support a certain load without permanent deformation. The great variety of extruded and roll-formed shapes complicates the structural design of aluminum extrusions. In the US, such design is conducted according to the rules outlined in the aluminum *Specifications*. The Aluminum Design System (ADS) software was commissioned by the Aluminum Association to automate the procedures in the aluminum *Specifications*. By automating the process, it can be performed more quickly and consistently than performing the calculations by hand.

ADS FEATURES

ADS contains five modules:

- Reference
- Geometric Properties
- Material Properties
- Structural Analysis
- Member Design

ADS operates in US or SI units as specified by the user.

Reference Module

The reference module contains the text of the *Aluminum Design Manual* which can be viewed, searched, navigated, and printed. Certain features are linked so that clicking on the text will immediately take the view to the section, table, or figure referred to in the text. For example, clicking on "section 6, Fabrication" in the table of contents takes the viewer to that section. Searching for the word "extrusion" can bring the viewer to the next (or previous) occurrence of that word in the text.

Geometric Properties Module

The geometric properties module contains the cross sectional properties of:

- Aluminum Association standard I beams
- Aluminum Association standard channels
- Pipes

The cross sectional properties include the designation for the shape (e.g., I 6 x 4.03 for the standard 6" deep I beam weighing 4.03 lb/ft), dimensions of the shape, area, weight per unit length, torsion constant, warping constant, and moment of inertia, section modulus, and radius of gyration about each of the two major axes of the shape. (For pipes, the warping constant is not applicable and so is not given.)

The geometric properties module can also calculate the cross sectional properties of 29 shapes with user-defined dimensions (including rectangles, solid and hollow regular polygons, and zees, to name a few). These properties include those in the following list that are appropriate for the given shape: area, location of

the centroid, location of the shear center, torsion constant, warping constant, weight per unit length, shear shape factor (ratio of average shear stress to maximum shear stress), orientation of principal axis, and moment of inertia, section modulus, and radius of gyration about each of the two major axes of the shape.

ADS can also calculate the section properties for any shape for which the width-to-thickness ratio of the elements is large. The elements of such arbitrary thin-walled sections are treated as lines. These elements are more common in cold-formed sheet sections, but some extrusions can be idealized as thin-walled without a significant loss in accuracy. Included in the section properties ADS calculates for thin-walled shapes is the circumscribing circle size and center location, useful properties for extrusions.

Material Properties

The material properties module contains a data base of properties for 135 aluminum alloy/temper/product combinations. The properties given are: for welded and unwelded material, minimum: tensile ultimate strength, tensile yield strength, compressive yield strength, shear ultimate strength, shear yield strength, bearing ultimate strength, and bearing yield strength; compressive modulus of elasticity, Aluminum Association ratings for: corrosion resistance, weldability, brazeability, machinability, and workability; and foreign alloy designations. The user may add his own alloys (for example, proprietary alloys) to the data base.

Structural Analysis

The structural analysis module calculates forces and moments for the following cases: single span and multiple span beams, beams with elastic support, curved beams, shafts, and rectangular plates. The results (forces and moments acting on the member) of these analyses can be used as input for the member design, the next module discussed.

Member Design

The member design module performs structural conformance checks. A structural conformance check shows if, as determined by the equations for strength given in the aluminum *Specifications*, a member is strong enough for a given application. This is probably the most useful aspect of ADS since no other commercially available software performs this function. ADS can perform this check for 13 cross sectional shapes: solid and hollow rectangles, solid and hollow circles, solid and hollow ellipses, angles (with equal or unequal legs), I sections (with equal or unequal width

flanges), channels, C sections, hat sections, zees, and tees. ADS accepts axial tension and compression, bending moments, torques, and shear loads (or any combination of these).

The aluminum *Specifications* provide two methods for conformance checks - allowable stress design (ASD) and load and resistance factor design (LRFD). LRFD is a more sophisticated method, but is used only for building type structures and requires additional input from the designer. ADS can perform whichever design method the user specifies.

The member design module also contains a feature that permits the user to study the effect of a change in a design parameter. Such a study is called parametric analysis. For example, the length of a member can be varied over a user-specified range and the longest length that is strong enough to carry the required axial compressive load for a given application can be determined.

LIMITATIONS

The aluminum *Specifications* do not provide rules for the structural design of all extruded shapes. The method used in the *Specifications* is to idealize shapes as a collection of curved or flat elements of constant thickness^[2], as shown in Figure 1.

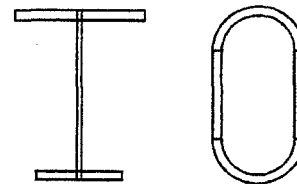


Figure 1. Idealizing shapes as collections of elements

If an element is connected to another element at its end, it is considered to be supported at that end. For example, the flange of an I beam is idealized as two elements, one on either side of the web. The tip of the flange is not connected to any other element of the cross section and thus is considered to be unsupported. Where the flange element is connected to the web, the flange element is considered to be supported. The strength of each element is a function of its width (or, in the case of curved elements, its radius), its thickness, the support conditions at its ends, and the variation of stress over its width. (Stress varies over the height of the web when the extrusion is subjected to bending, whereas stress is constant over the height of the web when the extrusion is subjected to axial compression, as in the case of a column).

This method is complicated when elements have intermediate stiffeners across their width or stiffeners

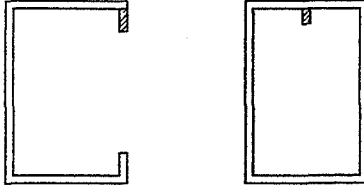


Figure 2. Edge and Intermediate Stiffeners

at their ends, as shown in Figure 2. These stiffeners are too small to be considered elements in their own right, but the strength of the extrusion is underestimated if they are neglected in the design. The aluminum *Specifications* contain rules for many of the possible cases arising with stiffeners, but do not address all, since the number of possibilities is quite large. For example, the *Specifications* address an element supported at one end and not at the other (the flange described above) with a stiffener at the unsupported edge. The *Specifications* do not, however, address the same element if an intermediate stiffener is added somewhere along the width of the flange. Furthermore, the *Specifications* do not address elements of varying thickness and other more extreme variations in shape, as shown in Figure 3.

Since ADS only performs designs by using the rules in the aluminum *Specifications*, there are extruded shapes that cannot be designed using ADS. Research co-sponsored by the Aluminum Association and the US Department of Energy is currently being conducted at

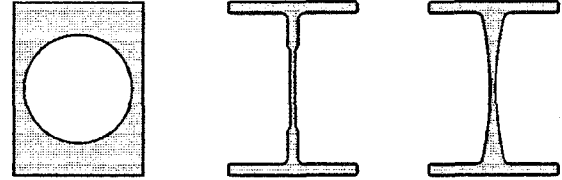


Figure 3. Extruded Shapes Not Addressed by the Aluminum *Specifications*

Cornell University to develop methods for determining the strength of shapes other than those already addressed by the aluminum *Specifications*. The finite strip method, a general method that can determine the strength of any shape, has shown promise.

CONCLUSION

The ADS software is a useful tool for quickly and accurately performing the structural design of many aluminum extrusions.

REFERENCES

1. Aluminum Association, *Aluminum Design Manual*, Aluminum Association, Washington, DC, 1994.
2. Kissell, J. R. and Ferry, R. L., *Aluminum Structures*, John Wiley, New York, 1995, p. 86-88.

**OPPORTUNITIES FOR RECYCLING OF ALUMINUM
FROM END-OF-LIFE VEHICLES**

M. P. Thomas

and

C. L. Wood, Jr.

The Aluminum Association, Inc.
Washington, D. C.

Opportunities for Recycling of Aluminum from End-of-Life Vehicles

M.P. Thomas and C.L. Wood, Jr.
The Aluminum Association Inc., Washington, D.C. U.S.A.

Abstract

Around 250 lbs (115 kg) of aluminum are used on current North American vehicles. When these vehicles are scrapped, the aluminum will be recycled by a highly successful industry that thrives on free market economics. Aluminum is an attractive candidate for use in future powertrain, chassis and structural applications, including body structures and closure panels. Aluminum's many product forms can help the designer to reduce tooling cost and assembly cost through parts consolidation. As the use of aluminum grows, and particularly with the increasing use of wrought alloys, there will be opportunities for methods to enhance the value of end-of-life vehicles, and particularly to optimize the recovery of the aluminum from these vehicles. The aluminum industry is working together to ensure that these methods are developed and implemented, and this paper will extend previous discussion of these activities in relation to existing and future recycling systems for automotive aluminum.

Introduction

Much effort is being applied to increase the use of lightweight materials in automobiles to improve performance and fuel efficiency. Aluminum is an attractive candidate for powertrain, chassis, body structure and closure sheet applications because of its lightweighting capability coupled with performance attributes. Currently about 250 lbs (115 kg) of aluminum is used in automobiles, mainly in the form of foundry alloy castings [1]. The main growth opportunity for aluminum lies in sheet and extruded wrought alloy for structures and closures, together with further growth in castings for engine blocks, cylinder heads and suspension components.

By the year 2006, the average usage of aluminum could reach over 400 lbs (180 kg) per vehicle, and aluminum intensive vehicles could easily have in excess of 900 lbs (400 kg). This growth in aluminum usage will have a significant impact on the downstream recycling of the manufacturing scraps generated during vehicle manufacturing and eventually of material from vehicles at the end of their life.

Aluminum has an excellent history of recyclability because it retains a high value in scrap form and because it is easy to recycle. For example, the present recycling system for automotive aluminum, through the application of shredding, sink-float separation technology and eddy current processing, recovers aluminum from scrapped automobiles with over 85% recovery. In this system, the aluminum is recovered from a mixed stream of metals and non-metallics and the intrinsic high value of the aluminum provides an incentive for the further development and implementation of separation technologies to improve yields and to upgrade the recovered material. Projections for the growth of aluminum used in automobiles and in the demand for secondary metal for automotive castings indicate that, on a weight basis, castings can continue to absorb aluminum automotive scrap well into the next decade [2]. However, as the market develops for closure sheet and aluminum body structures, it will be increasingly desirable to have these alloys segregated and recycled back into sheet products and, if possible, back into the same sheet applications from which they came. Moreover, the increasing fraction of wrought alloys in automotive scrap, coupled with increasingly tighter performance and hence metallurgical specifications for automotive castings, will put greater demands on the quality of the auto shred going back into foundry alloys. These issues are thus expected to provide increasing support for the demonstration and development of methods for ensuring that the future recycling of automotive aluminum follows a closed loop system.

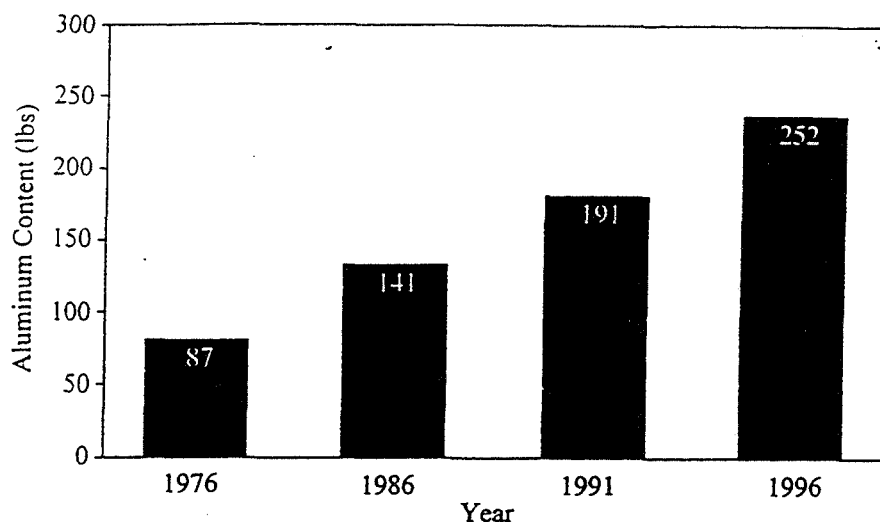


Figure 1. Average aluminum contained in passenger cars from 1976–1996 (approximate)

Existing Recycling Loop

As stated earlier, most of the aluminum in current automotive applications is in the form of foundry alloys for castings, used in powertrain components such as engine blocks, transmissions, cylinder heads and in wheels. Some wrought alloy is used in trim, in bumpers, in radiator and air conditioning components, and in closure panels, namely hoods and decklids. There are also a number of aluminum intensive vehicles in production at this time; examples include the Audi A8, the Jaguar XJ220, the Honda NSX, the Chrysler Prowler and the General Motors EV1. These vehicles can contain up to 900 lbs (400 kg) of aluminum. Of course, current production vehicles will not be retired for around ten years, and it is the vehicles manufactured in the mid 1980's that are currently being scrapped. Figure 1 shows the average aluminum content in passenger cars over the past 20 years. The mid-1980's car contains about 150 lbs (70 kg) of aluminum, of which an estimated 80% is in the form of castings, and the remaining 20% in wrought alloy products.

The current recycling process flow sheet for this scrap is given in Figure 2. About 94% of all end-of-life vehicles enter this recycling stream (the other 6% being lost to the system in the form of abandoned or discarded vehicles), and within this stream, about 90-95% of the available aluminum is captured for recycling. Therefore, the overall recovery rate for aluminum from vehicles is in the range 85 to 90%, a remarkably high number considering that it has developed entirely on the basis of free market economics. The key to aluminum's successful recycling record lies in its ease of recycling, durability and sustained value.

Recyclers benefit from the presence of aluminum at each step in the vehicle recycling process. First of all, during manufacturing of automotive components, scrap is generated in the form of machining chips and turnings, scrap castings, stamping skeletons etc., and these scraps are routinely fed back into the remelt loop. When the vehicles end their useful lives, they enter the recycling stream by way of the auto dismantlers. There are around 12000 of these in North America alone. The dismantlers remove useful components for resale purposes. At the same time, they will strip the vehicle of certain easily recognizable aluminum parts that are easy to remove but unsuitable for the resale market. Parts that are removed in this step include radiators, wheels and some powertrain components. These scrap items are generally segregated by the dismantlers according to type, because in this form they command a premium in the scrap market over mixed scrap. The stripped vehicles are commonly referred to as hulks at this stage, and they are sold on to the car shredders. There are around 200 of these in North America.

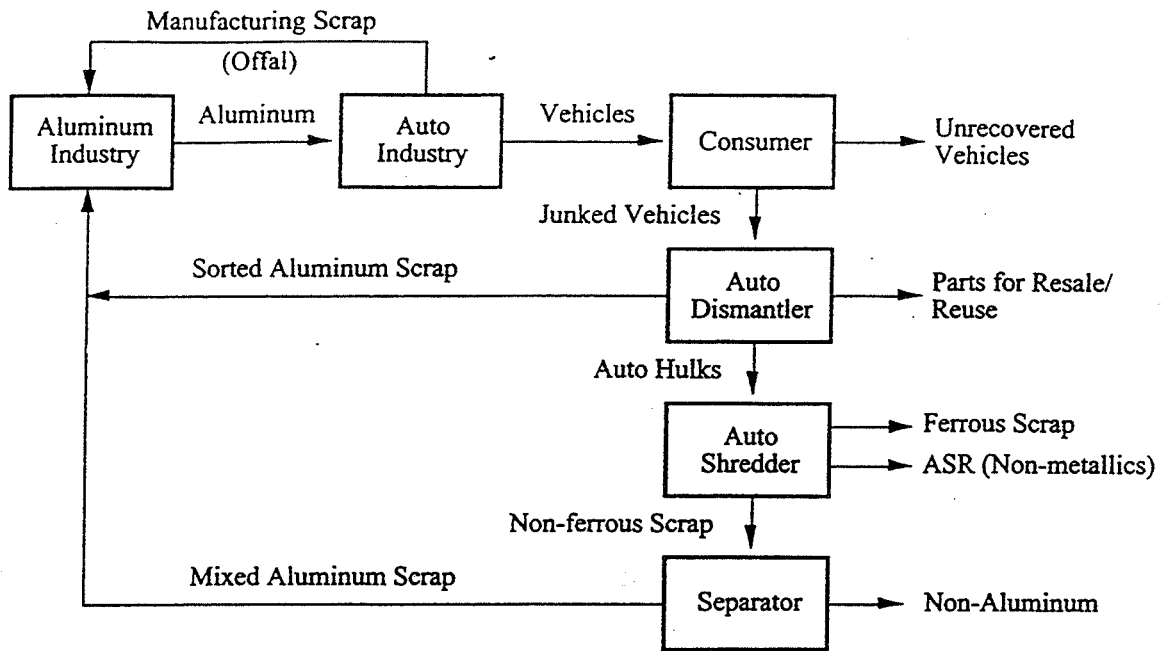


Figure 2. The current automotive aluminum recycling process

At the car shredders very high horsepower hammermills are used to reduce the hulks into fist sized scrap pieces. The raw product from this process is a mixture of iron and steel, plastics, glass, rubber, wood and various non-ferrous metals including magnesium, zinc and aluminum. The ferrous material is separated by magnets, for subsequent sale to the steel industry. A small amount of aluminum is lost to this ferrous fraction, in the form of scrap pieces which contain ferrous material joined to aluminum, for example screws, brackets, or hinges. Despite its loss to the aluminum recycling loop, this aluminum performs a valuable service as a deoxidant in the steel-making process. The non-metallic material, commonly referred to as automotive shredder residue, is a mixture of mainly polymers, wood, rubber and glass, which comprises around 25% of the vehicle's weight. Currently this material is either landfilled or incinerated, and it is the subject of significant research to identify other means of disposal or recycling. The remaining material is classified as the non-ferrous fraction. This is passed on to specialized separators, of which there are around 12 in North America. The non-ferrous processors separate the non-ferrous mixture into various densities, including fractions rich in aluminum, zinc, brass and copper. Further processing of the separated aluminum fraction can take place using eddy current separators to yield a premium grade product. This product consists of a clean, dry mixture of foundry and wrought alloys. It is sold to the secondary aluminum industry in bulk form for remelting into fresh secondary foundry alloy. In this manner the recycling loop is closed, because over 70% of the product of the secondary aluminum industry is foundry alloy for automotive castings. Overall, the aluminum present in current scrapped vehicles represents only a small percentage of the total vehicle weight, around 5% to 10%, yet it accounts for between 35% and 50% of the scrap value.

Growth in Aluminum Usage in Vehicles

As Aluminum Intensive Vehicles achieve a significant percentage of the total vehicle market, the recycling infrastructure will be presented with changes in the balance of materials arising from the recycling process. Not only will there be more wrought aluminum alloys, in the form of skin panels and structures, but there will be more primary alloy specification castings in the form of suspension components. Table 1 lists the major aluminum components that can be used in current (1996) vehicles,

as well as major aluminum components that could be specified for aluminum intensive vehicles. This is by no means an exhaustive list, as it omits those components with a cumulative weight of less than 4 pounds, so parts such as oil pump housings, seat pans, airbag components and the like are not listed. Even so, the list is impressive, and illustrates the diversity of potential application for aluminum in the automobile. Aside from potential decline in aluminum usage in certain components, such as intake manifolds (to plastic) and transfer cases (to magnesium), there is huge potential for growth in usage in many current applications such as engine blocks, suspension, wheels and brake components, and enormous opportunity for growth in new high volume structure and body applications.

In turn this mixture of new components offers opportunities and challenges for the automotive recyclers. The wrought alloys and the primary foundry alloys have premium metallurgical and economic value. Therefore there will be strong incentives for these alloys to be segregated during the recycling process.

Component	Number in Vehicle	Average Weight of 1996 Vehicle Component (lb)	% in 1996 Cars	Average Weight in lb (AIV Potential)	% Potential in AIV
Cylinder head	1	16	61	14	100
Intake manifold	1	17	83	0	0
Engine block	1	47	26	40	100
Engine pistons	6	1.2	100	1.2	100
Supercharger housing	1	16.2	0.15	16.2	100
Drivetrain cover	1	8.4	2	8	100
Transmission transfer case	1	36	99	30	20
Drive sprocket support	1	4.2	20	4	100
Trans. struc. side cover	1	9.3	20	9.3	100
Bumper, front	1	17	9	17	100
Bumper, rear	1	16	4.3	18	100
Deck lid	1	15.4	5.5	15.4	100
Hood	1	19.3	5.5	19.3	100
Body shell	1			320	100
Doors	4			16.4	100
Fender quarter panel	2			7.5	100
Roof	1			5	100
Front brake rotor	2	6.5	4	6.5	100
Rear brake rotor	2	4	4	4	100
Brake calipers	2	7	0.8	7	100
Cross member subframe	2	12.6	6.7	12.6	100
Differential carrier	1	9.5	20	9.5	100
Front knuckle	2	6.4	4.5	6.4	100
Rear knuckle	2	6.5	5.5	6.5	100
Condenser	1	14.3	98	7	100
Evaporator	1	4.2	98	4	100
Radiator	1	4.5	98	4	100
HVAC tubing/hardware	1	14.5	98	12	100
Wheels	4	18	45.8	13	100
Seat frames	1	20	3	20	100

Table 1. Major aluminum components of 1996 and potential aluminum intensive vehicles
Source: *The Aluminum Association*

All these new applications use aluminum to satisfy a number of performance criteria. Aluminum has more commercial product forms and alloys than any other structural material. The three broad classes of aluminum products are ingot, wrought products and castings. Ingot is cast from holding furnaces, in which alloying is carried out, and is the starting material for both cast and wrought products. Casting is employed to produce net shape products in which the mechanical properties are determined by the alloying elements and thermal treatments after casting. Wrought products are defined by the fact that they are given some mechanical deformation during production and achieve properties by some combination of that deformation, the alloy and thermal treatments, depending on the product. Wrought products are in turn grouped into flat rolled products (plate, sheet and foil), extrusions, forgings and wire, rod and bar. In common with castings, extrusions and forgings offer some net shape capability so that vehicle structure and components can be designed with fewer total parts and reduced tooling cost. In addition, these versatile product forms support new and innovative structures, such as the space frame construction exemplified by the Audi A8 and the weldbonded structure exemplified by the GM EV1. This variety of available forms has proved to be significant to the growth of aluminum usage and is expected to continue. Indeed, for the period 1990 to 2010 the growth of cast products has been forecast at 131 percent, while that of wrought products is put at 250 percent [4].

Sheet Alloys	Si	Fe	Cu	Mn	Mg	Cr	Zn	Ti
2011	0.40	0.7	5.0-6.0	—	—	—	0.30	—
2017	0.20-0.8	0.7	3.5-4.5	0.40-1.0	0.40-0.8	0.10	0.25	0.15
2117	0.8	0.7	2.2-3.0	0.20	0.20-0.50	0.10	0.25	—
3003	0.6	0.7	0.05-0.20	1.0-1.5	—	—	0.10	—
5052	0.25	0.40	0.10	0.10	2.2-2.8	0.15-0.35	0.10	—
5182	0.20	0.35	0.15	0.20-0.50	4.0-5.0	0.10	0.25	0.10
5454	0.25	0.40	0.10	0.50-1.0	2.4-3.0	0.05-0.20	0.25	0.20
5754	0.40	0.40	0.10	0.50*	2.6-3.6	0.30	0.20	0.15
6022	0.08-1.5	0.05-0.20	0.01-0.11	0.02-0.10	0.45-0.7	0.10	0.25	0.15
6061	0.40-0.8	0.7	0.15-0.40	0.15	0.8-1.2	0.04-0.35	0.25	—
6111	0.6-1.1	0.40	0.50-0.9	0.10-0.45	0.50-1.0	0.10	0.15	0.10
7072	†	—	0.10	0.10	0.10	—	0.8-1.3	—
7129	0.15	0.30	0.50-0.9	0.10	1.3-2.0	0.10	4.2-5.2	0.05

Casting Alloys

319	5.5-6.5	1	3.0-4.0	0.5	0.1	—	1	0.25
A356.0 (primary)	6.5-7.5	0.2	0.2	0.1	0.25-0.45	—	0.1	0.2
A356.0 (secondary)	6.5-7.5	0.6	0.25	0.35	0.2-0.45	—	0.35	0.2
A380	7.5-9.5	1.3	3.0-4.0	0.5	0.1	—	3.0	—

Extrusion Alloys

6063	0.20-0.60	0.35	0.1	0.1	0.45-0.90	0.1	0.1	0.1
7005	0.35	0.4	0.1	0.20-0.7	1.0-1.8	0.06-0.20	4.0-5.0	0.01-0.06

*Mn + Cr = 0.10-0.60 † Si + Fe = 0.7

Table 2. Chemical composition ranges for selected aluminum automotive alloys

The growth trend is further supported by technological development. In the forging and casting arenas, for instance, significant technology advances are occurring as, for instance, semi-solid forming in which the processing technique offers to net shape parts the internal structure and properties of a forging but uses a casting alloy. The implication of these trends is that there is not likely to be much diminution in the number of alloys in use and that the mix in alloys will continue to change. It isn't possible at this point to predict just how the product mix will change over time, but at least the recycling industry has the benefit of knowing in advance what they are facing. This new mixture of products offers challenges and opportunities to automotive recyclers. Table 2 gives the chemical composition of

selected alloys in current use. Ranges for the principal alloying elements are highlighted in **bold type**. Assuming that alloys cannot be kept completely segregated during product use, or during the recycling process, the mixtures that result will have a value and application that is entirely dependent upon the chemical composition of the mixtures. Different degrees of absorption are permitted between alloys depending upon their composition limits. Within the sheet and extrusion alloy families, for example, 6063 alloy is fully compatible as a metal source for 6111, because the alloying limits for all major elements in 6111 exceed those for 6063. For the same reason 6111 is unsuitable as a metal source for 6063, except in low concentrations blended with other alloys. In general, each alloy family will have limited chemical compatibility with other alloy families because there will be a conflict between the two or more major alloying ingredients, for example copper in the case of the 2xxx series, and zinc in the case of the 7xxx series. Within each alloy family there is a much better opportunity for absorption.

Mixtures that exceed the composition limits of any of the wrought alloy specifications are currently used in secondary casting alloys, typically A380 or A319. These alloys have higher than average tolerance for many alloying elements, with the exception of magnesium, which can, however, be removed in the melting furnace. Note that the casting alloys are not compatible with wrought alloy specifications because of their high silicon limits, silicon being added to foundry alloys to impart melt fluidity during the casting operation. Because of the wide chemical specifications of the casting alloys, and some of the non-automotive sheet alloys, all aluminum alloy mixtures arising from the post consumer stream are recycled. As a result aluminum is completely recyclable.

The design engineer working with aluminum may be able to maximize the metallurgical scrap value of a dismantled product by paying close attention to these compatibility issues. The aluminum industry recommends an integrated approach to design for recycling efficiency:

1. Avoid joining dissimilar materials where possible. Where aluminum alloys are joined with permanent joints, try to keep to one alloy family. If this cannot be done, try to use a joint that can be disassembled.
2. Design for ease of component removal from the vehicle.
3. Where possible specify recycling tolerant alloys or alloy combinations.
4. Avoid combining aluminum with substances of concern, for example heavy metals, or compounds that decompose to give rise to toxic or difficult-to-control emissions.

These design principles are only a partial answer to the overall process of recovering aluminum and returning it to producers for use in new product. Technology and economics will shape the recycling processes of tomorrow.

Future Automotive Aluminum Recycling Loop

We foresee a future recycling loop for aluminum that is an extension of the existing infrastructure (Figure 3). In order to ensure a closed loop, the wrought alloys must be substantially returned to wrought alloy applications, and the cast alloys to fresh castings. This will maximize the value of the recycled metal and make full use of the alloying ingredients in each of the scrap alloys. A closed loop also allows products to carry a significant recycled content, a desirable feature for economic and material conservation reasons. The increased use of aluminum presents a further business opportunity for the automotive dismantlers, with the use of many new components that may be easily accessible for dismantling. Examples of these components include doors, hoods, decklids fenders, and suspension components. Dismantling of these parts brings a significant benefit to the aluminum industry because the aluminum recycled by dismantling has the capability of being highly segregated by component type, and provided that the components are all of similar alloy families, the result will be a premium quality recycled metal source for making the same products over again. The second opportunity lies in upgrading the mixed scrap arising from the car shredder/non ferrous processors. This mixed scrap will

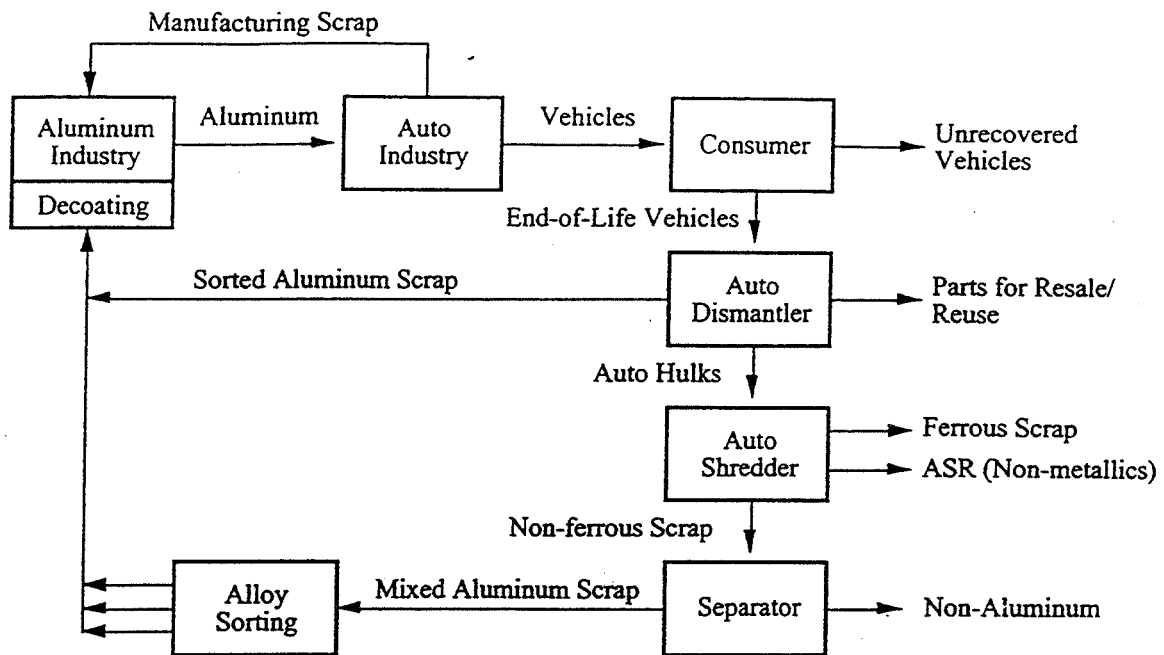


Figure 3. The future recycling loop for automotive aluminum.

represent the hard-to-dismantle components in the scrapped vehicle, and will likely be enriched by the presence of wrought alloys in the form of sheet and/or extrusions used in the vehicle structure.

New Processes and Technology

Several new approaches are being considered for assisting the recovery and recycling processes. They address the two points at which aluminum scrap will be generated in the future recycling loop, namely at the dismantlers and after the shredder/non-ferrous processors.

For the dismantling step, consideration is being given to the establishment of data showing the location and weight of aluminum used in vehicles. This type of information is already being used in databases in Europe to assist the dismantlers in removing polymeric parts for recycling. A database for aluminum would ideally list the alloys used, together with a target dismantling time which reflects the value of the recovered metal. The key here is to ensure that the maximum possible amount of aluminum is recovered by dismantling, subject, of course, to economic constraints. There will be a cutoff point where components are too small or too difficult to reach or disassemble and these will be left on the vehicle hulk for shredding. Of particular significance to the vehicle dismantler is the potential number of components over 4 lbs in weight (Table 1) that may be readily accessible for dismantling.

For the post-shredder scrap stream, new technologies offer the promise of being able to take a mixed alloy scrap stream and segregate it into its constituent alloys in a rapid, real-time process. A number of approaches have been proposed for the automatic sorting of aluminum alloys. A hot crush and screening method has been described for separating cast from wrought fractions in auto shred [5]. The method depends on the difference in embrittling temperature for different alloys and is generally restricted to the separation of two alloys or two classes of alloys. It should be noted that while such separation may facilitate the recycling of the cast fraction of auto shred back into foundry alloys, the wrought fraction thereby recovered would not be directly useable back into wrought materials. Eddy current techniques have been applied to the sorting of different metals in the non-ferrous fraction of auto shred [6]; the method is applicable in principle to the sorting of alloys but is limited by the magnitude of the conductivity differences between alloys and also requires the close sizing of the pieces to be separated.

Both of these technologies are technically viable and may find their economic niche in aluminum scrap recycling, possibly in isolation or in combination with other techniques such as shape and color recognition methods in order to achieve alloy separation.

Demands on the required degrees of separation for wrought alloy scraps are severe if these are to be effectively recycled back into wrought products. The greatest flexibility in dealing with the range of alloys likely to be encountered would be provided by a method that allows direct composition analysis of individual scrap pieces. The method of choice for composition analysis of aluminum alloys is optical emission spectroscopy (OES) which is used routinely in casting centers and foundries [7, 8]. However, in the conventional DC arc excitation mode of this technique, the need to contact differently shaped pieces moving at the required high speed would make application to scrap sorting very difficult. The use of a pulsed laser as the excitation source does, however, offer the potential for high rate, piece-by-piece analysis.

The feasibility of applying laser-induced OES to the sorting of elemental metals has been demonstrated [9]. Application of this technique to the sorting of different metals in the non-ferrous fraction of autoshred, as an alternative to conventional sink-float processing, has been tested at a pilot scale [10-12]. Several publications have addressed the feasibility of laser-induced OES composition analysis of shredded aluminum alloy scrap pieces [13,14] and a system for piece-by-piece, high speed sorting of aluminum alloys has been described [13] as well as a scrap sorting system configured around the technique.

Figure 4 is a schematic diagram of one concept of such a system after reference 13. Mixed shredded scrap, which has been mechanically cleaned or thermally decoated, is channeled into a stream of particles in single file. The stream passes under a sensor which triggers the laser firing system. Laser shots are used to evaporate a sample of the scrap surface, and the optical emission generated is detected by a spectrometer. The spectrometer is calibrated with reference to known alloy standards, and from this the scrap alloy is identified. A mechanical device is used to divert scrap pieces into collection bins

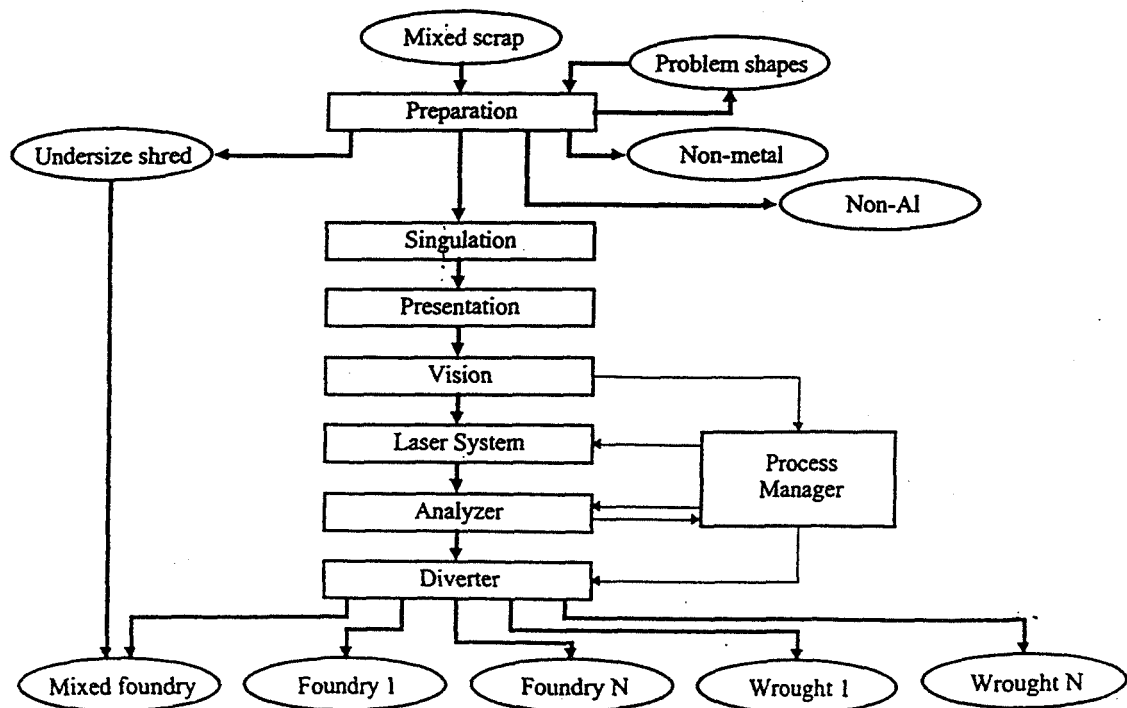


Figure 4. Schematic representation of an automated system for sorting aluminum alloy scrap

according to their alloy chemistry. While technologies like this are in the feasibility demonstration phase, they are, nevertheless, clearly the way ahead for achieving economically viable routes for segregating alloys from mixed scrap and as such are a key part of the future recycling infrastructure.

Legislation

It is important to understand that both the existing and proposed recycling routes for automotive aluminum are justifiable on the basis of economic benefits, and do not require recycling legislation to be successful. Legislation will impact aluminum recovery indirectly through restrictions on the disposal of other streams from the vehicle recycling process, for example auto shredder residue (ASR). In the Netherlands ASR is being banned from landfills, with the result that it must instead be disposed of for a fee in industrial incinerators. The net result is an increase in the cost to the recyclers of processing scrapped vehicles. Interestingly, as the cost of disposal of ASR increases, at the same time we see an increase in the amount of aluminum recovered, which means increased revenue for the scrap processors.

Recycled content legislation is another subject of discussion, and here there are some important statements to make on behalf of aluminum. While closed loop processes will ultimately allow a maximum amount of post-consumer recycled metal to be used in products, during the growth phase for new applications such as wrought alloy body and structure, the recycled content temporarily falls. This is because primary metal must be used the first time around in order to prime the market. However, this primary metal will eventually be fully recycled, preserving aluminum's excellent recycling record.

Conclusions

The existing recycling route for automotive aluminum is a highly successful example of a closed loop system. In the future, aluminum usage will grow and there will be changes in alloy mix, in the product forms used, and in the balance between cast and wrought alloys. These factors will present a challenge to maintain and enhance the closed loop process. Design considerations can play an important role in helping to achieve this, together with the establishment of new or enhanced dismantling practices and the selective application of new technology. Together, these activities offer promise of a future recycling loop that provides sustained value for automobile manufacturers, consumers and the recycling industry, as well as providing the means for the automakers to take full advantage of the lightweighting benefits and the design versatility of using aluminum.

References

1. Study to Determine Aluminum Content in North American Vehicles in 1996, The Aluminum Association, (1996).
2. L.E. Dastolfo and P.R. Bruggink "Preserving the Value Chain In Automotive Aluminum Recycling". Light Metals 1994. (TMS 1996). 1121-1127.
3. Automotive Aluminum Design Guidelines, The Aluminum Association, (1996).
4. M.B. Tessieri, "Overview of Automotive Aluminum Scrap Recycling in North America". 2nd International Aluminum Conference and Trade Exposition. (The Aluminum Association, Inc., 1997).
5. R.D. Brown Jr., F. Ambrose and D. Montagna, "Separation of Cast and Wrought Aluminum Alloys by Thermomechanical Processing", (Report RI-8960, U.S. Bureau of Mines, 1985).
6. R.R. Osterberg and R.B. Wolanski, "Method and Apparatus for Sorting Non-Ferrous Metal Pieces", U.S. Patent 4,834,870 (1989).
7. F. Kimmerle, P. Begin, J.-L. Fortier and G. Peloquin, "Quality Control of Aluminum Alloys: OES Hardware/Software Developments", Light Metals 1991. (The Minerals, Metals & Materials Society, 1990), 1077-1082.

8. B.P. Cochran, "Influence of Sampling Techniques on the Analysis of Aluminum Die Casting Alloys", 17th International Die Casting Congress and Exposition (North American Die Casting Association, 1993), 39-48.
9. D.A. Cremers, "The Analysis of Metals at a Distance Using Laser-Induced Breakdown Spectroscopy", Appl. Spectroscopy, 41 (1987), 572-579.
10. H.-P. Sattler, "Automatic Sorting of Non-Ferrous Metals from Automobile Shredders", Second International Symposium on Recycling of Metals and Engineered Materials (The Minerals, Metals & Materials Society, 1990), 333-341.
11. M. Potzschke, H.-P. Sattler, K. Hohla and T.R. Loree, "Scrap Detector", U.S. Patent 5,042,947, (1991).
12. H.-P. Sattler and T. Yoshida, "New Sorting System for Recycling of Magnesium and its Alloys After Use", First International Conference on Processing Materials for Properties (The Minerals, Metals and Materials Society, 1993), 861-864.
13. A. Rosenfeld, A. Gesing and B. Farahbakhsh, "Sorting of Aluminum Alloy Scrap by Laser Induced Optical Emission Spectroscopy", Third International Symposium on Recycling of Metals and Engineered Materials, 1995 (The Minerals, Metals & Materials Society, 1995), 751-763.
14. H.-P. Sattler, "The Laser Scrap Sorting Technique, New Developments and First Operational Experience", Proc. 3rd Int. Symp. on Recycling of Metals, ed. P.B. Queneau and R.D. Peterson (The Minerals, Metals & Materials Society, 1995), 57-64.

THERMOSET COMPOSITES (SMC & RRIM) FOR AUTOMOTIVE COMPONENTS

Ken C. Rusch

The Budd Company
Plastics Division
1850 Research Drive
Troy, Michigan 48083-2167

Telephone: 248-619-2235
e-mail rushkr@troyrd.buddcompany.com

Bruce Budde

LARSS Student
New Mexico State University

and

Carolyn Hamilton

LARSS student
University of New Mexico



Ken Rusch

Thermoset Composites (SMC & RRIM) For Automotive Components

**Ken Rusch
Technical Programs Manager
The Budd Company Plastics Division
Representing The Automotive Composites Alliance
November 1– 3, 1999**

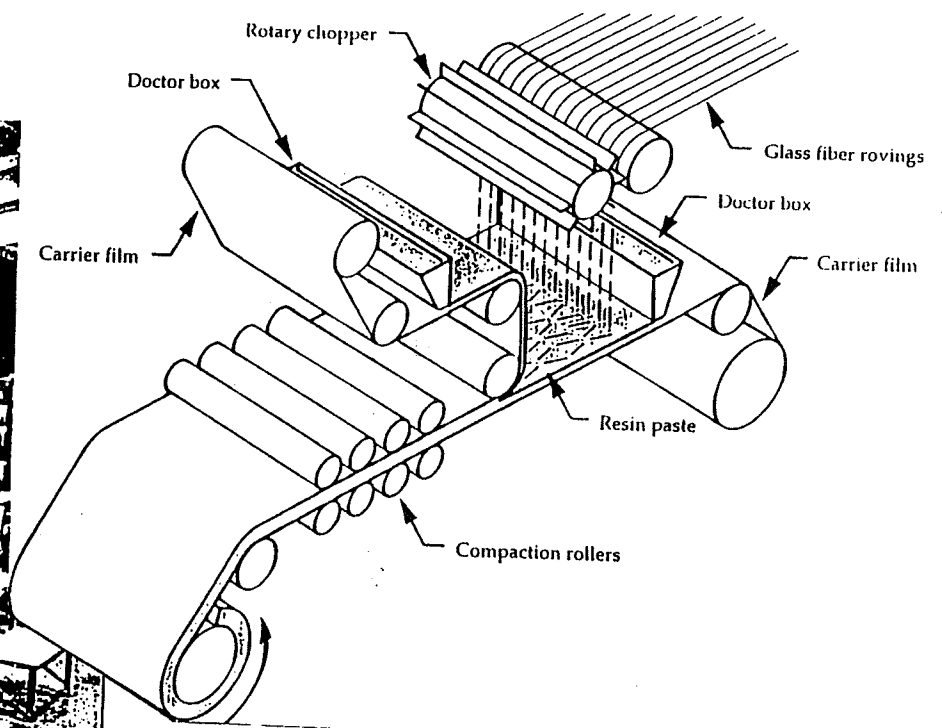
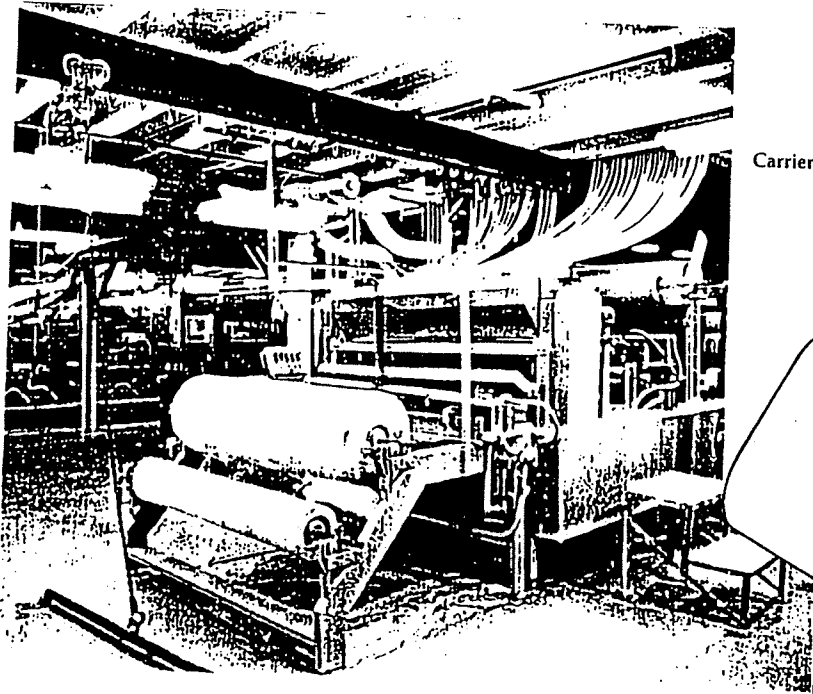
OUTLINE

- 1. What is Sheet Molding Composite (SMC)?**
- 2. Composition, Manufacture and Molding of SMC**
- 3. What is Reinforced Reaction Injection Molding (RRIM)?**
- 4. Composition and Molding of RRIM**
- 5. Annual Production of Composites for Automotive Components**
 - **SMC, BMC, LCM, RTM, RRIM & SRIM**
- 6. Why Use SMC/RRIM Composites for Automotive Components?**
- 7. Typical Automotive Components in Production Today**
 - **Grille Opening Panel/Reinforcement (GOP/GOR)**
 - **Hood**
 - **Fenders**
 - **Side Doors**
 - **Decklid**
 - **Van Cowl Panel**
 - **Radiator Support**
 - **Valve Covers/Engine Components**
- 8. Recycling and Recycled Content in Composites**
- 9. Next Generation of Composite Materials for Automotive**
 - **Low Density SMC**
 - **Carbon Fiber Reinforcement**
 - **Improved Surface Quality**
 - **Improved Structural Properties and Toughness**

TYPICAL SMC FORMULATION

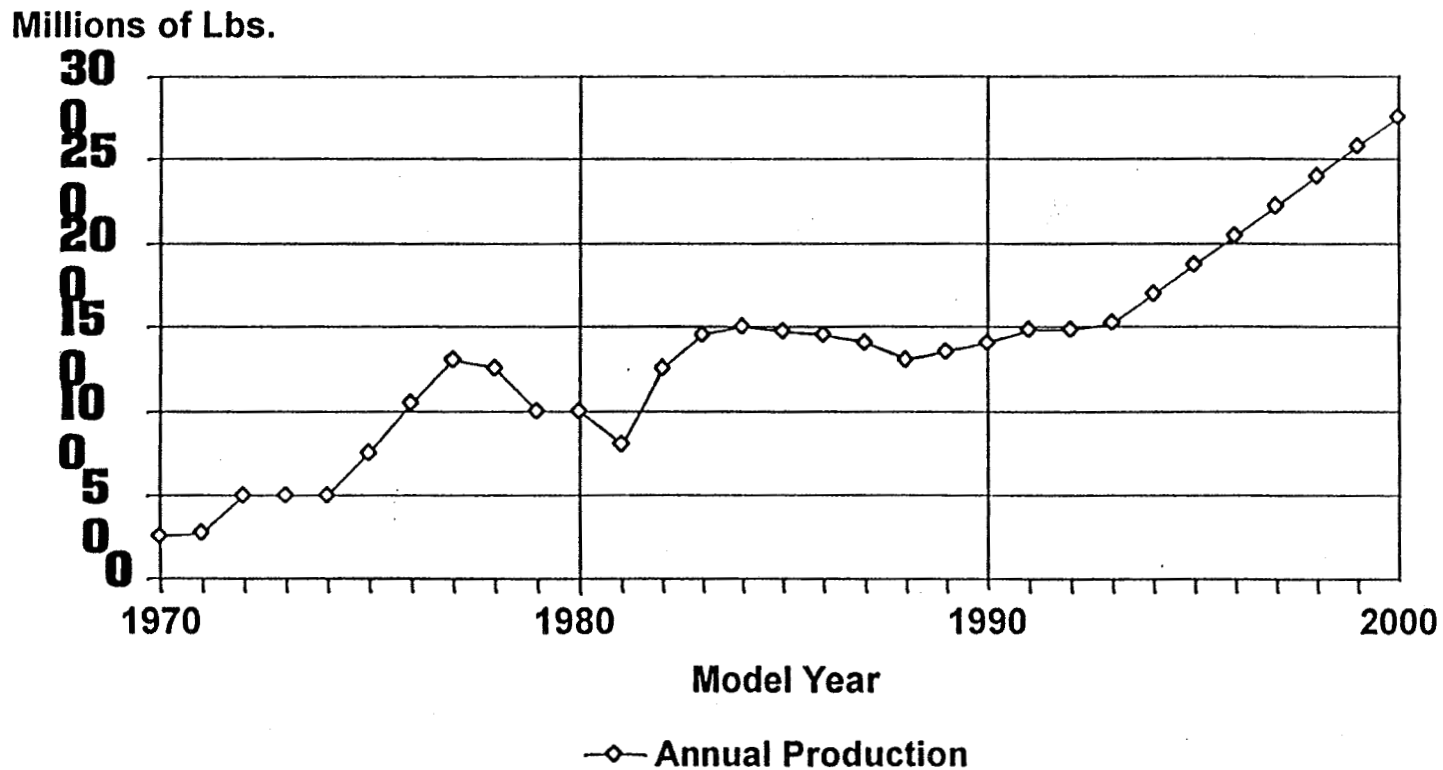
Material	Percent	Purpose
Calcium Carbonate	48%	Filler
Fiberglass (1 in. Lengths)	28%	Strength & Physical Properties
Polyester Resin	13%	Plastic Binder
Low Profile Additive	9%	Shrinkage Compensation & Class "A" Surface
Additives	2%	Catalyst, Mold Release, Pigment, Thickening Agent

SMC MACHINE PROCESS

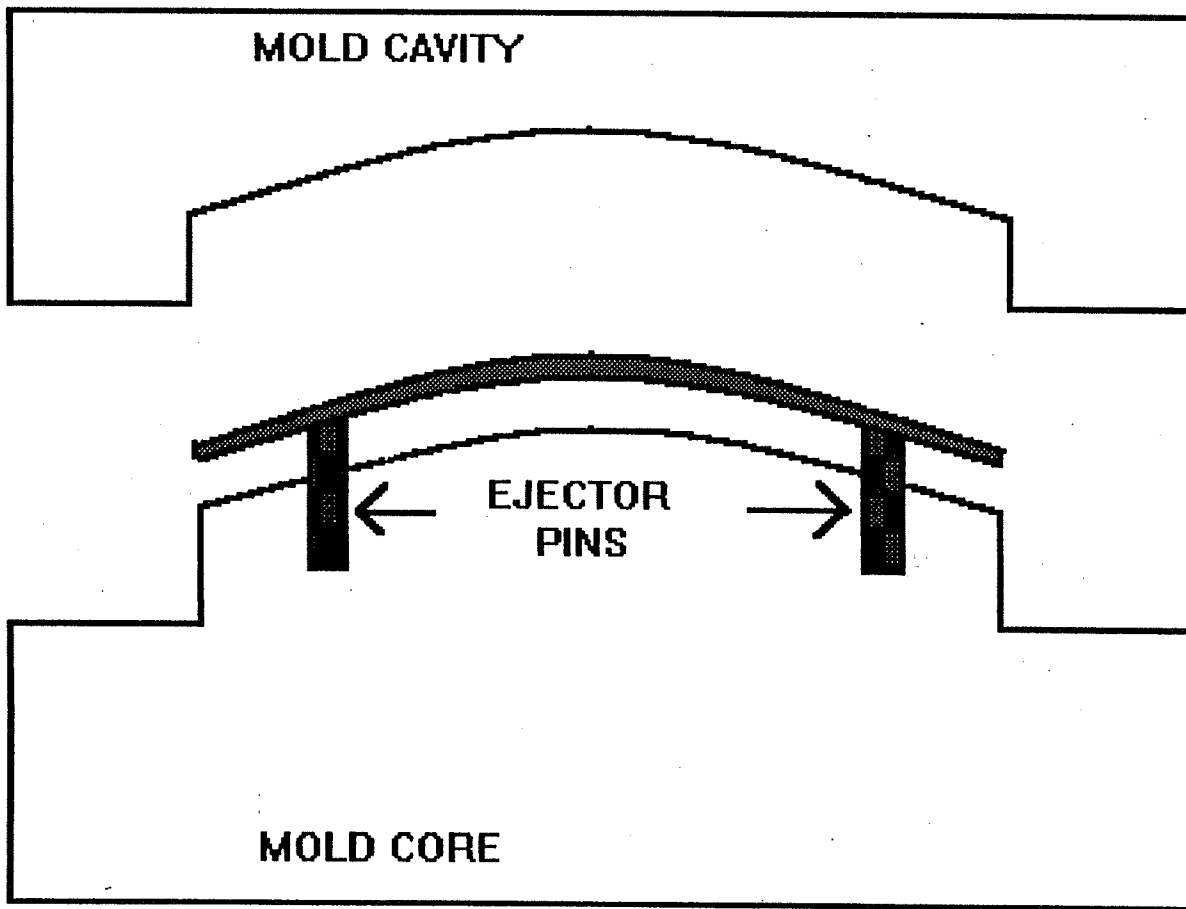


ANNUAL PRODUCTION OF SMC FOR AUTOMOTIVE

- Currently 300 Automotive Components On 110 Different Vehicle Models



MOLD CAVITY



DIE
DRAW

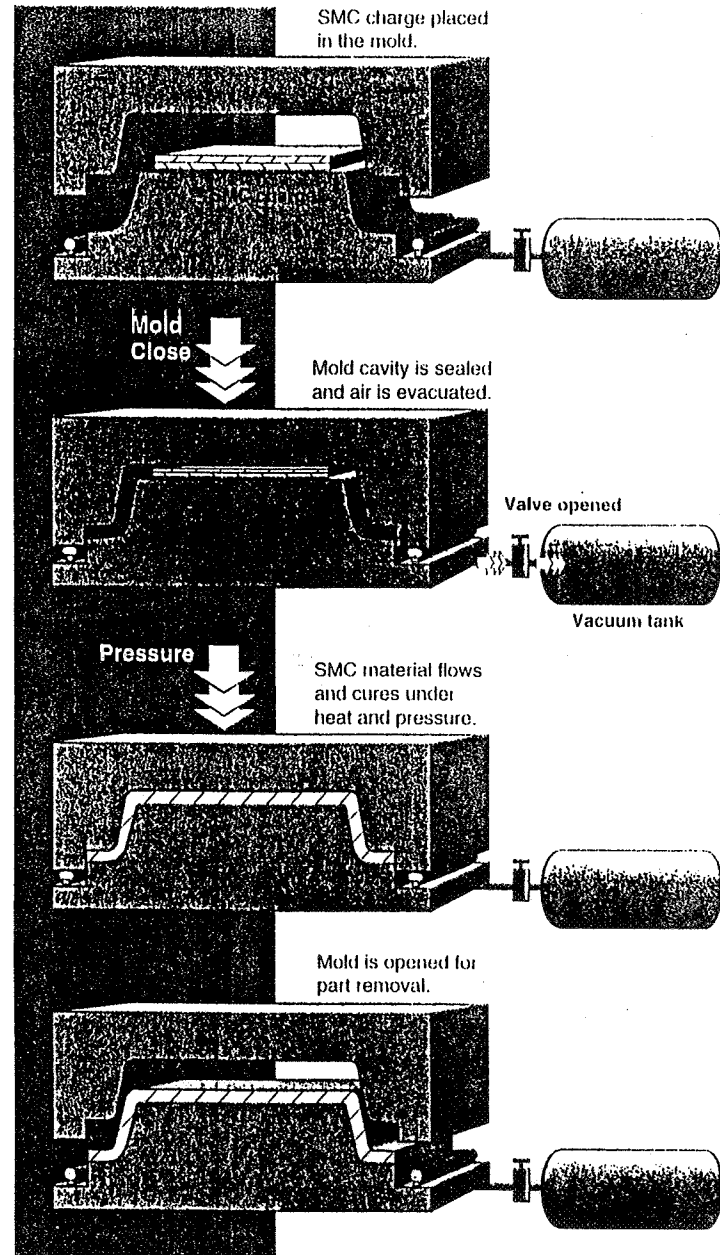
EJECTOR
PINS

MOLD CORE

MOLD OPEN

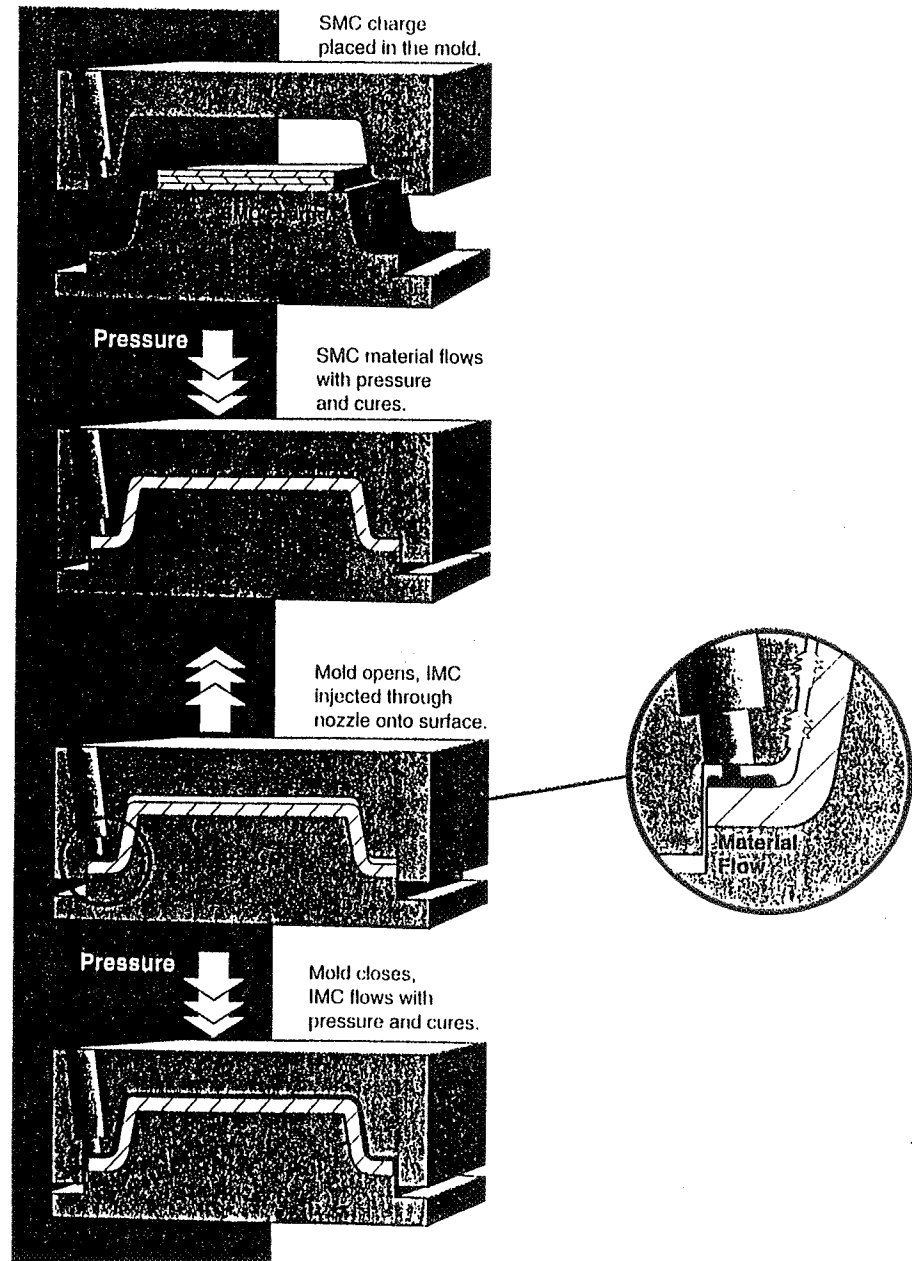
Vacuum Molding

- Seals the mold and pulls a vacuum.
- Minimizes porosity and voids caused by trapped air.



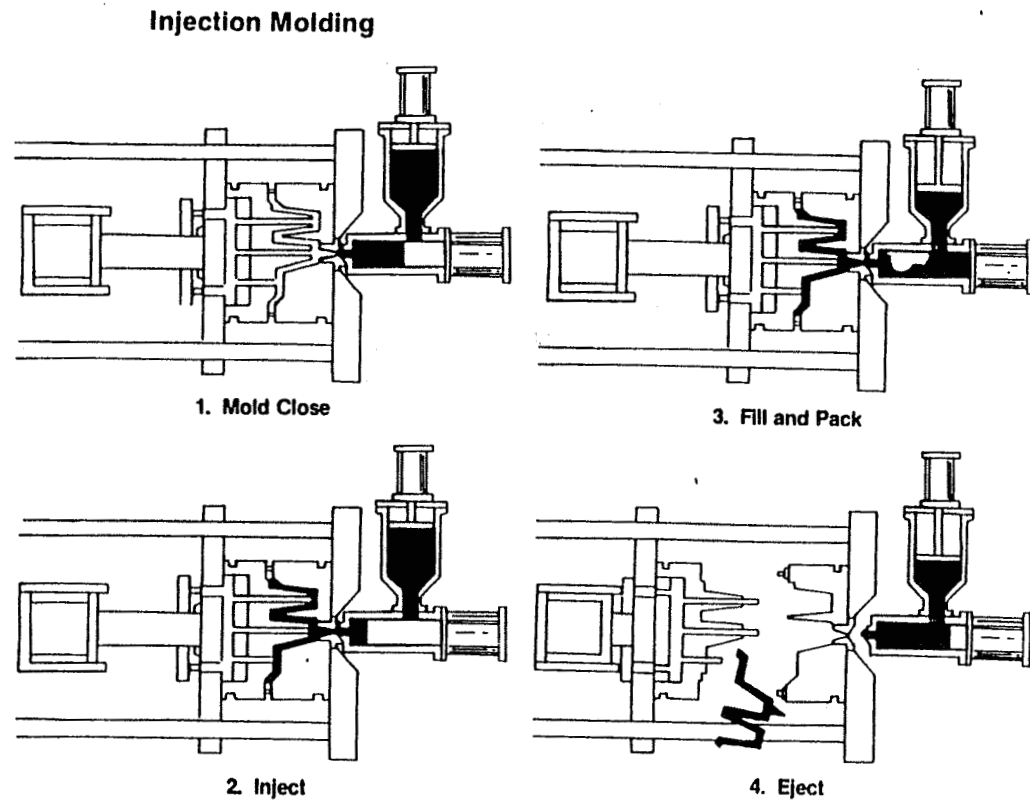
In Mold Coating (IMC)

- Coating applied to part in mold.
- Fills surface pits, porosity and small voids.
- Can replace a priming step.

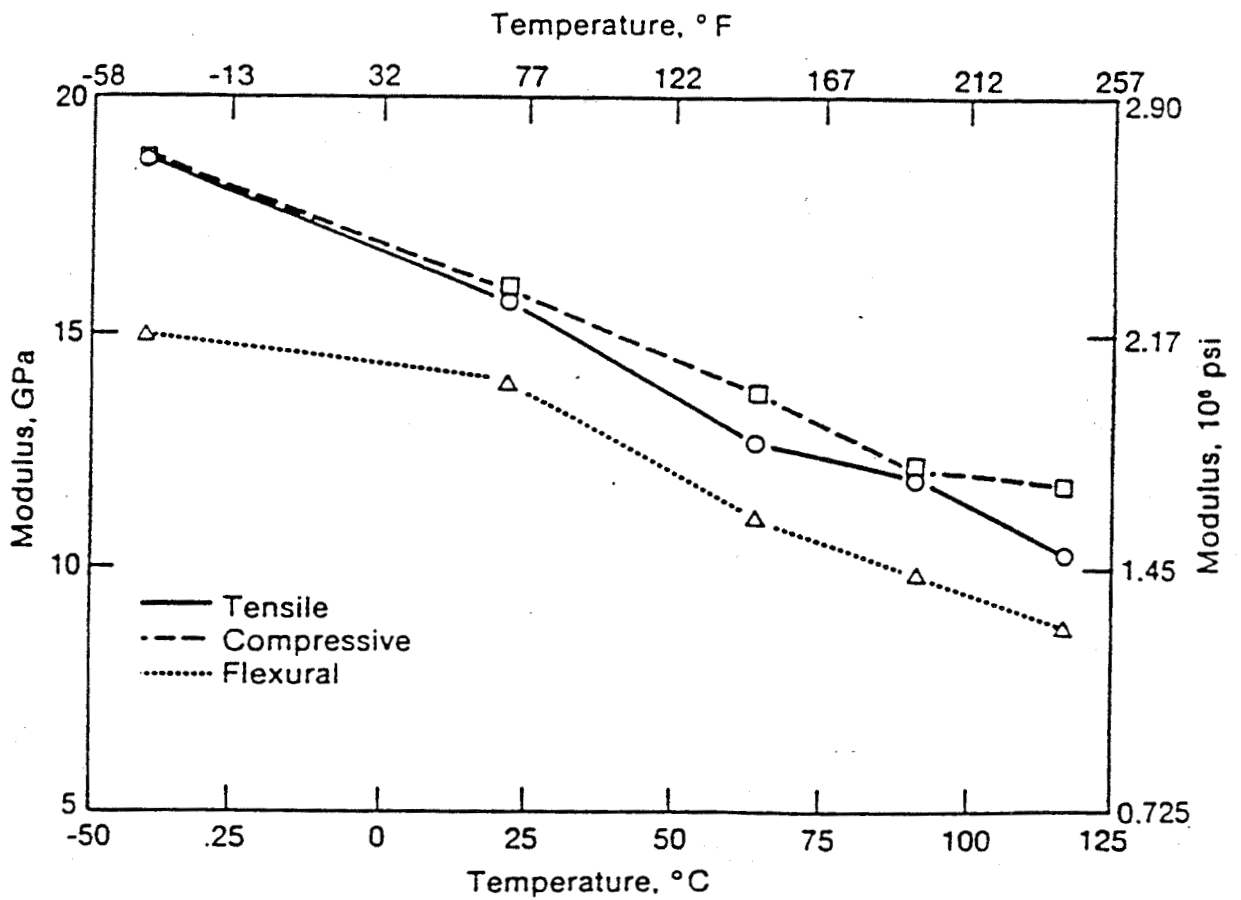


Injection Molding

- Advantages
 - Fast cycle time.
 - Precise part thickness.
 - Flashless parts.
 - Less operator variability
- Disadvantages
 - Lower mechanical properties

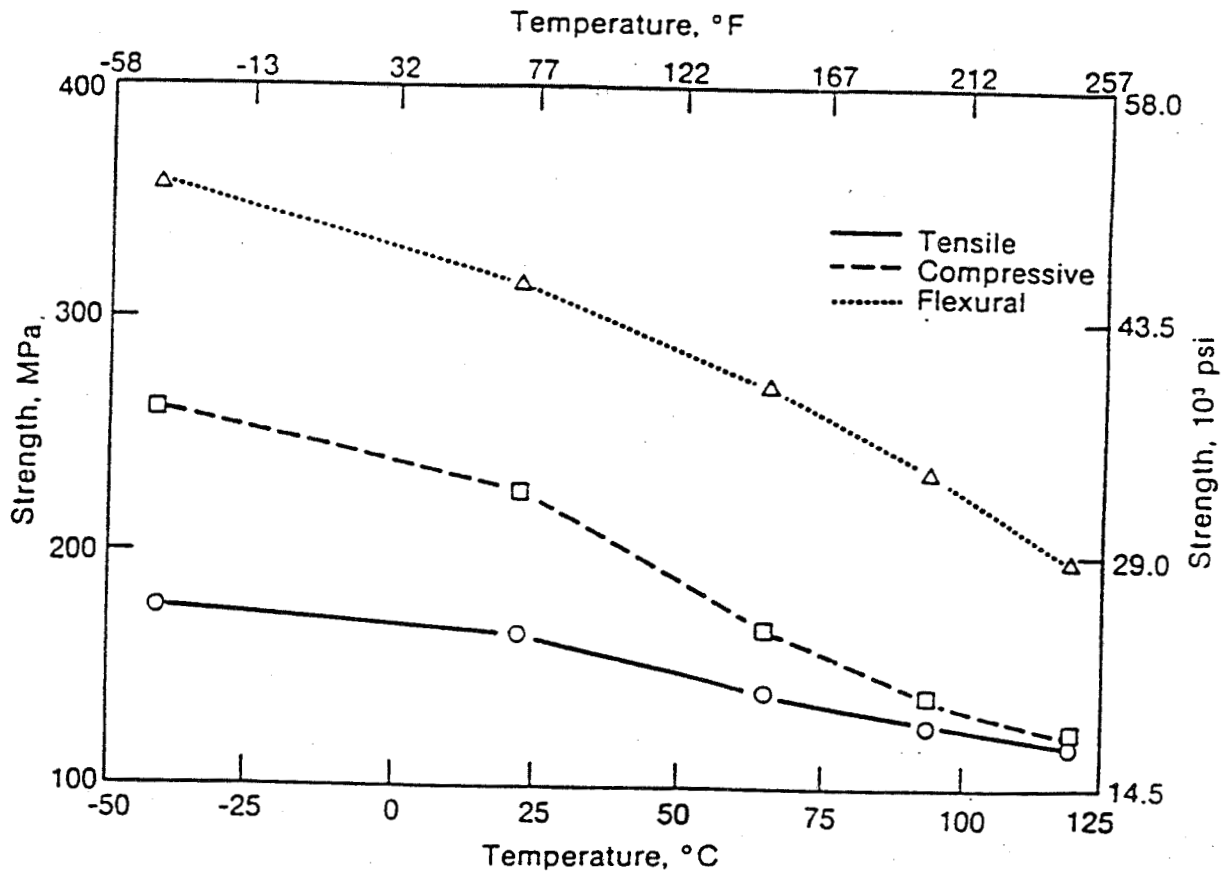


TYPICAL SMC R50 POLYESTER COMPOSITE



Tensile, compressive and flexural moduli vs temperature

TYPICAL SMC R50 POLYESTER COMPOSITE



Tensile, compressive and flexural strengths vs temperature.

Why Use SMC?

- Lower Program Cost
- Weight Reduction (vs. Steel)
- Design Features (Flexibility)
- Parts Consolidation (Complexity Reduction)
- Heat Resistance (Automotive Paint Ovens)
- Dimensional Stability/Integrity
- Linear Thermal Expansion Similar to Steel
- Corrosion Resistance
- Dent Resistance (vs. Sheet Metal)
- Structural Strength
- Recyclability



Ranger Light Truck Grille Opening Panel

•
Parts Consolidation

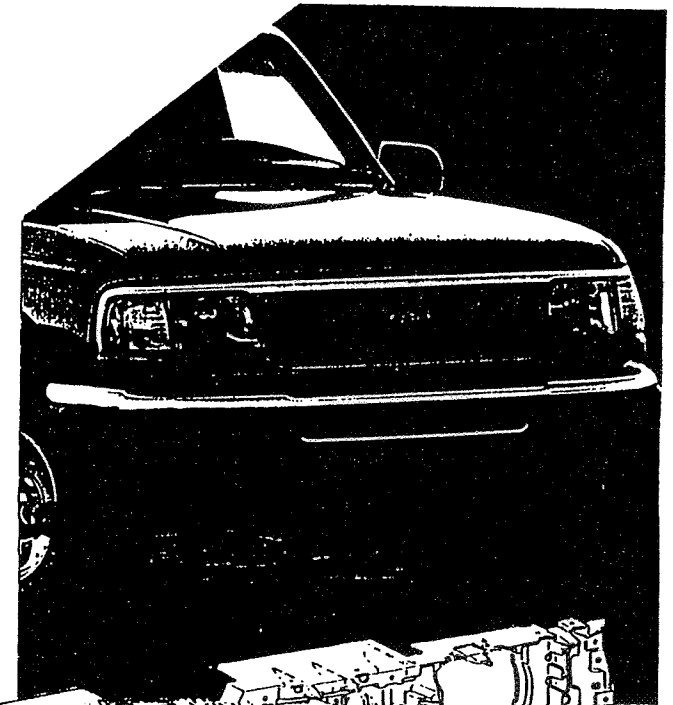
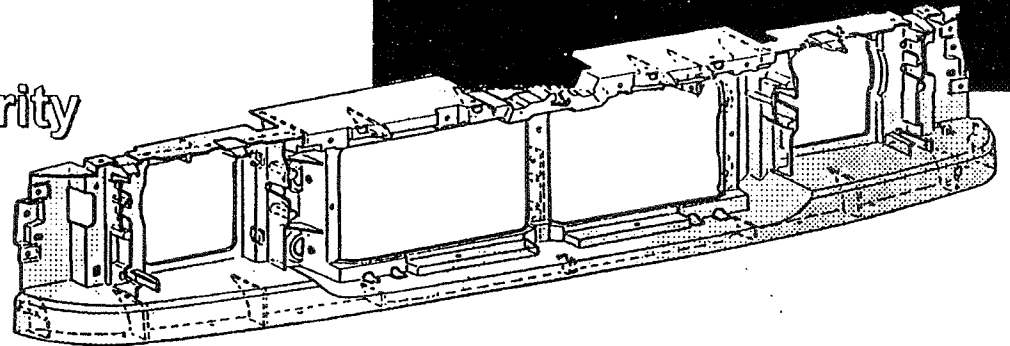
•
Front End Fit and Finish Control

•
Body Shop Assembly

•
E-Coat Compatibility

•
Front End Structural Integrity

•
Potential Cost Save





Mustang Hood

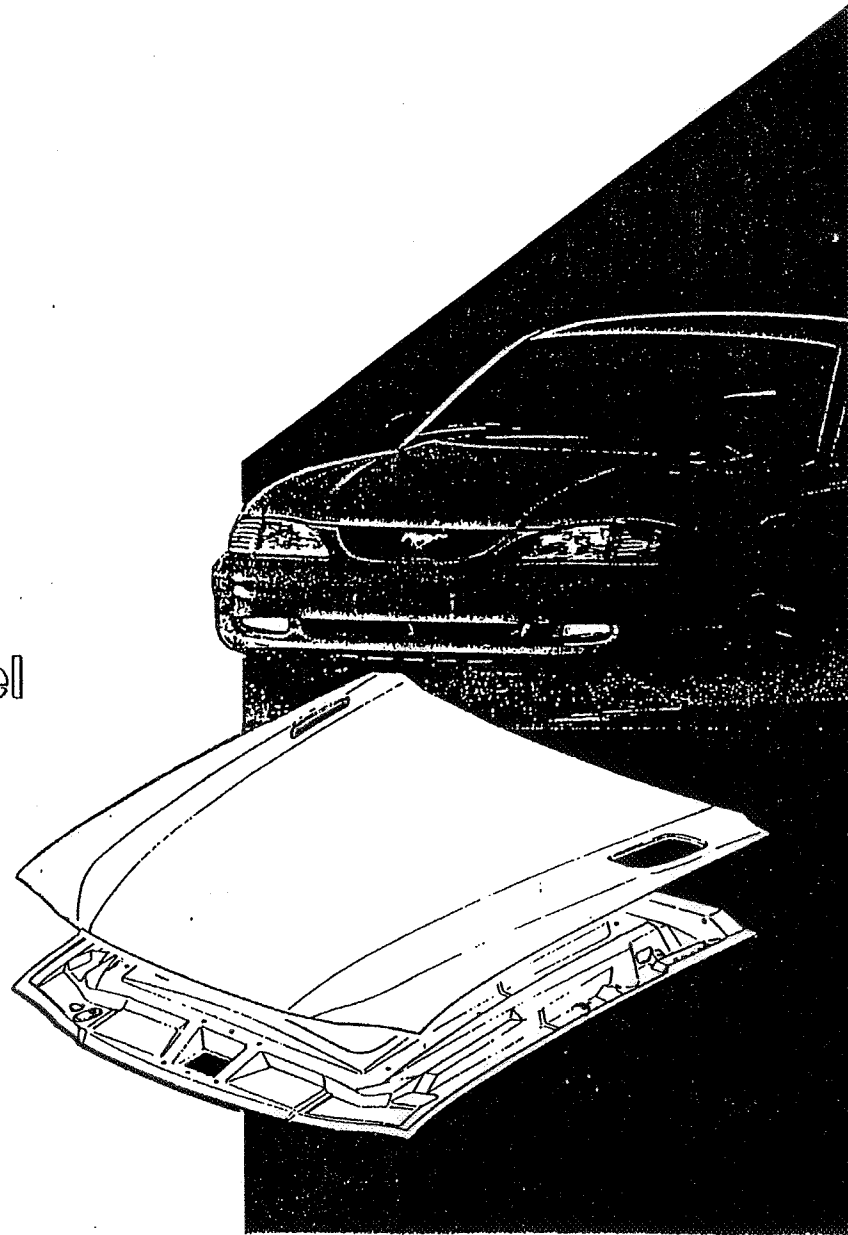
• Styling Flexibility

• 60% Tool Savings vs. Steel

• 20% Weight Savings vs. Steel

• Body Shop Assembly

• E-Coat Compatible





Continental Hi-Flex® Fenders

33% Weight Savings vs. Steel

Dent and Corrosion Resistant

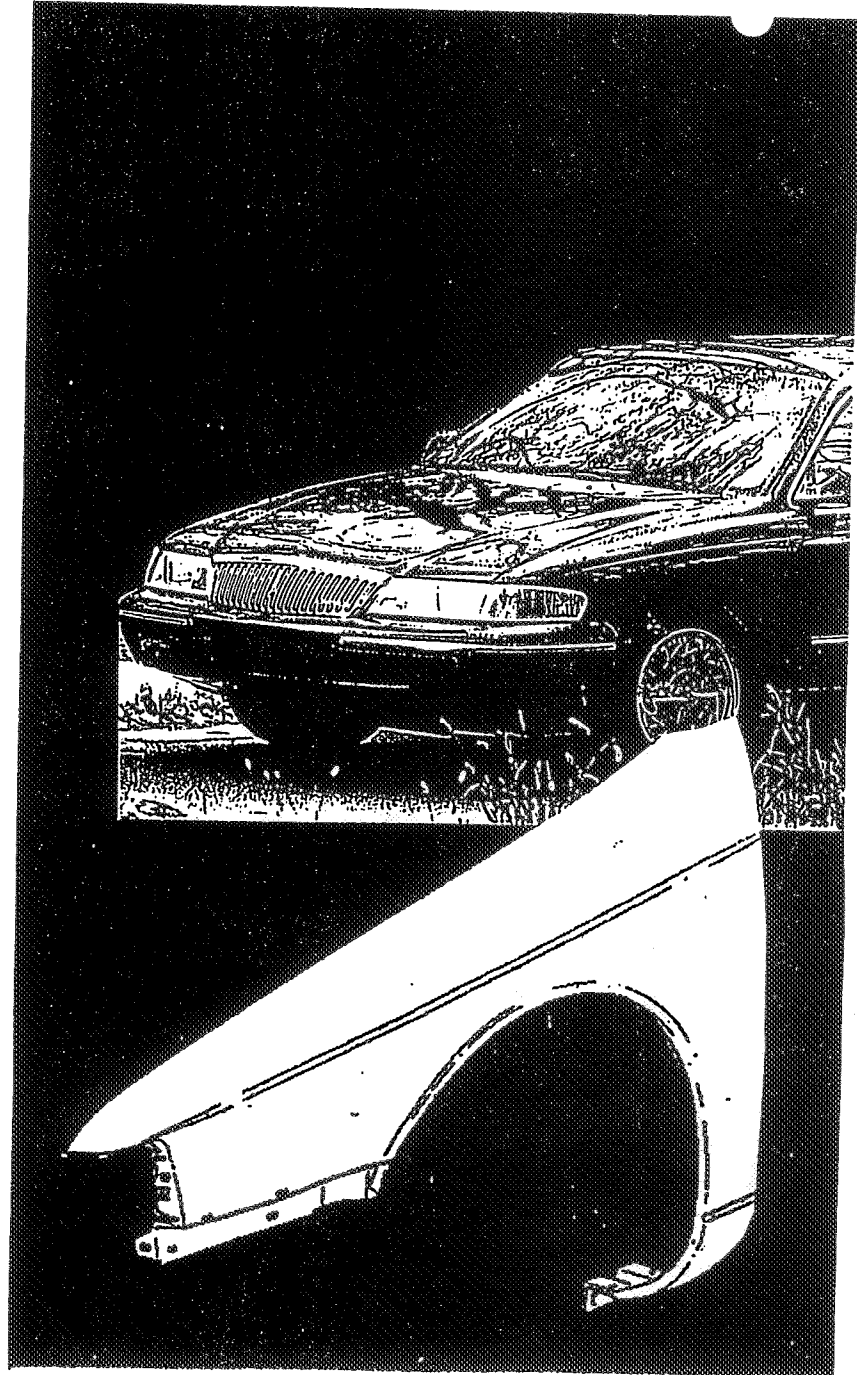
Styling Features

60% Tool Savings vs. Steel

Body Shop Assembly

E-Coat Compatibility

Budd Black Box Design





Camaro/Firebird Door Assembly

•
25% Weight Savings vs. Steel

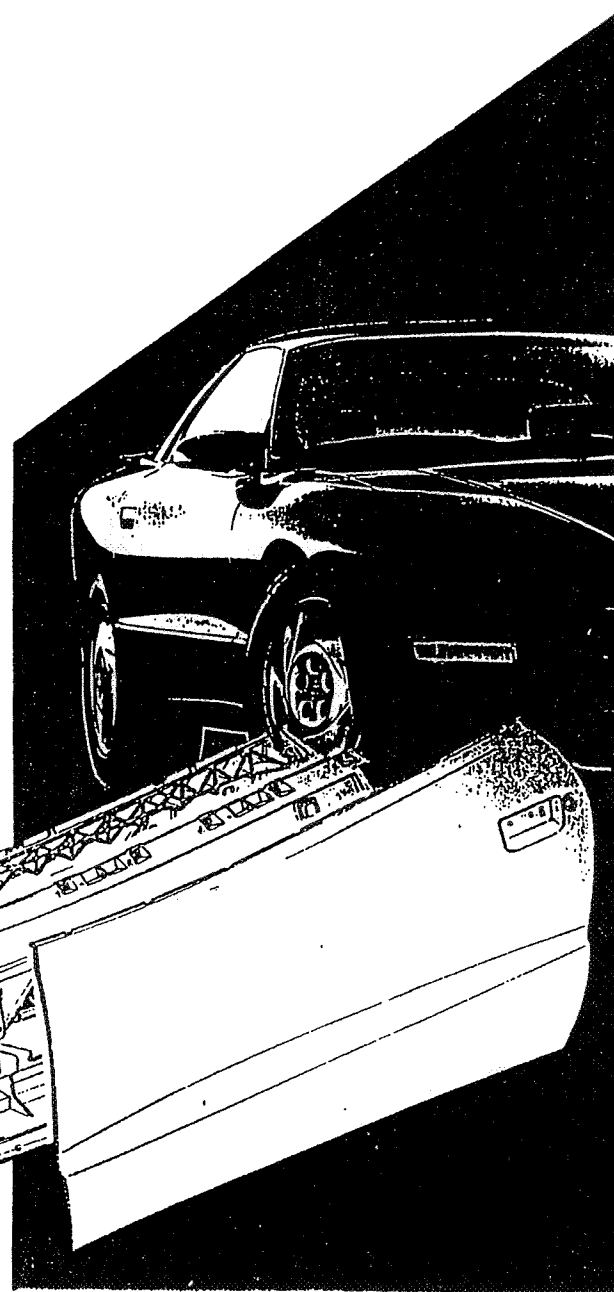
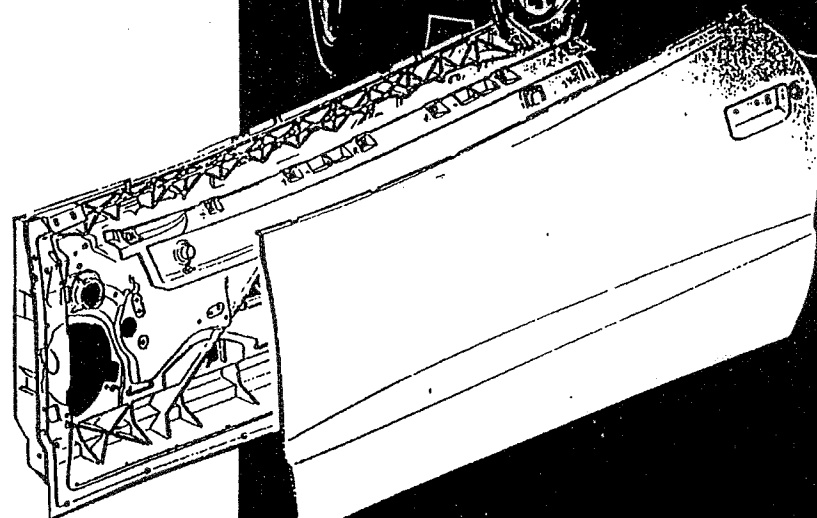
•
Dent and Corrosion Resistance

•
Styling Features

•
40% Tool Savings vs. Steel

•
Body Shop Assembly

•
E-Coat Compatibility





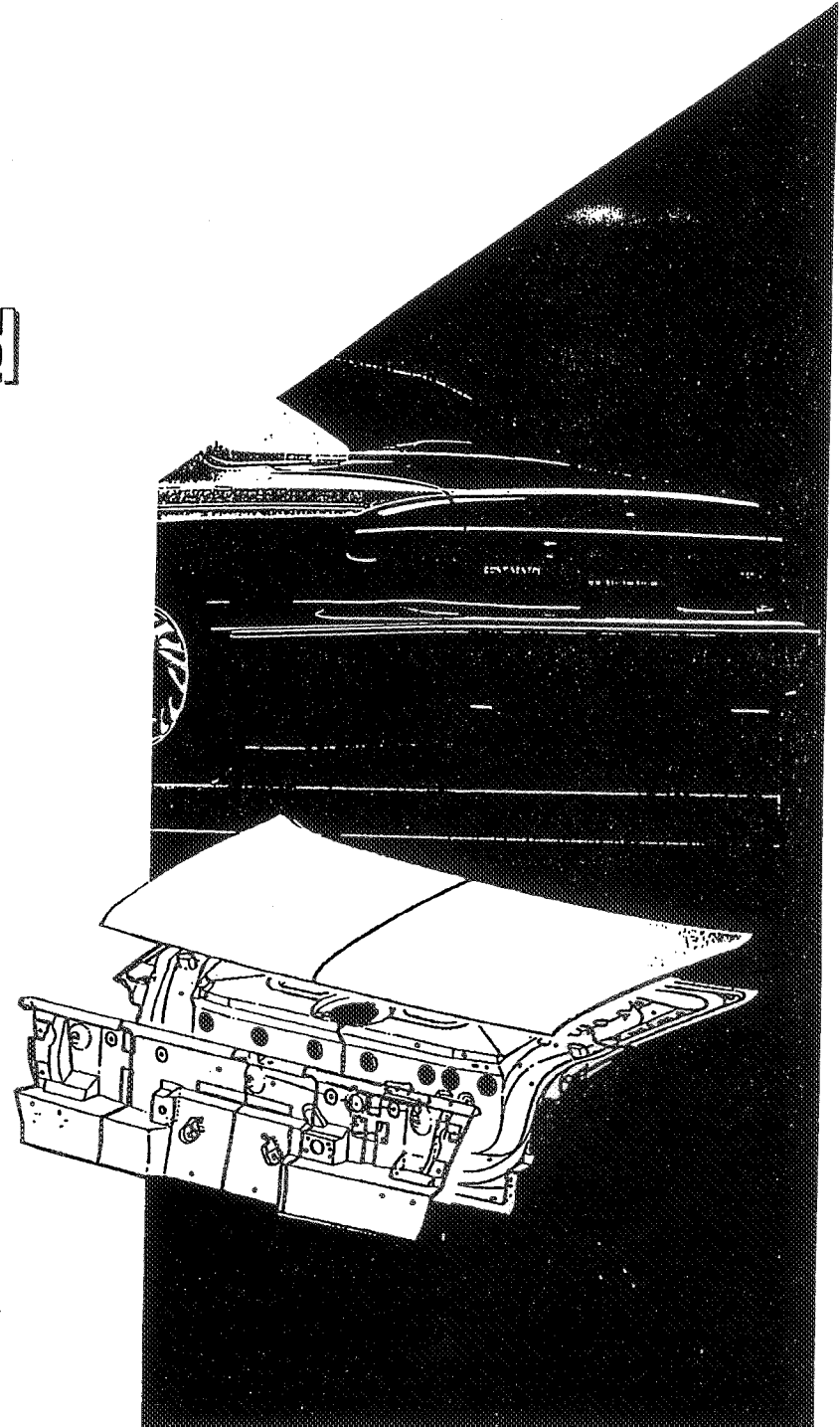
Continental Decklid

- Design Flexibility

- Part Consolidation

- Low Tooling Cost

- 25% Weight Savings





Windstar Van Cowl Panel

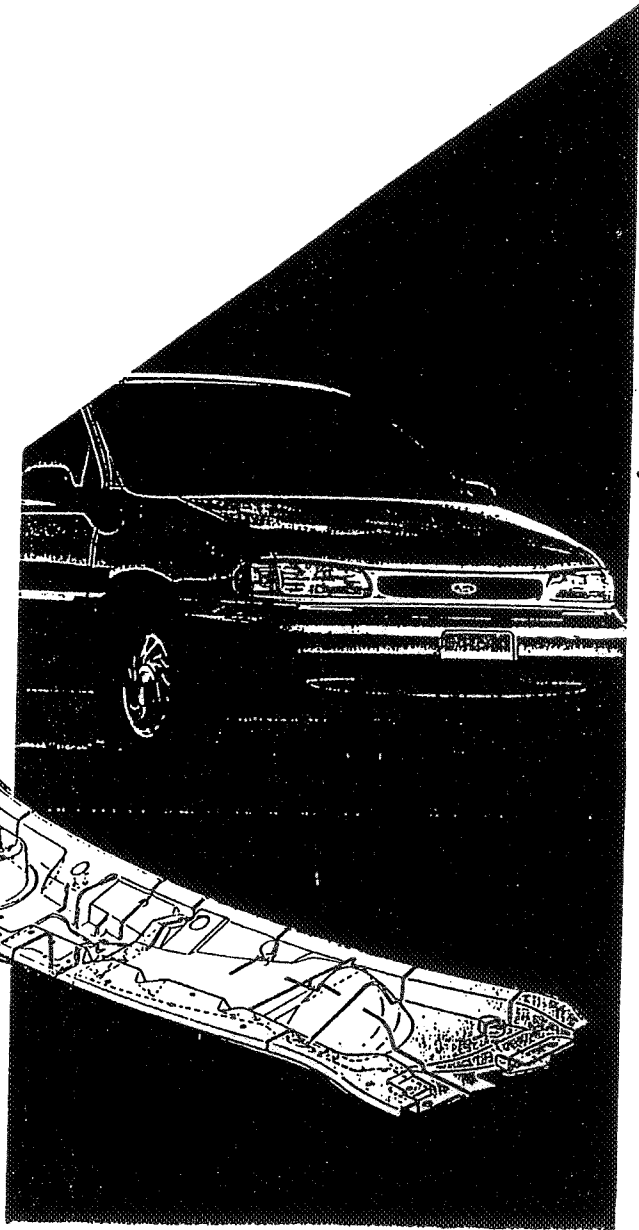
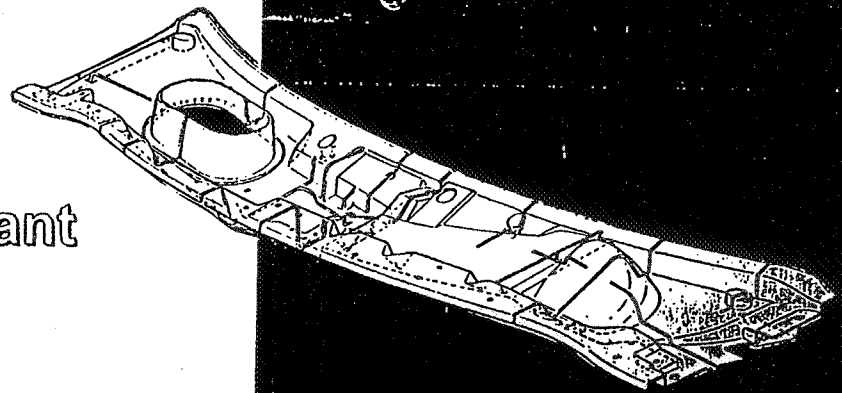
Wiper System Structural
Support Panel

Hood Seal

Supports Fresh Air Duct,
Water Drain, Leaf Screen

Abuse and Corrosion Resistant
Access Panel

285



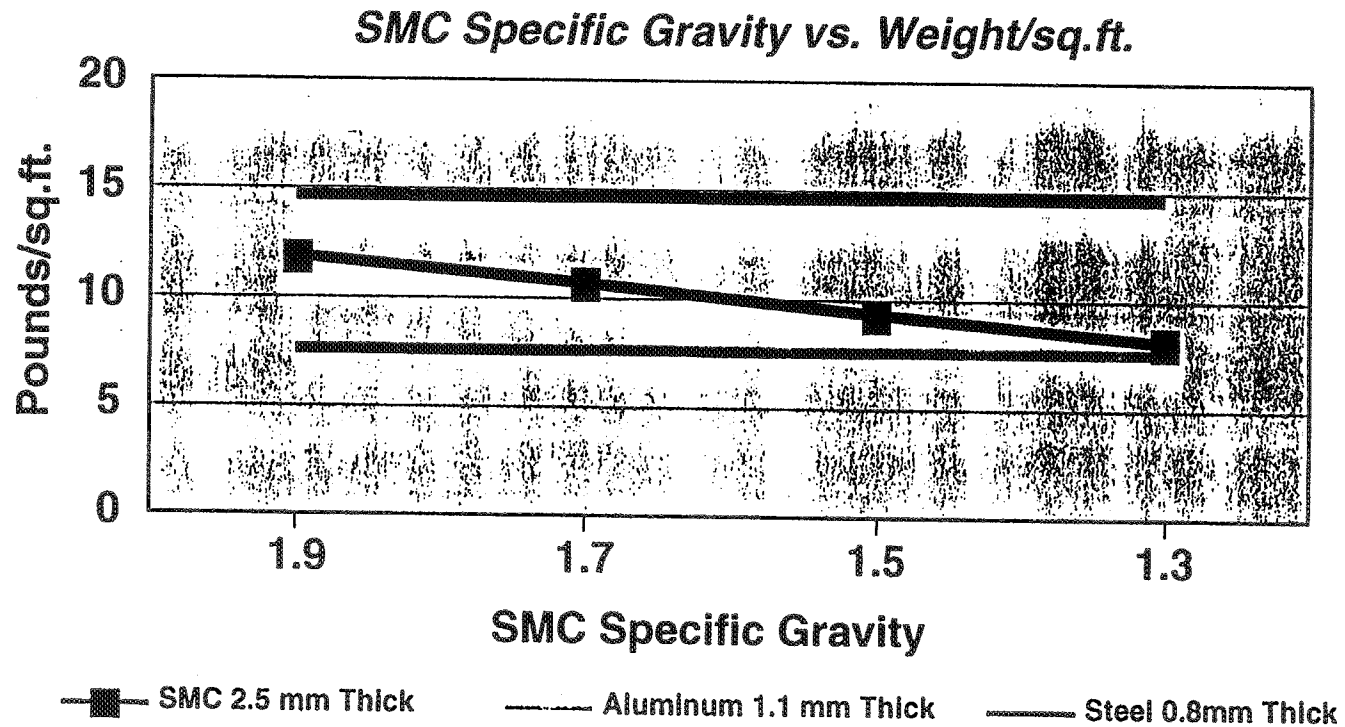
COMPOSITE MATERIALS COMPARISON

	SMC	LD-SMC	RRIM	SRIM	GMT
Weight (Specific Gravity)	1.9	1.3	1.3	1.5	1.2
Investment (Tooling)	~	~	Lowest	~	~
Total Program Cost	Lowest	~	~	Highest	~
Design Flexibility	~	~	Most	Least	~
Complexity Reduction	Most	Most	Least	~	~
Heat Resistance (degrees F)	400+	400+	375	350	250
Dimensional Integrity	Best	Best	~	~	Least
Thermal Expansion	Steel	Steel	Higher	Higher	Highest
Corrosion Resistance	High	High	High	High	High
Dent Resistance	~	~	High	~	Highest
Structural Strength	~	~	Lowest	Highest	~
Stiffness (Modulus)	1.8	1.5	0.3	1.2	0.8
Recyclable	Yes	Yes	Yes	Yes	Best
Surface Quality	Class A	Class A	Class A	Poor	Poor

Weight and Cost Implications

New low density SMC's promise more weight reduction:

- With hollow glass microspheres, 1.5 & 1.3 specific gravity SMC body panels are viable.



COST/WEIGHT COMPARISON

SMALL HOOD

Weight Comparison

Steel	38. lbs.	Base
SMC (sp. gr. 1.9)	26. lbs.	- 12. lbs.
SMC (sp. gr. 1.3)	19. lbs.	- 19. lbs.
Aluminum	19. lbs.	- 19. lbs.

Cost Comparison

	<u>Pc. Cost</u>	<u>Tooling</u>	<u>Amort.</u>	<u>Total Cost</u>	<u>Cost Diff.</u>
Steel	\$50.00	\$5. Mil	\$8.35	\$58.35	Base
SMC (sp. gr. 1.9)	\$53.00	\$2.9 Mil	\$4.85	\$57.85	-\$0.50
SMC (sp. gr. 1.3)	\$58.00	\$2.9 Mil	\$4.85	\$62.85	+\$4.50
Aluminum	\$75.00	\$5. Mil	\$8.35	\$83.35	+\$25.00

COST/WEIGHT COMPARISON

SMALL FENDER

Weight Comparison

Steel	19. lbs.	Base
SMC (sp. gr. 1.9)	14.5 lbs.	- 4.5 lbs.
SMC (sp. gr. 1.3)	10. lbs.	- 9.0 lbs.
Aluminum	10. lbs.	- 9.0 lbs.

Cost Comparison

	<u>Pc.Cost</u>	<u>Tooling</u>	<u>Amort.</u>	<u>Total Cost</u>	<u>Cost Diff.</u>
Steel	\$40.00	\$8.9 Mil	\$14.85	\$54.85	Base
SMC (sp. gr. 1.9)	\$45.00	\$4.0 Mil	\$6.65	\$51.65	-\$3.20
SMC (sp. gr. 1.3)	\$50.00	\$4.0 Mil	\$6.65	\$56.65	+\$1.80
Aluminum	\$60.00	\$8.9 Mil	\$14.85	\$74.85	+\$20.00

Note: The above costs are for engineering purposes only and do not represent a cost quotation. Tooling amortization assumes 2 year program at 300,000 units per year.

SMC CAN BE RECYCLED

SMC is recyclable at the end of its life cycle; and, new SMC can contain substantial quantities of recycled products (including resin, filler and additives). A projected 300 million pounds of SMC will be used by the auto industry by 2000. This has prompted the ACA (Automotive Composites Alliance), to resolve the technical challenges associated with recycling old SMC parts and incorporating recycled materials into new SMC parts.

Over the past ten years the ACA (previously SMCAA) has promoted the research and development activities necessary to establish economically viable processes for recycling, has demonstrated production applications for SMC with recycled content and has encouraged awareness of SMC recycling throughout the auto industry. To date, more than 20 automotive parts containing recycled SMC filler are used on production vehicles, and additional parts are scheduled for future cars and trucks (with recycled content as high as 25%). SMC molders have been successful in these recycling efforts because SMC is an easily recyclable plastic; there is no need to remove paint and adhesive from SMC prior to processing as recycled filler. In many respects, SMC is easier to recycle than thermoplastics; SMC recycling is less sensitive to contamination by dissimilar materials and there is no degradation of properties. The resin portion of SMC also can contain recycled PET (from recycled pop bottles).

Currently, the best SMC recycling approach is to grind up the SMC scrap (end-of-life parts or in-plant scrap) to provide a filler which can be used to replace the limestone filler in new SMC. The first commercial SMC recycling operation was Phoenix Fibreglas, a Canadian recycler partially owned and managed by Owens-Corning. Through Phoenix Fibreglas the technical feasibility of SMC recycling was established and several auto parts with Phoenix filler were put into production. The Phoenix process separated the ground SMC into filler and "fiber" fractions; the recycled fibers were found to be useful in friction materials, putty, one-coat stucco and BMC type of composites. Phoenix processed primarily in-plant scrap (over 6 million pounds); but, quantities of scrap SMC auto parts also were processed to demonstrate that the filler obtained is equivalent to that from in-plant SMC scrap.

Phoenix Fibreglas closed in April of 1996. SMC recycling was their only primary business, and the infrastructure to recycle SMC had not developed to a level sufficient to support the Phoenix operation. Although unfortunate, the closing of Phoenix will not retard the SMC recycling programs put in place, nor will it discourage continued use of recycled SMC. The R. J. Marshall Co. has been working with the ACA to process SMC scrap and to provide a recycled filler equivalent to that supplied by Phoenix. Since R. J. Marshall is in the business of producing specialty fillers, they will not be solely dependant on recycled SMC filler sales; this is a more stable business relationship. The ACA and R. J. Marshall are highly confident that recycling SMC is economically viable, as well as technically feasible.

The ease with which SMC can be recycled as a filler, and the capability to incorporate a number of different recycled products into the SMC formulation, without a cost penalty, are expected to make SMC even more competitive for auto components when compared to other plastic materials. As the infrastructure develops to collect scrap SMC, recyclability will be a major SMC advantage.

RECYCLING DEFINITIONS

(The Many Sides of the Recycling Picture)

❖ Recycled Content In A New Part

1. Post-Consumer Content
2. Pre-Consumer Content ("Post-Industrial")
3. Internal Reuse Of Scrap In The Manufacturing Process

❖ Part (Or Material) Is Recyclable At The End Of Its Primary Life-Cycle

1. Refurbish and Reuse Part (eg., Reuse Hood On Another Vehicle)
2. Primary Recycling (Reuse Material To Make A Similar Or Identical Part)
3. Secondary/Tertiary Recycling (Reuse Material To Make A Lesser Value Part, Recover Raw Material Ingredients or Recover Energy Content)

❖ Life Cycle Assessment ("Cradle To Grave" Analysis)

1. Life Cycle Inventory (eg., Total Energy Consumption From Raw Materials To Final Disposal Of Part)
2. Environmental Impact Assessment (Natural Resources Depletion, Toxic Emissions, Pollution, Etc. From Initial Manufacture To Final Disposal Of Part)

RECYCLING OPTIONS
Material Comparison For External Auto Body Panels
(Hood, Fender, Applique, Front End Panel, Bumper, Etc.)

	Thermosetting Composite SMC/BMC RRIM SRIM	Thermoplastic Composite Azdel GFN/GFPE	Engineering Thermoplastic PET/PBT Polycarbonate TPO	Sheet Steel	Sheet Aluminum
Recycled Content in New Part					
Post-Consumer	No (a)	No (a)	No (a)	No (a)	No (a)
Pre-Consumer	No (a)	No (a)	No (a)	Yes	Yes
Internal Reuse	No	Yes (b)	Yes (b)	Yes	Yes
Recyclable at End of Service Life					
Refurbish and Reuse	Yes (d)	No (e)	No (e)	Some (f)	Some (f)
Primary Recycling	No (a)	No (x)	No (x)	No (a)	No (a)
Secondary/Tertiary Recycling	No (a)	No (a)	No (a)	Yes	Some
Life Cycle Assessment					
Life Cycle Inventory (Energy)	Low	Low	Low	High	Med.
Environmental Impact	Med. (g)	Med. (g)	Med. (g)	Med. (g)	Med. (g)

- Notes:**
- a) Feasible, but not currently done because of cost penalty
 - b) Internal scrap used, but generally into "lower grade" parts
 - d) Bolt-On parts commonly dismantled and reused (if not damaged)
 - e) Generally not economical to reuse
 - f) Bolt-On parts can be reused if free of corrosion and/or damage
 - g) Generally no major differences between materials
 - x) Generally not feasible or large cost penalty

CURRENT AUTOMOBILE RECYCLING INFRASTRUCTURE

RECYCLING SEQUENCE

- ❖ Scrap Car Delivered To Dismantler
- ❖ Useful Or Recyclable Parts Are Removed
- ❖ "Hulk" Is Passed Through Shedder
- ❖ Ferrous Material Magnetically Removed; Remainder is ASR (Automotive Shredder Residue)
- ❖ ASR Passed Through Non-Ferrous Metal Separator (Removes Aluminum, Copper, Zinc, Magnesium, Etc.)
- ❖ Balance Of ASR Normally Goes To Landfill

TYPICAL RECOVERY RATES (By Material)

	<u>Dismantling</u>	<u>Ferrous</u>	<u>Non-Ferrous</u>	<u>Landfill</u>
1. Steel	35%	64%	1%	0
2. Cast Iron	90%	9%	1%	0
3. Aluminum	15%	0	65%	20%
4. Thermoplastics	1%	1%	5%	93%
5. SMC/BMC	15%	0	0	85%

NOTE: The percentage of Organic Materials (Plastics, Rubber, Fabrics, Etc.) in an average American vehicle is **15% by weight and 55% by volume.**

This is an important factor when considering the percentage of "Plastics" which currently ends up in Landfill.

REUSE OF AUTOMOTIVE PARTS (DISMANTLING)

(Sorted by Type Of Part)

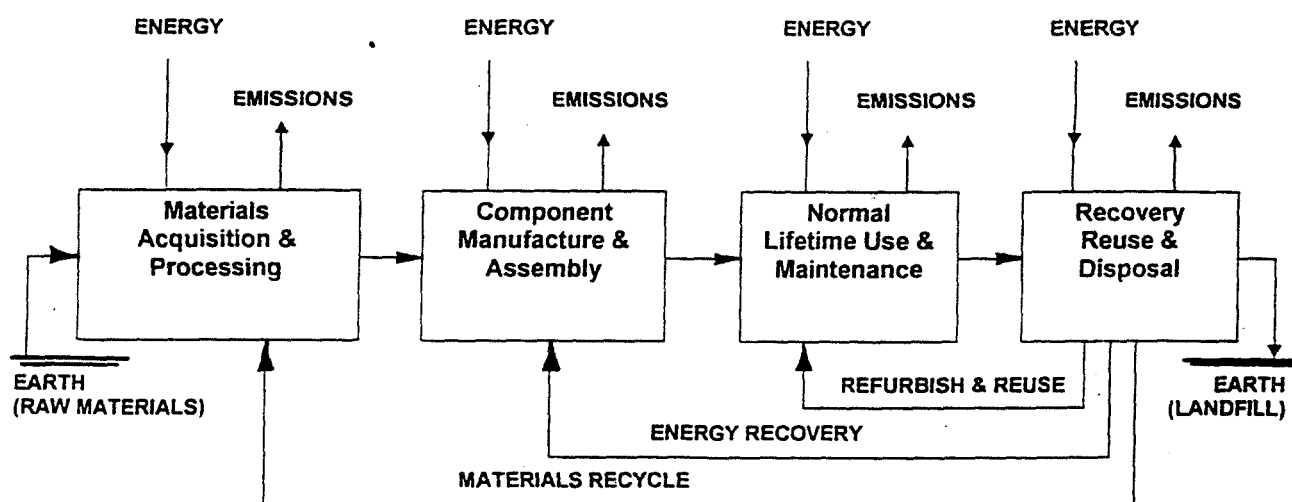
➤	Wheels	87%
➤	Transmissions	50%
➤	Engines	41%
➤	Doors	35%
➤	Bumpers	24%
➤	Fenders	22%
➤	Fuel Tanks	15%
➤	Deck Lids	15%
➤	Front End Panels	14%
➤	Hoods	12%
➤	Seats	12%
➤	Grilles/Exterior Trim	8%
➤	Instrument Panels/Interior Trim	2%
➤	Wiper Motor/Assemblies	1%

Note: Parts which could be SMC are shown in "Bold Type".
SMC parts are reused at higher rates than steel or aluminum.
The reuse rates shown above are averages for all vehicles.
Parts which are typically thermoplastic are reused at very low rates.

LIFE CYCLE INVENTORY (ENERGY)

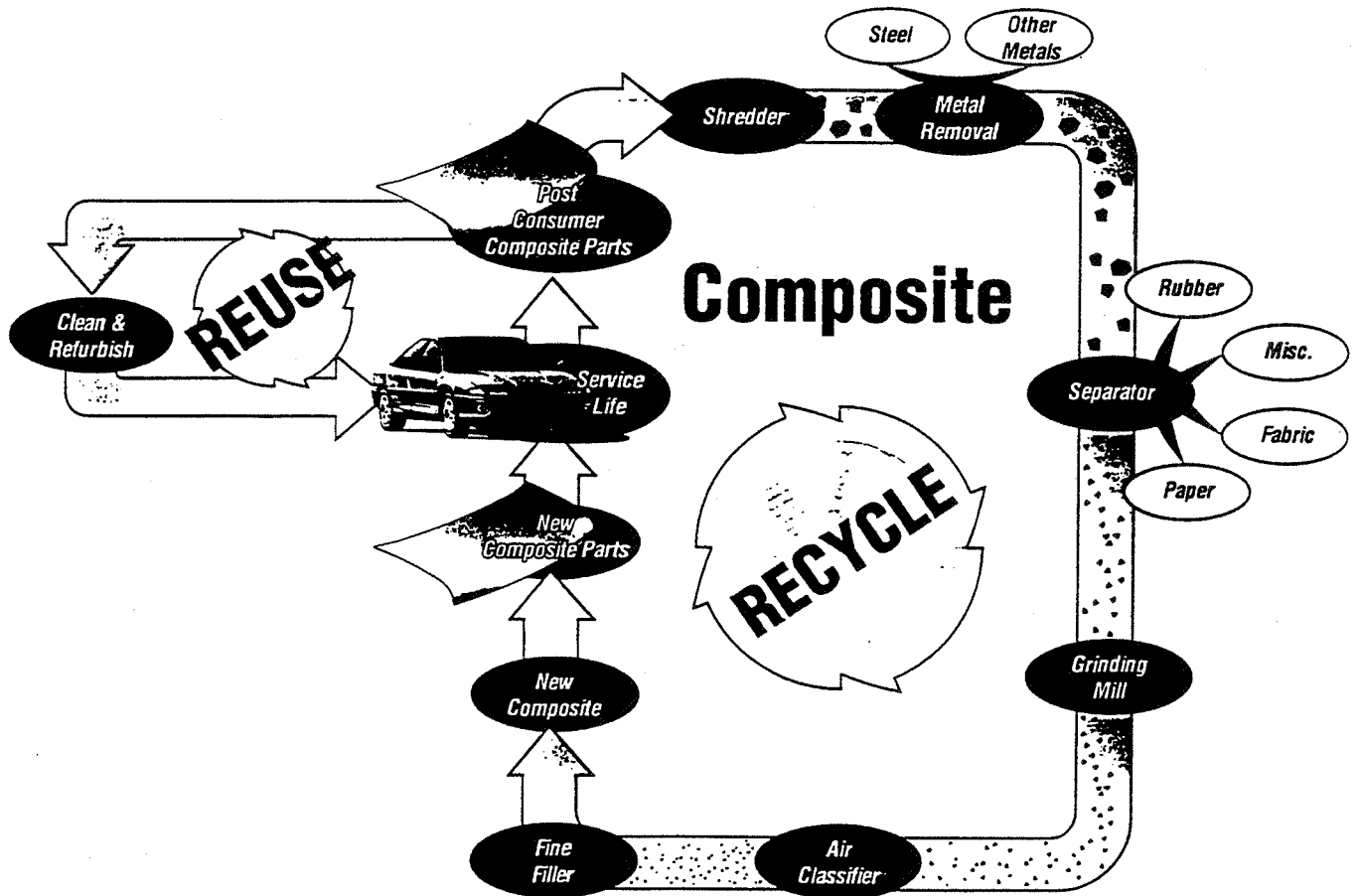
SMC AUTOMOTIVE BODY PANELS REDUCE USAGE OF FUEL RESERVES

- ❖ The Lincoln Continental uses 100 lbs. of SMC components, reducing vehicle mass by about 30 lbs. versus steel.
- ❖ This permits fuel savings of 24 gallons per 100,000 miles of driving.
- ❖ About 8.6 gallons of fuel are saved per vehicle in the materials acquisition, processing and manufacture of the SMC parts (versus comparable steel parts).
- ❖ SMC parts are more easily refurbished and reused when a vehicle is scrapped (versus steel), reducing the need to manufacture service parts and providing another 2 gallons of fuel saved per average vehicle.
- ❖ Recycling SMC scrap, end of lifecycle parts and introducing recycled content into new SMC material, can provide an additional 0.4 gallons of fuel saved.
- ❖ The total fuel savings potential per Continental vehicle over 100,000 miles is 35 gallons.



MAJOR LIFECYCLE STAGES FOR AUTOMOTIVE PART

Thermoset Composite Parts are being Recycled!



Over 20 different composite parts are on the road in North America with recycled filler content.

Reuse of composite parts from scrapped vehicles occurs more frequently with thermosets.

Recycled filler content up to 25% by weight results in no changes in composite physical properties.

Composites can be recycled and used as filler in making similar components (primary recycling).

Thermoset composite parts are more easily recycled than most decorated thermoplastic parts at the end of vehicle lifecycle.

First composite automotive parts with recycled filler appeared on the road in 1991 (Europe) and in North America since 1992.

ERCOM in Germany is a pioneer in recycling SMC Composite parts -- over 3 million vehicles with recycled composites are on the road in Europe.

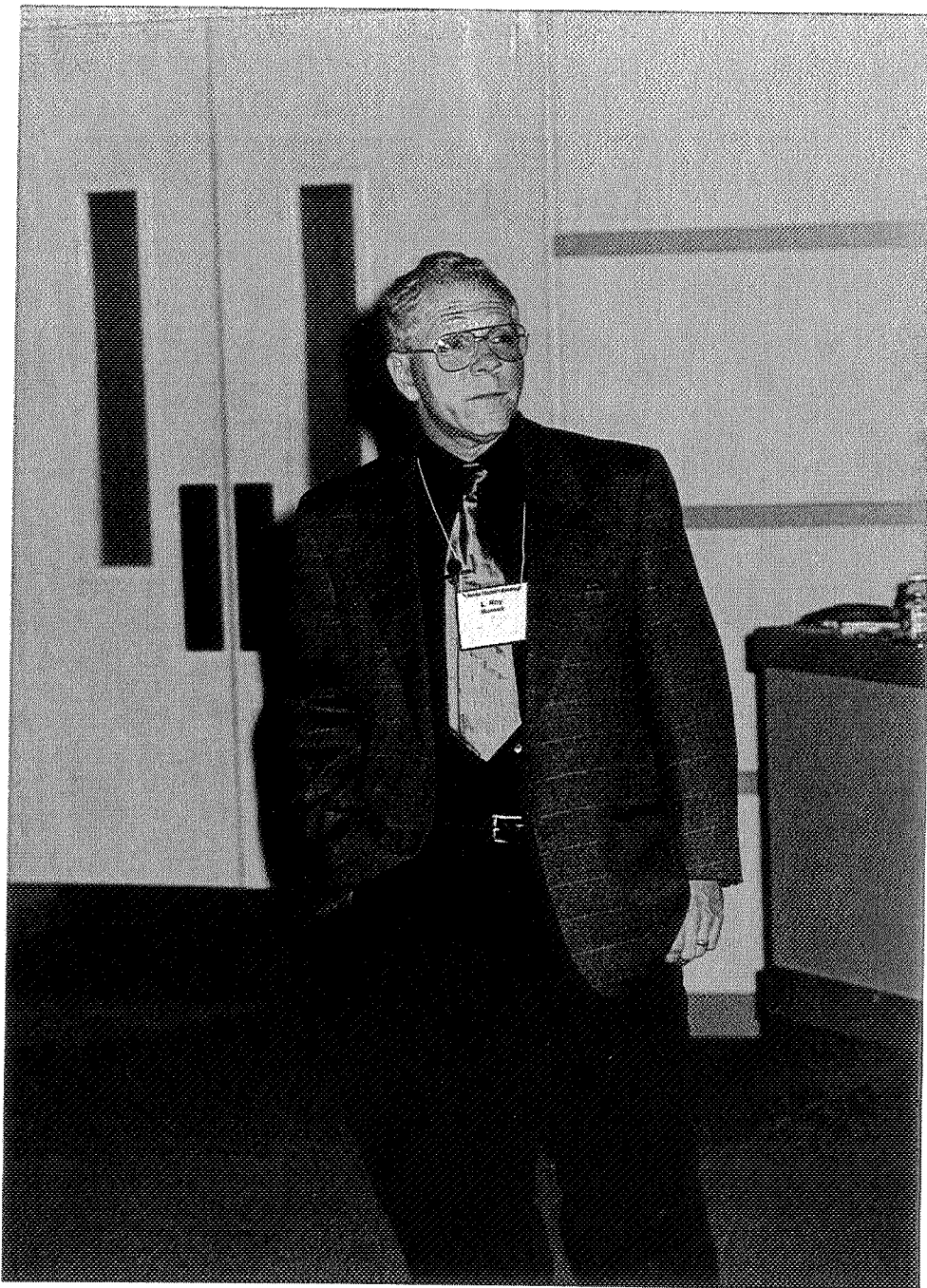
Unlike thermoplastics, composites can be recycled without removing paint, adhesives or other materials.

**SIMPLE AND INEXPENSIVE METHOD FOR
TESTING SHEAR STRENGTH OF
ADHESIVE BONDS**

L. Roy Bunnell

Southridge High School
Kennewick, WA 99338

Telephone 509-734-3800
e-mail Bunnro@ksd.org



L. Roy Bunnell

Simple and Inexpensive Method for Testing Shear Strength of Adhesive Bonds

L. Roy Bunnell
Southridge High School
Kennewick, WA 99338

Key Words: Shear Strength, Adhesive Bonds, Epoxy Resin

Prerequisite Knowledge: Students will have been instructed in the basics of epoxy resins and the importance of cleanliness in the surfaces to be bonded.

Objective: By testing adhesive bonds made under several different conditions, students develop an appreciation for the importance of proper batching of epoxy resins and the condition of surfaces to be bonded.

Equipment:

1. Torque Wrenches, probably 1 wrench/5 students, designed to measure torques from 0-200 N-m (0-150 ft-lb). A cheap beam-type wrench was used here, but a dial-gauge type would probably be more accurate and capable of showing subtle differences among specimen types.
2. Machine screws; 7/16 x 1-1/2 coarse threaded screws were used here. This size included enough bond area to give reasonable torque readings. Slightly larger screws could be used, but screws should probably be no smaller than this size. Each student should be supplied with one screw and matching nut.
3. Several bench vises, probably one vise/5 students to complete testing in one class period.
4. Epoxy resin and hardener, see text below for details.
5. Very light oil for contaminating surfaces, see text below for details.
6. Commercially available anaerobic thread locking compound if desired, see text for details.

Safety Precautions:

Follow label directions on the epoxy resins used, and remove resin from skin with soap and hot water, or methanol if that fails. When applying torque wrench to specimens, clamp the machine screw or nut securely and brace feet against reaction forces, and be cautious about sudden failure of the bond or screw.

Experiment Description:

Introduction: Adhesive bonds are finding increasing usage in the assembly of many manufactured products, from automobiles to passenger airplanes. This method of assembly has many advantages, including bonding of parts over large areas and the avoidance of stress-raising penetrations. However, adhesives must be chosen and used carefully, and surfaces to be bonded must be clean, dry and sound in order to develop consistently high bond strength.⁽¹⁾ Ideally, adhesively-bonded joints should be designed

so that the adhesive is placed in shear for best results. Similarly, testing of adhesively-bonded materials should be done so that the bond line is in pure shear. The testing method outlined in this paper provides a simple means for doing such testing.

Testing Method: Since the adhesively-bonded joint should be placed in pure shear, considerable thought was given to the testing method. Finally, the idea of using the adhesive between a standard machine screw and a corresponding nut occurred. By using this combination, the bond line would be placed in pure shear when the nut is rotated around the screw. Moreover, the torque for moving the nut could be easily measured by using a common torque wrench, as used previously by Nydam⁽²⁾ to show the differences in strength among bolts of several different classes. Since the shear strength of common epoxy resins was unknown (at least to this author), the size of machine screw to be used was determined by trial and error. In this work, the machine screws used were 7/16 x 1-1/2 inches, with coarse threads. When this size of screw was completely coated with adhesive and a nut applied, the torque necessary to break the bond was easily measured using a torque wrench of common size.

Preparation of Adhesive Bonds: In all cases except one, the adhesive used was Vinacron Epoxy.¹ This epoxy is a room-temperature-curing epoxy, is easy to batch, and has never produced a skin reaction in the hundreds of high school students who have used it. The variables tested are listed below; since there were five variables, the classes were divided into six teams and each student on a team prepared a screw-nut combination of one of the six types below:

- A. As-Purchased (cadmium-plated) fittings, epoxy resin and hardener mixed in proper (3:1) ratio by weight, cured overnight.
- B. Fittings Cleaned of any oily surface contamination that may have been present, by heating both nuts and screws to 500 deg. C, overnight. Fittings were bonded with properly batched epoxy, as in (A) above.
- C. Fittings Contaminated by spraying with WD-40² lubricant, then adhered by properly batched epoxy, cured overnight.
- D. As-Purchased fittings, epoxy and hardener mixed in 6:1 ratio, cured overnight.
- E. As-Purchased fittings, epoxy and hardener mixed in 1:1 ration, cured overnight.
- F. Loctite #271³ anaerobic thread lock, applied and cured overnight.

Students should be directed to label the head of their screw with an appropriate marker, using one of the letters above. In all cases, students coated the threads of the screw with adhesive by dipping, then applied the nut to full coverage of the screw.

¹ Industrial Arts Supply Company, Minneapolis, MN 55416-2594

² WD-40 Company, San Diego, CA 92110

³ Loctite Corporation, North American Group, Rocky Hill, CT 06067

Testing of Adhesive Bonds: On the day after preparing the specimens, students used a torque wrench to test their adhesive bonds, after first clamping the hex head of the machine screw in a vise. Students were directed to apply the torque wrench socket to the head of the nut and to turn very slowly, carefully noting the peak torque obtained before the adhesive bond failed. Students recorded torque values and reached team consensus as to the average peak torque value and the “feel” of the bond failure, i.e., whether the bond failed suddenly or gradually and whether further turning of the bolt met with continuing resistance. Results are shown in Figure 1.

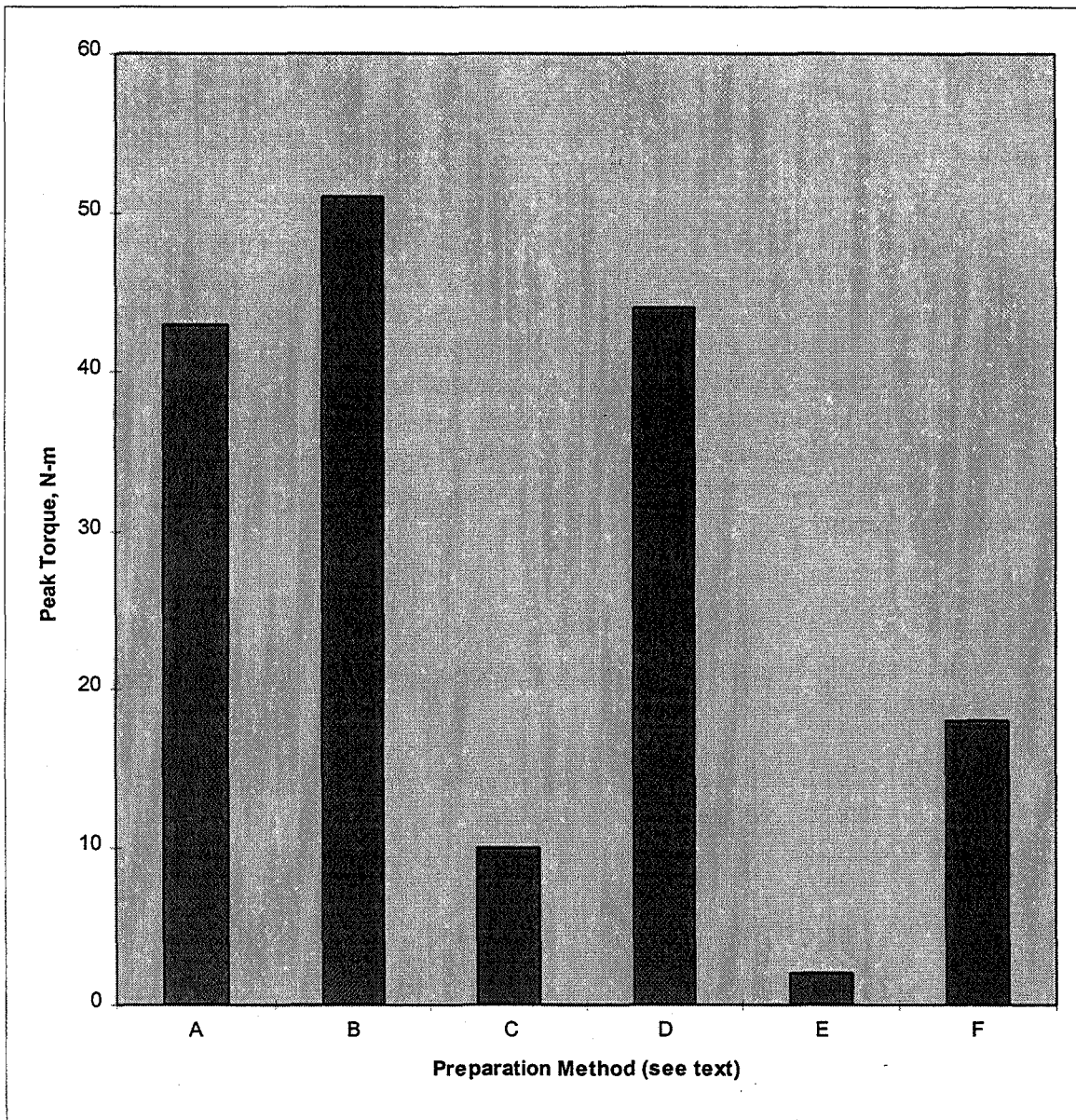


Figure 1. Measured Torque Values for Screw/Nut Combinations Bonded by the Six Methods as Described in the Text.

Discussion of the Results: By examining the results as presented in Figure 1, it appears that the as-received fittings (A) were quite free from contamination, because heating them to high temperature (B) did not produce a markedly higher bond strength. Deliberate contamination of the surfaces (C) produced much lower bond strength, as would be expected. The epoxy used was very tolerant of hardener-deficient batching errors, because specimens of this type (D) were as strongly bonded as as-received specimens. On the other hand, adding grossly too much hardener to the epoxy resin (type E) resulted in a non-hardening condition indicated by very low bonding strength. Type E specimens showed a viscous flow behavior in that torque values increased with shear rate. The epoxy bonds were strong enough that in one case not shown, when properly batched epoxy was applied to previously heated (type B) specimens and post-cured overnight at 60 deg. C, the machine screws actually failed by twisting during testing. On the other hand, the commercial thread-locking compound (F) produced a weaker bond than with properly prepared epoxy on clean surfaces, sufficiently strong for its intended use but unlikely to be unduly hard to remove or to cause screw failure.

Possible Variations and Extensions: The testing method in this paper appears applicable to evaluating the shear strength of epoxy. Other epoxies could be evaluated and compared, or mix ratio effects could be evaluated in more detail. If nonplated fittings were used, there would almost undoubtedly be oily contaminants present. The effects of different cleaning techniques might also be evaluated using the method of this paper. One might be tempted to use the method on other adhesives, but it should be kept in mind that solvent-based adhesives such as “airplane glue” or casein-based wood glues would not be appropriate because the solvent could not evaporate readily from the confined space of the threads.

References:

1. J. A. Jacobs, T. F. Kilduff, Engineering Materials Technology, Third Edition, Prentice-Hall, 1997
2. A. Nydam, “Low Dollar Tensile (Torsion) Tester”, Presented at National Educators’ Workshop: Update 97, NASA/CP-1998-208726

Biographical Information:

L. Roy Bunnell is a teacher of Materials Science Technology at Southridge High School in Kennewick, Washington. He received a Bachelor of Science degree in Ceramic Engineering from the University of Utah and worked at Pacific Northwest National Laboratory in Richland, Washington, where he worked on many materials-oriented projects and helped to develop the curriculum for a high school course in Materials Science. His major interests are glasses and composite materials. He has contributed papers to several National Educators’ Workshops.

MICROWAVE DRIVEN ACTUATORS POWER ALLOCATION AND DISTRIBUTION

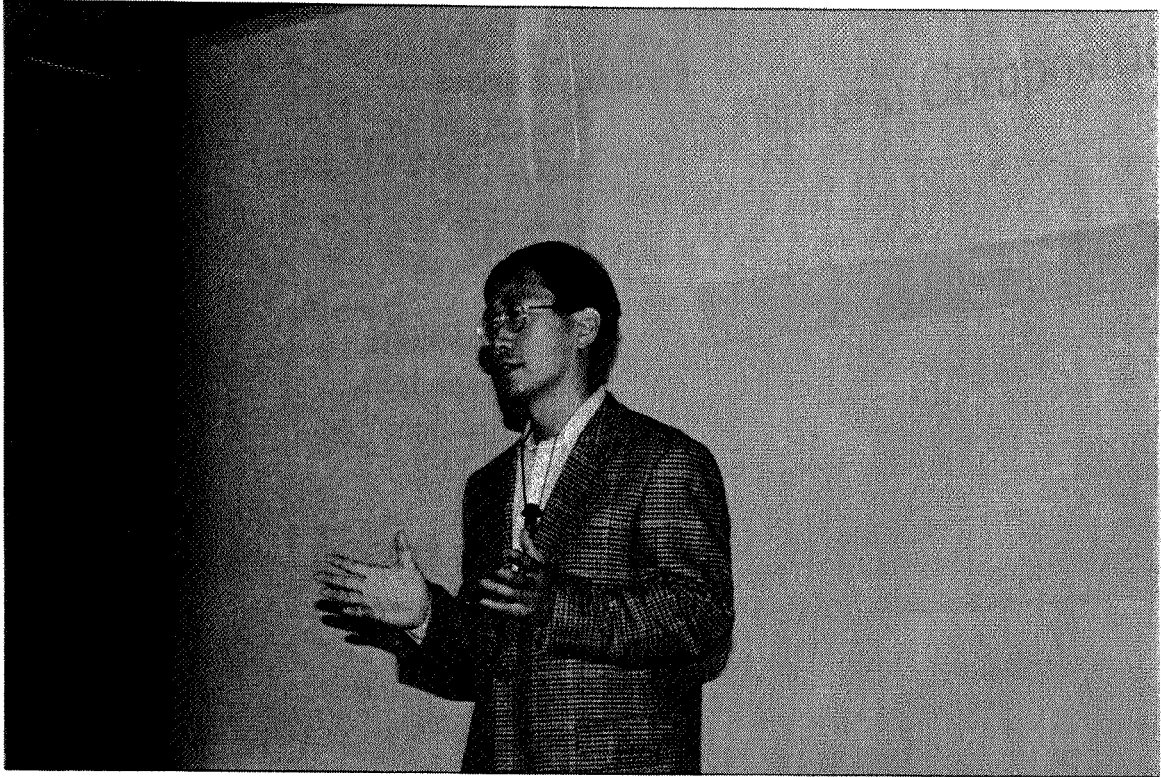
Timothy Forbes

and

Kyo D. Song

Department of Technology
Norfolk State University
2401 Corprew Avenue
Norfolk, Virginia 23504

Telephone: 757-683-8105
e-mail kdsong@vger.nsu.edu



Kyo D. Song

Microwave Driven Actuators Power Allocation and Distribution

Timothy Forbes and Kyo D. Song

*Norfolk State University
Department of Technology
Center for Materials Research
Norfolk, Virginia 23504*

Key Words: Microwave Driven Actuator, Voltage Up-Converter (VUC), Power Allocation and Distribution (PAD), Rectenna

Prerequisite Knowledge: Understanding of basic electronics principles, and Microwave Driven Actuators.

Objective: Develop a model system that will collect DC voltage from an array of rectenna and propagate the voltage to an array of actuators.

Equipment:

- PSPICE circuit design simulator
- Computer
- Infrared relay systems
- Resistors
- Nine-volt batteries
- Voltmeters
- Proportional Voltage Booster
- Resistors, light emitting diodes, mechanical switches
- 17"x12"x6" aluminum chassis box (2)
- 13.5x1.5" hinge
- Screws and nuts

Abstract

Design, fabrication and test of a power allocation and distribution (PAD) network for microwave driven actuators is presented in this paper. Development of a circuit that would collect power from a rectenna array amplify and distribute the power to actuators was designed and fabricated for space application in an actuator array driven by a microwave. A P- SPICE model was constructed initially for data reduction purposes, and was followed by a working real-world model. A voltage up – converter (VUC) is used to amplify the voltage from the individual rectenna. The testing yielded a 26:1 voltage amplification ratio with input voltage at 9 volts and a measured output voltage 230VDC. Future work includes the miniaturization of the circuitry, the use of microwave remote control, and voltage amplification technology for each voltage source.

Introduction

The development of microwave driven smart materials has caused a need for on – board power allocation and distribution to control individual rectenna. Microwave driven smart materials technology has been developed as a remote, wireless method of powering smart materials, specifically piezo-actuators for the Next Generation Space Telescope (NGST). Due to this fact, a power allocation and distribution (PAD) circuit must be integrated with the power source. Rectenna is a material that when bombarded with microwaves of certain frequency, generates voltage. This voltage must be collected, distributed, and amplified to control piezoelectric displacement actuators. The power allocation device and VUC integrated design makes this possible

Circuit Description (PSPICE model)

The power allocation circuit (PAC) is a model of a voltage distribution network used to collect and distribute DC voltage to a system of piezoelectric actuators as shown in Fig. 1. The design was tested and refined using PSPICE ICAP's 4Rx-circuit simulator. Stage one includes six nine-volt batteries and twelve solid-state switches (Fig 1a). Each set of switches represents relays (ICAP 4rx's parts library does not include relays) used to turn sources on or off. Stage two is a step-up transformer with a 26:1 voltage amplification ratio, which represents the voltage up – converter (Fig 1b). Stage three is a parallel network that includes nine switches and nine identical circuits; a resistor and capacitor in series (Fig 1c). The resistor and capacitor represent the electrical equivalent of a piezoelectric actuator.

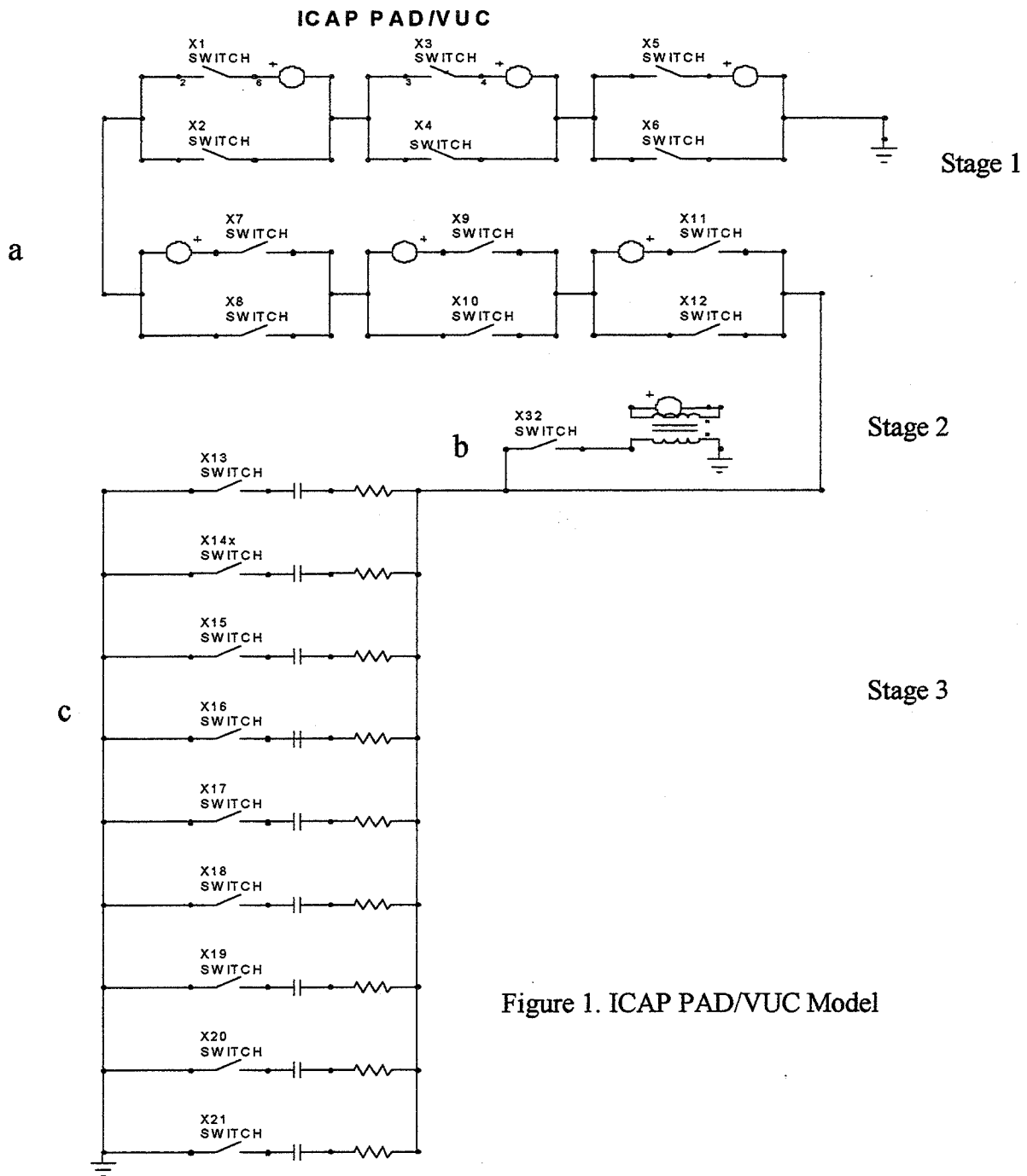


Figure 1. ICAP PAD/VUC Model

Theory of Operation (PSPICE model)

The power allocation model generally consists of stages one and two (Fig. 1a & b). Stage one provides a range of 9 to 54 volts DC in 9 - volt increments to the actuator array. The maximum voltage is achieved by linking voltage sources V1 –V6 in a series mode. V1 through V6 are each 9 – volt DC cells. Operating conditions with all sources on are X1

– X11 odd on, X2 – X12 even off. The actuator array is a parallel network (Fig 1c). The voltage across each branch is constant. All equivalent circuits may operate simultaneously, separately or in any combination. Switches S13 through S21 determine the on or off state of the equivalent circuits. The equivalent circuits represent piezoelectric actuators. DC operating point analysis is used to obtain data.

Voltage Up - Converter Circuit

The Voltage Up - Converter (VUC) circuit in the PSPICE simulator consists of a voltage booster (step - up transformer) and a voltage divider circuit. The transformer ratio is 26:1, in effect a voltage multiplier. The divider circuit is used to maintain a constant voltage across the array. The voltage divider circuit consists of a load resistor that is placed across the actuator array, and a potentiometer in series with the array. This configuration forms the voltage divider. Knowing that voltage is the same across parallel components, the voltage across load resistor will also be across the actuator array. The potentiometer is used to change the total resistance of the circuit as the output voltage from the voltage booster changes. As the total resistance of the divider decreases, the greater part of the voltage will drop across the load resistor. The potentiometer makes this possible. The voltage divider rule explains the relationship between voltage and resistance in a voltage divider circuit;

$$V_1 = R_1 V_o / R_t$$

Where V_1 is voltage across the load resistor, R_1 is a constant load resistance, V_o is the output voltage from the transformer, and R_t is the total resistance of the divider.

Equivalent Circuits

Figure 2 shows the equivalent circuit used in the power allocation and distribution circuit, a piezoelectric displacement actuator. Equivalent circuits for piezoelectric actuators vary by manufacturer. The difference between equivalent circuits is usually the state or mode of the actuator e.g. loaded, not loaded etc. Arbitrary values were used for ICAPs equivalent circuit.

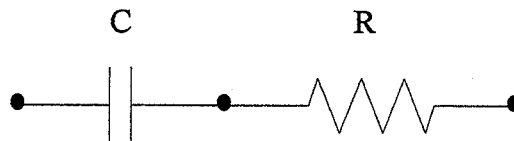


Figure 2. Actuator Equivalent Circuit.

Real World Model

The real world integrated PAD/VUC model functions in the same way as the ICAP's model. The real-world model mainly consists of a Vellman IR controlled fifteen – channel relay system, a Morgan Matroc IR controlled relay system, a proportional voltage booster from Piezo Systems, and three panel mount multi-meters. Six nine-volt batteries produce the voltage, and the VUC is powered by one nine-volt battery. Actuators are represented by green light emitting diodes and Rectenna (voltage sources) are represented by red LED's. Voltage sources and actuators are independently controlled by relays. The VUC is also controlled remotely by an independent IR channel and relay (Morgan Matroc Proportional voltage booster shown in Fig 3). The configuration of the PAD/VUC system is shown in Fig. 4.

Technical Issues

- Miniaturization

1. For conservation of space the PAD/ VUC will be produced at the microchip level
2. Fabrication would be specific to NASA Langley Research Center
3. Increased system reliability
4. Convenience
5. Increased speed and ease of production

- Infrared Interaction

1. 15 channel IR system produced by Vellman
2. Infrared remote control of relay state

- Microwave Remote Control

1. Eventually microwave RF will be used in stead of IR
2. Microwave allows for greater distance than IR.
3. RF control signal may be piggy backed along main wave
4. Development of multi – channel microwave system is needed.

- PAD/VUC – Circuit Interfacing
1. Circuit creates a common bus for each rectenna.
 2. Circuit can be imbedded in rectenna array.
 3. Allows bypassing or summing of rectenna power outputs.

Conclusions

During summer research at NASA Langley Research Center through the FAR Grant (NCC-1-280), development of a power allocation and distribution circuit (PADDC) was completed. Testing yielded maximum values of voltage at 54 VDC using six nine-volt cells. Future work includes interfacing and testing of the circuitry with Rectenna fabricated at NASA Langley. Testing aims to discover data such as design efficiency, maximum voltage and current levels, as well as maximum power values.

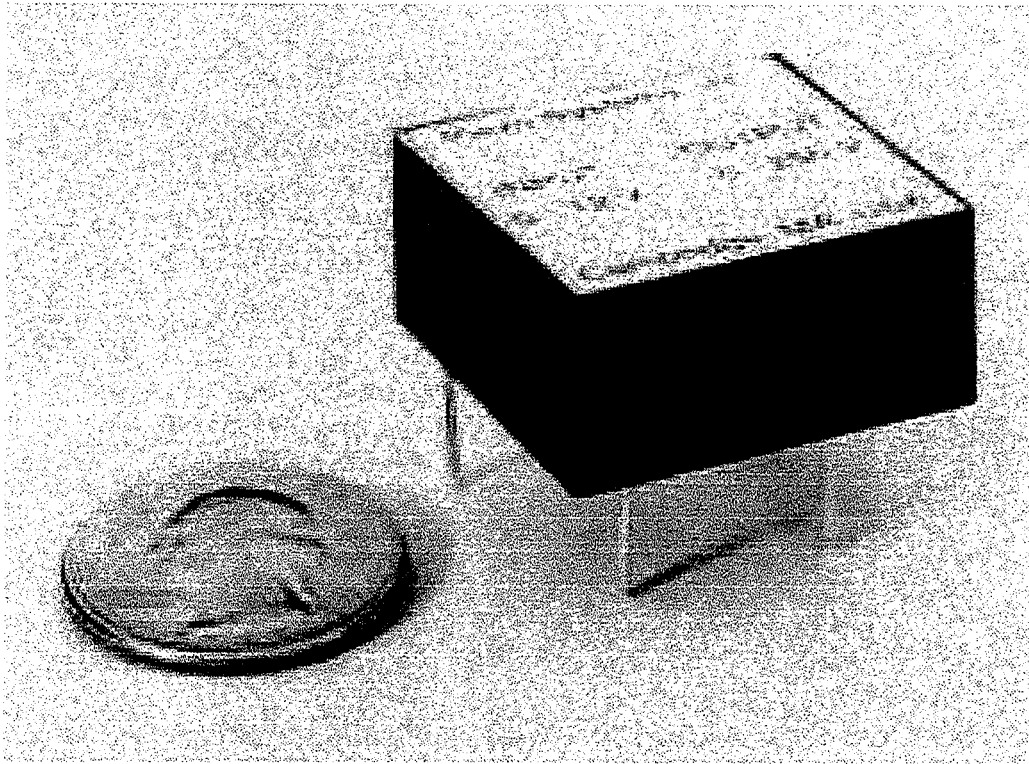


Figure 3 Morgan Matroc Proportional Voltage Booster

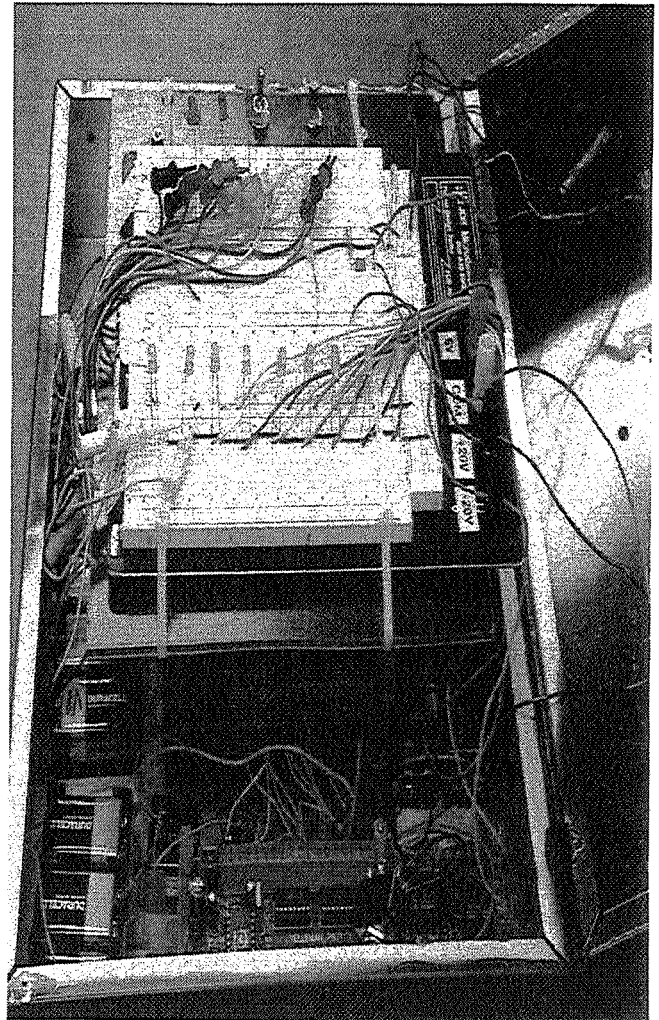
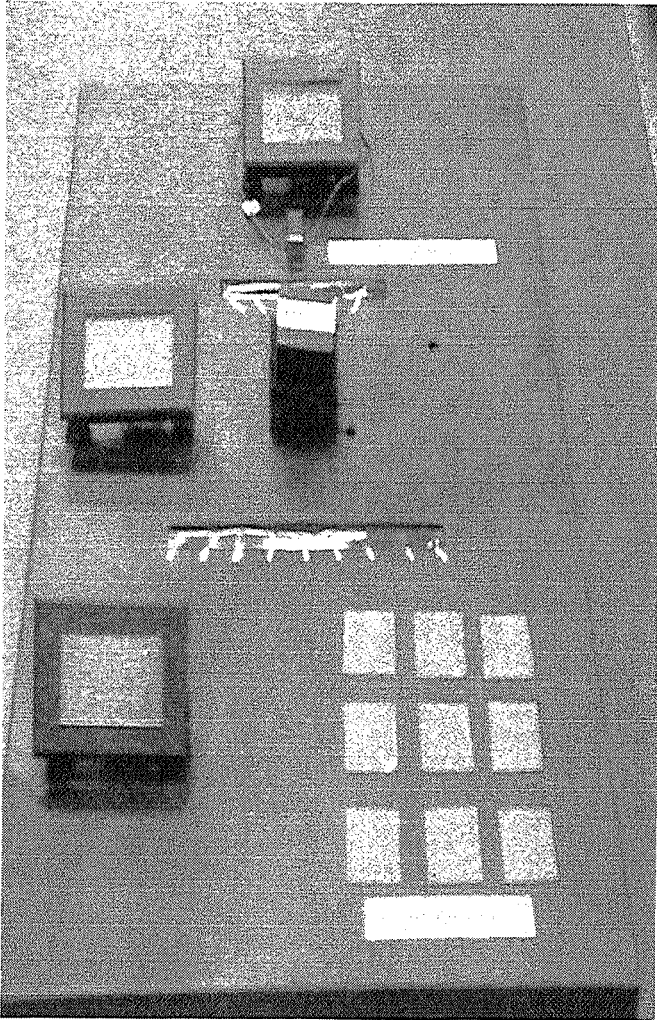


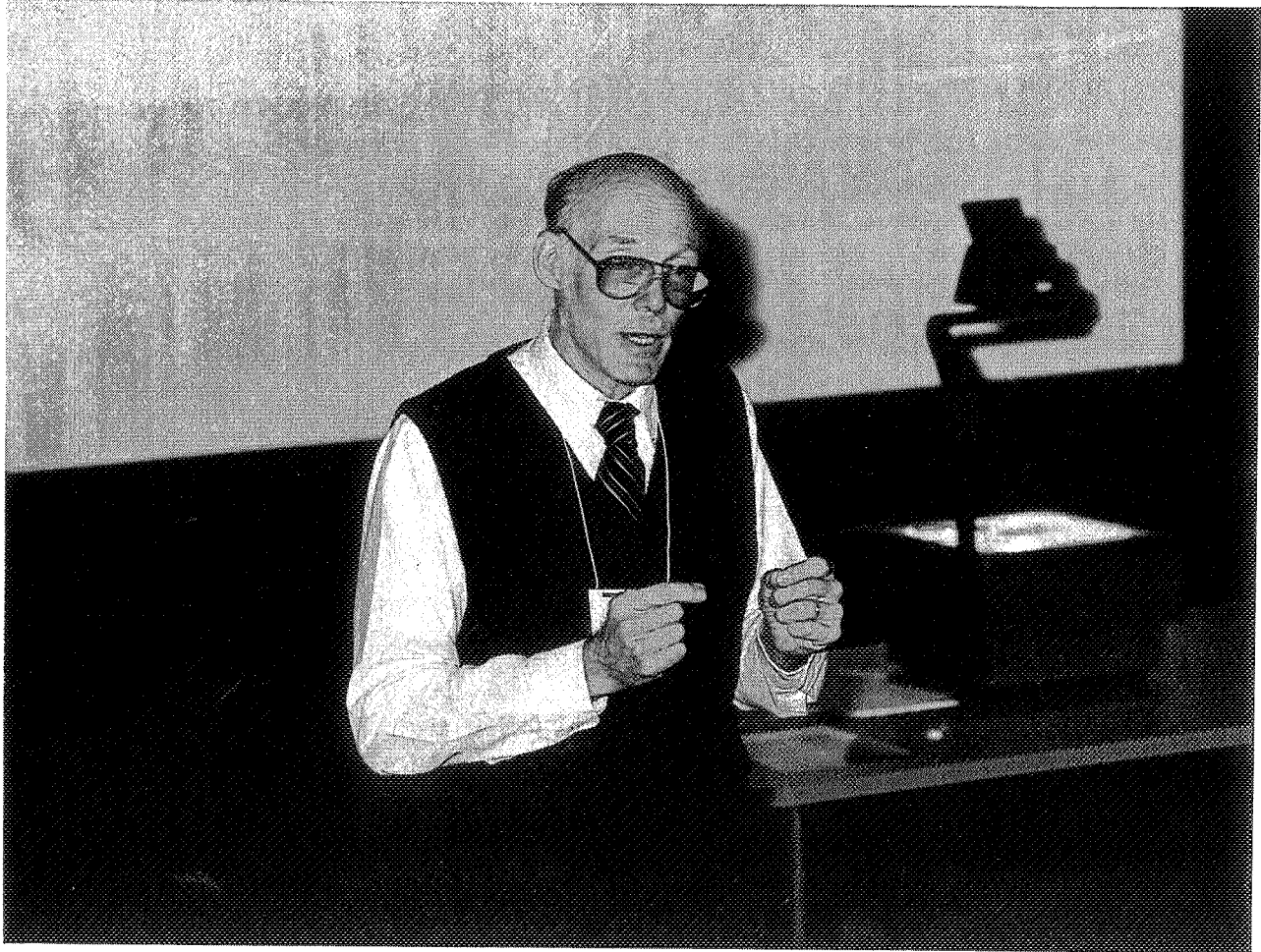
Fig. 4. Configuration of PAD/VUC System

STRETCHY "ELASTIC" BANDS III CONTAMINANT EFFECTS

Alan K. Karplus

Department of Mechanical Engineering
Western New England College
1215 Wilbraham Road
Springfield, Massachusetts 01119-2684

Telephone 413-782-1220
e-mail akarplus@wnec.edu



Alan K. Karplus

Stretchy “Elastic” Bands III Contaminant Effects

Alan K. Karplus
Department of Mechanical Engineering
Western New England College
Springfield, MA 01119-2684

Abstract:

Near constant rate loading and unloading of traditional number 33 rubber bands shows features which are unique to these elastic products, especially when a band is coated with a common household chemical. Tensile load - deflection tests are performed on a series of three and one half inch long rubber bands of 1/8 inch width in the “as-received” condition, coated with machine oil, castor oil, water, liquid hand soap, and talcum powder, respectively. Comparisons made include: 1. shape of loading and unloading paths for load/deflection plots, and 2. areas under stress/strain plots found by approximation. The applied load - deflection plots on the same graph show common features as well as differences due to coatings.

Key Words: Elastics, Tension Tests, Environmental Conditions

Prerequisite Knowledge: Have an idea about changes in the load an elastic band holds as it is stretched and unloaded and know that application of substances such as oils, soaps, and talcum powder can alter the load carrying capacity of some rubber bands.

Objective: To work as a team member in the collection of data, to make plots for near constant rate loading and unloading of traditional rubber bands, and to show features which are unique to these rubber band products in different conditions such as “as-received” condition, coated with a machine oil, liquid hand soap, or talcum powder.

Equipment:

1. A series of three and one half inch long rubber “elastic” bands of 1/8 inch width which are often referred to as number 33 rubber bands. Most office supply houses will stock these.
2. Yard Stick, or Tape measure or 30 inch long machinist’s measure.
3. Two, 2 inch size C - clamps.
4. Mounting board (2 in. by 1 in. by 30 inches) with a six penny nail inserted one inch from one end on the 2 inch by 30 inch face, and to which the machinist’s scale can be clamped. The zero of the machinist’s scale should be at the nail.

5. Vise to hold the mounting board.
6. Safety Goggles
7. Heavy work gloves
8. Load scale with a capacity to 10 pounds or 5 kg.
9. Micrometer or vernier caliper.
10. Household substances such as liquid hand soap, hydrogen peroxide, castor oil, machine cleaner oil and talcum powder.
11. Hand protection gloves, hand towels, and paper plates for coated rubber bands.
12. Half inch wide masking tape for making elastic band labels.
13. Data page with 25 lines with one line for a title and one line for units designation and twelve columns. Measurements are taken at one inch increments starting at a value of four inches listed in the first column. The next two columns are used to record load and unload while the remaining columns are used for computations of strain, stress, energy, etc. Be sure to label columns and include units of measure selected.
14. A Spreadsheet such as EXCEL™. All work performed on the spreadsheet can be done by hand.
15. When the computations are to be done by hand, computation paper and several pieces of linear graph paper with 20 divisions to the inch are needed.

Introduction:

Each rubber band is to be stretched at a near constant rate and unstretched at the same near constant rate while recording the load present at each stretch point. One team member does the loading and reads the load at each position while the second team member records the data. Try to load and unload the elastic at a constant rate, and about the same rate for each band so that meaningful comparisons between bands can be made. Both team members should work on the data analysis, make observations from the computations and plots, and formulate conclusions.

Testing and Load - Displacement Plot:

After the data has been collected and when a spreadsheet is used consider making a column of displacement that starts at four inches and ends at 24 inches. Then enter the loading at four inches and ends at 24 inches, and unloading that starts at 24 inches and returns to four inches. Increments of one inch are used. Enter the collected data into the spreadsheet and then make a plot for the entered displacement - load data.

Stress - Strain Plot:

At each displacement position make a computation for engineering strain and engineering stress. Engineering strain is the length (L) at any displacement minus a reference displacement (R) divided by the reference displacement (R) or $(L-R)/R$. Four (4) inches is chosen as the reference dimension (R) for this experiment. Engineering stress or (P/A) is the load (P) divided by the cross section area (A) of the band. Note that the band has two strands carrying load. Compute the strain and stress for the collected data. Make a second plot for the stress and strain found.

Hysteresis:

Compute increments for the area under the **LOADING** line separately from the **UNLOADING** line. This represents the energy used to stretch and unstretch the band. Now compute the area under the curves with trapezoidal increments; first the loading curve and then the unloading curve. A cell should be used to store each trapezoidal area increment. The trapezoidal increment is computed by forming the average of two stresses and multiplying by the change in strain. The total area under a curve can be found by adding the incremental areas in a column, and is the energy related to each curve. The difference between column totals found is the hysteresis. A ratio between this difference and the loading curve area when shown in percent finds the portion of energy lost to internal friction or hysteresis. Be sure to check **UNITS**.

Loading Data Ratio:

To learn about the constant loading rate and constant unloading rate, the loading rate ratio is computed when the change in loading (stress) values are divided by the change in displacement (strain) values for each increment. When this ratio is the same across increments, the rate is constant

Comparisons:

An informative comparison for rubber bands tested can be made by plotting and clearly labeling:

- A. the load deflection data for all elastics on one set of axes and
- B. the stress - strain data for all elastics on another set of axes.

Note how both the stress-strain plot curves compare favorably, how the load-displacement and stress-strain are comparable due to no changes in geometry of elastic bands evaluated, and how the percentage of energy allocated to hysteresis is seen to differ due to coatings while the load - displacement plot clearly shows the change in load carried by each band, again due to coatings applied to the elastic bands.

Once the above has been done for an "as-received" rubber band, select several common household materials such as machine oil, liquid hand soap, castor oil, talcum powder, and water, coat a new separate elastic band with each, and re - run the experiment with the coated band. Be sure to attach a label to each band. A piece of masking tape folded around the band and onto itself works nicely when the name of the contaminant is written on the label. When coating a band be sure to use hand protection gloves when immersing the band in a contaminant, and as appropriate, rubbing the contaminant into/onto the band.

Preparation:

Prepare the Mounting Board by placing a six penny nail into the 2 inch by 30 inch surface of the board one inch from the three surfaces at one end. Place the board into the vise and clamp the machinist's measure onto the top surface of the board. Clamps at six inches and 20 inches on the scale work well.

Figure 1 shows a possible set-up.

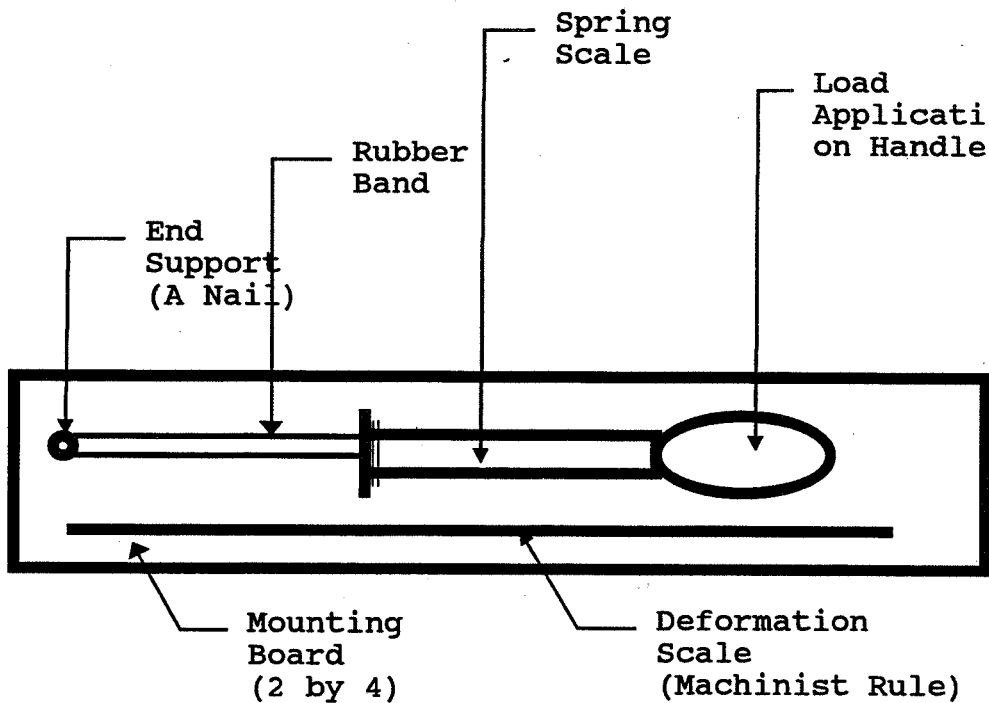


Figure 1
Example Test Apparatus Set-Up

Secure a rubber band for the size to be tested. A number 33 elastic band is selected. Measure the thickness and width of the band and record the results. Remember there are two strands of each band carrying load. Now compute the cross sectional area.

Prepare the data sheet with 25 lines and twelve columns. Add a title heading for each column on the first line and the units of the value on the next line. Leave a line empty and enter the first measurement. Load measurements are to be taken at one inch increments starting at a displacement value of four inches listed in the first column and end at the 24 inch position. The remaining columns are used in pairs to record loading and unloading for each elastic size. Be sure to label the load columns in pairs (LOADING and UNLOADING) and include units of measure selected. The first LOADING value is recorded in column two at the four inch position. A position is designated where the hook of the load scale attaches to the rubber band and is sited on the machinist's measure. The last LOADING value at 24 inches should be the FIRST UNLOADING value at 24 inches because the UNLOADING values are recorded for decreasing positions.

When the extension exceeds 20 inches for the larger bands you must make a *concentrated* effort to keep the current band under load. DO NOT UNLOAD or LOOSE LOAD on the scale on the loading because the band will be unloaded and the loading data will not be represent near constant rate loading. In case a band breaks when under test, COMPLETELY redo the test.

In preparation for a test run place a designated rubber band over the nail and through the hook of the load scale. Check that a load measurement can be made at the four inch mark on the machinist's measure. Be sure the operator of the load scale has safety glasses on and is wearing the heavy gloves.

These Safety Devices will protect the operator if the elastic breaks and the spring scale unloads and the elastic flies around. Be sure to have a four inch long piece of masking tape available to label the condition of the elastic band tested.

Procedure:

1. Tests:

Tensile load - deflection tests are to be performed on a series of number 33 rubber bands that are three and one half inch long and 1/8 inch wide. **Place safety glasses and gloves on the spring scale operator, prepared band AR on the loading apparatus, and prepare the record for writing the data on the data sheet.** The approach is to stretch a band and as this is done, at a near constant rate, record the load required to stretch the rubber band at each added inch. Start at four inches, which is one-half an inch past the three and one-half inch length of the rubber band. Continue until the length of the band is 24 inches. Next, unload the band at the same rate as was used to load the band, taking load measurements at each inch of reduced length. Remember the load value at the 24 inch position is the same for the **LOADING** and **UNLOADING** columns on the data sheet. The recorded data is defined as "raw data" for the "as-received" number 33 rubber band tested. "As-received" refers to the condition of the rubber band as it comes from the package. Be sure to label the rubber band tested "as-received", or **AR**, with a piece of masking tape placed around a leg of the band and taped onto itself with the name **AR** written on it, and then measure and record its elastic band width and thickness.

2. Load - Displacement Plots:

The first comparison to be made is for the shape of loading and unloading paths for load/displacement data. Enter the displacement data which starts at four inches and ends at 24 inches. At each displacement level, enter the load. Make an **XY¹** or **Scatter Plot** of the data. The horizontal axis should be Displacement in inches while the vertical axis is Load in pounds. Label the Load - Displacement line as **AR**.

Repeat the load-displacement test for each of the remaining coated rubber bands, plot the data on the **SAME** graph as for **AR** and label each curve as Band-Ade Machine Cleaner (**BA**), Castor Oil (**CO**), Liquid hand Soap (**S**), and Talcum Powder (**T**). Be sure to use hand protection gloves when coating bands, as appropriate.

The applied load - displacement plots on the same graph show magnitude changes. The largest load carried by each band should be clearly evident on the right hand end of the displacement axis at 24 inches. Note if a trend appears which shows which coating impacts the loading features the most.

3. Stress - Stain Plots:

The second comparison is dependent on two modifications made to the raw data. The first modification is to define the engineering strain as the ratio computed by taking the measured band displacement minus the starting displacement and dividing this quantity by the initial displacement.

¹ Be sure to make a plot of two variables and NOT a line chart as is the usual default setting on a spreadsheet.

For all samples use four inches as the initial displacement. This means that the first value of strain is zero with UNITS of inches/inch. The strain is to be plotted on the horizontal axis.

The second data modification is to divide the load by the cross-sectional area of the original rubber band. This computes the engineering stress in the band which has UNITS of pounds per square inch in the English system and is to be plotted on the vertical axis.

Again prepare an **XY** or **Scatter Plot** with the modified data. This will be a stress-strain plot for the uncoated rubber band. Label the line on the plot with the selected symbol such as **AR**.

Repeat the strain and stress calculations for the different coatings, make separate stress-strain plots for each, and add this data to the same stress-strain plot for **AR Elastic 33**. Be sure to label each line. Note the similarities between these curves. If the effect of initial elastic length and original cross sectional area are considered, the strain range of 5 times or 500 percent is the same for each rubber band and the stress ranges are changed due to the coatings, however, the "characteristic shape" of the curve does not appear to change significantly due to the coating.

4. Hysteresis:

Areas under each of the stress/strain curves are to be found by approximation. An approach is to represent the area between strain values as a trapezoid and to sum the areas of all the trapezoids to obtain the area under the **LOADING** line. The summing of trapezoids is repeated for the **UNLOADING** line. Note that the trapezoid has a 'height' in stress units of pounds per square inch and that the 'width' of the trapezoid has strain units of inches per inch. The product of stress times strain becomes inch-pounds per cubic inch. In summary, the difference between these sums is the residual often referred to as hysteresis. The hysteresis represents the energy consumed in the displacement process.

What can be presented about the energy differences between the **AR** and coated rubber bands? A rapid visual comparison is found when either the load-displacement (or the stress-strain plots) are super-imposed on one another. The plots show the common features such as the **LOADING** line differences such as and similarities for the **UNLOADING** lines between the coated rubber bands from four to 24 inches (or zero to 500 percent strain). Note that the area term represents **ENERGY**. When English units are used, the product of pounds times inches becomes in.- lbs. For the load-displacement plot (and for the stress-strain plot pounds per square inch times inches per inch becomes inch-pounds per cubic inch).

What relationship can be found between **LOADING** energy, **UNLOADING** energy, and hysteresis for the **AR** and various rubber band coatings? A summary table of rubber band coating with columns of maximum load and energy for **LOADING** and **UNLOADING** lines, and hysteresis can show that about half the energy is assigned to hysteresis for the **AR** condition.

5. Loading Rate Ratio:

Compute the loading rate ratios for each LOADING and UNLOADING line based on each displacement increment to learn about the constant loading rate and constant unloading rate. The loading rate ratio is computed when the change in loading (stress) values are divided by the change in displacement (strain) values for each increment. When this ratio is the same across increments, the rate is constant

Comments:

1. To aid the instructor in the execution of this experiment, a sample for Elastic 33 is shown below. **Figure 2** presents the data collected in columns one through three from the left and ensuing calculations in columns four through 12. Note the starting position for displacement at 4 inches with loading values to 24 inches and 24 inches to 4 inches. In **Figure 3** the loading and unloading curves are seen. **Figure 4** presents the stress-strain plot while in **Figure 2** are found the strain values in column four, loading stress, unloading stress in columns five and six and the trapezoidal areas between strain increments in columns seven and eight with energy values summed in the next two columns. The last two columns contain the rate of loading ratios.

To make a hand calculation for the 6 inch displacement: A. strain $[(L-R)/R]$ is $(6-4)/4 = 0.5$ and B. the loading stress (P/A) is 0.500 pounds / 0.0085 in. sq. or 58.82 psi. as seen in column five from the left in **Figure 2**. In column seven of **Figure 2** is C. the area under a part of the loading curve as 11.03 in.-lb. per cubic inch which is found by averaging 29.41 and 58.82 = $(88.23/2 = 44.12)$ psi. and multiplying 44.12 psi. by 0.25 in./in. which is the change in strain increment. For the incremental download the energy computed is 3.68 in.-lb./cubic inch shown in column eight and is found by averaging 29.41 and 0.00 and multiplying by 0.25. In column 11 is the loading rate ratio or $(59.82 \text{ psi.} - 29.21 \text{ psi.}) / 0.25 \text{ in./in.} = 117.65 \text{ psi.}$

A comparison of the total download energy of 591.91 in.-lb./cubic inches (found by adding all the incremental energies) to the loading value of 1119.49 in.-lb./ cubic inch shows a ratio of 0.5287 or 53 percent. The hysteresis value is likewise 47 percent which represents the energy consumed as shown at the bottom of the **figure 2**. **Figure 3** shows the stress-strain plot for the AR (as received) Number 33 elastic band. Note the similarity to **Figure 2**. The difference is the scales. Stress rather than load and strain rather than displacement are used. Since the same geometry elastic band is used for all bands in this experiment, future comparisons will be made with the load-deflection data which is collected and recorded data. Above the energy calculation was presented for stress - strain values. However, similar findings can be obtained with load - displacement values as follows: $(0.50 \text{ lbs.} + 0.25 \text{ lbs.})/2$ times one inch = 0.375 in. lbs. The percent hysteresis will be the same namely 100 times $(38.06 \text{ in.lbs.} - 20.13 \text{ in.lbs.}) / 38.06 \text{ in.lbs.} = 47.1\%$. A similar approach is used for the loading rate ratios. In place of the 117.65 psi. the value of the loading rate ratio is $(0.50 \text{ lbs.} - 0.25 \text{ lbs.}) / \text{one inch or } 0.25 \text{ lbs./in.}$

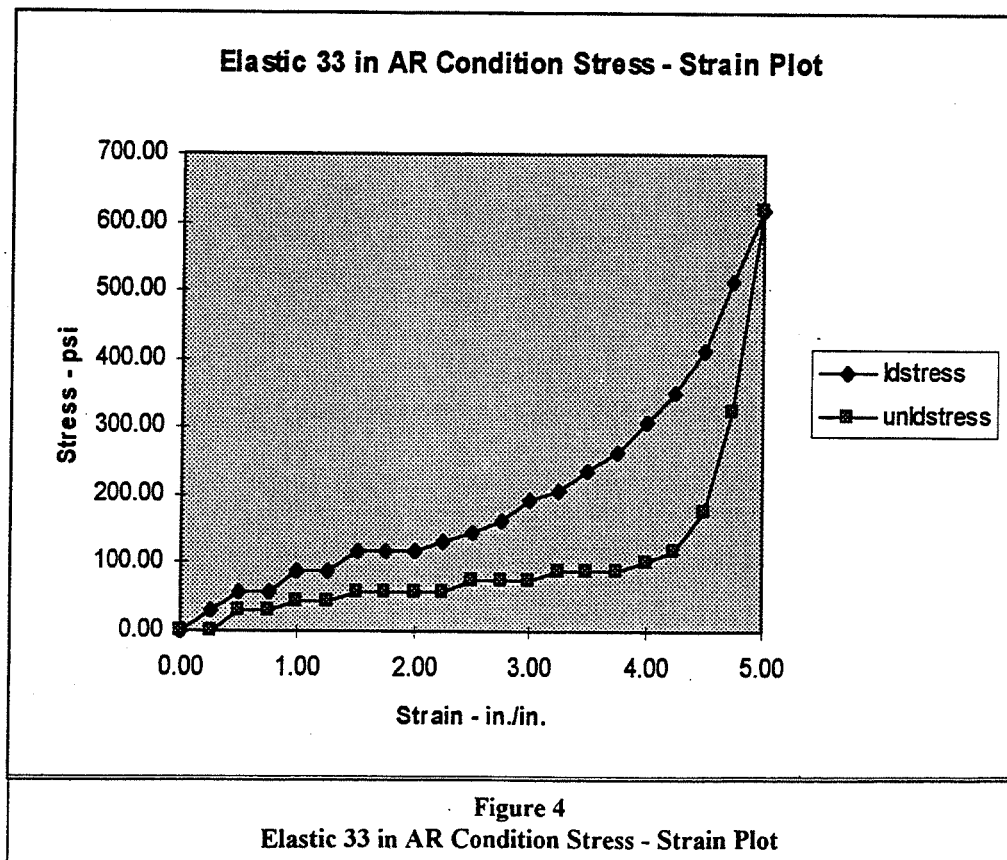
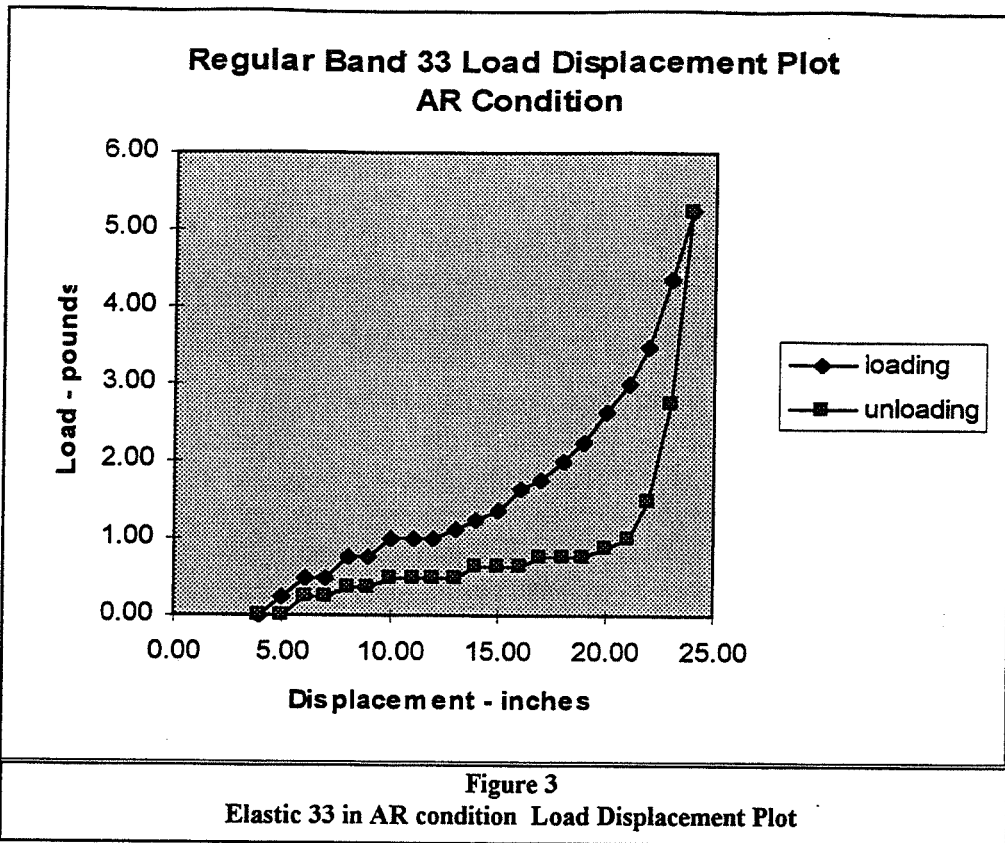
Stretchy"Elastic"Bands III - 33 with Gina

Cross section is 0.125 in. by 0.034in. with 2 tendons
 Cross section area = 0.0085 in.^2

Regular Band			AR Condition								
Displm't	Load	Unload	Strain	Up stress	Dw stress	Inwk up	Inwk dw	Work up	Work dw	Rate up	Rate dw
inches	pounds	pounds	in/in	psi	psi	in-lb per in^3	in-lb per in^3	in-lb per in^3	in-lb per in^3	psi	psi
4.00	0.00	0.00	0.00	0.00	0.00	0.00	0.00	0.00	0.00	0.00	0.00
5.00	0.25	0.00	0.25	29.41	0.00	3.68	0.00	3.68	0.00	117.65	0.00
6.00	0.50	0.25	0.50	58.82	29.41	11.03	3.68	14.71	3.68	117.65	117.65
7.00	0.50	0.25	0.75	58.82	29.41	14.71	7.35	29.41	11.03	0.00	0.00
8.00	0.75	0.38	1.00	88.24	44.12	18.38	9.19	47.79	20.22	117.65	58.82
9.00	0.75	0.38	1.25	88.24	44.12	22.06	11.03	69.85	31.25	0.00	0.00
10.00	1.00	0.50	1.50	117.65	58.82	25.74	12.87	95.59	44.12	117.65	58.82
11.00	1.00	0.50	1.75	117.65	58.82	29.41	14.71	125.00	58.82	0.00	0.00
12.00	1.00	0.50	2.00	117.65	58.82	29.41	14.71	154.41	73.53	0.00	0.00
13.00	1.13	0.50	2.25	132.35	58.82	31.25	14.71	185.66	88.24	58.82	0.00
14.00	1.25	0.63	2.50	147.06	73.53	34.93	16.54	220.59	104.78	58.82	58.82
15.00	1.38	0.63	2.75	161.76	73.53	38.60	18.38	259.19	123.16	58.82	0.00
16.00	1.63	0.63	3.00	191.18	73.53	44.12	18.38	303.31	141.54	117.65	0.00
17.00	1.75	0.75	3.25	205.88	88.24	49.63	20.22	352.94	161.76	58.82	58.82
18.00	2.00	0.75	3.50	235.29	88.24	55.15	22.06	408.09	183.82	117.65	0.00
19.00	2.25	0.75	3.75	264.71	88.24	62.50	22.06	470.59	205.88	117.65	0.00
20.00	2.63	0.88	4.00	308.82	102.94	71.69	23.90	542.28	229.78	176.47	58.82
21.00	3.00	1.00	4.25	352.94	117.65	82.72	27.57	625.00	257.35	176.47	58.82
22.00	3.50	1.50	4.50	411.76	176.47	95.59	36.76	720.59	294.12	235.29	235.29
23.00	4.38	2.75	4.75	514.71	323.53	115.81	62.50	836.40	356.62	411.76	588.24
24.00	5.25	5.25	5.25	617.65	617.65	283.09	235.29	1119.49	591.91	205.88	588.24

% Hysteresis = 47.13

Figure 2
 Collected Data and Computed Values for Elastic Band 33 in AR Condition



2. For a selection of bands wiped with a contaminant and tested and compared to the AR elastic band, the following: Liquid hand soap called Cormatic Soap from Georgia Pacific, Atlanta, GA 30306, increased the stress applied at 500 percent strain by forty-one percent, talc called Avon Bird of Paradise Perfumed Talc from Avon Products, Inc., N.Y., NY increased the load about ten percent while castor oil from CVS or Consumer Value Stores of Woonsocket, RI 02805 decreased the load about 20 percent while the Lenox Band-Ade Machine Cleaner from American Saw and Manufacturing Company of East Longmeadow, MA 01028 decreased the maximum load to 4.50 pounds or by 14% of the AR band. From figure 5 a plot of the load deflection curves for these cases shows the loading lines differ markedly with the 'highest curve for the liquid hand soap (S), decreasing to talc (T), the AR band, the Machine Cleaner (BA) and to the castor oil (CO) coated band. The total energy under the loading curves vary from 1182 in.-lb./in.^3 or 106% of the AR band for liquid hand soap to 95 percent of the AR band for talc to 75% of the AR for the machine cleaner and 761 in.-lb./in.^3 or 68 percent of the AR band for the castor oil. From Figure 5 it can be seen that after an initial load release the majority of the unloading lines appear to coincide. The hysteresis values are 52.3, 50.0, 48.8, 47.1, and 43.0 percent respectively for the liquid hand soap, talc, machine cleaner, "as-received" and castor oil coatings.

**** It is noted that no group runs to select an "average" or typical stretchy "elastic" band with a given coating have been made. The numbers presented here and the number you obtain will most likely be different. ****

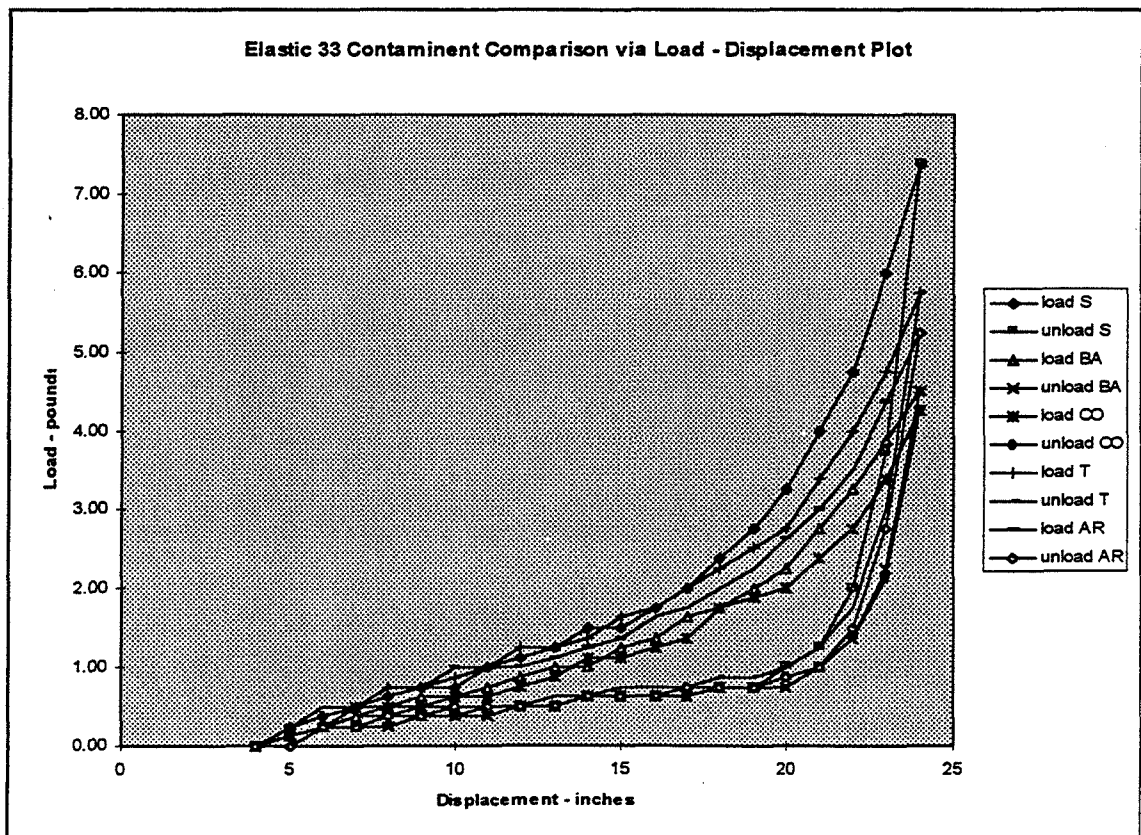
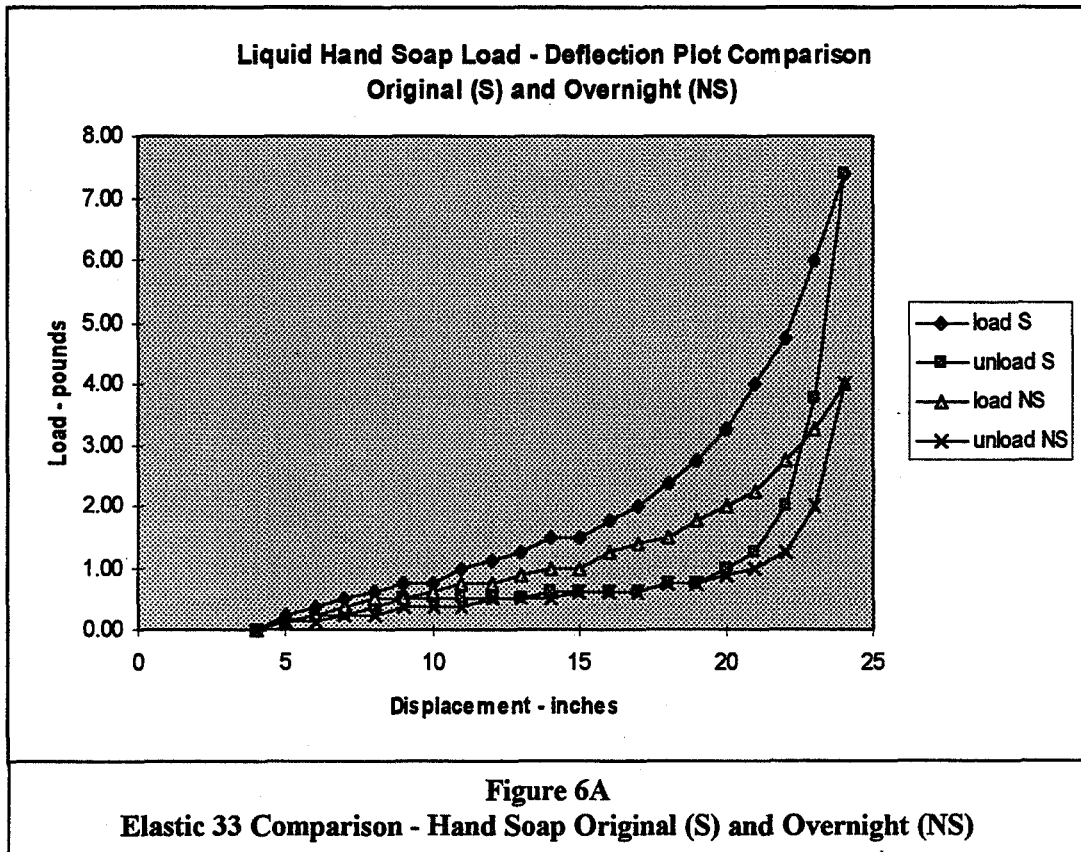


Figure 5
Elastic 33 Comparison of Contaminants
(S - hand soap, BA - machine cleaner, CO - castor oil, T - talc, AR - 'as-received' condition)

- Application of contaminants when left on the band prior to testing for 24 hours (one day designated by N) change the findings as shown in figures 6A, 6B, 6C, and 6D for the liquid hand soap (NS), talc (NT), machine cleaner (NB), and castor oil (NC), respectively. The overnight soaking produce new maximum loads which compare to the original maximum loads as follows: 54% for the hand soap, 104% for the talc, 147% for the machine cleaner, and 88% for the castor oil. Hysteresis values for the overnight load-deflection data are 44%, 49%, 50%, and 44% for the hand soap, talc, machine cleaner, and castor oil, respectively.

There are some notable items over the 24 hour period. The castor oil and the talc appear to maintain their respective impacts. This is interesting because talc is often used to coat a bicycle tire tube and its companion tire casings to improve compatibility while castor oil is used to lubricate the elastic rubber band used in an elastic rubber band powered model airplane to obtain longer flights by providing more turns in the powering band. For the liquid hand soap, it appears that the carrier for the soap has dried reducing the impact of this coating on the band. On the other hand, the machine cleaner appears to alter the elastic band such that after 24 hour soaking it becomes 'stronger'.



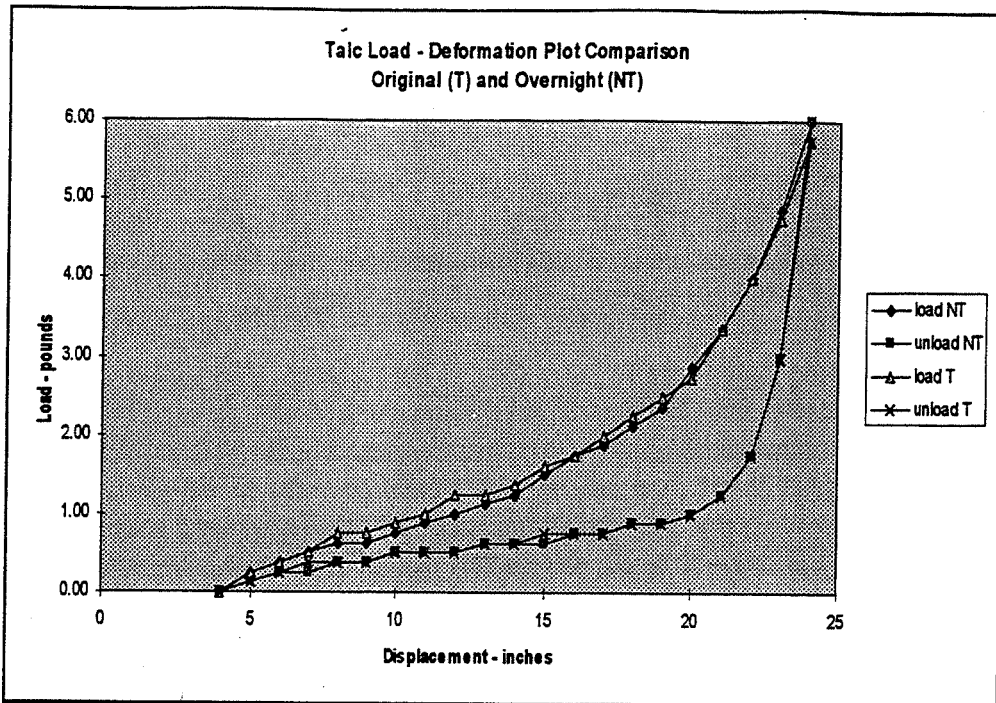


Figure 6B
Elastic 33 Comparison - Talc Original (T) and Overnight (NT)

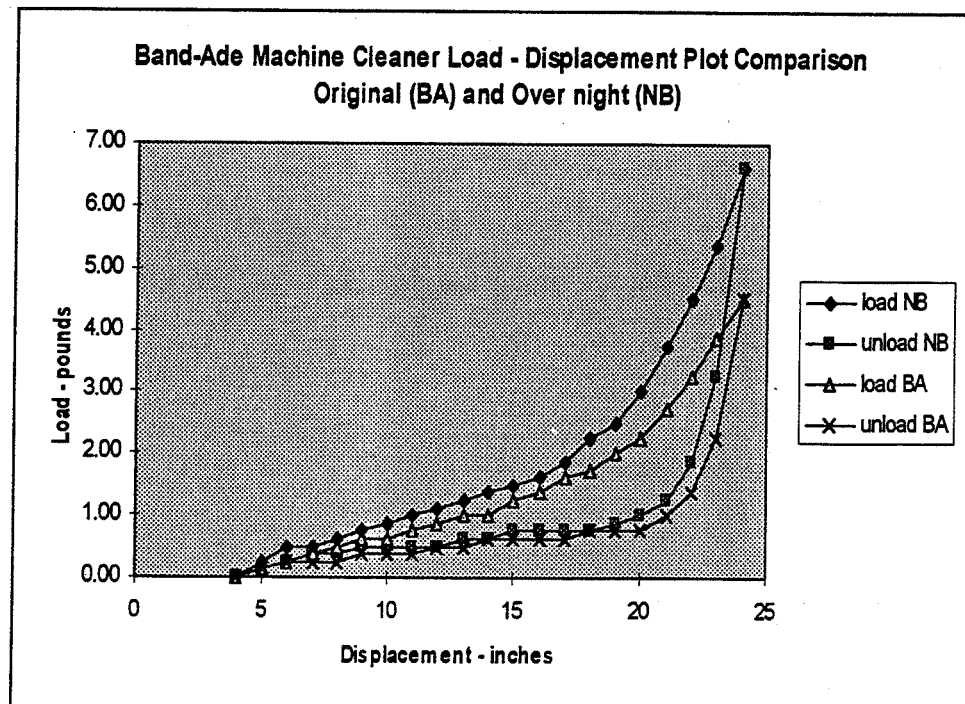
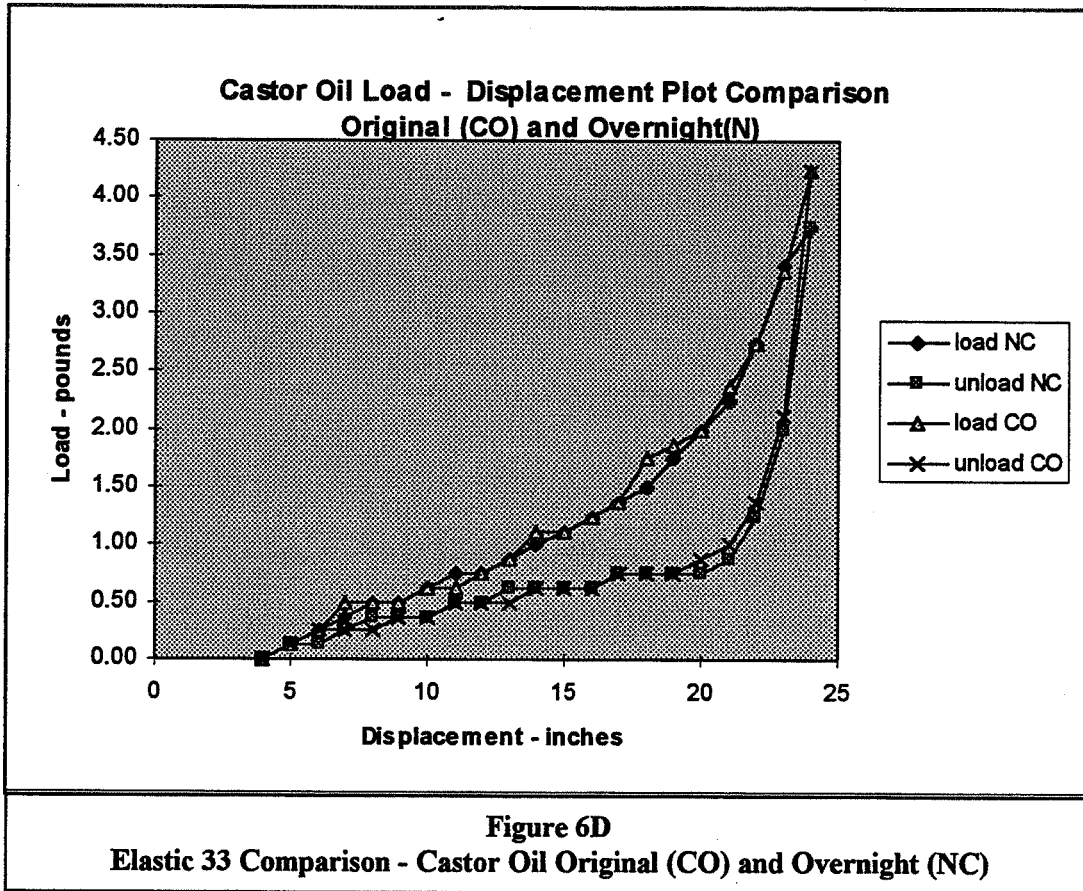


Figure 6C
Elastic 33 Comparison - Band - Ade Machine Cleanerl Original (BA) and Overnight (NB)



4. To provide added perspective a 1/16, 1/4 and 1/2 inch wide or number 19, 64, and 84 rubber bands can be tried with various coatings. The number 19 rubber band has not always attained the 500 percent elongation which the number 33, 64, and 84 bands achieve. It breaks! On the other hand, number 19 adds a fourth elastic to the data base. Information on the changes in 'as-received' elastic bands of varying cross-section but constant length can be found in Stretchy "Elastic" Bands which is part of NEW UPDATE '97, and changes due to evaluating constant cross-section bands of varying length can be found in Stretchy "Elastic" Bands II which is part of NEW UPDATE '98.

Acknowledgments:

The author is appreciative of the assistance provided by Mr. Richard DeCelle, Mechanical Laboratory Technician, in the finding of various rubber bands, selection of load scales, and the recording of data. Gina Ferrera, a junior WNEC electrical engineering student, assisted with several trials and made helpful suggestions as we prepared and analyzed test findings.

Bibliography:**ALAN K. KARPLUS**

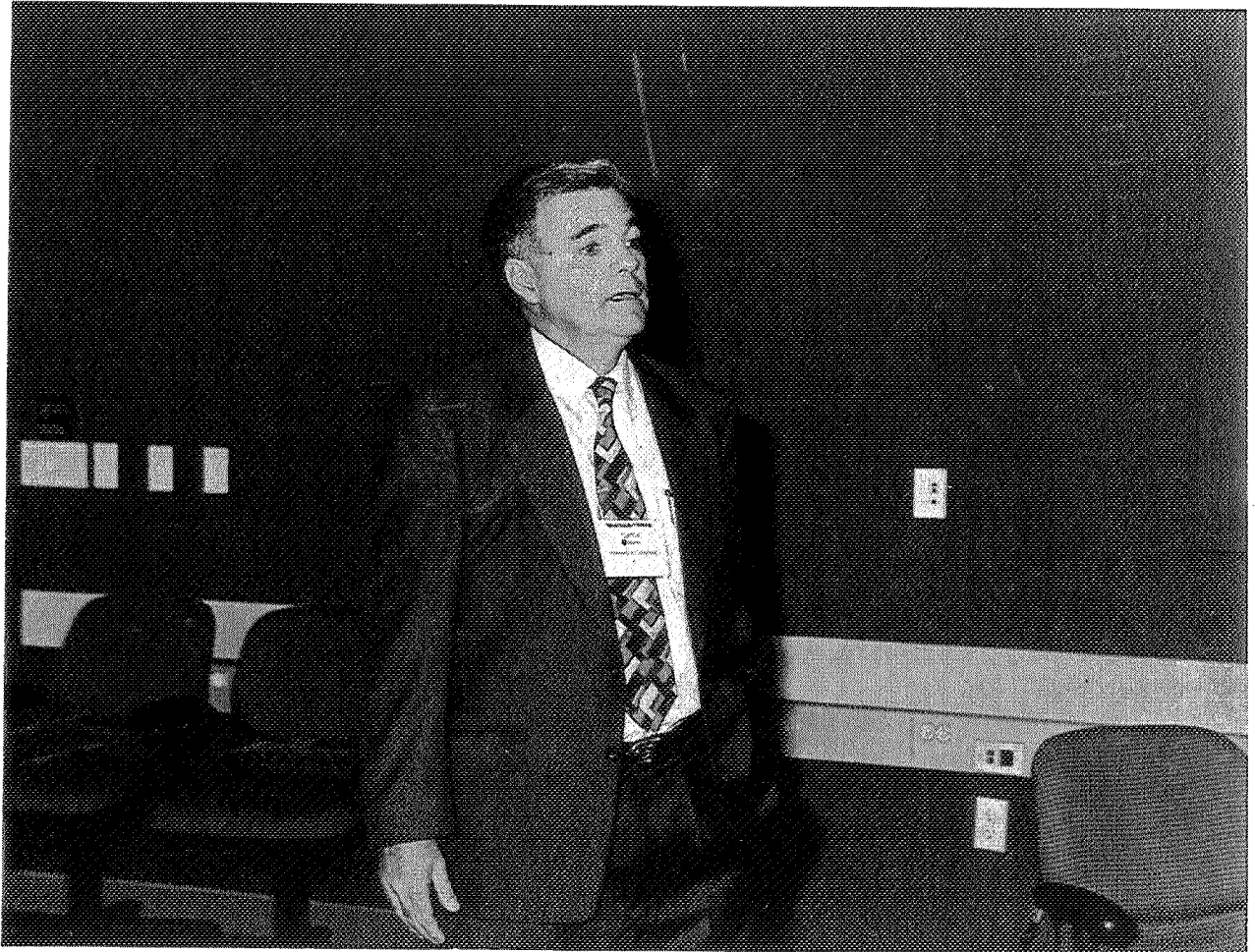
Alan K. Karplus is Professor of Mechanical Engineering at Western New England College, Springfield, Massachusetts. He has a Bachelor's degree from Tufts College, a Master's degree from Iowa State University and a Ph.D. from Colorado State University. He has been involved with the freshman engineering program, coordinates the senior mechanical engineering laboratory program, has taught Materials Science and supervises M.E. Senior Projects. His interests include materials and design. He is a member of ASME and ASEE. He has contributed to the National Educators' Workshop and ASEE Annual Conference for several years.

GALVANOSTATIC POLARIZATION CURVES FOR TEACHING PURPOSES PART II

Carlos E. Umana

Department of Materials
School of Mechanical Engineering
University of Costa Rica
San Jose, Costa Rica

Telephone: 506-207-4548
e-mail caruma@terraba.fing.ucr.ac.cr



Carlos E. Umana

GALVANOSTATIC POLARIZATION CURVES FOR TEACHING PURPOSES

PART II

Carlos E. Umaña
Departamento de Materiales
Escuela de Ingeniería Mecánica
Universidad de Costa Rica
San José, Costa Rica

KEY WORDS: Activation polarization, Tafel slopes and resistance polarization method.

PREREQUISITE KNOWLEDGE: A complete knowledge of the theory and experimental work involved in the first part of this experiment (Ref.1).
A basic course on calculus.

OBJECTIVES:

1. To introduce the basic concepts of the polarization resistance method (Ref. 2).
2. To use the polarization resistance method as a way to improve the exactness of the anodic Tafel slope.

EQUIPMENT AND SUPPLIES:

All the items listed in the first part (Ref.1).

Additionally:

1. A fine carbon steel brush
2. A brand new soft toothbrush
3. A stereomicroscope (15X magnification will be enough)

INTRODUCTION:

The first part of this experiment was presented at the NEW Update 98. In this second part polarization curves for mild steel are obtained following the same basic steps as in the first part but including the current range from 1 to 10 $\mu\text{A}/\text{cm}^2$. The low range data is used to introduce and apply the polarization resistance method. This method consists in plotting on a linear scale the lower anodic and cathodic overpotential values (ε) versus applied current density (i_{appl}) in order to obtain graphically the $\Delta\varepsilon/\Delta i_{\text{appl}}$ slope as ε approaches zero. This slope value is related with both the anodic and the cathodic Tafel slopes (β_a and β_c) and the corrosion current density (i_{corr}) by the polarization resistance equation as follows:

$$R_p = \left(\frac{\Delta\varepsilon}{\Delta i_{\text{appl}}} \right)_{\varepsilon \rightarrow 0} = \frac{\beta_a \beta_c}{2.3 i_{\text{corr}} (\beta_a + \beta_c)} \quad (1)$$

Where: R_p = polarization resistance

The demonstration of this equation is presented in the Appendix. The polarization resistance method is a technique normally used to estimate the corrosion current density without knowing the actual Tafel slopes. This is done by assuming common Tafel values. However in this work polarization resistance will be used

to improve the exactness of the anodic Tafel slope by assuming that the cathodic Tafel slope, the corrosion current density and the slope $(\Delta\varepsilon/\Delta i_{\text{appl}})_{\varepsilon \rightarrow 0}$ are more reliable experimental values than the anodic Tafel slope (Ref.2). From equation (1) an expression for β_a is obtained as shown below:

$$\beta_a = \frac{2.3R_p i_{\text{corr}} \beta_c}{(\beta_c - 2.3R_p i_{\text{corr}})} \quad (2)$$

In this way the main electrochemical techniques used in corrosion evaluation and control are introduced by performing simple but well based laboratory experiments.

PROCEDURE:

The same steps as in the first part except for the following points (the step numbers used here are the former numbers used in the procedure of the first part):

Step 3. To take into account surface defects and irregularities use a fine carbon steel brush to clean the surface before wet grinding with 240-400 grits SiC paper. Use a soft toothbrush to clean irregularities after wet polishing with 600 grits SiC paper.

Control the surface condition by using a stereomicroscope.

Each test requires a new working electrode surface or a new specimen.

Step 11. The data sheet is modified to include the lower experimental values.

Step 17. The open circuit potential E_{corr} is not necessarily -520 mv as in the first part. In this case a potential of $E_{\text{corr}} = -500$ mv was obtained.

Step 19. It takes around 80 minutes to complete each experiment for the cathodic or the anodic connection.

An additional step consists in plotting on a linear scale overpotential values (ε) versus applied current density i_{appl} for the 0-10 $\mu\text{A}/\text{cm}^2$ range in order to obtain the slope $(\Delta\varepsilon / \Delta i_{\text{appl}})_{\varepsilon \rightarrow 0}$.

EXPERIMENTAL RESULTS:

Table I show the values obtained in one polarization test and Figure 1 presents the cathodic and anodic curves and the Tafel extrapolations.

The corrosion potential is $E_{\text{corr}} = -500$ mv and the cathodic and anodic curve extrapolation corresponding to Tafel behavior give a corrosion current density of $i_{\text{corr}} = 19 \mu\text{A}/\text{cm}^2$. The cathodic Tafel slope is $\beta_c = -512$ mv/decade (1 cycle = decade) and the anodic Tafel slope is $\beta_a = 62$ mv / decade.

The overpotential values for low current density range are presented in Table II. Figure 2 shows a plot of these values from which it is graphically determined that $(\Delta\varepsilon / \Delta i_{\text{appl}})_{\varepsilon \rightarrow 0} \approx 3 \times 10^3 \Omega \cdot \text{cm}^2$.

Applying equation (2) gives a new value of $\beta_a = 176$ mv / decade, which corresponds to the modified anodic Tafel slope. The new anodic curve is shown in Figure 1. (Figures 1 and 2 were obtained using MATLAB[®] with Simulink V4.0, The MathWorks, Inc.).

Table I. Polarization Data Sheet

TEST N° 3 DATE 08/05/99
 REFERENCE ELECTRODE SCE
 WORK ELECTRODE Mild Steel Bolt AREA 1 cm²
 AUXILIARY ELECTRODE Graphite AREA 2 cm²
 ELECTROLYTE 20 g NaCl / 1liter DW pH _____ TEMP. 22 °C
 ELECTROLYTE TREATMENT
Boiled for 20 minutes, allowed to cool and N₂ bubbling to dissolve NaCl

CATHODIC REACTION

Corrosion Potential : $E_{corr} = -500$ mv

Initial time : 10:45 a.m. Final time : 12:10 p.m. Notes Final Resistance 39.2 KΩ

N°	1	2	3	4	5	6	7	8	9	10
I μA	1	2	3	4	5	6	7	8	9	10
E mv	-504	-506	-509	-510	-512	-516	-518	-521	-522	-524
N°	11	12	13	14	15	16	17	18	19	20
I μA	15	20	25	30	35	40	50	60	70	80
E mv	-539	-557	-574	-602	-624	-656	-704	-740	-774	-815
N°	21	22	23	24	25	26	27	28	29	30
I μA	90	100	125	150	175	200	250	300	350	400
E mv	-855	-891	-936	-975	-1008	-1029	-1054	-1074	-1091	-1105
N°	31	32	33	34	35	36	37	38	39	40
I μA	450	500	600	700	800	900	1000			
E mv	-1114	-1126	-1143	-1155	-1166	-1177	-1187			

ANODIC REACTION

Corrosion Potential : $E_{corr} = -500^*$ mv

Initial time: 4:45 p.m. Final time: 6:05 p.m. Notes: Final Resistance 41.1 KΩ. *After 87 Minutes

N°	1	2	3	4	5	6	7	8	9	10
I μA	1	2	3	4	5	6	7	8	9	10
E mv	-497	-494	-491	-491	-488	-487	-485	-484	-483	-481
N°	11	12	13	14	15	16	17	18	19	20
I μA	15	20	25	30	35	40	50	60	70	80
E mv	-475	-470	-466	-463	-460	-458	-454	-450	-448	-446
N°	21	22	23	24	25	26	27	28	29	30
I μA	90	100	125	150	175	200	250	300	350	400
E mv	-446	-447	-442	-438	-435	-432	-427	-422	-418	-416
N°	31	32	33	34	35	36	37	38	39	40
I μA	450	500	600	700	800	900	1000			
E mv	-414	-412	-407	-402	-398	-397	-395			

Table II. Anodic and Cathodic Overpotential for Low Current Density Values

Current Density $\mu\text{A}/\text{cm}^2$	Anodic Overpotential mv	Cathodic Overpotential mv
1	$-497 - (-500) = 3$	$-504 - (-500) = -4$
2	$-494 - (-500) = 6$	$-506 - (-500) = -6$
3	$-491 - (-500) = 9$	$-509 - (-500) = -9$
4	$-491 - (-500) = 9$	$-510 - (-500) = -10$
5	$-488 - (-500) = 12$	$-512 - (-500) = -12$
6	$-487 - (-500) = 13$	$-516 - (-500) = -16$
7	$-485 - (-500) = 15$	$-518 - (-500) = -18$
8	$-484 - (-500) = 16$	$-521 - (-500) = -21$
9	$-483 - (-500) = 17$	$-522 - (-500) = -22$
10	$-481 - (-500) = 19$	$-524 - (-500) = -24$

NOTES TO THE INSTRUCTOR:

1. Make sure that the aluminum-graphite connector contact surface is clean in order to have good electrical contact.
2. Repeatability requires a perfect control of the parameters involved. Even though it should be noticed that E_{corr} , β_c and i_{corr} differ a little from the values obtained for the experiment ran in the first part. These small changes are acceptable and in no way affect the validity of the experiment as a teaching aid.
3. It is important to observe by using a stereomicroscope the working electrode area before and after each test in order to establish the effect on the surface of each one of the following aspects:
 - a. Cathodic treatment.
 - b. Anodic treatment.
 - c. The shock wave effect of nitrogen bubbling.

REFERENCES:

1. Umaña, Carlos E.: Galvanostatic Polarization Curves for Teaching Purposes, NASA/ CP-1999-209549, National Educators' Workshop: Update 98, 1999.
2. Jones, Denny A.: Principles and Prevention of Corrosion, Second edition, Prentice Hall, Inc., 1996.

ACKNOWLEDGMENTS:

The author wishes to thank the Universidad de Costa Rica (Vicerretoría de Investigación), “La Fundación de la Universidad de Costa Rica para la Investigación” (FUNDEVI) and the Ministerio de Ciencia y Tecnología-Conicit for giving financial support to attend the NEW: Update 99.

The author also wishes to thank Prof. Mark Bloomfield for reviewing the grammar and vocabulary and Carlos Jiménez for helping in preparing this paper.

SOURCES OF SUPPLIES:

The same as in the first part (Ref.1).

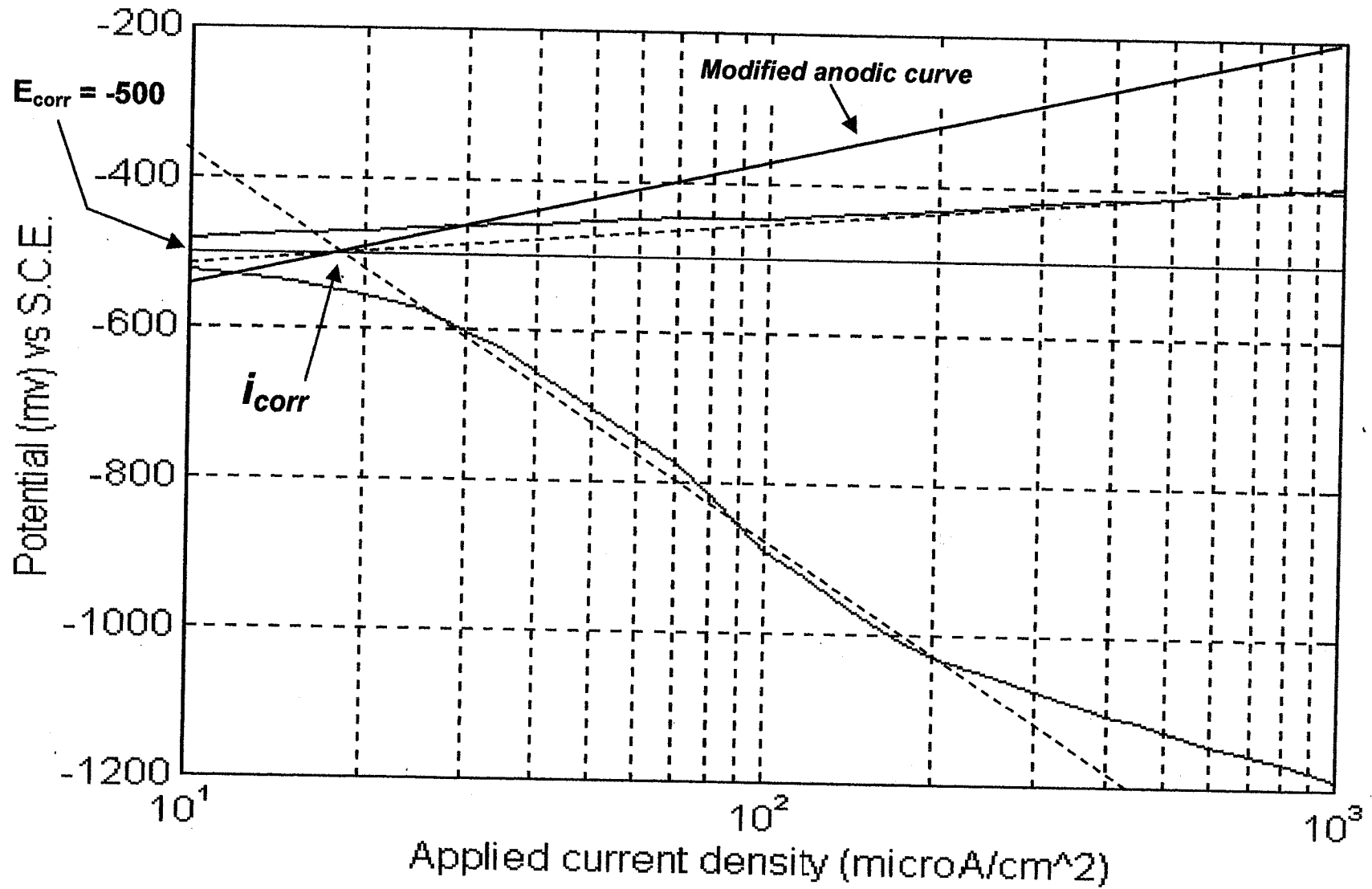


Figure 1. Experimental polarization curves for mild steel in a deaerated sodium chloride solution (20 g/liter).

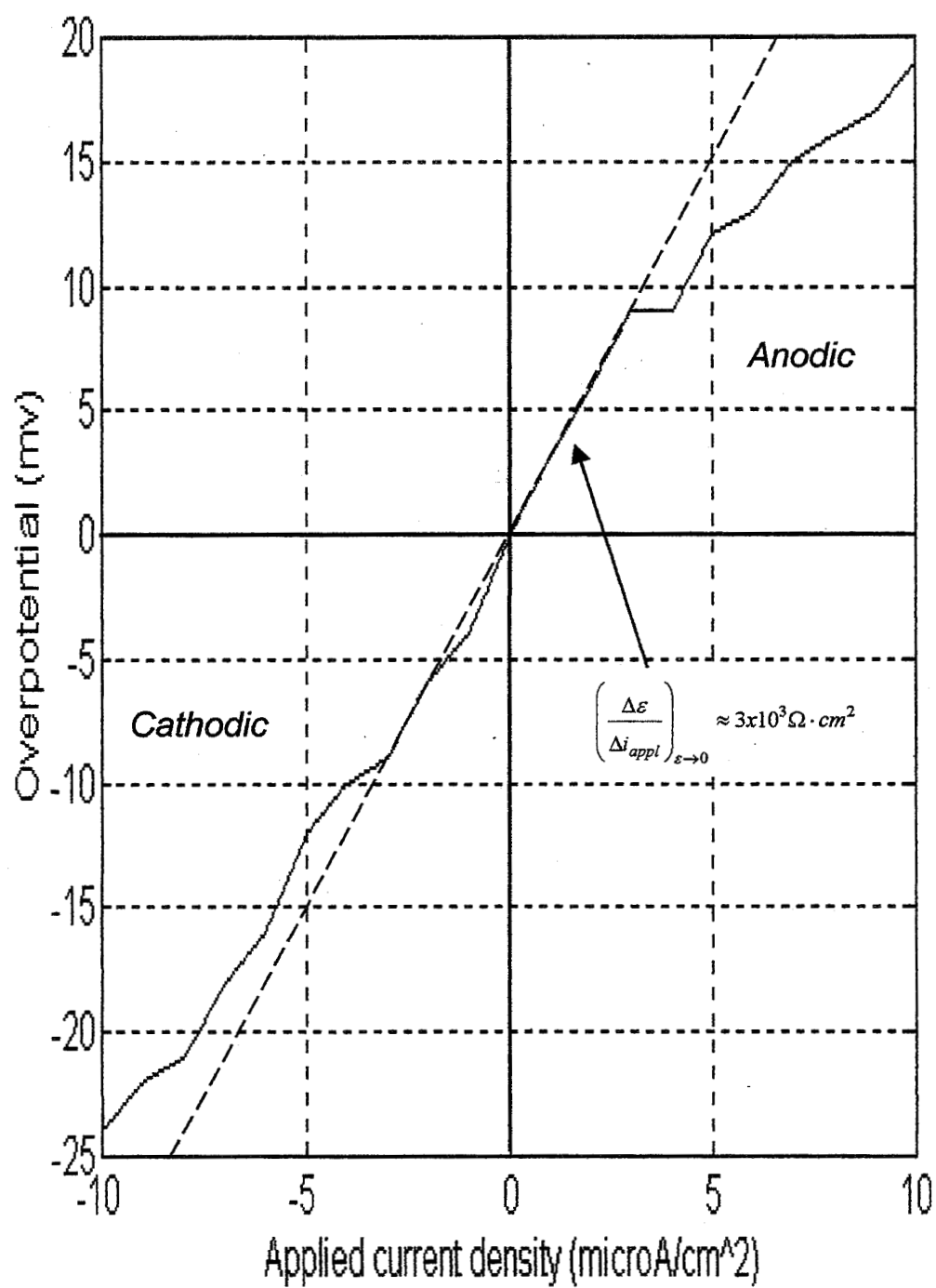


Figure 2. Overpotential vs low range applied current density

APPENDIX Demonstration of the resistance polarization equation

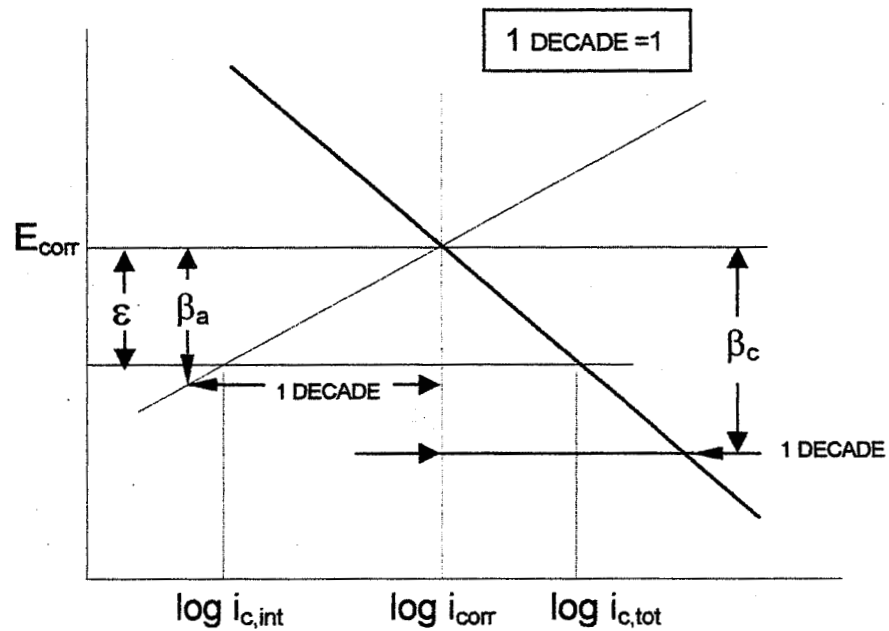


Figure A1. Schematic polarization diagram.

According to figure A1, the overpotential ε will be given by any of the following equations:

$$\varepsilon = \beta_a \log \frac{i_{corr}}{i_{c,int}} \quad (A1)$$

$$\varepsilon = -\beta_c \log \frac{i_{corr}}{i_{c,tot}} \quad (A2)$$

Multiplying both members of equation (A1) and (A2) by 2.3 to convert to natural logarithms, the following current density expressions are obtained:

$$i_{c,int} = i_{corr} e^{-\frac{2.3 \varepsilon}{\beta_a}} \quad (A3)$$

$$i_{c,tot} = i_{corr} e^{\frac{2.3 \varepsilon}{\beta_c}} \quad (A4)$$

In the first part of this experiment (Ref. 1), it was shown that for a given potential:

$$i_{c,appl} = i_{c,tot} - i_{c,int} \quad (A5)$$

Therefore combining equations A3, A4 and A5 and taking i_{appl} for $i_{c,appl}$ or $i_{a,appl}$:

$$i_{appl} = i_{corr} \left(e^{\frac{2.3 \varepsilon}{\beta_c}} - e^{-\frac{2.3 \varepsilon}{\beta_a}} \right) \quad (A6)$$

deriving equation (A6) with respect to ε :

$$\frac{di_{appl}}{d\varepsilon} = 2.3 i_{corr} \left(\frac{1}{\beta_c} e^{\frac{2.3\varepsilon}{\beta_c}} + \frac{1}{\beta_a} e^{-\frac{2.3\varepsilon}{\beta_a}} \right) \quad (A7)$$

as ε approaches zero the following expression is obtained:

$$\left(\frac{di_{appl}}{d\varepsilon} \right)_{\varepsilon \rightarrow 0} = 2.3 i_{corr} \left(\frac{\beta_a + \beta_c}{\beta_a \beta_c} \right) = \frac{1}{R_p} \quad (A8)$$

where R_p is the resistance polarization.

Therefore the resistance polarization equation will be given by:

$$R_p = \left(\frac{\Delta \varepsilon}{\Delta i_{appl}} \right)_{\varepsilon \rightarrow 0} = \frac{\beta_a \beta_c}{2.3 i_{corr} (\beta_a + \beta_c)} \quad (A9)$$

BIOGRAPHY

Carlos E. Umaña holds a Msc. in Metallurgy and Materials Science from Lehigh University (77) and a Mechanical Engineering degree from the Universidad de Costa Rica (72). Actually is the head of the Materials Department of the School of Mechanical Engineering of the Universidad de Costa Rica, where he has been in charge of a course in materials science and technology for twenty years. He has worked in industry and has much experience in hard chromium electroplating. As a consulting engineer he has dealt with more than thirty cases on failure analysis. In the field of materials science and engineering he is very interested in improving the teaching aids of basic concepts from a multidisciplinary point of view.

DIGITAL SHEAROGRAPHY AND APPLICATIONS

Michael Y. Y. Hung

John F. Dodge Chair Professor
Mechanical Engineering Department
Oakland University
Rochester Hills, Michigan 48309-4478

Telephone: 248-370-2238
e-mail hung@oakland.edu



Michael Y. Y. Hung

Digital Shearography and Applications

Y. Y. Hung

Department of Mechanical Engineering

Oakland University

Rochester, Michigan 48309, USA

Keywords: Shearography, interferometry, speckle pattern, phase determination, nondestructive testing, deformation measurement, residual stress measurement, steady state vibration, leakage detection, surface profiling, 3-D shape measurement.

Abstract

This article reviews shearography and its applications. Shearography is a laser-based technique for full-field, non-contacting measurement of surface deformation. Unlike holography, it does not require special vibration isolation; hence, it is a practical tool that can be used in a field/factory environment. Shearography has already received considerable industrial acceptance, in particular, for nondestructive testing. In nondestructive testing, shearography reveals defects in an object by identifying defect-induced deformation anomalies. Other applications of shearography include strain measurement, material characterization, residual stress evaluation, leak detection, vibration studies and 3-D shape measurement.

1. Introduction

Shearography is an interferometric technique developed to address several limitations of holography. Its significant advantages include (1) not requiring a reference light-beam, thus leading to simple optical setups, reduced coherence length requirement of the laser, and lax vibration isolation; and (2) direct measurement of surface strains (first-order derivatives of surface displacements). These distinct advantages have rendered shearography as a practical measurement tool and it has already gained wide industrial acceptance in nondestructive testing. For instance, the rubber industry routinely uses shearography for evaluating tires, and the aerospace industry has adopted it for nondestructive testing of aircraft structures, in particular, composite structures. Other applications of shearography include: measurement of strains, material properties, residual stresses, 3-D shapes, vibrations, as well as leakage detection.

Three versions of shearography are in existence using (1) photographic recording; (2) thermoplastic recording; and (3) digital recording. The photographic version^[1] uses a portrait camera with high-resolution photographic emulsion as the recording media. As shown in Figure 1(a), a roof-shape prism with a small wedge-angle is placed in front of the camera lens to produce a pair of slightly laterally-sheared images of an object. Conversely, two neighboring object points are brought to meet in the image plane (illustrated in Fig. 1(b)) The direction of the sheared images is known as the direction of image-shearing. Since the object is illuminated with laser light (light capable of interference), the two sheared images interfere with one another, forming a shearographic image containing a random interference pattern known as a speckle pattern. Shearographic measurement requires sequential recording of two speckle patterns on the

same photographic plate, one before and another after the object is slightly deformed. After being developed and chemically fixed, the photographic plate is optically Fourier-filtered for the reconstruction of a visible fringe pattern that depicts the derivatives of displacement with respect to the direction of image-shearing. This technique is also known as double-exposure shearography. Since double-exposure shearography requires subsequent Fourier filtering, it does not permit real-time applications. Another technique known as real-time shearography^[2] eliminates the Fourier filtering process and allows object deformation to be observed continuously in real-time. It involves recording of a single speckle pattern on a photographic plate before deformation. The photographic plate after being processed is returned to the original position in the camera, which serves as a filter for the live image of the object. When the object is deformed, a "live" fringe pattern is observed behind the plate. It is difficult to practise real-time shearography as it requires the precise reposition of the plate after developing. Major drawbacks of using photographic recording lies with the laborious and time-consuming wet photographic process, and the cost of high-resolution photographic plates has further discouraged industrial implementation.

The thermoplastic version^[3] uses a similar optical setup (Figure 1), except that the photographic plate is replaced by a reusable thermoplastic plate which may be instantly processed after recording. This bypasses the inconvenient wet photographic process, but Fourier filtering is still required. Hence, the thermoplastic version does not allow real-time measurements. The cost of the thermoplastic plates has deterred industrial use of the thermoplastic version. Furthermore, the production of thermoplastic plates of consistent quality is very difficult.

Digital shearography^[4] uses video sensors (such as CCD) as the recording media and digital processing technology for data acquisition and analysis. In addition to avoiding the use of consumables needed in the photographic and thermoplastic versions, digital shearography does not rely on Fourier filtering for fringe pattern reconstruction, thus enabling real-time measurements and inspection. The cutting edge of digital shearography is in direct and automated measurement of phase-changes (and, hence, strains) without having to rely on fringe pattern reconstruction. In this chapter, digital shearography and its applications will be discussed.

2. Principles Of Digital Shearography

2.1 Description Of The Technique

As illustrated in Figure 2, digital shearography requires the use of a laser point source for illuminating the test object and a video image-shearing camera connected to a microcomputer for recording and processing. The camera comprises a CCD image sensor and a double-refractive prism (a Wollaston prism, for instance) as the image-shearing device. The principle of image-shearing using a doubly-refractive prism is illustrated in Figure 3. Fig.3(a) shows that a light beam passing through this prism is split into two angularly separated beams. Conversely, through the image-shearing device, two non-parallel beams of light scattered from two different object points become nearly collinear,

and the resulting low spatial frequency of the interference fringes can be resolved with a low resolution image sensor such as CCD. This is illustrated in Fig. 3(b). The two sheared wavefronts transmitted by the two axes of the image-shearing device, however, are orthogonally polarized, hence they will not interfere with each other. To enable interference, a polarizer with its polarization axis oriented at an azimuth of 45° is required. As the illuminated object surface is generally optically rough, interference of the two sheared wavefronts will result in a speckle pattern embedded in the shearographic image. Fig. 4 shows a magnified speckle pattern.

The speckle pattern is slightly altered when the object is deformed. Practice of digital shearography involves digitizing sequentially two speckle patterns of the test object, one before and another after it is slightly deformed, into the microcomputer via a frame grabber (Figure 2). As will be shown in Section 2.2, the difference of the two speckle patterns will enable reconstruction of a visible fringe pattern that depicts displacement-derivatives with respect to the direction of image-shearing. The use of a frame grabber with on-board processing capability further allows real-time fringe pattern reconstruction at video rate. Although digital shearography may also be achieved using a Michelson shearing interferometer^[5,6], the author has preference for a double-refractive prism, as it is more light efficient; having wider field of view, and it produces higher quality fringes.

2.2 Principles Of Fringe Formation

A shearographic image may be mathematically represented as follows.

$$I = I_0 [1 + \mu \cos \phi] \quad (1)$$

where I is the intensity distribution of the speckle pattern received at the image plane of the camera; I_0 is the intensity of the laterally-sheared images (which may be perceived as the d.c. term); μ is the amplitude of modulation of the speckle pattern; and ϕ is a random phase angle. After the object is deformed, the intensity distribution of the speckle pattern is changed slightly to I' , which is described by the following equation.

$$I' = I_0 [1 + \mu \cos(\phi + \Delta)] \quad (2)$$

where Δ denotes phase-change due to surface deformation. Numerically, the difference of intensities I_d of the two speckle patterns (Eqs. (1) and (2)) yields the following equation.

$$I_d = 2I_0 \left[\mu \sin \left(\phi + \frac{\Delta}{2} \right) \sin \left(\frac{\Delta}{2} \right) \right] \quad (3)$$

where I_d manifests as a fringe pattern in which the dark fringes correspond to $\Delta = 2n\pi$, with $n = 0, 1, 2, 3, \dots$ being the fringe orders, and the bright fringes correspond to half

fringe orders. Figure 5(a) shows a typical shearographic fringe pattern for a fully-clamped rectangular plate under uniform lateral load when image-shearing is along the x-direction, and Figure 5(b) shows the corresponding fringe pattern when image-shearing is along the y-direction. Note that the absolute value of I_d is used in the display of the fringe patterns, as an image cannot have negative value.

2.3 Fringe Interpretation

The phase-change Δ in Eq. (2) is induced by the change in the relative optical path length of light scattered from two neighboring object points, $P(x,y,z)$ and $P(x+\delta x, y, z)$, considering that the direction of image-shearing is parallel with the x-axis and the amount of shearing is δx . It may be shown that Δ is related to the relative displacement ($\delta u, \delta v, \delta w$) of the two neighboring points as follows.

$$\Delta = \frac{2\pi}{\lambda} (A\delta u + B\delta v + C\delta w) \quad (4)$$

where (u,v,w) and $(u+\delta u, v+\delta v, w+\delta w)$ are, respectively, the displacement vectors of $P(x, y, z)$ and $P(x+\delta x, y, z)$; λ is the wavelength of the laser, and A, B, C are sensitivity factors that are related to the positions of the illumination point $S(x_s, y_s, z_s)$ and the camera $O(x_0, y_0, z_0)$ in the following manner.

$$\begin{aligned} A &= (x - x_0)/R_0 + (x - x_s)/R_s \\ B &= (y - y_0)/R_0 + (y - y_s)/R_s \\ C &= (z - z_0)/R_0 + (z - z_s)/R_s \end{aligned} \quad (5)$$

with $R_0^2 = x_0^2 + y_0^2 + z_0^2$ and $R_s^2 = x_s^2 + y_s^2 + z_s^2$

It is noted that $z = z(x,y)$ describes the object surface and is not an independent variable when surface points are considered. Equation (4) may be rewritten in the following form.

$$\Delta = \left(\frac{2\pi}{\lambda} \right) \left[A \frac{\delta u}{\delta x} + B \frac{\delta v}{\delta x} + C \frac{\delta w}{\delta x} \right] \delta x \quad (6)$$

Slight image-shearing gives rise to a small value of δx . The relative-displacement terms in Eq. (6) may subsequently be treated as the partial derivatives of u, v and w with respect to the direction of image-shearing x . Thus, Eq. (6) becomes

$$\Delta = \left(\frac{2\pi}{\lambda} \right) \left[A \frac{\partial u}{\partial x} + B \frac{\partial v}{\partial x} + C \frac{\partial w}{\partial x} \right] \delta x \quad (7)$$

Rotating the image-shearing device (Figure 2) about its optical axis will alter the direction of image-shearing, resulting in fringe patterns depicting displacement derivatives with respect to the current direction of image-shearing. Hence, if image-shearing is along the y-axis by an amount δy , Eq. (7) is modified to the following.

$$\Delta = \left(\frac{2\pi}{\lambda} \right) \left[A \frac{\partial u}{\partial y} + B \frac{\partial v}{\partial y} + C \frac{\partial w}{\partial y} \right] \delta y \quad (8)$$

The fringe patterns in Figures 4(a) and 4(b) for a laterally deflected plate therefore represent, respectively, $\frac{\partial w}{\partial x}$ and $\frac{\partial w}{\partial y}$. Subsequently, it is possible to use a multiple image-shearing camera^[7] for simultaneous recording of displacement derivatives with respect to x and y.

2.4 Automated Fringe Phase Determination

Traditional methods of shearographic analysis rely on the reconstruction of visible fringes and the correct identification of fringe orders (Eq. (3)). Therefore, only at locations where the dark and bright fringes appear can the fringe orders be correctly determined; elsewhere the fringe orders are generally estimated using linear interpolation, although the fringe-carrier method has been developed to alleviate the uncertainty. The following describes an automated process in which the phase-change Δ is directly determined at every digitized points without having to rely on fringe reconstruction and fringe order identification. It will be seen that this has constituted a significant advantage of digital shearography.

Perusal of Eqs. (1) and (2) shows four unknowns, namely, I_0 , μ , ϕ and Δ ; and by superimposing known phases to Eqs. (1) and (2), additional equations are generated to solve for these unknowns. This forms the basis of the phase-shift technique for automated phase determination in digital shearography. Several methods are available for effecting phase shifting: (1) tilting the object, (2) tilting the object beam, (3) translating the image-shearing device, (4) wavefronts manipulation by polarization, and (5) using a variable wave retarder. Among these methods, the author prefers the use of variable wave retarder.

Figure 6 shows an optical layout for phase shifting using a variable wave retarder that is made of liquid crystal and controlled by a computer. The wave retarder is placed in front of the image-shearing device, and at the same time, its slow and fast axes are aligned with the two polarization axes of the image-shearing device. This allows manipulation of the phase difference between two sheared wavefronts (see Eq. (9) below). Various algorithms for phase determination from multiple phase-shifted speckle

images are available^[8], but in this chapter, only the four-frame algorithm is described. Digitizing four speckle patterns of Eq. (1) with a phase-shift increment of $\frac{\pi}{2}$ generates the following four equations.

$$\begin{aligned}
 I_1 &= I_0 [1 + \mu \cos(\phi + 0)] \\
 I_2 &= I_0 [1 + \mu \cos(\phi + \pi/2)] \\
 I_3 &= I_0 [1 + \mu \cos(\phi + \pi)] \\
 I_4 &= I_0 [1 + \mu \cos(\phi + 3\pi/2)]
 \end{aligned}
 \tag{9}$$

The phase distribution ϕ is thus determined using the following equation.

$$\phi = \arctan (I_2 - I_4) / (I_3 - I_1) \tag{10}$$

The process is repeated for the deformed speckle pattern of Eq. (2), yielding

$$\phi + \Delta = \arctan (I'_2 - I'_4) / (I'_3 - I'_1) \tag{11}$$

The phase-change distribution Δ due to deformation is subsequently determined by subtracting Eq. (10) from Eq. (11). However, the computed phase-change Δ is wrapped into the range of $-\pi$ and $+\pi$, and the phase unwrapping algorithm proposed by Macy^[9] may be used to unwrap the phase. It should be noted that the determination of Δ is based upon the assumption that the random phase ϕ remains unchanged during deformation; otherwise ϕ cannot be totally cancelled from Eq.(10) and Eq.(11). A problem likely to encounter during the phase unwrapping process is the presence of noise. The iterative noise suppression algorithm^[10] is found to be very effective in alleviating the problem. Figure 7 shows a 3-D phase-change distribution plot for the fringe patterns of Figures 5(a) and 5(b).

3. Applications

3.1 General Surface Deformation Measurement

Equation (7) contains three displacement derivatives, namely, $\frac{\partial u}{\partial x}$, $\frac{\partial v}{\partial x}$ and $\frac{\partial w}{\partial x}$ so that three measurements with different sensitivity factors A, B, C, are required to separate these displacement derivatives. However, if the geometrical dimensions of the object are small compared to the distances of illumination and recording, the sensitivity factors may be approximated as follows.

$$A = \sin \alpha$$

$$B = \sin \beta \quad (12)$$

$$C = (1 + \cos \gamma)$$

where α and β are the angles of illumination made, respectively, with the yz-plane and the xz-plane; γ is the angle between the illumination beam and the z-axis, which is designated as the imaging direction.

Arranging the optical layout so that $\beta = 0$, the sensitivity factor B becomes zero and the measurement is insensitive to $\frac{\partial v}{\partial x}$. Therefore, the optical system measures the combination of $\frac{\partial u}{\partial x}$ and $\frac{\partial w}{\partial x}$. Likewise, for an optical layout with $\alpha = 0$, the combination of $\frac{\partial v}{\partial x}$ and $\frac{\partial w}{\partial x}$ is measured. However, it is not possible to isolate $\frac{\partial w}{\partial x}$, as the sensitivity factor C can never attain a zero-value.

Using a similar optical setup, the three displacement derivatives in Eq. (8) may also be determined. Thus, three-beam shearography is developed for the measurement of general surface deformation^[11].

3.2 Out-Of-Plane Displacement Measurement

If the illumination and imaging directions are both made parallel with the z-axis, the sensitivity factors A and B attain a zero-value. This optical arrangement, therefore, measures only $\frac{\partial w}{\partial x}$. The deformation fringes shown in Figure 5 are obtained with this optical arrangement.

3.3 In-Plane Strain Measurement

In-plane strains are expressed by the following two normal surface strain components and a shear strain component.

$$\begin{aligned} \epsilon_x &= \frac{\partial u}{\partial x} \\ \epsilon_y &= \frac{\partial v}{\partial x} \\ \gamma_{xy} &= \frac{\partial u}{\partial y} + \frac{\partial v}{\partial x} \end{aligned} \quad (13)$$

It is not possible to measure in-plane displacement derivatives free of out-of-plane displacement derivatives with the use of single-beam illumination (Section 3.1). This, however, is made possible with dual-beam shearography^[12]. As illustrated in Figure 8, the test object is alternately illuminated with two collimated laser beams inclined at equal angles with the z-axis (direction of recording), and the orientation of the beams depends on the in-plane strain component to be measured. In Figure 8, the directions of the illuminating beams are made symmetrical with respect to the yz-plane so that only \mathcal{E}_x is measured. During measurement, the deformation-related phase-change is determined for each illuminating beam using the phase-shift technique described in Section 2.4. With the same deformation, the difference of the two phase-changes due to different directions of illumination yields \mathcal{E}_x . Figure 9(a) shows the \mathcal{E}_x -fringes of an end-loaded cantilever. The theoretical fringe pattern in Figure 9(b) shows good agreement with the experiment.

The principle of dual-beam shearography is outlined as follows. The phase-change due to illumination from the right-hand side is given by the following equation.

$$\Delta_r = \left(\frac{2\pi}{\lambda} \right) \left[(\sin \alpha) \frac{\partial u}{\partial x} + (1 + \cos \alpha) \frac{\partial w}{\partial x} \right] \delta x \quad (14)$$

With the same deformation, the phase-change due to illumination from the left-hand side modifies Eq. (14) to the following expression.

$$\Delta_l = \left(\frac{2\pi}{\lambda} \right) \left[(-\sin \alpha) \frac{\partial u}{\partial x} + (1 + \cos \alpha) \frac{\partial w}{\partial x} \right] \delta x \quad (15)$$

Subtracting Eq. (15) from Eq. (14) yields the difference of phase-change Δ_d due to different illuminating directions. Thus,

$$\Delta_d = \Delta_r - \Delta_l = (4\pi / \lambda)(\sin \alpha) (\delta x) \frac{\partial u}{\partial x} \quad (16)$$

which, with reference to Eq. (13), is related to the normal strain component \mathcal{E}_x . Should the illuminations be made symmetrical with the xz-plane and the image-shearing direction parallel with y, the term $\frac{\partial u}{\partial x}$ in Eq. (16) is replaced by $\frac{\partial v}{\partial y}$, which represents

\mathcal{E}_y . In a similar manner, in-plane strain components along any direction may be measured through adjusting the orientation of the illuminating beams. With three different orientations of illumination, the measurement system is equivalent to a full-field strain rosette that enables determination of the complete state of in-plane strain.

The dual-beam scheme also allows the out-of-plane displacement derivatives to be deduced. This is achieved by adding Eqs. (14) and (15) together, allowing direct measurement of $\frac{\partial w}{\partial x}$, from the phase sum Δ_s , that is given by:

$$\Delta_s = \Delta_r + \Delta_l = (4\pi / \lambda)(1 + \cos\alpha)(\delta x) \frac{\partial w}{\partial x} \quad (17)$$

and $\frac{\partial w}{\partial y}$ may also be determined in a similar manner.

3.4 Comparison of Deformation of Two Different Objects

The optical arrangement of Fig. 10 can be used to compare the deformation of two different objects. In the setup, a point coherent light source simultaneously illuminates two different objects (a test object and a reference object), and a doubly-refractive shearing crystal with a large shear is used to bring the images of the two objects to combine and interfere in the CCD sensor of the camera. In this arrangement, one object serves as a reference for the other. When both objects are deformed, the fringe pattern generated depicts the difference of the deformations between the two objects. If only one object (test object) is deformed, the setup measures the surface displacement of the test object. Indeed, this yields the same results of holography or electronic speckle pattern interferometry (ESPI). The optical setup, however, is greatly simplified. Fig. 11 shows a fringe pattern obtained with the this method, which measures the deflection of a rectangular plate clamped along its boundaries and objected to a point load at the center.

3.5 Residual Stress Measurement^[13, 14]

The use of strain gage rosettes to determine the amount of strain released through controlled drilling of a blind hole is a common practice in residual stress measurement. This requires mounting of special strain gage rosettes and critical alignment of the drilled hole with respect to the positions of the gages. The finite size of the rosette discourages measurements close to the boundary of the drilled holes. For small test objects, such as those found in microelectronic packages, bonding of these rosettes is not possible. And for materials with low stiffness, strain gages would alter the real structural behavior. Shearography, being equivalent to a non-contacting optical strain rosette, has been applied to the measurement of residual stresses in plastics and composites^[15]. Figure 12 shows three fringe patterns, revealing different extent of residual stresses in the test structure when it is stress-released using hole-drilling.

Rapid shearographic residual stress measurement may be achieved using micro-indentation instead of hole-drilling. An image-shearing device with large shearing is used so that the speckle pattern is formed by light wave-fronts emitted from two remotely located areas on the test object. This is equivalent to comparing the deformation of two different areas with one acting as reference to the other. With localized deformation due

to stress releasing by micro-indentation, the area outside the indentation will hardly be affected by the stress-release and, hence, it appropriately acts as a reference surface. Thus, this technique measures absolute displacements in the neighborhood of the indentation.

Using micro-indentation, Figure 13(a) shows that, for a test object without residual stresses, the fringes are nearly axially symmetrical. However, the presence of residual stresses will give rise to an asymmetrical fringe pattern (Figure 13(b)). The directions of the principal stresses are those of the axes of symmetry, and the magnitude of the residual stresses is related to the degree of deviation from axi-symmetry. As the mechanics of stress redistribution due to stress releasing by micro-indentation is highly complex, research is currently being conducted to quantitatively determine the residual stresses. Nonetheless, this technique provides a quick means of qualitative analysis of residual stresses, and may be used in a field/production environment. Moreover, the indentation is so small and shallow (only several micrometers depth) that this technique may be considered as being non-destructive.

3.6 Study of Steady-State Vibration

3.6.1 Time-Integrated Shearography^[16,17]

For a test object undergoing steady state vibration, the phase-change Δ in Eq. (2) may be described by a sinusoidal function of time. The technique of time-integrated shearography is developed for measuring the derivative of vibrational amplitude. The optical setup similar to that shown in Figure 2 is used except that the object is vibrating in a steady state manner. In the recording, the CCD sensor of the image-shearing camera integrates the intensity of the vibrating object with an integration time longer than several vibrational periods. The integrated intensity I_a of the speckle patterns is given by the following equation.

$$I_a = I_o \left[1 + \mu \cos(\phi) J_o \left(\kappa \frac{\partial A}{\partial x} \right) \right] \quad (18)$$

where $\frac{\partial A}{\partial x}$ is the derivative of the vibrational amplitude; $\kappa = \left(\frac{2\pi}{\lambda} \right) (1 + \cos \gamma)$ is the sensitivity factor; and J_o is zero-order Bessel function of the first kind. In deriving Eq. (18), it is assumed that the vibrational displacement has only out-of-plane component and that the image-shearing direction is parallel with the x-axis.

Another fringe pattern with a phase-shift of π being superimposed onto Eq. (18) is digitized. Thus, the following equation is obtained.

$$I_a = I_o \left[1 + \mu \cos(\phi + \pi) J_o \left(\kappa \frac{\partial A}{\partial x} \right) \right] \quad (19)$$

Taking the difference of Eqs. (17) and (18) yields the following equation.

$$I_a = I_o \left[\mu \cos(\phi) J_o \left(\kappa \frac{\partial A}{\partial x} \right) \right] \quad (20)$$

which readily shows a visible fringe pattern. Dark fringes are formed when the following condition is satisfied.

$$\left[J_o \left(\kappa \frac{\partial A}{\partial x} \right) \right] = 0 \quad (21)$$

The variable $\frac{\partial A}{\partial x}$ is determined by equating the argument of the Bessel function to its roots. Figure 14(a) shows a typical fringe pattern, which depicts $\frac{\partial A}{\partial x}$, of a rectangular plate vibrating at its fundamental mode at 152 Hz. The fringe pattern in Figure 14(b) corresponds to $\frac{\partial A}{\partial y}$.

3.6.2 Stroboscopic Shearography^[18]

An alternative method of studying steady state vibration is the stroboscopic technique. In stroboscopic shearography, the vibrating object is strobed with the laser light such that the exposure of the CCD takes place at the vibrational peak and utilizes a low duty cycle (ratio of exposure time to period of vibration). Comparing with a reference image taken when the object is stationary, the difference yields a fringe pattern depicting the derivative of the vibrating amplitude. Note that time-integrated shearography yields a fringe pattern of diminishing fringe visibility (because of the Bessel function modulation) and its phase cannot be determined using the phase shift technique. The fringe pattern obtained with the stroboscopic technique is of sinusoidal form, and hence the phase shift technique can be applied to automate the fringe phase determination (Section 2.4). Figure 15 shows a sample result of stroboscopic shearography.

3.7 Time-Dependent Deformation Measurement

Time-dependent deformation may be measured by the technique^[19] which continuously digitizes the speckle patterns of a deforming object. The relationship between displacement-derivative and time at a point of interest is extracted from the time-varying phase-change map that is recorded and stored in the computer memory, and the total phase-change is subsequently obtained by integrating the phase-change curve with respect to time. For low strain-rates, a commercial video-cassette recorder may be used to record the speckle patterns at the speed of 30 frames/sec. For deformation with high strain-rates, high-speed shearography^[20] is developed using a high-speed digital image acquisition system. The image acquisition system used by the author is a Kodak EktaPro Model 4540 High Speed Motion Analyzer, which has the maximum frame speed

of 40,500 frames/sec. After recording, the images can be played-back at variable rates ranging from 2 frames/sec to 30 frames/sec. The playback images are then digitized with a microcomputer through a frame grabber. A fringe pattern may also be reconstructed from the difference of any two speckle patterns. Besides the measurement of time-dependent deformation, high speed shearography has been used for rapid evaluation of hermetic seals in microelectronic packages^[21].

3.8 Nondestructive testing^[22,23,24]

3.8.1 How does shearography detect flaws?

When a test object containing a flaw is loaded, strain concentration at the vicinity of the defect is induced. If the flaw is not too deeply embedded within the object, the induced strain concentration would cause anomalies in the surface strain distribution. Subsequently, these anomalies are translated into fringe-anomalies if two speckle patterns, taken one before and another after loading, of the object are compared. Thus, shearography reveals flaws, both surface and internal, through identification of anomalies in the fringe pattern; it also permits non-contacting full-field inspection.

3.8.2 Shearography vs Ultrasound

Shearography has found wide applications in nondestructive testing and it has already received industrial acceptance as a useful NDT tool, particularly for composite structures such as tires and honeycomb structures. It is particularly effective in revealing delaminations. Figure 16 shows a comparison of test result obtained using digital shearography and C-scan ultrasonic testing on a composite sample. Both techniques readily reveal an edge pullout and a delamination. With digital shearography, the flaws are revealed in one second, whilst the ultrasonic technique requires point-by-point scanning along the test surface and at the same time, proper fluid coupling between the transducer and the test surface is to be ensured. A limitation of shearography, however, is the need to apply suitable stress-increments to the test object during inspection, since the underlying principle of this technique is based upon changes in the state of the test surface.

3.8.3 Methods of stressing

The development of shearographic NDT procedures has therefore essentially become the development of a practical means of stressing the object that would readily reveal flaws. Ideally, the stress-increment should be similar to the service stresses so that flaws that are critical and detrimental to the service life of the object would be revealed, and cosmetic flaws that do not undermine the structural integrity of the test object can be ignored. This would minimize unnecessary rejects during inspection. In this regard, shearography has an advantage over ultrasonic testing, as the latter detects flaws by identifying inhomogeneities in the object and does not provide direct information on the criticality of the flaws. Exact duplication of the actual stress-increment for shearographic testing, however, is generally difficult. Therefore, various practical means of stressing the object must be developed. In developing these methods, an important precaution to be

taken is restricting rigid-body motion of the object during stressing, as excessive rigid-body motion would cause speckles de-correlation, resulting in degradation of fringe quality.

The various methods of stressing developed for holographic NDT^[25] may generally be used for shearographic NDT. The methods that are in current use and yet do not cause intolerable rigid-body motion of the test object include the use of pressure, vacuum, thermal, and acoustical and mechanical excitations. The use of microwave that excites water molecules is particularly effective for detecting moisture in plastics and non-metallic composites, but safety precautions must be taken seriously. The following are examples using various stressing methods.

Figure 17 shows that the use of internal pressurization to reveal two internal cracks in a steel pressure vessel. Figure 18 reveals several areas of separation in a large cord-reinforced rubber panel using partial vacuum stressing. Figure 19 illustrates successful crack-detection on a composite turbine blade when thermal stressing by heat-radiation is used. Figure 20 demonstrates shearographic inspection of adhesive-bonded composite assemblies using multi-frequency vibrational excitation^[26]. A perfectly bonded area should appear as dark, and any deviation from "perfect darkness" is indicative of a weak bond, whilst an unbonded area appears as bright. In Figure 16, there are two bond lines and a debond and several weak bond are seen.

3.8.4 Flaw recognition

Flaw characterization is a difficult task, as the signature of a fringe anomaly due to a flaw depends on the flaw's response to the applied stress. This depends on flaw nature, shape, size, location, and the state of applied stress at the location of flaw. So far, only debonds in composite laminates can be characterized with confidence. A simple model used to describe a debond is a circular plate clamped along its edges. When partial vacuum is applied, the debond behaves as a plate subjected to uniform pressure. The contour of the derivative of the plate deflection appears in the form of a butterfly. The size of a debond is approximately equal to the size of the butterfly. The depth of a debond can be estimated from the fringe density. For debonds of the same size, the one closer to the surface has a higher fringe density and vice versa. This is illustrated in Fig. 21, which shows four debonds of approximately same size but located at depths of 3, 6, 9, and 12mm from the surface. Notice that the one closest to the surface has the highest fringe density and vice versa. The plate theory predicts that the deflection derivative is inversely proportional to the flexural rigidity of the plate, and the flexural rigidity is proportional to the cube of the plate thickness. This means for equal size debonds, the density of the fringes is inversely proportional to the cube of the depth. An in-depth analysis of the response of debonds can found in Ref(27, 28).

3.9 Three-dimensional shape measurement

Shearography can be used to measure surface slopes $\frac{\partial Z}{\partial x}$ and $\frac{\partial Z}{\partial y}$ of a three-dimensional object surface, $Z(x,y)$. The following describes three shearographic methods for shape measurement.

3.9.1 Double Wavelength Method^[29]

This method requires the use of a laser of variable wavelength. A diode laser is one such laser whose wavelength varies with the controlling current. Using an optical arrangement similar to that shown in Figure 2, two speckle patterns of the test surface are sequentially digitized, one before and the other after the wavelength of the laser is changed incrementally from λ to $\lambda + \delta\lambda$. The difference of the two speckle patterns produces a fringe pattern depicting the derivative of the surface depth $Z(x,y)$ with respect to the direction of image-shearing, since the phase-change Δ is related to the surface slope by the following equation.

$$\Delta = 4\pi \delta x (\delta\lambda / \lambda^2) \frac{\partial Z}{\partial x} \quad (22)$$

where x has been considered as the direction of image-shearing.

As the surface slope along any direction may be measured through adjusting the direction of image-shearing, the $\frac{\partial Z}{\partial x}$ -term in Eq. (22) becomes $\frac{\partial Z}{\partial y}$ when the direction of image-shearing is made parallel with the y -axis. The phase-change Δ , and hence the surface slope, are automatically determined using the phase shift technique described in Section 2.4. Fig. 22(a) shows a fringe pattern depicting $\frac{\partial Z}{\partial x}$ of a light bulb, and Fig. 22(b) is a 3D plot of the $Z(x,y)$ obtained by integrating the slope information of (a).

3.9.2 Double Refractive Index Method^[30]

In the measurement, two speckle patterns are sequentially digitized when the refractive index of the medium surrounding the object is changed from n to $n + \delta n$ between digitization. A fringe pattern depicting the surface slope with respect to the direction of image-shearing is formed by subtracting the two digitized images. With image-shearing directed along the x -direction and with both the illumination and imaging directions along the z -axis, the phase-change Δ is related to the surface slope by the following equation.

$$\Delta = (4\pi / \lambda)(\delta x)(\delta n) \frac{\partial Z}{\partial x} \quad (23)$$

Again, the surface slope in any direction may be obtained by varying the direction of image-shearing, and the phase shift technique can be used to automated the phase determination.

3.9.3 Two Source Method^[31,32]

In this method, the object is illuminated with a collimated coherent beam in a direction oblique to the z-axis. Two speckle patterns are sequentially digitized when the illumination beam is slightly tilted between digitization. The fringe pattern resulted from subtracting the two digitized images contains information about the partial derivative of $Z(x,y)$ with respect to the direction of image-shearing.

3.10 Detection of Gas Leakage

The principle of this application is based on the phenomenon that gas leaking would change the refractive index of the ambient air around the leak, thus producing a phase-change that manifests as a visible fringe pattern. Figure 23 shows a leakage from the valve of a pressure vessel containing helium. It is seen that shearography not only detects gas leaks, but also reveals the location of leakage. To enhance the change in refractive index during inspection, it is preferable to use gas at the surrounding of the test object different from the gas within the object. A good combination is helium and air.

4. Limitations and Remedies

Being an optical method, shearography enjoys the desirable features of non-contact and full-field. Although the method is based on interferometric principles, it does not require critical optical alignment and extreme environmental stability. However, shearography suffers a severe drawback that is inherent in all speckle interferometric techniques. This drawback is the limited tolerance to rigid body motion. Excessive rigid motion including object translation and rotation produces a decorrelation of speckle patterns and it results in the deterioration of fringe visibility. The conventional speckle decorrelation theory^[33,34] predicts that total decorrelation will occur when the rigid body translation orthogonal to the line of sight exceeds a speckle size. (A speckle size is approximately 1.2 times the product of the f-number of the camera lens and the wavelength of laser light.) The author's experience has found that shearography's tolerance to rigid body translation is at least an order of magnitude greater than that theory's prediction. Generally, this tolerance depends on surface nature, surface roughness and magnitude of strain. Though more tolerant, decorrelation of speckle patterns limits its use for many real-world applications, especially for large objects as excessive rigid body motion due to the deformation of large structures is unavoidable. Rigid body translation in shearography may be negated by translating the image sensor or digital image shifting in the computer, as reported in Ref(35). However, decorrelation due to rigid body rotation is very difficult to compensate, unless the axis of rotation is known.

One effective method to alleviate the de-correlation problem is to attach the shearographic system (camera and illumination) to the test object. This eliminates the relative rigid motion (both translation and rotation) between the measurement system and the object, and hence only the deformation is measured. Of course, this arrangement requires the miniaturization of the shearographic equipment, which can be achieved by using a diode laser and a micro-camera.

5. Conclusion

A review of shearography and its applications is given in this chapter. Shearography is a practical technique and therefore, it has gained rapid acceptance by the industries as a useful tool for measurement and nondestructive testing. However, this technique is still relatively young and its full capability awaits further exploration.

6. Acknowledgement

The research reported in this article was sponsored by a National Science Foundation grant (CMS9601778). The author would like to thank Dr. Ken Chong of NSF for the support.

7. References

1. Hung, Y.Y. "Shearography: A New Optical Method for Strain Measurement and Nondestructive Testing", Optical Engineering, pp.391-395, May/June, 1982.
2. Y.Y. Hung, S. Tang and J.D. Hovanesian, "Real-time Shearography for Measuring Time-dependent Displacement Derivatives.," Experimental Mechanics, Vol. 34, No.1, pp 89-92, (March, 1994)
3. Hung, Y.Y. and J.D. Hovanesian, "Fast Detection of Residual Stresses in an Industrial Environment by Thermoplastic-based Shearography", Proceedings of the 1990 SEM Spring Conference on Experimental Mechanics, pp769-775, Albuquerque, New Mexico, June4-6, 1990.
4. Hung, Y.Y. " Nondestructive Evaluation by Electronic Shearography", presented at the 16th Symposium on Nondestructive Evaluation, San Antonio, Texas, April 21-23, 1987. Also, "Apparatus and Method for Electronic Analysis of Test Object", US Patent 4,887,899 (1989).
5. Y.Y. Hung, "A Speckle-Shearing Interferometer", Optical Communications, Vol.11, 732, 1974.
6. J.A. Leendertz and J.N. Butters, " An Image Shearing Speckle Pattern Interferometer for measuring bending moments", J. of Physics: E., 168-172, (July 1974).
7. Hung, Y.Y. and Durelli, A.J. "Simultaneous Measurement of Three Displacement-Derivatives Using a Multiple Image Shearing Interferometric Camera", J. of Strain Analysis, Vol. 14, No.3, 81-88, 1979.
8. K. Creath, "Phase-measurement techniques for nondestructive testing", Proceedings of SEM Conference on Hologram Interferometry and Speckle Metrology, 473-478, Baltimore, Maryland, November 5-8, (1990).
9. W.W. Macy, "Two-dimensional Fringe Pattern Analysis", Applied Optics, 22, 3898, (1983)

10. Jie Gu, Y.Y. Hung and Fang Chen, "Iteration Algorithm for Computer-aided Speckle Interferometry", Applied Optics, Vol.33, No.23, (August 1994).
11. K.W. Long "3-Beam Phase Shift Shearography for Simultaneous Measurement of In-plane and Out-of-plane Displacements and Its Applications to Residual Stress Measurements," PhD Dissertation, Oakland University, 1996.
12. Hung, Y.Y. and Wang, J.Q. "Dual-beam Phase Shift Shearography for Measurement of In-plane Strains" Optics and Lasers in Engineering, Vol.24, No.5-6, pp403-413, (May/June, 1996)
13. Y.Y. Hung, K.W. Long and J.W. Wang, "Measurement of residual stress by phase shift shearography," Optics and Lasers in Engineering, 1997, vol.27, no.1, pp.61-73.
14. Y.Y. Hung, K.W. Long, J.D. Hovanesian and R. Hathaway, "Fast detection of residual stresses by shearography," Proc. SPIE Industrial Laser Interferometry, Vol. 955, pp.26-35, Detroit, Michigan, June 27-28, 1988.
15. Y.Y. Hung, H.M. Shang, L. Lin, Yubei Zhang and Xinyu Wen "Evaluation of Residual Stresses in Plastics and Composites by Shearography," SAE Paper #1999-01-1254, 1999 SAE International Congress and Exposition, Detroit, Michigan, March 1-4, 1999.
16. J.D. Hovanesian, Y.Y. Hung and A.J. Durelli, "New Optical Method to Determine Vibration Induced Strains with Variable Sensitivity after Recording," Proceedings of the Conference on Experimental Stress Analysis, Smolenice, Czechoslovakia, October 16-18, 1978.
17. Y.Y. Hung and C.T. Griffen, "Digital Shearography versus TV-Holography for Vibration Measurement," Proc. The 15th Biennial Conference on Mechanical Vibration and Noise and 1995 ASME Design Engineering Technical Conferences, Vol. 3, Part C, pp1461-1470, Boston, Massachusetts, September 17-20, 1995.
18. F. Chen, C.T. Griffen and Y.Y. Hung, "Stroboscopic Phase Shifting Shearography for Automated Vibration Measurement", Proc. The 15th Biennial Conference on Mechanical Vibration and Noise and 1995 ASME Design Engineering Technical Conferences, Vol. 3, Part C, pp1399-1415, Boston, Massachusetts, September 17-20, 1995.
19. Y.Y. Hung, "Electronic shearography for measurement of time-dependent deformation," Proc VII Int. Congress on Experimental Mechanics, Vol.2, pp 674-678, Las Vegas, Nevada (June 1992).
20. Y.Y. Hung, C.T. Griffen and F. Chen "High Speed Shearography for Measuring Transient Deformation and Vibration", Proc VIII International Congress on Experimental Mechanics, pp206-207, Nashville, Tennessee, June 10-13, 1996.
21. Y.Y. Hung and Dahuan Shi, "Technique for Rapid Inspection of Hermetic Seals of Microelectronic Packages Using Shearography," Optical Engineering, Vol. 37(5), pp1406-1409, May, 1998.
22. Y.Y. Hung, "Shearography: a novel and practical approach to nondestructive testing," J. of Nondestructive Evaluation, Vol.8, No.2, PP55-68, 1989.
23. Y.Y. Hung, "Automated Shearography for Nondestructive Testing and Strain Measurement," Proc of SPIE Conference on Nondestructive Evaluation of Aircraft, Airports, Aerospace Hardware and Materials, Vol.2455, pp238-249, Oakland, California, June 6-8, 1995.
24. Y.Y. Hung, "Computerized Shearography and its Application for Nondestructive Evaluation of Composites" Chapter 17, Manual on Experimental Methods of Mechanical Testing of Composites, edited by C.H. Jenkins, published by Society for Experimental Mechanics (1998).

25. Holographic Nondestructive Testing, edited by R. K. Erf, Academic Press (1974).
26. Y.Y. Hung, "Automated Nondestructive Shearographic Inspection of Debonds in Composites Using Multi-frequency Vibrational Stressing," Proceedings of 1997 SEM Spring Conference, pp98-99, Bellevue, Washington, June 2-4, 1997.
27. H.M. Shang, S.L. Toh, F.S. Chau, V.P.W. Shim and C.J. Tay, "Locating and sizing disbonds in glassfibre-reinforced plastic plates using shearography," Transactions ASME, Journal of Engineering Materials and Technology, 1991, vol. 113, pp. 99-103.
28. H.M. Shang, L.M. Tham and F.S. Chau, "Shearographic and holographic assessment of defective laminates with bond-lines of different elasticities," Transactions ASME, Journal of Engineering Materials and Technology, 1995, vol. 117, no. 3, pp. 322-329.
29. J.R. Huang, H.D. Ford and R.P. Tatam, "Slope measurement by two-wavelength electronic shearography," Optics and Lasers in Engineering, 1997, vol. 27, no. 3, pp. 321-333.
30. Y.Y. Hung, J.L. Turner, M. Tafraian, J.D. Hovanesian and C.E. Taylor, "Optical Method for Measuring Contour Slopes of an Object," Applied Optics, Vol.17, No.1, pp128-131, 1978.
31. C.J. Tay, F.S. Chau, H.M. Shang, V.P.W. Shim and S.L. Toh, "The Measurement of Slope Using Shearography," Optics and Lasers in Engineering, Vol.14, pp13-24, 1991.
32. C.J. Tay, H.M. Shang, A.N. Poo and M. Luo, "On the Determination of Slope by Shearography," Optics and Lasers in Engineering, Vol.20, pp207-217, 1994.
33. M.O. Petersen, "Decorrelation and Fringe Visibility: on the limiting behaviour of various electronic speckle pattern correlation interferometers," J. Opt. Soc. AM, * (1991), 1082-1089.
34. H.T. Yura, S.G. Hanson, and T.P. Grum, "Speckle Statistics and Interferometric decorrelation effects in complex ABCD optical Systems," J. Opt. Soc, Am., 10, (1993), 316-323.
35. Y.Y. Hung and J.Q. Wang, "Technique for compensating Excessive Rigid Body Motion in NDT of Large Structures Using Shearography," Optics and Lasers in Engineering, Vol.26, pp249-258, 1997.

Figure Legends

Fig. 1 Schematic diagram of photographic shearography. (a) The image-shearing camera is equipped with a roof-shape prism which produces a pair of laterally-sheared images. (b) Conversely, the roof-shape prism (as shearing device) brings rays scattered from two neighboring object points to meet and interfere in the image plane.

Fig 2 Schematic diagram of digital shearography. Note that a double-refractive prism is used as a shearing device.

Fig. 3 Illustration of the doubly-refractive prism as a shearing device. (a) One light beam is split into two angularly separated and orthogonally polarized beams. (b) Conversely, two nonparallel rays scattered from two different points on the object are combined and become collinear.

Fig. 4 A magnified speckle pattern (random interference pattern).

Fig. 5 Fringe patterns depicting the deflection derivatives of a rectangular plate clamped along its boundaries and subjected to uniform pressure: (a) $\partial w / \partial x$, (b) $\partial w / \partial y$.

Fig. 6 Digital shearography with phase-shift capability. The phase shift device is a computer-controlled variable wave-retarder made of liquid crystal.

Fig. 7 Three-dimensional plot of: (a) $\partial w / \partial x$, (b) $\partial w / \partial y$ of the plate deformation of Figure 5 obtained by the automated phase determination algorithm.

Fig. 8 Schematic diagram of dual-beam technique for measuring in-plane strains.

Fig. 9 Fringe patterns depicting ϵ_x , the horizontal in-plane strain component of the cantilever beam. (a) result of the dual-beam shearography, (b) theoretical result.

Fig. 10 Optical arrangement for comparing deformations of two different objects. Note that if the reference object is not deformed, the setup is equivalent to ESPI which measures surface displacement of the test object.

Fig. 11 Fringe pattern depicting the deflection of a rectangular plate using the setup of Figure 10 with the reference object not deformed.

Fig. 12 Fringe patterns depicting three different levels of residual stresses in a composite panel.

Fig. 13 Fringe patterns using micro-indentation as a means of stress release. (a) without residual stress, (b) with residual stress.

Fig. 14 Time-integrated fringe patterns depicting (a) $\partial A / \partial x$ and (b) $\partial A / \partial y$, the derivatives of vibrational amplitude of a rectangular plate vibrating at its fundamental mode.

Fig. 15 Result of stroboscopic shearography of a vibrating plate at 3.07 KHz. (a-b) Phase maps before and after unwrapping, (c-d) 2D and 3D display of the amplitude derivative with respect to x.

Fig. 16 Comparison of shearography with C-scan ultrasound. An edge pullout and a delamination in a composite panel are revealed by both techniques. Time required: 10 minutes for ultrasound and 1 second for shearography. Moreover, fluid coupling is needed in ultrasonic testing.

Fig. 17 The use of internal pressurization detects two internal cracks in a steel pressure vessel.

Fig. 18 Fringe pattern reveals several areas of separation in a large cord-reinforced rubber panel. The method of stressing is partial vacuum.

Fig. 19 Detection of a crack on a composite turbine blade using thermal stressing. The object was heated with a hair dryer.

Fig. 20 Shearographic inspection of adhesive-bonded lines in composite assemblies using multi-frequency vibrational excitation. There are two bonded lines. Perfect bond lines should dark, and any deviation from darkness is indicative of weak bond.

Fig. 21 Fringe patterns of debonds at the various depths (3mm, 6mm, 9mm and 12 mm). Note that the one closest to the surface has the highest fringe density and vice versa.

Fig. 22 (a) Fringe pattern depicting $\partial Z / \partial x$ of a light bulb using the double wavelength method, and (b) A 3D plot of the surface shape (Z) obtained by integrating the fringe phase of (a).

Fig. 23 shows a leakage from the valve of a pressure vessel. The escaping gas is helium.

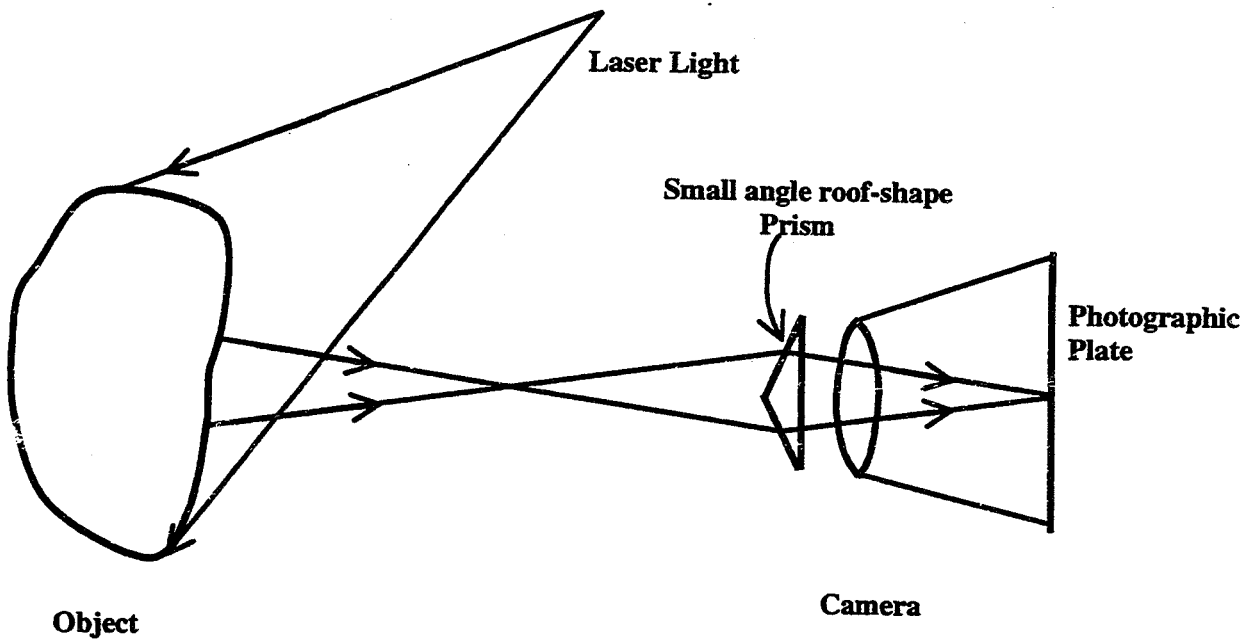
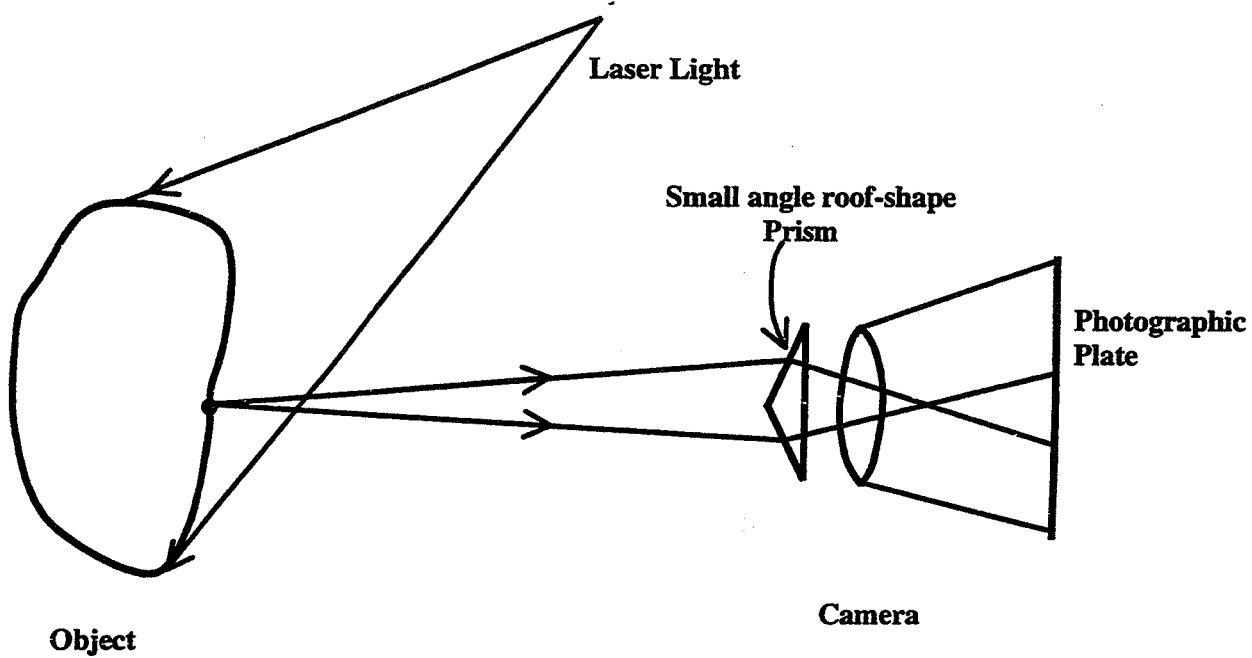


Fig. 1 Schematic diagram of photographic shearography. (a) The image-shearing camera is equipped with a roof-shape prism which produces a pair of laterally-sheared images. (b) Conversely, the roof-shape prism (as shearing device) brings rays scattered from two neighboring object points to meet and interfere in the image plane.

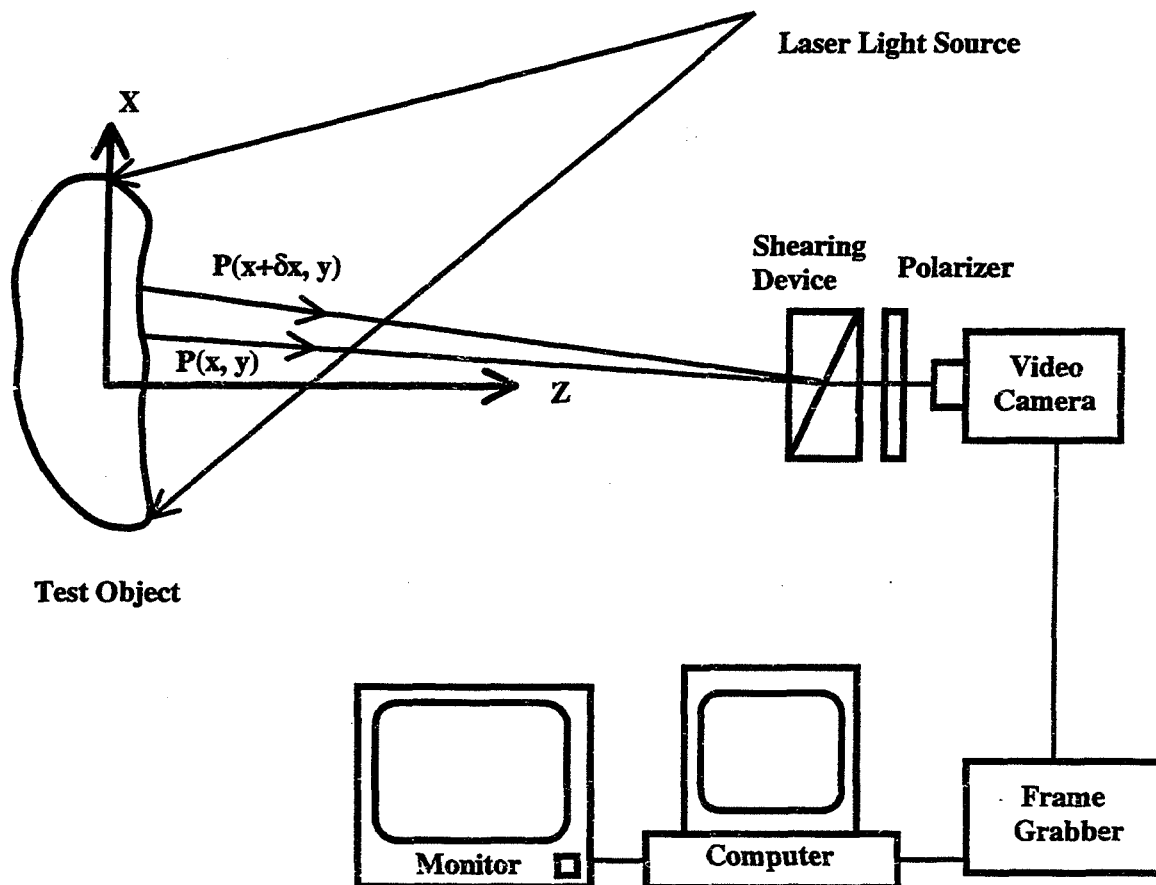
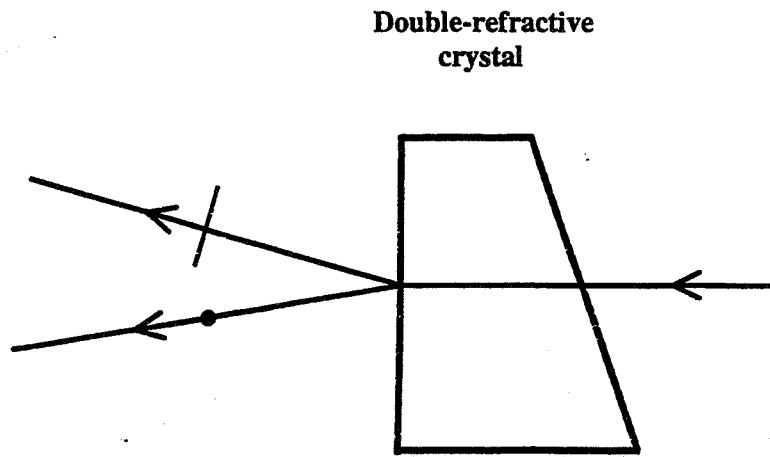
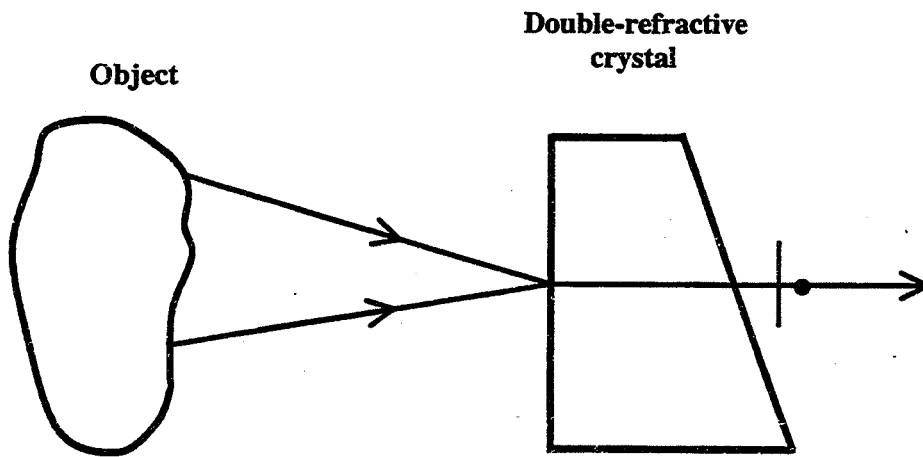


Fig 2 Schematic diagram of digital shearography. Note that a doubly-refractive prism is used as a shearing device.



(a)



(b)

Fig. 3 Illustration of the doubly-refractive prism as a shearing device. (a) One light beam is split into two angularly separated and orthogonally polarized beams. (b) Conversely, two nonparallel rays scattered from two different points on the object are combined and become collinear.

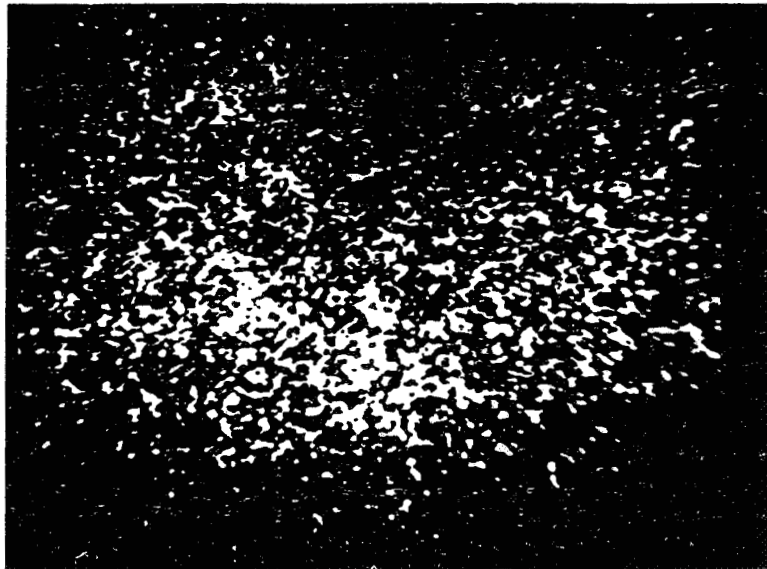
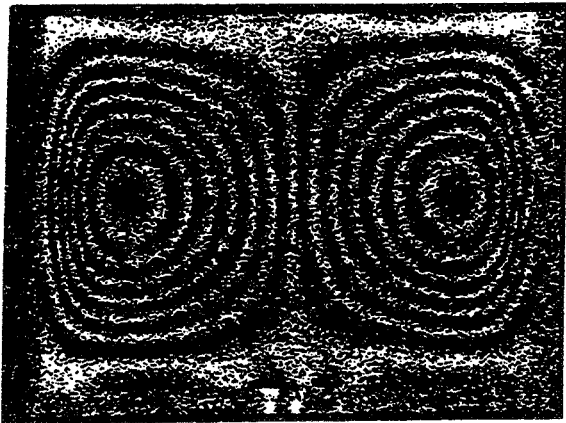
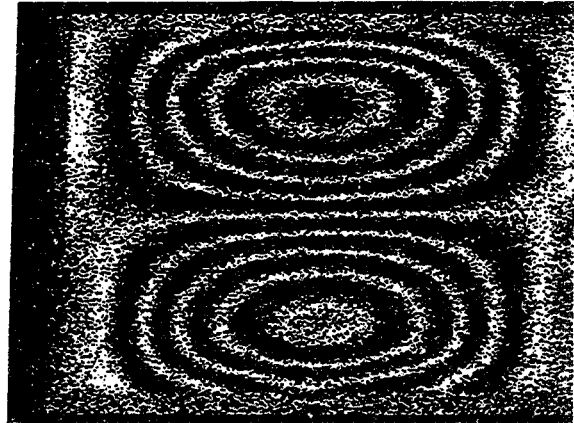


Fig. 4 A magnified speckle pattern (random interference pattern) of digital shearography.



(a)



(b)

Fig. 5 Fringe patterns depicting the deflection derivatives of a rectangular plate clamped along its boundaries and subjected to uniform pressure: (a) $\partial w / \partial x$, (b) $\partial w / \partial y$.

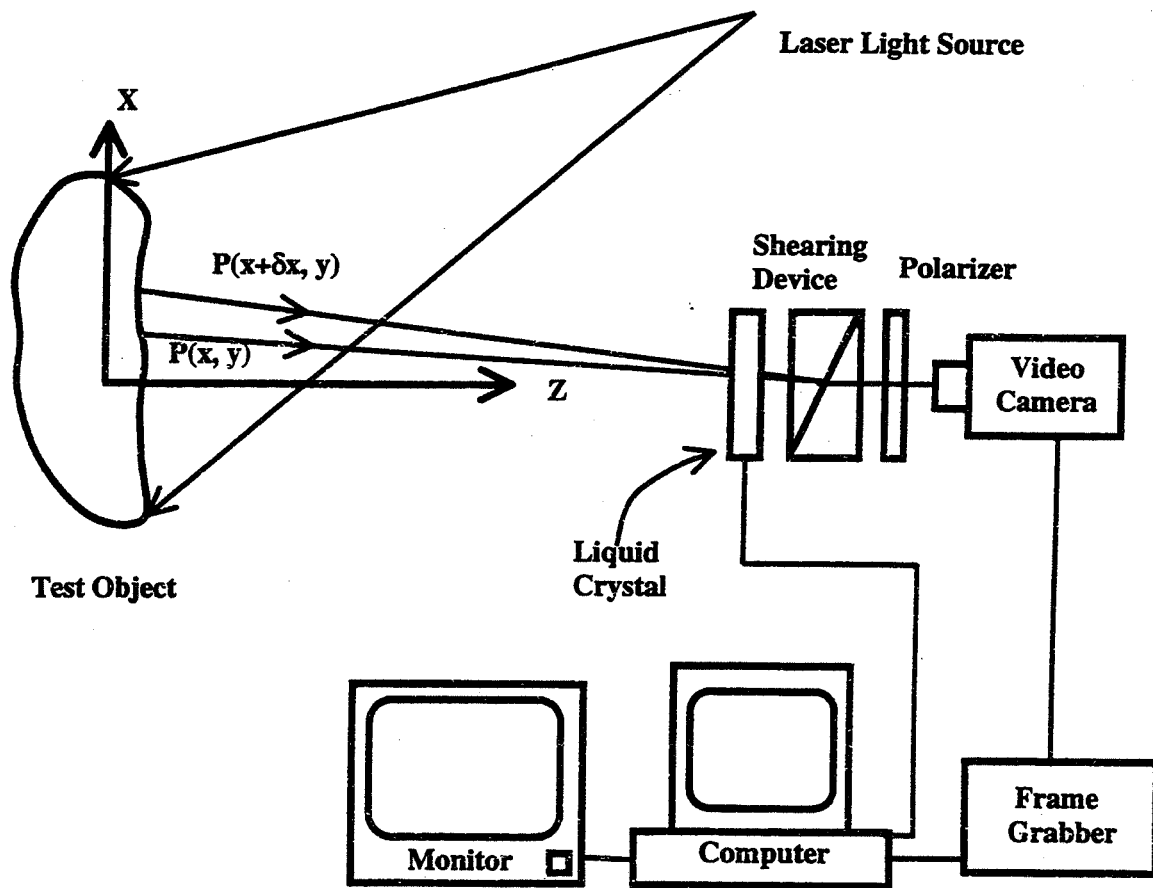


Fig. 6 Schematic diagram of digital shearography with phase-shift capability. The phase shift device is a computer-controlled variable wave-retarder made of liquid crystal.

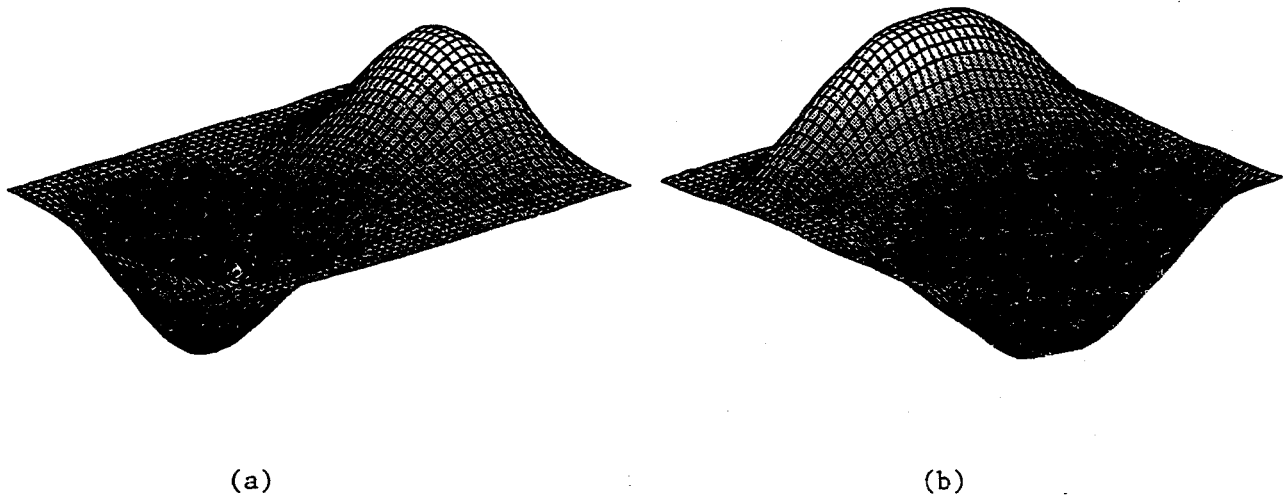


Fig. 7 Three-dimensional plot of : (a) $\partial w / \partial x$, (b) $\partial w / \partial y$ of the plate deformation of the fringe patterns of Fig. 5 obtained by the automated phase determination algorithm.

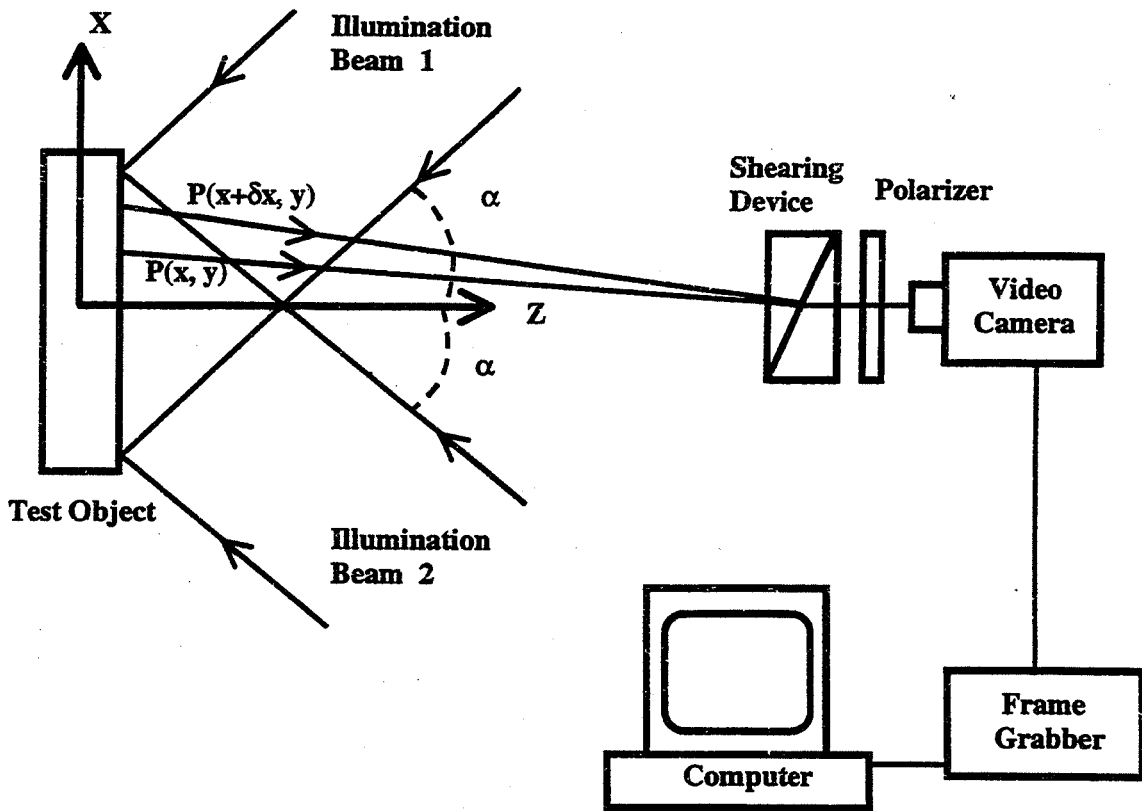
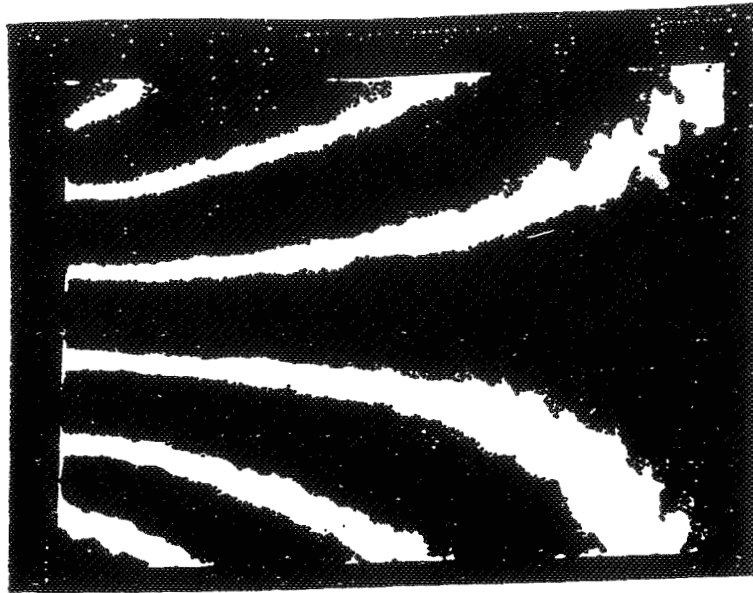
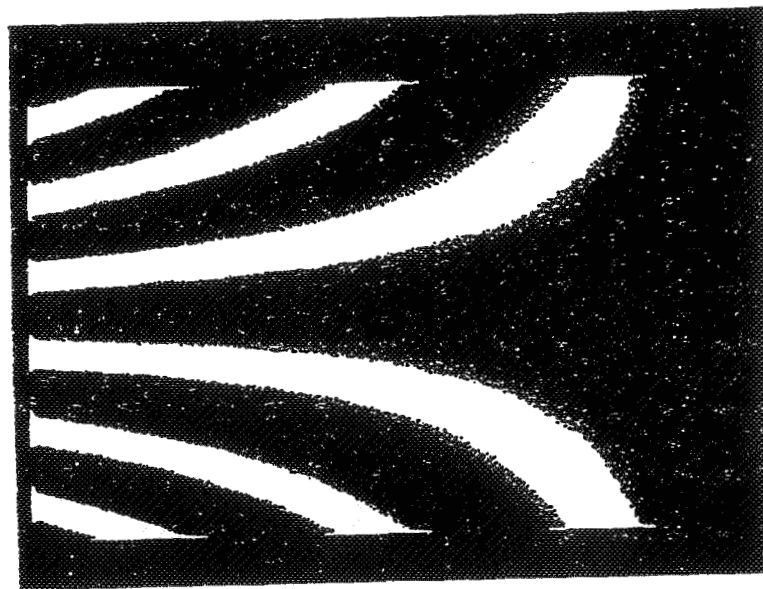


Fig. 8 Schematic diagram of dual-beam shearography for measuring in-plane strains.



(a)



(b)

Fig. 9 Fringe patterns depicting ϵ_x , the horizontal in-plane strain component of the cantilever beam. (a) result of the dual-beam shearography, (b) theoretical result.

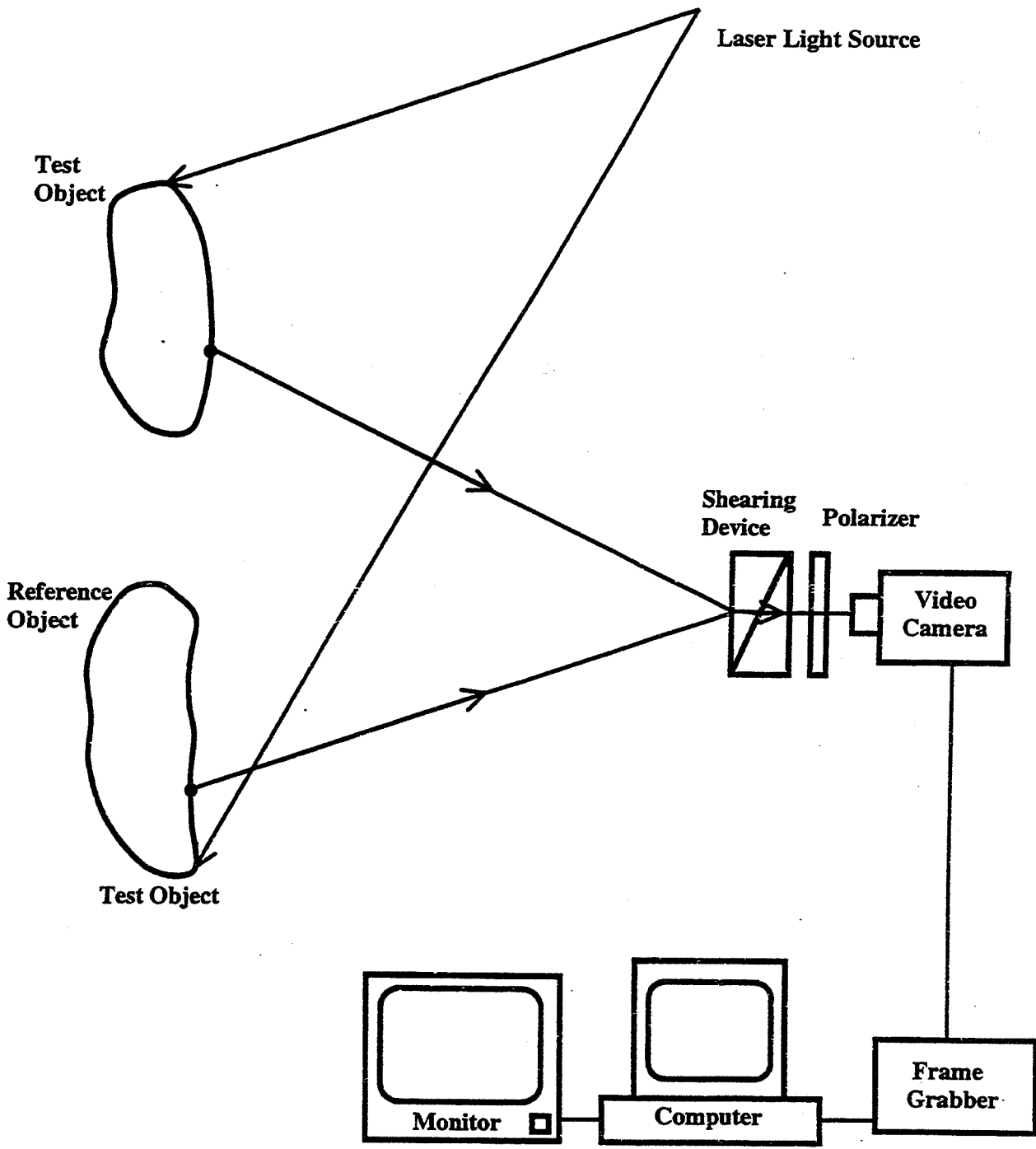


Fig. 10 Optical arrangement for comparing deformations of two different objects. Note that if the reference object is not deformed, the setup is equivalent to ESPI which measures surface displacement of the test object.

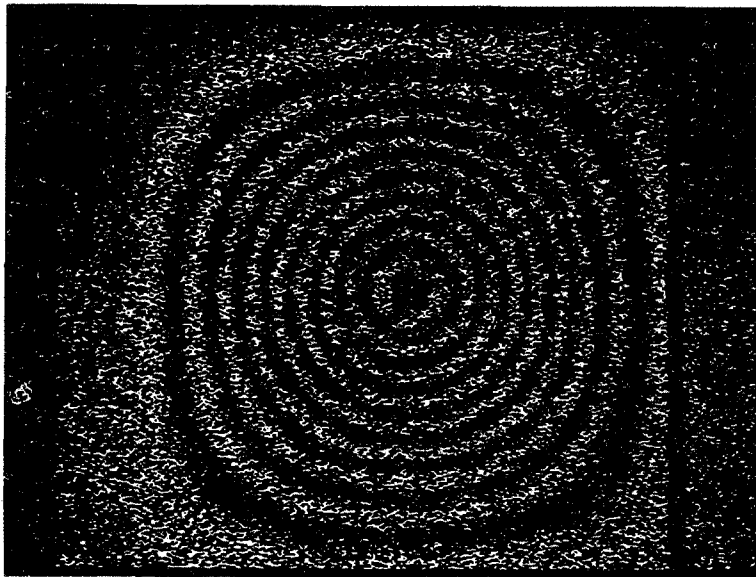
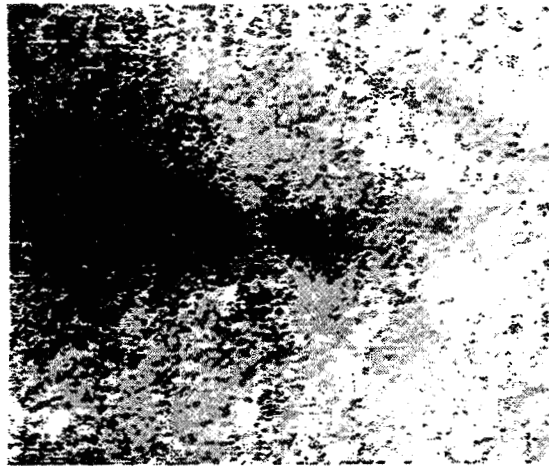
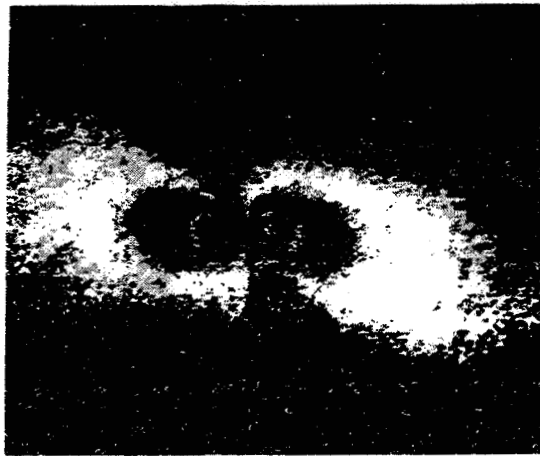


Fig. 11 Fringe pattern depicting the deflection of a rectangular plate clamped along its boundaries and subjected to a point load at its center, obtained by the setup of Fig. 10 with the reference object not deformed.



**Low Residual
Stress**

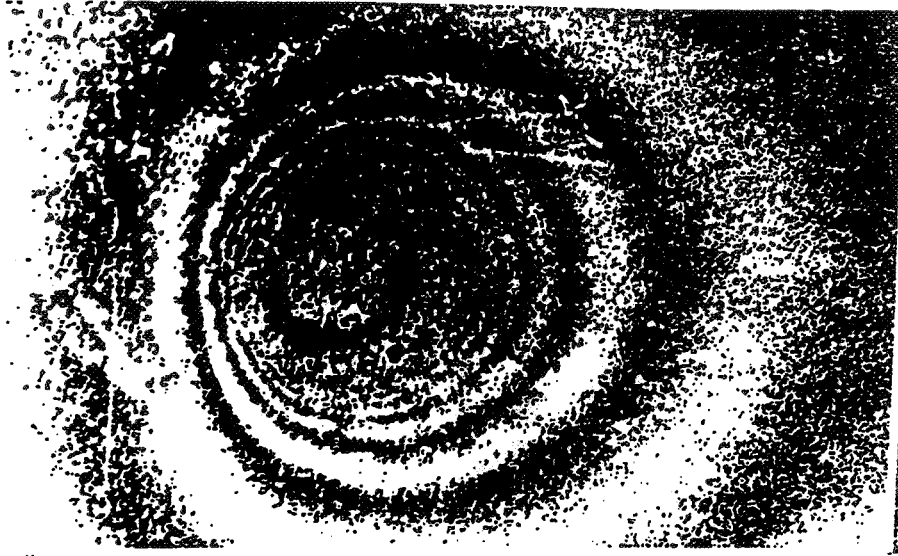


**Medium
Residual Stress**

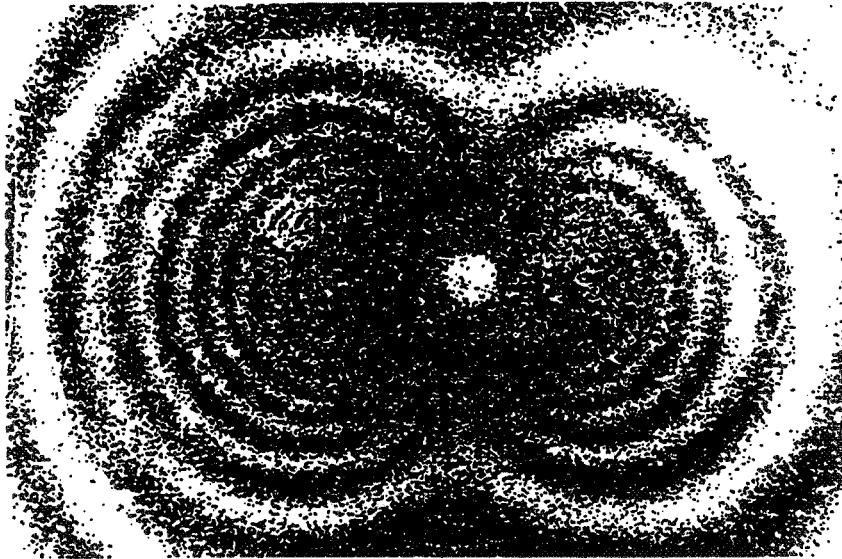


**High Residual
Stress**

Fig. 12 Shearographic fringe patterns depicting three different levels of residual stresses in a composite panel.

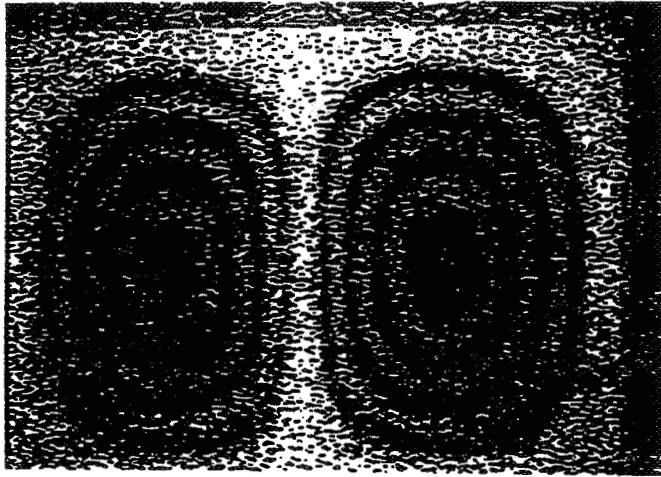


(a)

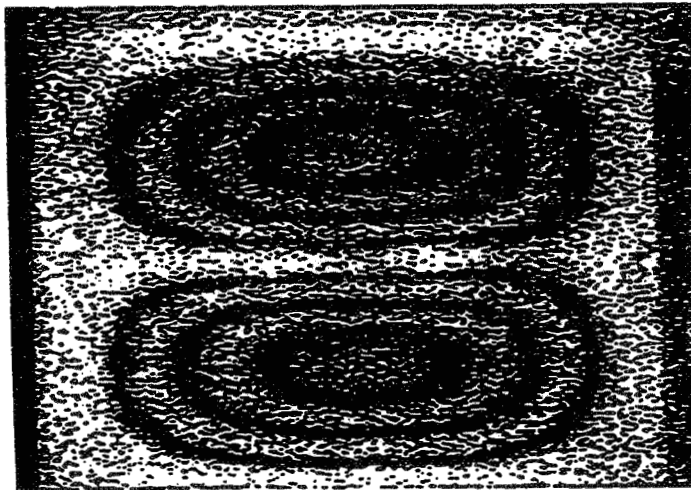


(b)

Fig. 13 Fringe patterns using micro-indentation as a means of stress release. (a) without residual stress, (b) with residual stress.



(a)



(b)

Fig. 14 Time-integrated fringe patterns depicting (a) $\partial A / \partial x$ and (b) $\partial A / \partial y$, the derivatives of vibrational amplitude of a rectangular plate vibrating at its fundamental mode.

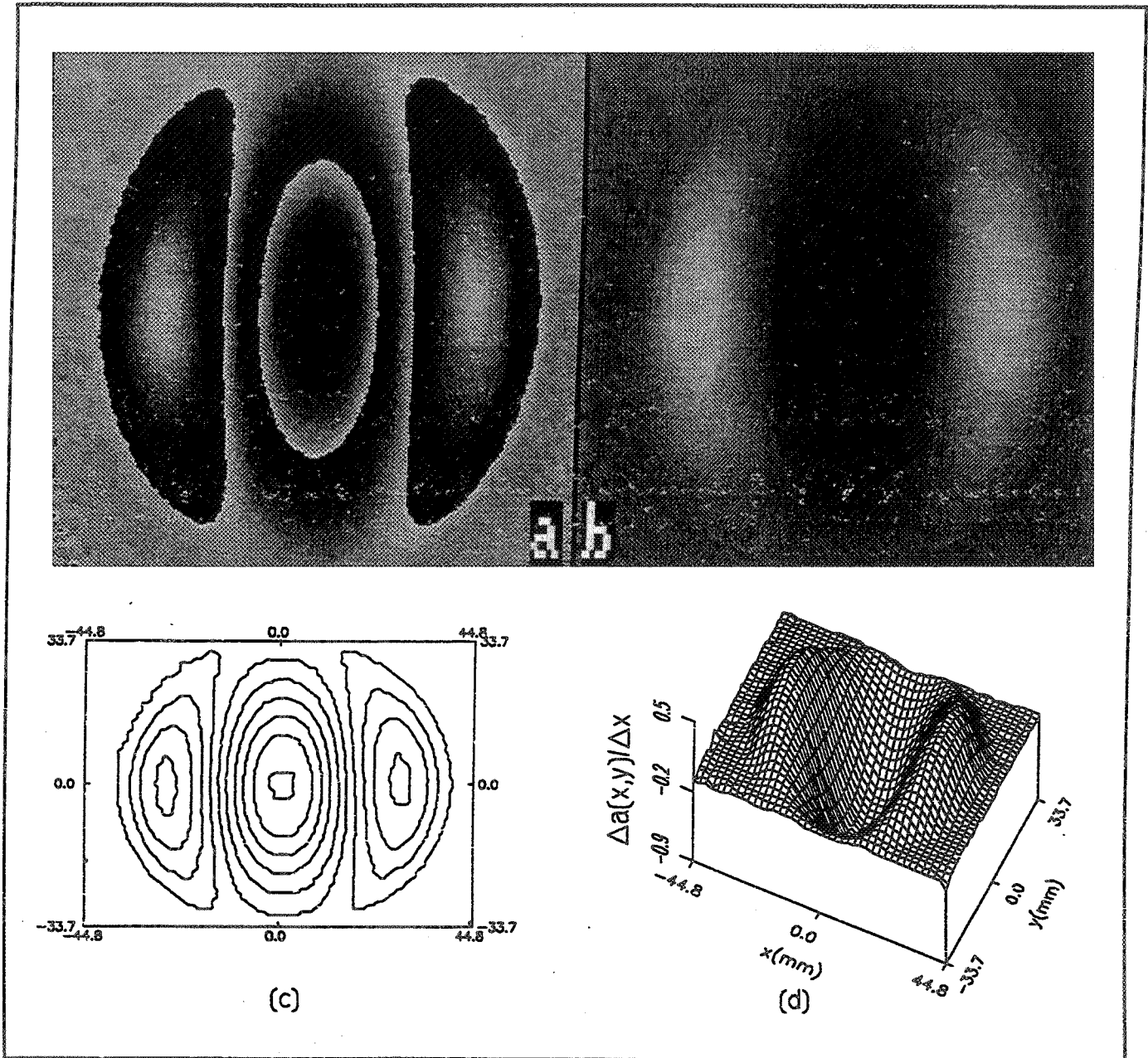
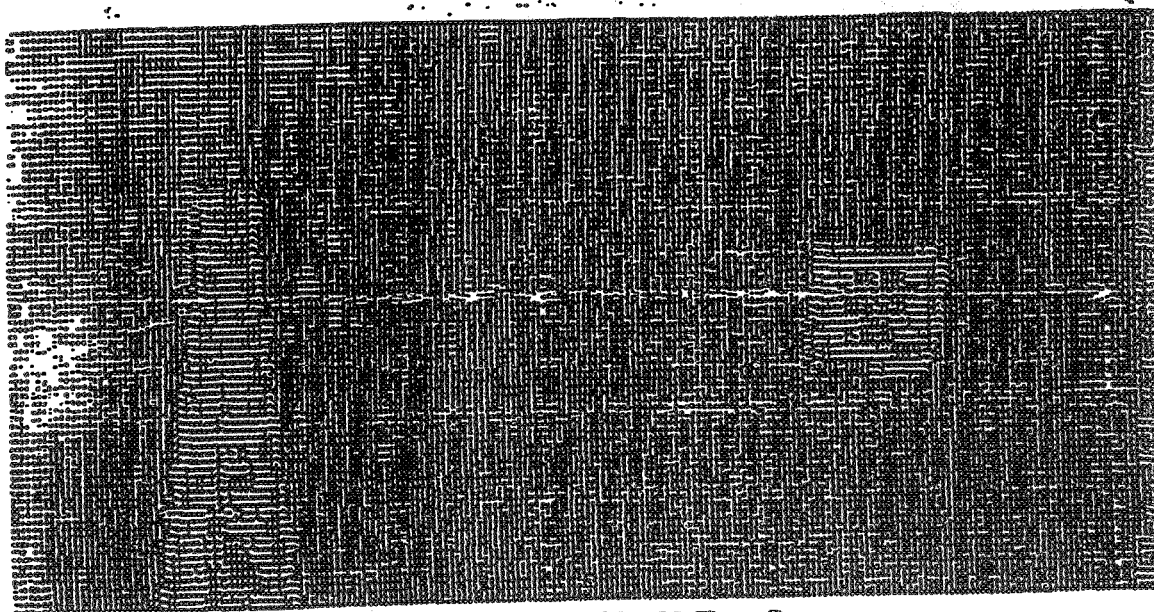
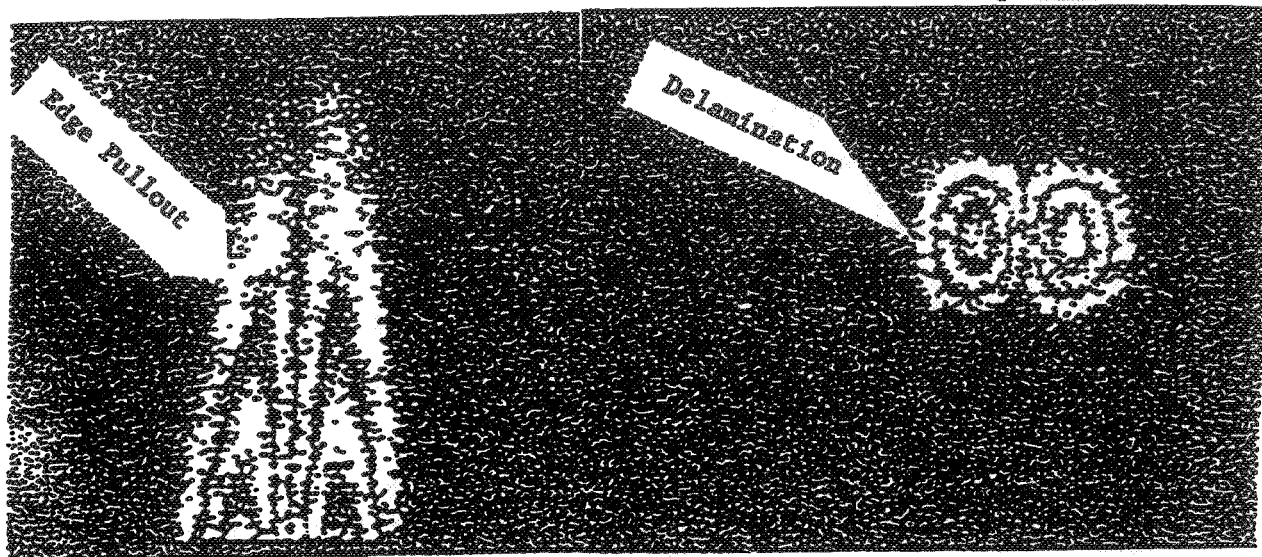


Fig. 15 Result of stroboscopic shearography of a vibrating plate at 3.07 KHz. (a-b) Phase maps before and after unwrapping, (c-d) 2D and 3D display of the amplitude derivative with respect to x.



C-Scan of 12" X 12" Test Part

Fig. 16 Comparison of shearography with C-scan ultrasound. An edge pullout and a delamination in a composite panel are revealed by both techniques. Time required: 10 minutes for ultrasound and 1 second for shearography. Moreover, fluid coupling is needed in the ultrasonic testing.

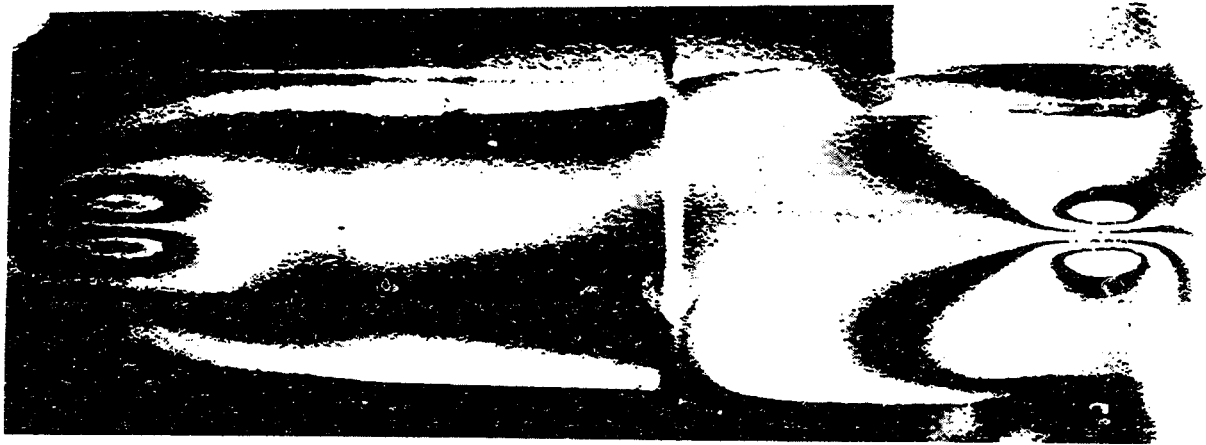


Fig. 17 Fringe pattern revealing two internal cracks in a steel vessel. The means of stressing is internal pressurization.

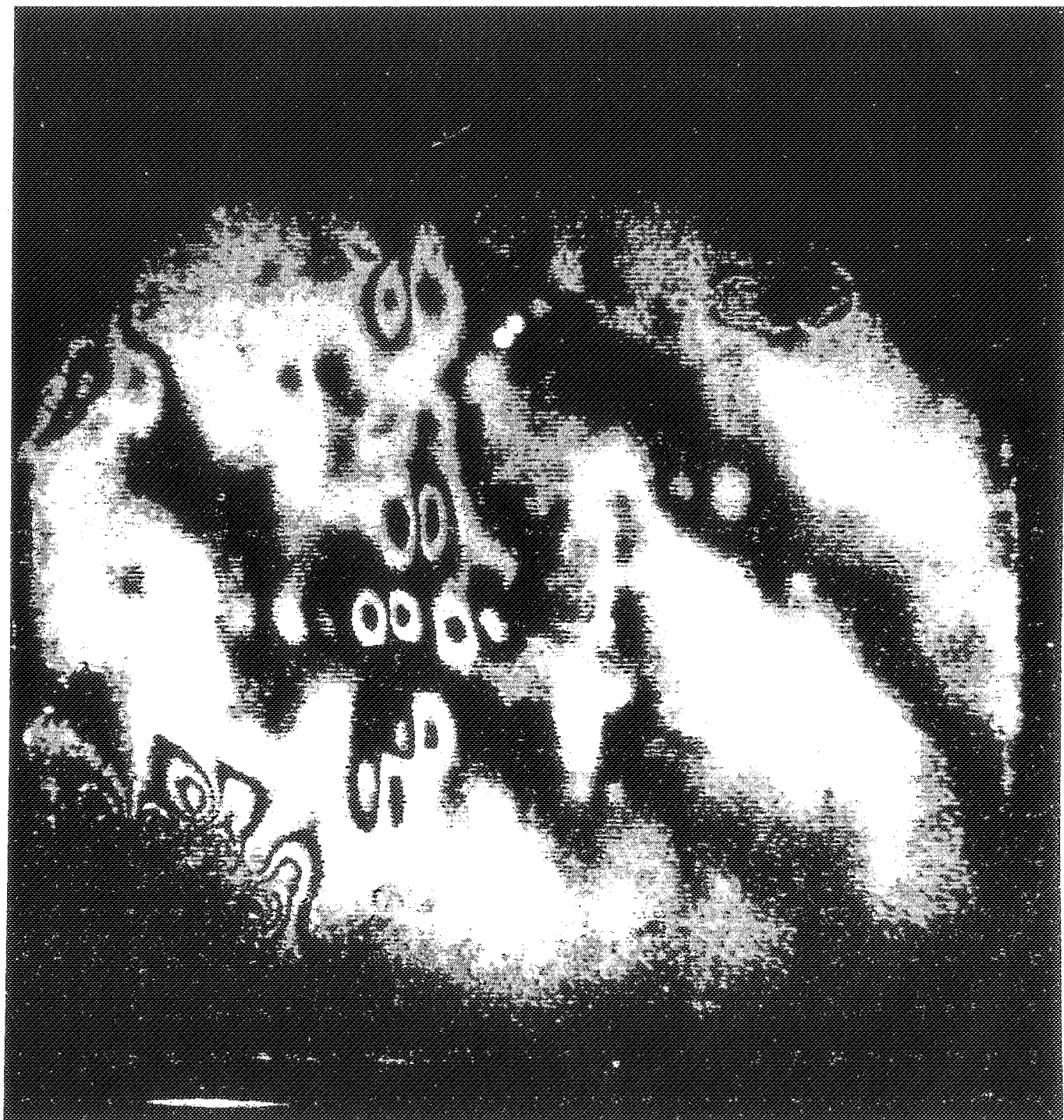


Fig. 18 Fringe pattern reveals several areas of separation in a large cord-reinforced rubber panel using partial vacuum stressing.

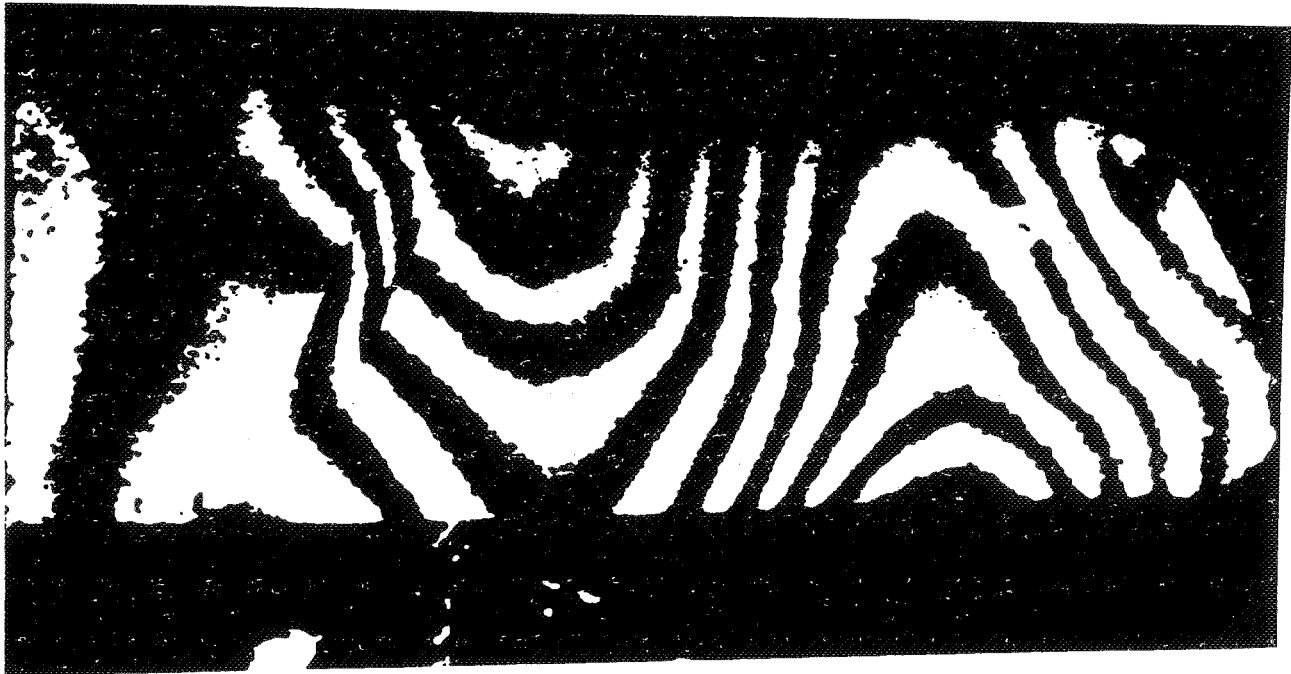


Fig. 19 illustrates detection of a crack on a composite turbine blade using thermal stressing. The object was heated with a hair dryer.



Fig. 20 Result of shearographic inspection of adhesive-bonded lines in composite assemblies using multi-frequency vibrational excitation. There are two bonded lines. Perfect bond lines should appear dark, and any deviation from darkness is indicative of a weak bond.

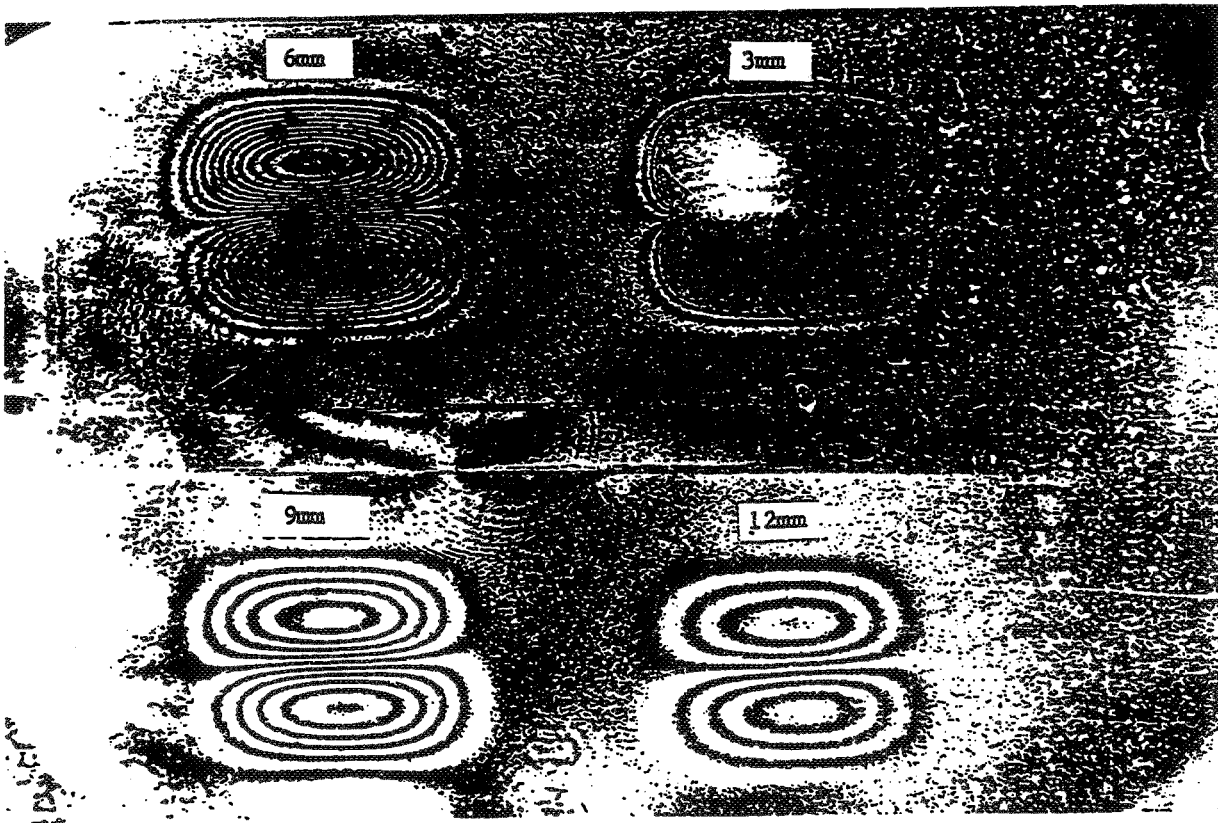
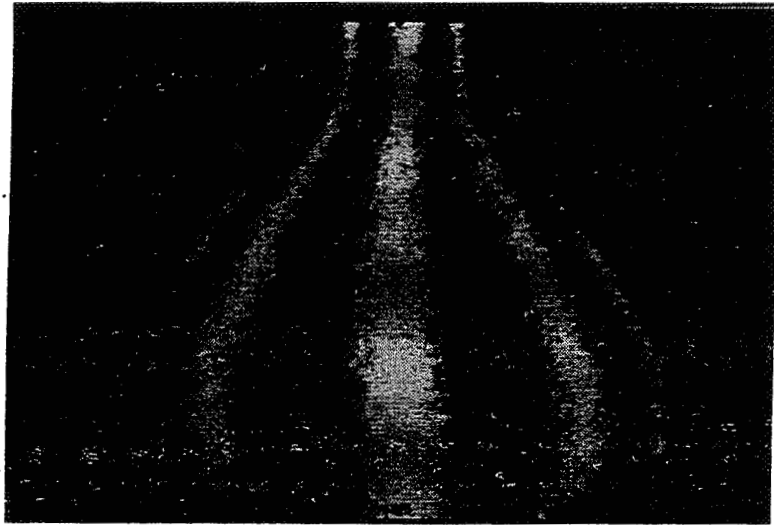
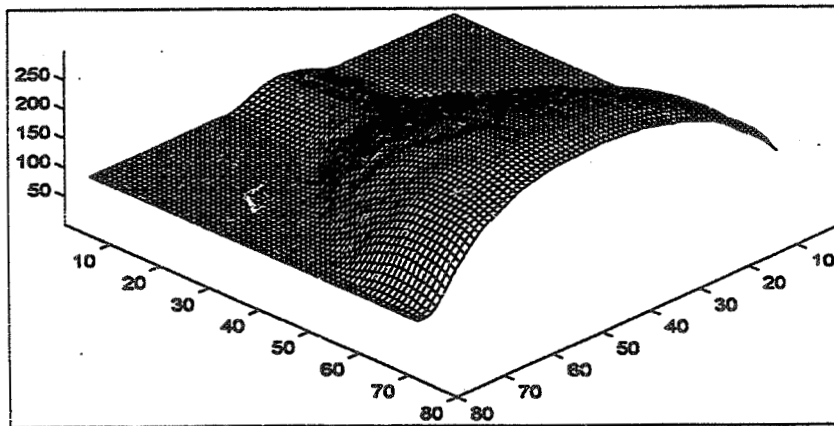


Fig. 21 Fringe patterns due to debonds at the various depths (3mm, 6mm, 9mm and 12mm). Note that the one closest to the surface has the highest fringe density and vice versa.



(a)



(b)

Fig. 22 (a) Fringe pattern depicting $\partial Z / \partial x$ of a light bulb using the double wavelength method. (b) A 3D plot of the surface shape (Z) obtained by integrating $\partial Z / \partial x$ of (a).

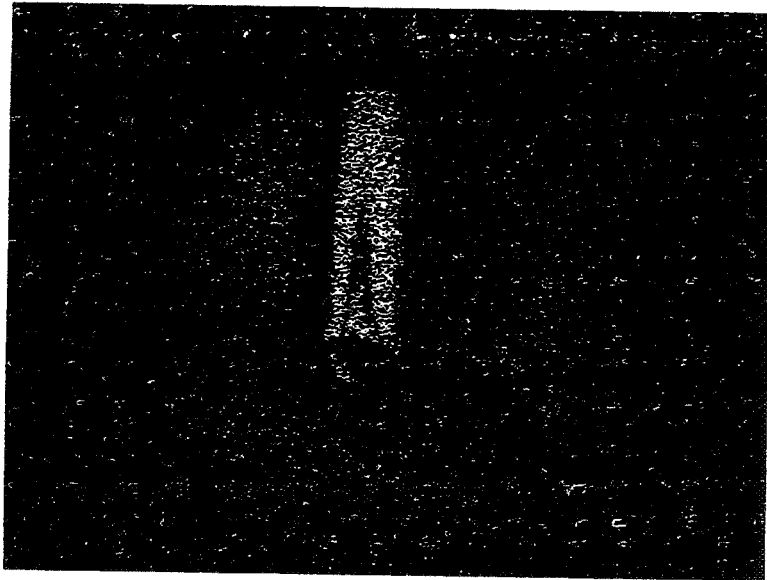


Fig. 23 shows a leakage from the valve of a pressure vessel. The escaping gas is helium.

**LARC™ RP46 POLYIMIDE
LOW COST HIGH TEMPERATURE TECHNOLOGY**

Ruth H. Pater

NASA Langley Research Center
Composites and Polymers Branch Materials Division
Research and Technology Group
Mail Stop 226
Hampton, Virginia 23681-2199

Telephone 757-864-4277
e-mail r.h.pater@larc.nasa.gov



Ruth H. Pater

LARC™ RP46 Polyimide Low Cost High Temperature Technology

The LARC™ RP46 polyimide was developed in 1991 at NASA Langley Research Center as an ultra-high-performance composite matrix resin for use in aircraft engine components, as well as a more environmentally friendly alternative to commercially available high temperature matrix resins. The LARC™ RP46 polyimide is prepared with non-toxic 3,4'-oxyldianiline(ODA). This chemistry has led to several improved performance characteristics over similar high temperature polyimides. These improvements include

- 700°F use temperature
- Significantly less moisture absorption
- Better chemical corrosion resistance
- Greater microcracking resistance
- Higher structural durability

The 700°F use temperature LARC™ RP46 is 150°F higher than that of commonly used PMR-type high temperature resins. In addition, it features significantly less moisture absorption and is therefore less susceptible to moisture induced damage. It also has better corrosion resistance to chemicals, greater microcracking resistance, and higher durability with regard to structural integrity.

The fabrication costs for Langley Research Center RP46 polyimide technology are expected to be significantly lower than similar because most of the rigid handling regulations established by the Occupational Safety and Health Administration(OSHA) can be eliminated because of the use of non-toxic 3,4'-oxyldianiline(ODA). The LARC™ RP46 polyimide technology is easy to process, with a cure cycle very similar to that of other commercially available PMR-type resins.

Commercial Uses

Langley Research Center RP46 polyimide technology can be used as a high-performance, high-temperature-resistant composite, adhesive, molding, coating material, foam, or film. Potential applications include high temperature printed circuit boards, wire coating, and molded hardware.

Benefits

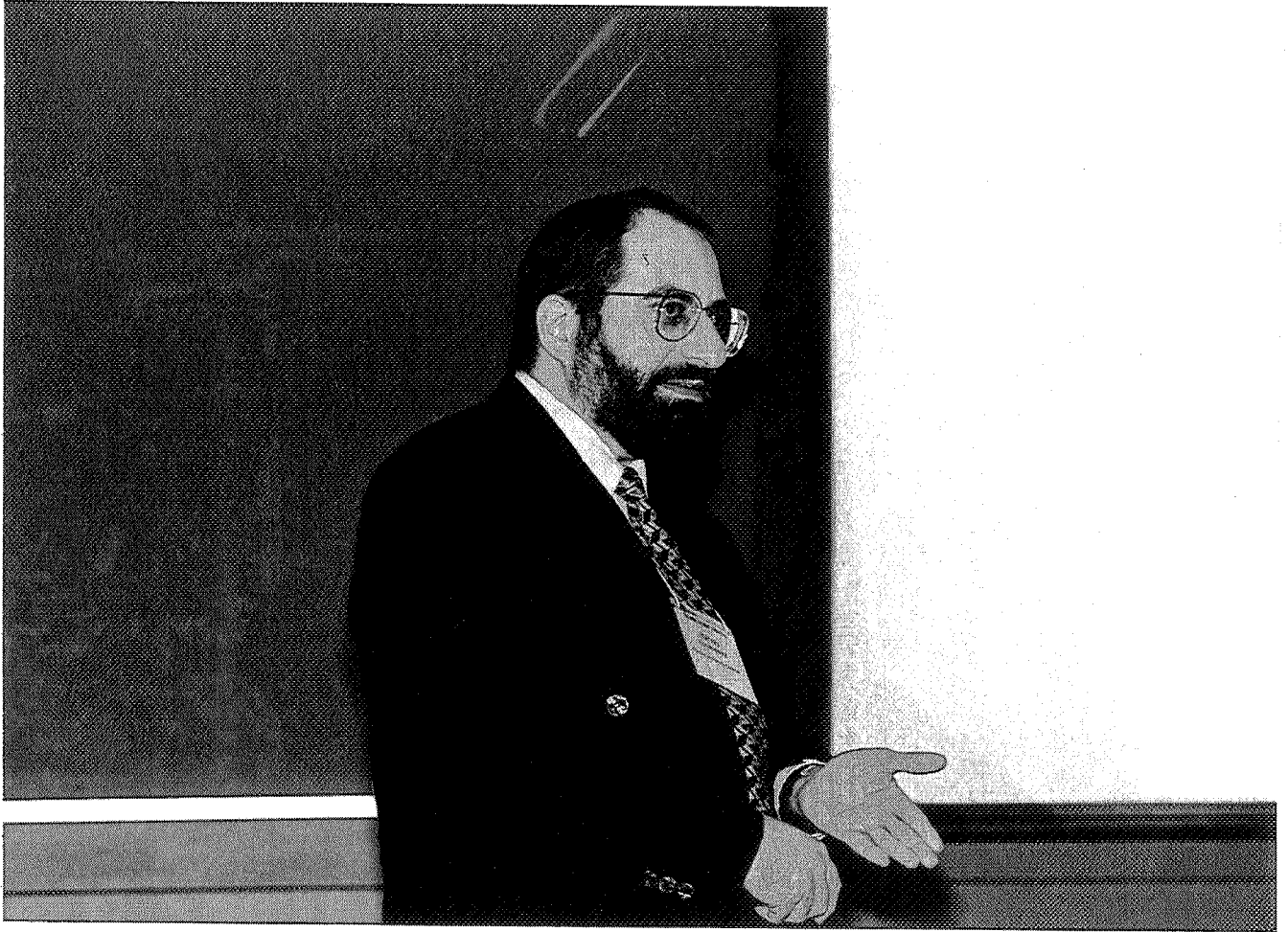
- Low cost
- Easy to process
- Non-toxic

MECHANICAL PROPERTIES OF SHEET STEELS USED IN STAMPING AND DRAWING

Harvey Abramowitz

Department of Engineering
Purdue University - Calumet
2200 169th Street
Hammond, Indiana 46323

Telephone: 219-989-2473
e-mail harveya@calumet.purdue.edu



Harvey Abramowitz

PREREQUISITE KNOWLEDGE

- **Stress – Strain Curves**
- **Tensile Testing - Experimental
Helpful, but not necessary**
- **Use of Dial Calipers, Micrometers**
- **PC's**
- **Spreadsheet Software**

EQUIPMENT/SUPPLIES

- Samples
 Various Types
- Micrometer
- Dial Calipers
- Tensile Tester
 with extensometer – 50%
- Ruler/Straight Edge
- Marker
- PC

INTRODUCTION

TO

SHEET STEELS

SHEET STEELS TESTED

DDS	Deep Drawing Steel
EDDS	Extra Deep Drawing Steel
HF	High Strength Formable
BH	Bake Hardenable

STEEL CHEMISTRIES (Typical)

Product	DDS	EDDS	HF	BH
Element				
C	0.005	0.003	0.06	0.04- 0.06
N	<0.005	<0.003	0.005	<0.005
Mn	0.20- 0.25	0.20- 0.25	0.3-0.6	0.4-0.6
P	0.01	0.01	0.02 max	0.05- 0.07
S	0.012	0.012	0.025	0.025
Ti	0.04- 0.06	0.06- 0.09	NA	NA
Cb	0.02- 0.03	NA	NA	NA
Si	<0.02	<0.02	<0.02	<0.02
Al	0.03- 0.08	0.03- 0.08	0.03- 0.08	0.04- 0.08

Nb-Ti

Ti Stab
alone

STEEL PROPERTIES

Product	DDS	EDDS	HF	BH
Property				
YS(ksi)	24	20	27 min	44 min
TS(ksi)	43	44	49 min	55 min
%EL	46	48	34 min	-----
n bar 6-12%	0.24	0.27	0.23	-----
r bar	1.9	2.0	1.6	-----

STEEL APPLICATIONS

DDS

OUTER PANEL

- Quarter Panel
- Side Panel Outer

INNER PANEL

- Rear Floor
- Fuel Tanks

STEEL APPLICATIONS

EDDS

OUTER PANEL

- Quarter Panel
- Side Panel Outer
- High Roof

INNER PANEL

- Quarter Inner
- Dashboard
- Wheelhouse

STEEL APPLICATIONS

HF

OUTER PANEL

- Hood Outer
- Tail Gate Outer
- Quarter Panel

INNER PANEL

- Cross Member
- Reinforcement

STEEL APPLICATIONS

BH

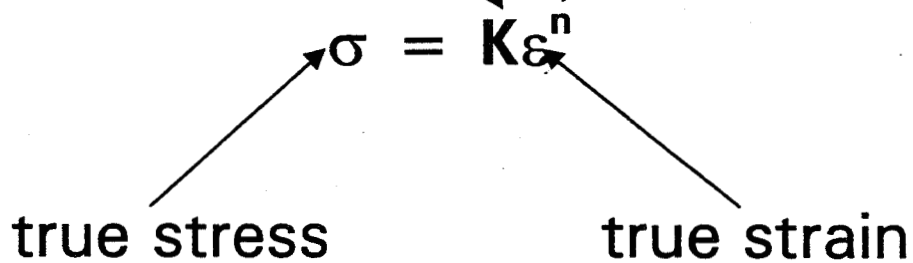
Appliances

TRUE STRESS – TRUE STRAIN CURVE

$$\sigma = K\varepsilon^n$$

strength coefficient

strain hardening
exponent



TRUE STRESS – TRUE STRAIN CURVE

$$\log \sigma = K + n \log \varepsilon$$

with

$$\sigma = S (1 + e) \quad \text{and} \quad \varepsilon = \ln(1 + e)$$

engineering stress

engineering strain

ASTM E 646

PLASTIC STRAIN RATIO, r

$$r = \frac{\epsilon_w}{\epsilon_t}$$

width thickness

$$R_m = (r_o + 2r_{45} + r_{90}) / 4$$

$$\Delta r = (r_o + r_{90} - r_{45}) / 2$$

ASTM E 517

Table 50—I. Approximate Values for Plastic-Strain Ratio of Sheet Steels.

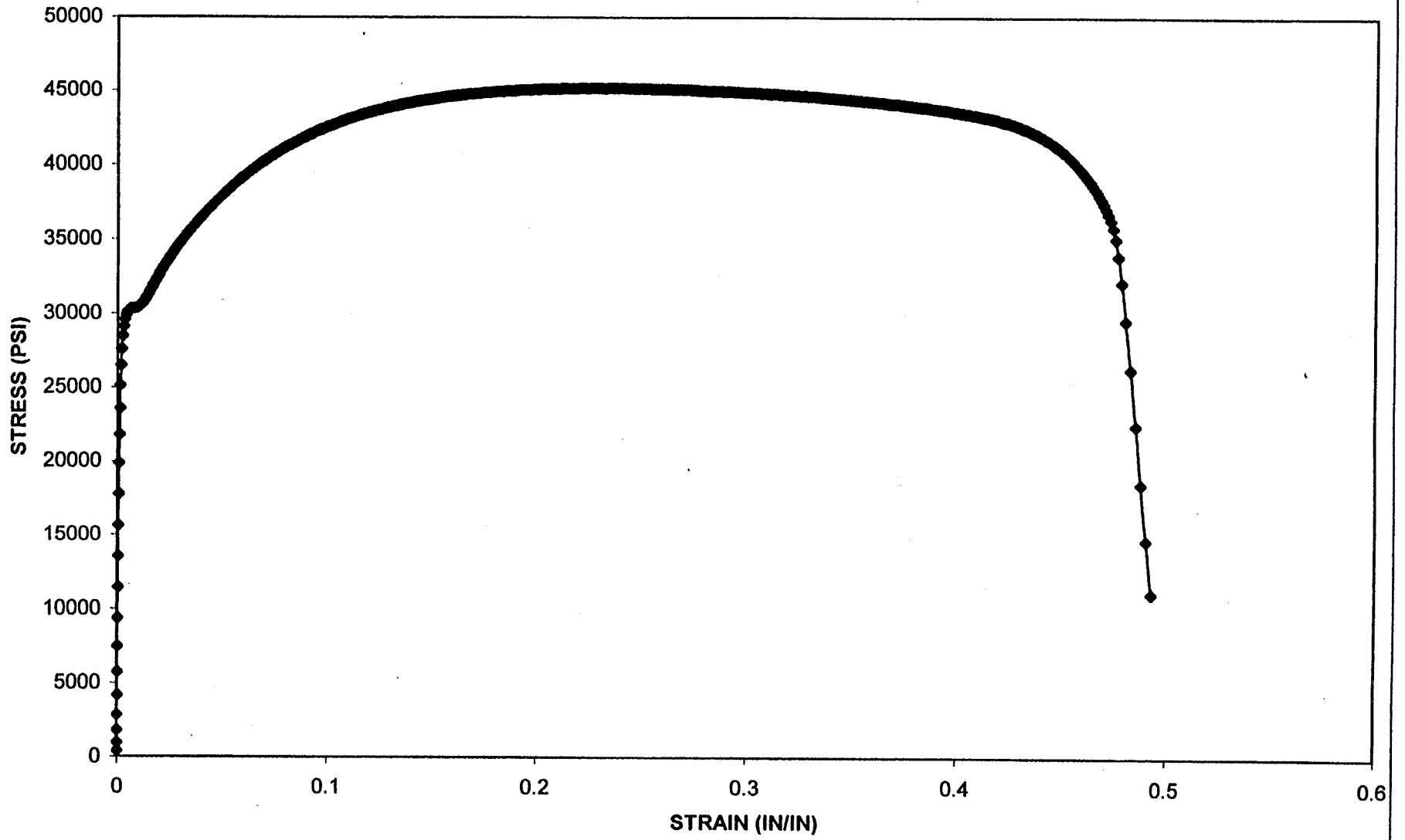
Steel	R_m	Δr
Hot-Rolled Sheet	~ 1.0	~ 0.0
DQ Sheet	~ 1.2	$\sim +0.4$
DQ SK Sheet	~ 1.6	$\sim +0.6$
Tin-Mill Products	Generally less than cold-rolled sheet.	Generally less than cold-rolled sheet and approximately zero.

TENSILE TEST

PROCEDURE

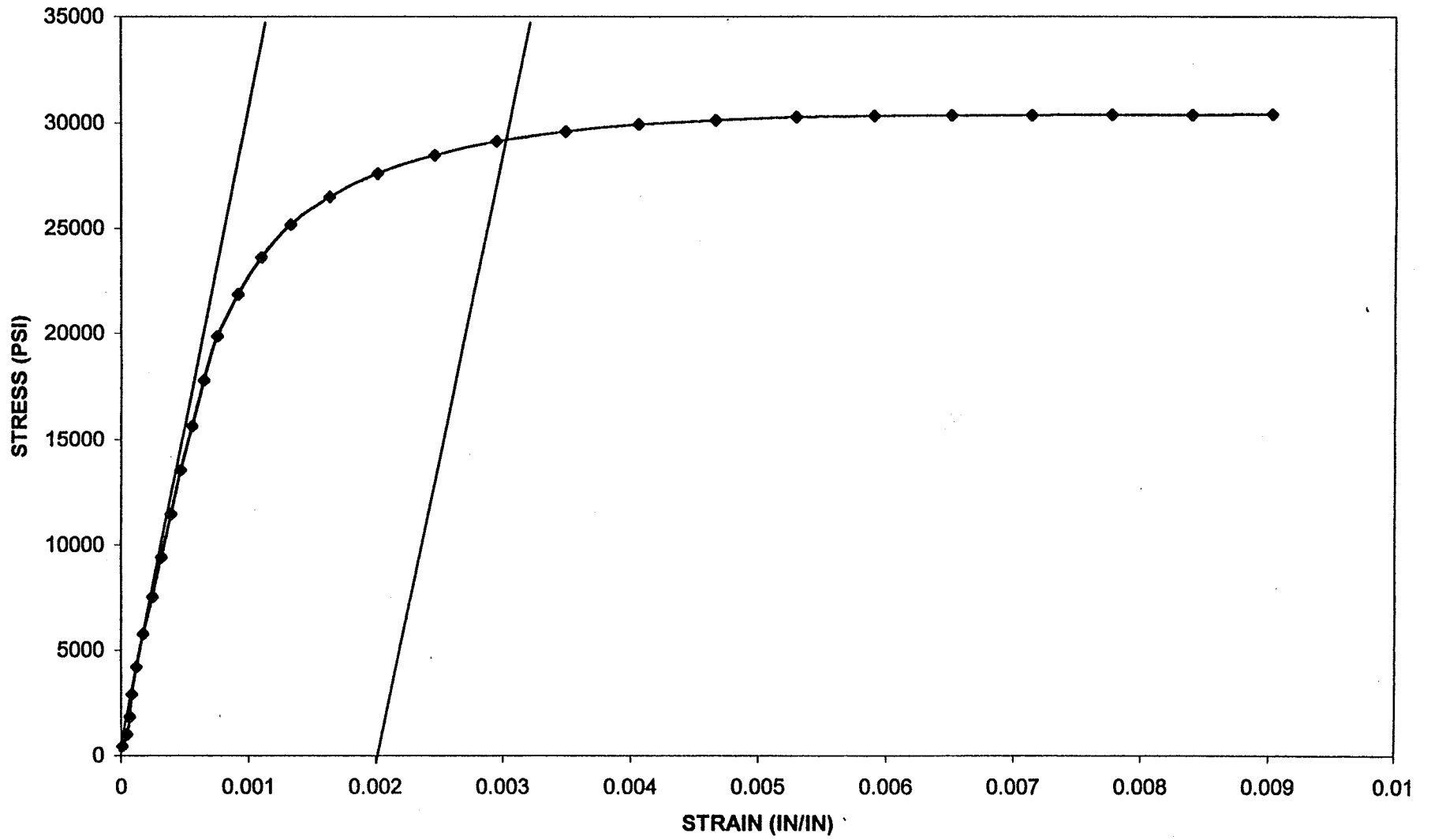
- Measure and mark gage length
- Place in tensile tester
- Run test
ASTM E 8
 - Analyze data

TENSILE TEST
DDS
SET1-#2

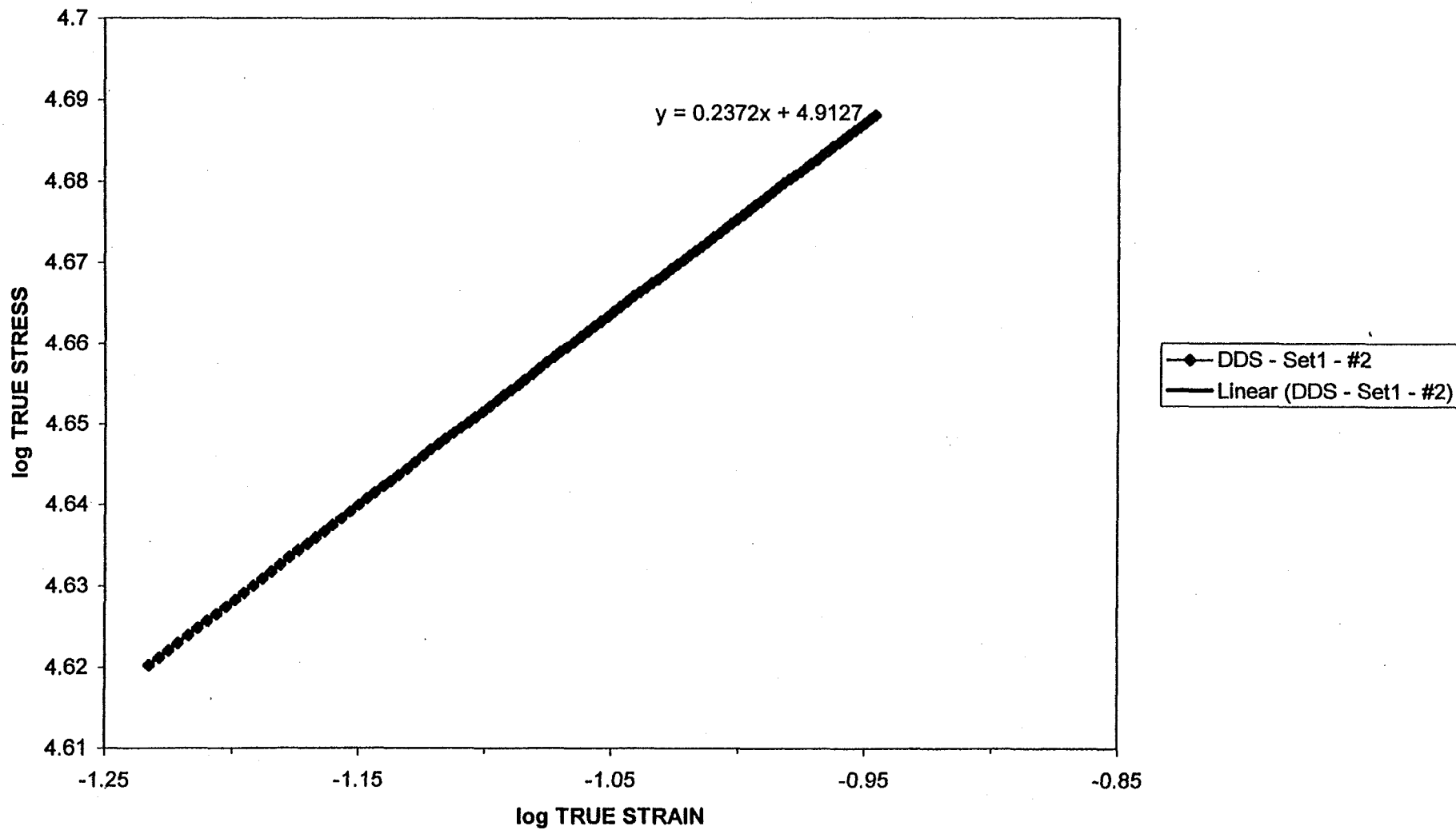


407

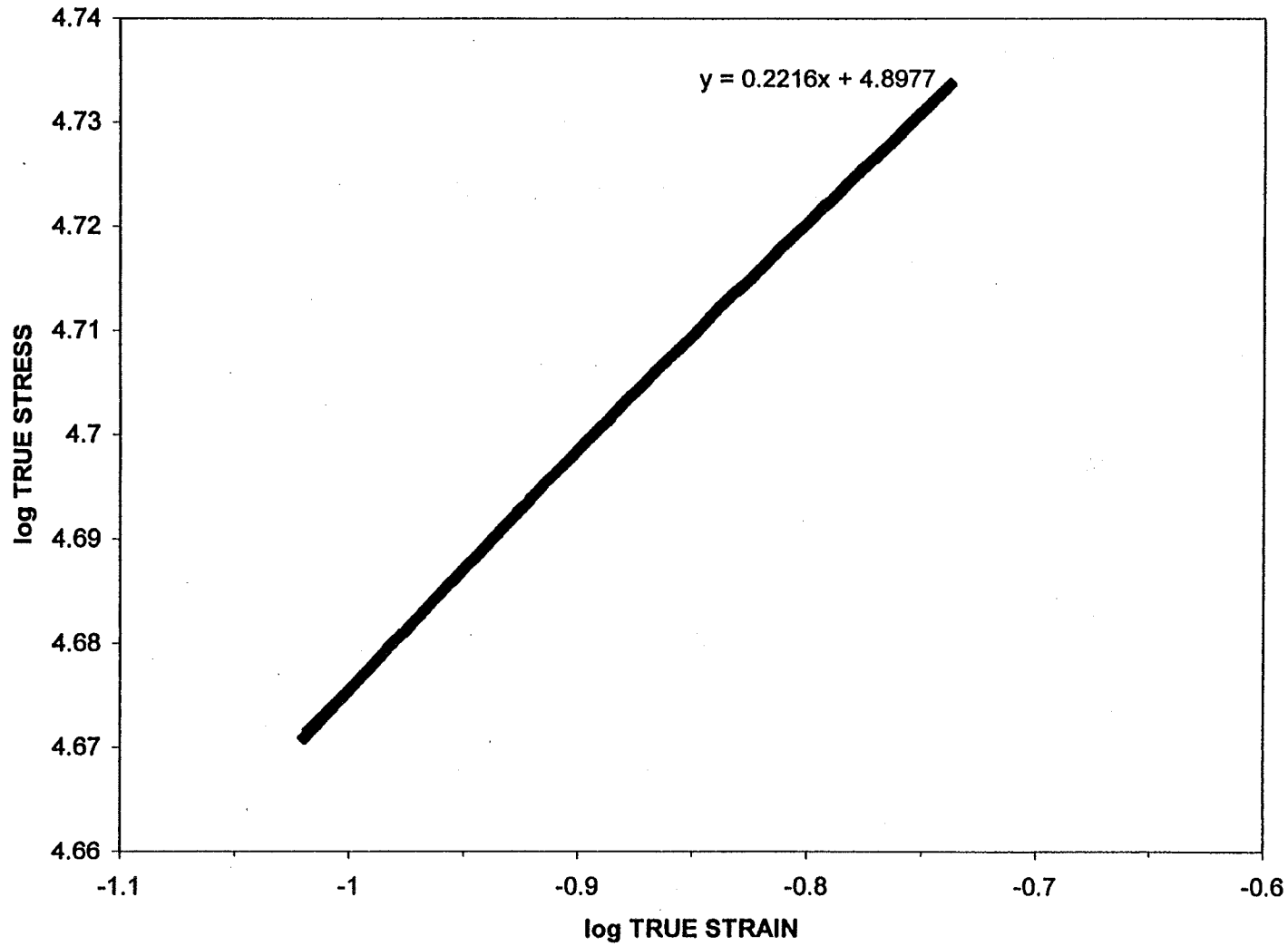
0.2%YS DDS
Set1-#2



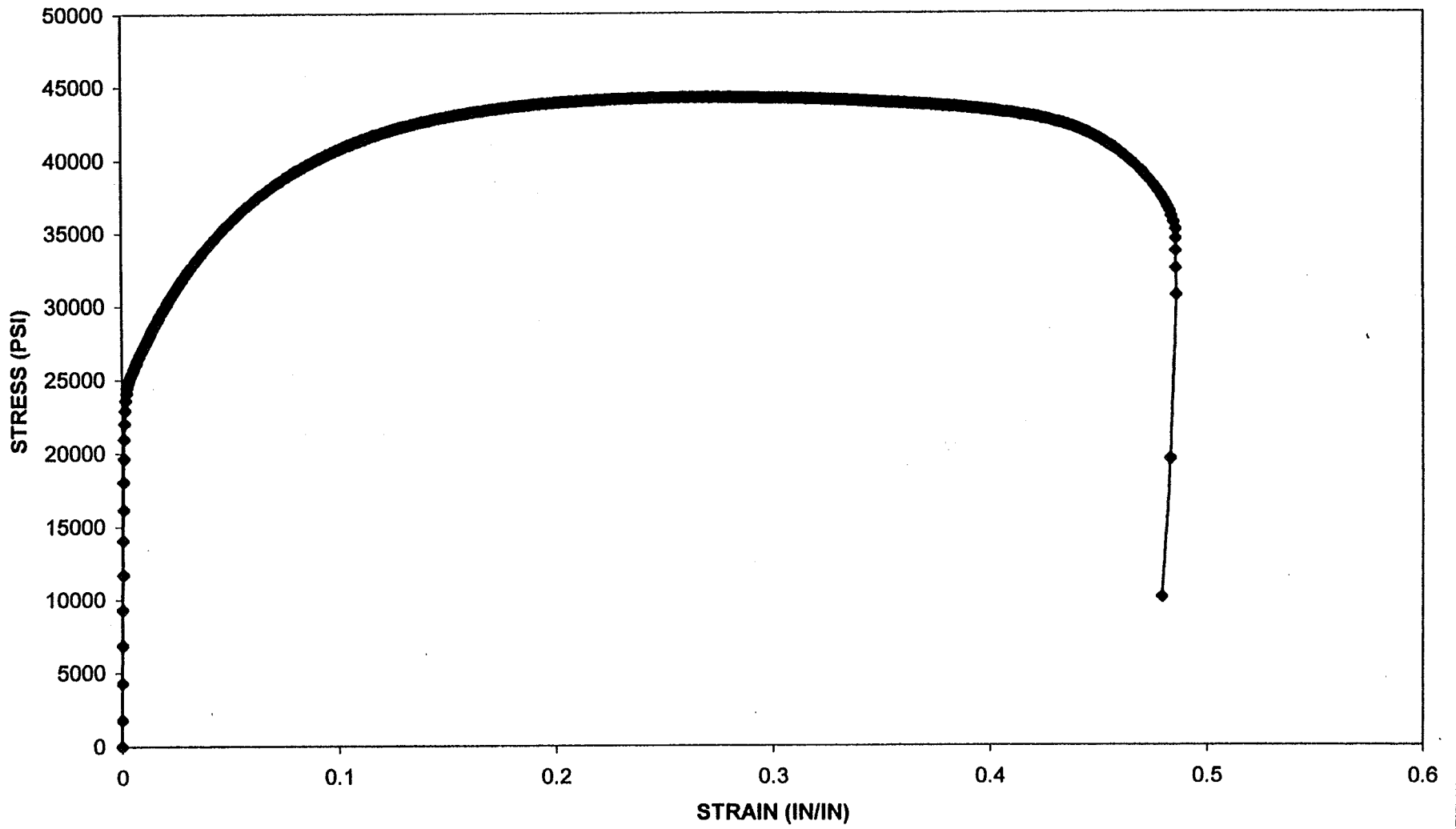
DETERMINATION OF n-VALUE (6-12%)
DDS



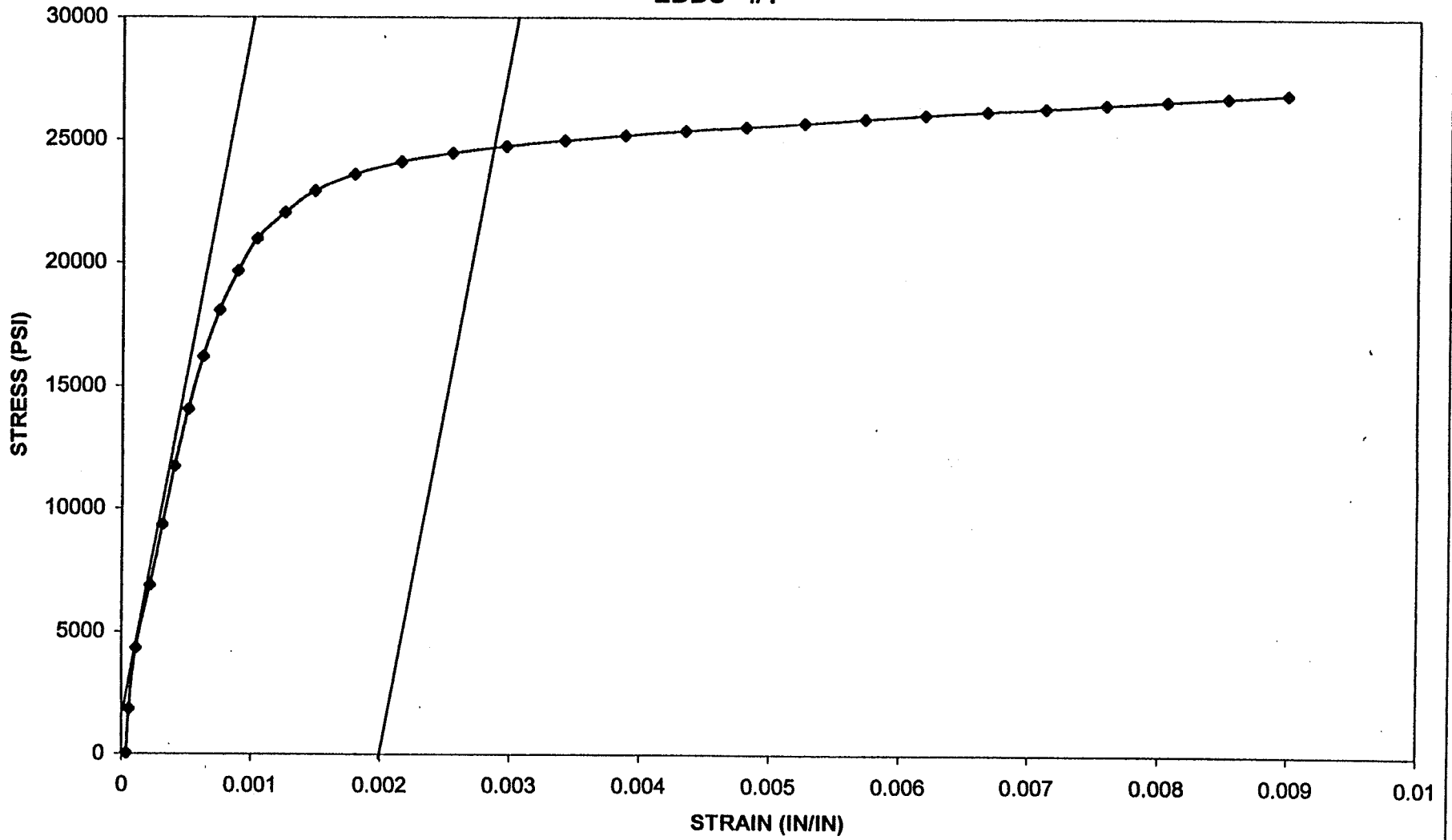
DETERMINATION OF n-VALUE (10-20%)
DDS



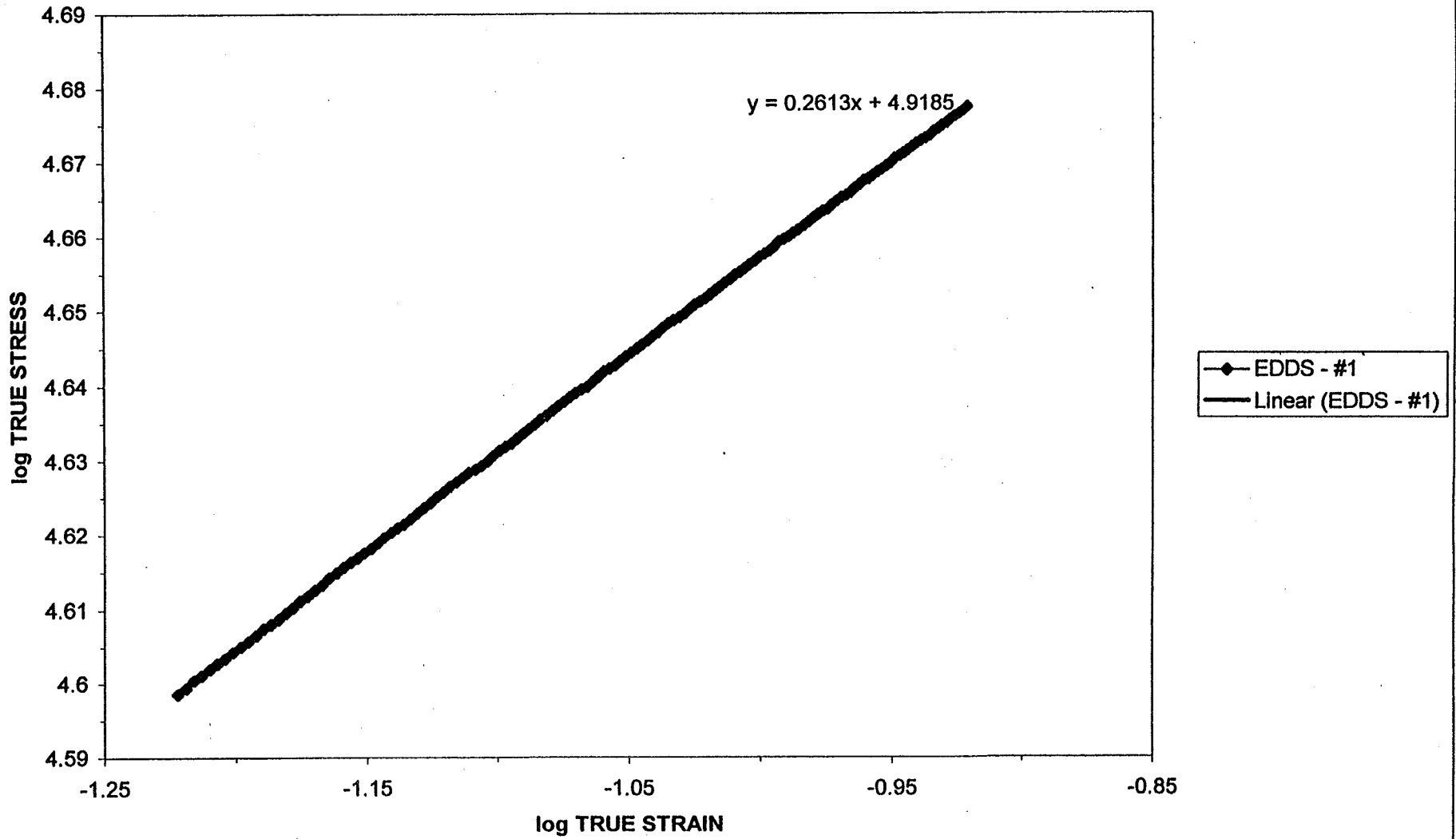
TENSILE TEST
EDDS #1



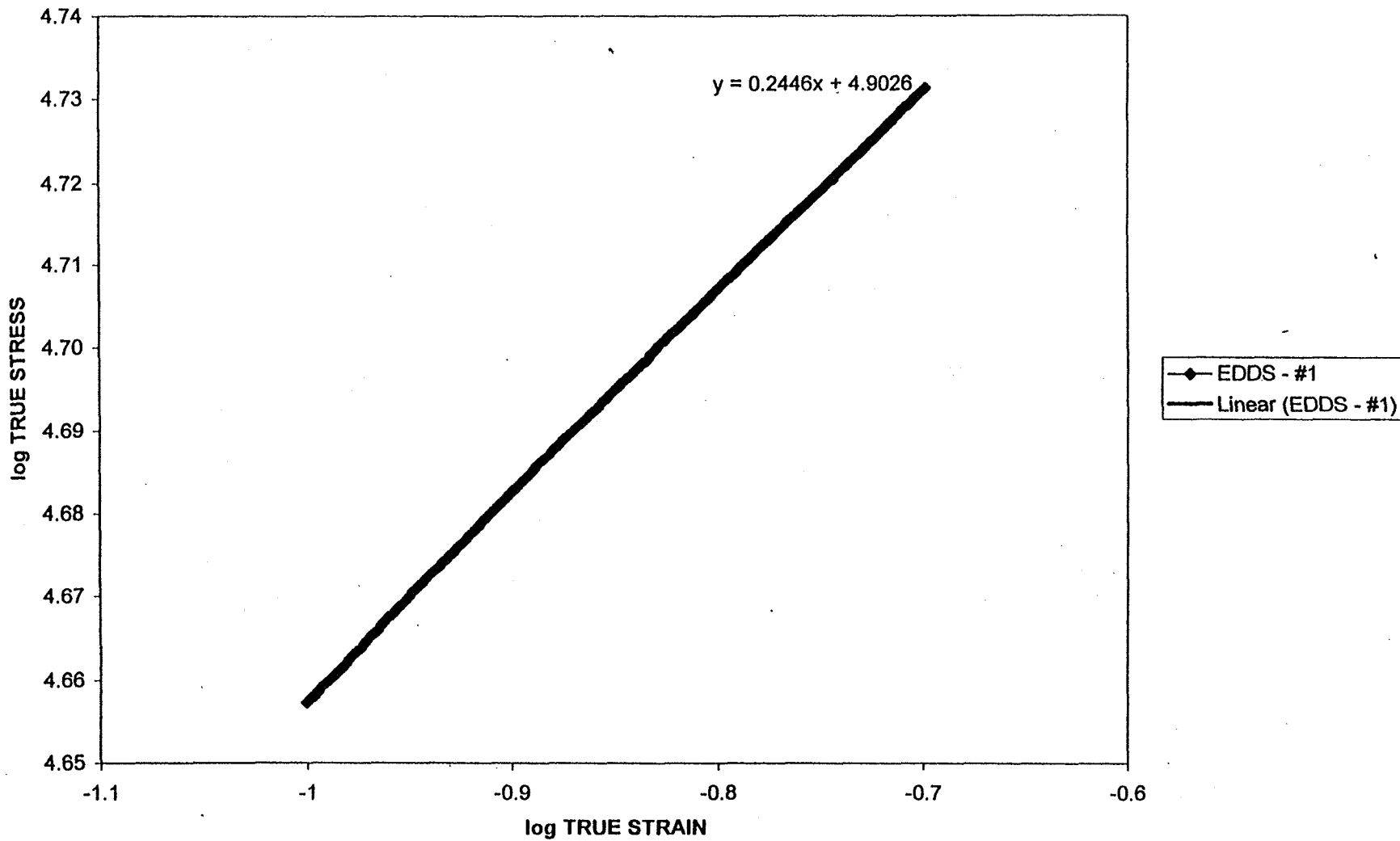
0.2% YS
EDDS - #1



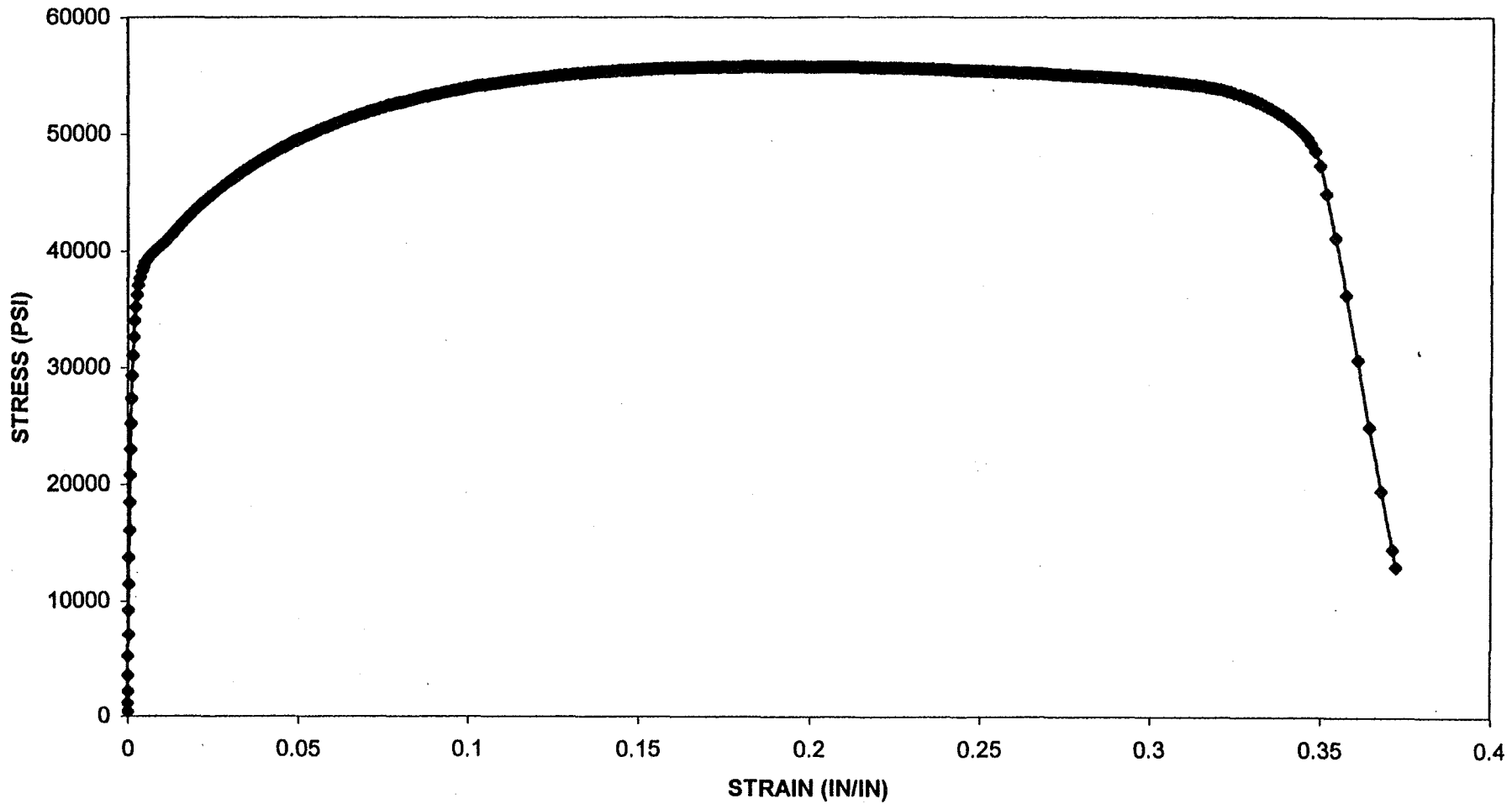
DETERMINATION OF n-VALUE (6-12%)
EDDS



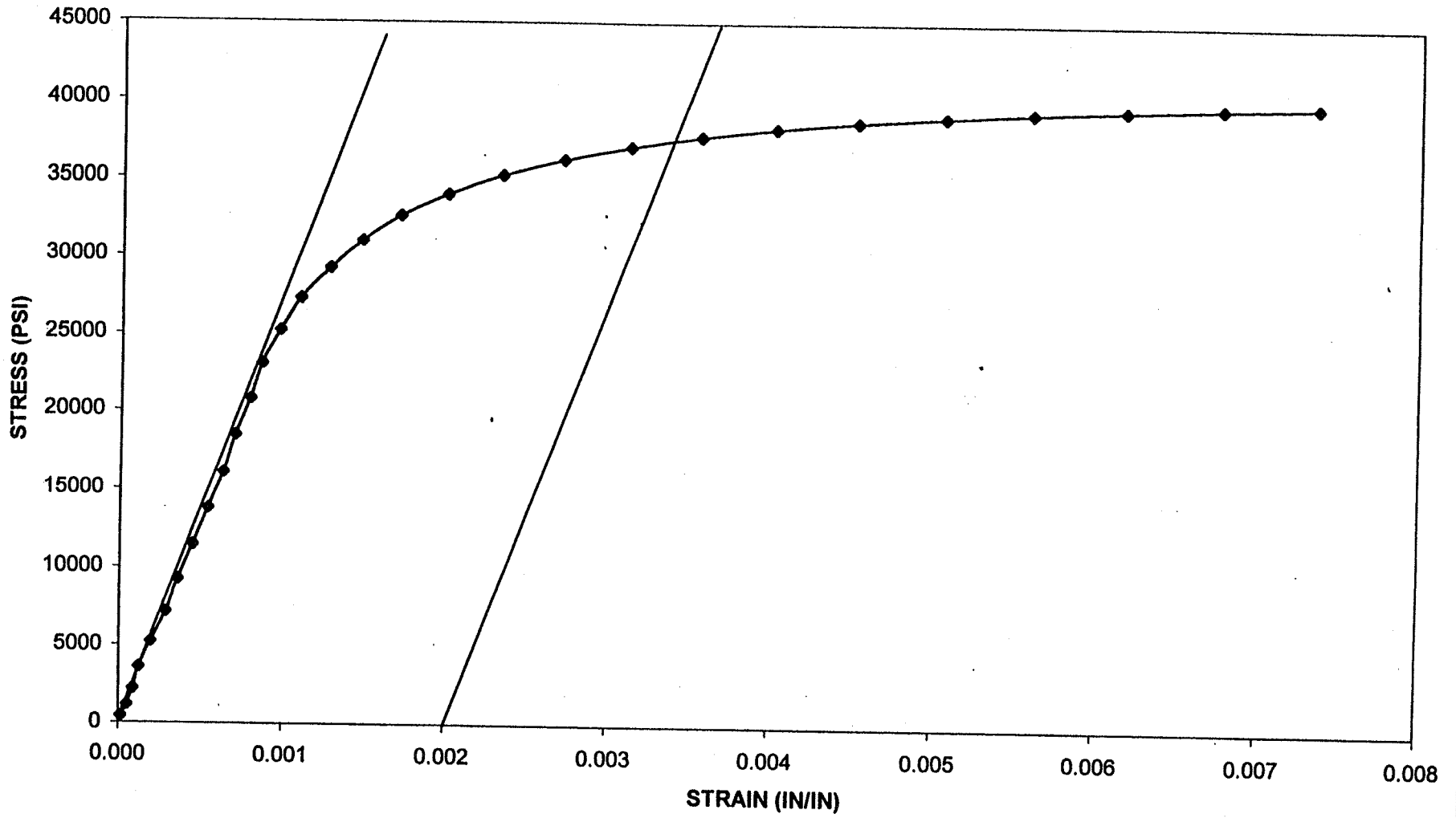
DETERMINATION OF n-VALUE (10-20%)
EDDS



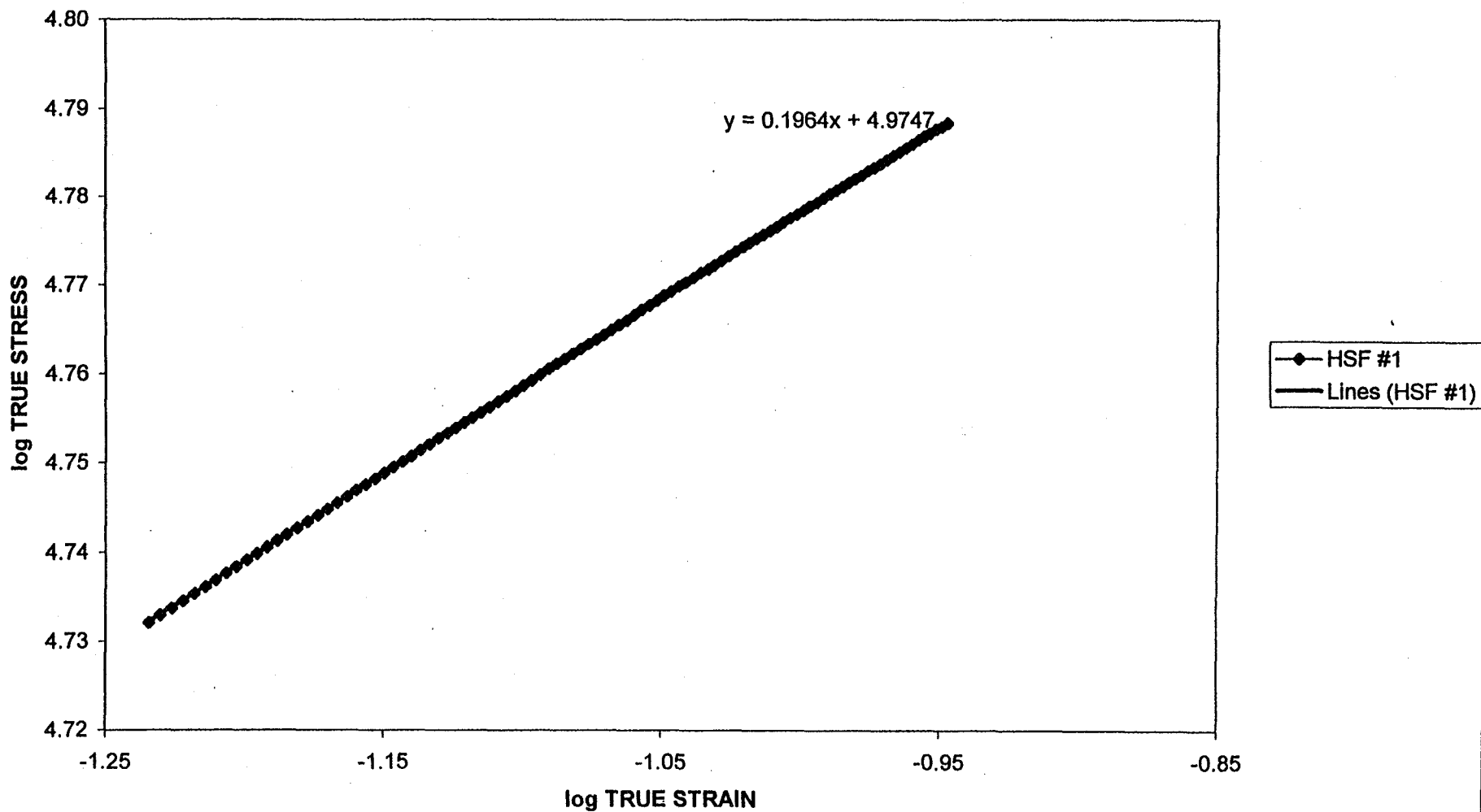
TENSILE TEST
HIGH STRENGTH FORMABLE
#1



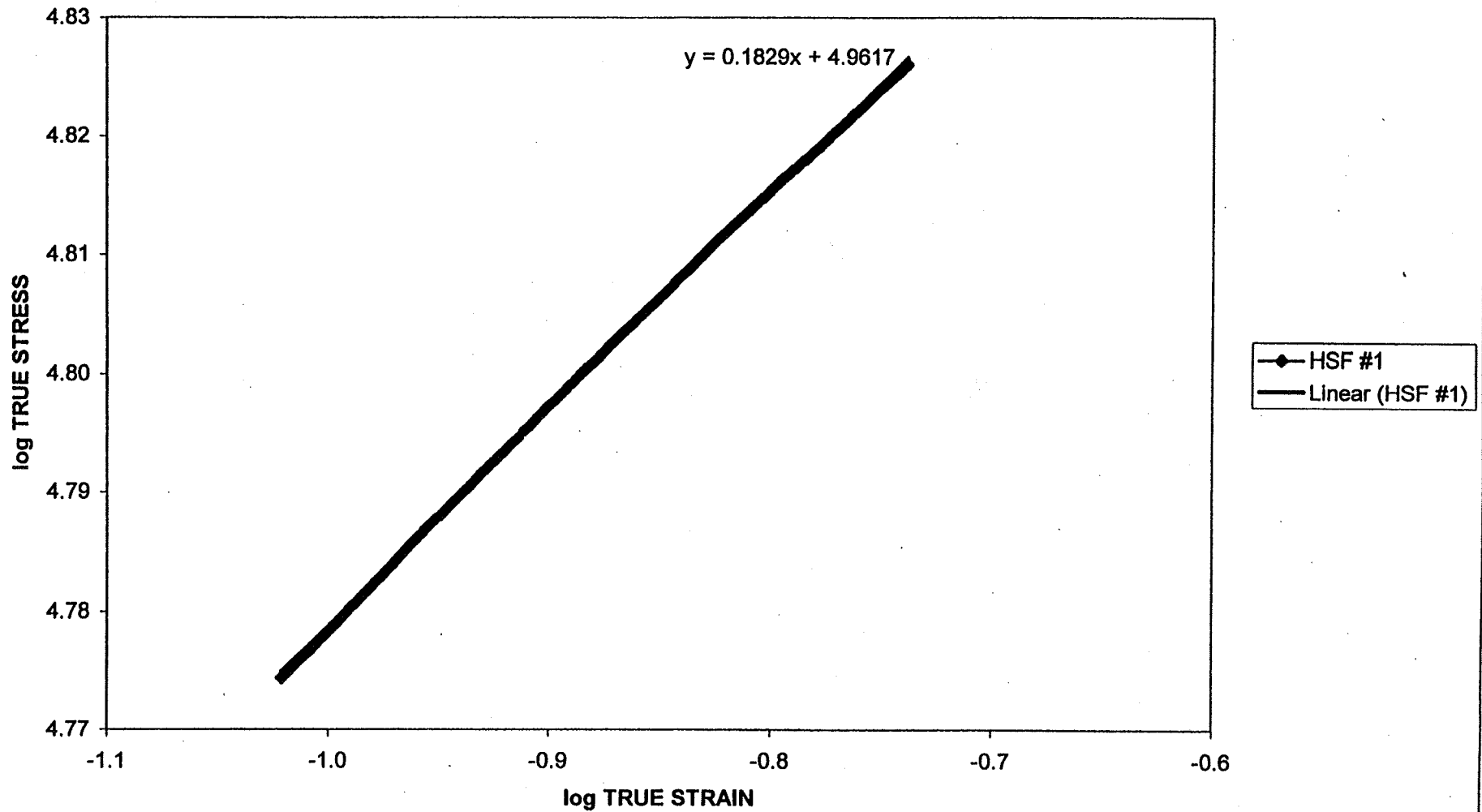
0.2% YIELD STRENGTH
HIGH STRENGTH FORMABLE
#1



DETERMINATION OF n-VALUE (6-12%)
HIGH STRENGTH FORMABLE
#1



DETERMINATION OF n-VALUE (10-20%)
HIGH STRENGTH FORMABLE
#1



RESULTS

<i>Product</i>	DDS	EDDS	HF	BH
<i>Property</i>				
0.2% offset YS (ksi)	29 (24)	25 (20)	36 (27min)	53→73 ** (44min)
TS (ksi)	46 (43)	44 (44)	55 (49min)	(55min)
% EL	46 (46)	47 (48)	34 (34min)	13 (----)
n (6-12%)	.24 (.24)	.26 (.27)	.20 (.23)	----- (-----)
K (ksi) (6-12%)	83	83	93	----- (-----)
N (10-20%)	.22	.24		----- (-----)
K (ksi) (10-20%)	79	80	91	----- (-----)

Notes: (a) () values from company, (b) ----- not taken ,
(c) ** heated at 100°C for 1h or 100°C for 1h
+ 170°C for 20 min

CONCLUSIONS

- Automotive sheet steels introduced to students
- Mechanical properties were measured and compared favorably with published values
YS, TS, %El, n-Value
- Properties of different steels compared

FUTURE ADDITIONS

- r – Value
- Hardness
 - Superficial (HR30T)
 - Microhardness
- Ductility
 - Olsen Cup Test
- Microstructure

**EVERY-DAY OBJECTS AND CLASS
DEMONSTRATION IN MATERIAL SCIENCE CLASS,
DESIGNED TO HELP STUDENTS LEARN**

Neda S. Fabris

Mechanical Engineering Department
California State University, Los Angeles
5151 State University
Los Angeles, California 90032

Telephone 213-343-5218
e-mail nfabris@calstatela.edu



Neda S. Fabris

Every-Day Objects and Class Demonstration in Material Science Class, Designed to Help Students Learn

Neda S. Fabris,

Department of Mechanical Engineering,

California State University, Los Angeles

Los Angeles, California 90032-8153

Key Words: Material Structure, Properties, Testing

Prerequisite Knowledge: Basic Chemistry Course, Enrollment in First Materials Class

Objective: To facilitate students' learning process, memorizing and visualization of three-dimensional concepts.

Equipment:

Styrofoam balls, piano wires, coat hangers, artists' nondrying clay, tricot cloth, striped cloth scraps, rubber band, chalk pieces, silly putty, small objects made from different material and using different manufacturing processes,

Introduction:

Based on my experience of teaching 27 different classes, Material Science or Engineering Materials classes require more facts to be remembered and more different concepts to understand than any other engineering class in the mechanical engineering curriculum.

In order to facilitate students' learning, I have applied for the California State University institutional grant and in 1994-95 received "Innovative Instruction Award" in the form of four units of released time and limited funding for student assistant support and supplies. For my project I collected samples, made models and developed a set of simple experiments that can be brought to the classroom and/or used in laboratories to demonstrate different properties of engineering materials.

I organized the material according to chapters 1-11 and chapter 18, of the textbook: The Science and Engineering of Materials by Donald Askeland,¹ that we cover in "Materials Science and Engineering," the sophomore class for mechanical and civil engineering students. Most other science and engineering books are organized in a similar way so the examples and demonstrations explained in this paper can be used by instructors teaching from other textbooks in almost the same order. Also, I am using several simple examples and associations that help me and hopefully my students, to remember the large number of terms, laws and relations. In this paper, I summarize the content of my "magic box" for Chapter 1 through Chapter 6 and share

some examples that I use to make teaching interesting and help students learn. While some demonstrations are new, others are adapted from presentations from other Materials educators.

The Chapters in the following text refer to chapters in Askelands' Material Science and Engineering of Materials¹ book.

Chapter 1.: Introduction to Materials

Chapter overview: In this chapter materials are grouped into different categories and the relationship between material structures, processing and environment on the properties of materials is briefly described. The basic guidelines for material selection are also outlined.

To illustrate different types of material, I have collected and organized material from five groups:

- a. Metals: steel (nail), aluminum (pan), copper (plate), brass (key), solder (wire) silver (spoon) gold (jewelry) and others
- b. Ceramics (substrate for electronics components, ceramic cup, chalk, clay, brick).
- c. Polymers: 1. Thermoplastics: polyethylene, (plastic bag, squeeze bottles), polyvinyl chloride (pipe, floor tile), polypropylene (piece of carpet, rope) polystyrene (Styrofoam – egg cartons and food container), 2. Thermosetting: phenolics (piece of Bakelite) epoxy, polyester (piece of clothing) 3. Elastomers (rubber band)
- d. Semiconductors (wafers used to make semiconductor chips), chips in integrated circuit.
- e. Composite (piece of wood, concrete, plywood, fiberglass, glass fiber composite, rapid prototyping composite, piece of honeycomb panel)

The objects are common objects found around the house, at trade shows and exhibits, and tours of companies. Also, for homework I assign students to bring objects from home made from each category of materials not shown in the class. Often these are scrap parts that students willingly donate to my collection.

Students are able to observe, touch, and weigh each material while their properties are discussed in class. Also, different manufacturing processes are introduced by the examples selected, i. e. pieces produced using different methods are exhibited: material cut, drawn, welded (aluminum-honeycomb), glued (paper-honeycomb), and manufactured using electro-discharge machining, to name a few.

The optical, thermal, electrical and acoustic properties of the materials are illustrated with selections of the different materials. Acoustic properties are discussed using wire coat hangers and strings adapted from Xavier³. By attaching string to the ends of coat hangers, it is easy to demonstrate the amplification of the sound in the more dense media. Hitting the coat hanger against the wooden surface (door) while the end of the rope is stuffed in the ears greatly amplifies the sound and resembles the ringing of metallic bells.

Memory Tip: Remember good heat conductors are also good electrical conductors. Good pots have copper bottoms!

Chapter 2: Atomic Structure.

This chapter is an overview of the material covered in chemistry class. The whole chapter is covered in one class period. To illustrate covalent bonding, a model of silica (SiO_2) is made using Styrofoam balls and piano wires. Similarly, ionic bonding is illustrated using a crystallographic model of sodium chloride made from different sizes of Styrofoam balls and piano wires. Also, students are asked to sort samples of different materials presented in Chapter 1 according to their bond energies presented in this chapter. I use my box of different materials to ask students which one has a higher coefficient of thermal expansion. I write their answers on the board. By going through atomic bonding and binding energy, we discuss the reasoning for low and high coefficients of thermal expansion and compare our findings with the students' estimate at the beginning of the class.

Memory Tip: To remember which ion is positive, cation or anion, I remind students that anion sounds like "onion" and you cry when you slice onions: therefore anions have to be negative!

Chapter 3: Atomic Arrangement

The crystallographic structure of different materials is illustrated using several models made of Styrofoam balls and piano wires. Points, directions, and planes in the crystals are much easier to comprehend if they are explained using the three-dimensional models than if drawn on the two-dimensional black board. Spatial presentation always represents problems to students, and different color models are the best visual aid possible. The largest amount of space in my "magic box" is occupied by crystallographic models.

Memory Tip: Planes are two-dimensional so their brackets are also "two-dimensional" (curved). Lines are straight so their brackets are made from straight lines. Planes and normal to planes have the same Miller indices.

Chapter 4: Imperfection in the Atomic Arrangement

The best way to illustrate the influence of imperfections in the crystallographic structure on the properties of materials is by simulating the dislocation movement, grain boundary influence and atomic slip with pieces of cloth. For example, the movement of dislocation can be illustrated by pushing the "bump" in a heavy cloth (like moving the heavy rug on the floor), or trying to move the "run" in nylon stocking. The strength of materials with small grain size can be illustrated with a piece of cloth made of the many pieces sewn in different directions and torn.

Surface tension can be easily explained with pieces of glass and water in between them. Also, throwing chalk on the floor can explain the energy absorbed in the creation of surfaces; throwing silly putty or piece on the floor can illustrate the energy absorbed in deformation.

To explain Schmid's Law, I make a model from the non-hardening clay, cut it with the ruler under an angle with respect to its axis and stick pencils into it to represent the line of loading, slip line and normal to the plane. On such a hand-made model, it is easy to explain angles λ (between the slip direction and the applied force) and ϕ (between the normal to the slip plane and the applied force).

To illustrate the grain boundary strengthening, I use two pieces of cloth one made from one piece, and the other sewn from different pieces. I compare the stitches with grain boundaries and

different directions of threads to crystal directions.

In this chapter I ask my students several fun and educational questions:

1. Why does water on a hot stove form a ball, **while on** a cold stove it makes flat puddle?(surface energy)
2. Why does baking soda absorb odors in the refrigerator?
3. If I throw two pieces of chalk from the same height, made from the same material and the same length but one with two times larger correction than the other, which one is going to break into more pieces assuming they both break perpendicular to their axis? Students have to equate the potential energy with the energy needed to break the bonds and create a new surface (Answer: both should break into an equal number off pieces).
4. I ask students what will be easier to tear one sweatshirt or one "cowboy's" shirt with many stitches and directions of threads?

Memory Tip: Remember my demonstrations and questions asked.

Chapter 5: Atomic Movement in Materials

Similar to the previous chapter, atom movement can be more easily explained on three-dimensional crystallographic models made from Styrofoam models, especially interstitial diffusion and the effect of the size of atoms. Samples of carburized material are collected to illustrate the practical applications of diffusion. Also, examples of bonded diffusion (sintered materials) are collected. To illustrate the time-temperature diffusion process, I use an example from my own experience, while working at Bell Laboratory on the accelerating testing of gold-plated contacts, i.e. testing at higher temperature to simulate the effect of twenty-year diffusion in a work environment.

.Memory Tip: Remember if you pour sugar water on an unsweetened cake, sugar will diffuse, and the whole cake will become sweet, but first the surface of it! Grated cheese (or chocolate) when heated will diffusion bond before they melt. Grains grow at a high temperature because the big grains absorb small, just like big fish eat small fish!

Chapter 6: Mechanical Testing and Properties

Although all mechanical and civil engineering students are required to take material testing laboratory in their junior year, this is the first class where they are exposed to this important aspect of engineering practice. In this class, I demonstrate many mechanical properties performing small experiments with simple objects.

1. Rubber band can illustrate elasticity, piece of clay plasticity, piece of "silly putty" creep.
2. Bending of the paper clip can illustrate fatigue properties of materials;
3. Twisting the chalk can illustrate the fracture of brittle materials;
4. Pulling the piece of elastic cloth (tricot) can illustrate the axial and longitudinal strains; Sketched square on the piece of cloth inclined 45 angle with respect to the axis of pull

can illustrate presence of shears in tension. Decrease in the width of the tricot illustrates Poisson effect.

5. Slow and fast deformation of "silly putty" can show the influence of strain rate on material properties.

In addition to all these experiments, I have collected many specimens that are broken in strength material laboratory to better explain the necking of the material, toughness testing and brittle fracture. Artist's nondrying clay is also very handy here: you can fast fabricate "tension" or "compression specimen" to illustrate the way the specimen is loaded, the effect of friction in compression, as well as how hardness, impact and fatigue testing are performed.

Using an elastic ball (rubber), a ball made from silly putty and a clay ball, I illustrate the effect of hardness on bouncing the ball. I then relate that to the measurement of the hardness using Scleroscope³ where the roles are inverted: indenter is rigid while the surface tested is softer and has a different hardness!

Memory Tip: Remember all tests are made from the necessity to compare different materials! Scientists did not develop equations to predict practical properties of real materials, so we engineers have to rely on testing. Remember the toughest guy in the class is not one who is the strongest but one who can take the most "beating". (This definition of toughness I got from one junior high school student during an "Open house" demonstration.). Then I ask them who is the tough teacher? The answer is often "You." It is true, I give them a lot of work, and they have to put lot of energy in this class to get a good grade.

REFERENCES:

1. Askeland R.A., *The Science and Engineering of Materials*, Third Edition, PWS Publishing Company, 1994
2. Spiegel, F.Xavier: "*Five Experiments in Materials Science for Less than \$10.00*", NASA Conference Publication 3151, November 1991, pp. 263-265
3. Kalpakjian S.: *Manufacturing Processes for Engineering Materials*, Third Edition, Addison Wesley 1997

Neda Saravanja Fabris, is Professor of Mechanical Engineering Department at California State University Los Angeles (CSULA). She has Bachelor's degree from University of Sarajevo, Bosnia and Herzegovina, MS and Ph.D. from Illinois Institute of Technology (IIT), Chicago Ill. She taught at the University of Sarajevo, at IIT, University of Illinois, and at CSULA (from 1979 till present). She was Research Fellow in Aachen, Germany in 1966-67 and member of Technical Staff Bell Telephone Laboratory, in Napperville Ill. 1976-1979. She teaches in the area of mechanics, materials and design and has developed four classes in manufacturing and automation. Her research activity and publications are in tool wear, self-excited chatter in metal cutting, cutting of honey-combs, and teaching methodology and recruitment of women in engineering. She has contributed to the National Educators' Workshop and ASEE Annual Conference for several years.

**ENGINEERING PLAN BEHIND THE
ULTRA LIGHT STEEL AUTO BODY
AND
AISI/CARS '98
OVERVIEW**

Darryl Martin

and

Samuel K. Errera

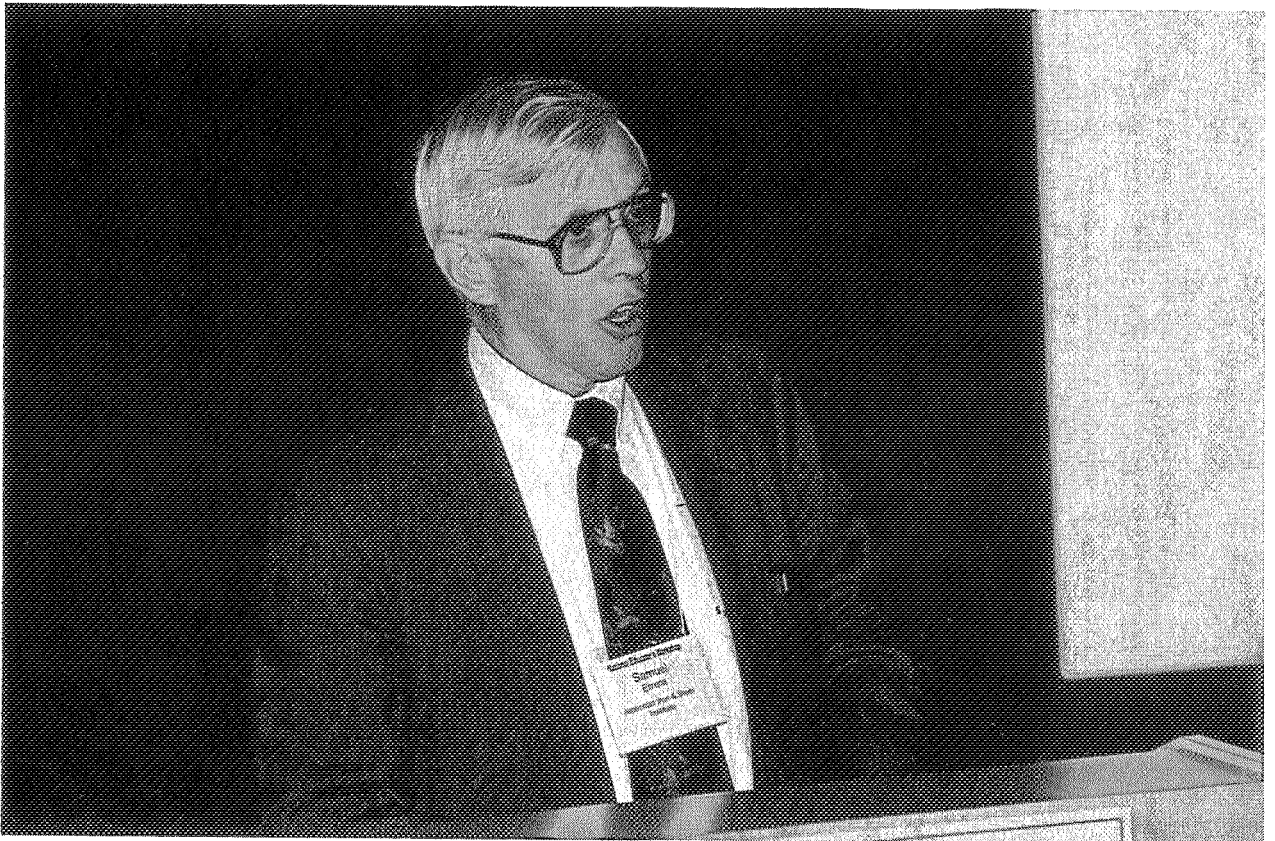
American Iron and Steel Institute
2000 Town Center
Suite 320
Southfield, Michigan 48075-1199

Telephone 248-945-4760
e-mail martin@autosteel.org

Telephone 248-945-4770
erreras@autosteel.org

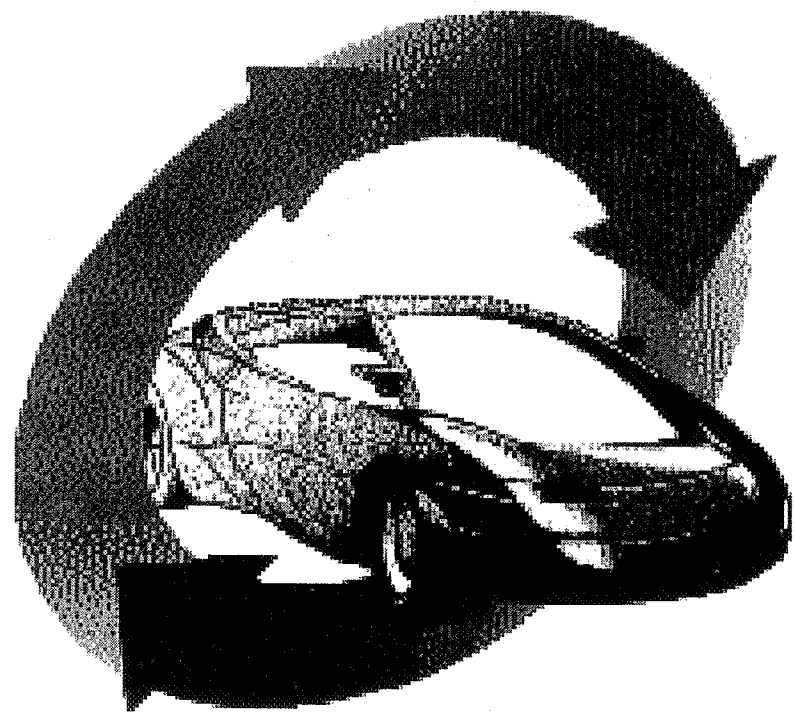


Darryl Martin



Samuel K. Errera

AISI/CARS '98 OVERVIEW



CARS FACTS

- ◆ **705 Pages of Text, Figures, Procedures, Equations & Tables**
- ◆ **Over 3,000 Hyperlinks**
- ◆ **92 Steel Materials Specified**
- ◆ **20 Different Material Properties**
- ◆ **35 Automated Design Procedures**
- ◆ **215 Design Equations**
- ◆ **31 Nominal Section Properties**
- ◆ **19 Effective Section Properties**
- ◆ **45 Megabytes of Information on CD**

AUTOMOTIVE STEEL DESIGN PROCEDURES

- ◆ **Straight Linear Members**
- ◆ **Curved Members**
- ◆ **Surface Elements**
- ◆ **Connections**

STRAIGHT LINEAR MEMBERS

- ◆ **Effective Width**
- ◆ **Section Properties**
 - **Nominal**
 - **Effective**
- ◆ **Member Capacity**
- ◆ **Web Strength**

EFFECTIVE WIDTH

- ◆ **Uniformly Compressed Stiffened Elements With or Without Circular Hole**
- ◆ **Webs and Stiffened Element With Stress Gradient**
- ◆ **Unstiffened Elements in Compression**
- ◆ **Uniformly Compressed Elements With Edge Stiffeners or Intermediate Stiffeners**
- ◆ **Effective Thickness of Curved Elements**

SECTION PROPERTIES

- ◆ **Nominal Properties Include:**
 - **Area**
 - **Centroid Location**
 - **Moment of Inertia (Local, Principal Axes)**
 - **Section Modulus (Local, Principal Axes)**
 - **Radius of Gyration**
 - **Shear Center Location**
 - **Shear Coefficient**
 - **Torsional Properties Including Torsion/Warping Constants**

- ◆ **Effective Properties Include All Except:**
 - **Torsion & Shear Properties**

MEMBER CAPACITY

- ◆ **Flexural Strength**
- ◆ **Lateral Buckling Strength in Flexure**
- ◆ **Flexural Capacity of Cylindrical Members**
- ◆ **Axial Capacity of Concentrically Loaded Compression Members**
- ◆ **Axial Capacity of Cylindrical Members**
- ◆ **Combined Axial Load and Bending of Member**
- ◆ **Torsion of Member**

WEB STRENGTH

- ◆ **Strength of Webs for Shear Only**
- ◆ **Strength for Combined Bending and Shear**
- ◆ **Transverse Load Web Capacity for Beams With Single Webs and Highly Restrained Webs**

CURVED MEMBERS

◆ **Webs in Plane of Curvature**

◆ **Curved Circular Tubular Members**

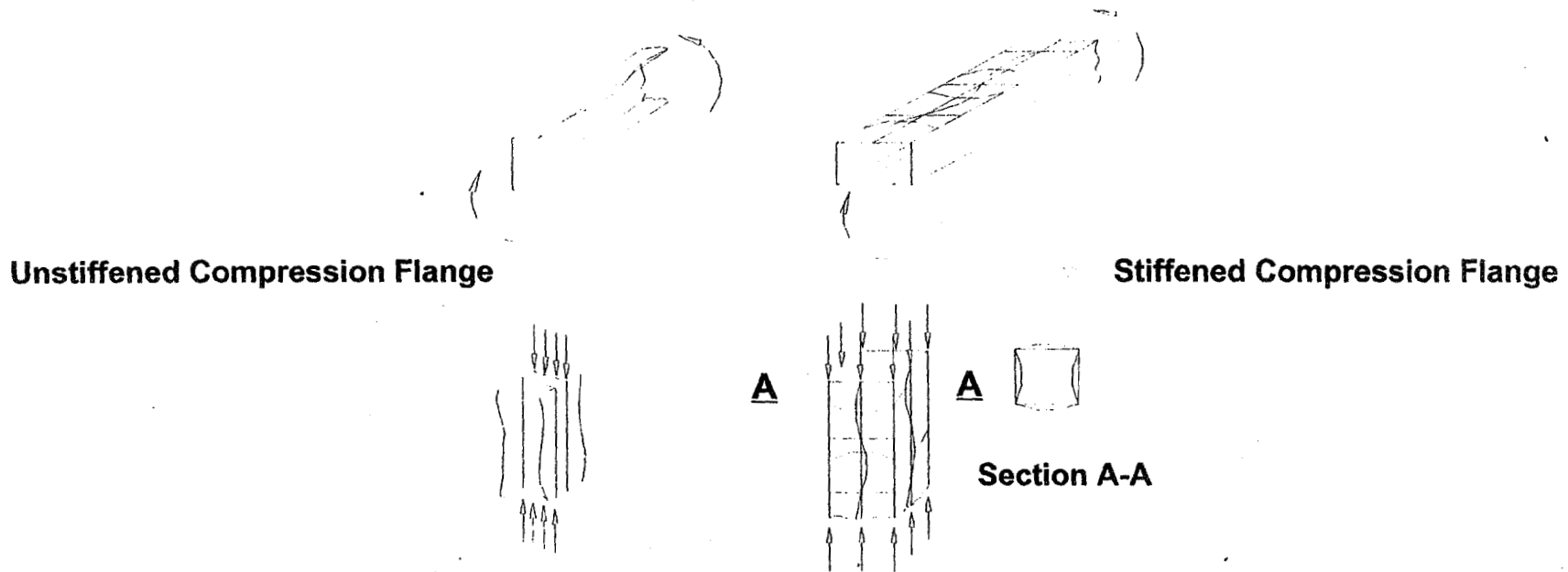
CONNECTIONS

- ◆ **Fastener Shear Integrity Considering Sheet Capacity**
- ◆ **Spacing Requirement of Mechanical Connections**

SURFACE ELEMENTS

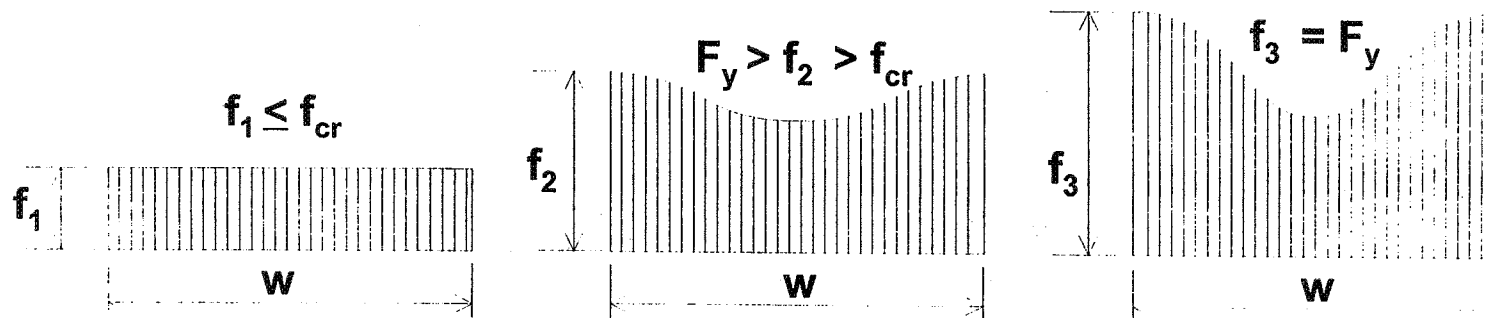
- ◆ **Deflection of Flat Plates**
- ◆ **Lateral Integrity of Curved Plates With Uniform Compression**
- ◆ **Dent Resistance**
 - **Denting Energy**
 - **Stiffness**
 - **Critical Oil Canning Load**

LOCAL BUCKLING OF COMPRESSION ELEMENTS



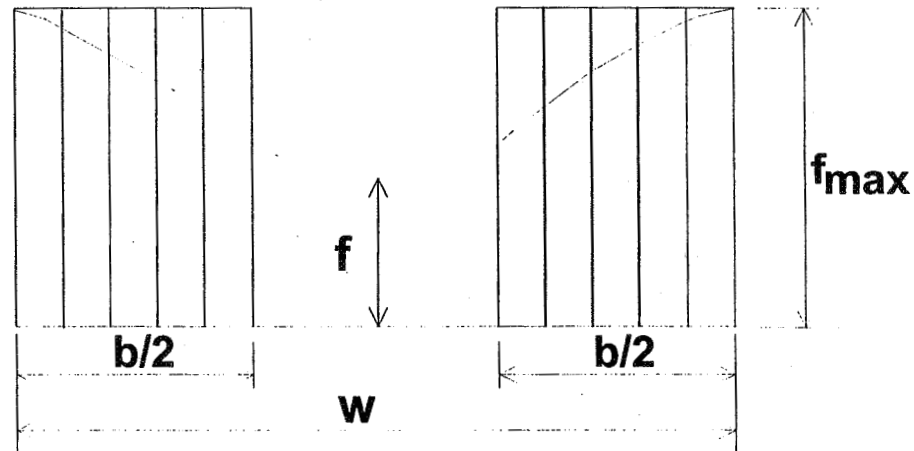
- ◆ **One Dimensional Structural Members Collapse When Buckling Stress Is Reached.**
- ◆ **Two Dimensional Plates With Large W/T Ratios Do Not Collapse but Experience Local Buckling and Post Buckling Strength.**

POST BUCKLING STRENGTH



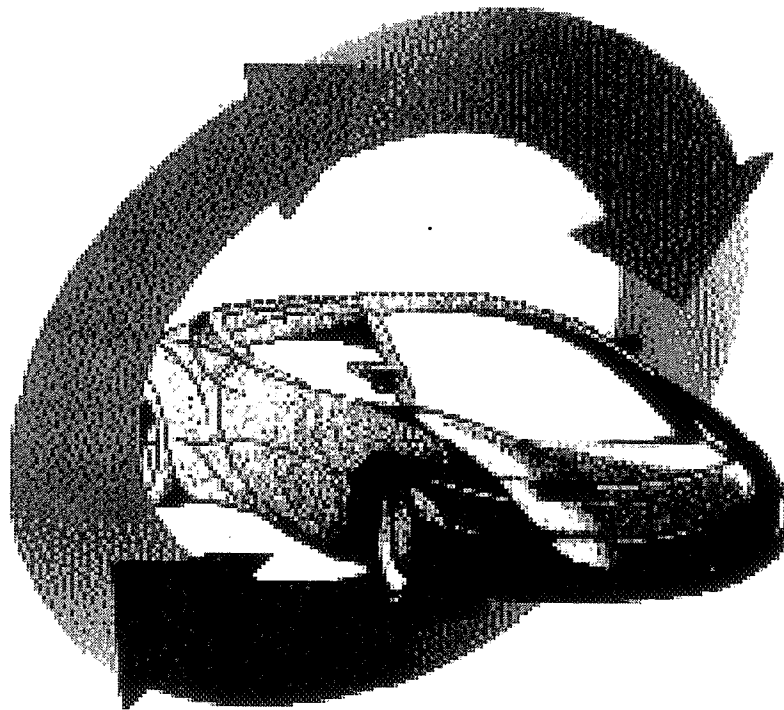
- ◆ **Additional Load Can Be Carried Due to the Redistribution of Stress.**
- ◆ **Member Fails When Edge of Element Yields.**

EFFECTIVE WIDTH



- ◆ It Is Assumed That the Total Load Is Carried by an Effective Width “b”.
- ◆ The Effective Width Is Calculated So That the Sum of the Areas of the Two Rectangles Equals the Area Under the Curve.

AISI/CARS '98 HOOD OUTER PANEL



HOOD OUTER PANEL

Geometric Properties

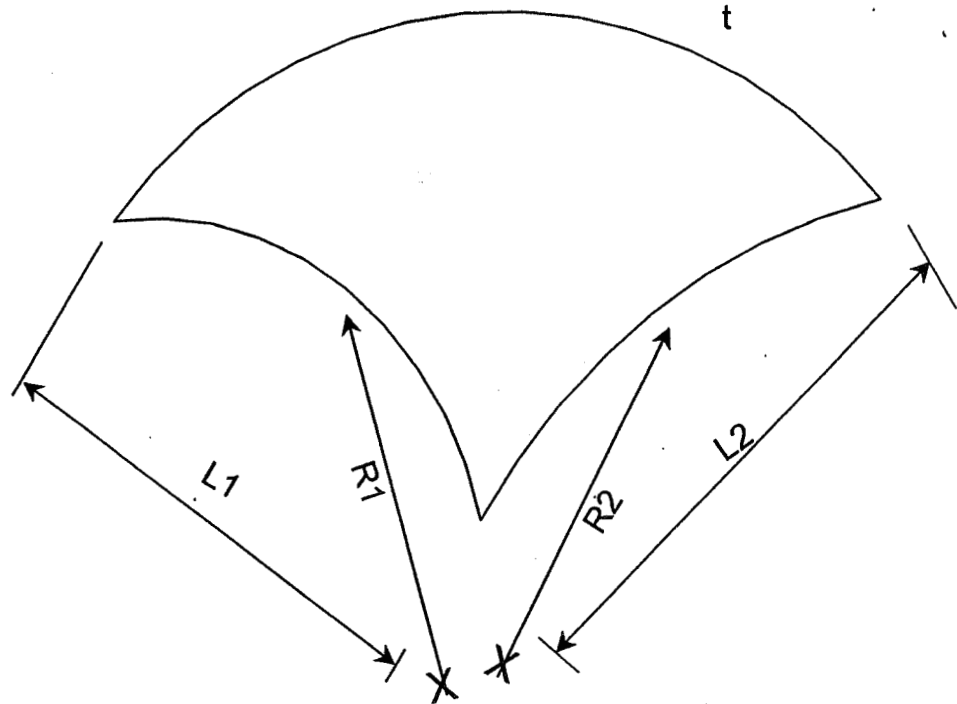
L1	=	660 mm	=	26 in
R1	=	5,715 mm	=	225 in
L2	=	762 mm	=	30 in
R2	=	15,748 mm	=	620 in
t	=	0.71 mm	=	0.028 in

Material Properties:

E	=	203,000 MPa	=	29,500 ksi
Fy	=	186 MPa	=	27 ksi
Fyd	=	298 MPa	=	43.2 ksi

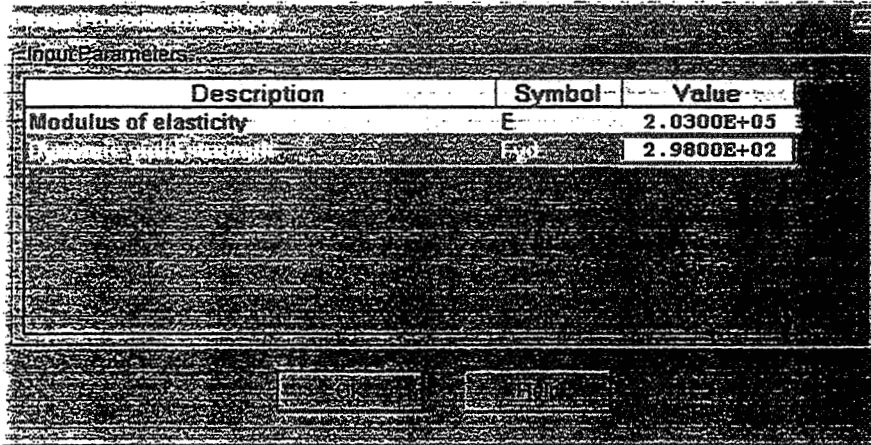
Structural Requirements:

Pcr	≥	53.4 N	=	12 lb
W	≥	26,560 N-mm	=	235 in-lb
K	≥	47.3 N/mm	=	270 lb/in

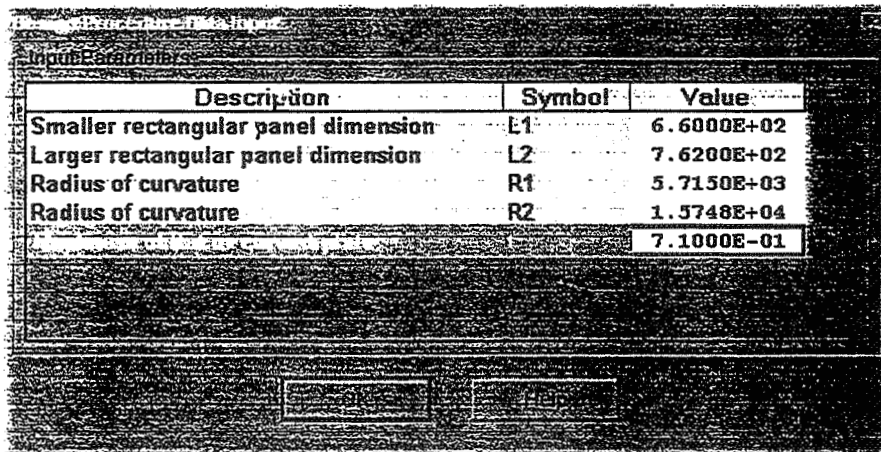


HOOD OUTER PANEL

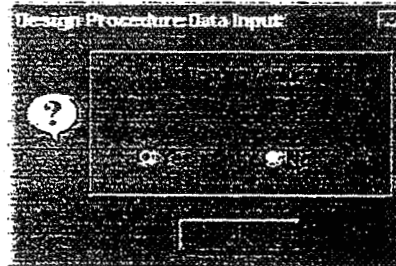
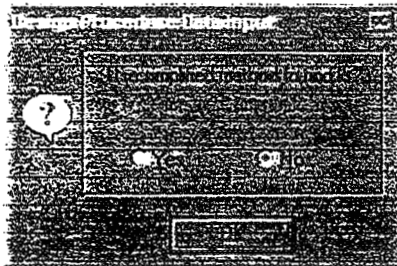
The hood outer case study is entered via the Design Expert by selecting Integrity of Surface Elements, then answering Yes to Dent Resistance. The program will then ask Enter Design Procedure 3.3-4, to which the answer should be Yes. This brings up the following panel, the modulus should come up as default (if units are set right) enter the F_{yd} value and mention that this value came a table in the ASDM hit OK.



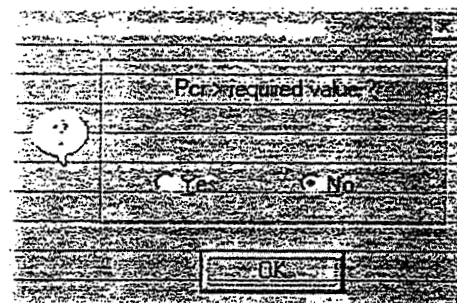
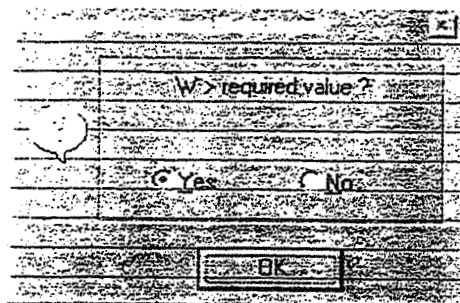
The following is the next input panel and the values should be entered as shown (have someone in class call out input numbers). Once input is complete hit OK to continue.

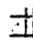


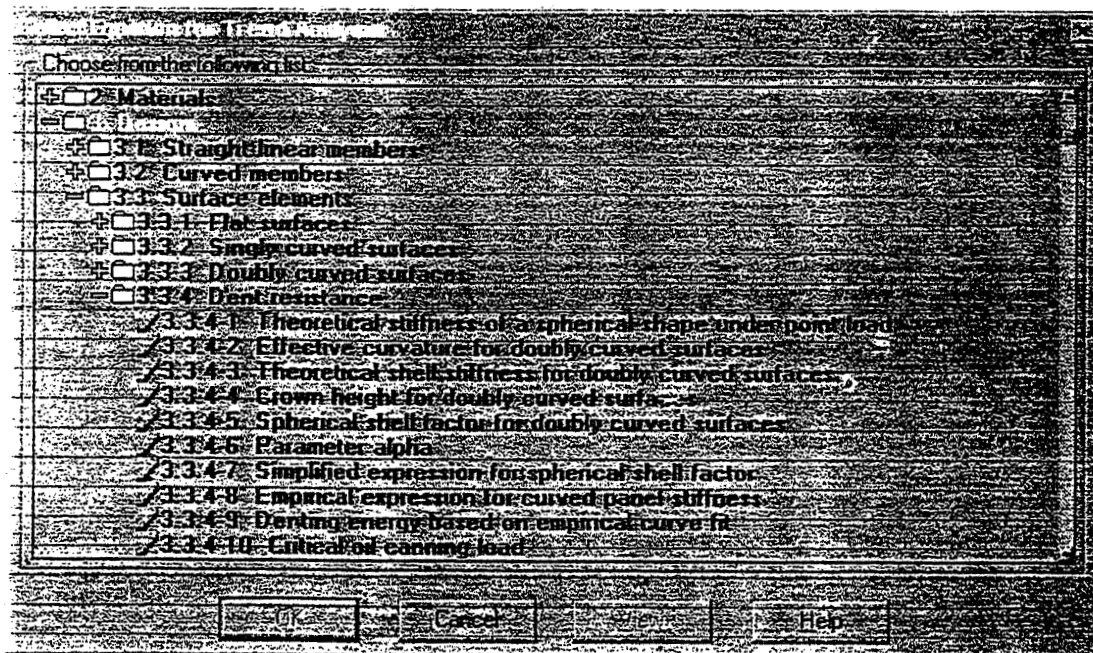
Answer the following panels as shown, then hit OK. K is actually less than the required value at 42.84 N vs 47.3 N, but the answer has to be Yes to continue the procedure (point this out).



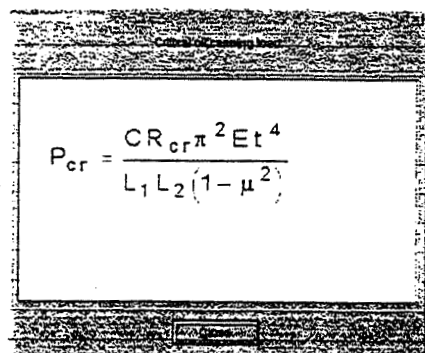
HOOD OUTER PANEL



By answering 'No' to the last panel this will step back in the procedure to the Design Procedure Data Input panel to allow parameters to be change that would improve the result. Change the thickness to 0.8mm and repeat the procedure as above. Now all values are well above the requirements and thus there is a need to optimize to save mass. Leave the procedure as is and hit  Equation/Trend Analysis button on the tool bar and go through list and select equation 3.3.4-10 Critical oil canning load.



Enter this equation and first display the equation by hitting the View button and point out that t is to the power 4, therefore it has a large influence on the Critical load for oil canning.



HOOD OUTER PANEL

Close the equation panel out and proceed with the Trend Analysis using the input data shown :

Critical Oil Canning Load

Description	Symbol	From	To
Shorter plate dimension	L1	5.6000E+02	
Larger plate dimension	L2	7.6200E+02	
Poisson's ratio	μ	3.0000E-01	
Modulus of elasticity	E	2.0300E+05	
Thickness of flat or curved plate	t	6.5000E-01	9.0000E-01
Radius of curvature - R1	R1	5.7150E+03	
Radius of curvature - R2	R2	1.5748E+04	

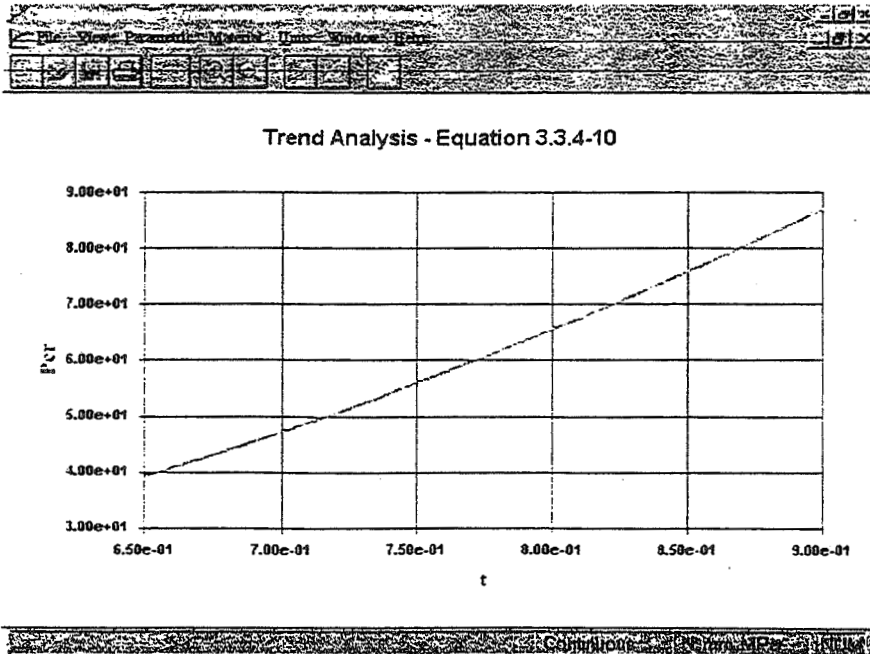
Numerical and graphical results provided for:

Critical oil canning load **Pcr**

Solve Equation Close Help

Continuous Numerical

Hit the solve button and take a look at the trend graph full window to pick off a good point.



HOOD OUTER PANEL

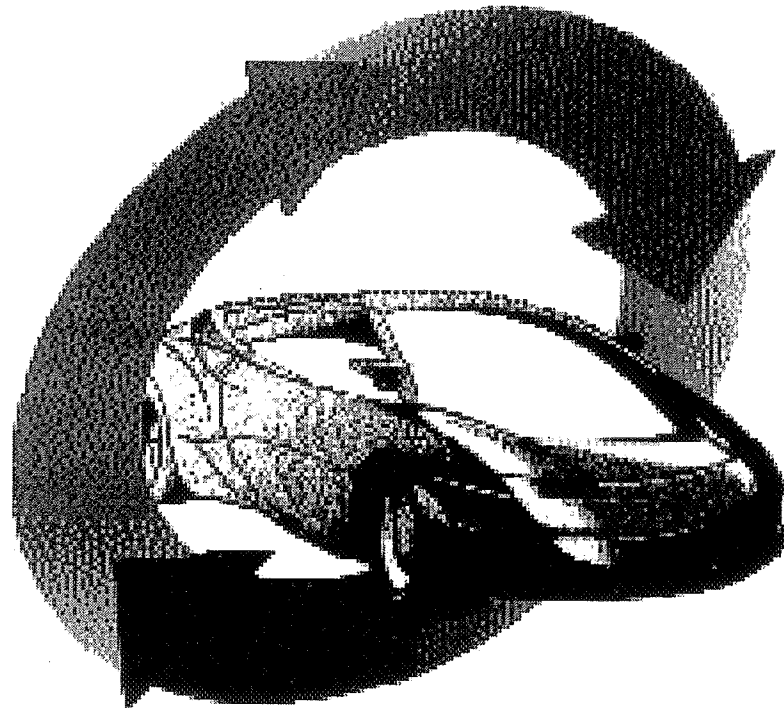
Also by looking at the numerical results a more accurate number can be determined. A gauge of 0.735mm gives a Pcr of 53.23 N, a gauge of 0.74 mm gives 54.1 N however for supply reasons the engineer may be forced to go as high as 0.75 mm for the final gauge.

Close out the Trend Analysis and return to the design procedure which should be waiting for an answer to the is Pcr > required value question. Answer No. thus returning to the Design Procedure Data Input panel and change the gauge from 0.8 mm to 0.75 mm and run the procedure as before noting for the class the values at each stage. The values should now be 47.77 N/mm for K, just over the requirement of 47.3 therefore the engineer would stay with the 0.75mm gauge. 33410 N-mm for W, well over the requirement and 55.95 N for Pcr just over the requirement.

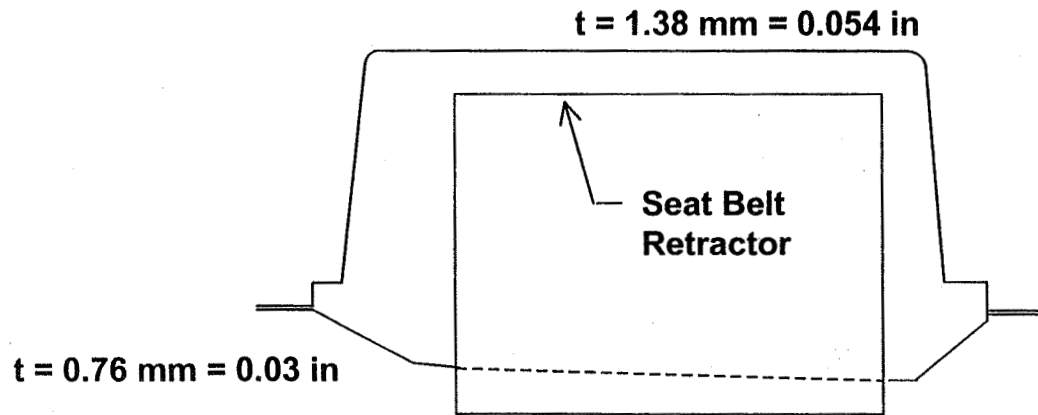
The Hood Outer Panel case study is now complete therefore answer Yes to the last panel and the flow chart will show Finish.

AISI/CARS '98

B-PILLAR



FOUR DOOR LOWER B-PILLAR



Y Outside of car
X Rearward in car

Material Properties:

$E = 203,000 \text{ MPa} = 29,500 \text{ ksi}$

$F_y = 175 \text{ MPa} = 25 \text{ ksi}$

Structural Requirements:

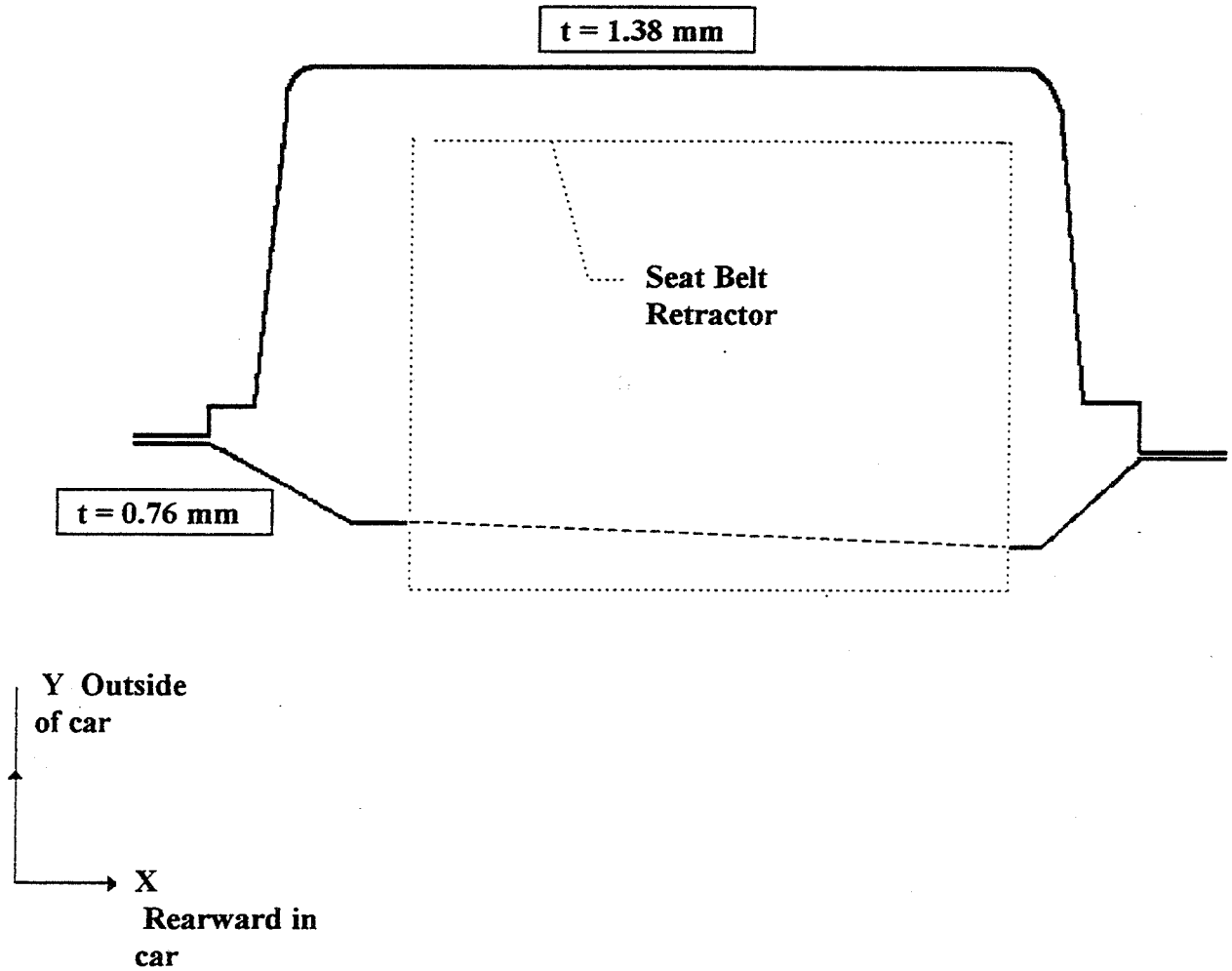
$I_{xx} \geq 466,180 \text{ mm}^4 = 1.12 \text{ in}^4$

$I_{yy} \geq 208,120 \text{ mm}^4 = 5.00 \text{ in}^4$

$M_x \leq 1,627 \text{ Nm} = 1,200 \text{ ft-lbs}$

(M_x load simulates quasi static side door intrusion test FMVSS 214.)

FOUR DOOR LOWER 'B' PILLAR



MATERIAL PROPERTIES:

$$E = 203,000 \text{ Mpa (29,500 ksi)}$$

$$F_y = 175 \text{ Mpa (25 ksi)}$$

STRUCTURAL REQUIREMENTS:

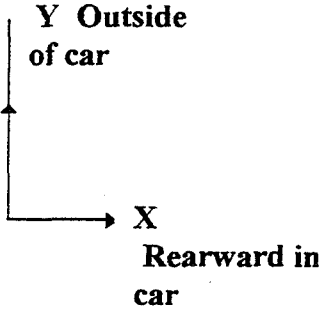
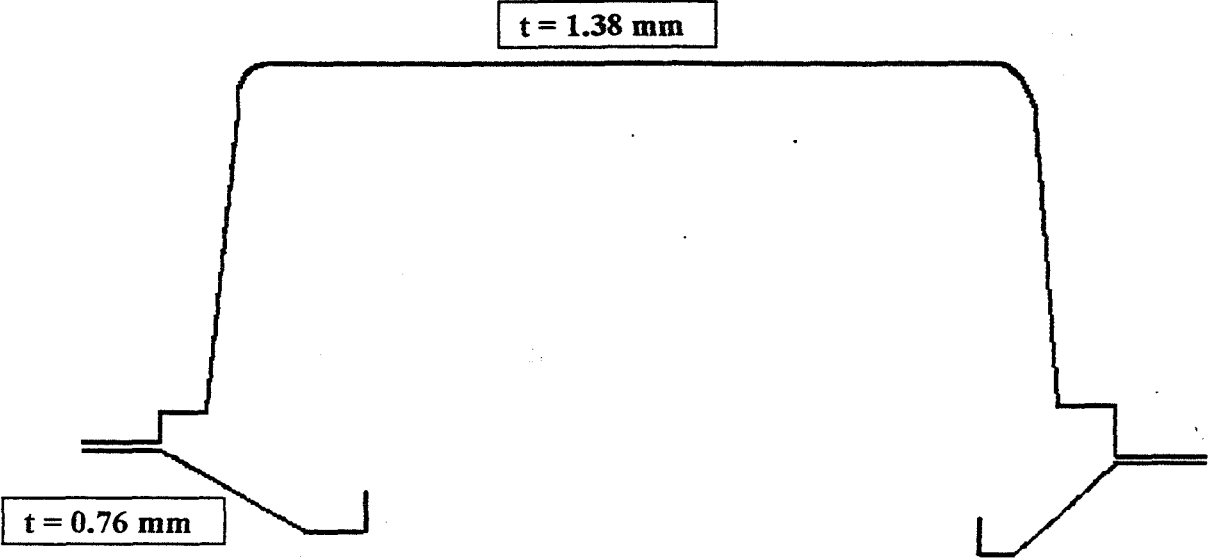
$$M_x + \leq 1600 \text{ Nm (1200 ft - lb)}$$

$$I_{xx} \geq 4.66 \text{ E}+5 \text{ mm}^4 \text{ (1.12 in}^4\text{)}$$

$$I_{yy} \geq 2.08 \text{ E}+6 \text{ mm}^4 \text{ (5.00 in}^4\text{)}$$

$M_x +$ load is due to quasi static side door intrusion test FMVSS 214.

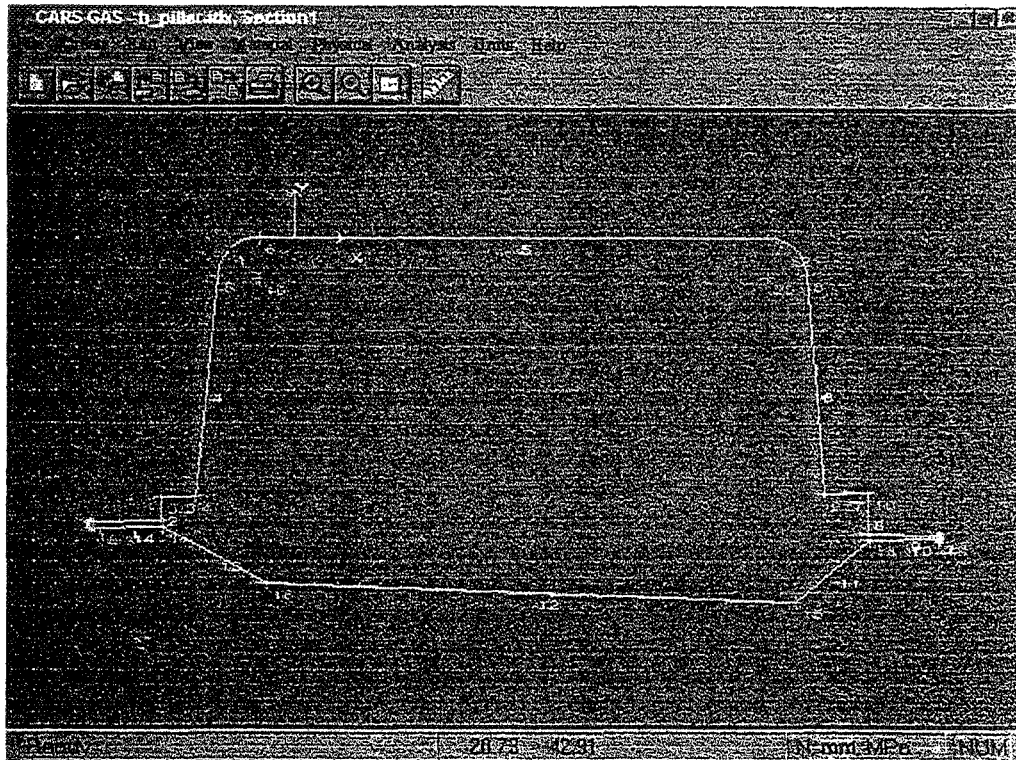
FOUR DOOR LOWER 'B' PILLAR



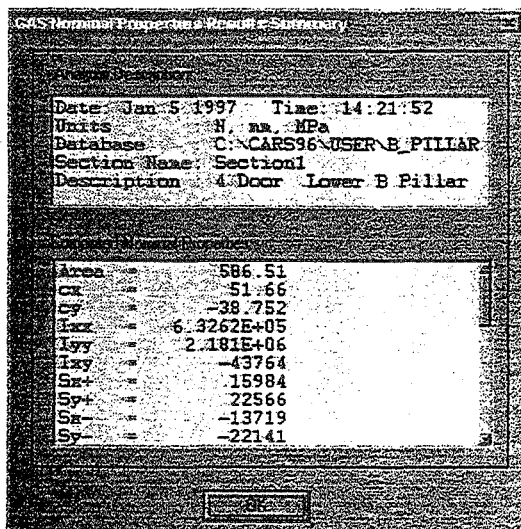
Return flange added around hole to stiffen section.

FOUR DOOR LOWER 'B' PILLAR

The 'B' pillar case study is begun by making sure the units and the default material is set the correctly. Material ID 19 should be used for this case study. Once these are set bring in the first 'B' pillar section by selecting New Database on the File menu and under the sub-directory user select file b_pillar.idx. hit OK. There is then a need to select Get section in the same menu and select Section 1. the baseline section will come up on the screen as shown below. There is also an actual 'B' pillar that should be show to the class and it should then be explained that the intent is to package a seat belt retractor in the base of the pillar.

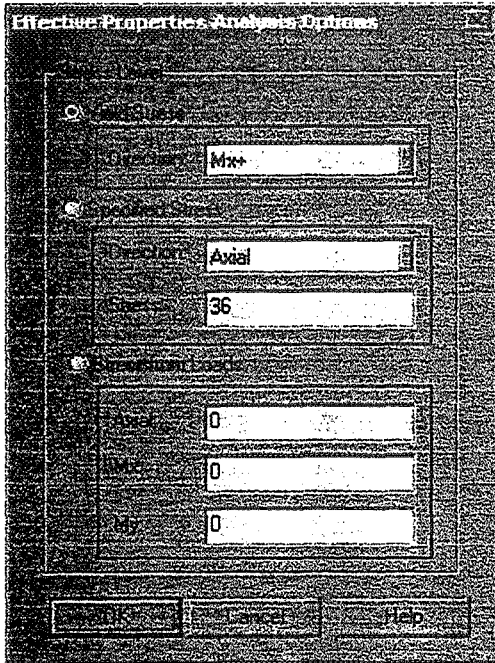


Explain that first the baseline section should be checked to make sure it currently meets the requirements. Also zoom-in to one of the areas where the welds are to show the section is welded. Return section to full screen then enter the Analysis menu and perform a Nominal Property, Single Calculation analysis. Show results summary which should have the following results, which are well above the Ixx and Iyy section property Structural Requirements. Answer OK and close results using File menu. do not save results.

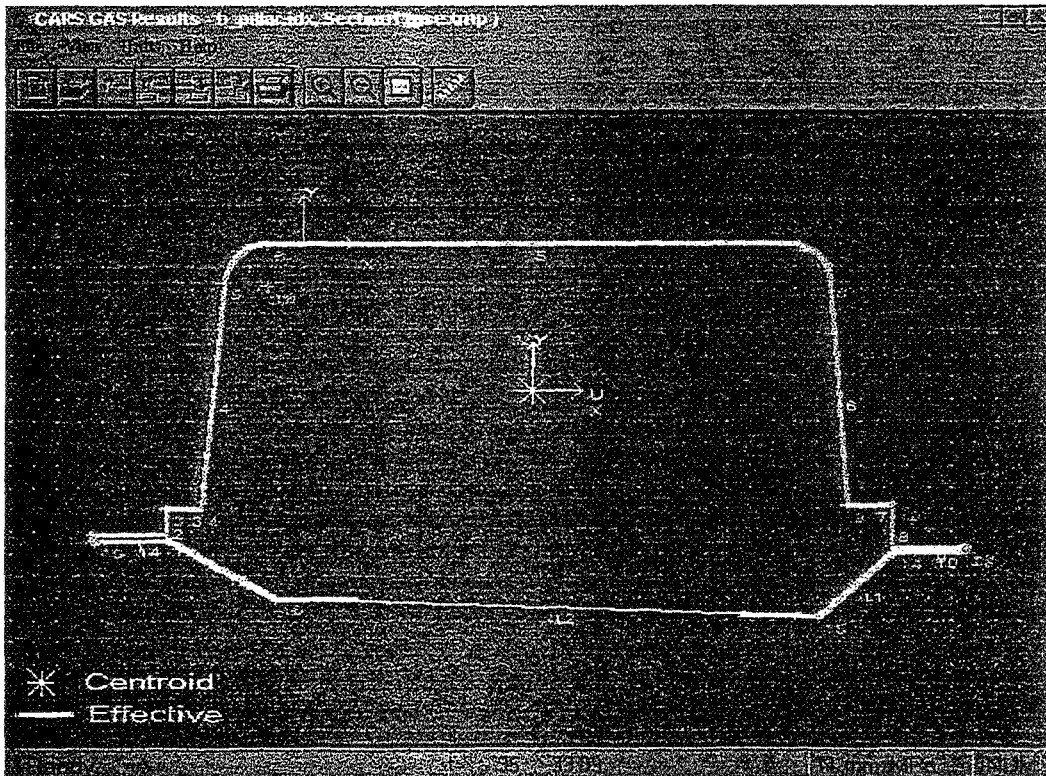


FOUR DOOR LOWER 'B' PILLAR

The first section will now return to the screen. "The section properties are however only one part of the picture, the other being the bending moment capacity. To do this there is a need to calculate the effective section properties under the $M_x +$ moment. save them and move over the Design Key to calculate the bending moment capacity". Using the Analysis menu perform an Effective Property, Single Calculation analysis and enter $M_x +$ in the panel as shown, then enter OK to continue.

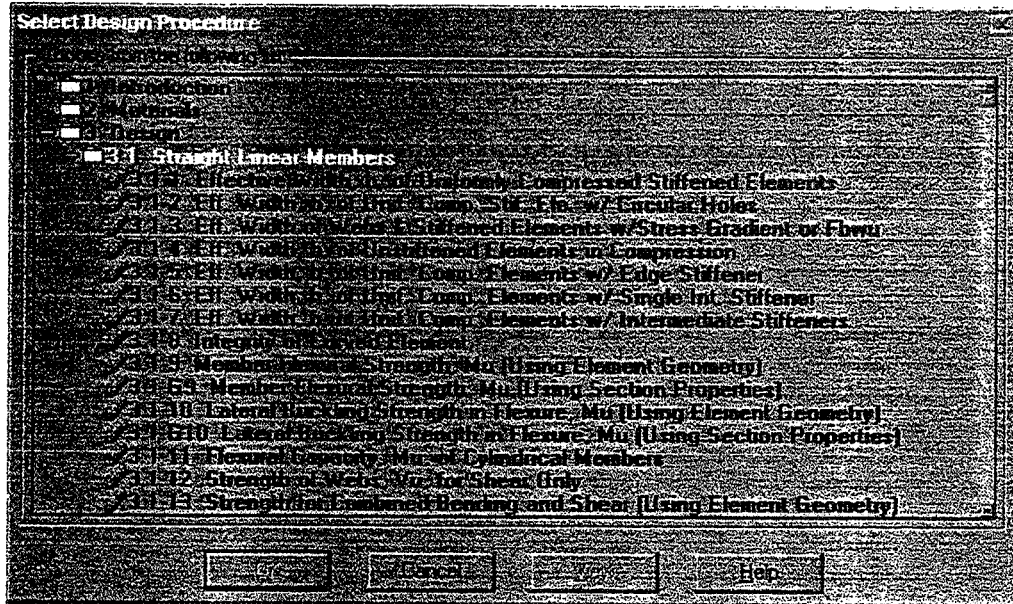


The section will then come on the screen highlighting the effective portion of the section.

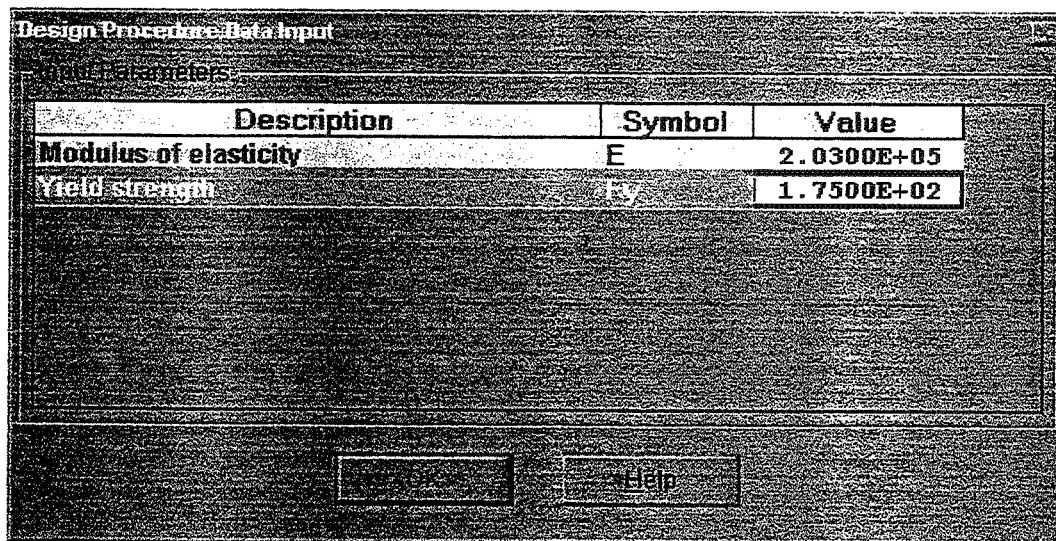


FOUR DOOR LOWER 'B' PILLAR

This shows the material that is to be removed for the retractor is ineffective for this load case and thus can be removed without any immediate concerns. However there is still the need to check the current capacity by first saving the results using Save Results As in the file menu and typing in an appropriate filename. Minimize GAS down to the toolbar and bring back up Design Key. select New Design and select the procedure 3.1-G9 as shown.

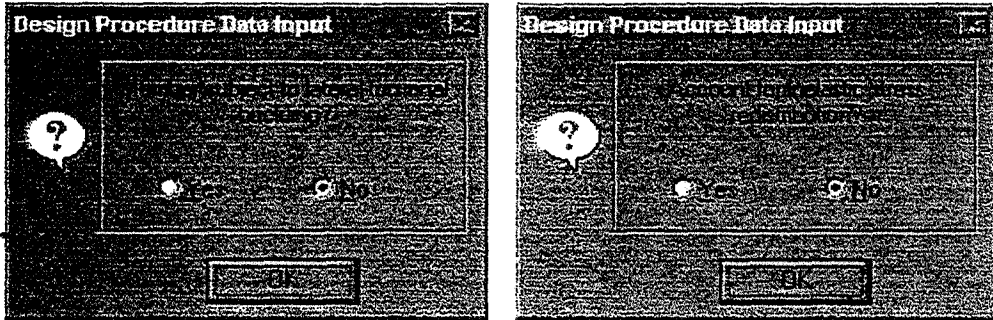


Hit OK and enter that procedure and select from the appropriate directory the just saved GAS file. Answer No to the first panel question Cylindrical tube ? and fill in the following panel as shown .

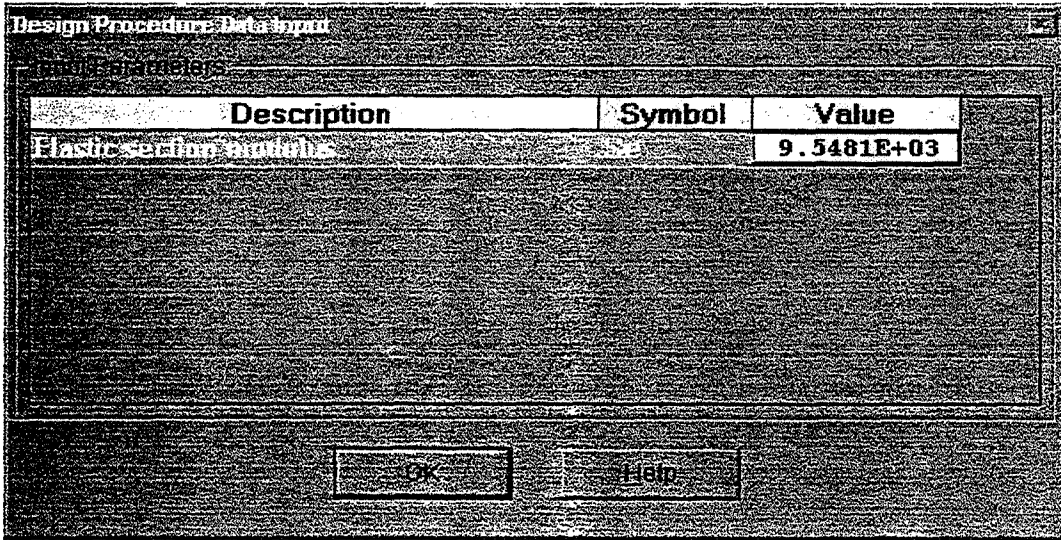


Hit OK and then answer the next two panels as shown on the following page.

FOUR DOOR LOWER 'B' PILLAR



The Elastic section modulus is coming from the Effective Section calculation from GAS and this value should be accepted by hitting OK.



This then leads to the Mu (bending moment capacity) being calculated at 1671 Nm which is just above the structural requirement thus the baseline section is ok. Once this is complete move back to the GAS module and close out results if they are open. Then using Get section retrieve the second 'B' pillar section with the hole for the retractor added and proceed as above to calculate Nominal Properties, Single Calculation. This will show that the I_{xx} is now 460450 mm⁴ which is below the structural requirement, because of this the bending moment capacity will not be calculated at this point, this is not necessary until the requirement for I_{xx} is met.

It should then be mentioned that a return flange around the hole was suggested, pull up the third section using the steps stated above and perform the Nominal Property, Single Calculation again. Look at the results summary and show that I_{xx} is now above the requirement at 481680 mm⁴.

Because of this move on to the Effective Property, Single Calculation, as with Section 1, by closing out the Nominal results and following the steps detailed above. Once again save these results in an appropriate file and move over to the Design Key module. Repeat the same procedure as before in the Design Key and show that result of 1621 Nm is above the requirement of 1600 Nm.

**MST ONLINE: THE DESIGN OF AN INTERNET
GATEWAY FOR EDUCATIONAL RESOURCES IN
MATERIALS SCIENCE AND TECHNOLOGY**

S. Raj Chaudhury

Matthew Sanders

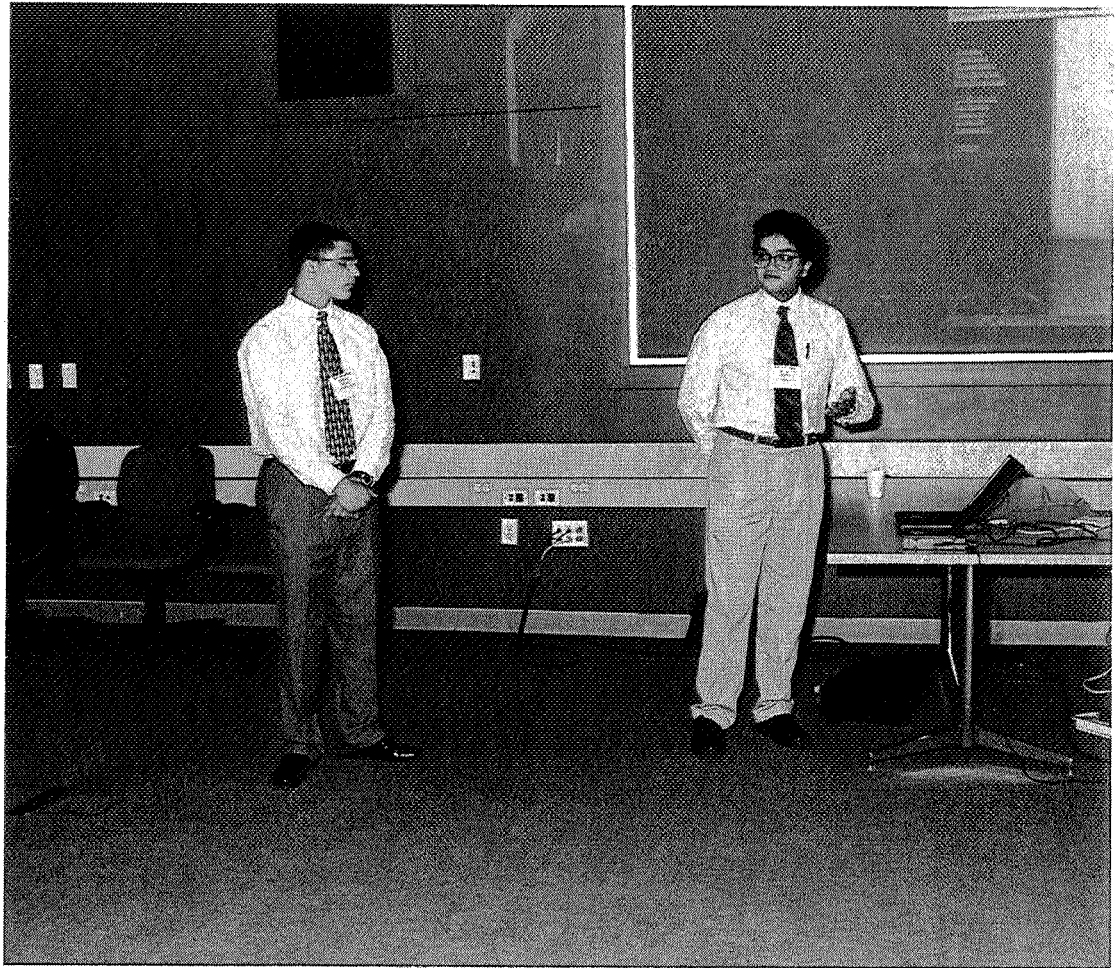
Curtiss Wall

and

James A. Jacobs

Norfolk State University
700 Park Avenue
Norfolk, Virginia 23504

Telephone: 757-823-2381
e-mail srchaudhury@nsu.edu



Matthew Sanders and S. Raj Chaudhury

MST-Online : the design of an internet gateway for educational resources in Materials Science and Technology

S. Raj Chaudhury, Matthew Sanders, Curtiss Wall and James Jacobs

Norfolk State University
700 Park Avenue
Norfolk, VA 23504

schaudhury@nsu.edu
<http://vigyan.nsu.edu/mstonline>

Abstract

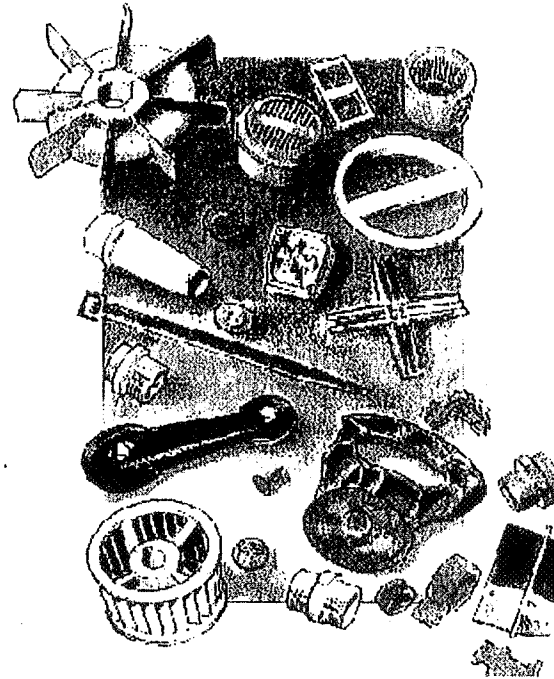
MST-Online is a web site that is being designed with an eye to the future of internet technologies and the future needs of materials science educators and students. With the support of NASA Langley Research Center, this project is combining the traditional collection of useful links with actual content adapted especially for this purpose from a variety of sources. Textbook resources are being provided (Jacobs and Kilduff) as an overview to different types of materials. Valuable, out-of-print references such as Elizabeth Wood's manual on single crystals and Laue diffraction are being digitized for easy access. In addition, Java applets are being collected and showcased for applications of visualization to the study of materials science. In this talk we shall present our overall design philosophy and methodology and discuss features of the growing website.

**MS
ONLINE**

**INTRODUCTION
CERAMICS
POLYMERS
COMPOSITES
MATERIALS
METALS
TESTING
MANUFACTURING
HOT LINKS
OTHERS**

Welcome to MST Online

Sponsored By NASA Langley Research Center



Ceramics

Page Contents

[\[Porosity and Density\]](#) [\[Structure, Bonding, and Properties\]](#) [\[Wear Resistance\]](#)
[\[Stress Concentrations and Fracture Toughness\]](#) [\[Designing Ceramics\]](#) [\[Ceramic Processing\]](#)

Nature of Ceramics

Ceramics are loosely defined as crystalline solids composed of metallic and nonmetallic materials. They are inorganic materials; that is, they do not contain carbon and are derived from mineral sources. Ceramics are crystal structures made of metallic ions. Bonding is either partially or completely ionic. Variables involved are (1) the magnitude of the electrical charge on the ions, and (2) the relative size of the ions. The crystal must be neutral; that is, all the cation positive charges must be balanced by an equal number of anion negative charges. The oxidation state or oxidation number designates the number of electrons an atom loses or gains or otherwise uses in joining with other atoms in compounds. The total of the oxidation states of all atoms in a molecule or formula unit is zero. Na has an oxidation state of + 1; Cl has an oxidation state of -1. When they join to form the compound expressed by the formula unit NaCl, their oxidation states must add up to 0.

Some of these ceramics are intermetallic compounds. Originally, ceramics were clay-based materials. The word ceramic comes from the Greek *keramos*, meaning "burnt earth." Glass, a rigid liquid with an amorphous molecular structure, is sometimes classified as a ceramic. Silicon carbide, a very popular ceramic, does not meet the definition of a ceramic material given above. Ceramics are inexpensive compared with competing materials. Consisting primarily of forms of silicon, aluminum, and oxygen, the most abundant elements in the earth's crust, ceramics can be produced at less cost than that of competing metal-alloy components. Further, many, if not all, of the strategic minerals, including cobalt, that are needed to produce sophisticated metal alloys, such as the superalloys presently used in high-temperature applications, are not found in the United States. AerMet 100, is one such recently developed superalloy steel. What sets ceramics apart is their set of properties common to nearly all forms: (1) extreme hardness, (2) heat resistance, (3) corrosion resistance, (4) low electrical and thermal conductivity, and (5) low ductility, or brittleness. Table 7-1 is a comparison of these and other properties of ceramics with those of metals. Table 7-2 provides an additional comparison of the properties of ceramics and those of competing materials.

Table 7-2

The Knoop hardness cubic boron nitride (CBN) is 5000 kg/mm²; that of diamond, the hardest known material, is about 7500 kg/mm². Partially stabilized zirconia (PSZ), to be discussed in more detail later, can withstand a pressure of 78,000 psi for about 2000 hours without any appreciable effect. Its coefficient of friction α with steel is only 0.17 at room temperature, and its coefficient of thermal expansion has very nearly the same value between 00 and 10000C.

Polymers

Page Contents
[Polymerization]

What is a "Polymer"

The word Polymer comes from the Greek "poly" meaning many, and "meros", parts or units. A polymer is a chainlike molecule made up of smaller units "monomers". The "monomers", made up of atoms, bond together covalently to form a polymer that usually has a carbon backbone.

Nature of Polymers

Polymers can include many type of industrial materials, as seen in Figure 6-2 page 327 (below).

Figure 6-2

The basic markup of polymers consists of smaller units "mers" joined together either naturally or synthetically to produce polymers or macromolecules. The initial step in polymer production is achieved by petrochemist or petrochemical engineers, engineering technicians and engineering technologist, or other with chistry in their education and training. This nitial step involves breaking down raw materials such as crude oil, coal, limestone, salt, natural gas, and air. With cellulose plastics, the raw material is cotton or wood; however, they are not broken down, as are most other polymer ingredients. Whether it be the cracking of natural gas, distillation of coal or crude oil, or the esterification of cotton or wood, processing the basic organic (carbo base) raw materials yields the element carbon together with hydrogen. Other basic elements are also obtained in the initial stage, including oxygen, nitrogen, silicon, fluorine, chlorine, and sulfur.

Polymer is often used as a synonym for "plastic", but many biological and inorganic molecules are also polymeric. All plastics are polymers, but not all polymers are plastics. Plastic more commonly refers to the way a material behaves under applied forces, or behaves when it melts and flows. Commercial polymers are formed through chemical reactions in large vessels under heat and pressure. Other ingredients are added to control how the polymer is formed and to produce the proper molecular length and desired properties. This chemical process is called "polymerization". A "homopolymer" results from polymerizing only one kind of monomer. A "copolymer" results from using different monomers. Homopolymers have the same repeating unit while copolymers (which can be random, block, or graft) can vary have different numbers of repeating units. A "terpolymer" results from using three different monomers.

[Back](#) [Home](#) [Next](#)

Reproduced by permission of Prentice-Hall, Inc.
From James A. Jacobs & Thomas F. Kilduff's
Engineering Materials Tectnology, 1997 pgs. 323-433

Composites

Page Contents

[Development of Composites] [Constituents of Fiber-Reinforced Composites]
[Fiber] [Matrix]

INTRODUCTION

A composite material or composite is a complex solid material composed of two or more materials that, on a macroscopic scale, form a useful material. The composite is designed to exhibit the best properties or qualities of its constituents or some properties possessed by neither. The combining of the two or more existing materials is done by physical means, as opposed to the chemical bonding that takes place in the alloys of monolithic solid materials. A true composite might be considered to have a matrix material completely surrounding its reinforcing material in which the two phases act together to produce characteristics not attainable by either constituent acting alone. Note that the insoluble phases or main constituents in a composite do not lose their identity. This is not true of solids, which are metallic alloys or copolymers whose phases are lost to the naked eye because these phases are formed as a result of natural phenomena. In other words, steel is a multiphase metal alloy but is not considered a composite. A metallic alloy of Al and Cu, with the addition of Al₂O₃, is considered a dispersion-strengthened copper composite in which a dilute copper/aluminum alloy powder is exposed to an oxidizing environment and the aluminum is oxidized within the copper matrix. The aluminum oxide particles are inert and act as inhibitors of dislocation movement and thus strengthen the alloy at high temperatures. By adding niobium (10%) to this same extruded composite in the form of a uniformly distributed powder, even greater hardness and strength are produced with only a minimal reduction in electrical conductivity. Two phase alloys are not considered composites by some because their phases are not formed in separate processes but originate in a single manufacturing process.

The above discussion reveals that the definition of a composite is still somewhat arbitrary. A broad definition of composite materials includes the naturally occurring composites, such as wood, as well as the synthetic or human-made composites. A recent example of the development of composites in the medical field is cited. A mineral paste composed of monocalcium phosphate monohydrate, alpha-tricalcium phosphate, and calcium carbonate, dry mixed, to which a sodium phosphate solution is added to form a paste, is surgically implanted into acute bone fractures and hardens within ten minutes after injection. This paste holds fractured bones in place while the native bone remodeling process replaces the implant with living bone. This process causes the in-situ formation of the mineral phase of bone. Attaining a compressive strength greater than that of long bones, the paste's tensile strength of about 2.1 MPa is comparable to long bones. This new material eliminates the need for heavy and uncomfortable casts.

In answer to the question, Why use composites? one can reply, in part, as follows:

Metals

Page Contents
[\[Phase\]](#) [\[Phase Diagrams\]](#)

NATURE OF METALS

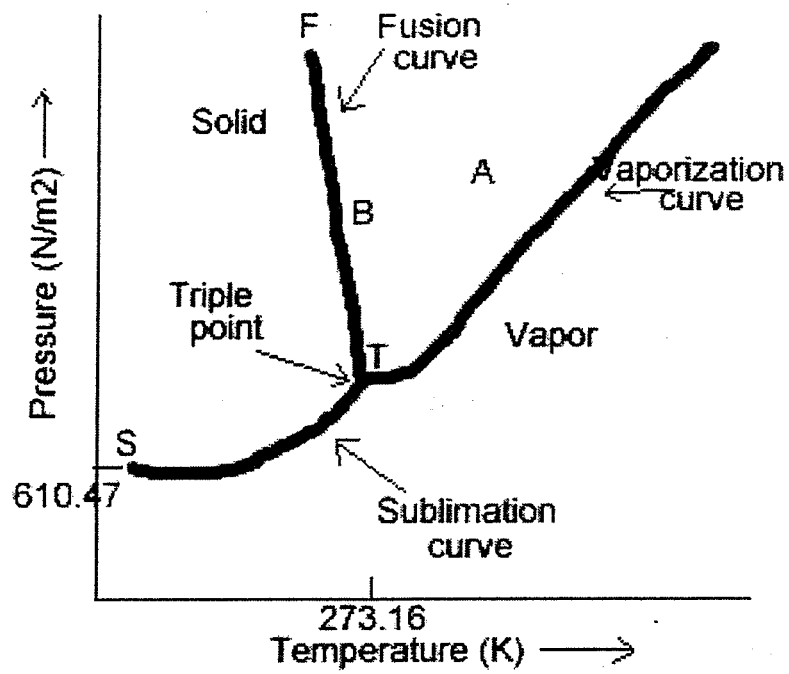
Metals have been useful in humanity through the ages because they are "strong" when subjected to the external forces encountered under service conditions, yet they become "soft" enough to yield to a machine cutting tool or to a compressive shaping force. Above a certain temperature, they melt and become liquids capable of being shaped by casting. Only in recent times have we realized that the properties of all types of solid materials, including metals, arise from their atomic architecture, that is, from the manner in which their atoms arrange themselves into a crystalline order, from the number and types of imperfections found in this structure, and from the bonding forces that keep the collection or structure of atoms bound or joined together.

The "softness" quality of metals can be explained by an understanding of the atomic structure and metallic bond of the metal atoms to form a crystalline structure. We recall that the electrons in the metallic bond are free to move about their positive ions in an electron cloud or gas, which acts to glue or bond the ions together. This free movement, within limits, also allows for the movement of the atoms under the influence of an external load. This slight movement, visible only under the most powerful microscopes, is called elastic deformation or elastic strain. Once the external force, such as a bending force, is removed, the internal electrical forces that cause the atoms to move will decrease, allowing the atoms to return to their normal position; they leave no sign of ever being moved. If you bend a piece of spring steel such as a machinist's rule or vegetable knife, it will return to its original shape, thus experiencing elastic deformation.

If you were not careful and applied too much external force by excessively bending the rule or knife, the atoms might move too far from their original positions to be able to move back again when you released the external force. Consequently, the rule or knife would be permanently bent and no longer fit for use. This permanent deformation is known as plastic flow, plastic slip, plastic deformation, or permanent set. When automakers stamp out a metal car body from low-carbon steel in a huge die press, they use this softness quality of metals. The term cold working (defined later) is applied to this stamping operation and many other metalworking processes that produce plastic deformation in a metal. Cold-working operations include rolling, heading, spinning, peening, bending, pressing, extruding, drawing, and others.

The microstructure of metals can be modified in a number of ways. By now we know that this last statement can be interpreted to mean that, through advances in metals technology, we can affect the atomic structure of metals in a precise, controlled manner in the design of metal alloys with the desired properties. In this module we classify, for learning purposes, the basic methods of changing a metal's

Figure 5-9 Unary phase diagram for water



Back

Reproduced by permission of Prentice-Hall, Inc.
From James A. Jacobs & Thomas F. Kilduff's
Engineering Materials Tectnology, 1997 pg. 223

- [Material Science and Engineering Education Forum](#)
- [Materials Research Science and Engineering Center at Arizona State University](#)
- [Cal Poly Materials Engineering Department](#)
- [Composites Manufacturing Science Laboratory at the University of Delaware](#)
- [Center for Materials Science James Madison University](#)
- [The Composite Materials Research Group at the University of Mississippi](#)
- [The Materials Systems Laboratory at MIT](#)
- [New York State College of Ceramics](#)
- [Materials World Module](#)
- [Science Nextwave](#)
- [National Academy of Engineering](#)
- [Materials Science Library](#)
- [Franklin Institute Science Museum](#)
- [Smithsonian Institutio](#)
- [National Geographic](#)

MST Online

- * [Introduction](#)
- * [Polymers](#)
- * [Electronic & Optical](#)
- * [Hot Links](#)
- * [Structure & Testing](#)
- * [Ceramics](#)
- * [Manufacturing](#)
- * [Metals](#)
- * [Composites](#)
- * [Curriculum](#)

Links

- * [Ceramics](#)
- * [Composites](#)
- * [Manufacturing](#)
- * [Materials Education](#)
- * [Metals](#)
- * [Plastics](#)
- * [Polymers](#)
- * [Technical Societies](#)

- [A & M Composites Corporation](#)
- [Advanced Composites Engineering](#)
- [Advanced Stitching Machine](#)
- [Cade AutoAir](#)
- [CARBON COMPOSITES](#)
- [Composite Materials Inc.](#)
- [Composite Registry](#)
- [HUBER+SUHNER](#)
- [SCI's composite](#)
- [STORAGETE](#)
- [Stoughton Composite](#)
- [The Composites Corner](#)
- [THE COMPOSITES NEWS SUPERSITE](#)

**MST
Online**

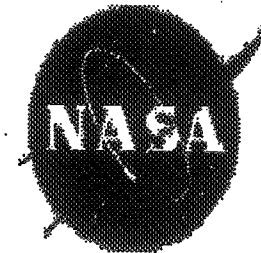
- * Introduction
- * Polymers
- * Electronic & Optical
- * Hot Links
- * Structure & Testing
- * Ceramics
- * Manufacturing
- * Metals
- * Composites
- * Curriculum

Links

- Ceramics
- Composites
- Manufacturing
- Materials Education
- Metals
- Plastics
- Polymers
- Technical Societies

NASA Facts

O N L I N E



FS-1997-08-31-LaRC
August 1997

The Advanced Stitching Machine:

NASA Facts

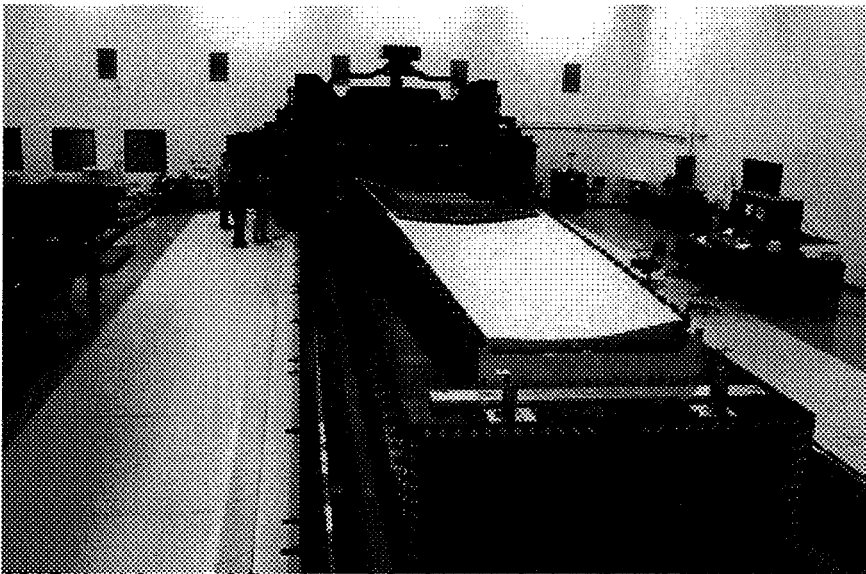
O N L I N E



FS-1997-08-31-LaRC
August 1997

The Advanced Stitching Machine:

Making Composite Wing Structures Of The Future



NASA's Advanced Stitching Machine is located at the Marvin B. Dow Stitched Composites Development Center--a new Boeing facility that will produce low-cost composite wing structures.

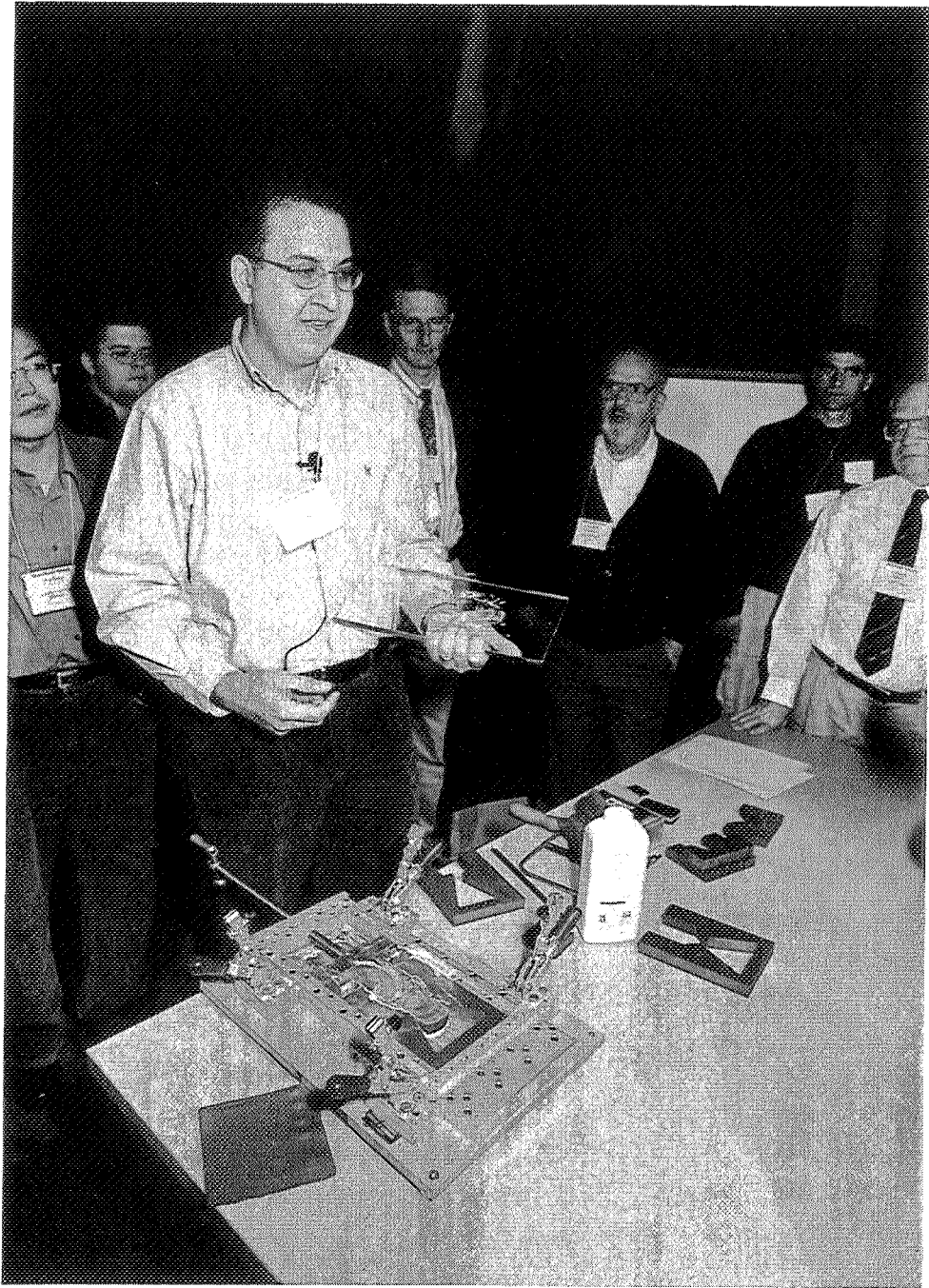
From the World War II image of "Rosie the Riveter" bolting together war planes to the jets flying overhead today, Americans have always associated metal airplanes with strength. However, aircraft designers today are turning to composite materials to meet the growing challenge of maintaining safety and economy for commercial air travelers. Anticipating this challenge, NASA and Boeing have joined forces under the NASA Advanced Composites Technology (ACT) program to make large composite airplane structures a reality.

VISIO-PLASTIC MODELING OF METAL FORGING AND EXTRUSION

Ghassan T. Kridli

Department of Industrial and
Manufacturing Systems Engineering
University of Michigan-Dearborn
Dearborn, Michigan 48128-1491

Telephone: 313-593-5467
e-mail gkridli@umich.edu



Ghassan T. Kridli

Visio-Plastic Modeling of Metal Forging and Extrusion

Ghassan T. Kridli

Department of Industrial and Manufacturing Systems Engineering
University of Michigan-Dearborn
Dearborn, Michigan 48128-1491

Abstract

Visio-plastic modeling is a technique that uses soft materials, such as plasticine, to demonstrate material flow, and to study the strain distribution in plane strain and axisymmetric upset forgings and extrusions. This technique is a useful tool that can be used during die design, especially in the case of progressive dies. Due to the low stress requirements necessary to cause deformation in plasticine, testing dies are inexpensive to machine and may be machined in short periods of time.

During the experiment, plasticine strips of equal thickness and of two different colors, are stacked with alternating color, so as to represent the initial shape of the forging stock or extrusion billet. The plasticine is then placed in the die and formed. Sections of severe deformation and material folding may be observed. Strain can be evaluated by comparing the initial and final strip thicknesses at different regions in the formed piece.

Keywords

Extrusion, visio-plastic modeling.

Prerequisite Knowledge

An understanding of the fundamentals of metal plasticity and the basics of the extrusion process and its limitations.

Objectives

The objectives of this experiment are to physically model the extrusion process and to visually identify the flow path taken by different sections of the starting billet. In addition, it demonstrates: (a) the effects on the material flow of die parameters such as the die half angle and the extrusion ratio; and (b) failures that may be associated with the process.

Equipment and Materials

1. A visio-plastic forming press (schematically represented in Figure 1) with a tempered glass cover that allows for material flow visualization during forming.
2. Plasticine modeling material in at least two colors, that can be sliced into 3.0 in. x 0.75 in. x 0.25 in. billets. These may be purchased at hobby stores.
3. A miter box to slice the plasticine into the desired thickness.

4. Talcum powder to be used as a lubricant and to prevent the plasticine from sticking to the walls of the miter box.
5. PVC forming dies that have been machined to a shape and geometry so as to produce the desired flow effects (i.e., dead metal zone, extrusion defects, etc.)
6. A digital camera to record flow patterns
7. Safety goggles.

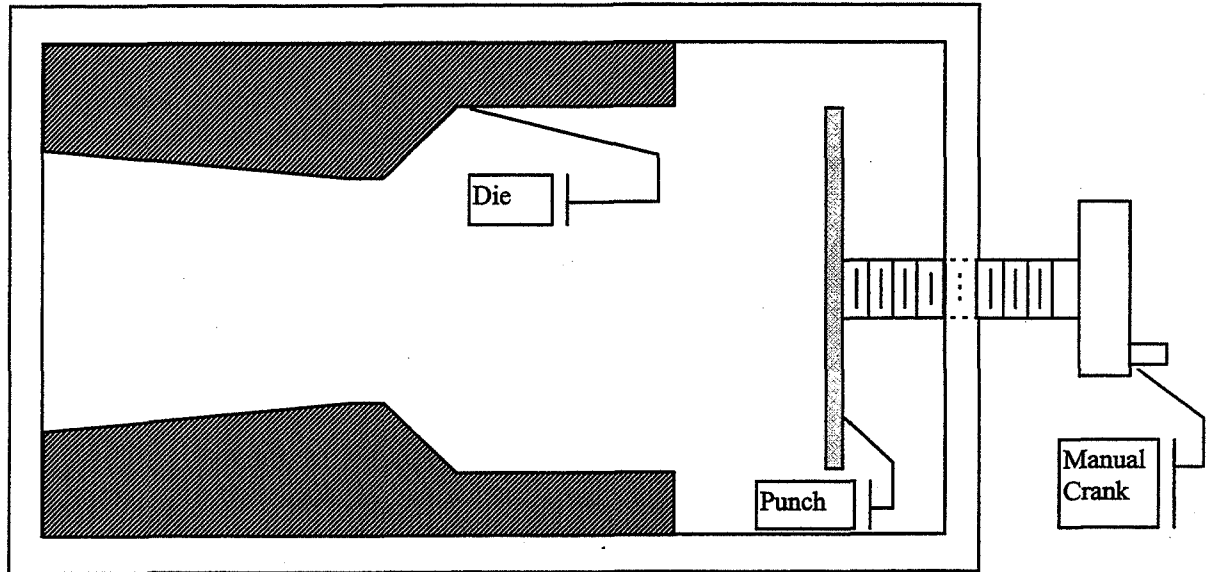


Figure 1. Schematic of the visio-plastic extruder

Introduction

Visio-plastic modeling is a visual technique in which a soft material, such as plasticine, is used to model material flow and strain distribution patterns for conditions of plane strain, axisymmetric extrusion, or forging. This technique is similar to etching a grid pattern on a metallic billet and observing the distorted grid during and after deformation. Plasticine is selected because of its low yield strength, which allows for the use of inexpensive manually driven presses and dies made of PVC. Pearson and Parkins (1960) reported that plasticine could be used effectively in modeling the flow of hot metals.

Both internal and external defects in extruded pieces are generally affected by die half angle and extrusion ratio. The most severe internal defect is a centerline burst, also called a "chevron" crack, an arrowhead crack, or a cuppy core (Hosford and Caddell, 1993). Centerline bursts occur under low cross-sectional reductions and large die half angles for plane strain extrusion. This defect is caused by a high level of hydrostatic tension near the mid-plane (Hosford and Caddell, 1993). These internal cracks affect the in-service mechanical properties of extruded components, and they are important in predicting form conditions under which they occur. External defects are usually in the form of: (a) piping,

which occurs at the back face of the billet (in contact with the ram), or (b) enfolding of the oxidized layer at the back face of the billet. In this demonstration, only external type (b) defects will be modeled.

The demonstration also models the effects of friction, and die shape and geometry of the flow of materials during extrusion. The technique also demonstrates the need to use progressive die extrusion or forging.

Billet Preparation

To prepare the billet, talcum powder is sprinkled in the miter box to prevent the plasticine from sticking to it. Two plasticine blocks of different colors are sliced in the miter box into strips of equal thickness (i.e., 0.25 in.) The width of the miter box should represent the desired width of the starting billet (in this case 3 in.). The billet is then prepared by stacking the sliced strips in the form of transverse bands of alternating colors as shown in Figure 2(a). This billet layout is appropriate for demonstrating the strain distribution for sliding between the billet and the container. For the case where sticking between the billet and container walls occurs (i.e., material shearing), the billet is prepared by stacking square bars (0.75 in. x 0.25 in. x 0.25 in.) of clay in a checkered pattern, as shown in Figure 2(b).

Procedure

1. Four type A billets [Figure 2(a)], and one type B billet [Figure 2(b)] are prepared.
2. Safety glasses are to be worn. Even though the press is covered with tempered glass and manually operated, the students need to protect their eyes in the event of glass failure.
3. Using the PVC die with a 90° half angle, an A type billet is extruded; talcum powder is used as a lubricant. The different stages of material flow into the die are observed and videos of the formation of the dead metal zone, and the steady state flow are taken. An image at the end of the punch stroke is recorded. Students are to write down their observations.
4. Using the PVC die with a 45° half angle, an A type billet is extruded; again, talcum powder is used as a lubricant. The different stages of material flow into the die are observed and videos of the formation of the dead metal zone, and the steady state flow are taken. An image at the end of the punch stroke is recorded. Students are to write down their observations.
5. A strip of plasticine of a third color is added to the last A-type billet so as to represent an oxidized layer of material. The billet in the die with a 45° half angle is extruded, and the students observe the flow of the oxidized layer into the extruded component.
6. The 90° half angle die is cleaned with alcohol to remove all traces of the lubricant; the last type A billet, and also the type B billet are extruded under dry conditions. Videos of the flow of these two billets are taken and the images are compared.
7. The students are to comment on their observations.

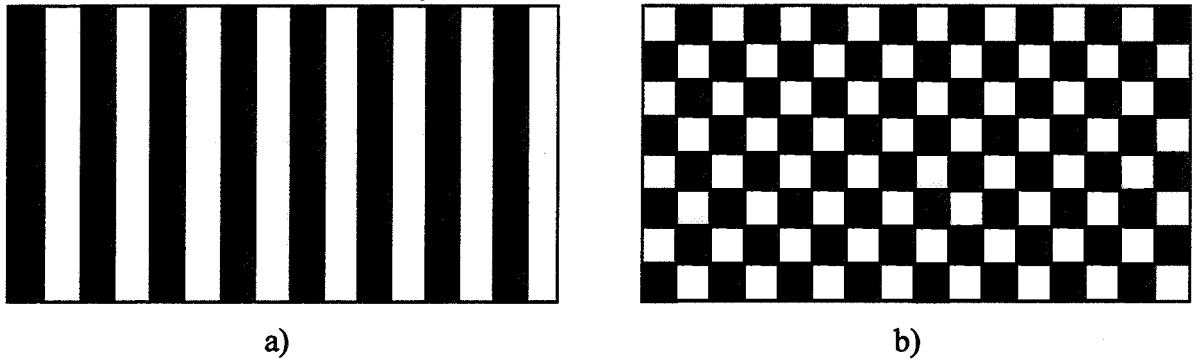


Figure 2. Composite billet (a) rectangular strips, and (b) checkered blocks

Summary

The exercise provides a visual tool to demonstrate material flow during extrusion and upset forging. It shows the effects of the process parameters (die half angle and extrusion ratio) on the formed part. The effect of forming speed can also be investigated by using rate sensitive modeling materials.

References

1. Hosford, W. F., and Caddell, R. M., *Metal Forming*, 2nd edition, Prentice-Hall, 1993.
2. Pearson, C. E. and Parkins, R. N., *The Extrusion of Metals*, 2nd edition, John Wiley & Sons, 1960.

Biographical Information

Ghassan T. Kridli is an Assistant Professor of Industrial and Manufacturing Systems Engineering at the University of Michigan-Dearborn. He received his Bachelor's and Master's degrees in Mechanical Engineering from the University of Miami, and his Ph.D. from the University of Missouri-Columbia. He teaches manufacturing related courses and supervises manufacturing senior design projects. His interests include manufacturing process simulation, and light weight material processing and characterization. He is a member of SME, ASME, and TMS.

**CORPORATE PARTNERSHIPS:
WIN-WIN-WIN**

David H. Devier

**Industrial & Engineering Technologies
Owens Community College
P. O. Box 10,000
Toledo, Ohio 43699**

**Telephone: 419-661-7459
e-mail ddevier@owens.cc.oh.us**



David H. Devier

CORPORATE PARTNERSHIPS: WIN-WIN-WIN

David H. Devier, Ph.D.

Industrial & Engineering Technologies
Owens Community College
Toledo, OH 43699

INTRODUCTION

As we approach the turn of the twenty-first century in America we find a dynamic educational environment at all levels. The demands on educational institutions, kindergarten through adult, are higher than ever before. The types of work available to entry level workers today are considerably different than just a generation ago. The low skill-high paying factory jobs of the past are no longer easily attainable to young workers, or displaced workers for that matter. Today, more than ever before, entry level workers must have special skills to be employable in any position which offers high compensation. The only work remaining for the unskilled and under skilled work force is in the service and raw labor sector which offers compensation at only the minimum way level.

This is true for the types of positions which historically did not require advanced college training such as auto mechanics and diesel technicians. Today one cannot learn on the job the high tech skills required to diagnose and repair a \$30,000 sport utility vehicle or trouble shoot an electronic problem on a \$100,000 farm tractor. The days of the backyard mechanic who can walk into an auto dealership and sign on as a technician are gone. Now these dealers demand entry level employees who already have the required skills and corporations are demanding that the dealers have certified, well trained workers for all warranty work.

To make matters more difficult, the young people of today do not generally see such positions as auto technicians as desirable while at the same time the demand for such workers is overwhelming. There in lies the focus of the corporate programs which have been developed at Owens Community college and other two year institutions. The goal of each program is to meet the demand for high skilled entry level employees for occupations where it is difficult to fill the positions.

The corporate partnerships bring together the corporation, such as John Deere or General Motors, the dealerships, and the college to recruit, support, and train the students. Most programs are full two-year associate degrees with summer internships at the dealerships. The remainder of this paper will discuss the details of the Owens Community College corporate partnerships and make suggestions for similar endeavors at other institutions.

OCC CORPORATE PARTNERSHIPS:

The Industrial & Engineering Technologies Division at Owens Community College is made up of more than twenty major programs ranging from traditional mechanical and electrical

engineering technologies through auto and diesel technician programs. The seven corporate partnership programs are housed in the Transportation Technologies Department (auto and diesel) and include John Deere Agricultural Equipment, Caterpillar Construction Equipment, Mitsubishi-Caterpillar Towlift, General Motor ASEP, Ford ASSET, Freightliner, and Williams-Detroit Diesel/Allison. While there are differences among the programs, the general approach is the same. The curriculums for each are a specialized version of the general auto or diesel technician associate degrees. In each case, there is corporate and dealer involvement ranging from cash contributions to equipment/tool gifts and loans to off term internship employment of students. Some of the programs such as the ASEP, ASSET, and John Deere are widely known as national programs with sites around the U.S. On the other hand, programs such as the two Caterpillar endeavors and Williams-Detroit Diesel/Allison are unique to Owens Community College. In all cases, the goal is the same — establish win-win-win-win (corporation-dealers-college-students) situations where the corporations and dealers acquire skilled workers, the college provides much needed training and the students gain employment in well paid, high skilled jobs. The various programs at Owens have been implemented during the late 1980's and throughout the 1990's. The most recent being the Mitsubishi-Caterpillar Towlift program initiated for the Fall of 1998.

HOW TO ESTABLISH A CORPORATE PARTNERSHIP

The process of establishing a corporate partnership is multifaceted. The first step is to determine what the needs are of a given corporate-dealer group. Generally, the basic need is for well trained, entry level service technicians who have a solid background in the given product line, i.e., John Deere ag, Caterpillar construction, etc., and the desire to pursue a career in the field.

This relationship between the corporation, the dealers, and Owens Community College may begin in any number of ways including the corporation contacting the college, the dealer(s) coming to the college, or the college reaching out to make the contact. The history of the programs at Owens is that once the first successful program was created the others came along based on the similar needs of other corporation-dealership groups.

Once the initial contact has been made, the second step is to pull together all the interested parties in an ad hoc advisory committee. These parties include corporate management, dealership personnel, and college administrators and faculty. At these first meetings, a strong commitment must be voiced by all concerned because the total success of the program is based on the sincere interest of each party. If even one of the subgroups such as the dealers lack this deep commitment, the program will not develop. Generally, an official agreement is developed and signed off on by all parties to insure this commitment and outline the responsibilities of each. Confidentiality will not permit the inclusion of an example agreement here, but suffice it to say that it includes an outline of what each party will provide and/or do throughout the life of the program.

After the formal agreement has been signed, additional meetings are held with a select group of college faculty and administrators, corporate training/education personnel, and dealership technician/service personnel to determine the curriculum outline and courses, as well as, the equipment, tools, and training aid requirements of the developing program. The curriculum begins with one of the current college auto or diesel outlines and modifications are made as needed. For instance, all programs have an engines course, but the given corporate program will require work on the engines related to that product line. New courses may need to be developed such as electric motor operation and maintenance for the Mitsubishi-Caterpillar Towlift program.

The final pre-program step is the finalization of the kick-off and student recruitment activities. The college plans and hosts an official kick-off event where corporate and dealer personnel meet with college officials to act-out the signing of the agreement, show corporate product, etc., for the news media. There is a news release sent to all the local media in the location of all the dealers to facilitate recruitment.

The recruitment phase is the most important element to the success of the program, because simply stated — no students - no program. The dealers must accept the lead in this process, because they are recruiting future employees and generally they are high school students from the schools in their area. It will not work to have an Owens admission counselor visit a school in an area where no dealerships exist and attract students into a given program. It is well known that two-year college students generally do not want to relocate after college. The Owens responsibility in this process is to facilitate student enrollment and advising and help with financial aid and housing. Many times, an Owens faculty member or administrator will attend a recruitment event at a dealership.

Figure 1, outlines a Corporate Partnership Startup Check Sheet which will serve to identify the various steps in the process in more detail.

- Inform relevant College departments of company/dealer intent to collaborate
- Initial discussions with company/dealer interested
- Initial tour of facility for company/dealer management
- Determine minimum number of students to justify program
- Tentative commitment from company/dealer to proceed - estimate likely enrollment
- Brief College Relations on activity
- Form advisory committee to provide guidance on curriculum and other issues such as curriculum, financial aid, and equipment/tools.
- Discuss need for student housing
- Determine what equipment and or software company/dealer will provide and what College will provide
- Obtain commitment from company/dealer for needed enrollment
- Determine if company/dealer is willing to provide financial aid
- College submits program proposal to state higher education governing board
- Decide who monitors field experiences, if they are required
- Agree on when to start program
- Determine need for instructor training
- Formal company/dealer and college approval (of all above issues) to proceed
- Submit any required new course information, i.e., catalog, schedule, etc.
- Request assistance from public relations units of college and company
- Purchase orders for required start up lab equipment/computers
- Kickoff held
- Promote at dealerships - line up students
- Administer assessment testing to sponsored students
- Register students - begin program
- Conduct regular advisory committee meetings to continuously improve

Figure 1
Corporate Partnership Startup Check Sheet

It may be necessary to submit information to the State Board of Regents for Higher Education for formal program approval if the new program is considerably different than currently approved programs. New courses and the new program outline need to be submitted for the college catalog and various publications. Facilities may also need to be developed/modified to incorporate the new program. This is an area where early discussions by the college faculty and administration will head off problems.

SUMMARY:

Corporate partnerships are an excellent way for any two-year college to provide much needed training to serve the needs of industry and students. It goes almost without saying that there must be a sincere commitment on the part of all parties. If anyone of the three; corporation, dealers, or college fail to do their part, then the partnership will not be successful. The most important element is the recruitment of students by and with the dealers. It is almost impossible to attract students to the program without the dealer involvement. Faculty currency is also an important element and here the corporation must help to provide the specialized training required. The specialized equipment, tooling, software, etc., must also be provided by the corporation and dealers on a lend-lease agreement.

In conclusion, let it be said that corporate partnerships at two-year colleges are an excellent opportunity to serve the needs of the community and broaden the scope of programming. The results are effective programs which challenge the college faculty, increase enrollment, expand student employment opportunities, and serve industries' needs.

Dr. David H. Devier is Dean, Industrial and Engineering Technologies, Owens Community College, Toledo, Ohio. Prior to assuming this position, he was Chair and Professor, Department of Technology, Ohio Northern University, Ada, Ohio. He has twenty-two years of teaching and administrative experience in technical higher education

A SIMPLE EXPERIMENT FOR DETERMINING ELASTIC PROPERTIES OF POLYMERS

P. K. Mallick

Department of Mechanical Engineering
University of Michigan-Dearborn
Dearborn, Michigan 48128

Telephone 313-593-5119
e-mail pkm@umich.edu

and

Subrata Sengupta



P. K. Mallick



Subrata Sengupta

A Simple Experiment for Determining Elastic Properties of Polymers

P. K. Mallick
Department of Mechanical Engineering
University of Michigan-Dearborn
Dearborn, MI 48128

Key Words: Modulus of Elasticity, Poisson's Ratio, Hooke's Law, Internal Pressure

Prerequisite Knowledge: Knowledge of mechanics of materials, including Hooke's Law that describes the stress-strain relationship in two-dimensional loading conditions.

Objective: The objective of this paper is to describe a simple experiment for determining the modulus of elasticity and Poisson's ratio of polymers using Hooke's Law for a two-dimensional stress condition.

Equipment:

1. One 2-liter soft-drink bottle
2. A bicycle pump
3. Two strain gages
4. Pressure gage
5. Miscellaneous items, such as rubber stopper, brass tube, etc.
6. Two portable strain indicators (one may also work)

Introduction:

Modulus of elasticity and Poisson's ratio are the two most basic material properties that describe the elastic response of a structure subjected to external loads. In general, they are determined using a uniaxial tension test with either a solid round specimen or a flat rectangular specimen. The flat rectangular specimen of the shape shown in Fig. 1 is preferred for polymers. They are either machined from extruded sheets or injection molded to the dimensions specified by the ASTM Standard D-638. An extensometer is used to measure axial (longitudinal) strain, which is then used to plot the axial stress vs. axial strain diagram. The modulus of elasticity of the material is determined from the initial slope of the elastic portion of this diagram. To determine the Poisson's ratio, the transverse strain must also be measured. For a flat specimen, either a transverse extensometer or a transverse strain gage is used to determine the transverse (or width-direction) strain. The Poisson's ratio is calculated from the slope of the transverse strain vs. axial strain diagram.

In most engineering programs, students in courses on mechanics of materials, mechanical properties of materials or mechanical design conduct uniaxial tension test and determine tensile properties of materials, including modulus of elasticity. However, the Poisson's ratio is usually not determined, since it requires additional instrumentation to measure the transverse strain.

This principal objective of this paper is to show the application of Hooke's Law in determining the modulus of elasticity and Poisson's ratio of a material. In this experiment, a 2-liter plastic soft drink bottle is strain gaged and internally pressurized using a bicycle pump. The pressure-strain data are used to calculate the modulus and Poisson's ratio of the polymer used in the soft drink bottle.

Theory

The Hooke's law describes the strain-stress relationships, which for a linear elastic isotropic material under a biaxial stress condition (Fig. 2) are given by the following two equations:

$$\epsilon_{xx} = (1/E) [\sigma_{xx} - \nu \sigma_{yy}] \quad (1)$$

$$\epsilon_{yy} = (1/E) [\sigma_{yy} - \nu \sigma_{xx}] \quad (2)$$

where, σ_{xx} and σ_{yy} = normal stresses in the x and y directions, respectively
 ϵ_{xx} and ϵ_{yy} = normal strains in the x and y directions, respectively
 E = modulus of elasticity
 ν = Poisson's ratio

Solving Equation (1) and Equation (2) simultaneously gives the Poisson's ratio:

$$\nu = \frac{\epsilon_{xx} \sigma_{yy} - \epsilon_{yy} \sigma_{xx}}{\epsilon_{xx} \sigma_{xx} - \epsilon_{yy} \sigma_{yy}} \quad (3)$$

Knowing the Poisson's ratio, the modulus of elasticity E can be determined using Equations (1):

$$E = \frac{\sigma_{xx} - \nu \sigma_{yy}}{\epsilon_{xx}} \quad (4)$$

The Hooke's Law, given by Equations (1) and (2), is taught in the first course on Mechanics of Materials and is included in all textbooks on this subject. However, the application of Hooke's law is seldom demonstrated in laboratory experiments.

Experiment

The experimental setup is shown in Fig. 3. It consists of a 2-liter soft drink bottle positioned horizontally inside a protective plastic shield. Strain gages are mounted at the mid-length of the bottle, one in the axial (x) direction and the other in the hoop (y) direction (Fig. 4). A bicycle pump is used for increasing the internal pressure inside the bottle. The bottle mouth is sealed with a hollow rubber stopper and a brass tube passing

through the rubber stopper carries air from the bicycle pump to the inside of the bottle. Two strain indicators are used, one for the axial strain (ϵ_{xx}) measurement and the other for the hoop strain (ϵ_{yy}) measurement.

The steps in this experiment are as follows:

1. Increase the pressure in steps of 5 psi.
2. Read both hoop and axial strains on the strain indicators at each pressure increment.
3. Do not exceed 30 psi.
4. After reaching 30 psi, reduce the pressure in steps of 5 psi and read strains at each pressure value.
5. Plot hoop strain vs. pressure and axial strain vs. pressure for both increasing pressures as well as decreasing pressures.
6. Assuming a thin-walled closed-ended tube to represent the bottle, calculate hoop stress and axial stress using the following equations;

$$\sigma_{xx} = pr/2t \quad (5)$$

$$\sigma_{yy} = pr/t \quad (6)$$

where, σ_{xx} = axial stress
 σ_{yy} = hoop stress
 p = internal pressure
 r = internal radius
 t = wall thickness

7. Using Equations (3) and (4), calculate the modulus of elasticity and Poisson's ratio of the bottle material.

Results

Hoop and axial strain data from an actual laboratory test conducted by a student in Applied Mechanics in Design (ME 260) are shown in Fig. 5. Both strains increased linearly with increasing internal pressure and, although not shown, they returned back to zero along the same pressure-strain line as the internal pressure was released. This indicates that the bottle material remained in the elastic state. The outer diameter of the bottle is 4.33 in. and the wall thickness is 0.014 in. Based on these dimensions, the hoop stress and the axial stress at the highest internal pressure of 30 psi are calculated as 4609.2 and 2304.6 psi, respectively. Both these stresses are tensile in nature and, since there are no shear stresses in bottle wall, these are also the principal stresses. The von Mises equivalent stress is 3991.7 psi and using the maximum distortion energy theory of yielding, it can be shown that the material in the bottle wall did not yield.

Using the data at 30 psi and Equations (3) and (4), the Poisson's ratio (ν) and the modulus of elasticity (E) of the polymer used in the soft drink bottle are determined as 0.299 and 0.745×10^6 psi, respectively. For a more accurate determination of ν , an Excel spreadsheet may be set up to plot $(\epsilon_{xx} \sigma_{yy} - \epsilon_{yy} \sigma_{xx})$ vs. $(\epsilon_{xx} \sigma_{xx} - \epsilon_{yy} \sigma_{yy})$. The slope of this

plot is the Poisson's ratio ν . The modulus of elasticity can then be determined using Equation (4).

Conclusions

This paper has described a simple test method to determine the modulus of elasticity and Poisson's ratio of polymers. It also demonstrates the use of Hooke's Law to students who have learned the principles of Hooke's Law in their mechanics of materials course. The test equipment is very simple and it does not involve a testing machine. One obvious limitation is that the test can only be performed with bottles or closed-ended tubes that can act as pressure vessels. The other limitation is that the bottle material may not be isotropic, since many plastic bottles are manufactured using a process called stretch blow molding. As a result of this particular processing method, the polymer molecules may be somewhat oriented in the axial direction, making the bottle material non-isotropic. Equations (1) and (2) assume isotropy.

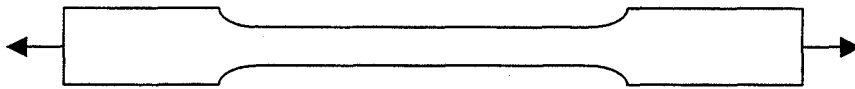


Fig. 1:
Typical
tensile test
specimen

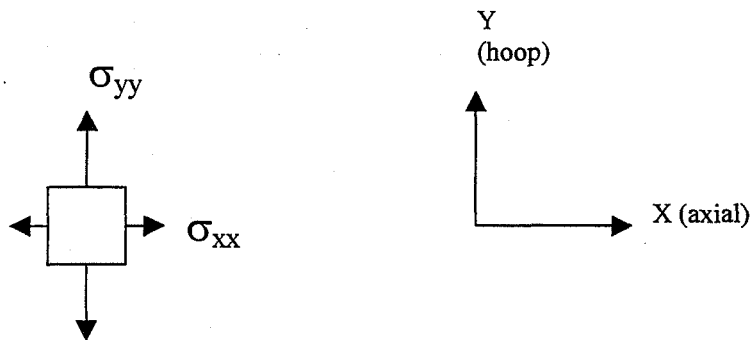


Fig. 2:
Biaxial
stresses
defined

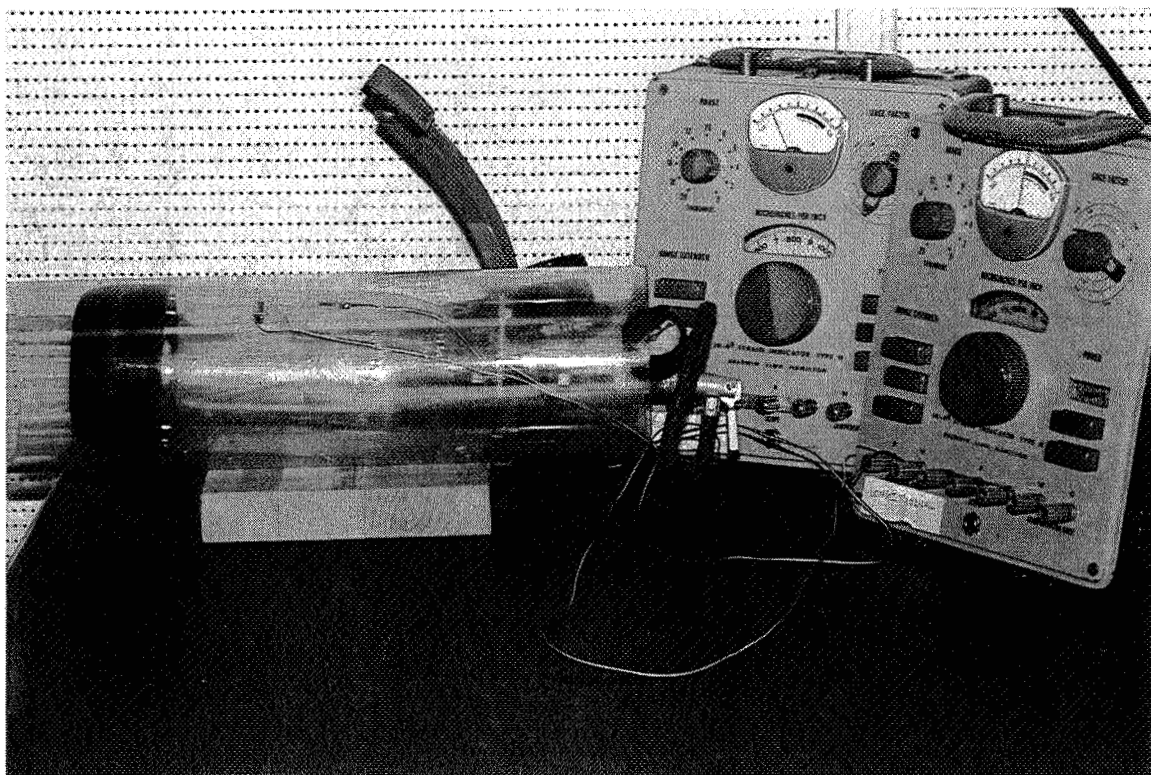


Fig. 3: Photograph of the biaxial test arrangement

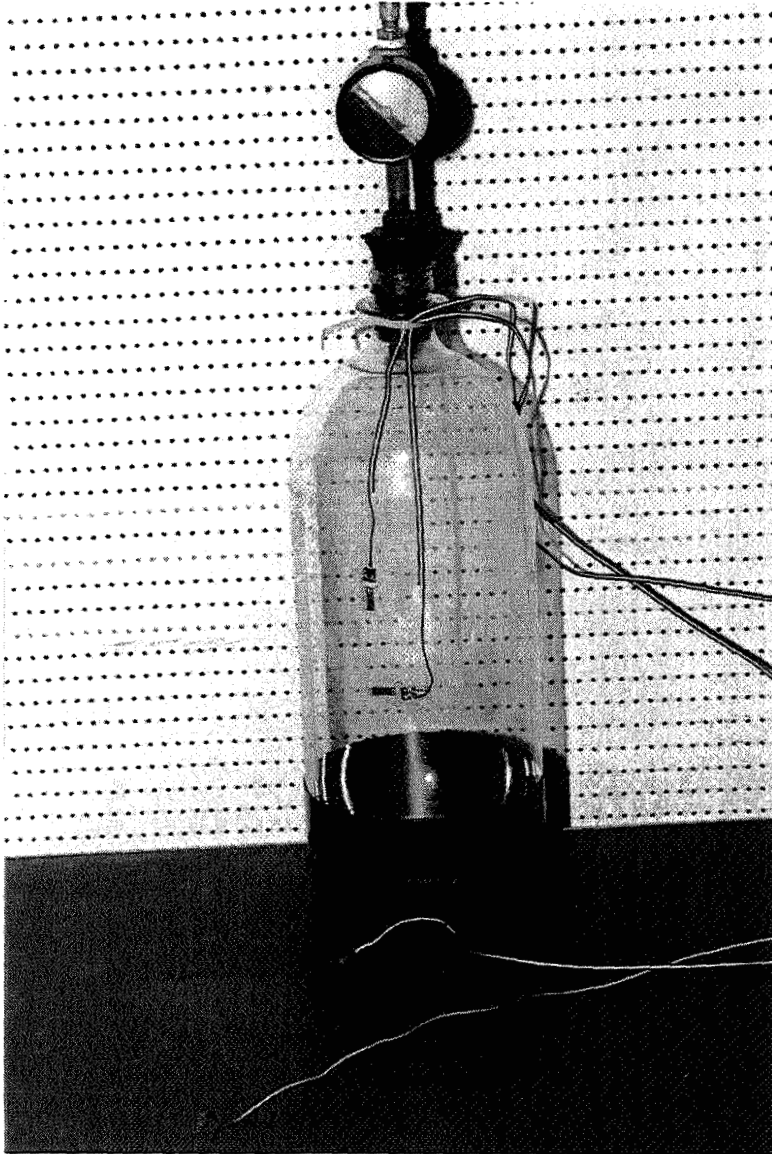


Fig. 4: A close up view of the strain gaged bottle

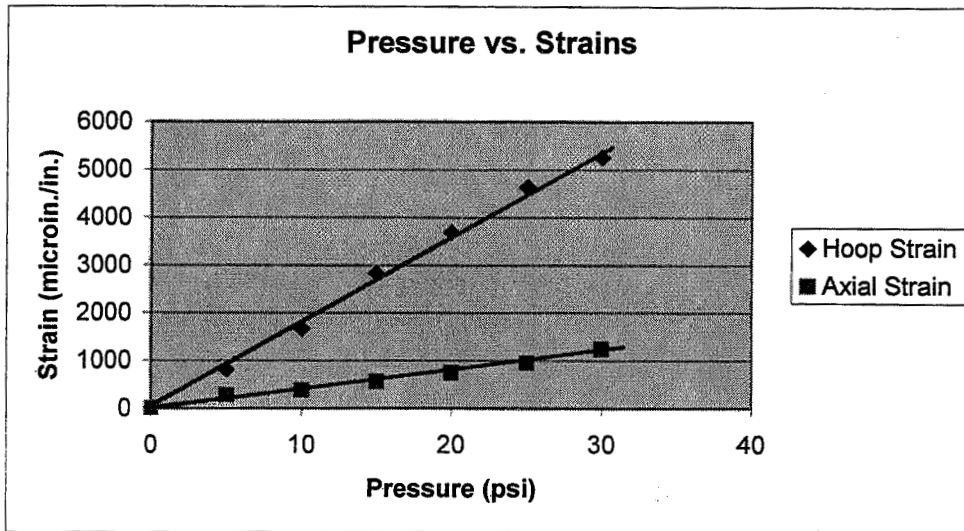


Fig. 5: Hoop strain and axial strain vs. internal pressure in the soft drink bottle wall

Biography

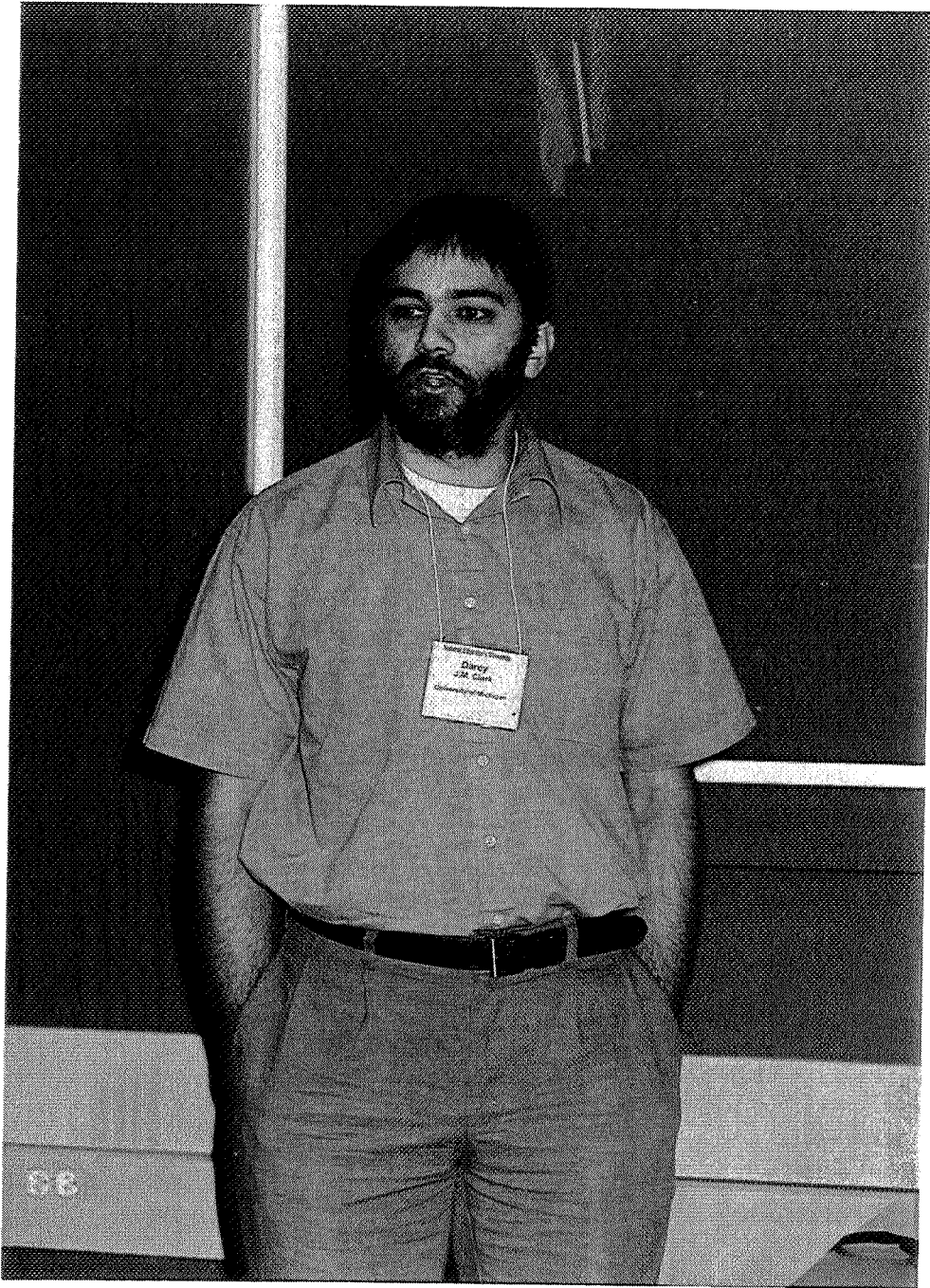
P. K. Mallick is a professor of mechanical engineering and the director of the Interdisciplinary Programs at the University of Michigan-Dearborn. He is also the director of the Center for Lightweight Automotive Materials and Processing. He received his Ph. D. in mechanical engineering from the Illinois Institute of Technology in 1974. His teaching and research interests are mechanical properties, design and processing of polymers, composites and other lightweight materials. He is the author of a textbook, *Fiber reinforced Composites*, co-author of a reference book *Composite Materials Technology* and editor of the recently published *Composites Engineering Handbook*. He is a fellow of the American Society of Mechanical Engineers and a recipient of the university's outstanding faculty research award in 1997.

**THE MATERIALS EDUCATION LIBRARY:
SHARING EDUCATIONAL RESOURCES VIA
THE WORLD WIDE WEB**

Darcy J. M. Clark

Materials Science and Engineering Department
University of Michigan
H. H. Dow Building
2300 Hayward Street
Ann Arbor, Michigan 48104-2136

Telephone: 734-764-3377
e-mail darcyc@engin.umich.edu



Darcy J. M. Clark

The Materials Education Library: Sharing Educational Resources via the World Wide Web

Darcy J. M. Clark
Materials Science and Engineering Department
University of Michigan
Ann Arbor, MI 48104-2136

Keywords : World Wide Web, Multimedia

Prerequisite Knowledge Required : Some experience with the use of a web browser (such as Netscape Communicator³ or Microsoft's Internet Explorer⁴) is assumed.

Objective : The Materials Education Library (MEL) is an online library of multimedia content for materials educators. It's main objective is to promote the sharing of educational content amongst the materials education community. The objective of this article is to demonstrate how the MEL operates, e.g. how do you get content out of the library, how do you contribute your own content ?

Equipment and Materials :

Hardware

1. A relatively modern personal computer capable of running a web browser (e.g. an Apple Mac 7x00 or a Pentium PC or better)
2. An internet connection (modem or ethernet)

Software

- Netscape Communicator (3.0 or greater, 4.x recommended)³
- or
- Microsoft Internet Explorer (3.0 or greater, 4.x recommended)⁴

Optional(but recommended)

1. Apple Quicktime 3.0 or greater⁵

Introduction

The Internet and the World Wide Web (WWW) both have enormous potential to change how educational resources are developed and distributed. Indeed the WWW was first developed to enable more efficient exchange of scientific information between geographically-separated researchers. Capitalizing on this capability, the Materials Education Library (MEL) is a website that provides mechanisms for the sharing of educational resources amongst materials educators.

Content within the library can be searched by keyword or media format and used within multimedia lectures (e.g. via Netscape or Powerpoint). This content can be rated online, providing users with valuable information from their peers about the useability and educational

usefulness of individual objects with the library. Content can be contributed to the library by simply filling out an online form.

Resources already available in the library include (but are not limited to) images, animations and java applets for use in course websites. Links to many external resources such as simulation software and materials-related websites are also cataloged. A prototype catalog of in-class demonstrations has also been developed.

For a more in-depth coverage of the philosophies and motivations behind the development of the MEL, the reader is referred to previous articles ^{1,2}.

Procedures

1. Accessing the site

To access the site, open the following address with your preferred web browser :

<http://msewww.engin.umich.edu/MEL/> (see Figure 1., label A)

2. Basic Site Navigation

A : type address here

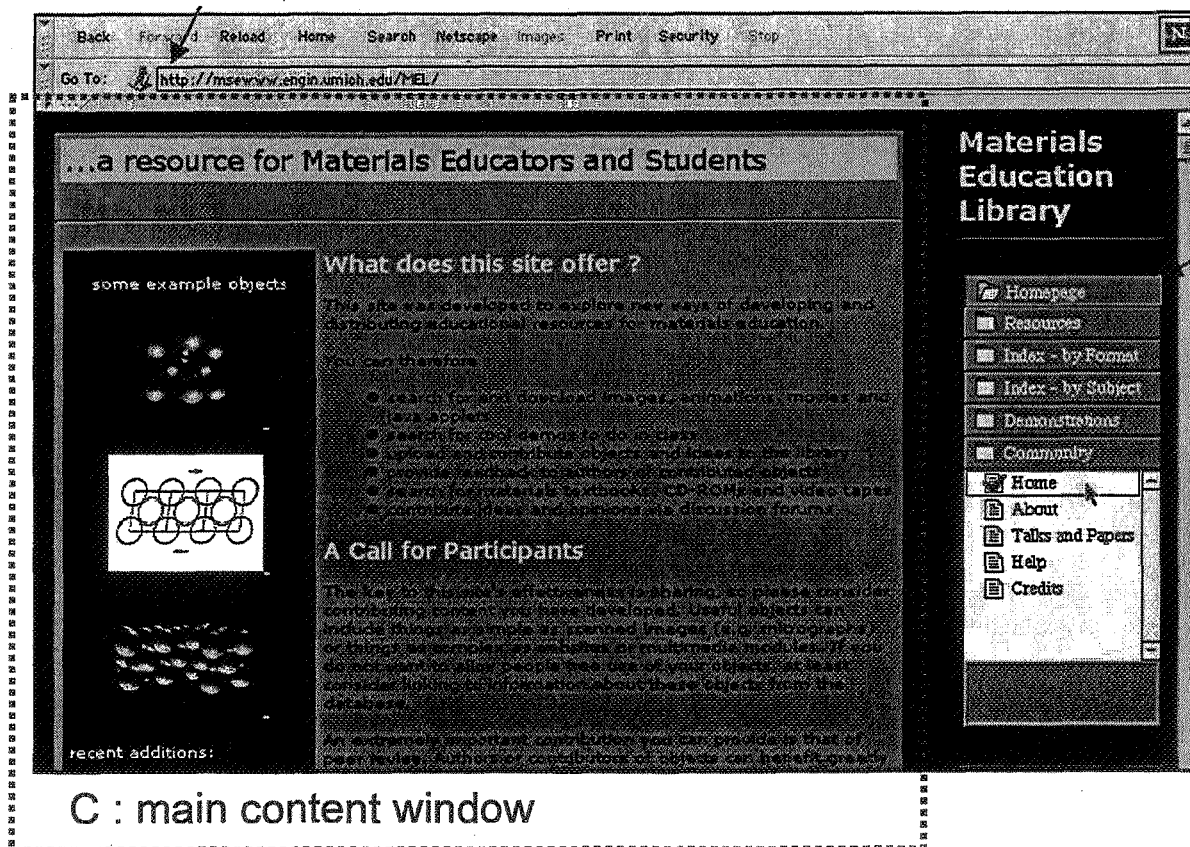


Figure 1. Basic layout of the MEL website

The MEL utilizes a frames-based layout in order to simplify navigation throughout the site. The menu bar (label B in Figure 1.) on the right side of the screen allows the user to jump to one of six main areas. These main areas contain sub-areas that are listed and described below :

- Homepage
 - Home – go to the MEL front page
 - About – about the site
 - Talks and Papers - some links to talks and papers about the MEL
 - Help
 - Credits

- Resources
 - List All – list every resource within the library
 - Search – search using criteria such as keyword and media class
 - Develop – some tips on producing content for the library
 - Contribute – fill-out form for contributing content to the library
 - Evaluate – instructions on contributing peer review

- Index – by Format : this section allows quick access to content by media format
 - Webpages
 - Digital Text
 - Digital Video
 - Digital Animation
 - Digital Image
 - etc, etc.

- Index – by Subject : this section allows quick access to content by subject
 - Atomic Bonding
 - Case Studies
 - Ceramics
 - Composites
 - Corrosion and Degradation
 - Crystallography
 - etc, etc.

- Demonstrations – a prototype in-class demo database
 - Add a Demo
 - Search
 - List All

- Community - a bulletin board for online discussions and a member listing
 - Discussions
 - Members

3. Finding content

There are a number of ways to find content within the MEL. The menu bar on the right side of the screen (see label B in Figure 1.) provides a very quick way to find content by either subject or media format. By clicking the “Index – by Subject” button, you can select from a number of sub-areas within the materials science field (e.g. Composites, Crystallography, Defects etc..). By clicking the “Index – by Format” button, you can search for multimedia content by its media format (e.g. images, websites, java applets, animations etc..).

For ‘finer-grained’ searching of the library, use the “search” facility found under the “Resources” button in the menu bar. As shown below in Figure 2., it is possible to combine search criteria.

Search for Objects

Type search criteria in one or more fields below (not entering any criteria will return with no objects).
N.B. Because of the way that Filemaker Pro works, the search doesn't match **exactly**, but finds words which are contained in the field. So, for example, to search for a certain URL, just type in a few words which are in the URL, not the whole thing.

Find Objects

URL:

Name:

Media Class: digital animation

Description: fcc

Subject: Any
atomic bonding
case study
ceramics
composites
corrosion and degradation
crystallography
defects
demonstration
design

Author Name:

Author Email:

Source Avail?: Don't Care Yes No

Submitter Name:

Submitter Email:

Sort by: Date Entered Descending

Find Objects **Show Every Object**

Figure 2. Combining search criteria to find specific content. In this case we are looking for a digital animation in the crystallography subject area that deals with FCC unit cells.

Once you have entered your search criteria into the form, press the “Find Objects” button on the lower part of the screen. Objects that match the criteria are returned as shown in Figure 3. By clicking the underlined object name, you can preview objects (see Figure 4.).

Objects Found			Search
Displaying records 1 thru 2 of 2 records found (2 records displayed)			
Object Name	Subject Area/s	Media Class	Description
4xfcc.mov	crystallography	digital animation	shows generation of structure from unit cells, fcc lattice
FCCrotate.mov	crystallography	digital animation	rotation of FCC unit cell while changing from ball-and-stick to hard sphere

Figure 3. The search criteria shown in Figure 2. returns the following resources. By clicking on the underlined object name, you can then examine the object (shown in Figure 4.)

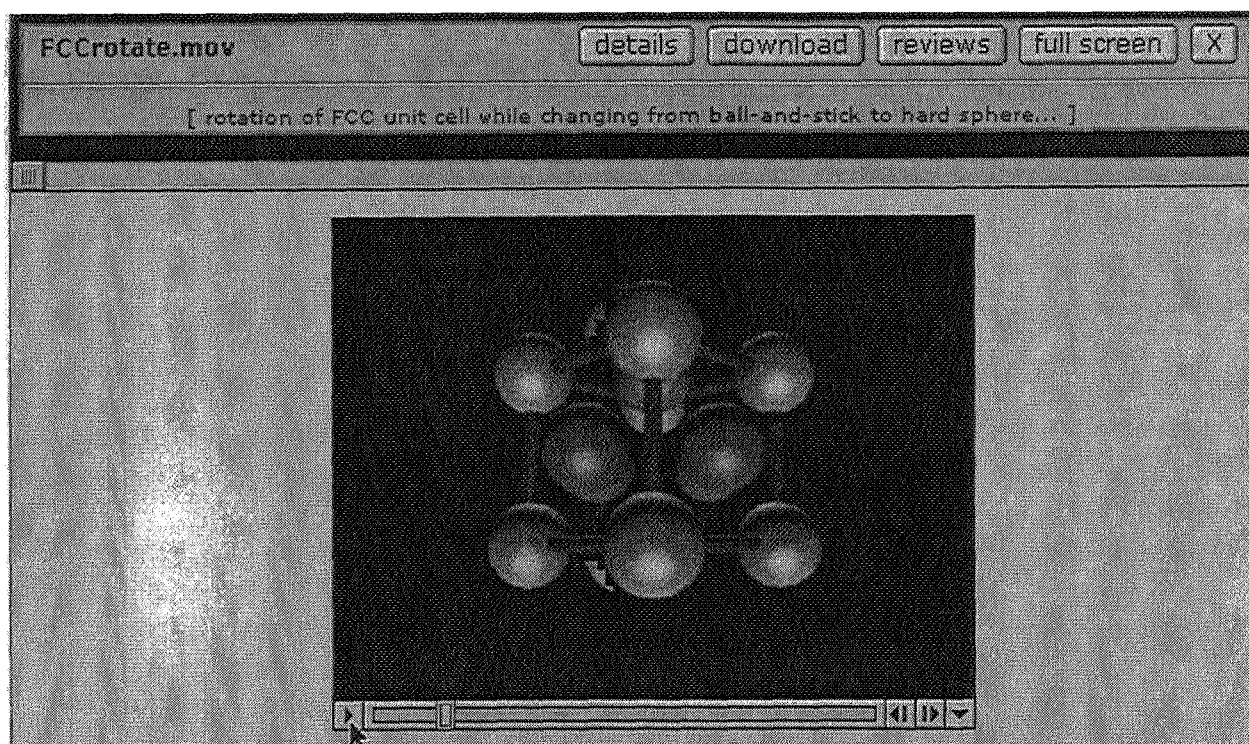


Figure 4. By clicking the object name (as shown in Figure 3.), we can preview the object. In this case, FCCrotate.mov is a Quicktime⁵ movie showing the rotation of an FCC unit cell while changing from a ball-and-stick to hard sphere representation.

To obtain detailed information about a particular object, click the “details” button (see Figure 4.). This detailed information includes important authorship and copyright information.

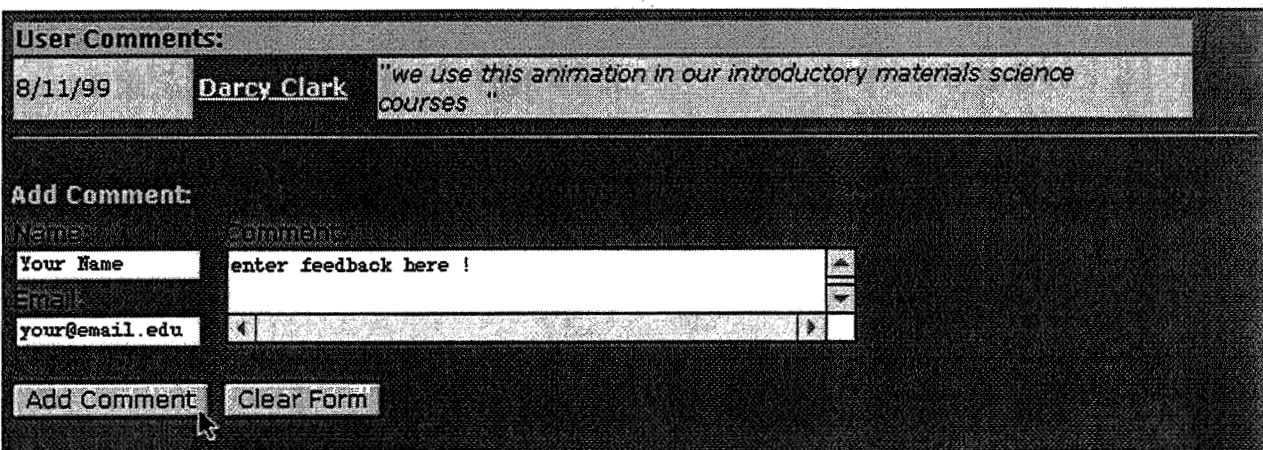
To download an object for use in Powerpoint or your own websites, press the “download” button (instructions on how to download and then subsequently use content in your own class presentations are provided in section 5).

To peruse any contributed peer comments about the object, press the “reviews” button (instructions on how to contribute your own feedback are detailed in section 4).

To preview the object in a full screen mode, press the “full screen” button. To close the object window, press the “X” button on the far right of the screen.

4. Peer Review

An important concern of educators using the WWW for teaching is the quality of online content. Unlike books or journals, peer review of content before publication online is not part of the typical *modus operandi*. However it is most definitely possible to incorporate significant peer review mechanisms into web publications. The MEL accomplishes this by allowing users to both peruse and contribute peer review regarding individual objects within the library. This feature is enabled by pressing the “reviews” button (shown in Figure 4.), which both brings up any peer review comments as shown below in Figure 5., and prompts you for your own feedback about the content in question.



The screenshot displays a web interface for user comments. At the top, a header reads "User Comments:". Below this, a comment is shown with a date of "8/11/99", the name "Darcy Clark", and the text "we use this animation in our introductory materials science courses". Underneath, there is a section titled "Add Comment:" which includes a "Name:" field with the placeholder "Your Name", an "Email:" field with the placeholder "your@email.edu", and a "Comment:" text area containing the text "enter feedback here !". At the bottom of this section are two buttons: "Add Comment" and "Clear Form".

Figure 5. A simple peer review mechanism provides valuable feedback about content within of the MEL.

5. Using content

Objects that are actually contained in the library (including images, animations and movies) can be downloaded to your personal computer and incorporated into your own websites or Powerpoint presentations. Obviously external content referenced in the library (including websites, textbooks and CD-ROMs) will not be able to used in this way. Clicking the “download” button (shown in Figure 4.) brings up the following instructions and dialog boxes.

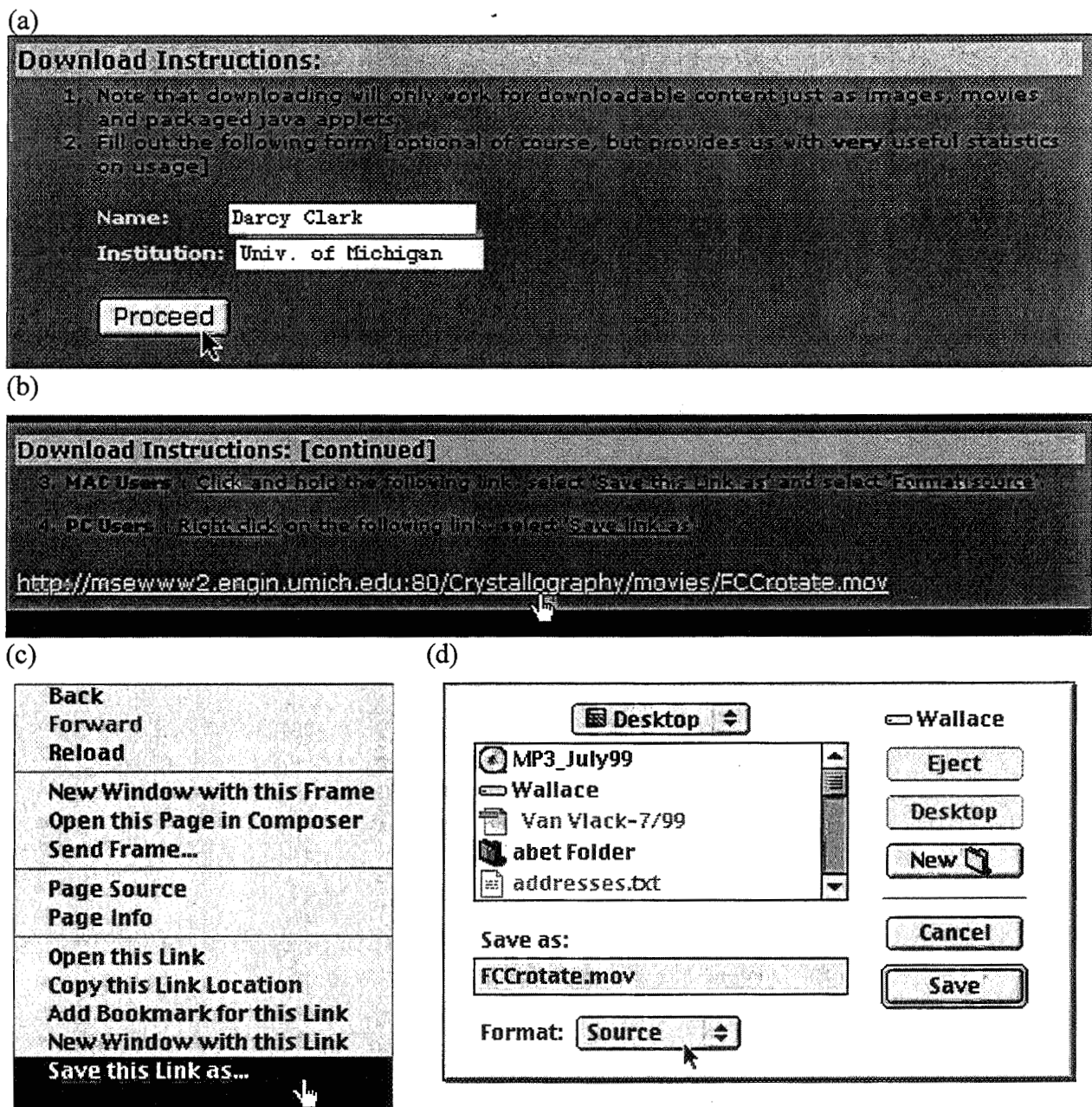


Figure 6. (a)-(d) Steps involved in downloading content from the library to your local machine. Content can then be incorporated into your own WWW or Powerpoint presentations. Make sure you save the content as 'source' as shown in 6(d).

Once you have the downloaded object on your local machine, it is very simple to embed this object into your own Powerpoint presentations, as shown in Figure 7., by using the "Insert / Movies and Sounds / Movie From File" command. Images can be utilized in a very similar fashion by using the "Insert / Picture / From File" command sequence.

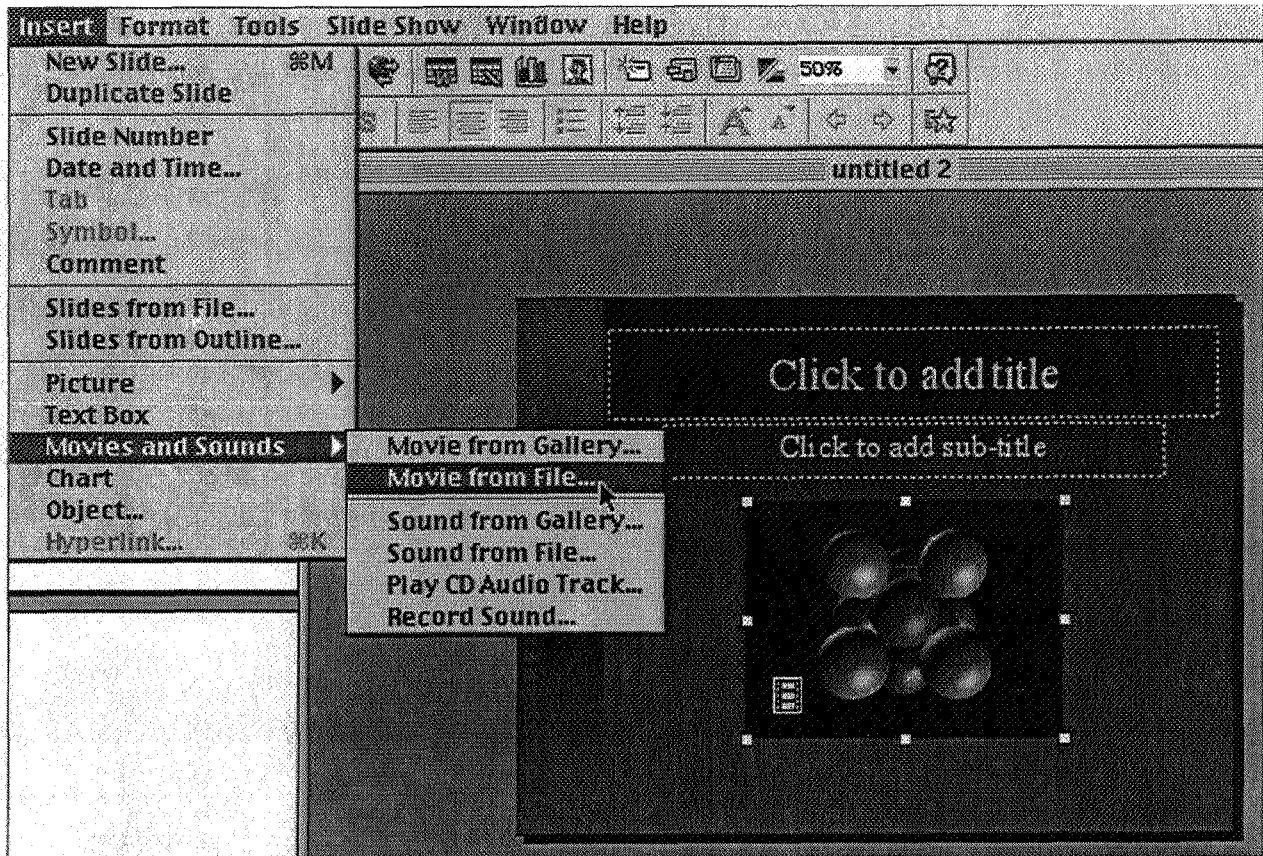


Figure 7. Incorporating downloaded content from the MEL into your own Powerpoint presentations, by the "Insert / Movies and Sounds / Movie From File" command (note: Microsoft Powerpoint 98 for MacOS is shown).

6. Contributing Content

So far we have only examined how content can be found and used, and briefly covered how the peer review mechanism works. In this section we will detail how to contribute your own educational content to the MEL. Suitable content might include images, animations, short Quicktime movies or archived (.zip, .hqx or .bin) Java applets. Other suitable content includes interesting web sites, textbooks and CD-ROMs. The value of the MEL to educators can only grow if there is an active group of contributors to the library.

There are 4 basic steps involved with becoming a contributing member of the MEL. If you want to contribute your own content to the server, follow steps a through d. If you are hosting your won content within your own web space, then follow steps a,b and d. If you simply adding a reference to textbook, CD-ROM or an external web site, then you can jump to part d.

- a. Sign up as a member
- b. Decide to host content locally or on the MEL server ?
- c. Transfer files to MEL server (if necessary)
- d. Add contributed content to the MEL database

a. Sign up as a member

Becoming a member is accomplished by clicking the “Community” button in the main menu (see Figure 1.), and then by clicking the “Members” sub-area. On this page a complete list of members is shown. By clicking the “Add Yourself” button on this page, you will be presented with a form to fill out, containing a few contact information fields and a short questionnaire. The purpose of the questionnaire is to identify members who want to contribute to the library. Those who do will then receive an email with instructions on how to contribute their original content to the MEL server. By signing up as a member, you will also receive semi-regular email updates on the latest contributed content.

b. Decide to host content locally or on the MEL server ?

The choice between storing your content on your own web server space or on the MEL server is completely dependant on the you, the contributor. Most educators will have web server space assigned to them by their respective institution. As space is limited on the MEL server, then the hosting your content within your own web space is the preferred option. Contact your local systems administrator for assistance with this. If you do decide to host your own content locally, then jump to section d.

c. Transferring content to the MEL server (if necessary)

If you want to transfer your content to the MEL server, then the following instructions address this. Each contributing member will receive a username and a password via email that will allow them to use the File Transfer Protocol (FTP) to transfer files to the MEL server. There are numerous FTP clients available for all platforms⁶. Using your chosen FTP client, open a connection to the MEL server at this address : [msewww2.engin.umich.edu](ftp://msewww2.engin.umich.edu), using the username and password that was provided to you. Once you have a connection, you will see a list of directories. Open the directory that corresponds to your account and upload your content. Verify the success of the upload by opening the following address in your web browser : <http://msewww2.engin.umich.edu/contrib/your@email.edu/content> , replacing your@email.edu with your own email address, and [content](#) with the filename of your content (e.g. image.gif, movie.mov or archive.zip).

d. Add contributed content to the MEL database

Once you have uploaded your content to either your local server or the MEL server, then you can add the relevant meta-data that describes your content to the MEL database. Under the “Resources” menu (see Figure 1.), there is a “Contribute” menu item. You will be first asked for the name of your content – this name will be checked against the existing database for duplicates. If all goes well, you will be presented with a fill-out form that prompts you for information about your contributed content. Enter the URL of your content into the URL field, and complete the various other fields. Be sure to enter an accurate, yet succinct description of your content into the “description” field. This will help MEL users find your content when searching using appropriate keywords.

URL:	http://msewww2.engin.umich.edu/contrib/your@email.edu/content
Name:	content name -
Media Class:	digital animation
Description:	enter a short description here
Subject:	<ul style="list-style-type: none"> atomic bonding case study ceramics composites corrosion and degradation crystallography defects demonstration design diffusion
Author Name:	Your Name
Author Email:	your@email.edu

Figure 8. Entering your content into the MEL database.

7. Prototype Demonstration Database

In-class demonstrations can be a key component in making materials science classes interesting for students. Many such demonstrations and experiments have been presented at previous NEW workshops. The prototype demonstration database is briefly presented here as a possible way of widening the publication audience and increasing the accessibility of a collection of interesting and informative demonstrations and experiments for materials science. Access the demo database by pressing the "Demonstrations" menu item (see Figure 1.). The demo database is designed and can be utilized in the same manner as the rest of the MEL site.

8. Conclusion

The MEL is very much a work in progress. The concepts it embodies are very dependent on the idea of an active community of members/users. To date most users have been content to simply 'use' content from the library, but the future success of the MEL depends on a continual growth of the content contained in the library.

References

1. Journal of Metals (Electronic Edition) Volume 50 (5), 1998. URL : <http://www.tms.org/pubs/journals/JOM/9805/Clark/>
2. Shared Educational Resource Development for Materials Science and Engineering, J. Mater. Ed., volume 20, numbers 1 and 2 (1998).
3. Netscape Communicator, URL: <http://home.netscape.com/computing/download/>
4. Microsoft Internet Explorer, URL: <http://www.microsoft.com/windows/ie/default.htm>
5. Apple Quicktime, URL: <http://www.apple.com/quicktime/>
6. Downloadable FTP clients for PC and MAC, URL: <http://www.tucows.com/ftp95.html> and URL: <http://www.allmacintosh.com/ftpmac.html>

Biographical Information

Darcy Clark is a Research Investigator at the University of Michigan (Ann Arbor, MI), Materials Science and Engineering Department. He has a Bachelor's degree and Ph.D from the University of Queensland (Brisbane, Australia). His work deals with the application of technology and new media to the process of teaching materials science. For more information, please visit this URL : <http://www-personal.engin.umich.edu/~darcyc/Work/>.

**TEACHING THE PRINCIPLES OF MATERIALS
SCIENCE USING OUR NATURAL SURROUNDINGS:
SPIDER SILK**

Robert J. Scheer

Composite Materials Engineering
Winona State University
Winona, Minnesota 55987-5838

Teaching the Principles of Materials Science using our Natural Surroundings: Spider Silk

Robert J. Scheer
Assistant Professor
Composite Materials Engineering
Winona State University

Key Words: Biomimetics, spider silk

Prerequisite Knowledge: None

Objective: To help students incorporate new concepts in materials science into their knowledge base using their understanding of our natural surroundings.

Equipment: None

Materials: sample of spider silk, sample of Kevlar®, 16-long rubber bands of equal length, 20-one inch (1") lengths of craft sticks, 40-small binder clips, rubber cement, and test frame (see instructions)

Introduction:

Nature has evolved many materials that have properties superior to those developed by humankind. Among the most widely studied of these are the abalone shell, spider silk, bone, and wood (or trees). Using these materials, the concepts of toughness, elasticity, and "intelligence" can be investigated and understood.

Tree and bone growth occurs in response to external stimuli (intelligent materials). As tree trunks and bones are strained a corresponding growth occurs to compensate for or neutralize the increased strain (Woodward et. al.). This is evidenced by larger growth rings on trees and by denser mineral deposits on bone.

Abalone shell and spider silk exhibit extraordinary specific mechanical properties. Considering that these materials are manufactured in an aqueous environment at moderate temperatures, we could learn a great deal from the study of them.

This demonstration/workshop hopes to increase students' understanding of the concepts of stiffness and toughness using simple models and the example of spider silk.

Procedure/Discussion:

Background

Spider dragline silk is nature's high-performance fiber. Its combination of tensile strength and elasticity gives the silk a higher energy to break than that of other natural or synthetic fibers. See properties listed in Table 1. It is a semicrystalline material made of amorphous flexible chains reinforced by strong and stiff crystals. The crystals are

made of hydrophobic polyaniline sequences arranged into beta-pleated sheets. The amorphous part is attributed to oligopeptide chains rich in glycine.

Table 1. Important mechanical properties of engineering materials. (Tirrell, Hinman)

Material	Strength (MPa)	Elasticity (%)	Energy to Break (kJ/kg)
Dragline silk	1000-4000	35	100
Kevlar®	4000	5	30
Rubber	1	600	80
Tendon	1000	5	5

Silk properties are routinely modulated by orb spiders, which can spin up to seven distinct fiber types having mechanical properties ranging from low modulus and highly extensible “elastomers” to high modulus and high toughness “filaments”. Such broad functionality is often achieved by seemingly subtle changes in amino acid sequence, composition, and mechanical processing (O’Brien, Simmons). Figure 1 is a two dimensional representation of one accepted way in which spider’s achieve a variety of properties in their silks.

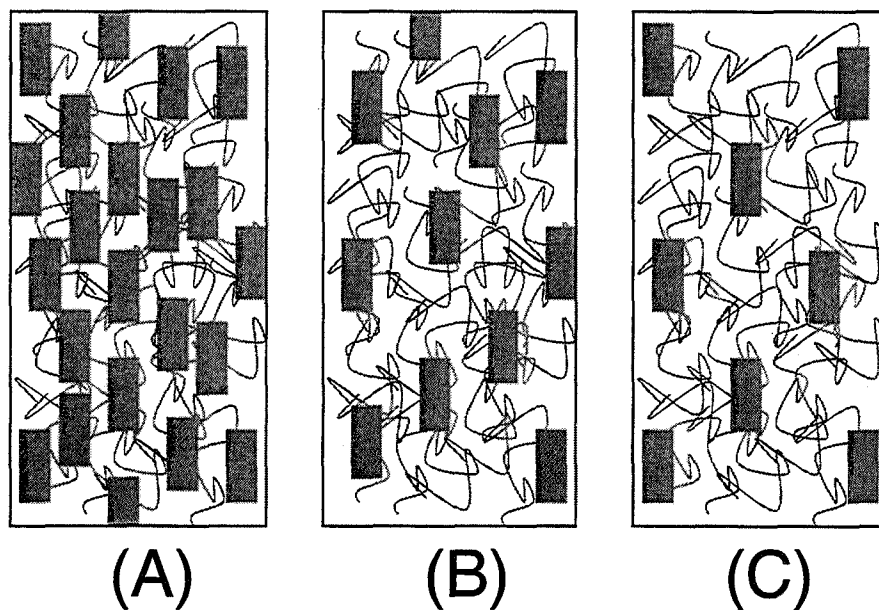


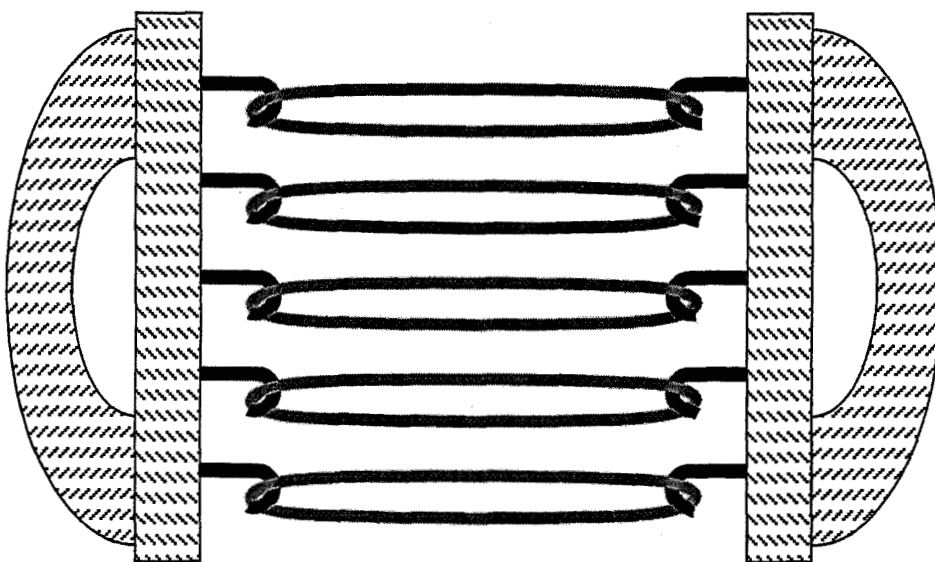
Figure 1. Three models representing hard (crystalline) and soft (amorphous) regions of different types of spider silks. (A) represents the stiffest silk showing the most crystalline regions, (B) represents the middle stiffness silk showing and intermediate number of crystalline regions, and (C) represents the lowest stiffness silk showing the fewest number of crystalline regions. (O’Brien et. al., Thiel, Simmons)

Demonstrations

1. Have the students handle and stretch the spider web, rubber bands and Kevlar®. Review the mechanical properties of each one.
2. Place five rubber bands in the test fixture and have the students apply a tensile load to “feel” its properties. Describe this as the low modulus, high elasticity spider silk.
3. Attach 8 sets of “crystals” to the rubber bands. Distribute them evenly throughout the structure. Have the students apply a tensile load to “feel” its properties. Describe this as the intermediate modulus, medium elasticity spider silk.
4. With a new set of rubber bands, attach 12 sets of “crystals” to the rubber bands. Distribute them evenly through the structure. Have the students apply a tensile load to “feel” its properties. Describe this as the high modulus, high elasticity spider silk.

Special Instructions:

This test frame is designed to allow simple attachment of the five rubber bands and application of a tensile load.



“Crystals” are attached by aligning the rubber bands, placing rubber cement on one side of two craft stick segments, and binding them to two or three adjacent rubber bands.

References:

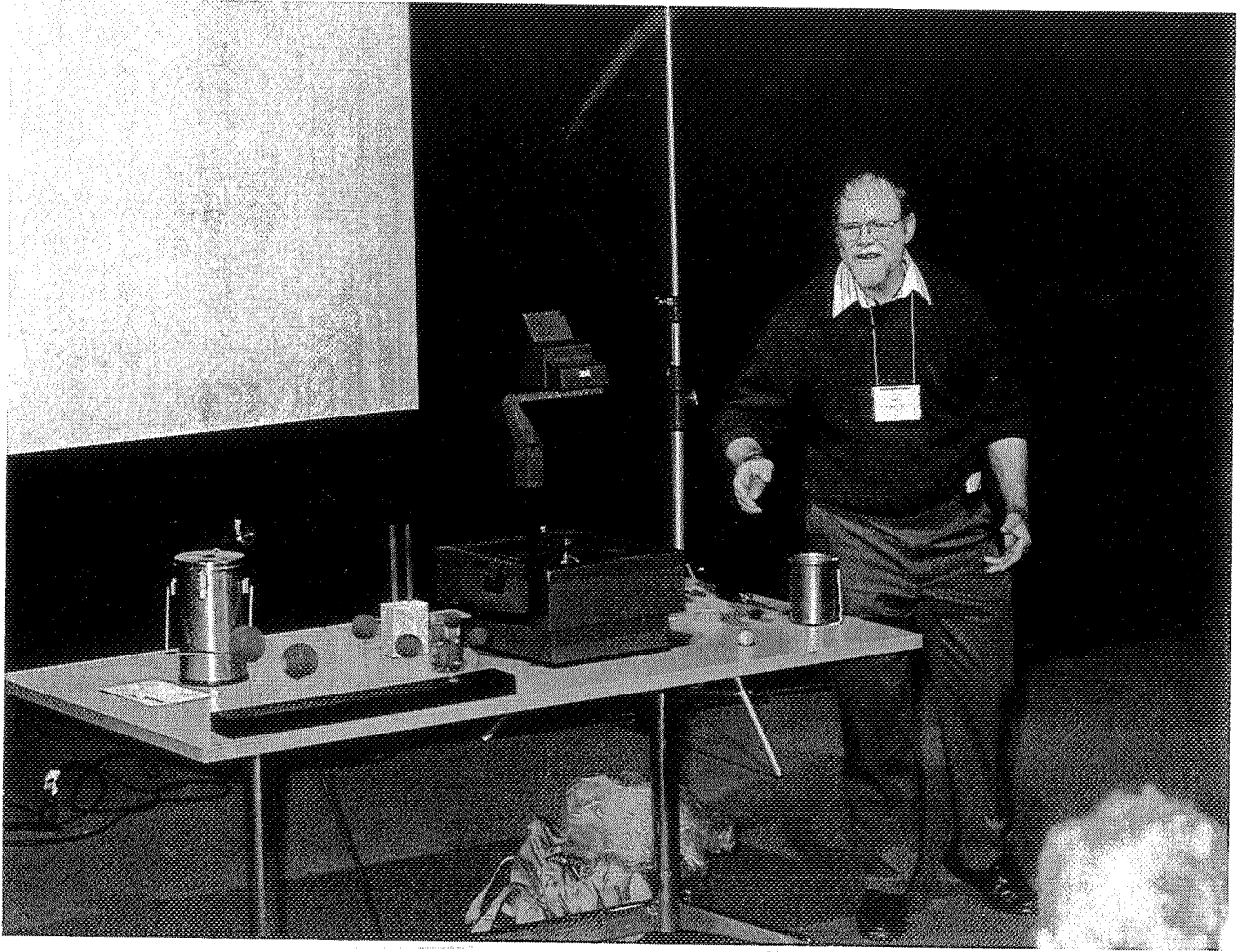
- Berenbaum, M.R. "Spin Control." *The Sciences*, Sept-Oct **1995**, v35, n5, p13.
- Colgin, M.A. and R.V. Lewis. "Spider silk: a biomaterial for the future." *Chemistry and Industry*. 18 December **1995**, pp1009-1012.
- Fox, D. "The Spinners." *New Scientist*, 24 April **1999**, pp38-41.
- Hinman, M.; Z. Dong; M. Xu and R. Lewis. "Spider Silk Proteins." in *Mat. Res. Soc. Symp. Proc.* Vol. 292, eds C. Viney, S.T. Case and J.H. Waite. **1993** Materials Research Society: Pittsburgh, PA.
- Lewis, R. "Unraveling the weave of spider silk: One of nature's most wondrous chemical structures is being dissected so that it can be used in human inventions." *BioScience*, Oct **1996**, v46, n9, p636.
- Lipkin, R. "Artificial Spider Silk." *Science News*, 9 March **1996**, v149, pp152-153.
- O'Brien, J.P.; S.R. Fahnestock, Y. Termonia and K.H. Gardner. "Nylons from Nature: Synthetic Analogs to Spider Silk." *Adv. Mater.* **1998**, v10, n15, pp1185-1195.
- Osaki, S. "Spider Silk as Mechanical Lifeline." *Nature*, 5 Dec. **1996**, v384, p419.
- Seidel, A.; O. Liivak, and L.W. Jelinski. "Artificial Spinning of Spider Silk." *Macromolecules* **1998**, v31, pp6733-6736.
- Shen, Y.; M.A. Johnson and D.C. Martin. "Microstructural Characterization of *Bombyx mori* Silk Fibers." *Macromolecules* **1998**, v31, pp8857-8864.
- Simmons, A.H.; C.A. Michal and L.W. Jelinski. "Molecular Orientation and Two-Component Nature of the Crystalline Fraction of Spider Dragline Silk." *Science*, 5 January **1996**, v271, pp84-87.
- Termonia, Y. "Molecular Modeling of Spider Silk Elasticity." *Macromolecules* **1994**, v27, pp7378-7381.
- Thiel, B.; D. Kunkel; K. Guess and C. Viney. "Composite Microstructure of Spider (*Nephila Clavipes*) Dragline." in *Mat. Res. Soc. Symp. Proc.* Vol, 330, eds M. Alper, H. Bayley, D. Kaplan and M. Navia. **1994** Materials Research Society: Pittsburgh, PA.
- Tirrell, D.A. "Putting a New Spin on Spider Silk." *Science*, 5 January **1996**, v271, p39.
- Vollrath, F. "Spider Webs and Silks." *Scientific American*. March **1992**, pp70-76.
- Woodward, S.C. and T.N. Salthouse "The Tissue Response to Implants and its Evaluation by Light Microscopy." in *Handbook of Biomaterial Evaluation*, ed. Von Recum. **1986**. (Woolf's Law explained)

SIMPLE CLASSROOM DEMONSTRATIONS IN CHEMISTRY AND MATERIALS SCIENCE

John B. Hudson

Materials Science and Engineering Department
Rensselaer Polytechnic Institute
Troy, New York 12180

Telephone: 518-276-6447
e-mail hudsoj@rpi.edu



John B. Hudson

Simple Classroom Demonstrations in Chemistry and Materials Science

John B. Hudson, Materials Science and Engineering Department, Rensselaer Polytechnic Institute,
Troy NY 12180

Abstract

Six classroom demonstrations developed for a freshman level course in Chemistry and Materials Science are described, and the message to be drawn from each is presented.

Key Words

Conservation of energy, atomic vibrations, polymer structure, glass transition, diffusion, heat treating.

Introduction

At Rensselaer, all engineering freshmen take a two-semester course sequence, Chemistry of Materials, that combines material traditionally taught in freshman general chemistry and beginning materials science. This course sequence is taught in an interactive studio mode, which combines the presentation of new material, student problem solving and laboratory work in two, two-hour class sessions per week. In the process of developing this sequence, we have developed a large number of classroom demonstrations that are used to illustrate points relevant to topics covered in class. In the material that follows, I will describe a number of these demonstrations, and show how they relate to an understanding of the chemical and physical principles involved.

In all cases, we have tried to keep the demonstrations as simple as possible, and use materials that are cheap and readily available.

Conservation of Energy

Near the beginning of the first semester, we review basic principles, including both the concept of conservation of energy, and the fact that all energies are relative, requiring a reference point in order to specify a numerical value of energy. To demonstrate this, we use a ball of glazier's putty, about an inch in diameter. The ball is first placed on a desktop, which is taken as our reference "zero of energy". Students are then asked about the potential energy of the ball when it is held either above or below the table top. This leads in to the concept of decreasing potential energy when electrons are bound to a nucleus, or chemical bonds are formed. For example, the ground state potential energy of an electron in a hydrogen atom is -13.4 eV relative to a free electron. The putty ball is then raised above the desk top, and students are asked "Has the energy of the ball increased?" (Yes - its potential energy is higher.) "Where did the energy come from" (The instructor did work on the ball - energy transfer from instructor to ball.) The ball is next dropped back onto the table top, and students are asked "Did the energy of the ball change while

it was dropping?" (No - energy was converted from potential to kinetic.) and "Is the energy after the ball lands lower than before it was dropped?" (Yes - it has no kinetic energy relative to the table top, and its potential energy has decreased.) Finally, the students are asked "Where did this energy go?". This will generate a range of answers - heating of the ball or table, generation of sound waves, deformation of the ball or table.

When this discussion is finished, two concepts should be clear to the students:

1. All energy values are relative to some arbitrary reference energy.
2. Energy can neither be created or destroyed, only changed from one form to another.

Dependence of Atomic Vibration Frequency on Mass and Bond Strength

This demonstration is used as part of a module on infrared spectroscopy, which is discussed as part of our study of chemical bonding. This demonstration uses a model constructed from a piece of 2x4; six styrofoam balls, two at 1.5" diameter, two at 2" diameter, and two at 3" diameter (more or less); twelve 1/2" hex nuts and 6 pieces of 0.040" diameter molybdenum wire. (High strength steel would do - I just happened to have some molybdenum wire of the right stiffness around.) The model constructed is shown in Figure 1 below. It consists of the six foam balls, each

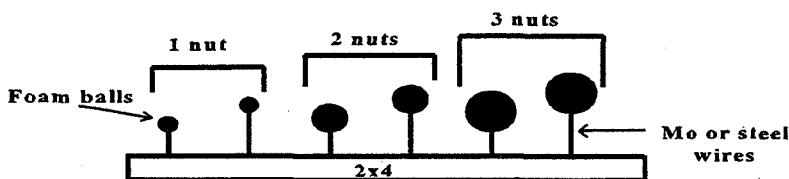


Figure 1

Demonstration of effect of atomic mass and bond strength on atomic vibration frequency. The styrofoam balls contain stainless steel hex nuts to reduce the resonant frequency to a readily observable value

containing one or more of the hex nuts, mounted on a piece of the wire, with the other end of the wire inserted in a hole in the 2x4. The nuts are recessed into the balls by carving out appropriate sized holes. The nuts are glued directly onto the wires using epoxy glue, and the balls then glued over the nuts. Six combinations of wire length (which represents bond strength - short wire = strong bond) and number of hex nuts (which represent atomic mass) were used. The wire and nut combinations I used are:

Short wire (about 3")

- 1 nut
- 2 nuts
- 3 nuts

Long wire (about 6")

- 1 nut
- 2 nuts
- 3 nuts

These combinations give a wide range of resonant frequencies, all of which are low enough for the motion to be readily visible by students in the classroom. The various frequencies, which are given by the harmonic oscillator expression

$$v = \frac{1}{2\pi} \left(\frac{f}{m} \right)^{1/2}$$

relating the frequency, v , to the force constant, f , and the mass, m , can be demonstrated by tweaking the balls, one at a time. This will show that the short wire, 1 nut combination has the highest natural frequency, while the long wire, 3 nut combination has the lowest. You can also demonstrate the concept of energy absorption at the resonant frequency by rhythmically shaking the whole 2x4 at various frequencies and watching the various balls respond.

At the end of the demonstration, the students should understand that:

1. Vibrational frequency increases as bond strength increases.
2. Vibrational frequency decreases as atomic mass increases.

Model of a High Molecular Weight Linear Polymer

This demonstration is used at the beginning of our study of polymers, and is intended to give students a feeling for just how long a polymer chain is, relative to its diameter. It consists of a string of wooden or plastic beads, held together with a strong string. This is basically a model of linear polyethylene, with each bead representing a single CH_2 unit. To represent a polymer with a molecular weight of 100000 Daltons requires about 7000 beads, so fairly small beads should be used. We used 3/16" diameter plastic beads and monofilament nylon fishing line. In the demonstration, the string of beads is put in a large wide mouth jar or beaker, taking care to avoid tangles. At the start of the demonstration, one end of the chain is removed from the jar, and allowed to drop to the floor, pulling the rest of the chain out of the jar. Depending on the length of the chain, this will take from one minute to several minutes. When all of the chain has fallen from the jar, it can be picked up, to emphasize the flexibility of the chain, and the extent to which segments of the chain become entangled. You can keep talking about polymers while this is going on, to emphasize the amount of time required.

The points made by this demonstration are:

1. Polymer molecules are very long.
2. Linear polymers such as polyethylene are very flexible

3. Polymer chains are easily entangled, making it hard to produce single crystal polymers.

Solid State Diffusion by a Random Walk Process.

This demonstration is used in connection with the study of solid state diffusion, specifically in connection with diffusion in a crystalline solid by a vacancy mechanism. It requires a 6x10 grid of squares on an overhead transparency, 29 pennies, 30 large washers, and a means of generating random numbers, such as a hand calculator. At the start of the demonstration, the transparency is put on an overhead projector, with the pennies and washers arranged as shown in Figure 2.

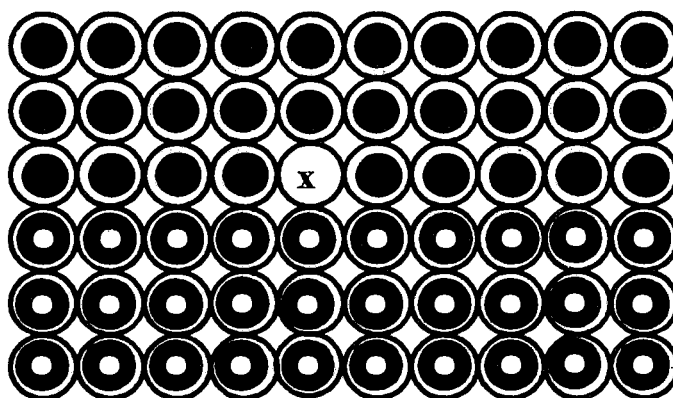


Figure 2

Setup to demonstrate atom migration in a solid by a random walk process

The point of using washers, with a hole in the middle, is that they are more easily distinguished from the pennies than other size coins would be. Begin the demonstration by marking an "x" in the vacant square. This will enable you to show how far the vacancy has migrated in the course of the demonstration. Appoint one student to generate random numbers using the calculator. Multi digit numbers can be used one digit at a time. As the student calls out the numbers, move the pennies and washers as follows:

Random Number	Direction of Vacancy Motion
1 or 2	Up
3 or 4	Down
5 or 6	Left
7 or 8	Right
9 or 0	Disregard

As an additional rule, ignore any motion that would move the vacancy out of the grid.

You will find that this is a very inefficient process, as often the result of a given step will be to reverse the action of the previous step, but in time you will see both vacancy migration and mixing across the penny-washer interface. At the end of the demonstration, mark the site where the vacancy has ended up. Then remove the pennies or washers to indicate how far the vacancy has moved in the course of the demonstration. At this point, the concept of a random walk may be introduced, along with the formula for the average displacement (x) as a function of time (t) and diffusivity (D) shown below:

$$x = (2Dt)^{1/2}$$

The points to be made by this demonstration are:

1. Random motion of a vacancy can lead to net displacement of both vacancies and atoms, even in the absence of a chemical driving force (cf. self diffusion.)
2. The only thermodynamic driving force involved is the change in entropy associated with the mixing of different atomic species.
3. This is a very inefficient process. The average displacement of the vacancy is very small compared to the sum of the lengths of the individual steps.

Glass Transition Temperature of an Elastomer

This demonstration requires a racquet ball, a flask of liquid nitrogen and a pair of tongs. To demonstrate the properties of the ball at room temperature, drop it or throw it against some hard surface, and observe the bounce. Then chill the ball in the liquid nitrogen, remove it with the tongs, and again drop or throw it against a hard surface. This time, if you throw hard enough, the ball will shatter. (Dropping is probably safer, but throwing is more spectacular - this is a good demonstration for waking people up.)

Make sure that the surface you throw against is both strong and rigid, as the frozen ball can damage surfaces such as drywall or plaster, and the energy absorbing qualities of carpeting will not lead to fracture of the ball. To show that the change induced by freezing is reversible, another ball may be frozen and then allowed to warm up, then thrown to demonstrate the reversibility of this effect. A variant on this demonstration is to drop the cold ball from a relatively low height and to observe how the sound the ball makes and the amount of bounce change as it warms through the glass transition temperature.

The change in behavior can be explained in terms of the restricted mobility of the polymer chains that make up the ball as the temperature is lowered. You can also cite the Challenger space shuttle disaster in 1985 as a practical consequence of using an elastomer below its glass transition temperature. Other examples of polymers that show very different behavior at room temperature are polyethylene (above T_g at room temperature) and polystyrene (below T_g at room temperature).

Students should understand from this demonstration that:

1. Polymer mechanical behavior is strongly temperature dependent.
2. Restricted molecular motion at low temperature makes polymers brittle.
3. The glass transition temperature of a polymer depends on its molecular structure.

Age Hardening in an Aluminum Alloy

This demonstration can be used either as part of a discussion of solid state reaction kinetics (precipitation reactions) or in connection of the study of heat treating of non-ferrous alloys. The apparatus used is shown in Figure 3. It consists of two pieces of an age-hardenable aluminum alloy, such as 6061, each about 1" by 6" by .030" thick, mounted on a piece of 2x4. One piece of the aluminum should be optimally heat treated for maximum hardness, the other fully annealed to be as soft as possible. The difference in behavior can be shown by holding the 2x4 over the overhead projector so that the aluminum alloy strips are seen edge on. Hold the strips over a reference mark on the surface of the overhead projector. One at a time, bend each strip down to a second reference mark, then release it. Note the difference in springback between the hardened sample (little or no permanent deformation) and the annealed sample (much permanent deformation). Make the point that the two samples are identical in composition, and were cut from the same sheet of material. They differ only in their thermal history. After the

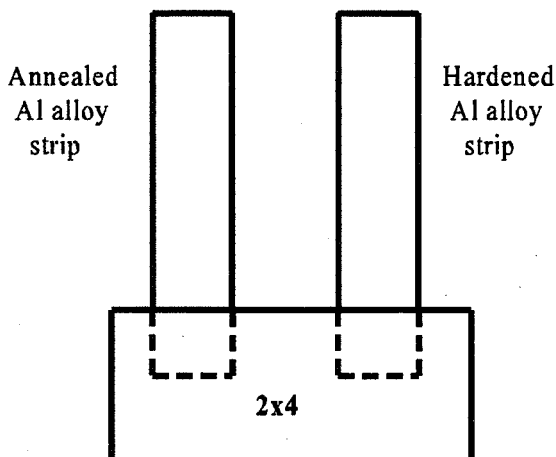


Figure 3

Apparatus used to demonstrate the age hardening of an aluminum alloy

demonstration, pass the sample assembly around the classroom, so that the students can see for themselves the difference in yield point. At the end of class, retrieve the sample, and show the class that the annealed sample is now much harder than at the start of the demonstration. This leads into a discussion of other hardening mechanisms, and the concept of work hardening.

Points illustrated by this demonstration are:

1. Mechanical properties of metal alloys can be markedly affected by thermal history.
2. Formation of very small precipitate particles has a strong strengthening effect; the large particles formed in the annealing process are ineffectual.
3. Plastic deformation is another effective way to increase the strength of metal alloys.

Acknowledgment

The glass transition temperature demonstration was first suggested by Professor Linda Schadler of the Materials Science and Engineering Department at Rensselaer

John B. Hudson is Professor of Materials Engineering at Rensselaer Polytechnic Institute. His areas of research interest include chemical reactions a surfaces, instrumentation for surface analysis and nanocrystal growth. In recent years he has been actively involved in the modernization of the undergraduate curriculum in Materials Science and Engineering at Rensselaer, and has developed studio techniques for the teaching of basic courses in Chemistry and Materials Science. He is also the author of textbooks on Surface Science and Thermodynamics.

ARTIFACTS IN X-RAY DIFFRACTION EXPERIMENTS

Bruce J. Pletka

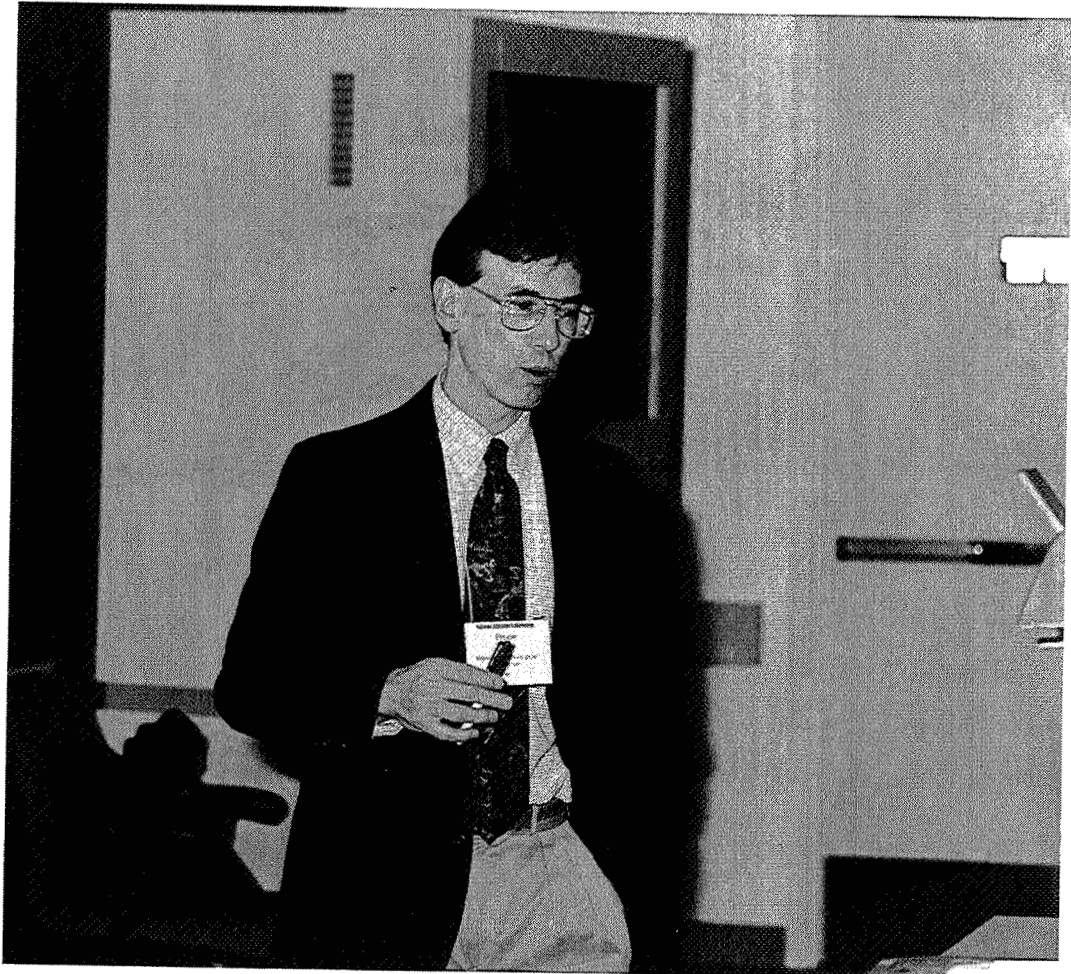
Ruth I. Schultz Kramer

and

Edward A. Laitila

Department of Metallurgical & Materials Engineering
Michigan Technological University
1400 Townsend Drive
Houghton, Michigan 49931

Telephone: 906-487-2639
e-mail bjpletka@mtu.edu



Bruce J. Pletka

Artifacts in X-Ray Diffraction Experiments

Bruce J. Pletka, Ruth I. Schultz Kramer and Edward A. Laitila
Department of Metallurgical & Materials Engineering
Michigan Technological University
Houghton, MI 49931

Abstract

An experiment is described in which alloys within the Pb-Bi system are prepared and used to demonstrate that non-equilibrium structures can be obtained even when slow cooling rates (i.e., furnace cooling) are employed from the liquid state. The non-equilibrium structures occur for alloys on the Pb-rich side of the phase diagram. These alloys are then used to demonstrate that improper preparation of specimens can lead to erroneous conclusions regarding the microstructure present within a specimen. Two different etches are used to prepare the alloys for examination with optical microscopy and x-ray diffraction. X-ray diffraction experiments performed after using these different etches reveal dramatically different relative amounts of the phases that exist in the microstructure. Observations of the specimens using optical and scanning electron microscopy show that this artifact results from differential etching of the phases within the microstructure.

Key Words: X-Ray Diffraction, Artifacts, Non-Equilibrium Structures

Prerequisite Knowledge: An understanding of phase equilibria and x-ray diffraction principles.

Objectives: To examine the non-equilibrium structures that can form in material systems and to demonstrate that improper specimen preparation can lead to artifacts in material characterization experiments such as x-ray diffraction.

Equipment and Materials:

1. Lead and bismuth of 99.999% purity, a balance to weigh out various alloy compositions in the Pb-Bi system, crucibles, and furnace to melt the alloys.
2. Metallographic facilities to prepare the alloys for microscopic examination and x-ray diffraction experiments. This should include preparing and applying different etches to the specimens.
3. Optical microscope.
4. X-ray diffractometer.

Safety Precautions: The use of the etchants and x-ray diffraction equipment require that the students be properly informed of the hazards of preparing and using etchants and the safety issues involved in using equipment that produces x-rays.

Introduction:

X-ray diffraction experiments are performed often in undergraduate laboratory courses to demonstrate how this technique can be used to determine the identity of various phases present in the microstructures of materials, establish solvus phase boundaries, and other structural characteristics. However, improper preparation of specimens can lead to erroneous conclusions regarding the microstructure present in a specimen. We have developed an experiment to demonstrate this effect by using different etches to prepare the surfaces of specimens that will be examined using x-ray diffraction and optical microscopy techniques.

Specimens within the Pb-Bi system are used in this experiment because Pb and Bi are low melting elements (melting temperatures of 327.5 and 271.4°C, respectively) which makes it easy to prepare any desired composition. In addition, the Pb-Bi system contains two invariant reactions as shown in Fig. 1: a peritectic reaction at 184°C on the Pb-rich side of the phase diagram and an eutectic reaction at 125°C on the Bi-rich side of the phase diagram. We have found that alloys with bulk compositions passing through the eutectic reaction isotherm (i.e., compositions greater than 41.8 wt% Bi) display structures predicted for equilibrium cooling when specimens are either furnace or air cooled from the liquid state. Alloys with bulk compositions less than about 41.8 wt% Bi, however, exhibit non-equilibrium structures that are not predicted by the phase diagram even when furnace cooled from the liquid state. This results because an incomplete reaction of the peritectic takes place and significant coring in the solid produces a dramatically expanded freezing range. It can be seen from the phase diagram in Fig. 1, that only a Pb-rich solid solution should be present at room temperature in alloys containing less than about 17 wt% Bi under equilibrium cooling conditions. Because of the expanded freezing range, eutectic liquid is still present when solidification is completed (even under furnace cooling conditions) for compositions with as little as 5 wt% Bi. As a result, an essentially 100 wt% Bi phase (the terminal phase on the Bi-rich side of the phase diagram) is present in these alloys as part of the the eutectic microconstituent, which is composed of the Bi phase along with the intermediate β phase (Pb_7Bi_3).

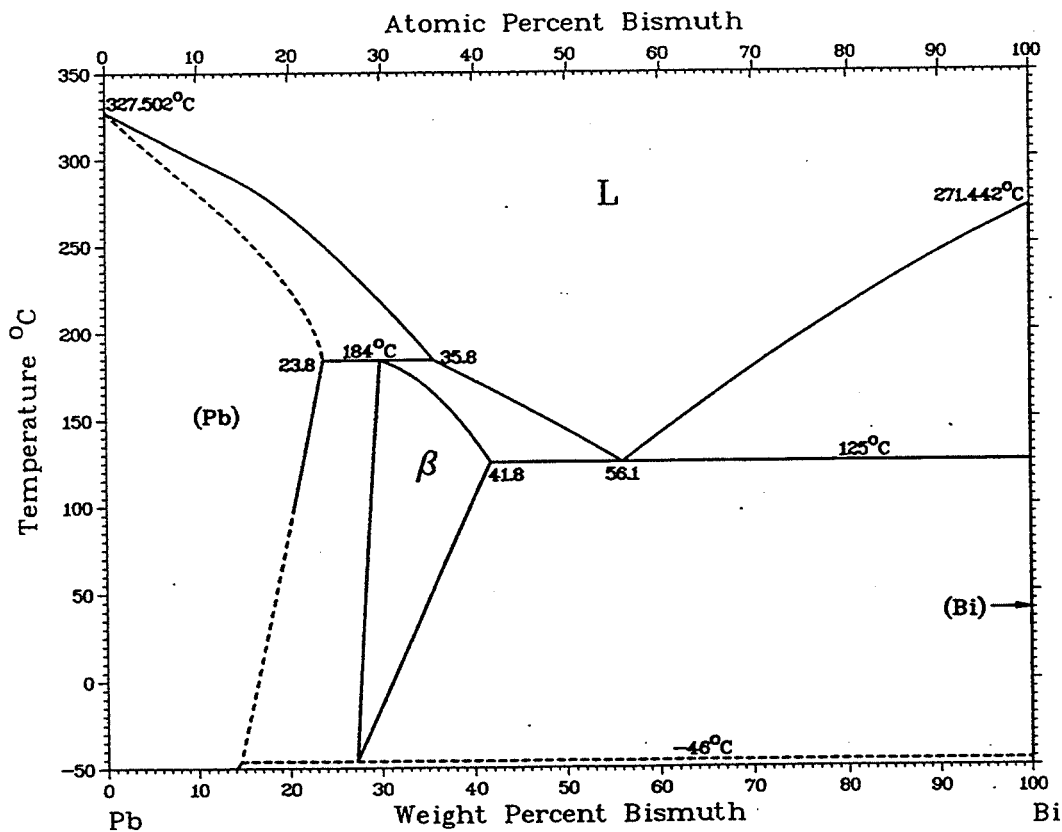


Fig. 1 The Pb-Bi phase diagram [1].

Based upon the different solidification behavior of the Pb-rich and Bi-rich alloys, we typically perform two distinct laboratory experiments using this alloy system. The first set of experiments involves preparing alloys which have bulk compositions greater than 41.8 wt% Bi. These alloys solidify with structures composed of proeutectic β or Bi along with the eutectic microconstituent as shown in Fig. 2 for a hypereutectic alloy. The microstructures in these alloys can be readily interpreted in terms of equilibrium cooling. This allows the students to gain confidence in using the phase diagram, and the concepts of cooling paths and the lever rule to predict the microstructures which should occur in a given composition on cooling from the liquid state.

A second laboratory exercise involves examining alloys on the Pb-rich side, typically ranging from 5 to 35 wt% Bi. These alloys undergo sufficient coring and an incomplete peritectic reaction on solidification so that non-equilibrium microstructures result as discussed previously. We use this second set of alloys to demonstrate that non-equilibrium cooling can lead to structures not predicted by the phase diagram (although the phase diagram can still be used to interpret their development) and to show that errors can be induced in x-ray diffraction experiments if improper specimen preparation occurs; namely, utilizing an etchant that attacks one (or more) of the phases present in the microstructure much more aggressively than the other phases.

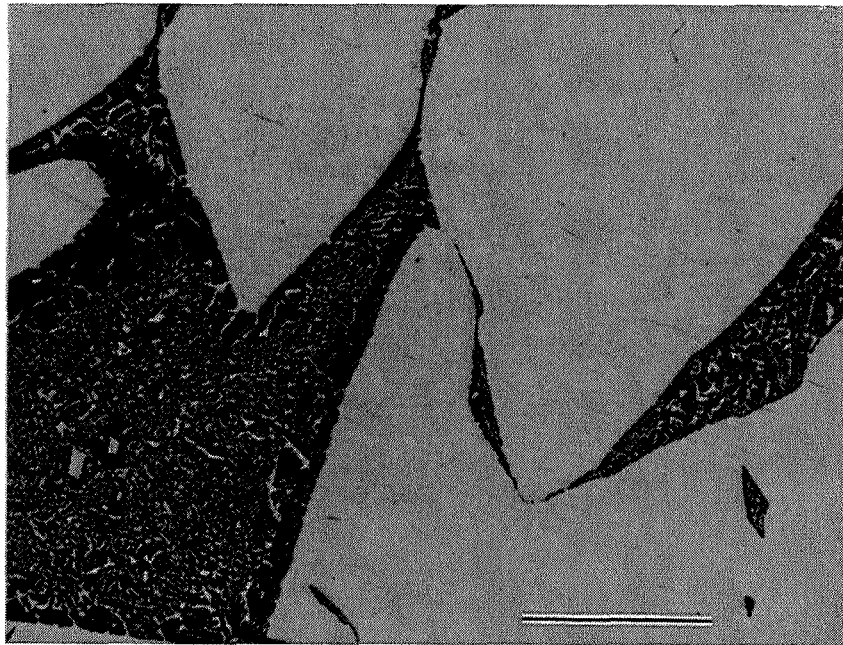


Fig. 2 Typical microstructure of a Pb-84 wt% Bi alloy which is composed of primary Bi (the light phase) dispersed in a Pb₇Bi₃ (dark phase) plus Bi eutectic microconstituent. Marker bar equals 500 μm .

Procedure:

The samples are prepared by first weighing out the proper amounts of Pb and Bi to form the desired composition and placing the charge material in crucibles. The crucibles are placed in a furnace which is $\sim 100^\circ\text{C}$ higher than the liquidus temperature; after the charges have become molten, the crucibles are removed from the furnace and the liquid alloy is stirred to insure homogeneity is achieved in the melt. The crucibles are allowed then to air cool or are placed back in the furnace and allowed to furnace cool (making

sure the alloy has time to re-equilibrate at the furnace temperature). After solidification is completed, the samples are removed from the crucible and sectioned into two pieces.

Metallographic specimen preparation of Pb-rich samples is conducted by alternately abrading the sample surface and then chemically etching to remove deformation and embedded abrasive. Wet grinding using 120, 240, 320, 400, and 600 grit SiC smears the lead to fill in the scratches produced during each grinding step. This deformed layer is removed by lightly etching in 75% acetic acid- 25% H_2O_2 (30%). As the surface becomes pitted from loosening of the coarse abrasive, the specimen is re-ground at 600 grit for several seconds to fill the pits, then re-etched until all the coarse abrasive is removed. It is necessary to repeat this step several times to prevent over etching of the Pb-rich phases, which are aggressively attacked by the etchant, yet to successfully remove the abrasive. Coarse polishing with 6 μm diamond on nylon and etching with 4% nital is alternated until the surface is free of diamond. The final polish is produced by alternately polishing with 0.05 μm Al_2O_3 and etching with 4% nital. The same procedure was used for the Bi-rich specimens, except the only etchant used was 4% nital.

In our experiment, two different etchants are utilized. As discussed in the polishing procedure, the final etch used on the specimens is a 4% nital solution. This etchant attacks all the phases at roughly the same rate. An examination of the microstructures is then performed to illustrate that the structures obtained in the specimens are not predicted by the phase diagram. (The students had been instructed to determine what the equilibrium microstructures should look like prior to coming to the laboratory session.) For example, as discussed earlier, the microstructure of a Pb-5 wt% Bi alloy should be a single phase Pb solid solution. Fig. 3, however, contains three phases; coarse dendrites of lead (light) are surrounded by a darker phase, which is the intermediate Pb_7Bi_3 phase, and some Pb_7Bi_3 plus Bi eutectic is included in the interdendritic regions (identifiable by the presence of the white Bi phase).

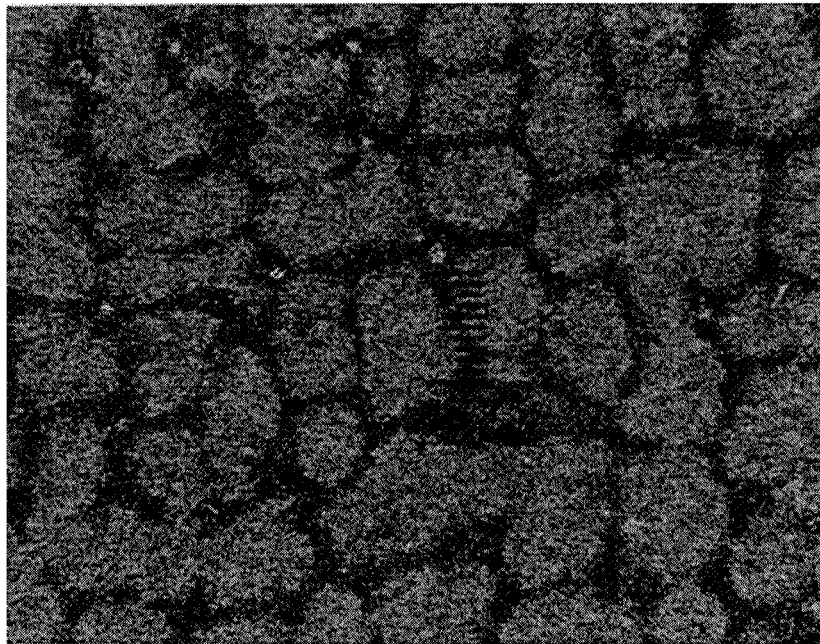


Fig. 3 The microstructure of a Pb-5 wt% Bi alloy after air cooling and etching with 4% nital. If this alloy was solidified under equilibrium conditions, the microstructure should consist of only a lead solid solution. However, three distinct microconstituents are present as described in the text. Scale = 100 μm .

When it is obvious to the students that the structures in these alloys are not what they predicted, we then discuss how x-ray diffraction can be used to determine the identity of the phases and that this information can be used in conjunction with their microstructural observations to determine what phases and microconstituents are present in the structure.

X-ray diffraction patterns are obtained by performing scans between 2θ angles of $25\text{-}40^\circ$. This range of 2θ angles is selected because the only three equilibrium phases that can occur in this system are the terminal Pb-rich solid solution and Bi phases and the intermediate phase of Pb_7Bi_3 . The students are instructed to look up the d spacings for these three phases and to determine the 2θ angles for the two most intense peaks of each phase using the alphabetical index provided by the Joint Committee on Powder Diffraction Standards (JCPDS). The two most intense peaks for Pb and Bi and three of the five most intense peaks for the Pb_7Bi_3 phase occur in the angular range of $25\text{-}40^\circ$ 2θ . A step scan is used in obtaining the diffraction patterns; a counting time per step of 5 seconds and a step size of 0.03° 2θ are utilized to insure that statistically valid data are obtained.

A typical diffraction pattern for the Pb-5 wt% Bi alloy that was obtained using the 4% nital etch is shown in Fig. 4. The peak positions and relative peak intensities for the Pb, Bi and Pb_7Bi_3 phases are included on the pattern, and it can be seen that the two most intense peaks in Fig. 4 correspond to Pb, although the peak positions are slightly shifted with respect to the JCPDS data. The shift in peak positions allows us to spend some time discussing how putting solute atoms of different size into a solvent can cause expansion or contraction of the solvent unit cell. The peak positions for the Pb solid solution are shifted to lower 2θ angles compared to pure Pb, indicating that the unit cell has expanded when Bi was added. (This conclusion is based on the Bragg law, $\lambda = 2d\sin\theta$. If the d spacing for a crystallographic plane increases, the Bragg angle for that plane must decrease in order to satisfy the Bragg law for a given wavelength of radiation.) These shifts in peak position are in agreement with data in the literature which show that the lattice parameter of the Pb-solid solution increases as Bi is added [2]. Much less intense peaks for the Pb_7Bi_3 phase also are present in the pattern. The difference between the predicted and experimental relative peak heights of both phases is due to texture (orientation) and/or grain size effects being present in the sample.

The same specimen was then etched for five seconds using 75% acetic acid- 25% H_2O_2 (30%), and the diffraction scan was repeated on the same region of the specimen. The resulting diffraction pattern, shown in Fig. 5, now contains peaks corresponding to the Bi phase. In addition, the intensity of the Pb solid solution and Pb_7Bi_3 phase peaks have decreased and increased, respectively, compared to Fig. 4. In fact, the relative peak heights in Fig. 5 suggest that only a small amount of the Pb-rich phase is present in the microstructure. (This comparison can be made because Pb and Bi are adjacent to one another in the periodic table and would have similar atomic scattering factors.) The diffraction pattern in Fig. 6, obtained after etching for an additional 5 seconds with acetic acid/hydrogen peroxide, shows that the Bi peak heights have increased even more when compared to the other two phases and that the peak heights of the Pb solid solution have decreased dramatically compared to those same peaks in Fig. 4.

A more quantitative evaluation of the change in peak height for the various phases as a function of etch type/time was obtained by determining the area under the peaks. The relative peak areas for the phases present in Figs. 4-6 are given in Table 1. It is clear that

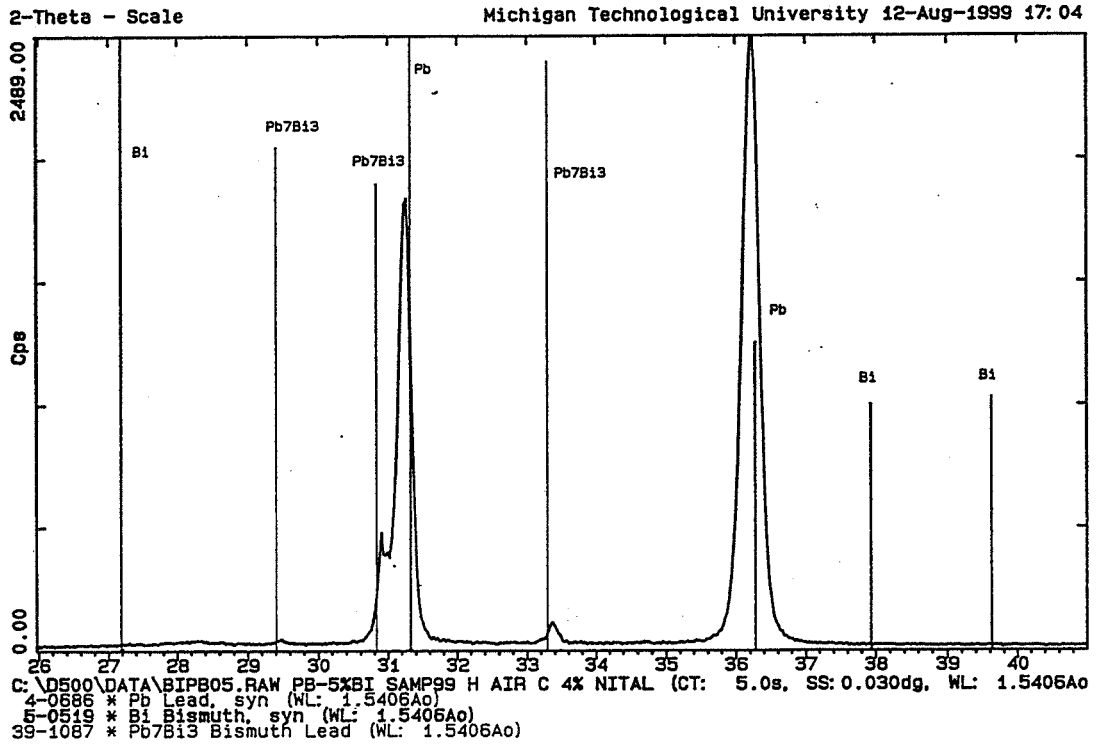


Fig. 4 Typical x-ray diffraction pattern after etching a Pb-5 wt% Bi alloy with 4% nital.

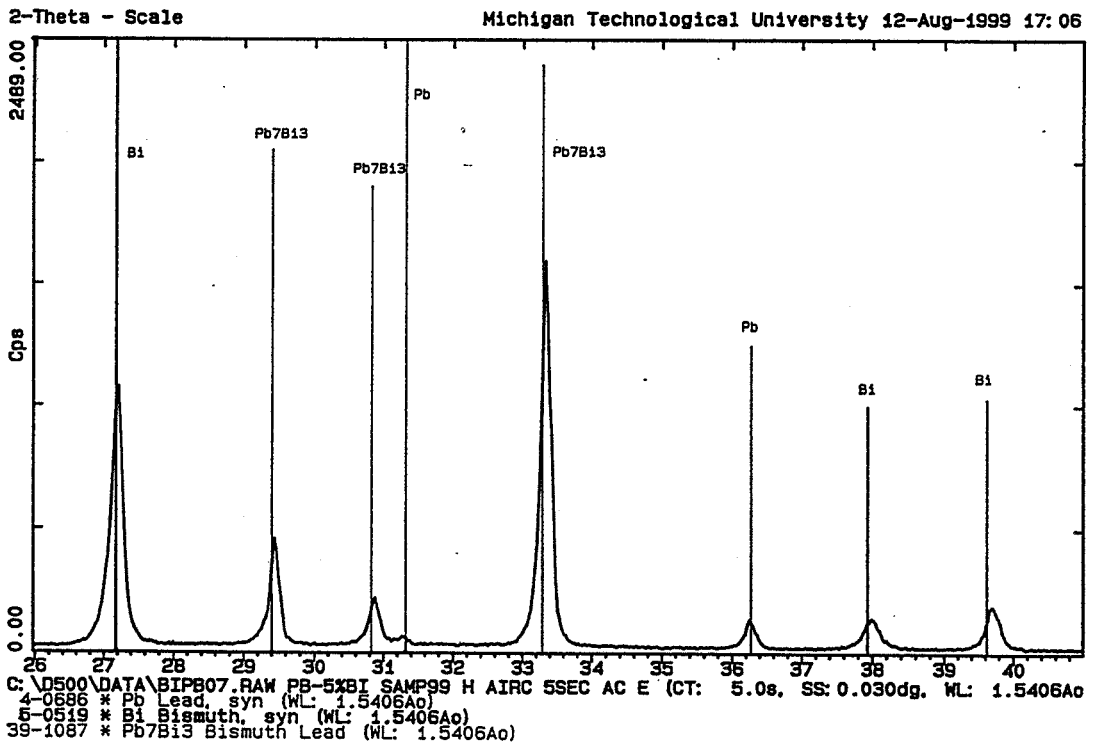


Fig. 5 X-ray diffraction pattern of the same Pb-5 wt% Bi alloy after etching 5 seconds with acetic acid/hydrogen peroxide.

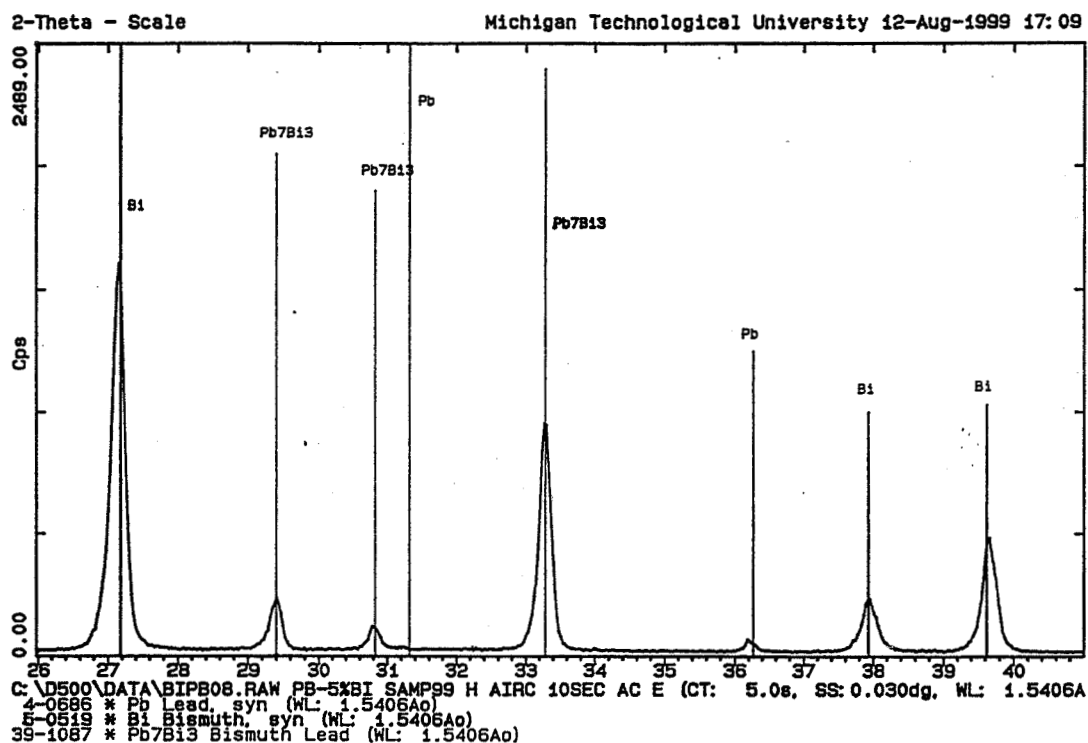


Fig. 6 X-ray diffraction pattern of the Pb-5 wt% Bi alloy after etching for a total of 10 seconds with acetic acid/hydrogen peroxide.

the peak areas increase for the Bi phase either as the acetic acid/hydrogen peroxide etch is used or the time for that etch is increased while the peak areas decrease for the Pb solid solution phase. The peak areas for the Pb_7Bi_3 phase increase when the acetic acid/hydrogen peroxide etch is first used but then decrease in intensity with further etching time. Thus, the x-ray diffraction data indicate that the apparent amount of the Bi phase in the microstructure increases while that of the Pb-rich phase decreases as the specimen is etched with acetic acid/hydrogen peroxide.

Table 1 Relative Areas Under the Peaks for the Various Phases in Figures 4-6

Approximate Peak Angle (2θ) and Phase Type	Area under Peak 4% Nital Etch	Area under Peak Acetic Acid/H.P. 5 seconds	Area under Peak Acetic Acid/H.P. 10 seconds
27.2 - Bi	N.D.*	261	403
29.4 - Pb_7Bi_3	N.D.	81	47
30.9 - Pb_7Bi_3	50	39	21
31.3 - Pb	465	9	3
33.3 - Pb_7Bi_3	20	312	212
36.3 - Pb	765	24	8
38.0 - Bi	N.D.	35	60
39.7 - Bi	N.D.	45	120

*Not Detected

Discussion of the Artifact Observed in the X-Ray Diffraction Patterns:

The x-ray diffraction data indicate that the apparent amount of the Bi phase in the microstructure of the Pb-5 wt% Bi alloy increases while the amounts of the other two phases decrease as the specimen is etched with acetic acid/hydrogen peroxide. This result can be explained if one or more of the phases is being etched more rapidly than the other phases, which causes the various phases to exist at "different levels" within the microstructure.

Fig. 7 shows a sketch in which the three phases exist at different levels in the microstructure. Assume that the Pb solid solution phase is attacked more aggressively than the other two phases and that the Bi phase is attacked the least. When a bulk specimen is placed in the x-ray diffractometer, the specimen position relative to the x-ray optics of the diffractometer is fixed using the top the specimen. That is, the specimen is placed on top of a substance like clay in the specimen holder, and a glass plate is pressed on the specimen surface until the plate contacts the sides of the holder. Thus, the focal plane of the specimen is fixed by the "highest features" in the specimen. When x-rays are scattered from this surface, those x-rays scattered by the Bi (far left in Fig. 7) can reach the x-ray detector unimpeded. X-rays scattered from the Pb_7Bi_3 or the Pb solid solution phases will either not satisfy the x-ray optics for they do not lie in the focal plane and/or the x-rays scattered beneath the focal plane are absorbed by phases lying closer to the surface; the latter situation is depicted for a x-ray scattered from the Pb solid solution phase on the right hand side of the figure. Another way of thinking about this effect, is that with continued etching using acetic acid/hydrogen peroxide, more Bi is exposed to the x-ray beam in the focal plane, effectively increasing the "apparent volume fraction" of the Bi with respect to the other two phases.

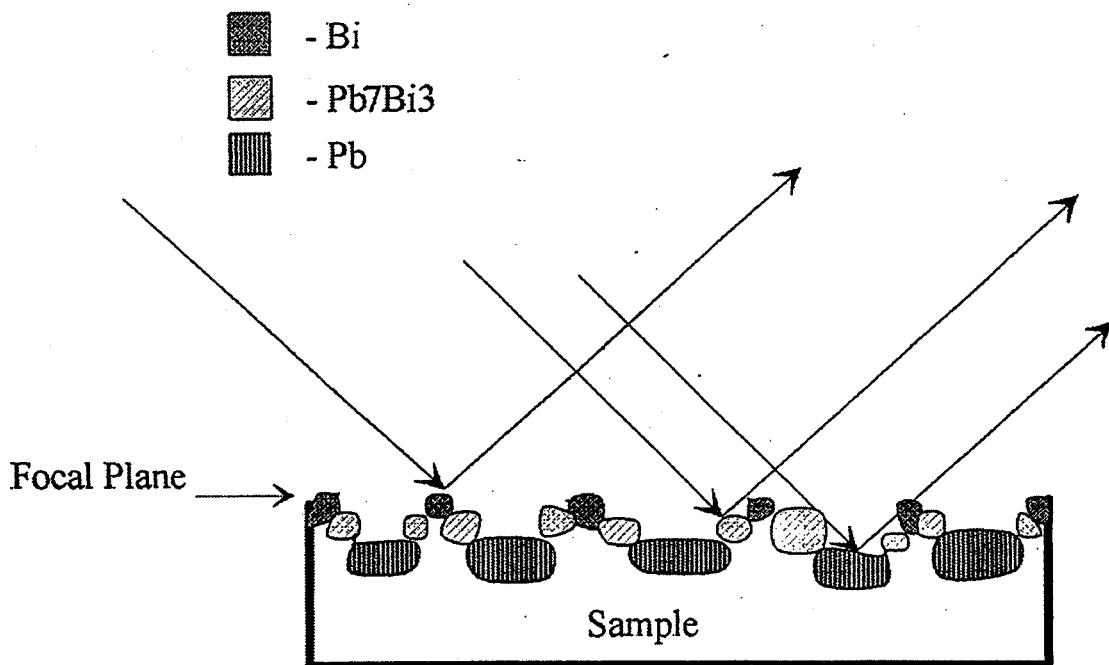


Fig. 7 Schematic figure of the three phases lying at different levels in the microstructure. In this figure, it is assumed that the Bi is attacked the least by the etchant and the Pb solid solution is attacked the most.

The differential etching of the phases was verified by examining the Pb-5 wt% Bi alloy with optical microscopy after etching with acetic acid/hydrogen peroxide, changing the focus, and imaging the same area again. Fig. 8(a) was obtained by bringing into focus the four Bi particles present in this field of view. (It should be pointed out that the density of Bi particles in this figure is not representative of the distribution in the alloy.) The darker intermediate phase and the lighter Pb solid solution are not in focus in this image. Fig. 8(b) is a micrograph of the same area but the light Pb solid solution was brought into focus so that the four Bi particles in the micrograph are now underfocused relative to the Pb solid solution. These micrographs illustrate qualitatively that the phases are attacked at a different rate by the acetic acid/hydrogen peroxide etch, consistent with the sketch in Fig. 7.

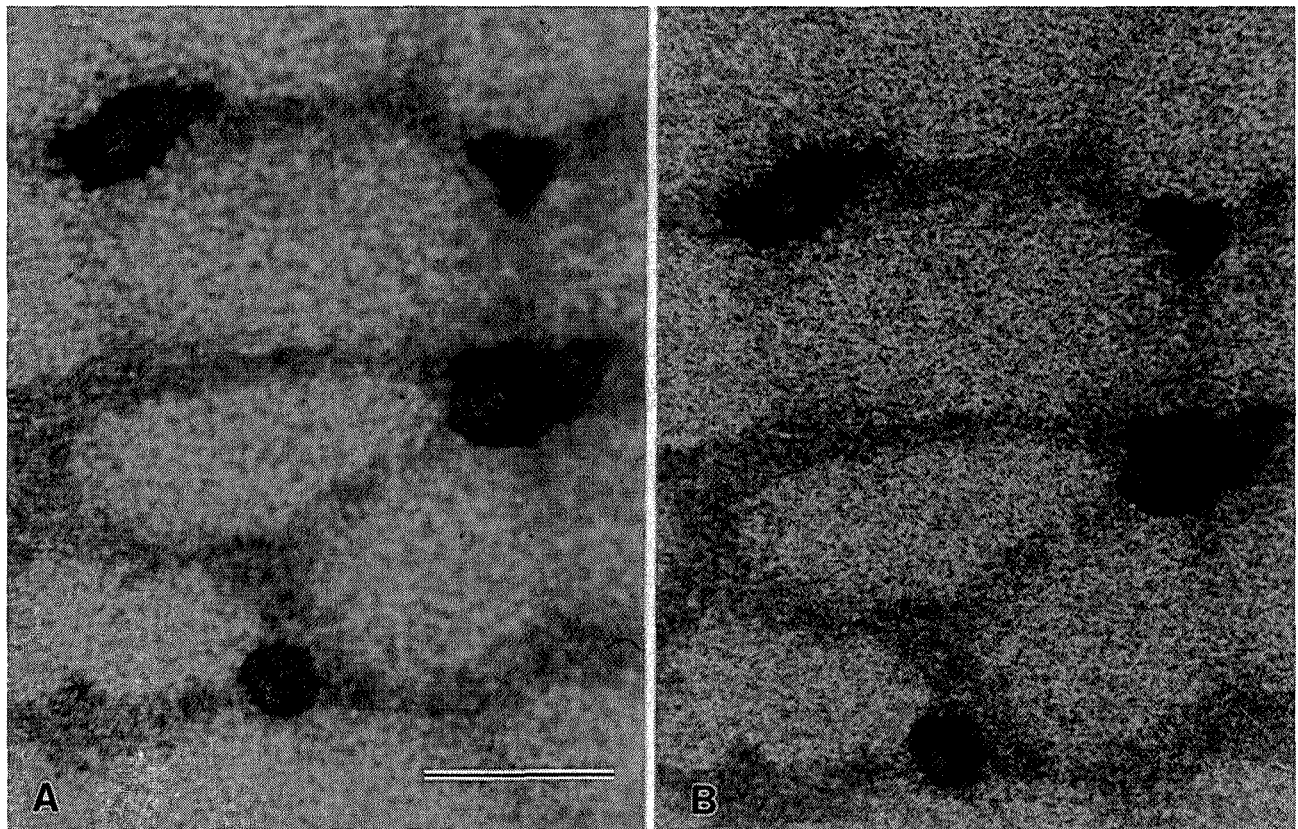


Fig 8. Optical micrographs taken of the same area but changing the focus between (a) and (b). The four Bi particles are in focus in (a) whereas the Pb solid solution phase is in focus in (b). These observations support the contention that the Bi is not attacked as aggressively as the Pb-rich phases. Marker bar is equal to 50 μm .

Further evidence of this differential etching attack was obtained by taking stereo pair micrographs in a scanning electron microscope. A micrograph was taken and then the specimen was tilted 10° towards the secondary electron detector where a second micrograph of the same area is obtained. A stereo pair originally taken at a magnification of 500X is shown in Fig. 9 of a specimen etched with acetic acid/hydrogen peroxide for 20 seconds. When these stereo pairs are viewed under a stereoviewer, it becomes very evident that the Pb solid solution is attacked the most while the Bi is attacked the least.

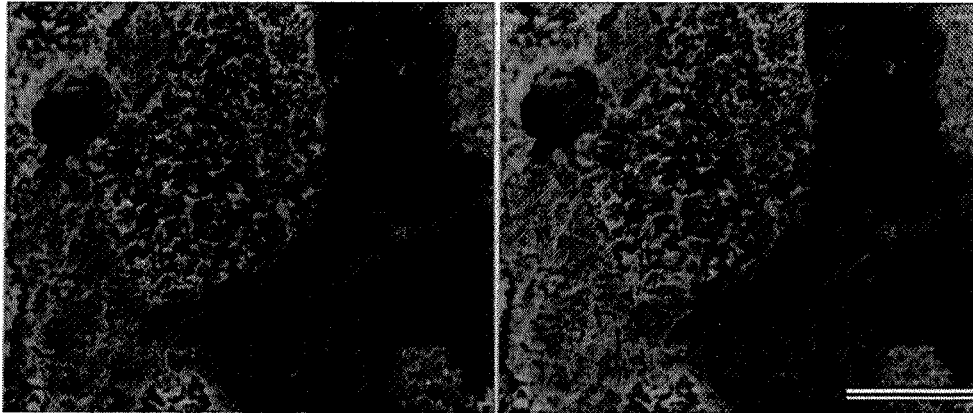


Fig. 9 SEM stereo pair micrographs of a Pb- 5 wt% Bi alloy etched for 20 seconds with acetic acid/hydrogen peroxide. A Bi particle is in the upper left of the micrograph. The lighter phase adjacent to it is the Pb_7Bi_3 intermediate phase and the darker phase on the right hand side of the micrograph is the Pb solid solution. Marker bar equals $50\mu m$.

A word of caution in performing these experiments, is that etching for too long with hydrogen peroxide/acetic acid can cause the relative Bi peak heights to decrease in intensity with respect to the Pb-rich phase peaks as shown in the x-ray diffraction pattern in Fig. 10. This is apparently caused by the etchant attacking the Pb-rich phases that lie under the Bi phase causing the Bi to be removed from the sample surface. Indications of this effect were detected from the presence of holes observed on the surface of the specimen using optical microscopy.

In summary, examining a series of alloys in the Pb-Bi system allows the students to observe the equilibrium structures obtained on cooling Bi-rich alloys while also gaining an appreciation of the non-equilibrium microstructures that can result from incomplete phase reactions and extended freezing ranges on solidifying Pb-rich alloys. More importantly, etching Pb-rich alloys with a 4% nital and then an acetic acid/hydrogen peroxide solution demonstrates how selective etching of one (or more) phase(s) in a multiphase microstructure can lead to erroneous interpretation of the microstructures in x-ray diffraction experiments.

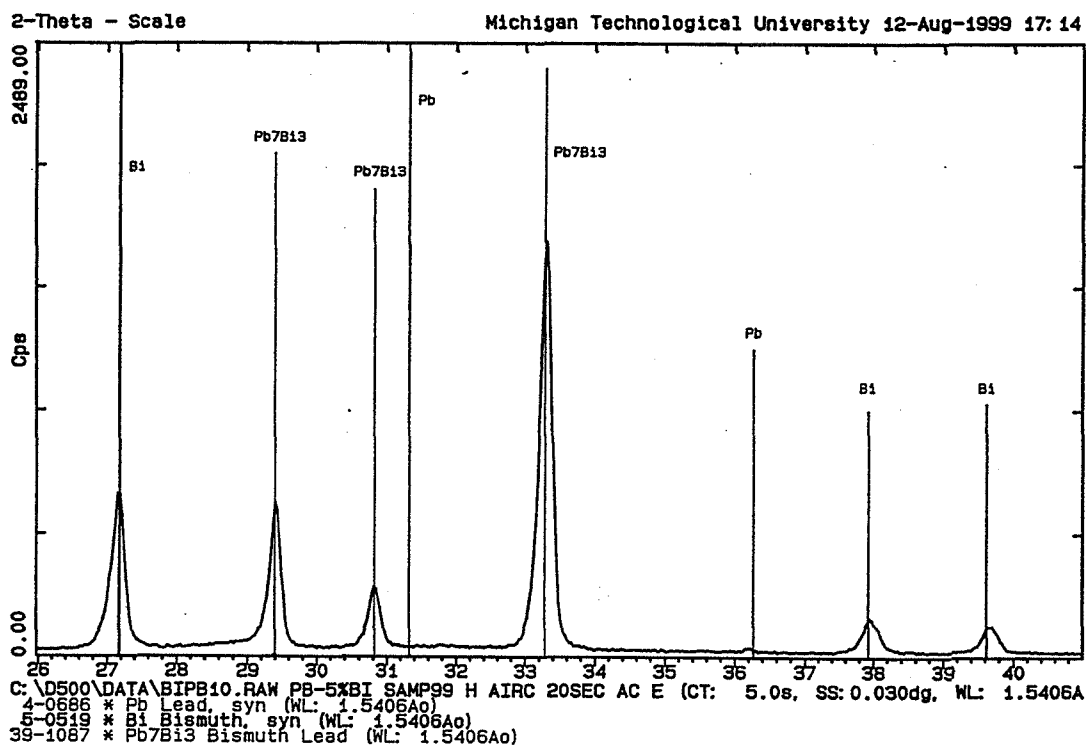


Fig. 10 X-ray diffraction pattern of the Pb-5 wt% Bi alloy after etching for a total of 20 seconds with acetic acid/hydrogen peroxide. Notice the change in the relative peak heights for the Bi and Pb_7Bi_3 phases compared to those in Fig. 6.

References

1. T.B. Massalski, editor in chief, Binary Alloy Phase Diagrams (ASM, Metals Park, OH, 1986).
2. W.D. Pearson, A Handbook of Lattice Spacings and Structures of Metals and Alloys (Pergamon Press, Oxford, 1964).

BRUCE J. PLETKA

Bruce J. Pletka is a Professor of Metallurgical and Materials Engineering at Michigan Technological University. He has a bachelors degree in Metallurgical Engineering from Cleveland State University and obtained his M.S. and PhD degrees in Ceramic Science from Case Western Reserve University. His research interest include examining the structure-properties of materials, particularly ceramics. More recently, he has become involved with the powder processing of metals and ceramics with an emphasis on mechanical alloying of metallic alloys. He has taught a variety of undergraduate courses including ones dealing with materials characterization.

RUTH I. SCHULTZ KRAMER

Ruth Kramer is a Scientist in the Department of Metallurgical and Materials Engineering at Michigan Technological University. She holds a B.S. in geology from the University of Oregon and a M.S. in geology from Michigan Tech, and her interests are in microscopy and characterization. She teaches electron microscopy and microprobe laboratories, a course in ore characterization methods, and supervises the metallographic and optical microscopy laboratories.

EDWARD A. LAITILA

Edward A. Laitila is an Engineer/Scientist in the Department of Metallurgical and Materials Engineering at Michigan Technological University. He has a Associate in Applied Science degree in Electrical Engineering Technology, a Bachelor of Science degree in Electrical Engineering, and is currently completing a Master of Science degree in Metallurgical and Materials Engineering, all from Michigan Technological University. He has 15 years experience in x-ray diffraction and materials characterization and is heavily involved in laboratory teaching in addition to training users in the operation and various data analysis techniques used in x-ray diffraction.

**THE ADVANCED MATERIALS AND
PROCESSING EDUCATION CENTER**

R. S. Goldman

D. Clark

A. Ghosh

L. P. Kendig

J. F. Mansfield

K. McIntyre

X. Pan

and

K. Worth

Department of Materials Science and Engineering
University of Michigan
Ann Arbor, Michigan 48109-2136

e-mail rsgold@engin.umich.edu



R. S. Goldman

The Advanced Materials and Processing Education Center

R.S. Goldman, D. Clark, A. Ghosh, L.P. Kendig, J.F. Mansfield, K. McIntyre, X. Pan,
and K. Worth

Department of Materials Science and Engineering
University of Michigan
Ann Arbor, MI 48109-2136

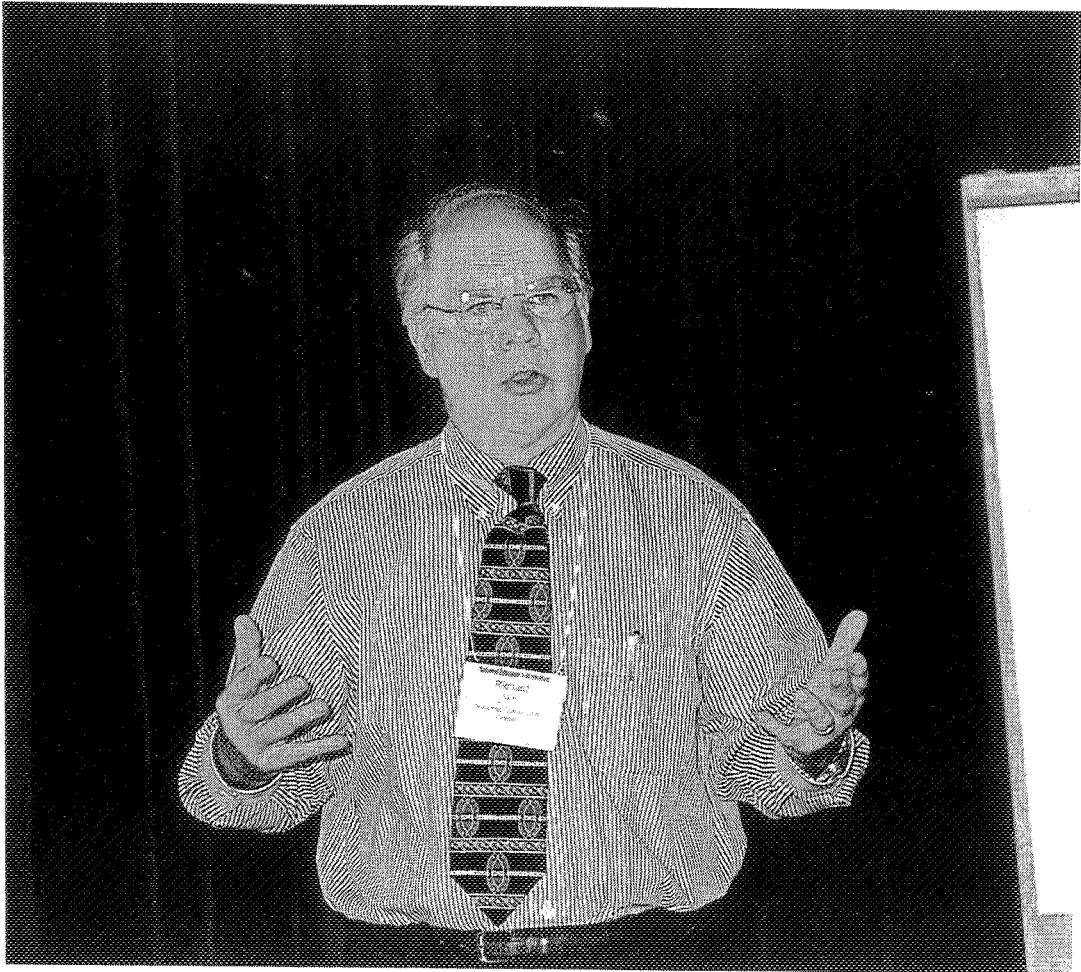
We are developing a state-of-the-art Materials Education Facility, the Advanced Materials and Processing Education Center (AMPEC) by expanding our current laboratory capabilities and incorporating the latest in computer technology. AMPEC includes modern facilities for metallography, microscopy, heat treatment, mechanical testing, scanning electron microscopy, and injection molding. In the past year, we have added a number of undergraduate facilities, including a Workstation Center, an X-ray Facility, a Scanning Probe Microscopy Facility, and an Electronic Properties Laboratory. In this talk, I will discuss the new laboratory modules we have begun to incorporate into our undergraduate curriculum, particularly in the area of electronic, magnetic, and optical materials. I will also discuss some of our future plans, include the addition of both a Dielectric Measurements Laboratory and a Casting Facility.

PREVIEW OF NEW:UPDATE 2000

Richard E. Lee

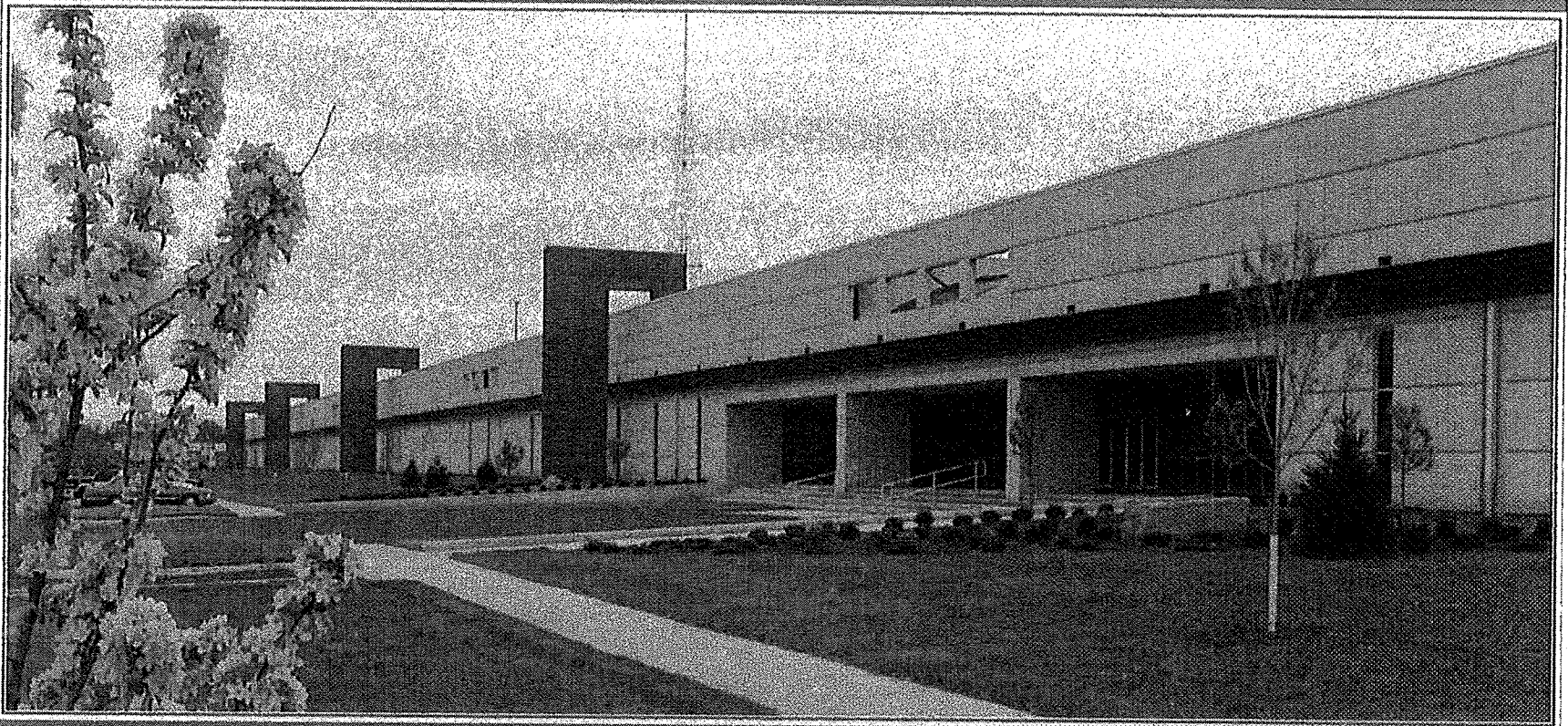
National Composites Center
200 Composites Drive
Kettering, Ohio 45420

Telephone: 937-297-9453
e-mail teamelks@ix.netcom.com



Richard E. Lee

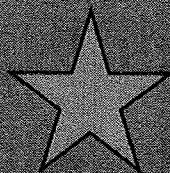
National Composite Center



Site for N.E.W. 2000

- History of the National Composite Center
- NCC Facilities
- NCC Operations

History

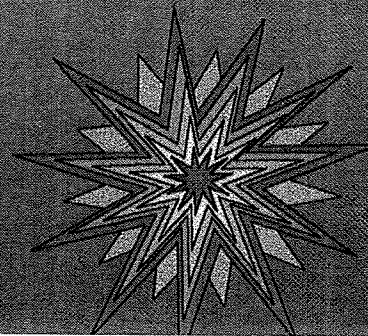
- Area survey
- U.S. and Miami Valley have has leadership in advanced composites
- Area support
 - Wright Labs 
 - Automotive industry
 - Colleges & Universities

History

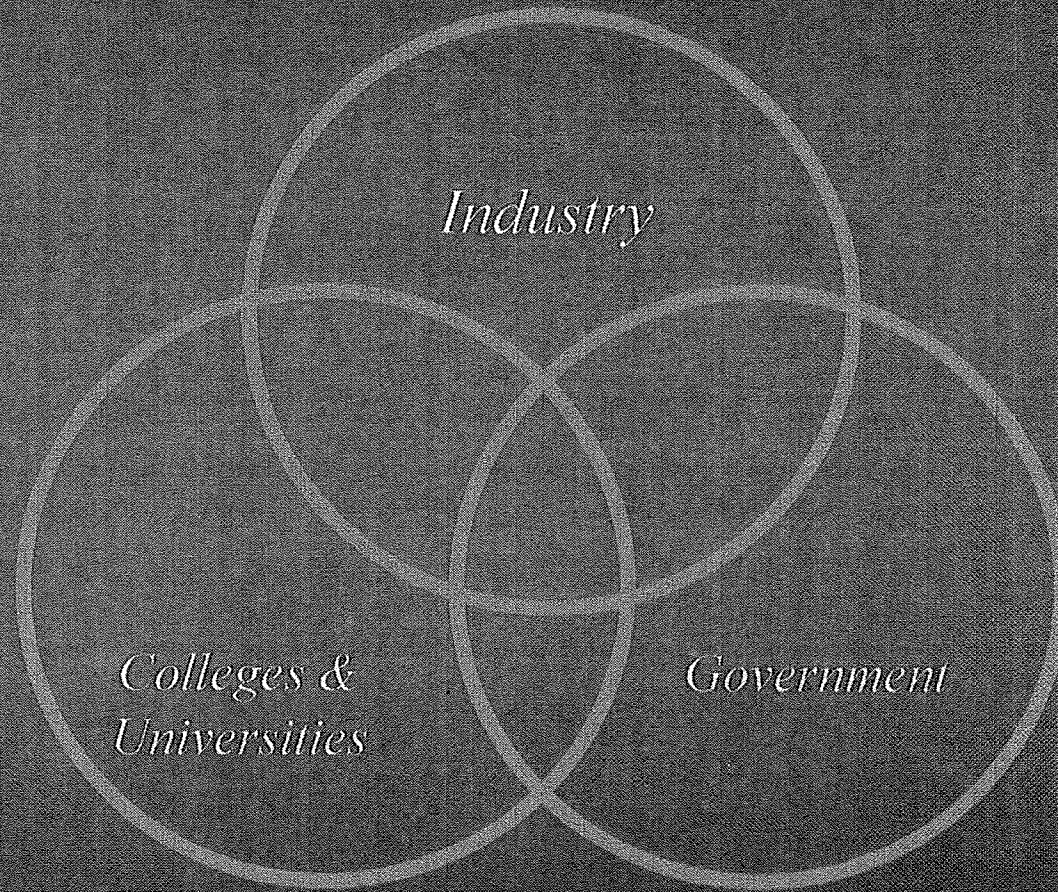
- Financial commitment secured from Ohio & Montgomery Co.
- Incorporated the National Composite Center in 1996

Composite Center Mission

“To promote, develop, demonstrate and support commercialization of composite materials and processes that provide significant commercial advantages through partnerships with industry, academia and government.”



Encouraging Partnerships



Encouraging Partnerships

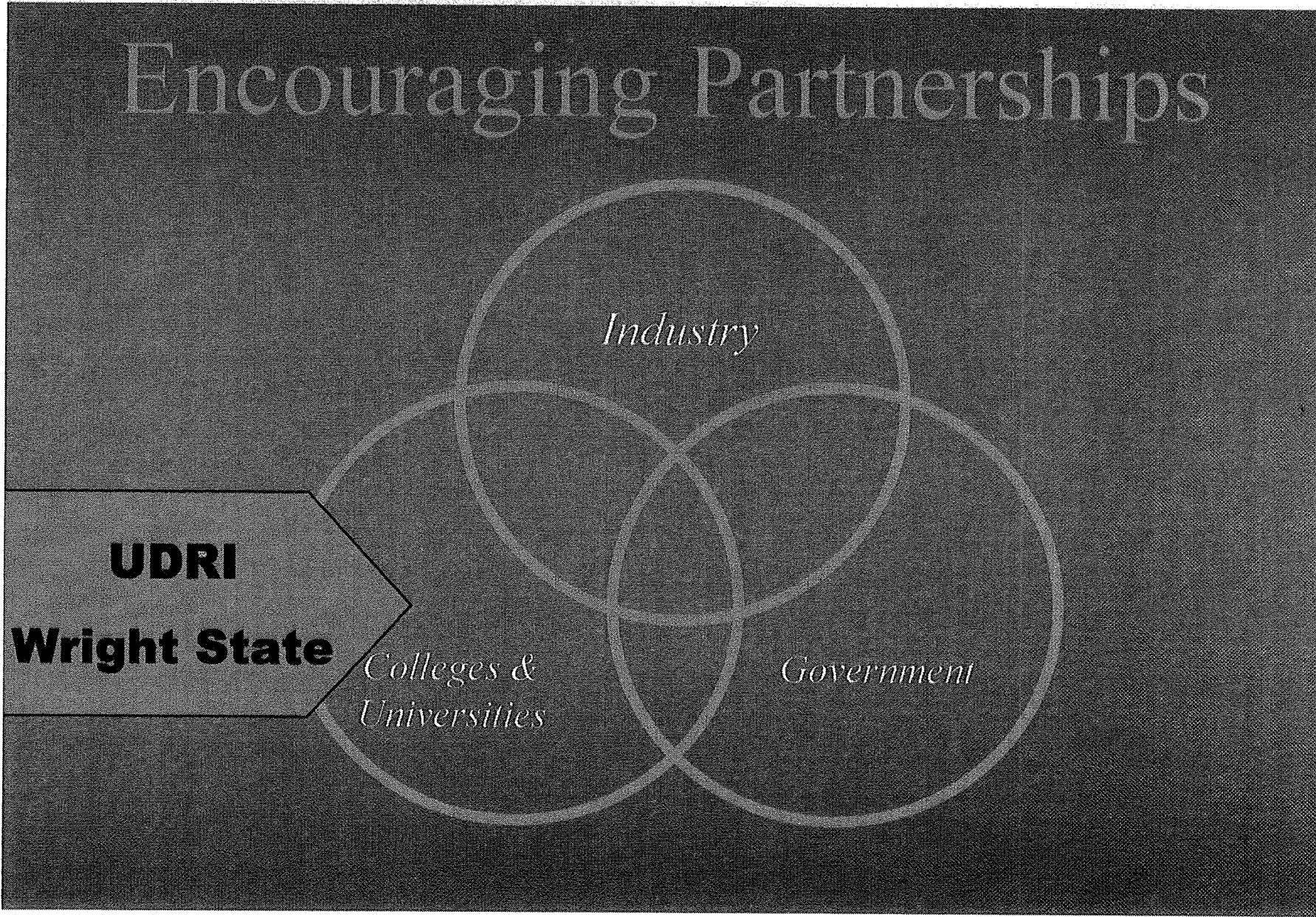
Industry

*Colleges &
Universities*

Government

UDRI

Wright State



Encouraging Partnerships

Boeing
Daimler Chrysler
Owens Corning
Ashland

Industry

*Colleges &
Universities*

Government

Encouraging Partnerships

Industry

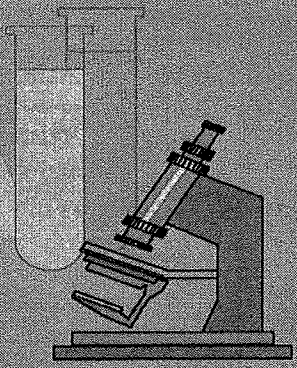
*Colleges &
Universities*

Government

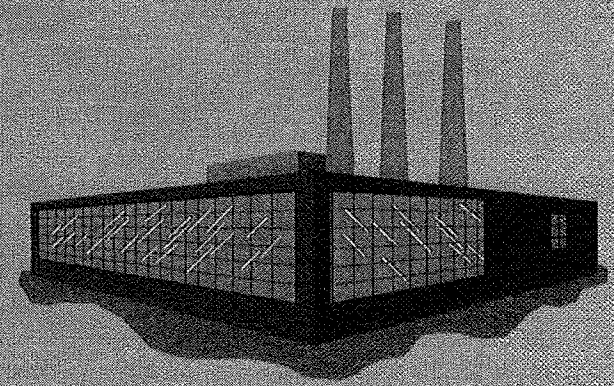
**State of Ohio
Mont. Co.**

We are not

A research facility

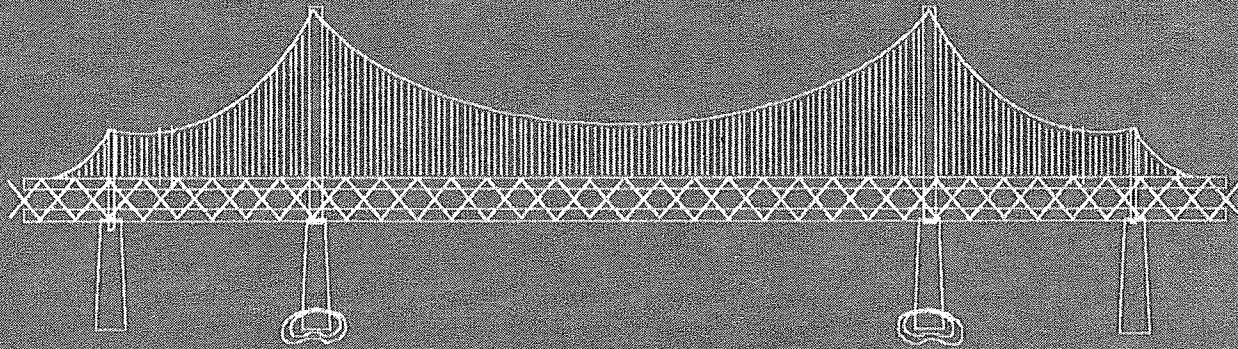


or



A production company

We are a bridge between . . .



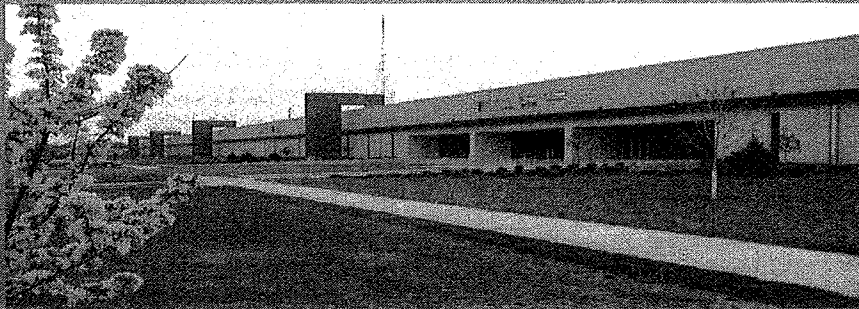
NICC Role

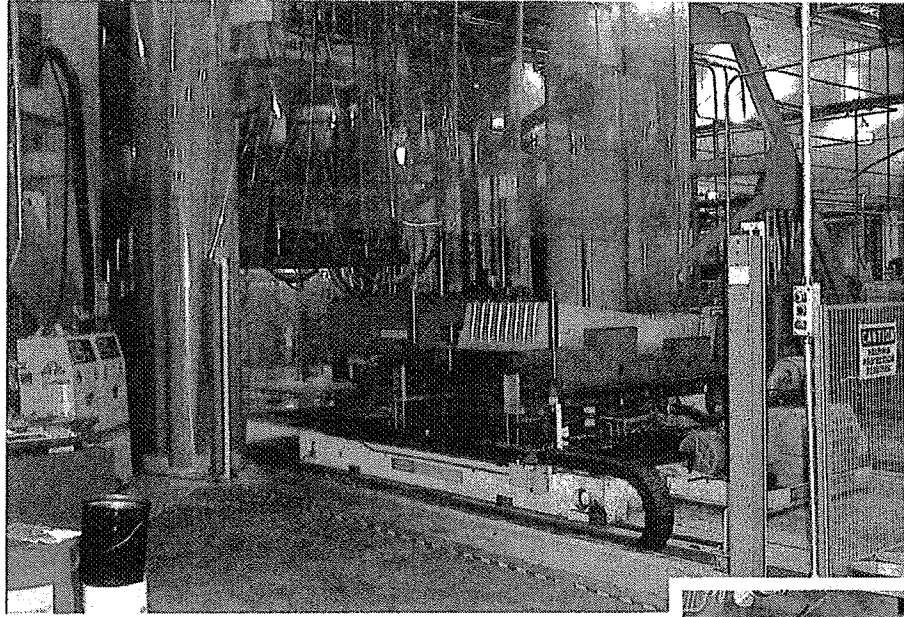
Provide:

- Project development expertise
- Project management expertise
- A neutral/confidential site
- Office, training and classroom space

National Composite Center

- 200,000 sq.ft.
 - 120,000 sq.ft. prototype development / manufacturing
 - 60,000 sq.ft lab / shop
 - 40,000 sq.ft office / training

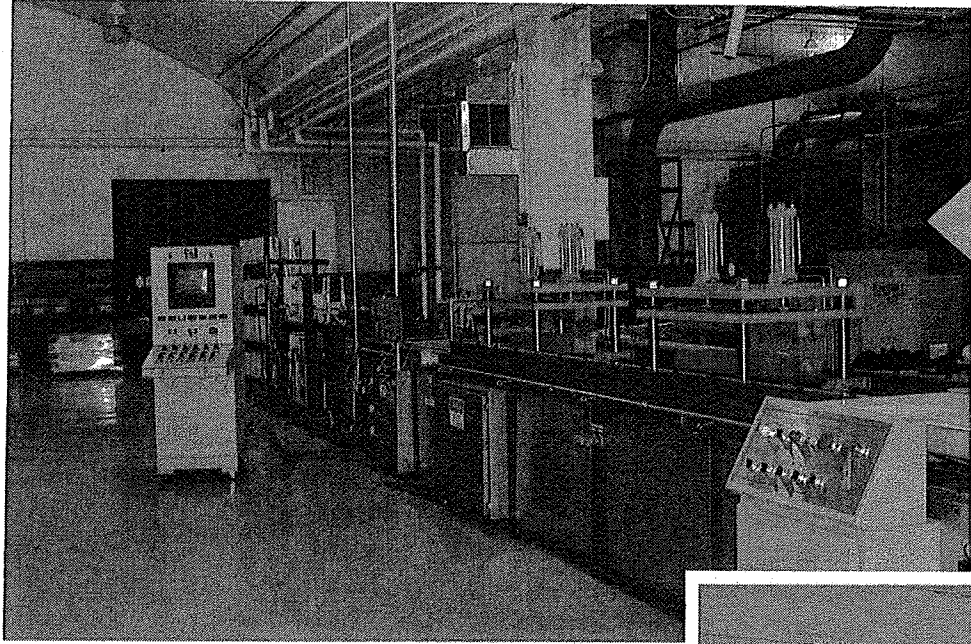




PRESS OPERATIONS

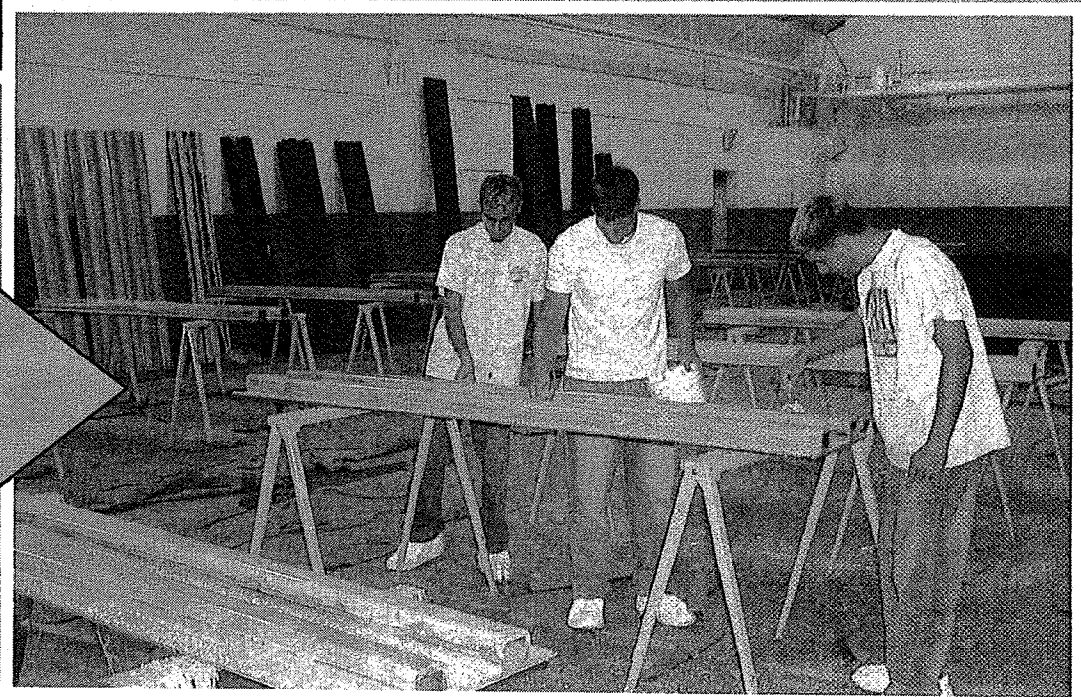
PREFORMING OPERATIONS

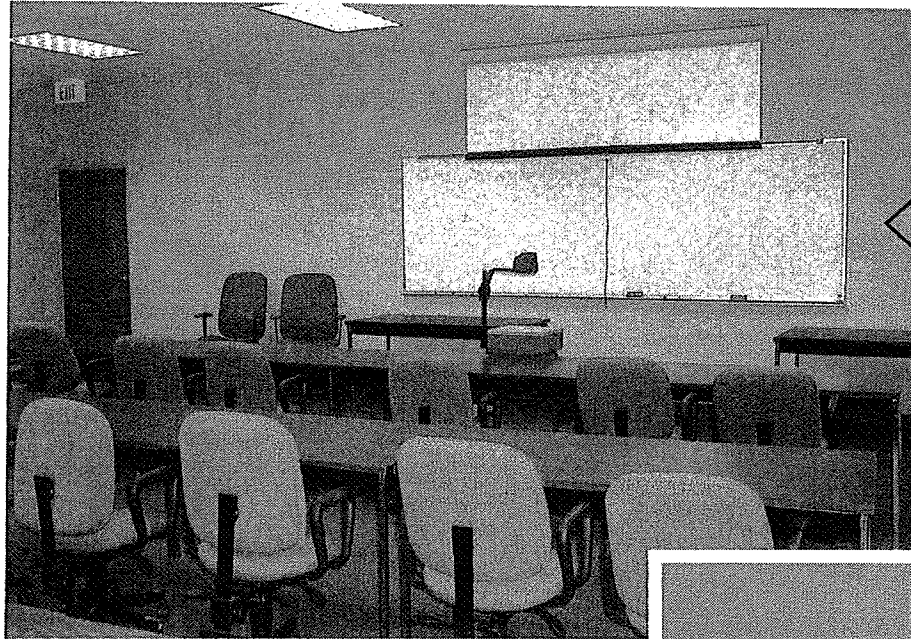




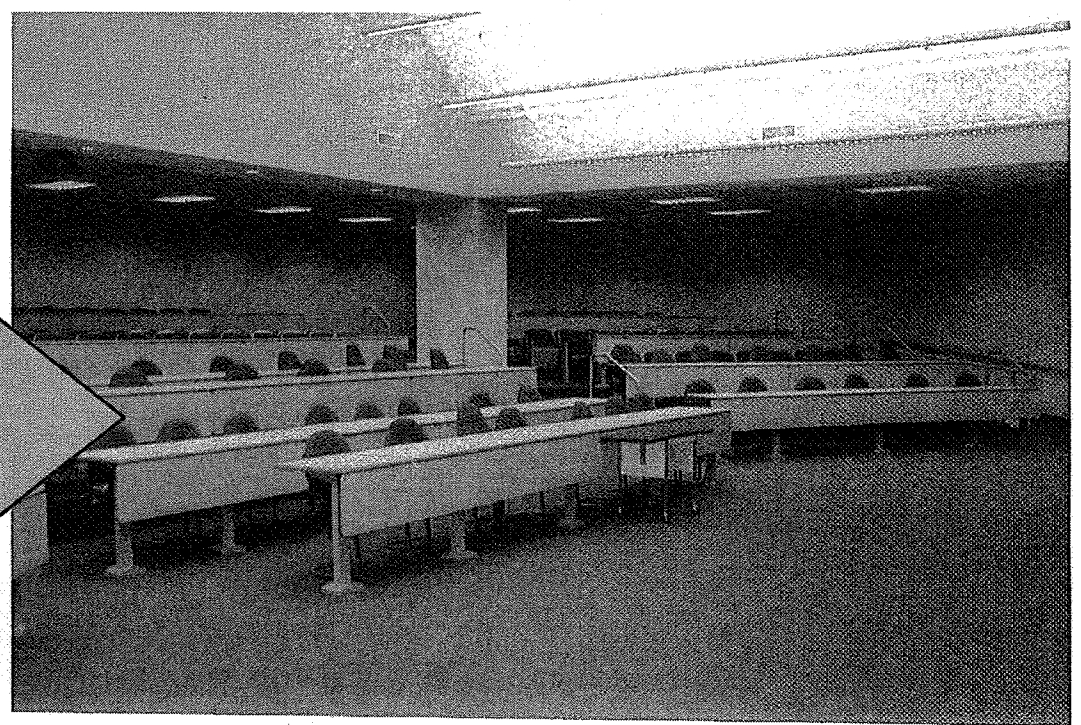
PULTRUSION OPERATIONS

BRIDGE DECK PREPARATION

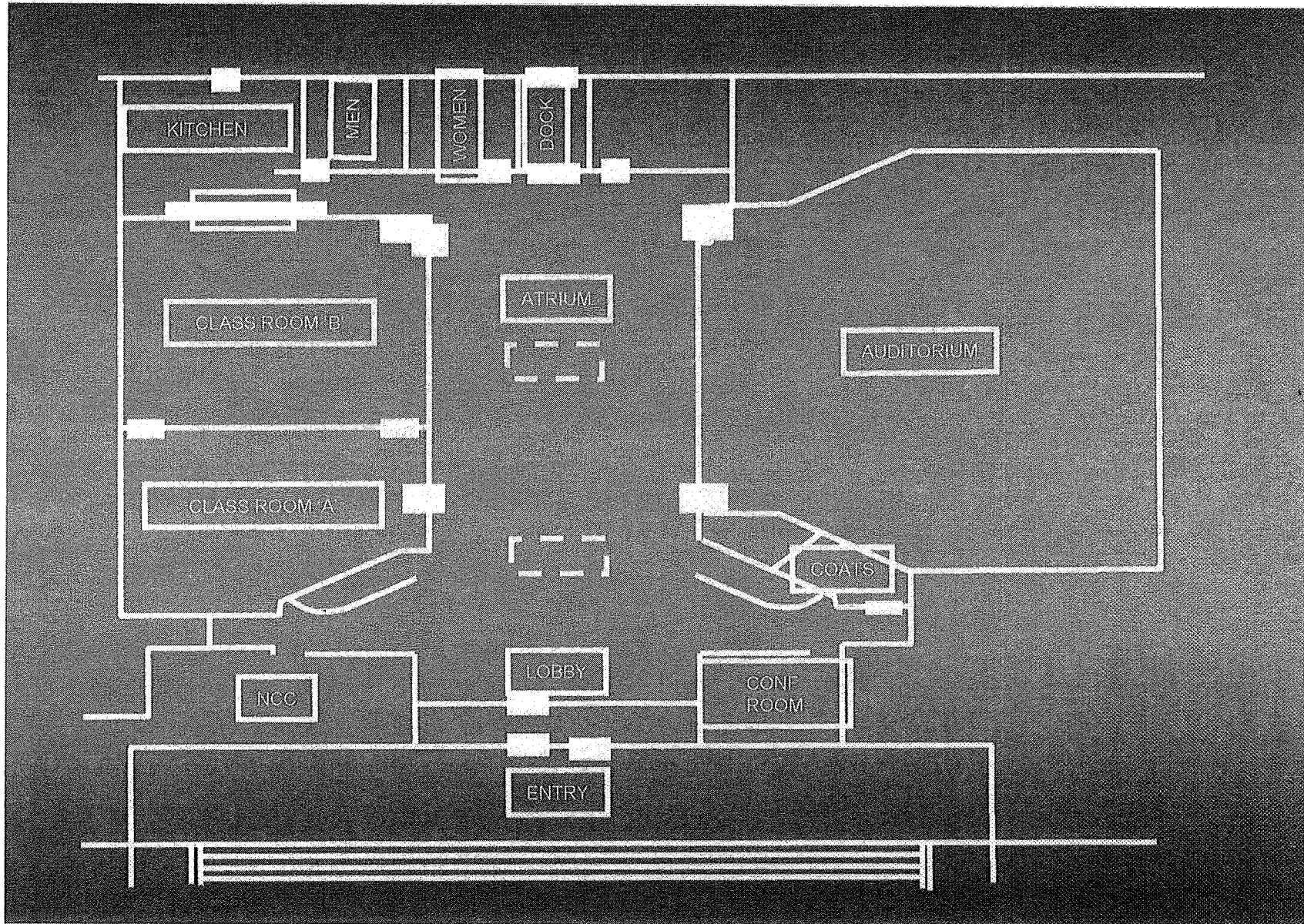




CLASSROOM



AUDITORIUM



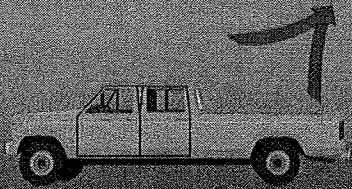
A Member Oriented

- Designed to foster a broad committed organization
- Benefits
 - Use of a neutral site
 - Access to a broad range of composite knowledge
 - Availability of office, lab, and manufacturing space for project development

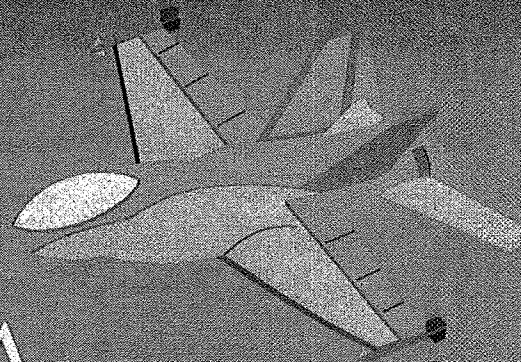
Automotive Consortium Project

- Replace a steel structure with a composite structure
- Economical replacement
- Weight savings
- Improved corrosion
- Eliminate the need for other parts

*The successful transfer of
technology . . .*



P4



P4A

Air Force Chopped Carbon

- Builds from the automotive glass program
- Oriented chopped carbon fiber preform
- Tail cone test part

Other Current Projects

- State of Ohio Project 100
 - 100 state and county bridge decks
 - Cost parity with current materials
- Major pleasure boat manufacturer
- Emergency medical cots
- Armored vehicles

We look forward to seeing

you

NEW 2000

USCAR LIFE CYCLE INVENTORY STUDY GENERIC VEHICLE LCA

**J. L. Sullivan, Ford
R. W. Williams, GM**

Susan G. Yester

DaimlerChrysler Corporation
800 Chrysler Drive
Auburn Hills, Michigan 48326

**S. Hentges, APC
S. Pomper, AA
S. Chubbs, AISI**



Susan G. Yester

LCA - Why

- Need to assess the overall environmental performance of vehicles
 - Want to quantify environmental burdens over a vehicle's entire life cycle
 - Life Cycle Assessment is the tool of choice
- Consistent with US Automaker efforts to improve the environmental performance of vehicles
- It is highly visible internationally
- ISO is attempting to standardize it
- Maybe used for Ecolabeling



SHARING TECHNOLOGY FOR A STRONGER AMERICA

USAMP -- Life Cycle Inventory

- Objective
 - To assess the cradle to grave environmental performance of vehicles
 - Conduct an LCI for an entire vehicle, in this case, the generic family sedan.
 - An LCI quantifies energy and material flows over a product's life cycle
 - Due to immaturity, an LCIA is not considered at this time
- Use of Results
 - To serve as a benchmark for future vehicles, eg. PNGVs
 - To communicate with the public and private sector
 - Not intended for material comparisons
 - It is stressed that cost and performance must also be considered.

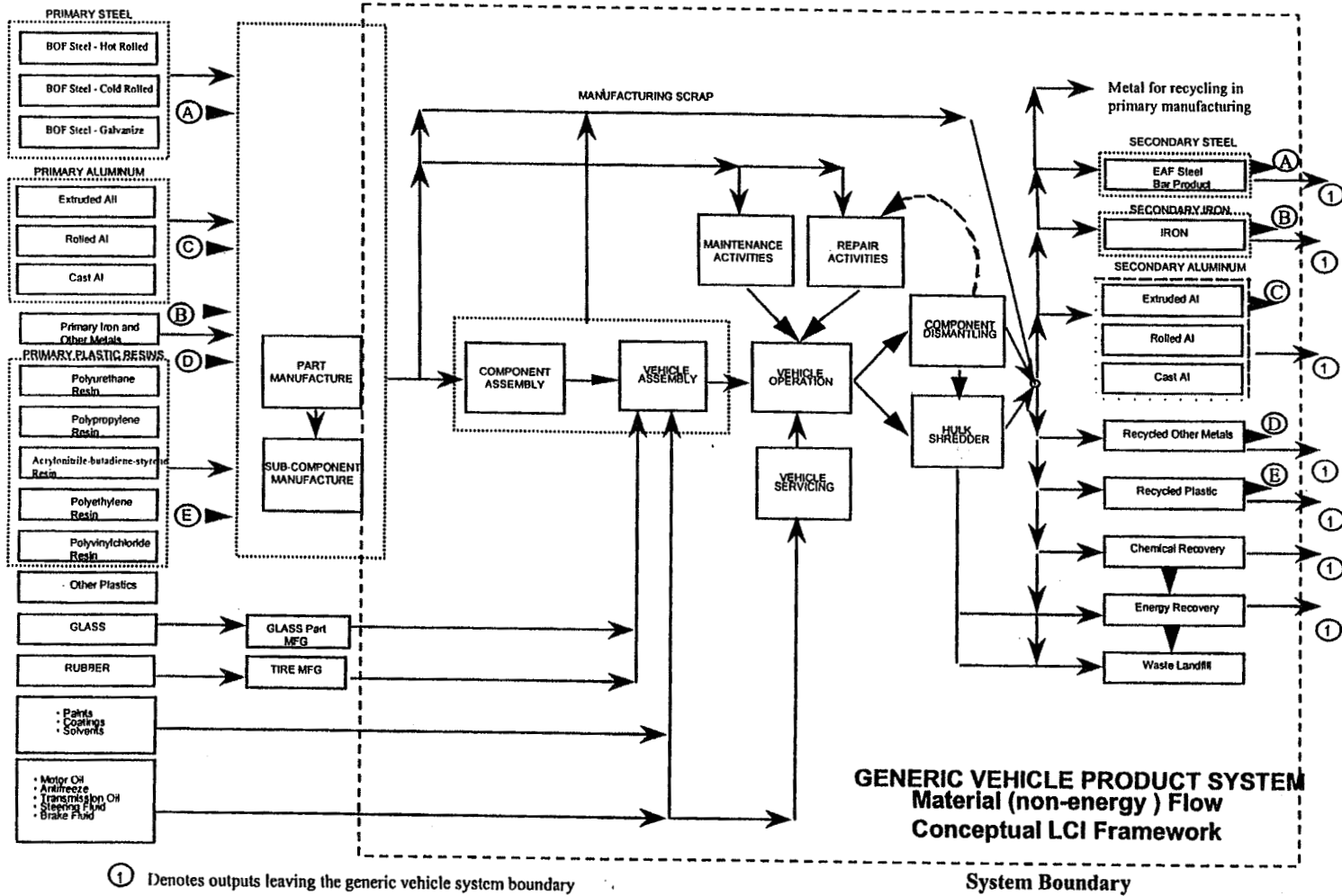
Brief History of USAMP/LCI Efforts

- Conducted a Scoping and Project Definition study to define a suitable life cycle project.
 - Initiate development of a methodology
 - Decided to conduct a generic vehicle LCI
- Preliminary Modeling stage
 - Methodology completed
 - OEM data need identified
- Each industry group participant to conduct its own LCI
- Conduct a final roll-up study for the generic vehicle

USAMP Life Cycle Study Outline

- The generic family sedan is an entire vehicle comprised of components from the Taurus/Lumina/Intrepid vehicle lines
- Have our major materials suppliers provide the most up to date LCI material production information, i.e. for aluminum , plastics, and steel
 - Invite AA, AISI, and APC to join the project.
- OEMs to pool their data
 - Use available data on appropriate vehicle lines
- Acquire remaining LCI data from existing databases
- Use available recycling data; sources include AAMA and VRP

579



Vehicle Sub-System Layout

- Each OEM wanted to keep its own parts organization code proprietary.
- Hence, the USAMP code was developed
- The USAMP organizational code divides the vehicle into 7 vehicle systems:
 - Powertrain
 - Suspension
 - Body
 - Interior
 - HVAC
 - Electrical
 - Fluids
- They are further sub-divided into 19 sub-systems and 77 sub-subsystems, and 644 discrete parts

Data Gathering

- Material suppliers provide data on 4 types of steel, 3 types of aluminum, and 5 types of plastics.
- The OEMs gather data on:
 - Alternator
 - Brakes
 - Electronics
 - Engine
 - Transmissions
 - Aluminum Casting
 - Forgings
 - Glass
 - Iron Casting
 - Plastics Molding
 - Stamping
 - Vehicle Assembly
- The vehicle is characterized by 74 materials weighing 1532 Kg.
 - Lifetime drive distance is 120,000 miles



SHARING TECHNOLOGY FOR A STRONGER AMERICA

USAMP -- Life Cycle Inventory

Data Categories

- Energy
 - Fossil and non-fossil
 - Process
 - Transportation
 - Feedstock
 - Total
- Water Consumption
 - Ground
 - Surface
- Air Emission
 - CO₂, CO, SO_x
 - NO_x, CH₄, HCL
 - HF, NMHC, Pb
 - Dust and particulates
- Water Effluents
 - Dissolved Solids
 - Suspended Solids
 - Heavy metals
 - Oils and greases
 - PO₄ & NH₃
- Solid Wastes
 - Sanitary and municipal
 - Total solid waste
- Raw Materials



SHARING TECHNOLOGY FOR A STRONGER AMERICA

USAMP -- Life Cycle Inventory

Generic Vehicle Description

Plastics			Metals (Ferrous)		
Material	Mass (kg)	Mass (%)	Material	Mass (kg)	Mass (%)
ABS-PC (acrylonitrile butadiene styrene-polycarbonate blend)	2.8	0.18%	Ferrite (Fe)	1.5	0.10%
Acetal	4.7	0.31%	Cast Iron (Fe)	132	8.59%
Acrylic Resin	2.5	0.16%	Pig Iron (Fe)	23	1.48%
Acrylonitrile Butadiene Styrene (ABS)	9.7	0.64%	Steel (cold rolled)	114	7.46%
Acrylonitrile Styrene Acrylate (ASA)	0.18	0.012%	Steel (EAF)	214	13.94%
Epoxy Resin	0.77	0.050%	Steel (galvanized)	357	23.29%
PA 6-PC (polyamide-polycarbonate blend)	0.45	0.030%	Steel (hot rolled)	126	8.23%
Phenolic Resin	1.1	0.072%	Steel (stainless)	19	1.23%
Polyamide (PA 6)	1.7	0.11%	Total Metals (Ferrous): 985 64%		
Polyamide (PA 66)	10	0.67%	Fluids		
Polybutylene Terephthalate (PBT)	0.37	0.024%	Material	Mass (kg)	Mass (%)
Polycarbonate (PC)	3.8	0.25%	Automatic Transmission Fluid	6.7	0.44%
Polyester Resin	11	0.75%	Engine Oil (SAE 10w-30)	3.5	0.23%
Polyethylene (PE)	6.2	0.40%	Ethylene Glycol	4.3	0.28%
Polyethylene Terephthalate (PET)	2.2	0.14%	Glycol-Ether	1.1	0.069%
Polypropylene (PP)	25	1.6%	Refrigerant (R 134a)	0.91	0.059%
Polypropylene (PP, foam)	1.7	0.11%	Unleaded Gasoline	48	3.1%
Polystyrene (PS)	0.0067	0.00044%	Water	9.0	0.59%
Polyurethane (PUR)	35	2.3%	Windshield Cleaning Additives	0.48	0.031%
Polyvinyl Chloride (PVC)	20	1.3%	Total Fluids: 74 4.8%		
PP-EPDM (polypropylene-ethylene propylene diene monomer blend)	0.10	0.0067%	Other Materials		
PPO-PC (polyphenylene oxide-polycarbonate blend)	0.025	0.0017%	Material	Mass (kg)	Mass (%)
PPO-PS (polyphenylene oxide-polystyrene blend)	2.2	0.14%	Ethylene Propylene Diene Monomer (EPDM)	10	0.68%
Thermoplastic Elastomeric Olefin (TEO)	0.31	0.020%	Adhesive	0.17	0.011%
Total Plastics: 143 9.3%			Asbestos	0.4	0.026%
Metals (Non-Ferrous)			Bromine (Br)	0.23	0.015%
Material	Mass (kg)	Mass (%)	Carpeting	11	0.73%
Aluminum Oxide	0.27	0.018%	Ceramic	0.25	0.016%
Aluminum (cast)	71	4.663%	Charcoal	0.22	0.014%
Aluminum (extruded)	22	1.438%	Corderite	1.2	0.081%
Aluminum (rolled)	3.3	0.2%	Desiccant	0.023	0.0015%
Brass	8.5	0.55%	Fiberglass	3.8	0.25%
Chromium (Cr)	0.91	0.060%	Glass	42	2.8%
Copper (Cu)	18	1.1%	Graphite	0.092	0.0060%
Lead (Pb)	13	0.85%	Paper	0.20	0.013%
Platinum (Pt)	0.0015	0.00010%	Recycled Textile Fibers	12	0.78%
Rhodium (Rh)	2.9E-04	0.000019%	Rubber (except tire)	23	1.5%
Silver (Ag)	0.0034	0.00022%	Rubber (extruded)	37	2.4%
Tin (Sn)	0.067	0.0044%	Sulfuric Acid (H2SO4)	2.2	0.14%
Tungsten (W)	0.011	0.00073%	Tire	45	3.0%
Zinc (Zn)	0.32	0.021%	Wood	2.3	0.15%
Total Metals (Non-Ferrous): 138 9.0%			Total Other Materials: 192 13%		
			Total Weight of Generic Vehicle: 1532 100%		



SHARING TECHNOLOGY FOR A STRONGER AMERICA

USAMP -- Life Cycle Inventory

Ancillary Materials Modeled in the Generic Vehicle Life Cycle

Acetic Acid Glacial	Methanol (CH ₃ OH)
Acetone (CH ₃ COCH ₃)	Methyl Ethyl Ketone (MEK, CH ₃ COCH ₂ CH ₃)
Acetylene	Mineral Spirits
Adipic Acid (HOOC(CH ₂) ₄ COOH)	n-Butanol (CH ₃ CH ₂ CH ₂ CH ₂ OH)
Aluminum Oxide	n-Butanol
Ammonia (NH ₃ with CO ₂ recovery, 100%)	n-Butoxy Propanol (C ₄ H ₉ O(CH ₂) ₃ OH)
Argon (Ar)	Naphtha
Bauxite (Al ₂ O ₃)	Nitrogen (N ₂)
Benzene (C ₆ H ₆)	Oil
Carbon Black	Oxygen (O ₂)
Carbon Dioxide (CO ₂)	Petroleum Distillate
Cardboard	Phenol (C ₆ H ₅ OH)
Chlorine (Cl ₂)	Phenolic Resin
Coke	Potassium Chloride (KCl)
Diethylene Glycol (HOCH ₂ CH ₂ OCH ₂ CH ₂ OH)	Propylene Oxide (CH ₃ C ₂ H ₃ O)
Diisopropanol Amine	Sand
Dolomite (Crude)	Silica
Ethylene Glycol (HOCH ₂ CH ₂ OH)	Sodium Carbonate
Ethylene Oxide	Sodium Chloride (NaCl, Chlorine Use)
Feldspar	Sodium Hydroxide (NaOH, 100%)
Formaldehyde	Sodium Sulfate
Glycol Monobutyl Ether (C ₄ H ₉ OCH ₂ CH ₂ OH)	Solder Alloy
Hydrochloric Acid (HCl, 100%)	Solder Flux
Iron Ore	Styrene (C ₆ H ₅ CHCH ₂)
Isopropyl Alcohol	Sulfuric Acid (H ₂ SO ₄ , 100%) (1)
Kaolin	Titanium Dioxide (TiO ₂ , 100%)
Lime	Toluene (C ₆ H ₅ CH ₃)
Limestone	Wood (55% Dry): Supply
Melamine Formaldehyde Resin	Xylene (C ₆ H ₄ (CH ₃) ₂)

Form of Results

- Results of the study and the model can be expressed in the following ways:
 - Overall
 - by subsystem
 - by life cycle stage
 - by material



SHARING TECHNOLOGY FOR A STRONGER AMERICA

USAMP -- Life Cycle Inventory

LCI of the Generic Vehicle (Raw Materials Use)

<i>Environmental Flow</i>	<i>Units</i>	<i>Generic Vehicle</i>	<i>Materials Production</i>	<i>Manufacturing & Assembly</i>	<i>Use & Operation</i>	<i>E-O-L</i>
Inflow						
(r) Bauxite Rich Soil	kg	222	222			
(r) Bauxite (Al ₂ O ₃ , in ground)	kg	32	32	0.0026	0.02	
(r) Chromium (Cr, in ground)	kg	0.91	0.91			
(r) Coal (in ground)	kg	2,473	997	618	848	11
(r) Copper (Cu, in ground)	kg	23	23			
(r) Ilmenite (FeO.TiO ₂ , in ground)	kg	0.97	0.32	0.65	9.9 E-05	
(r) Iron (Fe, in ground)	kg	1,443	1,440	0.38	3.	0.045
(r) Lead (Pb, in ground)	kg	33	13	0.26	20	
(r) Limestone (CaCO ₃ , in ground)	kg	441	182	95	162	2.0
(r) Manganese (Mn, in ground)	kg	24	23		0.76	
(r) Natural Gas (in ground)	kg	1,775	458	216	1,098	2.2
(r) Oil (in ground)	kg	16,255	402	87	15,731	35
(r) Olivine (in ground)	kg	8.3	8.3		0.0032	
(r) Perlite (SiO ₂ , in ground)	kg	2.4	2.3	0.056		
(r) Platinum (Pt, in ground)	kg	0.0015	0.0015			
(r) Pyrite (FeS ₂ , in ground)	kg	13	13		4.3 E-05	
(r) Rhodium (Rh, in ground)	kg	2.9 E-04	2.9 E-04			
(r) Sulfur (S)	kg	0.10	0.08	0.022	4.0 E-05	
(r) Tin (Sn, in ground)	kg	0.48	0.067	0.41		
(r) Tungsten (W, in ground)	kg	0.012	0.011		6.8 E-04	
(r) Uranium (U, in ground)	kg	0.043	0.014	0.0089	0.02	2.5 E-04
(r) Zinc (Zn, in ground)	kg	18	18	-1.0 E-04	4.3 E-04	
Iron Scrap	kg	243	200	0.05	43	
Natural Rubber	kg	25	8.8		16	
Raw Materials (Iron Casting Alloys)	kg	12	12			
Raw Materials (unspecified)	kg	16	6.2	9.2	0.32	
Steel Scrap	kg	474	428	-1.0 E-03	46	
Water Used (total)	Liter	76,834	59,556	9,817	7,457	4.0



SHARING TECHNOLOGY FOR A STRONGER AMERICA

USAMP -- Life Cycle Inventory

LCI of the Generic Vehicle (Outflows and Energy Use)

<i>Environmental Flow</i>	<i>Units</i>	<i>Generic Vehicle</i>	<i>Materials Production</i>	<i>Manufacturing & Assembly</i>	<i>Use & Operation</i>	<i>E-O-L</i>
Outflow						
(a) Dust and Particulates	g	53,483	26,430	8,235	18,572	247
(a) Carbon Dioxide (CO ₂ , fossil)	g	59,051,700	4,401,500	2,561,990	51,944,900	143,273
(a) Carbon Monoxide (CO)	g	1,942,190	63,776	5,914	1,871,820	683
(a) Sulfur Oxides (SO _x as SO ₂)	g	133,146	30,319	14,917	87,595	315
(a) Nitrogen Oxides (NO _x as NO ₂)	g	253,924	12,619	8,295	232,204	806
(a) Non-Methane Hydrocarbons	g	256,043	12,059	7,348	236,465	170
(a) Methane (CH ₄)	g	65,366	11,359	5,534	48,330	144
(a) Hydrogen Chloride (HCl)	g	725	277	10	431	5.7
(a) Hydrogen Fluoride (HF)	g	113	59	1.1	52	0.71
(a) Lead (Pb)	g	115	50	1.2	64	0.015
(w) Dissolved Solids	g	7,684	4,526	1,118	2,023	17
(w) Suspended Solids	g	74,313	2,771	2,450	69,034	58
(w) Heavy Metals (total)	g	39	29	7.5	3.1	0.0013
(w) Oils and Greases	g	7,599	118	516	6,957	7.4
(w) Other Organics	g	79	76	0.37	2.4	2.2 E-04
(w) Phosphates (as P)	g	15	7.2	7.8	0.42	1.6 E-05
(w) Ammonia (as N)	g	2,354	115	17	2,220	1.9
Waste (total)	kg	4,211	2,438	386	1,060	326
Waste (municipal and industrial)	kg	414	21	56	41	296
Energy Reminder						
E (HHV) Total Energy	MJ	961,486	82,734	39,212	837,378	2,164
E (HHV) Fossil Energy	MJ	955,410	78,988	38,408	835,866	2,147
E (HHV) Non-Fossil Energy	MJ	6,079	3,745	803	1,515	16
E (HHV) Process Energy	MJ	928,609	68,642	36,686	822,535	746
E (HHV) Feedstock Energy	MJ	25,534	16,246	951	8,337	
E (HHV) Transportation Energy	MJ	11,033	1,355	1,574	6,686	1,418



SHARING TECHNOLOGY FOR A STRONGER AMERICA

USAMP -- Life Cycle Inventory

Ferrous Material Use per Vehicle Subsystem

Material	Units	Total	Vehicle Subsystem						
			Body	Electrical	Fluids	HVAC	Interior	Powertrain	Suspension
Ferrite (Fe)	kg	1.5		1.5					
Iron (Fe)	kg	25						25	
Iron (Fe, cast)	kg	138						96	42
Steel (cold rolled)	kg	175	46	8.9		6.0	51	41	22
Steel (EAF)	kg	232	47	3.1		0.10	7.1	70	105
Steel (galvanized)	kg	597	546	1.9		5.1	2.2	42	0.35
Steel (hot rolled)	kg	197	82					5.3	110
Steel (stainless)	kg	32	0.23			1.2		30	
Total:	kg	1,397	721	15		12	60	309	279

Non-Ferrous Material Use per Vehicle Subsystem

Material	Units	Total	Vehicle Subsystem						
			Body	Electrical	Fluids	HVAC	Interior	Powertrain	Suspension
Aluminum (automotive, cast)	kg	71	0.0068	2.2		5.2		61	2.7
Aluminum (automotive, extruded)	kg	22		0.0033		11	3.1	7.6	
Aluminum (automotive, rolled)	kg	5.6				0.89		4.7	
Brass	kg	8.5		0.43		1.1		6.9	
Chromium (Cr)	kg	0.91	0.91						
Copper (Cu)	kg	18	0.68	12				4.4	
Lead (Pb)	kg	13		13					0.28
Platinum (Pt)	kg	0.0015						0.0015	
Rhodium (Rh)	kg	2.9 E-04						2.9 E-04	
Silver (Ag)	kg	0.0034		0.0034					
Tin (Sn)	kg	0.067		0.0045				0.063	
Tungsten (W)	kg	0.011		0.011					
Zinc (Zn)	kg	0.32	0.32						
Total:	kg	140	1.9	28		19	3.1	85	2.9



SHARING TECHNOLOGY FOR A STRONGER AMERICA

USAMP -- Life Cycle Inventory

Plastic Material Use per Vehicle Subsystem

Material	Units	Total	Vehicle Subsystem						
			Body	Electrical	Fluids	HVAC	Interior	Powertrain	Suspension
ABS-PC (Acrylonitrile Butadiene Styrene Polycarbonate blend)	kg	2.9				0.015	0.40		2.5
Acetal	kg	4.7	2.6	0.38		0.045	1.0	0.52	0.18
Acrylic Resin	kg	2.5		2.5					
Acrylonitrile Butadiene Styrene (ABS)	kg	9.8	0.74	3.5		1.3	2.5		1.7
Epoxy Resin	kg	0.77						0.14	0.63
PA 6-PC (Polyamide Polycarbonate blend)	kg	0.47						0.47	
Phenolic Resin	kg	1.1		0.0045			1.1	0.0052	
Polyamide (PA 6)	kg	1.7	0.10			0.77	0.68		0.13
Polyamide (PA 66)	kg	10	0.32	2.1		0.16	3.1	3.8	0.95
Polybutylene Terephthalate (PBT)	kg	0.37		0.37					
Polycarbonate (PC)	kg	3.8	1.6	1.6		0.0091	0.51	0.052	
Polyester Resin	kg	11					11		
Polyethylene (PE)	kg	6.2	4.1	1.5			0.62		
Polyethylene Terephthalate (PET)	kg	2.2	0.65	0.045			1.2	0.27	
Polypropylene (PP)	kg	26	3.9	0.46		8.4	12	1.2	0.11
Polypropylene (PP, foam)	kg	1.8	1.8						
Polystyrene (PS)	kg	0.0067		0.0067					
Polyurethane (PUR)	kg	35	13	0.026		3.9	18		0.58
Polyvinyl Chloride (PVC)	kg	21	3.5	10		0.43	5.3	0.16	0.91
PP-EPDM (Polypropylene Ethylene Propylene Diene Monomer blend)	kg	0.10	0.10						
PPO-PC (Polyphenylene Oxide Polycarbonate blend)	kg	0.026		0.026					
PPO-PS (Polyphenylene Oxide Polystyrene blend)	kg	2.2		2.2					
Total:	kg	144	32	25		15	57	6.6	7.8

USAMP -- Life Cycle Inventory

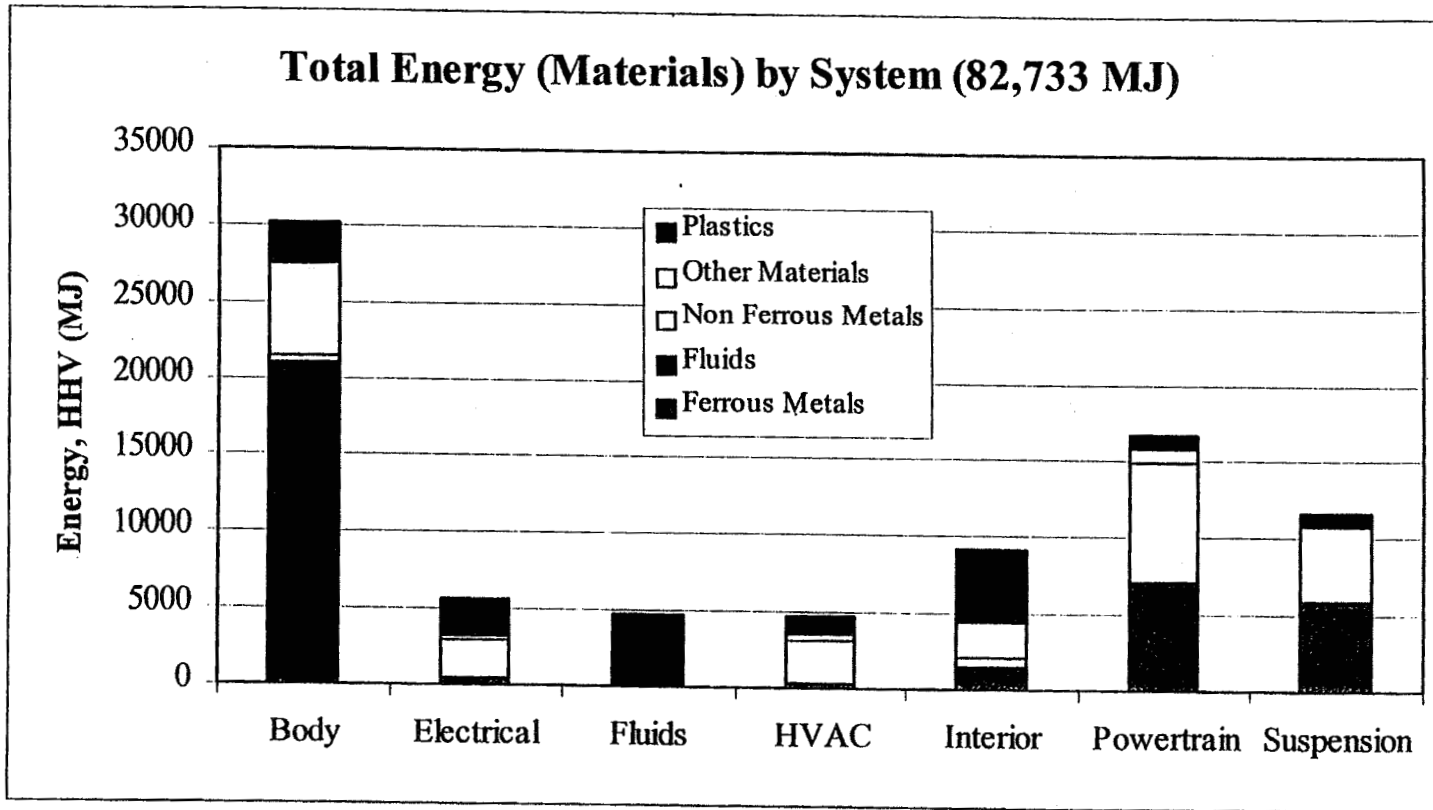
Fluid Material Use per Vehicle Subsystem

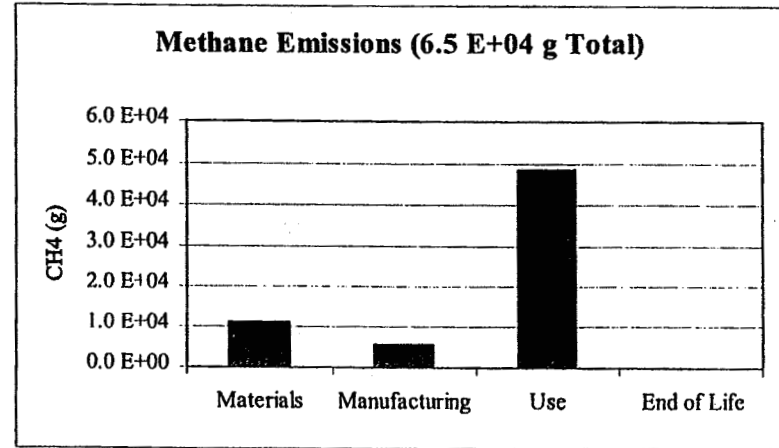
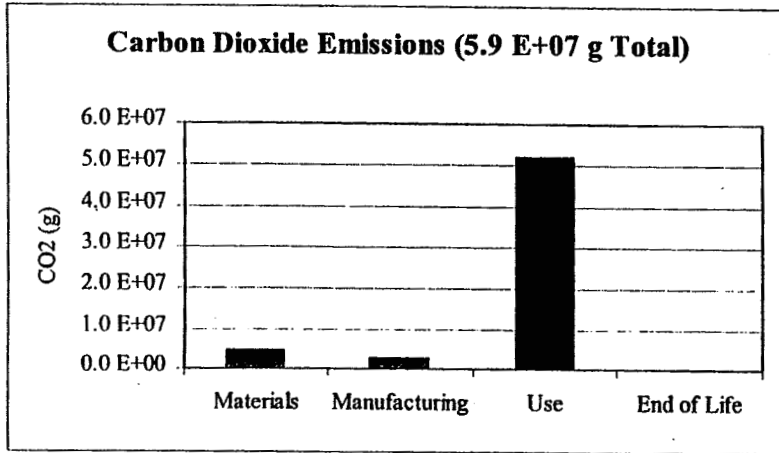
Material	Units	Total	Vehicle Subsystem						
			Body	Electrical	Fluids	HVAC	Interior	Powertrain	Suspension
Automatic Transmission Fluid	kg	8.6			8.6				
Engine Coolant	kg	9.3			9.3				
Engine Oil (SAE 10w-30)	kg	3.9			3.9				
Gasoline	kg	64			64				
Refrigerant	kg	0.91			0.91				
Total:	kg	87			87				

Other Material Use per Vehicle Subsystem

Material	Units	Total	Vehicle Subsystem						
			Body	Electrical	Fluids	HVAC	Interior	Powertrain	Suspension
Carpeting	kg	11	0.44				11		
EPDM (Ethylene Propylene Diene Monomer)	kg	10	4.2	0.69			2.8	2.8	
Fiberglass	kg	3.8	0.59	0.72			2.3		0.13
Glass	kg	42	41	0.99					
Paper	kg	0.20		0.015					0.19
Rubber	kg	23	0.83	0.13		3.0	11	0.43	7.7
Rubber (extruded)	kg	37	31			0.91		2.1	3.3
Sand	kg	1.3		1.2					0.027
Sulfuric Acid (H2SO4, 100%)	kg	2.2		2.2					
Tire	kg	45							45
Wood	kg	2.6	1.8	0.15			0.51	0.15	
Total:	kg	179	80	6.1		3.9	27	5.7	57

Total Energy (Materials) by System (82,733 MJ)





Results Summary

- In its life cycle, the generic family sedan:
 - consumes 961 GJ of energy
 - consumes 46,000 pounds of hydrocarbon
 - generates 130,000 pounds of carbon dioxide
- The operational stage:
 - consumes 86% of the LCE
 - generates 87% of the LC-CO₂, 94% of LC-CO, 90% of LC-NO_x and 62% of LC-SO_x
 - others
- The production stage:
 - consumes 14% of the LCE
 - generates 65% of particulates and 34% of LC-SO_x

Comparison to Previous Work

Study	Vehicle mass (Kg)	Fuel Efficiency	E_{pr}	E_{op}	E_{mn}	E_{tot}
Generic Vehicle	1532	23.6	118.2 ^d	821.9 (86.0%) ^a	16.6	957
Sullivan & Hu	1395	24.3	80.8	788 (89.1%)	15.5	884
Schuckert et al ^b	1040	29.1	70	612 (89.7%) ^c	----	682

^a Percentage of total

^b Results adjusted to 120,000 miles lifetime distance.

^c Gasoline fuel production burdens have been added to the operational life cycle stage

^d Adjusted for gasoline energy content for a full tank.

- Differences in E_{op} (34 GJ) are due to different fuel production and vehicle fuel efficiencies
- E_{pr} equal to 80.8 becomes 106.8 when an offal burden energy, a corrected E_{assm} , and vehicle weight adjustments are applied.
- For energy, the two studies are in good accord
- However, the generic vehicle study is much more comprehensive.

Results Reliability

- For energy, hydrocarbon, carbon dioxide , and carbon monoxide, they are quite good.
- For NO_x, SO_x, and particulates, they are also expected to be quite good
- For other emission, they are expected to be good estimates
- Results reliability generally depends on category, system or the material in question

Gratitude

- The OEMs want to thank our Material Industry Partners for their support in this endeavor.
 - They are: Aluminum Association, American Iron and Steel Institute, and the American Plastics Council
 - This study was about the generic family sedan and not aluminum, plastics, or steel.
- In cash and sweat equity, this study cost around \$2.7 million to complete.
- The project is the first of its kind:
 - It is a landmark study.
 - Four competing industry groups successfully worked together, agreed on a methodology and procedures, and published results.
 - Many of the results apply to other product systems

**USE OF A WEBSEM
(REMOTE SCANNING ELECTRON MICROSCOPE)
TO CHARACTERIZE AUTOMOTIVE
WEAR DEBRIS**

Stephen K. Kennedy

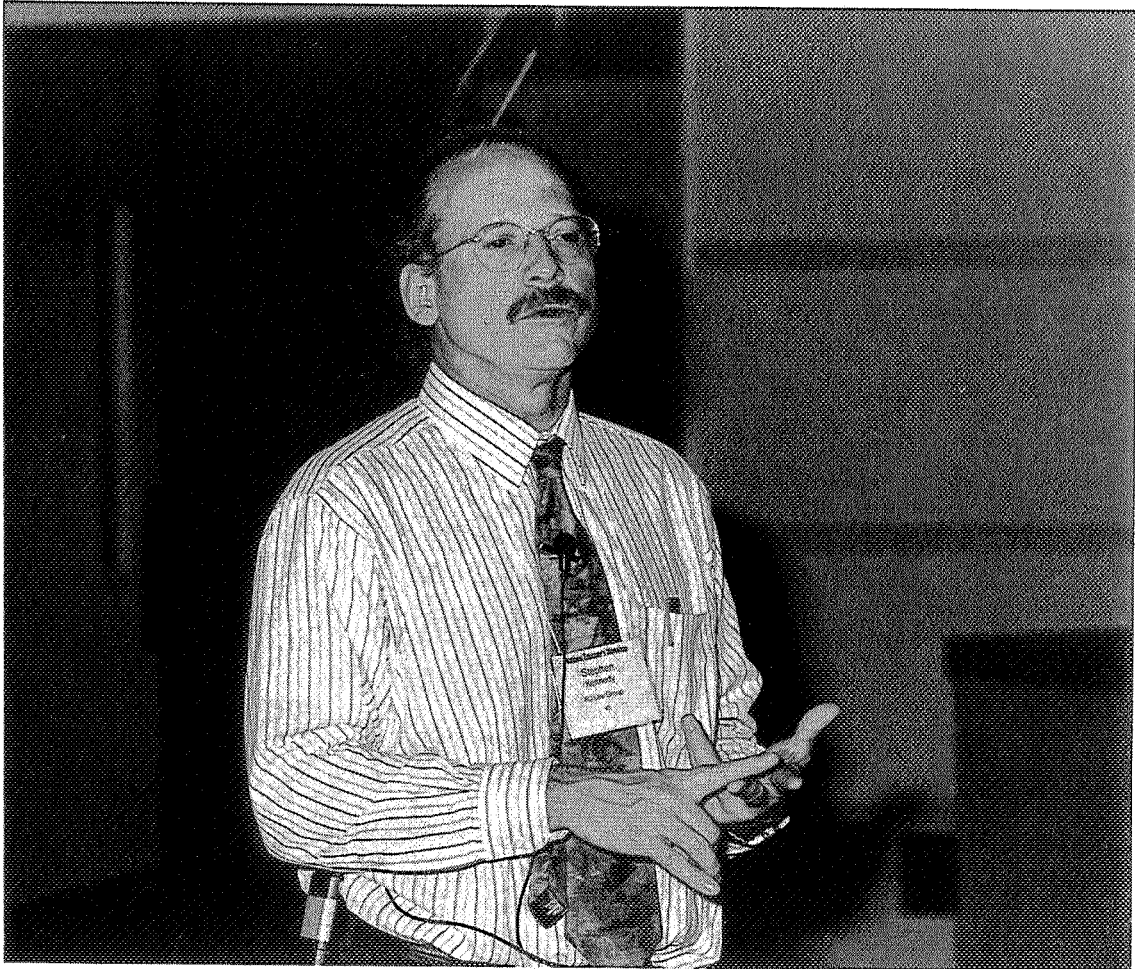
RJ Lee Group, Inc.
350 Hochberg Road
Monroeville, Pennsylvania 15146

Telephone: 724-325-1776
e-mail www.rjlg.com

and

Michael Gaston

West Greene High School
RD 5, Box 36B
Waynesburg, Pennsylvania 15370



Stephen K. Kennedy

USE OF A WEBSEM (REMOTE SCANNING ELECTRON MICROSCOPE)
TO CHARACTERIZE AUTOMOTIVE WEAR DEBRIS

Stephen K. Kennedy, Ph.D., PG
RJ Lee Group, Inc.
350 Hochberg Road
Monroeville, PA 15146
e-mail: skennedy@rjlg.com

and

Michael Gaston
West Greene High School
RD 5, Box 36B
Waynesburg, PA 15370

Key Words

wear debris, oil filter, scanning electron microscope

Objectives

To illustrate characterization of wear particulate in automotive oil filters through the use of a remote scanning electron microscope.

Materials and Equipment

Used automobile oil filter from vehicle with known mileage
Large diameter pipe cutter
Razor blade knife
Hexane and 250 ml beaker
Hood, gloves and protective eyewear
Tweezers
Ultrasonic bath
Vacuum filtration system with polycarbonate filters
WEBSEM access

Introduction

Wear debris particulate is present in a wide variety of systems, (e.g., lubricating, cooling, hydraulic). Analysis of such particulate can be used in an ongoing program of wear monitoring to predict or prevent failure (in the field or in the design/testing stage), or can be used in post-failure determination of probable cause. Particle size and morphology help to assess mode of wear, and particle composition can assist in the identification of the component undergoing wear. Images obtained using a scanning electron microscope (SEM) can be used to characterize such features. In addition, the SEM with an energy dispersive spectrometer (EDS) is capable of determining elemental composition and can be used to identify source of debris. This model is relevant for use in education because modern SEMs are simple to use with point and click

interfaces, and students regard them as fun to operate. Furthermore, the Internet now permits the SEM to be operated from distant locations.

This laboratory model was developed as a cooperative exercise for high school and voc-tech students, and illustrates one example of using the SEM to characterize debris in automotive oil filter. This model can be modified to examine debris in other systems.

The Scanning Electron Microscope

How it works:

The SEM rasters a focused beam of electrons in an area resulting in the emission of secondary and backscattered electrons which can be used for imaging, and characteristic x-rays which can be used to determine elemental composition. Secondary electrons are ejected from inner shells of specimen atoms and images produced by them have a three dimensional aspect. Backscattered electrons are beam electrons that elastically rebound from the specimen. The brightness in backscattered electron images is proportional to the average atomic number and these images are useful for general phase differentiation. That is, a carbon-rich particle will appear relatively dark and an iron-rich particle will appear significantly brighter. The ejection of secondary electrons is accompanied by the emission of x-rays whose energy is directly related to the specific electronic configuration of the atoms in the sample and so are characteristic of the specimen elemental composition. The elements are identified using an energy dispersive spectrometer (x-ray analyzer). The combination of imaging and spot chemical analysis allows the size, morphology and composition of particulate to be determined.

Availability:

Although prevalent in research laboratories of academia and industry, few SEMs are available for student use. Universities generally reserve their use for faculty and graduate student research, and such instruments are *very* rare in colleges and high schools. Many of today's SEMs are digital and can be made amenable to remote operation. Remote access to the SEM (as well as other high cost digital instruments) would result in distributing the cost over a large number of users making it affordable to a broader number of potential users. One such instrument with remote capabilities is the RJ Lee Instruments PERSONAL SEM[®] (or PSEM[®]) and will be described for illustrative purposes.

In the remote mode, the SEM is referred to as the "host" and the "client" observes and controls the SEM using a personal computer connected by phone modem or higher rate line to the host. After dialing up the IP address for the host, the client logs in. At the host location, the samples are loaded into the sample chamber and the SEM is turned on and ready for operation. The client will see a screen where the left side contains controls and the right side shows the SEM image. The magnification and field location are selected and displayed on the left image. When the cursor is moved onto the left image, a rubber band box appears on that image and the contents of that box is displayed on the right image. The size and location of the rubber band box is controlled using the mouse. When the cursor is moved onto the right image, the EDS mode is activated. A point and click starts the collection of an EDS spectrum. Peaks are identified and labeled using keyboard commands. Images can be saved and later downloaded to the client.

An alternative to actual or remote access to the SEM is to review off-line the data that were collected on-line. Using available programs, particle images can be inspected to characterize size and morphology. Spectra with peaks labeled can be reviewed. Alternatively, unlabeled spectra may be provided and the student will be required to identify the elemental composition.

Background

Wear debris particles displaying a variety of morphologies and compositions are presented as examples in Figure 1. In each illustration, a low magnification image (100 to 230x) is shown in the upper left, a higher magnification image (280 to 2000x) is shown in the upper right, and an EDS elemental spectrum is shown below. Figure 1A and 1B are gold debris from a slip ring assembly. Figure 1C and 1D are lead and copper debris from a hydraulic break assembly. Figure 1E and 1F are from a common oil reservoir of a large construction tractor showing wear debris from a steering and transmission assembly respectively.

Experimental Procedure

The following tasks are performed by groups of two or three students. Data and/or samples can be archived to provide a data base from which additional conclusions can be derived.

Sample Preparation:

Use the large diameter pipe cutters to open the oil filter at the end near the threads. Use a razor blade knife to remove a small portion of the paper filter material; say 1 cm x 10 cm. Measure the area of the oil filter sample. Under a laboratory hood and using gloves and eye protection, place the filter sample in a 250 ml beaker with about 50 ml of hexane. Agitate using tweezers and an ultrasonic bath if available. For this experiment, we are only interested in the larger particles so carefully decant the hexane leaving the deposited particulate. Rinse several times until the hexane remains clear. Using vacuum filtration, filter the solvent through a pre-weighed polycarbonate filter. After the filter has dried weigh it to determine the weight of the particulate. Calculate the weight of particulate matter per unit area of oil filter. Mount the polycarbonate filter on an SEM stub and coat with carbon.

Sample Analysis:

Place the sample into the SEM using the backscattered electron imaging mode and select a field for analysis. For each particle in the field, measure its size and describe its general morphology. Collect an EDS spectrum, identify the elements present and summarize the composition. Save representative images and spectra as shown in Figure 2. Tabulate all data. Randomly select another field and repeat the analysis. Continue until a specified number of particles have been analyzed.

NOTE: If the available SEM has automated analysis capabilities (such as computer controlled or CCSEM), you may easily characterize 1000 particles in an hour or two.

Interpretation:

Group the particles into compositional classes such as those described in Figure 2. Figure 2A is a field view. Figure 2B is a 100 micrometer particle containing sulfur, calcium, phosphorus, magnesium, zinc, oxygen and carbon. This general particle type contains a variable amount of

carbon and comes in another morphology (Figure 2C). Metallic iron, lead and tin are shown in Figures 2D, 2E, and 2F respectively. Compare results among all student groups and modify the classification as needed. Combine results and determine the mean and standard deviation for particle size for each compositional group. Determine the number of particles per unit area of original oil filter sample for each compositional group.

Compare results for the filters for cars of various ages. Does the number or size distribution correlate with age? Relate the data to specific automotive components.

CCSEM Results

The manual SEM analysis is repetitive, relatively slow, but amenable to automation. The sample was analyzed by computer controlled methods (CCSEM). In this analysis, the particles larger than 5 micrometers were sized and imaged, and the EDS composition was determined. A total of 1492 particles were characterized in 2 hours and 15 minutes. A summary distribution by compositional class is given in Table 1 and a size distribution is given in Table 2.

Table 1 – Summary distribution by compositional class

Classes	#	Number %	Wt %
C/S/Ca/P	566	36.46	51.15
C-rich	551	38.89	22.77
S/Ca/P	64	4.03	6.64
Si-rich	59	3.76	2.15
Fe Metal	73	4.92	5.30
P/Ca/Mg	63	4.22	2.90
Ca/S	26	1.65	2.51
Misc.	43	2.76	3.56
Fe-bearing	22	1.51	1.16
Pb Metal	21	1.47	1.82
Sn-rich	3	0.26	0.01
Zn Metal	1	0.06	0.01
Totals	1492	100.00	100.00

Table 2 - Mass Percent by Average Diameter (microns)

Classes	Mass %	5.0	7.8	15.6	31.0	50.0	62.5	>>>
		-	-	-	-	-	-	
		7.8	15.6	31.0	62.5	100.0	125.0	
C/S/Ca/P	51.2	0.3	7.6	38.9	41.3	11.9	0.0	0.0
C-rich	22.8	1.6	9.1	33.2	44.4	11.8	0.0	0.0
S/Ca/P	6.6	0.1	13.6	47.7	38.6	0.0	0.0	0.0
Si-rich	2.2	0.8	17.2	57.6	24.3	0.0	0.0	0.0
Fe Metal	5.3	2.4	17.8	67.7	12.1	0.0	0.0	0.0
P/Ca/Mg	2.9	1.6	20.7	53.7	24.0	0.0	0.0	0.0
Ca/S	2.5	0.2	5.3	33.6	60.9	0.0	0.0	0.0
Misc.	3.6	0.8	16.1	30.7	52.4	0.0	0.0	0.0
Fe-bearing	1.2	2.1	24.2	73.7	0.0	0.0	0.0	0.0
Pb Metal	1.8	2.5	22.6	74.8	0.0	0.0	0.0	0.0
Sn-rich	0.0	100.0	0.0	0.0	0.0	0.0	0.0	0.0
Zn Metal	0.0	0.0	100.0	0.0	0.0	0.0	0.0	0.0
Totals	100.0	0.8	10.2	41.2	39.1	8.8	0.0	0.0

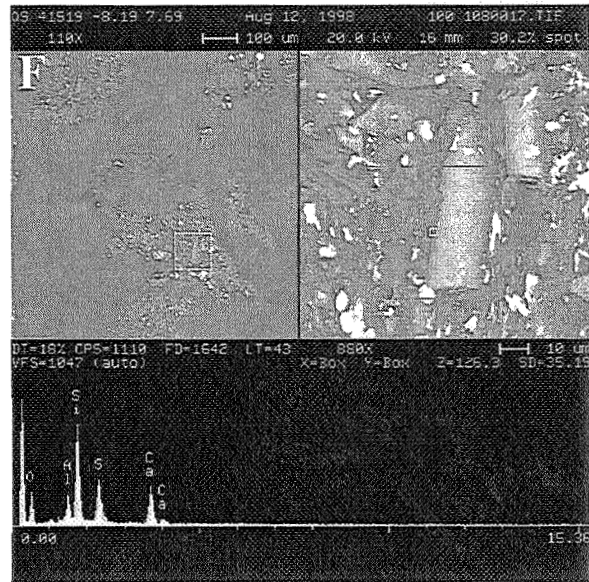
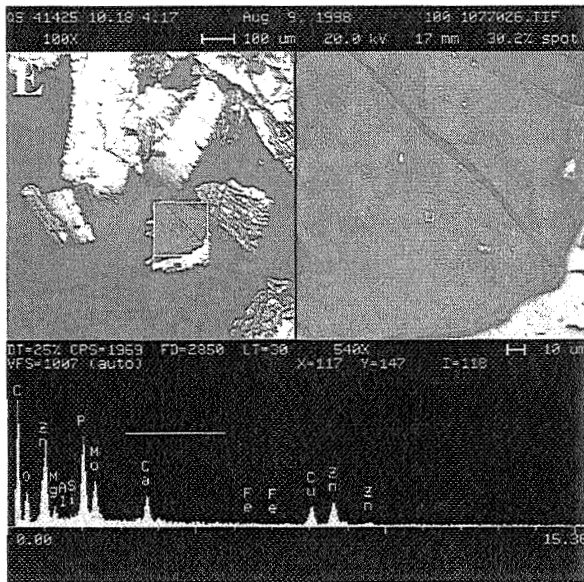
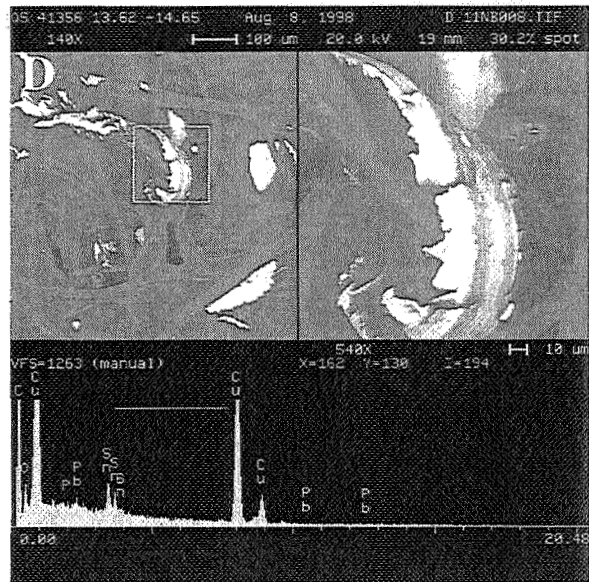
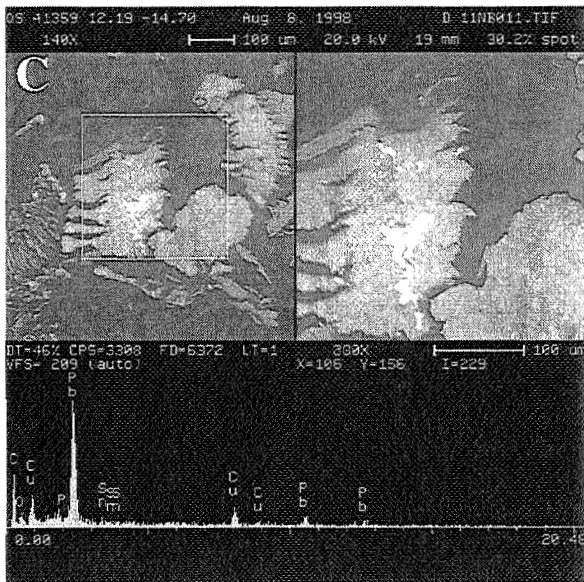
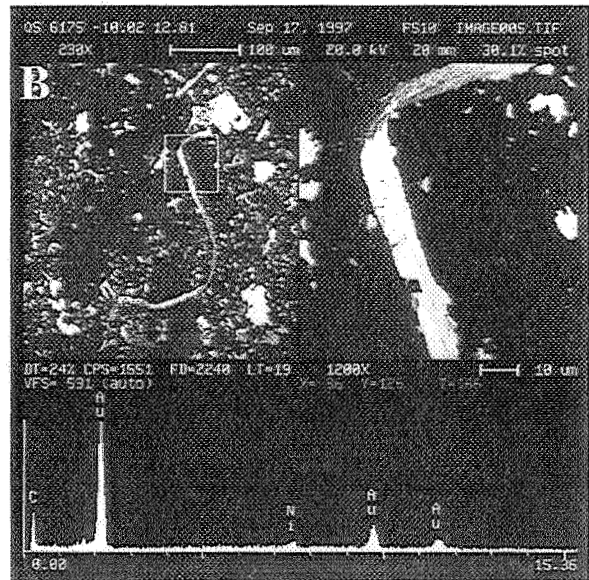
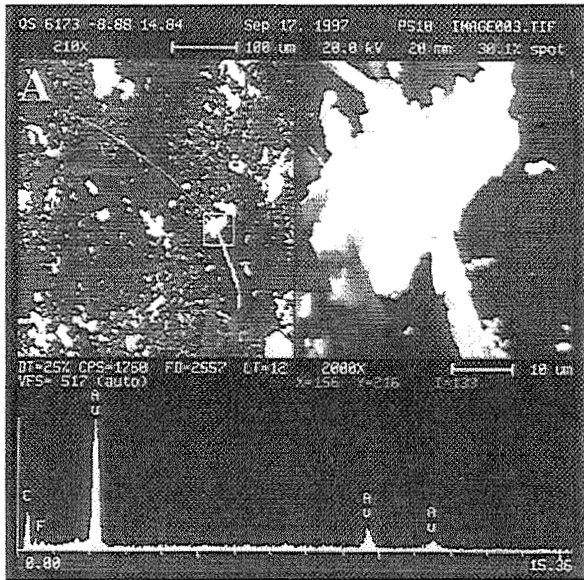


Figure 1 – Example wear debris

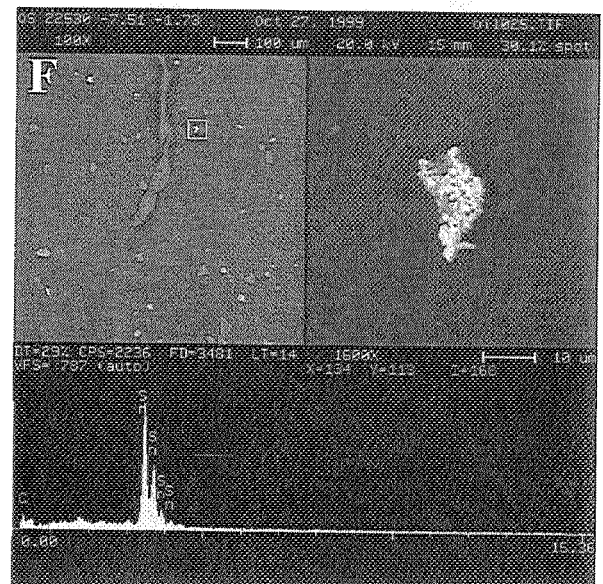
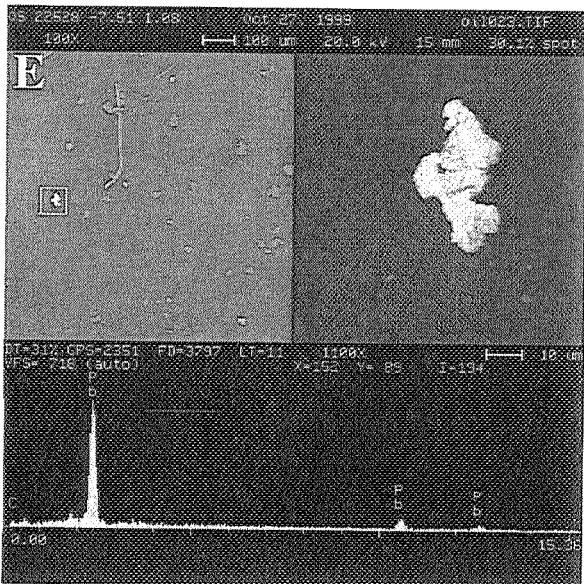
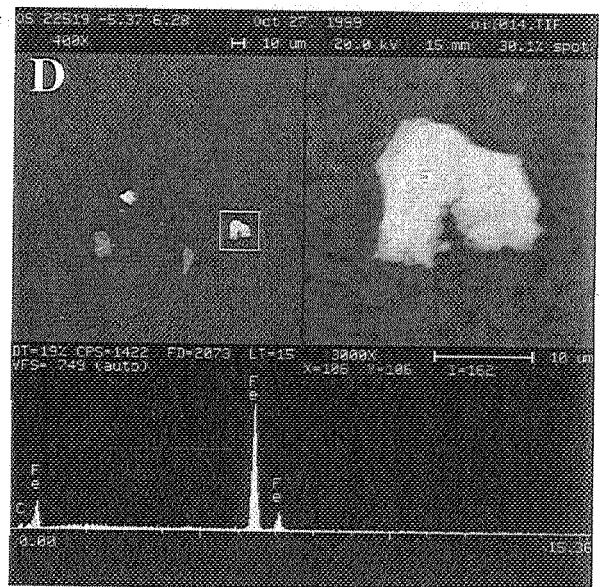
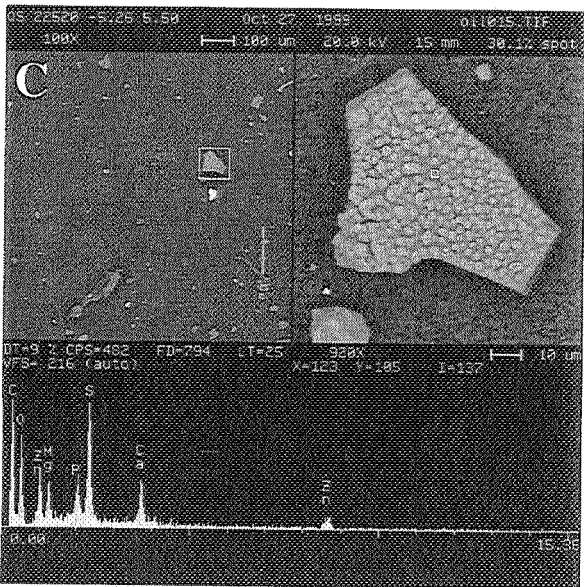
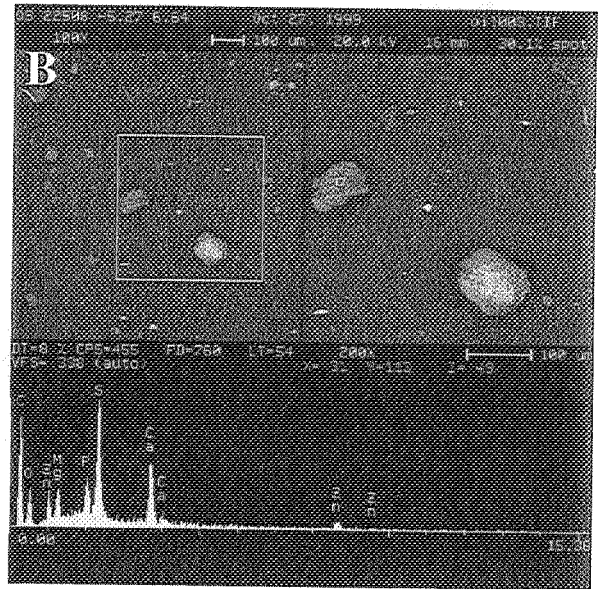
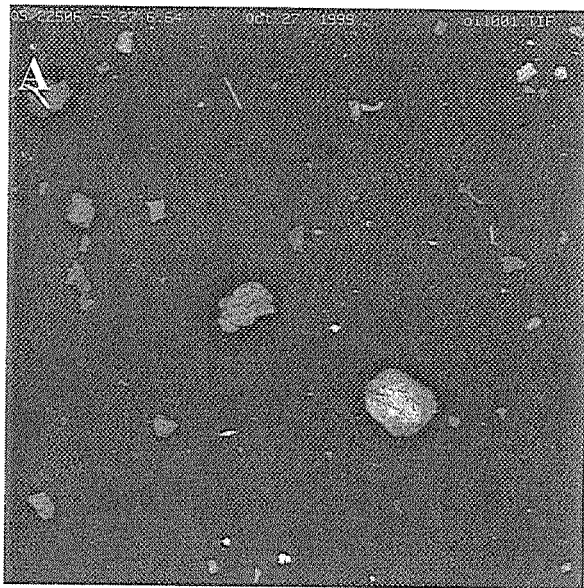


Figure 2 – Wear debris from automotive oil filter.

TEENAGED MATERIALS SCIENCE

Joanna Mirecki Millunchick

Department of Materials Science and Engineering
University of Michigan
2300 Hayward Street
Ann Arbor, Michigan 48109-2136



Joanna Mirecki Millunchick

Teenaged Materials Science

Joanna Mirecki Millunchick
University of Michigan



Michigan**Engineering**

Teenaged Materials Science

Joanna Mirecki Millunchick
University of Michigan



Michigan**Engineering**

- **One week day program on the University of Michigan campus for 7th and 8th grade girls interested in engineering, science and technology.**
- **Main activities**
 - **Ethics in Science**
 - **Web page design**
 - **Career Panels**
- **Focus groups**
 - **Physics Aerospace Physics Genetics**
 - **Materials Chemistry Biology Medicine**
- **Sponsored by**
 - **Women in Science and Engineering**
 - **Center for the Education of Women**
 - **GM Foundation**

Purpose: To introduce Materials Science to teens

Approach: Demonstrate how Materials issues impact their daily lives

Day One:

- Introduction
- Glass Labs

● **Day Two: Materials Science of Sports**

- Materials Issues in Sporting Equipment
- Hot Air Balloon Demo
- Bouncing Balls

● **Day Three: Materials Science of Make Up**

- Materials Issues in Cosmetics
- Nail Polish Formulation
- Testing of Commercial Products

- **Materials classes**
 - **Metals Ceramics Polymers**
 - **Composites Semiconductors**
 - **Demonstrations of mechanical behavior**
 - **F.X. Spiegel “Elasticity Plasticity and Anelasticity: Demonstrations,” National Educator’s Workshop: Update 96 and**
- F.X. Spiegel “Demonstrations in Materials Science from the Candy Shop,” National Educators’ Workshop: Update 94**
- **Glassblowing Demo- Harald Eberhart**
 - **Glass Blowing Experiments**
 - Supplies:**
 - **Soda lime glass tubes**
 - **Propane torch**
 - **Water bucket**
 - **Wood board**
 - **Safety glasses**

- **Materials Issues in Sporting Equipment**
 - **Questions for discussion:**
 - What is the function of different kinds of sporting equipment?
 - What materials fit that function?
 - **Examples:**
 - Softball bats
 - Skis
 - Balls
 - Protective gear
- **Hot Air Balloon Demo**
 - **Set up, inflate, and fly a hot air balloon!**
Keith McIntyre- Wind Drifters Inc.

- **Materials Issues in Cosmetics**

- **Questions for discussion:**

- **What is the function of different kinds of cosmetics?**
 - **What materials fit that function?**

- **Demos:**

- **Miscibility**
 - **Surfactants**
 - **Emulsions**
 - **Colloids**

- **Nail Polish Formulation**

- Supplies:

- Nitrocellulose
 - Butyl Acetate
 - Pigment
 - Beakers
 - Mortar and Pestle
 - Eye droppers
 - Bottles

- **Testing of commercial vs homemade nail polish**

- Adhesion tests
 - Wear tests
 - Examination under the SEM

- **Examination of Commercial Cosmetics**

- Lipstick
 - Mascara
 - Foundation

- **WISE/CEW Facilitators**
 - Cinda Sue Davis
 - Margaret Krasnoff
- **Materials Science Personnel**
 - Laraba Kendig, Instrument Analyst
 - Keith McIntyre, Facilities Engineer and Balloon Pilot
 - Harald Eberhart, Master Glass Blower
 - Kevin Worth, Computer Systems Specialist
 - Mike Johnson, Graduate Student
 - Chris Reilly, Graduate Student
 - Ruth Cleveland, Graduate Student
 - Karmen Lappo, Undergraduate Student

INTRODUCTION TO EMSET2

James A. Jacobs

Norfolk State University
700 Park Avenue
Norfolk, Virginia 23504-8060

Telephone 757-823-8109
e-mail jajacobs@nsu.edu

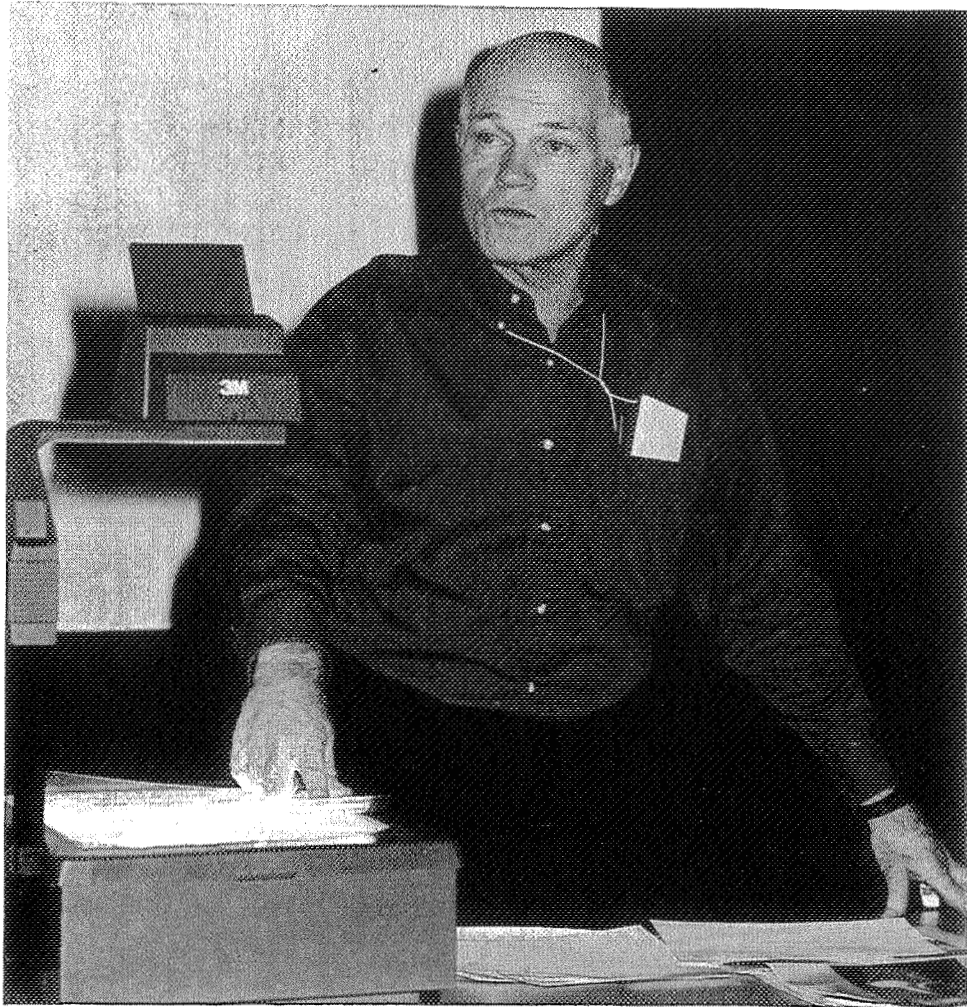
Alfred E. McKenney

516 Fairfax Way
Williamsburg, Virginia 23185

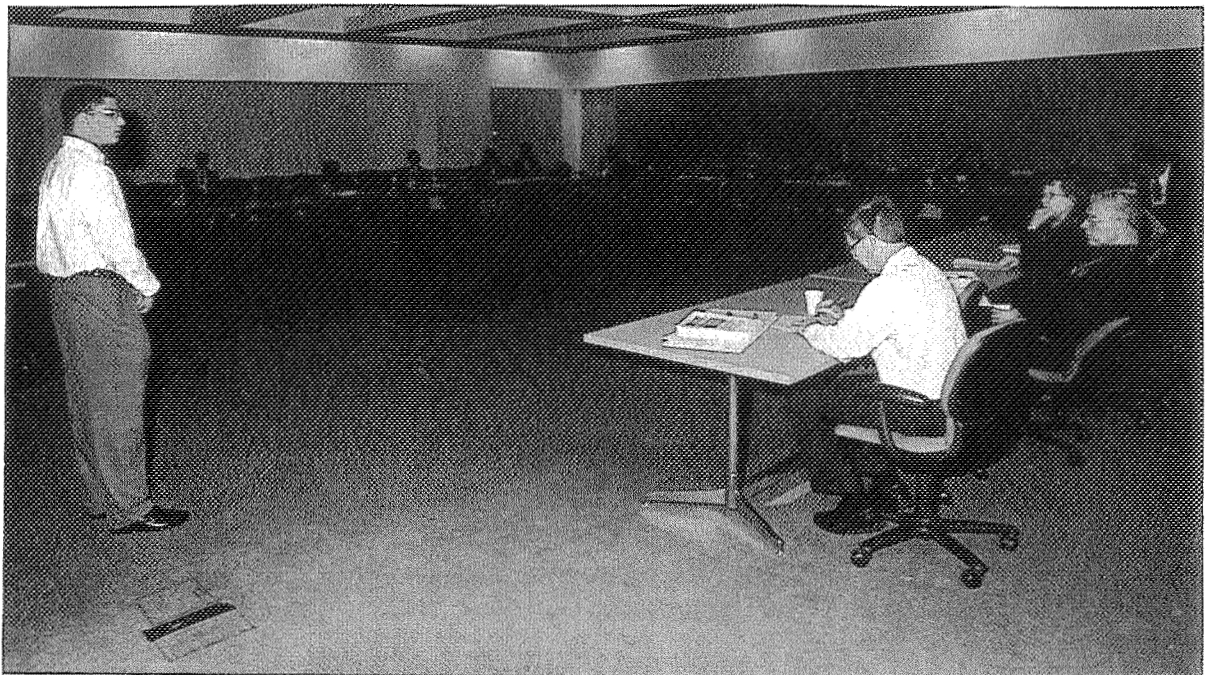
Telephone 757-221-0476
e-mail aem2@prodigy.net

Matthew Sanders
(student)

Norfolk State University
700 Park Avenue
Norfolk, Virginia 23504-8060



James A. Jacobs



Introduction to **EMSET2**

Getting Started

Additional Resources

Experiments & Demonstrations

Twelve Years of Experiments and Demonstrations from the National Educators' Workshops



(Main)

[Return to Main Menu](#)

- 1. Structure, Testing & Evaluation**
- 2. Metals**
- 3. Polymers**
- 4. Ceramics**
- 5. Composites**
- 6. Electronic & Optical Materials**
- 7. Materials Curriculum**



(TOC)

EXPERIMENTS AND DEMONSTRATIONS IN STRUCTURE, TESTING AND EVALUATION

MEASUREMENT OF SPRINGBACK ANGLE IN SHEET BENDING

J. Hilden, K. Lewis, A. Meamaripour and Guna Selvaduray San Jose State University

EFFECT OF TEMPERATURE ON WETTING ANGLE

Richard Brindos and Guna Selvaduray - San Jose State University

TRANSPIRATION COOLING EXPERIMENT

Kyo D. Song and Heidi R. Ries - Norfolk State University and
Stephen J. Scotti and Sang H. Choi - NASA Langley Research Center

THE APPLICATION OF COMPUTERS TO THE DETERMINATION OF CORROSION RATES FOR METALS IN AQUEOUS SOLUTIONS

R. B. Griffin, L. R. Cornwell, and Holly E. Ridings - Texas A&M University

EXPERIMENTS SHOWING DYNAMICS OF MATERIAL INTERFACES

Robert F. Benjamin - Los Alamos National Laboratory

FROM RUGS TO DEMONSTRATIONS IN ENGINEERING MATERIALS CLASS

Neda S. Fabris - California State University

HYSTERESIS LOOPS AND BARKHAUSEN EFFECTS IN MAGNETIC MATERIALS

Luke Ferguson and Thomas Stoebe - University of Washington

ELASTICITY, PLASTICITY AND ANELASTICITY: DEMONSTRATIONS.

F. Xavier Spiegel - Spiegel Designs

RELAXATION AND RESISTANCE MEASUREMENTS

Daniel W. Koon - St. Lawrence University

THE EFFECT OF SURFACE FINISH ON TENSILE STRENGTH

Julie Chao, Selene Currotto, Cameron Anderson, and Guna Selvaduray - San Jose State
University

A MAGNETIC DILEMMA: A CASE STUDY

F. Xavier Spiegel - Spiegel Designs

TENSILE TEST EXPERIMENTS WITH PLASTICS

Michael G. Thorogood - Norfolk State University

A "PROBLEM BASED LEARNING" APPROACH TO REFLECTION AND REFRACTION

Amy Wilkerson, Donna Self, Waldo J. Rodriguez, and Heidi R. Ries - Norfolk State Univ

EXPERIMENTS AND DEMONSTRATIONS IN COMPOSITES

COMPOSITE OF GLASS FIBER WITH EPOXY MATRIX

Ping Liu and Tommy L. Waskom - Eastern Illinois University

STRENGTH TESTING OF COMPOSITE MATERIALS

John and Eric Cadwell and Steven Piippo - Richland High School

EFFECTIVENESS OF ULTRASONIC TESTING METHOD IN DETECTING DELAMINATION DEFECTS IN THICK COMPOSITES

Glen C. Erickson - Ground Systems Division and
W. Richard Chung - San Jose State University

COMPOSITES: FIBERGLASS HAND LAMINATING PROCESS

James A. Nelson - Battelle, Pacific Northwest Laboratories

THE ASSESSMENT OF METAL FIBER REINFORCED POLYMERIC COMPOSITES

Wenchiang R. Chung, San Jose State University

SIMPLE STRESSED-SKIN COMPOSITES USING PAPER REINFORCEMENT

L. R. Bunnell - Battelle Pacific Northwest Laboratories

FIBER REINFORCED COMPOSITE MATERIALS

Harvey A. West and A. F. Sprecher - North Carolina State University

COMPOSITE COLUMN OF COMMON MATERIALS

Richard J. Greet - University of Southern Colorado

CONTINUOUS UNIDIRECTIONAL FIBER REINFORCED COMPOSITES: FABRICATION AND TESTING

M. D. Weber, Pennsylvania State University, F. X. Spiegel, Loyola College, and Harvey
A. West, North Carolina State University

USING TEMPLATE/HOT-WIRE CUTTING TO DEMONSTRATE MOLDLESS COMPOSITE FABRICATION

Mario J. Coleman

FABRICATION AND EVALUATION OF A SIMPLE COMPOSITE STRUCTURAL BEAM

Myron J. Schmenk - Miami University

MECHANICAL PROPERTIES OF COMPOSITE MATERIALS

H. Richard Thornton and L. R. Cornwell - Texas A&M University

Composite of Glass Fiber with Epoxy Matrix

Ping Liu and Tommy L. Waskom
School of Technology
Eastern Illinois University
Charleston, IL 61920

Key Words: Epoxy, glass fiber, laminate.

Prerequisite Knowledge: Thermoset plastics, polymeric matrix composite, reinforcement fibers.

Objective:

1. Understand the concept of composite materials by combining two or more different materials to obtain a new material.
2. Examine the process of making composites using the simplest method: hand lay-up.

Equipment and Materials:

1. Fiberglass
2. Scissors
3. Epoxy resin (two part kit)
4. Paper measuring cups, 4-6 oz.
5. Brush (1 in.)
6. A polyethylene sheet, 8 x 36 in.
7. Acetone
8. Disposable stirring sticks
9. Plastic gloves

Introduction:

Polymeric matrix composites have found wide applications in products such as airplanes and even fishing rods. Epoxy is the most often used matrix and glass fiber is the most economical reinforcing fibers on the market. Glass fiber reinforced epoxy matrix composites are popular composites used for such products as racing boats.

In this experiment, students used a simple hand lay-up method to make the composite. Students are encouraged to apply their innovative ideas to make the material with the highest specific strength.

Procedure:

!!! Wear Safety goggles before the experiment.

1. Cut five 2" x 30" fiberglass strips with scissors.
2. Weigh the batch of strips to be used in the composite.
3. Approximately 2 oz of epoxy resin is needed for this experiment. Follow the directions on the back of the resin can, measure the ingredients into a paper cup. Thoroughly mix contents with a stirring stick for 3-5 minutes.
4. Place a polyethylene sheet on table top to protect the table.
5. Pour a small amount of resin onto the polyethylene sheet surface. *Note:* resin does not stick to polyethylene. Spread with brush to an area of 2" x 30".
6. Place one fiberglass mat on the resin.
7. Dip brush into resin. Paint the resin into the fiberglass mat by gently stroking the brush over the fiberglass. Begin brushing in the middle, and stroke toward the outer edges. The fiberglass will absorb the previously poured resin. Apply only enough resin with the brush to saturate the fiberglass.
8. Place second fiberglass mat (dull side up) onto the first layer. Apply resin with brush, working from the center out to prevent air bubbles. Add only enough resin with the brush to wet or saturate the fiberglass.
9. Repeat the process with each additional fiberglass laminate.
10. Upon completion, place brush into empty cup
11. Cover the fiberglass laminate with a polyethylene sheet. Apply a flat weight onto the laminate using books, wood or metal slab.
12. Observe the contents of the cup and brush to verify that the resin is curing. The cup will feel warm from an exothermic reaction that is taking place. An odor will be increasingly noticeable as a chemical reaction occurs.
13. Clean the brush with acetone. Discard the cup and clean the table top
14. Let the composite cure until rigid.
15. Measure a final weight of the composite, record the weight in a log book.

Instructor's Notes on Competition Rules:

1. Each group will submit three specimens for the competition.
2. The laminated specimen will be tested for cantilever bending strength,
3. Load will be applied by pouring sand into a bucket until the specimen is bent to break. The maximum load will be recorded for each specimen.
4. The maximum load will be divided by the weight of the specimen, to obtain specific loading capacity (or specific strength) for each specimen.
5. The average of the three results in terms of specific loading capacity will be used for each team.
6. The score for each group was used as follows.

First place:	100
Second place:	95
Third place:	90
Fourth place:	85
No show:	0

Supplier:

1. Most of the consumables can be purchased from the following vendor:

Industrial Arts Supply Co. (IASCO)
5724 West 36th Street
Minneapolis, MN 55416-2594
1-800-328-4827, Ext. 2662

2. Acetone can be purchased from any painting store or paint department at Wal-Mart.
3. Polyethylene sheets and stirring sticks (craft department) are available at Wal-Mart.

References:

1. A. B. Strong, Fundamentals of Composite Manufacturing, Society of Manufacturing Engineers, Dearborn, MI (1989).
2. Materials Science and Technology Handbook, Pacific Northwest Laboratory, pp 8.1-8.11.

Structural
Laboratory
Manual

Dr. Jack Kayser

Lafayette College

1997

INDEX

<u>Experiment</u>	<u>Topic</u>	<u>Page</u>
1	Properties of Metals in Tension	3
2	Evaluation of Bolts and Bolted Connections	6
3	Flexural Beam Test	10
4	Compressive Strength of Columns	13
5	Evaluation and Testing of Welded Connections	16
6	Material Properties of Balsa Wood	20
7	Selecting Proportions for Normal Weight Concrete	24
8	Mixing, Testing and Casting of Fresh Concrete	36
9	Mechanical Properties of Concrete	41
10	Batching and Testing of Mortar Specimens	46
11	Testing and Evaluation of Coarse Aggregate	50

Experiment 1: Properties of Metals in Tension

References:

ASTM E-6 Standard Definitions of Terms Relating to Methods of Mechanical Testing

ASTM E-8 Standard Test Methods of Tension Testing of Metallic Materials

“Structural Steel Design LRFD Method,” Jack McCormac, 2nd Ed., Section 1-7

Description:

Two of the most important items involved in the engineering of a structure are the deflections the structure will undergo when loaded, and the amount of load the structure can take before failing. These two fundamental measures of performance depend upon the behavior of the material the structure is composed of.

This experiment examines the behavior of metals in tension. Steel, aluminum, and cast-iron specimens will be tested. The following outline describes the properties which will be studied.

1. Stress-Strain Diagram: A plot of the stress-strain values which were recorded during a tension test. The plot will be created using the data file which was down loaded from the Instron computer, modified and plotted using Quattro.
2. Ductility Based on Reduction of Area: The ability of the material to deform plastically. It is calculated as the ratio of the change in cross sectional area due to rupture divided by the original cross sectional area. Units of percent.
3. Ductility Based on Elongation: Another way of measuring the ability of a material to deform plastically. It is calculated as the ratio of the change in gage length due to rupture divided by the original gage length. Units of percent.
4. Tensile Strength: The maximum tensile stress that can be applied to a specimen. It is based on the ratio of ultimate load divided by the original cross section. Units of ksi.
5. Modulus of Elasticity: The ratio of stress over strain in the linear elastic region of the stress-strain diagram. Units of ksi.
6. Yield Strength: The stress level beyond which the material will permanently deform. In some materials this limit is defined by using the 0.002”/” strain offset. Units of ksi.
7. Modulus of Resilience: The energy absorbed by a specimen when it is loaded to its proportional limit. It is the area under the stress-strain diagram from zero to the proportional limit. Units of ksi.
8. Modulus of Toughness: The energy absorbed by a specimen when it is loaded to the point of rupture. It is the area under the stress-strain diagram from zero to the point of rupture. Units of ksi.

Name: _____

Date: _____ Section: _____

Experiment 1 Data Sheet

Specimen 1

Material: _____

Initial Diameter: _____

Gage Length: _____

Final Diameter: _____

Final Gage Length: _____

Specimen 2

Material: _____

Initial Diameter: _____

Gage Length: _____

Final Diameter: _____

Final Gage Length: _____

Specimen 3

Material: _____

Initial Diameter: _____

Gage Length: _____

Final Diameter: _____

Final Gage Length: _____

Specimen 4

Material: _____

Initial Diameter: _____

Gage Length: _____

Final Diameter: _____

Final Gage Length: _____

EMSET CD ROM
EXPERIMENTS IN MATERIALS SCIENCE, ENGINEERING & TECHNOLOGY
ISBN: 0-13-648486-7

James A. Jacobs

A Multimedia Tool of Laboratory Experiments and Classroom Demonstrations

FEATURES:

- Over 200 laboratory experiments and classroom demonstrations which you can modify to suit your teaching objectives, environment, and students' needs.
- Access to instructional aids developed by hundreds of materials educators and industry specialists in the field of materials science, engineering and technology.
- Provides students with "hands-on" activities that cover the full range of materials science and technology: topics such as woods, metals, and emerging technologies including processing and structures of advanced composites and sol-gel ceramics.
- Flexibility: emphasis is placed on low-cost, multi-concept exercises in recognition of the many settings in which materials education occurs.
- The CD-ROM allows you to read, navigate, search for other experiments/documents, print, and edit.

CATEGORIES OF EXPERIMENTS:

TESTING & EVALUATION, POLYMERS, METALS, CERAMICS, COMPOSITES, ELECTRONIC MATERIALS & MATERIALS CURRICULUM

A BONUS CD OF VIDEO CLIPS:

A bonus CD provides video segments on selected concepts.

STM & AFM MICROSCOPY, POLYMERS, CERAMICS, AND COMPOSITES

PLATFORMS SUPPORTED:

This CD-ROM can be used on Windows and Macintosh platforms. Acrobat Reader and QuickTime software is included on the disk for Windows 3x, Windows 95 and Macintosh. The disk may be used on other platforms provided the appropriate software is installed.

TO ORDER A COPY

Call: 1 (800) 947-7700 OR Visit our web site: www.prenhall.com

OR simply fill out and mail this to:

Prentice Hall, Order Processing Dept.
200 Old Tappan Road, Old Tappan, NJ 07675

Date _____

P.O. Number _____

Tax Exempt Cert. No. _____

BILL TO:

Account No. _____

Name _____

Dept. _____

School/Org. _____

Address _____

City _____

State, Zip _____

SHIP TO:

Cust. Key No. _____

Name _____

Dept. _____

School/Org. _____

Address _____

City _____

State, Zip _____

CD-ROM Price: \$150.00

**A METHOD FOR THE MEASUREMENT OF
MAGNETOSTRICTION IN FERROMAGNETIC
ALLOYS**

O. Garcia-Hernandez

R. Galindo

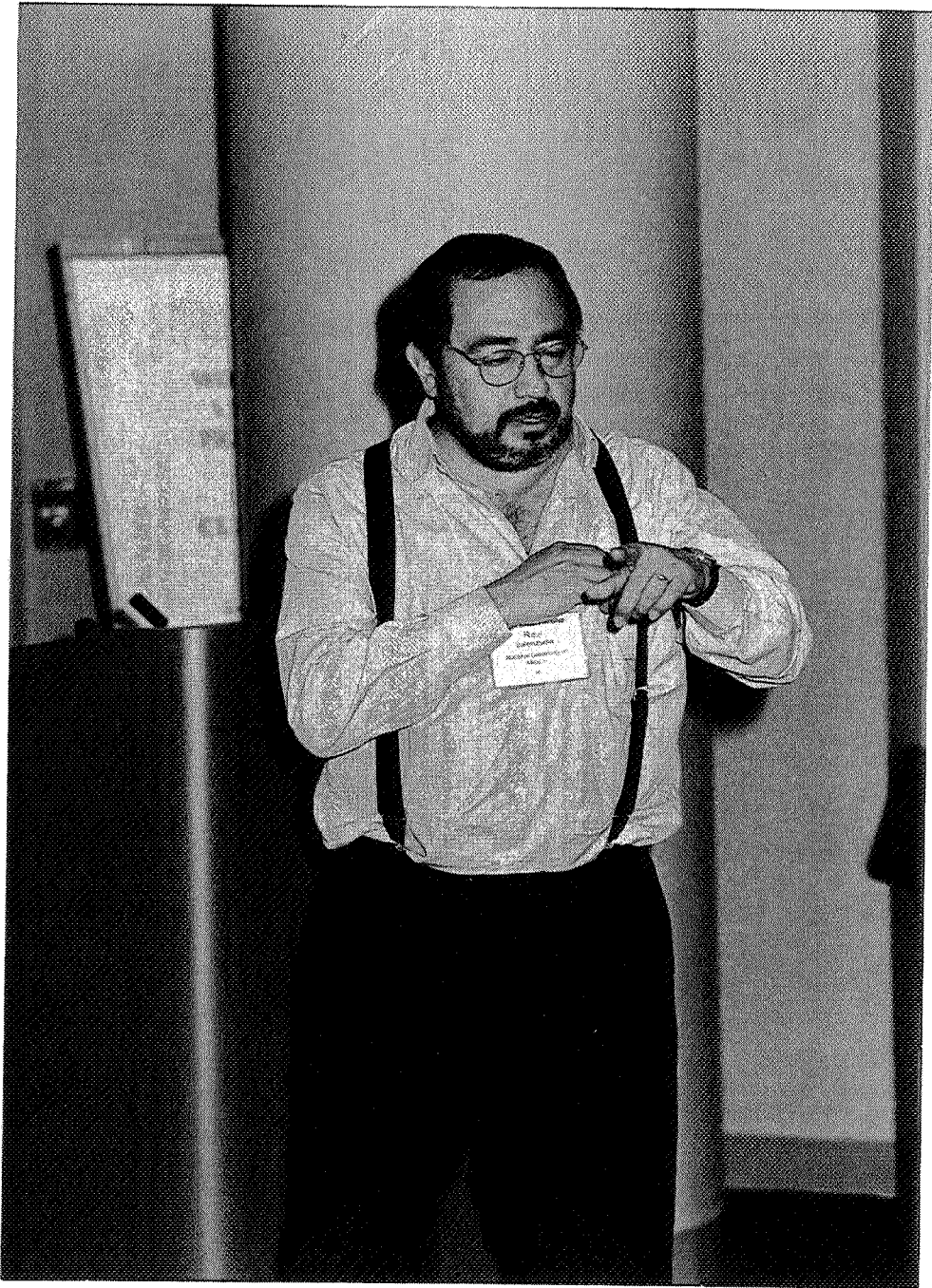
K. L. Garcia

and

R. Valenzuela

Institute for Materials Research
National University of Mexico
P. O. Box 70-360
Mexico 04510

Telephone: 525-622-4653
e-mail monjaras@servidor.unam.mx



R. Valenzuela

A Method for the Measurement of Magnetostriction in Ferromagnetic Alloys

O. García-Hernández¹, R. Galindo², K.L. García and R. Valenzuela^{1,*}
National University of Mexico P.O. Box 70-360, Mexico D.F., 04510 Mexico
¹Institute for Materials Research, ²Faculty of Chemistry

Key Words: Ferromagnetism, Magnetostriction

Prerequisite Knowledge: Have the basic notions about magnetically ordered materials (ferromagnetism), magnetization, magnetic hysteresis, domains, domain walls.

Objective: To obtain ferromagnetic hysteresis loops, observe the effects of mechanical stresses on them, and thereby understand the interaction between magnetic and elastic energies; finally, to evaluate the magnetostriction constant.

Equipment:

1. A standard oscilloscope (we used a Hameg® HM-205-3).
2. Two primary coils 150 turns each; for our experiments, they were solenoids 2 cm diameter and 14 cm long, made of 85 mm copper wire.
3. Two secondary coils 600 turns each; they were directly coiled on the primary coils, and made of 85 mm copper wire.
4. Electronic components to fabricate an integrator circuit, as follows: an integrated circuit IC μ A 741 CN, a 0.33μ f capacitor, and resistors of $1 \text{ M}\Omega$, $6.8 \text{ k}\Omega$, $15 \text{ k}\Omega$, 560Ω , and 50Ω ; all of them with a dissipation of 0.25 W , except for the latter, which has a dissipation energy of 100 W .
5. A weight and pouly system to apply tensile stress on measuring samples. The system here detailed is planned for ferromagnetic materials with the shape of ribbons. The sample is clamped on its two ends; one end is fixed to the table, and the other one is clamped to a wire which, through a pulley, allows the addition of weights to control the tensile stress. The sample should be placed within one of the coil systems in order to apply simultaneously the magnetic field and the tensile stress.
6. A Variac to control the electric current flowing through the primary circuit.
7. Micrometer or vernier caliper.
8. A photographic camera with a tripod to obtain images of hysteresis loops from the oscilloscope screen.
9. The use of the Origin™ program is recommended for plotting and slope calculations. However, due to the usual small number of points, all plots and calculations can easily be made by hand.

Introduction:

The magnetization process, i.e. the change of magnetization state of a ferromagnetic material from the demagnetized state ($M = 0$) to the maximum magnetization value (saturation magnetization, M_s) under a magnetic field, H , involves a change in the dimensions of the sample. These changes are very small (usually a few parts per million), but they can be important in many aspects. For instance, the most common manifestation of this phenomenon is the "humming" from transformers, where the core is submitted to an *ac* current that magnetizes and demagnetizes it (at a rate twice the current frequency).

Since the core dimensions change with the change in magnetization state, it "vibrates" at twice the current frequency. These vibrations can easily be heard near a transformer.

The saturation magnetostriction constant, λ_s , quantifies these changes, and is defines as:

$$\lambda_s = (L - L_0) / L_0 \quad (1)$$

where L_0 is the initial length of the sample in the demagnetized state, and L the length in the magnetically saturated state, both in the same direction than the applied field, as shown in Fig. 1. λ_s is adimensional and can be positive when the material stretches during magnetization; or negative, when it shows a contraction in the field direction.

A simple model to explain magnetostriction is to recall that ferromagnetic materials involve the presence of atoms with incomplete 3d orbitals, since these orbitals have unbalanced spins, as well as the possibility of strong interactions leading to magnetic order. Due to the spin-orbit coupling, the orientation of spins and that of 3d orbitals is related. When a change in direction occurs (as a consequence of an applied field), the change in orientation of 3d orbitals is associated with an increase in length, as shown in Fig. 2. To explain a negative magnetostriction constant, this model can also be used, simply by changing the spin orientation to the minor axis direction. The magnetoelastic energy can be calculated [1] as the work done by rotating the magnetization vector by an angle θ against the opposition of a tensile stress σ as:

$$E_{ME} = (3/2) \sigma \lambda_s \sin^2 \theta \quad (2)$$

In most ferromagnetic materials, the total magnetic energy is reduced to a minimum by the formation of domains, separated by domain walls to retain all the magnetic flux inside the sample, Fig. 3 (a). Domains disappear when a strong magnetic field is applied, leading to the saturated state, Fig. 3 (b). The magnetization process, from 3 (a) to 3 (b), involves the displacement of domain walls to promote the growth of domains with the same orientation than the applied field, and the decrease of domains with the opposite orientation. This process involves some energy dissipation, since domain wall displacements proceed by spin rotations and this needs energy. Also, any structural defect in the sample represents an obstacle to domain wall movement, and energy is needed to displace domain walls through them. Domain wall displacement is therefore an irreversible process, leading to hysteresis loops. Here, the magnetization value depends on the path followed; the hysteresis loop is described in one direction. The total energy needed to describe the hysteresis loop is simply the area encompassed by the loop, or

$$E_m = \int H dM. \quad (3)$$

In the demagnetized state, there are domains in all the orientations that compensate each other (the global magnetization is zero), and therefore the differences in length associated with the orientation in 3d orbitals also compensate each other. However, when the sample is saturated, there is no longer compensation since all spins are oriented in the same direction, and the expansion due to the assymetry in 3d orbitals becomes additive, producing a macroscopic increase in length.

Basis of the Measurement:

Since the expansion due to magnetization is small (λ_s typically ranges between 10^{-8} to 10^{-6}), a direct determination of magnetostriction constant is difficult. An alternative method consists in the measurement of hysteresis loops under different values of applied stress. If all the other parameters are kept constant, the differences in loop area, A , depend only on the magnetoelastic energy, and therefore can be evaluated by

$$\Delta A = \Delta E_{ME} = (3/2) \Delta \sigma \lambda_s \quad (4)$$

The magnetostriction constant can then be determined from measurements of hysteresis loop area as a function of applied stress.

Electric Circuit

The electric circuit is shown in Fig. 4 and is formed by a Variac connected to the mains ($f = 60$ Hz); a high dissipation resistor (1 k Ω) in series provides a voltage proportional to the current, which is connected to the X-axis of the oscilloscope. The sample is placed inside a primary coil (solenoid with 150 turns). An identical primary coil is connected in series. A secondary coil (600 turns, on the primary coil) "receives" the magnetic flux produced by the sample (and the primary coil) and feeds this voltage into an integrator circuit (741 OpAmp), which in turn, is connected to the Y-axis of the oscilloscope, Fig. 5. The secondary coil is also connected to another secondary coil in phase opposition, to compensate the effects of empty coils and have only the sample effects. All the component values are indicated in Fig. 4.

To calculate the absolute values of magnetic field, H , (X-axis in the oscilloscope) and magnetic induction, B , (Y-axis of oscilloscope), we use the following equations:

$$H = n_p v_p / R_p S \quad (5)$$

$$B = R C V_a / n_s t x \quad (6)$$

Where n_p is the number of turns in the primary coil, v_p is the voltage across the series resistor R in the primary circuit, and S is the length of the coil; R and C are the resistor and capacitor, respectively, in the integrator circuit, V_a is the integrated voltage, n_s is number of secondary coil turns, t is the sample thickness and its x width.

Preparation:

Once all the electric connections have been done, fix the one end of the sample to the support on the table, Fig. 5. Then, place it in one of the primary-secondary coil systems. The sample should have a maximum length of 12 cm, in order to be completely contained within the coil system. At the other end of the sample, fix the plastic wire to apply the tensile stress.

A first step is to fix the applied field level to have a magnetized state close to saturation. This is easy to monitor on the oscilloscope, when the ends at maximum field show a quasi-horizontal line.

Procedure:

1. Fix a convenient level of applied field. A low field leads to a magnetized state far from saturation, producing an incomplete change of dimensions in the sample. On the other hand, an excessive field can produce heating on the dissipation resistors in the primary coil circuit. As a simple rule of thumb, the quasilinear part should not be larger than the width of the loop.
2. Adjust the X- and Y- axis gain of the oscilloscope to have the hysteresis loop on most of the screen, to facilitate loop area measurements. Register these values as G_x and G_y .
3. Take a photo of the $\sigma = \text{zero}$ loop (see Fig. 6)
4. Put a small weight on the pulley system to apply a stress on the sample and observe the loop. If the change is not noticeable, add another weight.
5. When you obtain a small but noticeable change in the loop, take another photo (see Fig. 6). Register the weight.
6. Add some more weight, and repeat the process. Be careful with weights, since samples can fail and weights fall!
7. Usually, four to five points are enough to find a clear linear behavior and determine the slope.
8. On photo prints, measure the loop areas (a simple method: carefully cut the loop and weight it in a balance; the area can then be calibrated by weighing a 1 cm^2 square cut from the same paper).
9. Plot the area values as a function of applied stress; calculate the stress in each point by taking into account that the force depends on the weight and the gravity ($F = wg$, where F is the force produced by a weight w with a gravity constant g), and the cross-section area (thickness t by width x), $\sigma = wg/tx$ (see Fig. 7. In this case, we used a negative magnetostriction material, since the slope is negative).
10. Calculate the magnetostriction constant from the slope, as $\lambda_s = 2 A / 3 \sigma$, and transform this value into absolute units by taking into account Eqs (5) and (6). Use always the SI unit System, where magnetic field H is given in A/m, magnetic induction B in T (or Wb/m^2)

Comments

The presented system was conceived to measure amorphous alloys in ribbon shape but it can easily be used to measure laminated cores, as far as they fit into the coils. For ceramic magnetic materials such as ferrites, measurements under tensile stress are not feasible because these materials fracture very easily. They can be measured under compression only, which changes considerably the sample holder.

References

- [1] B.D. Cullity. Introduction to Magnetic Materials (Addison Wesley, 1972), p. 267.

Raul Valenzuela

Raul Valenzuela is Professor of Materials Science at the Institute for Materials Research, National University of Mexico. He has a bachelor degree (Chemical Engineering) from the National University of Mexico, a Master's degree (Ceramic Engineering) from the Ecole Nationale Supérieure de Céramique de Sèvres, France, and a Ph.D. (Materials Science) from the Université de Paris VI, France. He has been involved in research on magnetization processes in ferrites and amorphous alloys, and teaching in the Materials Science program at the University of Mexico, supervising M. Sc. and Ph. D. Projects. He is the author of the book "Magnetic Ceramics", edited by Cambridge University Press (1994). He is a member of MRS and is currently coordinator of the new graduate program on Materials Science and Engineering at the National University of Mexico.

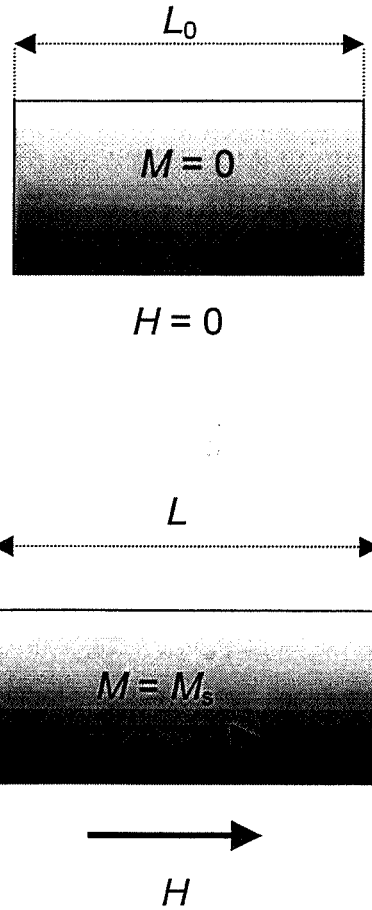
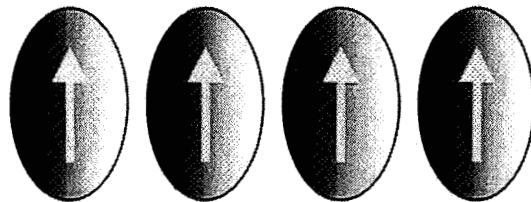
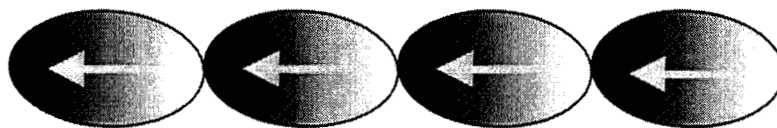


Fig. 1. Schematic representation of increase in length of a ferromagnetic sample upon the application of a magnetic field H .



$H = 0$



H

Fig. 2. Simplified model for the increase in length with magnetization, based on 3d orbitals.

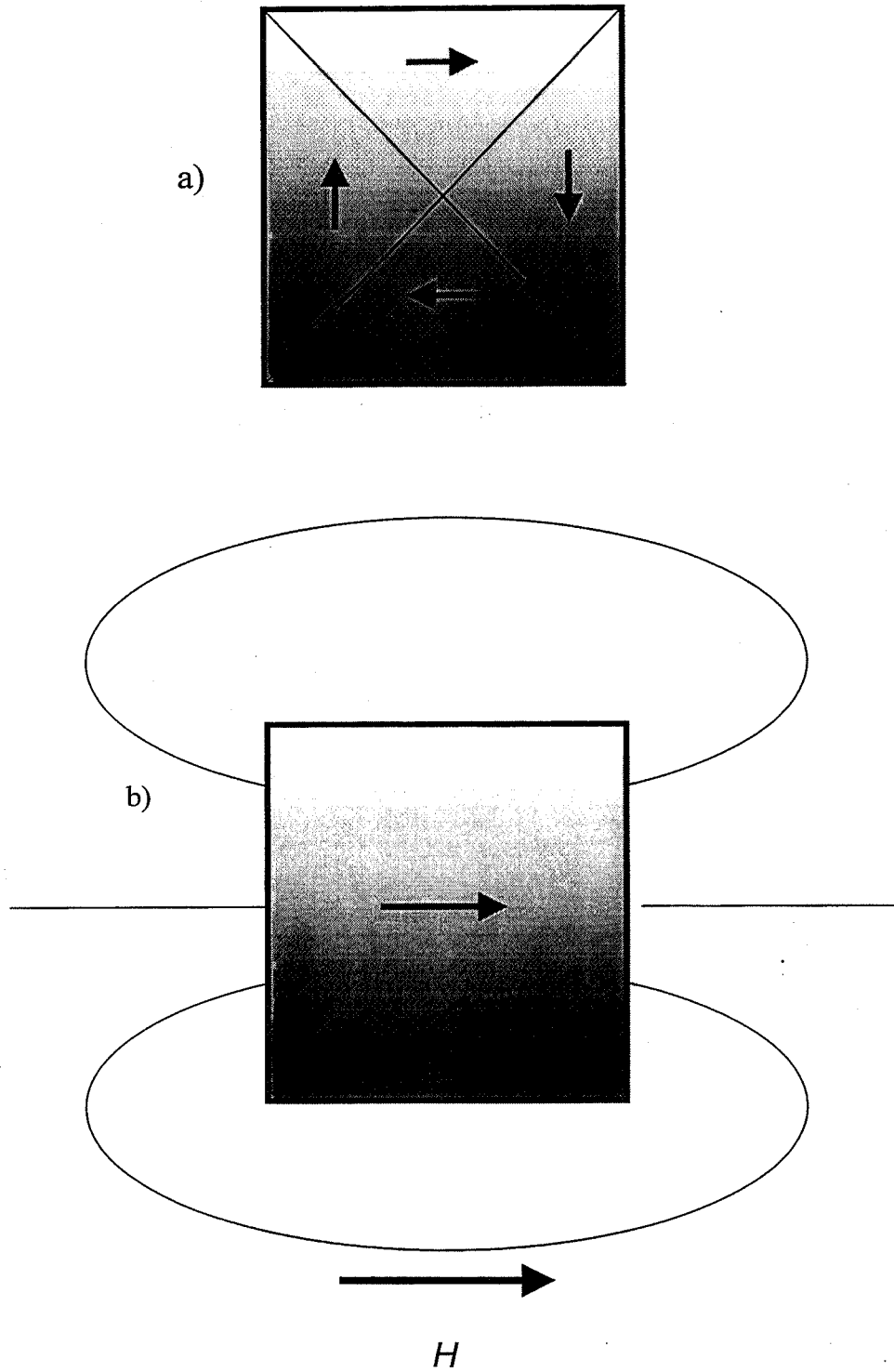


Fig. 3. Magnetic structure, a) in the demagnetized state, showing the domain structure, and b), in the saturated state, under a strong applied field.

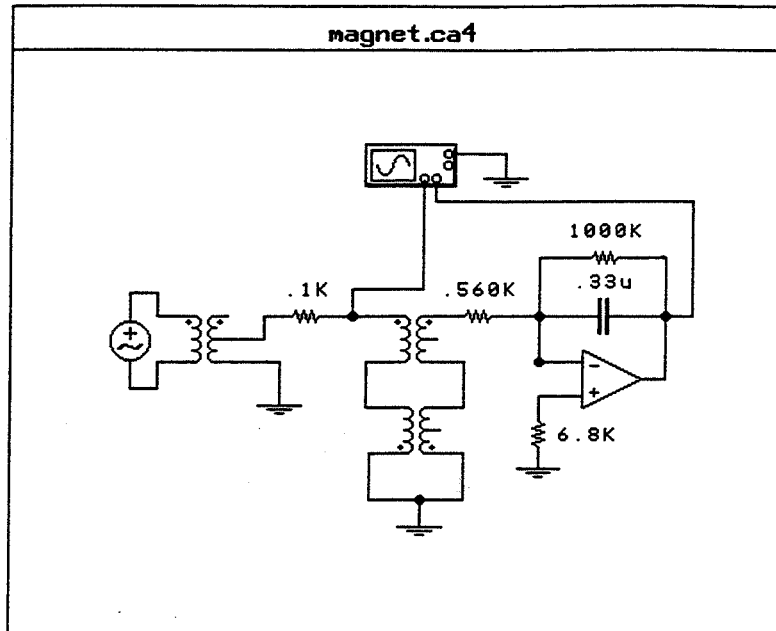


Fig. 4. Layout of the electric circuit.

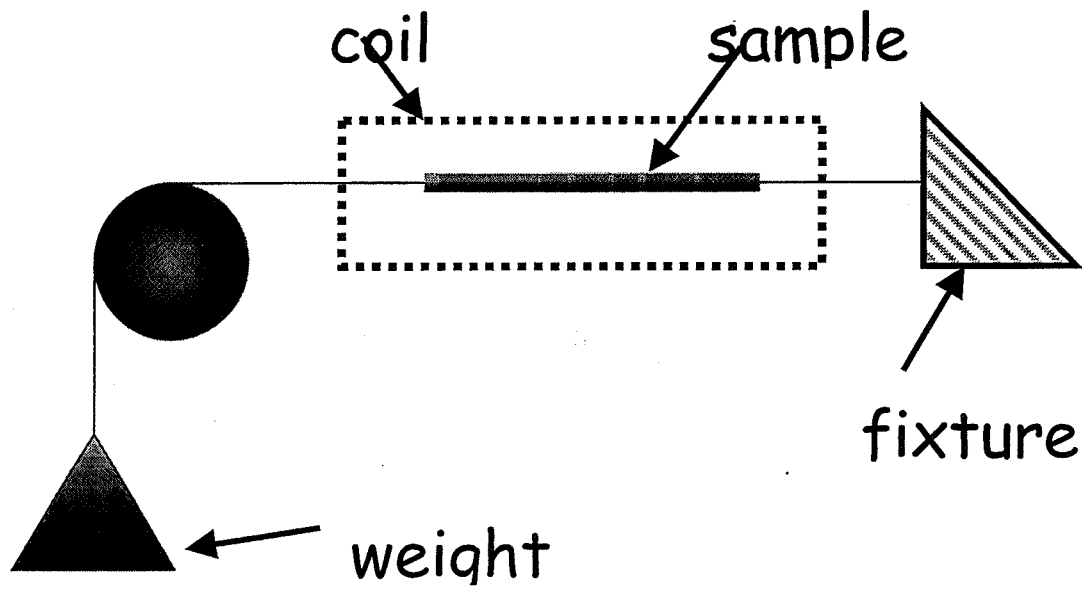
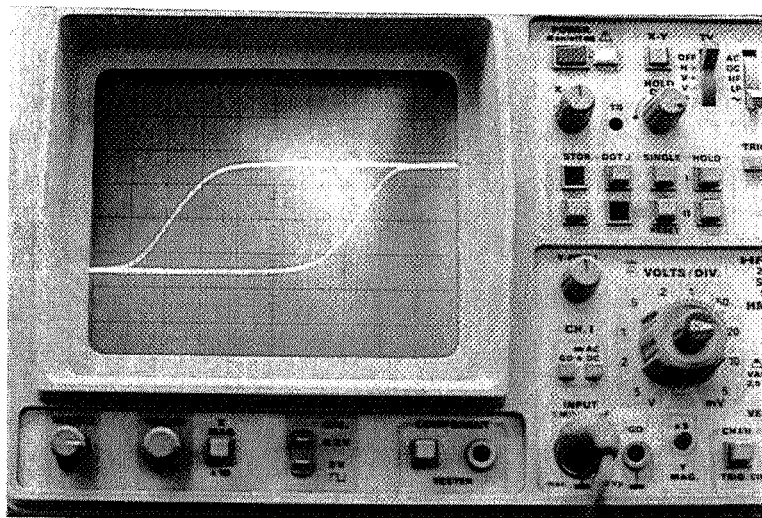
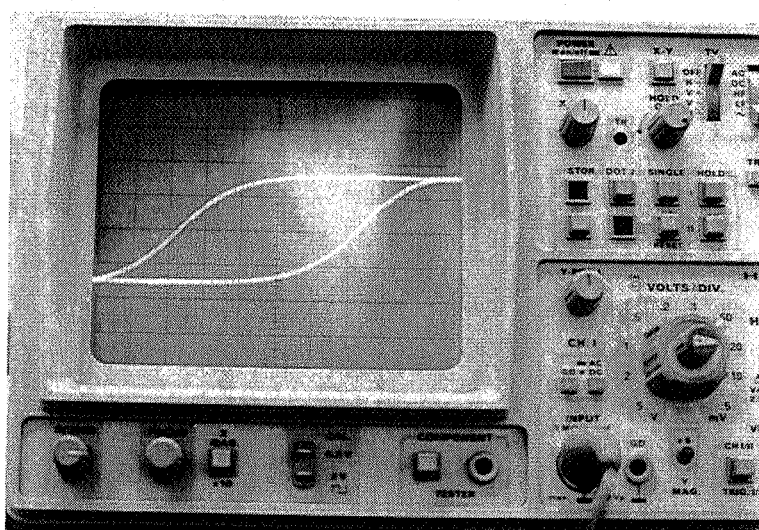


Fig. 5. Layout of the system to apply tensile stress.

a) $\sigma = 0$



b) $\sigma = 16.3$ MPa



c) $\sigma = 26.13$ MPa

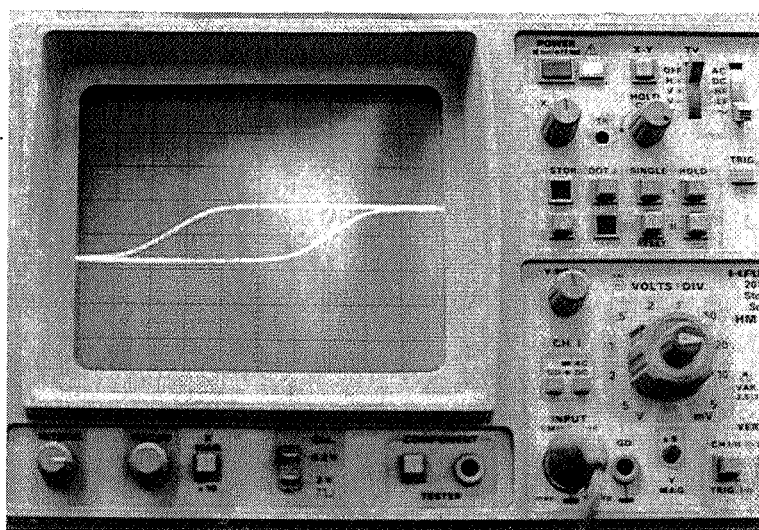


Fig. 6. Change of hysteresis loops of a Vitrovac® 2605 SC ribbon at a) $\sigma = 0$, b) $\sigma = 16.3$ MPa, and c) $\sigma = 26.13$ MPa.

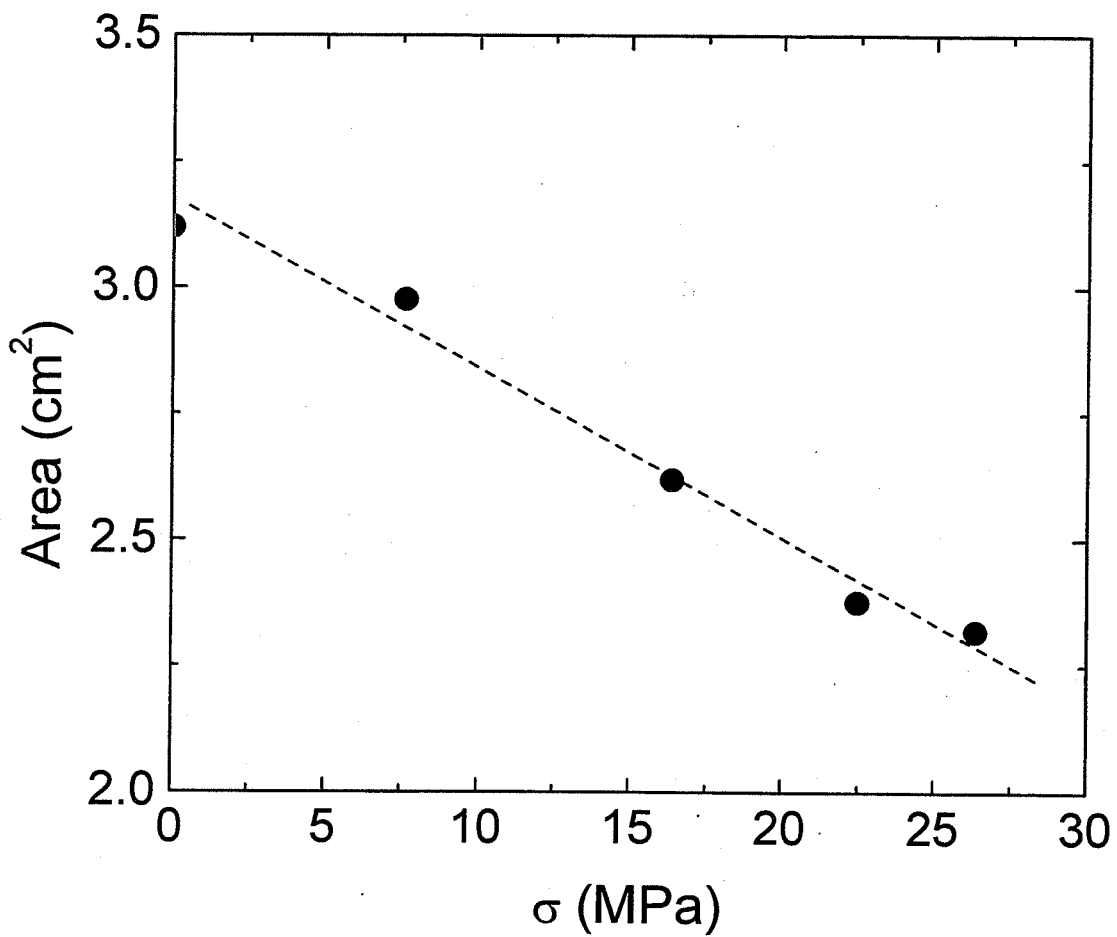


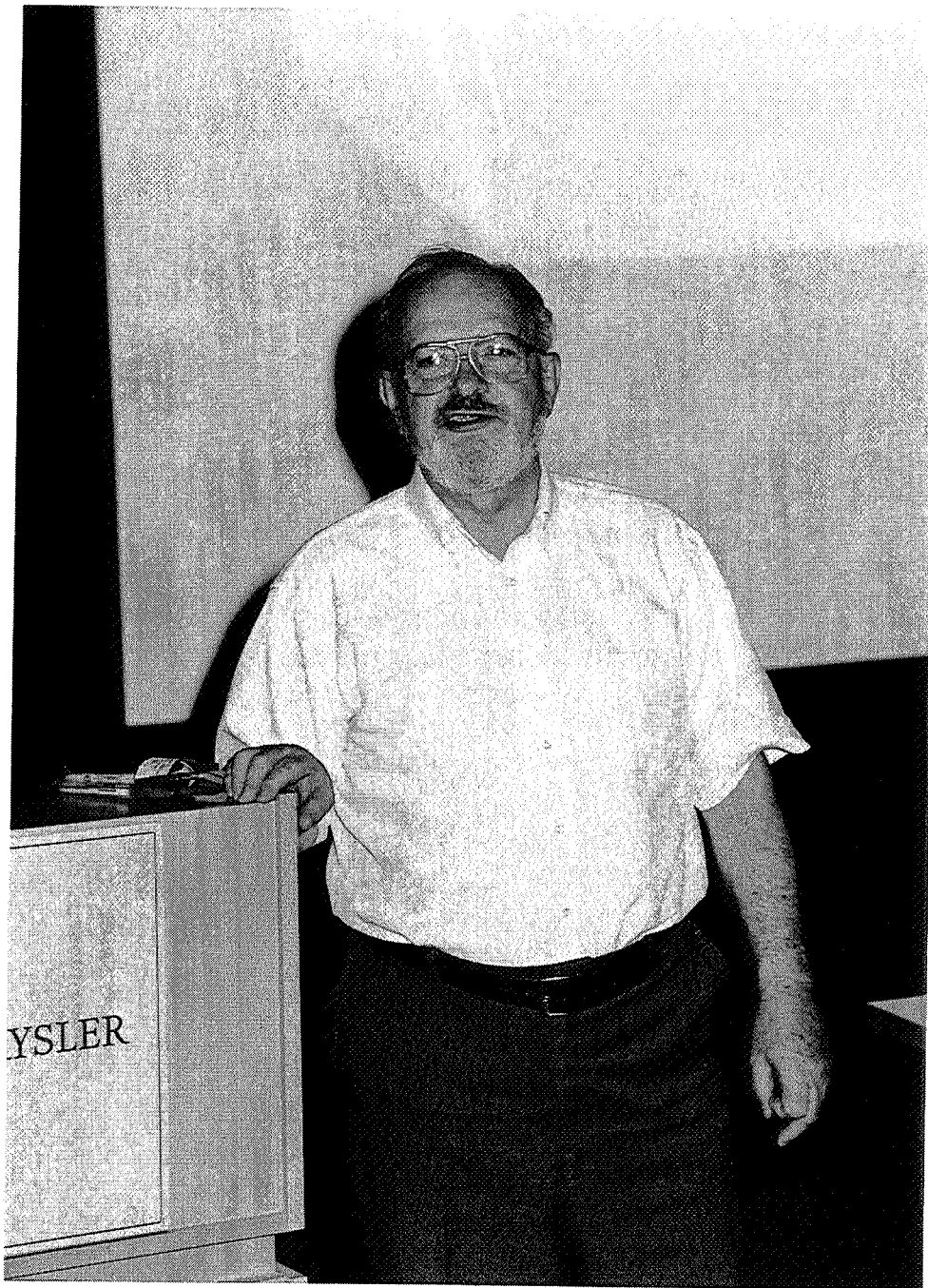
Fig. 7. Results obtained on the Vitrovac® 2605 SC ribbon when plotting the loops area as a function of applied stress.

CORKING AN OPEN-ENDED TANK

Edward L. Widener

School of Technology
Mechanical Engineering Technology
Purdue University
1417 Knoy Hall, Room 145
West Lafayette, Indiana 47907-1317

Telephone: 765-494-7521
e-mail elwidener@tech.purdue.edu



Edward L. Widener

CORKING AN OPEN-ENDED TANK

Edward L. Widener
Mechanical Engineering Technology
Purdue University, W. Lafayette, IN 47907

Key Words: Storage Tanks, Air Pollution, Volatile Emissions, Topology

Prerequisite Knowledge: Basic math (arithmetic, geometry, trigonometry) and physics (buoyancy, capillarity, evaporation).

Objective: To promote creative problem-solving. To see more than one path to a solution. To cope with inadequate information. To recognize an optimal solution, considering constraints of time, cost or accuracy. To meet accreditation criteria for design skill.

Equipment and Materials:

- 1) Containers (cans, pans, bowls, beakers, or jars). Try several sizes between 2 to 8" diameter (say 5-20 cm) and 1 to 6" tall (say 3 to 15 cm).
- 2) Liquids (water or milk). Pour into container, enough to float corks off bottom.
- 3) Floats (several dozen corks, disks, or spheres). Try several sizes, between $\frac{1}{4}$ " – 1" diameter (say 5 to 25 mm). Punched paper holes (6 mm dia) will float. Puffed cereals (foam balls) like Reese's Corn puffs or Kellogg's Fruit-Loops, which are oily & thus water-resistant.
- 4) Ruler (US or SI) to measure containers and floats.

Note that bottle corks (2 cm dia.x 5 cm lg.) may be cut 1 cm long (makes 5 floats). All floats (in a given container) should be the same size (diameter, shape).

Introduction: Here is an open-ended problem, solvable by multiple approaches. Assume your boss needs a quick, cheap answer to an EPA mandate for only 10% uncovered area.. You must find the Open-Area of any Solvent-Tank, subject to Evaporation, after covering the Surface with small Corks in close-packed Pattern. The tank diameters are unknown. All corks are the same, but much smaller than any of the tanks. You try several experiments with specific tanks and floats. Then try a general geometric approach, select a simple "unit-cell", and find the minimal open area is under 10%.

Procedure:

- 1) Tank Shapes – A thin, shallow reservoir has large perimeter, excess surface, but small volume. A tall, narrow cylinder has less perimeter, smaller surface, and relatively more volume. Select a small bowl of milk, sprinkle some cereal-balls, and note the natural

“close-packing” of balls. Surface tension at first will cause 3-ball groups to form, then stirring leads to hex-cell clusters. This 7-ball pattern repeats until liquid is “covered”. Fruit-Loops, with “flowers” in hex-cell shapes, are more convenient (for counting the floats); but sugary cereals may crumble or draw flies.

- 2) Floats – Cork spheres are preferable to cereals, but harder to find. Cork cylinders (boles) are an acceptable substitute, but they float like logs in a pond. Rectangles cannot cover as efficiently as circles. So a popular confection, originally paste from the marsh-mallow plant, comes to mind.
- 3) Miniature marshmallows, floating in a cup of cocoa, are also truncated cylinders. Each cylinder should float upright, with center-of-gravity below center-of-bouyancy. So, cut each cork in half, then into fourths. The larger the container, the more corks needed to cover, but with less edge-effect. Then, since all dimensions are known, count all the disks, calculate the disk-areas, and then subtract from the total tank area. Although tedious and complicated, this suggests that open-area can be reduced to 10%.
- 4) Common Cents – Instead of packing floats inside a given tank, a graphical ploy involves starting with 2-cents and circumscribing with a “circle template” (or compass). Continue with 3-cents (encircling a triangle), then 4-cents (encircled square), 5-cents (encircled body-centered square), 6-cents (enclose larger triangle), 7-cents (enclose hex-cell), 8-cents (double square), 9-cents (5+4), 10-cents (5+5), 12-cents (4+4+4), 13-cents (7 + 6), etc. Measure the enclosing diameter (D), measure the cent diameter (d), count each set of cents (times area of a cent), and figure the open-area (dA). Then, plotting the % open-area (y-axis) vs D/d ratio (x-axis) should produce a curve, which approaches a limit (dA about 10%). This is a dimensionless plot, independent of units.
- 5) Calculus – To find a minimum value for this curve, get an equation for Area Difference (dA) as a function of D/d, set it equal to zero, as D/d approaches infinity, and integrate. However, this confuses most novices needlessly. and is certainly time-consuming.
- 6) Unit Cell Solution – Simply recognize each hex-cell is composed of 6-equilateral triangles. An equilateral triangle contains 3-segments of a cork (60-degree arc). Eureka! Each side of our triangle is twice the radius of our cork. So calculate the triangle’s area, subtract half a circle’s area, and find dA to several decimal places.
- 7) Assume diameters, pi, and dA all have the same significant figures. Assume edge-effects can be ignored.

References:

- 1) Conway, John H., Sloane, N.J.A., et al, “Sphere Packings, Lattices & Groups”, Springer-Verlag Inc., New York, NY, 1998
- 2) Rafson, Harold (ed.), “Odor & VOC Control Handbook”, McGraw-Hill Inc., New York, NY, 1998
- 3) Jacobs, James A., & Kilduff, Thomas F., “Engineering Materials Technology”, 3rd ed., Prentice-Hall Inc., Upper Saddle River, NJ, 1997, pp 184, 402 (Volatile Organic Compounds).
- 4) Degarmo, E. Paul et al, “Materials & Processes in Manufacturing”, 7th ed., Macmillan Co., New York, NY, 1988, p 972 (Chemical Cleaning).
- 5) “Webster’s New Collegiate Dictionary” 2nd ed., G. & C. Merriam Co., Springfield, MA, 1956, p 185 (Cork Oak, quercus suber).

6) Richardson, Terry L. & Lokensgard, Erik, "Industrial Plastics", 3rd ed., Delmar Inc. (ITP), Albany, NY, 1997, p 101 (Foaming/Flowing Polymers).

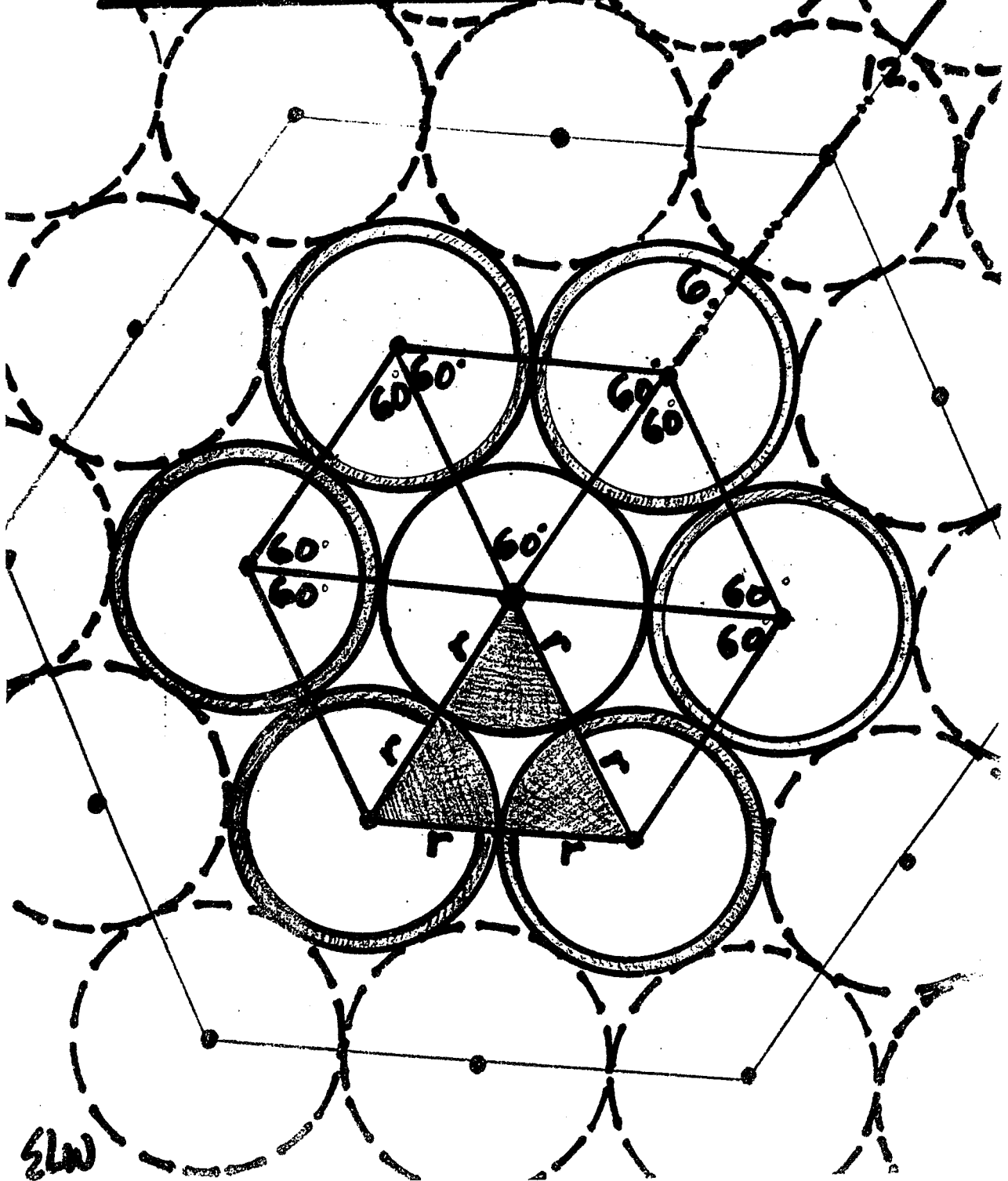
7) Parker, Sybil P. (ed.), "Dictionary of Scientific & Technical Terms", 5th ed., McGraw-Hill Inc., New York, NY, 1994, p 2043 (Topography, Topology).

Biography:

Prof. Widener has taught at Purdue University since 1978, concentrating on mechanics, materials, recycling, and communicating. Ed was in Malaysia from April 1995 – June 1996, teaching Metals Lab for new technology teachers. Memberships include ASEE, ASM, ASME, ISA, TAPPI. A registered P.E. in New York and Indiana, he was ABET accreditation visitor from 1983-1990; and NSF lab-grants reviewer in 1989 and 1990. Between 1974-1977, he had night classes in Indianapolis, IN (IUPUI) and Danville, IL (Jr. College). Degrees from Purdue are BS '49 (physics) and BS '51 (ME); MSEM '62 (Hydraulics) is from University of Kansas. Between 1952-1978, Ed was a process or project engineer for Continental Group, Baker-McHenry-Welch, Kimberly-Clark, E.I. DuPont, Union Carbide, and U.S. Steel. In WWII, he was U.S. Navy S1/c, aboard light-cruisers Vicksburg and Astoria.

2-D CLOSE PACK

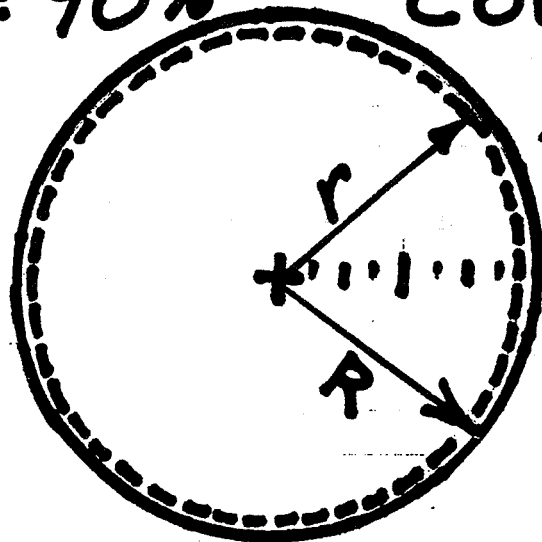
24



SLW

10% OPEN AREA (max.)

= 90% COVER:



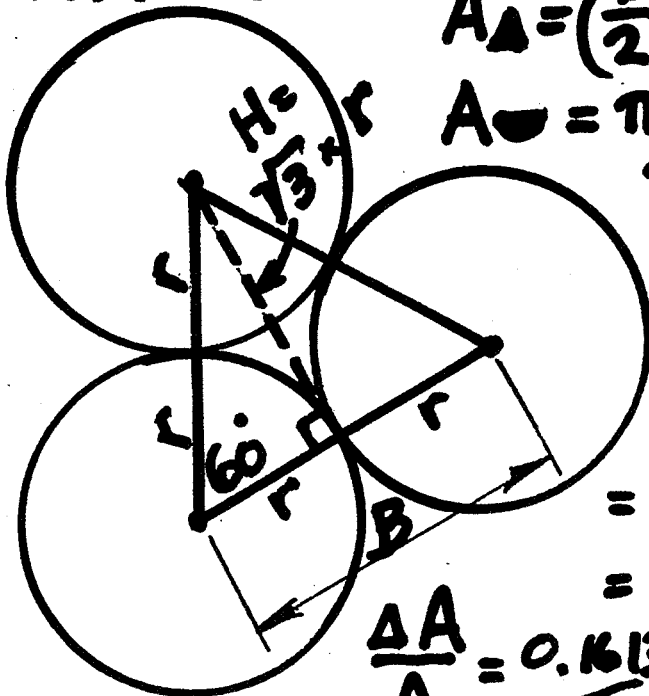
$$a = 0.9A$$

$$\pi r^2 = 0.9 \pi R^2$$

$$r = R \sqrt{0.9}$$

$$\approx 0.95 R$$

UNIT CELL:



$$A_{\Delta} = \left(\frac{B}{2}\right)H = r \cdot r \sqrt{3}$$

$$A_{\circ} = \pi r^2 / 2, \text{ say } r=1.$$

$$\therefore A_{\Delta} - A_{\circ} = \Delta A$$

$$= \sqrt{3} - \frac{\pi}{2}$$

$$= 1.73205 - \frac{3.14159}{2}$$

$$= 1.7321 - 1.5708$$

$$= 0.1613$$

$$\frac{\Delta A}{A} = \frac{0.1613}{1.7321} (100) =$$

$$\boxed{9.31\%}$$

MEASUREMENT OF VISCOSITY: CLASSROOM DEMONSTRATION

Richard B. Griffin

and

Lance Terrill
(student)

Department of Mechanical Engineering
Texas A&M
College Station, Texas 77843

Telephone 409-845-9779
e-mail rgriffin@mengr.tamu.edu



Richard B. Griffin

Measurement of Viscosity: Classroom Demonstration

Dr. Richard Griffin, Faculty
Lance Terrill, Student
Department of Mechanical Engineering
Texas A&M University
College Station, TX 77843

Key Words: Material science, Thermally activated process, Viscometer, Viscosity

Prerequisite Knowledge

Freshmen chemistry, physics, thermally activated processes, mechanical behavior of crystalline solids.

Objective

To demonstrate viscous behavior. To determine the activation energy for a thermally activated process.

Equipment

1. Rotational Viscometer with spindles. The one used in this demonstration is a Cole-Parmer 98936-20/25 Rotational Viscometer.
2. Three glass 600 ml standard beakers.
3. Digital thermometer.
4. Stopwatch.
5. Heater or refrigerator.
6. Three insulating containers to keep the fluids at preset temperature.
7. Spreadsheet computer program.
8. 1200 ml glycerin or other moderately viscous test fluid.

Introduction

Texas A&M University has been part of a National Science Foundation Coalition for more than six years. During this time period, a series of sophomore engineering courses have been developed that are built around the use and application of conservation principles.^{1,2,3} In an effort to provide students with some hands-on experience, several laboratory and demonstration experiments have been developed. In 1998, we reported on a four-point bend experiment that had been developed and used in the classroom.⁴ Similarly in 1998 at the ASEE meeting in Seattle, Washington, we presented a poster describing the development of a 1-D thermal conductivity experiment.⁵ Additionally, we are developing a remote experiment facility for use by the students in the classroom. Currently, we have a tension and a torsion experiment.⁶

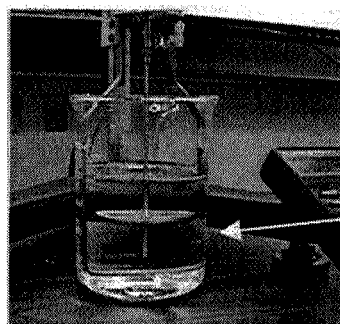
The sophomore sequence consists of five courses: mechanics, thermodynamics, materials, continuum mechanics, and an introduction to electrical engineering. The experiments mentioned above have been used in the materials and the continuum mechanics course. This is an effort on the faculties' part to integrate course material, which is one of the Foundation Coalition's thrusts.

One of the concepts that students struggle with is the idea of viscoelastic behavior. Generally, they are comfortable with elastic behavior, and for many of them they have a reasonable idea of how a component made from metal is suppose to behave. However, when discussing plastics and the idea of a material relaxing under a strain or continuing to elongate under a load is not quite so intuitive. In an effort to increase the understanding of this behavior, a viscosity experiment was developed. The approach is to use a rotational viscometer and to measure the viscosity of the test fluid at several different temperatures.

The educational objective is to measure the viscosity of a fluid at several temperatures and to calculate the activation energy associated with the process.

Procedure

The process involves setting up the viscometer, and selecting the correct rotational speed and spindle for the solution and temperature range of interest. The solutions, contained in 600 ml beakers, are at a known temperature. A thermocouple has been attached to the spindle guard; this is shown in Figure 1. The spindle is lowered into the solution, and the viscosity is read from the digital readout located on the front face of the viscometer.



Thermocouple

Figure 1. Beaker containing the glycerin, spindle, and thermocouple.

Glycerin or glycerol was chosen as the test fluid for two reasons. First, it fit the range of the viscometer that was available. Second, it was clear and the students can see the test being conducted. The measured viscosity of glycerin has been taken from the 69th edition of the handbook of Chemistry and Physics and several of the values are shown in Table 1.⁷

Table 1. Viscosity values for glycerin. (Ref. 7)

T (°C)	Viscosity (P)
-10.8	355
-4.2	149
0	121
6	62.6
15	23
20	14.9
25	9.54

For glycerin, the test was conducted at room temperature or below to stay within the Cole-Parmer Rotational Viscometer's range of 3 – 90,000 Poise(P).

Measurements may be made at any spindle/speed combination, however for accuracy, it is best to follow the suggested combinations in the instruction manual for the viscometer. In the example glycerin experiment, spindle/speed combinations other than the suggested ones were used for thoroughness, however this is not necessary for a demonstration.

Demonstration

Place the viscometer on a level surface and adjust the legs of the viscometer until the bubble level on the top of the instrument shows that it is level. Prepare the viscometer by attaching the spindle guard and connecting the instrument to an appropriate power source. The setup is shown in Figure 2.

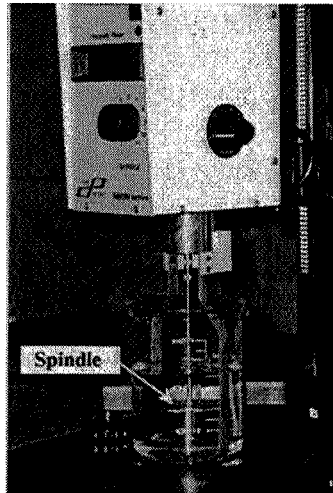


Figure 2. Rotational viscometer showing the setup.

Fill three beakers with 400 ml of glycerin per beaker. Certainly more than three test temperatures may be used, but for time considerations and convenience only three temperatures were used during the classroom demonstration. Refrigerate one at 0°C, one at 10°C, and leave the last one at room temperature. As soon as possible before the experiment, remove the beakers from the refrigerators and place in an insulating holder. The beakers may also be placed in a water bath chilled to the desired temperature before testing, if the demonstration site is very far from a refrigerator.

Turn the “spindle” and “RPM” dials to the appropriate settings. These are located on the instrument. For glycerin over the temperature tested, the R2, R3 and R4 spindles were used and the results are shown in Table 2.

Table 2. Test temperature, spindle speed and spindle used during the test.

Temperature (°C)	Speed RPM	Spindle
0	50	R3
5	20	R2
6	100	R3
9	50	R2
10	100	R3
11	100	R2
23	100	R2

Because of the considerable overlap between the ranges of the R2 and R3 spindles, their use is alternated for some of the testing temperatures. Note that it is important to measure the fluid temperature immediately before each data value is measured.

Attach the appropriate spindle to the viscometer (left-hand threaded screws), and lower it into the glycerin sample up to the fluid level notch on the spindle. Take care to ensure that there are no bubbles trapped beneath the spindle and that the spindle is in the center of the beaker.

Turn the viscometer on. Readings should begin immediately, but wait 30 seconds to record the data. The speed may be changed during instrument operation. When the desired values are obtained, turn off the viscometer and change the spindle or fluid. Record the values under the appropriate column of the spreadsheet.

A double dashed line on the dial of the instrument indicates a viscosity value out of the range of the viscometer. Recheck the speed and spindle dials to ensure that a mistake has not been made.

In the current classroom computers are available for the students to use, and Excel is an easy way for the students to plot the data and determine the activation energy.

Results

The values that were obtained during the experiment are listed in Table 3.

Table 3. Viscosity data for glycerin obtained using a rotating viscometer.

Temperature (K)	Temperature (C)	Viscosity (P)	1/T (1/K)	ln Viscosity
273	0	92.5	0.00366	4.527
278	5	57.5	0.00360	4.052
279	6	50	0.00358	3.912
280	7	41.5	0.00357	3.726
282	9	38.1	0.00355	3.640
283	10	32	0.00353	3.466
284	11	30	0.00352	3.401
296	23	9.45	0.00333	2.246

The data may be plotted as viscosity vs. temperature on a Cartesian coordinate graph or a natural logarithm of viscosity vs. inverse temperature graph to help evaluate the activation energy.

The following plot, shown in Figure 3, is a Cartesian plot of the data collected that illustrates the exponential nature of the relationship between viscosity and temperature.

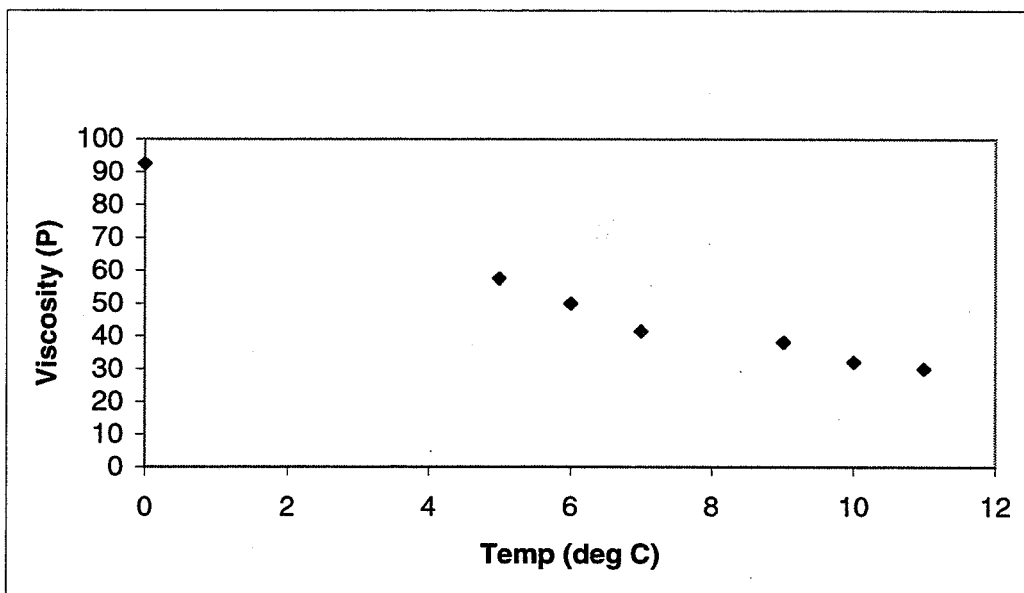


Figure 3. A plot of the data obtained during the viscosity experiment with glycerin.

The following plot, Figure 4, is the natural logarithm of viscosity vs. inverse temperature plot that shows a linear correlation between the data. This is an excellent example for the students to observe a thermally activated process or a process that can be described using the Arrhenius equation.⁸

$$\eta = \eta_0 e^{(Q/RT)}$$

Rate or viscosity

η_0 - constant or pre-exponential term

Q- activation energy

R- gas constant

T- temperature (K)

The slope of the line shown in Figure 4 may be used to determine the activation energy, and it is determined to be 15,900 cal/mol.

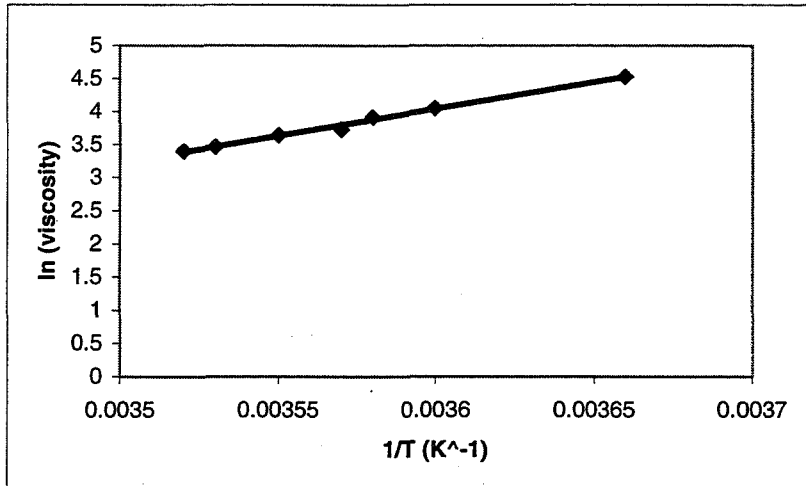


Figure 4. Arrhenius plot of the viscosity data

As a comparison, calculating the activation energy for the data shown in Table 1 gives an activation energy of 15,700 ca/mol.⁷

Conclusion

A viscosity experiment was developed for use in the classroom. The results obtained from the experiment for glycerin compares favorably with published data. The data fit an Arrhenius equation or thermally activated process and the activation energies were in close agreement.

Acknowledgement

The authors would like to thank the National Science Foundation for their support through the Foundation Coalition, Director Karen Friar, University of Alabama. Project No. NSF EEC-9221460.

References

- ¹ Griffin, R. B., Everett, L. J., Keating, P., Lagoudas, D., Tebeaux, E., Parker, D., Bassichis, W. and Barrow, D., "Planning the Texas A&M University College of Engineering Sophomore Year Integrated Curriculum," Fourth World Conference on Engineering Education, Oct. 95, St Paul, MN, vol. 1 pp. 228-232.
- ² Griffin, R. B., Everett, L., and Lagoudas, D., "Development of a Sophomore Year Engineering Program at Texas A&M University," FIE, Pittsburgh, PA, Nov. 1997.
- ³ Glover, C., "Conservation Principles and the Structure of Engineering," McGraw-Hill, New York, NY, 1996.
- ⁴ Griffin, R. B., Cornwell, L. R., Yapura, C., Krishnan, S., and Hallford, J., "Use of a Four-Point Bend Apparatus to Determine the Modulus of Elasticity," National Educators Workshop Update 98, Brookhaven, NY, 1-4 November, 1998.
- ⁵ Griffin, R. B., Ragupathi, P., Johnson, E., "Development of a Thermal Conductivity Experiment for Use in Class," ASEE, Seattle, WA, 1998.
- ⁶ Yapura, C. L. Richard Griffin, R. B., Lagoudas, D. L., "Mechanics of Materials Experiments Via the Internet," National Instruments Week, Austin, TX, Aug. 1999.
- ⁷ Handbook of Chemistry and Physics, Weast, R. C., ed., 69th edit., CRC Press, Inc., 1988.

⁸ "The Science and Design of Engineering Materials," Schaffer, Saxena, Antolovich, Sanders, & Warner, Irwin (McGraw Hill), Chicago, 1995.

Biographical Information

Richard Griffin has been at Texas A&M in Mechanical Engineering since 1977. His research area is aqueous corrosion, and he received a NACE Technical Achievement Award in 1992. For the past five years, he has been a member of the Sophomore Team-Foundation Coalition that developed the core engineering science courses, which have been adopted at Texas A&M University.

Lance Terrill is an undergraduate student in Mechanical Engineering at Texas A&M University. We met during a materials science class and Lance has helped me for the past nine months. For the fall semester, he is working as a co-operative education student.

THE ROLE OF PLASTICS IN THE AUTOMOBILE

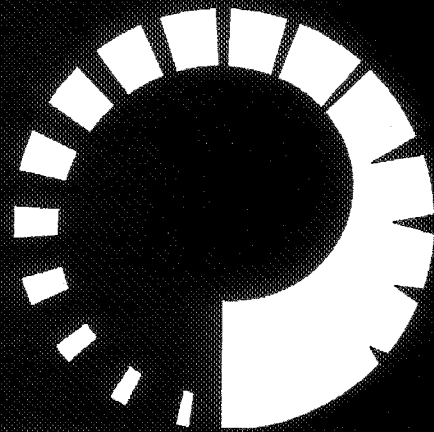
Bruce Cundiff

Director of Automotive
American Plastics Council
1800 Crooks Road, Suite A
Troy, Michigan 48084

e-mail bcundiff@ameriplas.org



Bruce Cundiff



American
Plastics
Council®

*The Role of Plastics in the
Automobile*

Bruce Cundiff

Director of Automotive

November 3, 1999



American
Plastics
Council

What will automobiles be like in 10 years?

- ▶ Pretty much the same
- ▶ Yet completely different!
- ▶ Lower emissions
- ▶ Greater fuel economy
- ▶ Higher safety standards



American
Plastics
Council

The 2007 Automobile & Lt. Truck

- ▶ **Fueled by alcohol (5%), natural gas (2%), electricity (2%), hybrid (5%), diesel (5-10%), gasoline(76-81%)**
- ▶ **10%/6% lighter (pass. car/lt. truck)**
- ▶ **Electronic content from 13 to 19% of total vehicle cost**

Source: Delphi IX, OSAT, U of Michigan



American
Plastics
Council

Pounds of Material in a Typical Family Vehicle

Source: 99 Ward's, OSAT, American Metal Market

Material	1998	2009 @ 35 mpg
Aluminum	219 lbs.	257 (+17.5%)
Cast Iron	359	287 (-20%)
Copper	46	43 (-6%)
Glass	95	94 (-1%)
Magnesium	6.5	7.8 (+20%)
Plastic/Composite	243.5	292 (+20%)
Powdered Metal	32.5	35 (+7%)
Rubber (incl. Tires)	139.5	138 (-1%)
Steel	1810	1540 (-15%)
Zinc die castings	13.5	14 (+4%)
Total	3261	2710



American
Plastics
Council

What are the Drivers?

- ▶ **Societal**
 - **EPA (CAFÉ), NHTSA**
 - **PNGV**
- ▶ **Global Competition (costs, performance)**
- ▶ **Global (European) Standards**



American
Plastics
Council

Why Plastics?

Light Weight

- Reduced fuel consumption
- Reduced emissions
- Reduced material usage
- Longer tire wear
- Smaller engine requirements
- Reduced suspension requirements
- Reduced fuel consumption for parts delivery



American
Plastics
Council

Why Plastics?

Durability

- Longer, more reliable vehicle life
- Better economy to the owner
- Reduced landfill demand
- Reduced material usage

Manufacturability

- “Net Shape” engineering minimizes material usage
- Efficient part manufacturing
- Parts consolidation, conserves resources

Design Flexibility

- More streamlined shapes
- More complex shapes



American
Plastics
Council

Plastics Usage in Automobiles (North America)

Year	Lbs./vehicle	Total Lbs. (billion)
1970	70	
1999	257	4.0
2009	313	5.1

Source: Automotive Plastics Report – 1999, *Market Search, Inc.*



American
Plastics
Council

Plastics Applications

Segment	1999	2009
Body Panels	TBD	
Bumper System		
Electrical		
Mechanical, Engine, Chassis, Int.		
Flexible Components		
Fuel System		
Int. Trim/Other Lg. Functional		
Structural		
Transparent Parts		
Exterior Trim		
Upholstery		



American
Plastics
Council

Automotive Plastics

The Challenges - and Opportunities

- ▶ **Total Energy Management**
- ▶ **Safety**
- ▶ **Recycling/Life Cycle Analysis**



American
Plastics
Council

Plastics Trade Associations Meeting the Challenge

- ▶ The Automotive Learning Center's Expanding Role
 - Recycling Technology
 - SPE Strategic Collaboration
 - The "4-Wheel Strategies"

Bruce T. Cundiff
Director of Automotive
American Plastics Council
Automotive Learning Center

Bruce Cundiff joined the American Plastics Council (APC) April 15, 1998, as Director of Automotive, replacing the retiring Al Maten. He directed the highly successful startup of APC's new Automotive Learning Center, located in Troy, MI. The overall goal of this new facility is to become a center of knowledge and expertise on the current and future use of plastics for automotive applications.

Bruce joined the APC after having nearly 32 years' experience in plastics manufacturing, research, finance, product management, and marketing with the DuPont Company. In 1986, he relocated from Wilmington, DE to the Detroit area as a Senior Marketing Programs Manager, where he focused on selling and marketing plastics to the automotive industry.

Bruce has a BSME and an MS in Industrial Administration (Krannert School of Management) from Purdue University.

REPORT DOCUMENTATION PAGE			Form Approved OMB No. 0704-0188	
Public reporting burden for this collection of information is estimated to average 1 hour per response, including the time for reviewing instructions, searching existing data sources, gathering and maintaining the data needed, and completing and reviewing the collection of information. Send comments regarding this burden estimate or any other aspect of this collection of information, including suggestions for reducing this burden, to Washington Headquarters Services, Directorate for Information Operations and Reports, 1215 Jefferson Davis Highway, Suite 1204, Arlington, VA 22202-4302, and to the Office of Management and Budget, Paperwork Reduction Project (0704-0188), Washington, DC 20503.				
1. AGENCY USE ONLY (Leave blank)	2. REPORT DATE October 2000	3. REPORT TYPE AND DATES COVERED Conference Publication		
4. TITLE AND SUBTITLE National Educators' Workshop: Update 99 <i>Standard Experiments in Engineering, Materials Science, and Technology</i>			5. FUNDING NUMBERS WU 251-10-01-01	
6. AUTHOR(S) Compiled by Ginger L. F. Arrington, James E. Gardner, James A. Jacobs, John E. Fillion, and P. K. Mallick				
7. PERFORMING ORGANIZATION NAME(S) AND ADDRESS(ES) NASA Langley Research Center Hampton, VA 23681-2199			8. PERFORMING ORGANIZATION REPORT NUMBER L-18010	
9. SPONSORING/MONITORING AGENCY NAME(S) AND ADDRESS(ES) National Aeronautics and Space Administration, Washington, DC 20546-0001; Norfolk State University, Norfolk, VA 23504; Department of Defense, Washington, DC 20301-1000; National Institute of Standards and Technology, Gaithersburg, MD 20899 DaimlerChrysler Corporation, Auburn Hills, MI 48326 University of Michigan, Dearborn, MI 48128			10. SPONSORING/MONITORING AGENCY REPORT NUMBER NASA/CP-2000-210325	
11. SUPPLEMENTARY NOTES Arrington and Gardner: Langley Research Center, Hampton, VA; Jacobs; Norfolk State University, Norfolk, VA; Fillion: DaimlerChrysler, Auburn Hills, MI; and Mallick: University of Michigan, Dearborn, MI.				
12a. DISTRIBUTION/AVAILABILITY STATEMENT Unclassified-Unlimited Subject Category 23 Availability: NASA CASI (301) 621-0390			12b. DISTRIBUTION CODE Distribution: Standard	
13. ABSTRACT (Maximum 200 words) This document contains a collection of experiments presented and demonstrated at the National Educators' Workshop: Update 99, held at DaimlerChrysler, Auburn Hills, Michigan, from October 31–November 3, 1999.				
14. SUBJECT TERMS Materials; Experiments; Education			15. NUMBER OF PAGES 706	
			16. PRICE CODE A99	
17. SECURITY CLASSIFICATION OF REPORT Unclassified	18. SECURITY CLASSIFICATION OF THIS PAGE Unclassified	19. SECURITY CLASSIFICATION OF ABSTRACT Unclassified	20. LIMITATION OF ABSTRACT UL	